Wind and Seismic Effects

Proceedings of the 32nd Joint Meeting

NIST Special Publication 963

Stephen A. Cauffman, Editor

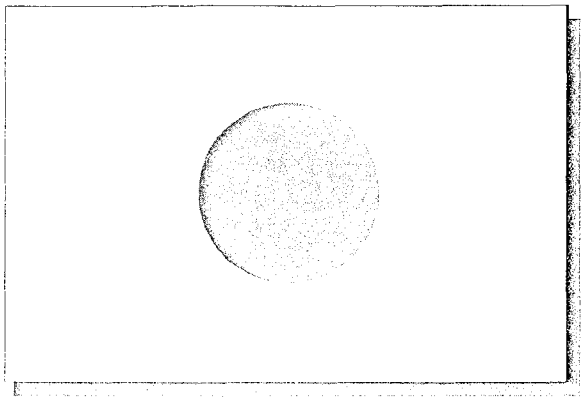

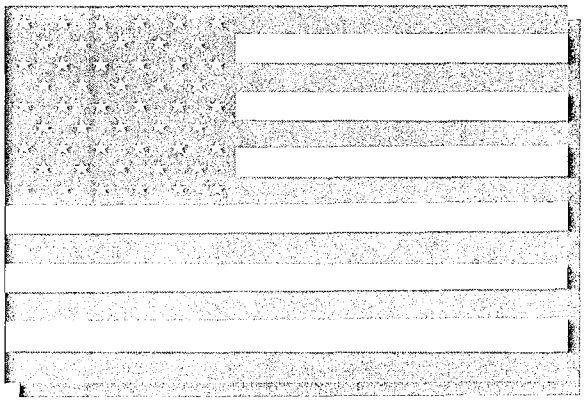

National Institute of Standards and Technology
Technology Administration, U.S. Department of Commerce

NIST CENTENNIAL 1901-2001

The National Institute of Standards and Technology was established in 1988 by Congress to "assist industry in the development of technology . . . needed to improve product quality, to modernize manufacturing processes, to ensure product reliability . . . and to facilitate rapid commercialization . . . of products based on new scientific discoveries."

NIST, originally founded as the National Bureau of Standards in 1901, works to strengthen U.S. industry's competitiveness; advance science and engineering; and improve public health, safety, and the environment. One of the agency's basic functions is to develop, maintain, and retain custody of the national standards of measurement, and provide the means and methods for comparing standards used in science, engineering, manufacturing, commerce, industry, and education with the standards adopted or recognized by the Federal Government.

As an agency of the U.S. Commerce Department's Technology Administration, NIST conducts basic and applied research in the physical sciences and engineering, and develops measurement techniques, test methods, standards, and related services. The Institute does generic and precompetitive work on new and advanced technologies. NIST's research facilities are located at Gaithersburg, MD 20899, and at Boulder, CO 80303. Major technical operating units and their principal activities are listed below. For more information contact the Publications and Program Inquiries Desk, 301-975-3058.

Office of the Director
- National Quality Program
- International and Academic Affairs

Technology Services
- Standards Services
- Technology Partnerships
- Measurement Services
- Information Services

Advanced Technology Program
- Economic Assessment
- Information Technology and Applications
- Chemistry and Life Sciences
- Materials and Manufacturing Technology
- Electronics and Photonics Technology

Manufacturing Extension Partnership Program
- Regional Programs
- National Programs
- Program Development

Electronics and Electrical Engineering Laboratory
- Microelectronics
- Law Enforcement Standards
- Electricity
- Semiconductor Electronics
- Radio-Frequency Technology[1]
- Electromagnetic Technology[1]
- Optoelectronics[1]

Materials Science and Engineering Laboratory
- Intelligent Processing of Materials
- Ceramics
- Materials Reliability[1]
- Polymers
- Metallurgy
- NIST Center for Neutron Research

Chemical Science and Technology Laboratory
- Biotechnology
- Physical and Chemical Properties[2]
- Analytical Chemistry
- Process Measurements
- Surface and Microanalysis Science

Physics Laboratory
- Electron and Optical Physics
- Atomic Physics
- Optical Technology
- Ionizing Radiation
- Time and Frequency[1]
- Quantum Physics[1]

Manufacturing Engineering Laboratory
- Precision Engineering
- Manufacturing Metrology
- Intelligent Systems
- Fabrication Technology
- Manufacturing Systems Integration

Building and Fire Research Laboratory
- Applied Economics
- Structures
- Building Materials
- Building Environment
- Fire Safety Engineering
- Fire Science

Information Technology Laboratory
- Mathematical and Computational Sciences[2]
- Advanced Network Technologies
- Computer Security
- Information Access
- Convergent Information Systems
- Information Services and Computing
- Software Diagnostics and Conformance Testing
- Statistical Engineering

[1] At Boulder, CO 80303.
[2] Some elements at Boulder, CO.

Wind and Seismic Effects

NIST SP 963

PROCEEDINGS OF
THE 32ND JOINT
MEETING OF
THE U.S.-JAPAN
COOPERATIVE PROGRAM
IN NATURAL RESOURCES
PANEL ON WIND AND
SEISMIC EFFECTS

Issued April 2001

Stephen A. Cauffman,
EDITOR

Structures Division
Building and Fire Research Laboratory
Gaithersburg, MD 20899-8610

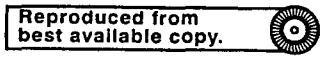

U.S. Department of Commerce
Donald L. Evans, Secretary

National Institute of Standards and Technology
Karen H. Brown, Acting Director

National Institute of Standards and Technology Special Publication 963
Natl. Inst. Stand. Technol. Spec. Publ. 963, 549 pages (April 2001)
CODEN: NSPUE2

U.S. GOVERNMENT PRINTING OFFICE
WASHINGTON: 2001

For sale by the Superintendent of Documents, U.S. Government Printing Office
Internet: bookstore.gpo.gov — Phone: (202) 512-1800 — Fax: (202) 512-2250
Mail: Stop SSOP, Washington, DC 20402-0001

PREFACE

This publication contains the proceedings of the 32nd Joint Meeting of the U.S.-Japan Panel on Wind and Seismic Effects. The meeting was held at the National Institute of Standards and Technology (NIST), Gaithersburg, Maryland (USA), during May 16-19, 2000. The proceedings include the program, list of members, task committee reports, and technical papers submitted to the Joint Panel Meeting, and a summary of the technical site visits.

BACKGROUND

Responding to the need for improving engineering and scientific practices through exchange of technical data and information, research personnel, and research equipment, the United States and Japan in 1961 created the U.S.-Japan Cooperative Science Program. Three collateral programs comprise the Cooperative Science Program. One of the three, the U.S.-Japan Cooperative Program in Natural Resources (UJNR), was created in January 1964. The objective of UJNR is to exchange information on research results and exchange scientists and engineers in the area of natural resources for the benefit of both countries. UJNR is composed of 18 Panels, each of which is responsible for specific technical subjects.

The Panel on Wind and Seismic Effects was established in 1969. Seventeen U.S. and seven Japanese agencies participate with representatives of private sector organizations to develop and exchange technologies aimed at reducing damage from high winds, earthquakes, storm surge, and tsunamis. This work is produced through collaboration between U.S. and Japanese member researchers working in eleven task committees. Each task committee focuses on specific technical issues, e.g., earthquake strong motion data. The Panel provides the vehicle to exchange technical data and information on design and construction of civil engineering lifelines, buildings, and waterfront structures, and to exchange high wind and seismic measurement records. Annual meetings alternate between Japan and the U.S. (odd numbered years in Japan; even numbered years in the U.S.). These one-week technical meetings provide a forum to discuss ongoing research and research results; they are followed by a series of technical site visits.

The National Institute of Standards and Technology (NIST) provides the U.S.-side chairman and secretary-general. The Public Works Research Institute (PWRI) provides the Japan-side chairman and secretary-general.

Annual meetings provide the mechanism for interaction between U.S. and Japanese researchers in wind and seismic engineering, creating opportunities to gain valuable information and to engage in cooperative research. Through these opportunities, the Panel member organizations have realized important advances in building and structures technology. The Panel's activities have resulted in improved building and structures codes and standards in both countries; for example, the Panel:

- created and exchanged digitized earthquake records used as the basis of design and research for Japan and the United States;
- transferred earthquake engineering information and strong-motion measurement techniques for use by seismically active countries, e.g., Australia, Canada, Italy, Mexico, Peru, Taiwan, Turkey, and North Africa;
- produced data that advanced the design and construction of bridge structures;
- produced large-scale testing data that advanced the seismic design standards for buildings;
- improved in-situ measurement methods for soil liquefaction and stability under seismic loads;
- created a database on storm surge and tsunamis and verified mathematical models of tsunami and storm surge warning systems;
- established a library resource of current research on wind and earthquake engineering and on storm surge and tsunamis;
- published proceedings of Panel Meeting and Task Committee Workshops;
- provided earthquake science and technology expertise to the U.S.-Japan Natural Disaster Reduction Initiative of the U.S.-Japan Framework for New Economic Partnership (Common Agenda);
- created a web site for promoting the Panel's activities widely.

The Panel's efforts are exemplary of effective joint research and technology delivery between researchers from the U.S. and Japan. Since its creation, more than 1900 papers have been presented in 32 Joint Meetings, more than 60 Task Committee Workshops were held, and over 200 guest researchers have participated in exchange programs. The Panel provides important information about the U.S. and Japan's civil engineering thrusts, which influence both countries' research and provide the basis for improvements in building and structures codes and standards.

HIGHLIGHTS OF THE 32nd JOINT PANEL MEETING

- Technical presentations:
  - Forty-four papers were presented during ten sessions.
  - Important knowledge was exchanged for research and practice, e.g., information systems for risk assessment and disaster response using Geographical Information Systems; performance-based design of buildings, bridges, and port facilities; wind and earthquake engineering for buildings, bridges and other structures; research findings and lessons learned from recent natural disasters; and research findings on public health issues following natural disasters.

- Task Committee activities:
  - The T/C structure is an extremely effective vehicle to explore in depth the technologies and methods being used by both countries.
  - Five Task Committee Workshops and Meetings were held in the past year.
  - Five Task Committee Workshops/Committee Meetings are planned for the coming year.

- Strategic Plan Development:

Recognizing its strengths and accomplishments and a desire to position itself functionally and organizationally to address future challenges, the Panel agreed to appoint a Joint Ad-Hoc Planning Committee to develop a strategic plan for the Panel. The Joint Ad-Hoc Planning Committee will:

- Evaluate the current organization, task committee structure, annual technical meeting and site visit program, cooperative research projects, and related operating procedures.
- Assess current and emerging technical needs and interests of government agencies in the two countries.
- Review options for streamlining and increasing the efficiency of Panel operations and for moving toward more effective operating procedures.
- Develop a joint strategic plan for the Panel and present it to the Panel for adoption in early 2001.

John L. Gross, Secretary-General
U.S.-side Panel on Wind and Seismic Effects

CONTENTS

AGENDA

AGENDA
32ND JOINT MEETING
PANEL ON WIND AND SEISMIC EFFECTS
16-19 May 2000

May 16 (Tuesday)

10:00 Opening Ceremonies

Call to order by John GROSS, Secretary-General, U.S.-Side Panel on Wind and Seismic Effects

Welcome by James HILL, Deputy Director, Building and Fire Research Laboratory, National Institute of Standards and Technology

Opening Remarks by Takao KURAMOCHI, Counselor for Science and Technology, Embassy of Japan

Opening Remarks Donald FERGUSON, U.S.-side Coordinator, UJNR, International Relations Advisor, U.S. Department of Agriculture

Remarks by S. Shyam SUNDER, Chairman U.S.-Side, Panel on Wind and Seismic Effects and Chief, Structures Division, National Institute of Standards and Technology

Remarks by Tomomitsu FUJII, Chairman Japan-Side, Panel on Wind and Seismic Effects and Director-General, Public Works Research Institute

Introduction of Japan Members by Japan Panel Chairman

Introduction of U.S. Members by U.S. Panel Chairman

Election of Joint Meeting Chairman

Adoption of Agenda

Adjourn

11:45 Group Photograph

12:00 Session 1 (Information Technology for Land Management and Natural Disaster Prevention Countermeasures) Chairman - Mr. Tomomitsu Fujii

12:00 Web-Based GIS Support to Disaster Response; William ROPER, (NIST)
12:20 Draft Manual for Seismic Information System Development; Hideki SUGITA and Tomofumi NOZAKI, (PWRI)

12:40 Lunch: Hosted by John Filson, Manager, Earthquake Hazards Program, U.S. Geological Survey

13:40 Session 1 (Information Technology for Land Management and Natural Disaster Prevention Countermeasures) – Continued

13:40 The US Tsunami Mitigation Initiative, Michael BLACKFORD (NOAA)
14:00 Discussion

14:20 Break

14:40 Session 2 (Wind Engineering) Chairman – Mr. Tomomitsu Fujii

14:40 Design for Wind/Rain Response of Bridge Cables; Harold BOSCH (FHWA)
15:00 Study on Performance-Based Design Methods for Wind Effects on Bridges, Hiroshi SATO and Ken-ichi OGI (PWRI)
15:20 Safe Rooms/Shelters; Cliff OLIVER (FEMA)
15:40 Discussion

16:00 Break

16:20 Task Committee Meetings

A: Strong Motion Data and Applications
B: Testing and Evaluation Procedures for Building Systems
C: High-Performance Structural Systems and Auto-Adaptive Media
D: Earthquake Engineering for Dams
E: Design for Wind and Wind Hazard Mitigation
F: Disaster Prevention Methods for Lifeline Systems

17:30 Adjourn for day

19:00 Banquet hosted by US-Side (National Academy of Sciences)

May 17 (Wednesday)

8:30 Session 3 (Special Topics: Natural Disasters in the World and the Lessons Learned, 1) Chairman - Dr. S. Shyam Sunder

8:30 Urbanization and Urban Disaster Prevention; Tomomitsu FUJII (PWRI)
8:50 Effects of the 17 August 1999 Kocaeli (Izmit) Earthquake and the 12 November 1999 Duzce Earthquake, Turkey on Dams; Ellis KRINITSKY, Mostafiz CHOWDHURY, and Ghassan AL-CHAAR (USACE)

9:10 Damage of Transportation Facilities in the 1999 Kocaeli, Turkey Earthquake and the Chi Chi, Taiwan Earthquake; Kaszuhiko KAWASHIMA and Gaku SHOJI (Tokyo Institute of Technology)

9:30 The Performance of the Trans European Motorway Structures During the Nov. 12, 1999 Düzce Earthquake; Hamid GHASEMI, James Cooper (FHWA), Roy IMBSEN (Imbsen & Associates, Inc.)

9:50 Building Damages in Taiwan Chi Chi Earthquake; Masaomi TESHIGAWARA, Hiroshi FUKUYAMA, Hiroto KATO, and Mizuo INUKAI (BRI)

10:10 Discussion

10:40 Break

11:00 Session 4 (Special Topics: Natural Disasters in the World and the Lessons Learned 2)
Chairman - Dr. S. Shyam Sunder

11:00 Bridge Lessons in Taiwan – W. Phillip YEN (FHWA)

11:20 Damage of Earth Retaining Structures During the 1999 Chi-Chi Earthquake; Ken-Ichi TOKIDA, Osamu MATSUO, and Shinya NAKAMURA (PWRI)

11:40 Information Infrastructure and Reconstruction After Hurricane Mitch; William ROPER (NIST)

12:00 Storm Surge Disaster by Typhoon No. 18 in 1999; Hiroyasu KAWAI (PHRI) (presented by Takashi NAGAO)

12:20 Discussion

12:50 Lunch: Hosted by Priscilla Nelson, Director, Division of Civil and Mechanical Systems, National Science Foundation

13:50 Session 5 (Earthquake Engineering 1) Chairman – Dr. S. Shyam Sunder

13:50 Seismic Testing of a 1/20-Scale 2D Model of Koyna Dam; Robert HALL and Mostafiz CHOWDHURY, Enrique MATHEU (USACE)

14:10 Development of Smart Materials and Structural Systems – Research Plan on Structural Systems, Sensing, and Effectors; Shunsuke OTANI (University of Tokyo), Hisahiro HIRAISHI (BRI), Mitsumasa MIDORIKAWA (BRI), Masanori IIBA (BRI), Masaomi TESHIGAWARA (BRI)

14:30 Nonlinear Analysis of Concrete Dams; Luis DEBEJAR, Robert HALL (USACE)

14:50 Pre-Analytical Study on Damage Detection Test of Five-Story Steel Frame with Simulated Damage; Masaomi TESHIGAWARA, Takashi KAMINOSONO, Mizuo INUKAI, Hiroshi ISODA, Koichi MORITA, and Kazuya NOGUCHI (BRI)

15:10 Limiting Pore Pressures in Deep Soil Deposits, M.E. HYNES and Richard LEDBETTER (USACE)

15:30 Soil Amplification Factor for Seismic Design of Buildings; Izuru OKAWA, Masanori IIBA, Mitsumasa MIDORIKAWA, Shin KOYAMA (BRI), and Kenji MIURA (Kajima Corp.)

15:50 Discussion

16:20 Break

16:30 Task Committee Meetings
G: Seismic Information Systems
H: Soil Behavior and Stability during Earthquakes
I: Storm Surge and Tsunami
J: Wind and Earthquake Engineering Systems for Transportation Systems

17:30 Adjourn for Day

19:00 Individually hosted dinners

May 18 (Thursday)

8:30 Session 6 (Earthquake Engineering 2) Chairman – Mr. Tomomitsu Fujii

8:30 Probabilistic Analysis of Liquefaction of Soils; M. E. HYNES and Don YULE (USACE)
8:50 Construction of a Base-Isolated House for Observation of Isolation Effects During Earthquake and Wind; Yasuyuki YAMANOUCHI, Mitsumasa MIDORIKAWA, Masanori IIBA (BRI), Masayoshi IKENAGA (Oiles Corp.), and Kenichi MACHIDA (Sumitomo Forestry Co., Ltd.) presented by Izuru OHKAWA)
9:10 Structural Control; Michael RILEY and Fahim SADEK (NIST)
9:30 Seismic Design Ground Motion for Strait-Crossing Projects in Japan; Keiichi TAMURA, Shojiro KATAOKA, Yoshihiro NAKAO (PWRI) and Masahiko YASUDA (HSBA)
9:50 Discussion

10:20 Break

10:40 Session 7 (Earthquake Engineering 3) Chairman – Mr. Tomomitsu Fujii

10:40 Development of Seismic Isolation Technology for Underground Structures and the Application; Shigeki UNJOH, Jun-Ichi HOSHIKUMA, Kazuhiro NAGAYA (PWRI), Takeyasu SUZUKI (Kumagai-gumi Corp.)
11:00 Earthquake Motions at an Embankment Dam Base and an Estimation Method of Incident Seismic Waves Using the Observations; Yoshikazu YAMAGUCHI and Tomoya IWASHITA (PWRI)
11:20 Reproduction of Large-Scale 1G Test on Dry Sand Deposit and Pile Foundation using Centrifuge Modeling (Step-2); Tikahiro MINOWA (NRI), Masayoshi SATO (Shimizu Co.), Yukiko SAITO (PWRI), Takaaki KAGAWA (Wayne State University), and Akio ABE (Tokyo Soil Research Co.)
11:40 Discussion

12:10 Break

12:20 Session 8 (Performance Based Design Methods 1) Chairman –Mr. Tomomitsu Fujii

12:20 Comparison of Performance-Based Design Codes for Bridges in Various Countries; Michio OKAHARA and Masahiro NISHITANI (PWRI)
12:40 Recommended Changes to the AASHTO Specifications for the Seismic Design of Bridges (NCHRP Project 12-49); Ian FRIEDLAND (ATC), Ronald MAYES

13:00 Lunch: Hosted by Jack Snell, Director, Building and Fire Research Laboratory, National Institute of Standards and Technology

14:00 Session 8 (Performance Based Design Methods 1) - Continued

14:00 Performance-Based Design – The Big Picture; Tim SHECKLER, (FEMA)
14:20 Earthquake Resistant Design of Port Facilities; Takashi NAGAO and Atsushi NOZU (PHRI)
14:40 GIS and Pre- and Post-Disaster Risk Assessment, Stuart NISHENKO (FEMA)
15:00 Discussion

15:30 Break

15:50 Session 9 (Performance-Based Design Methods 2) Chairman –Mr. Tomomitsu Fujii

15:50 Structural Housing Systems; Fahim SADEK (NIST)
16:10 Performance-Based Damage Assessment and Design Verification of U.S. Housing in Extreme Earthquake and Hurricane Events; Jay CRANDALL (NAHB Research Center) and William FREEBORNE (HUD)
16:30 American Lifeline Alliance and Performance-Based Guidelines for Lifelines and Utilities; Woody SAVAGE (FEMA)
16:50 Discussion

17:10 Adjourn

18:15 US-Side Hosted Dinner at Smokey Glen

May 19 (Fri)

8:30 Session 10 (Public Health) Chairman – Dr. S. Shyam Sunder

8:30 A Proposed Model for Multidisciplinary Needs Assessment in Post Disaster Settings; Josephine MALILAY (CDC)
8:50 Living Difficulties After Earthquakes and the Related Phenomena; Keishi SHIONO (Nagaoka College) (presented by Keiichi TAMURA)
9:10 Predictors for People's Response to Tornado Warning, Arkansas, March 1, 1997; Lina BALLUZ (CDC)

9:30 Post-Disaster Carbon Monoxide Poisoning; An Emerging Health Problem; Randolph DALEY (CDC)
9:50 Assessment of Public Health Needs Among Displaced Persons Residing in a Temporary Camp Following the August 1999 Earthquakes in Turkey; Dahna BATTS-OSBORNE (CDC)
10:10 Wind-Related Climactic Disaster-Related Deaths in the United States, 1994-1998; Julie JACOBSEN (CDC)
10:30 Discussion

10:50 Break

11:05 Workshop Reports

12:00 Reports of Task Committees 1

13:00 Lunch: Hosted by Craig Wingo, Director of the National Earthquake Program, Federal Emergency Management Agency

14:00 Reports of Task Committees 2

15:00 Adoption of Final Resolutions

15:50 Break

16:00 Closing Ceremonies

Call to Order by John GROSS, Secretary-General, US-side Panel

Closing Remarks by Tomomitsu FUJII, Chairman Japan-side Panel

Closing Remarks by S. Shyam SUNDER, Chairman US-side Panel

16:30 Conclusion of 32nd Joint Panel Technical Sessions

19:00 Japan-Side Hosted Dinner at Japan Inn

Technical Site Visits
32nd Joint Panel on Wind and Seismic Effects

Saturday, 20 May	Depart Washington Dulles at 9:20 am on United Airlines Flight UA1919 Arrive San Juan, Puerto Rico 1:11 pm (local time) Sightseeing in Old San Juan Stay at Marriott Condado Beach Hotel
Sunday, 21 May	Visit Arecibo Observatory Radio Telescope (NSF) Cultural visit to Rio Camuy Cave Park Travel to Ponce, Puerto Rico Stay at Holiday Inn in Ponce
Monday, 22 May	Visit Cerrillos and Portugues dam projects (USACE) Cultural tour of Serralles Castle and Parque de Bombas Return to San Juan Stay at Caribe Hilton in San Juan
Tuesday, 23 May	Visit Tren Urbano (mass transit system – under construction) Japan-side delegation departs from San Juan

List of Panel Members

JAPAN-SIDE PANEL ON WIND AND SEISMIC EFFECTS
MEMBERSHIP LIST

STEERING COMMITTEE MEMBERS

Mr. Tomomitsu Fujii
Chairman, Japan-side Panel on Wind and Seismic Effects
Director-General, Public Works Research Institute
Ministry of Construction
1, Asahi, Tsukuba-shi, Ibaraki-ken 305-0804
Tel: 0298-64-2211
Fax: 0298-64-2148
E-mail: fujii310@pwri.go.jp

Dr. Michio Okahara
Secretary-General, Japan-side Panel on Wind and Seismic Effects
Director, Structure and Bridge Department
Public Works Research Institute
Ministry of Construction
1, Asahi, Tsukuba-shi, Ibaraki-ken 305-0804
Tel: 0298-64-2211
Fax: 0298-64-0565
E-mail: okahara@pwri.go.jp

Mr. Hiroshi Akiyama
Director, Geographic Department
Geographical Survey Institute
Ministry of Construction
1, Kitasato, Tsukuba-shi, Ibaraki-ken 305-0811
Tel:0298-64-1111
Fax:0298-64-1804

Mr. Yoshitoki Hashimoto
Director, Disaster Countermeasure Office
Coast Administration Disaster Prevention Division
Ports and Harbors Bureau
Ministry of Transport
2-1-3, Kasumigaseki, Chiyoda-ku, Tokyo 100-0013
Tel: 03-3580-7021
Fax: 03-5511-8280

Dr. Hisahiro Hiraishi
Director, Codes and Evaluation Research Center
Building Research Institute
Ministry of Construction
1, Tatehara, Tsukuba-shi, Ibaraki-ken 305-0802
Tel: 0298-64-6633
Fax: 0298-64-6773
E-mail: hiraishi@kenken.go.jp

Dr. Susumu Iai
Director, Earthquake Disaster Prevention Laboratory
Port and Harbour Research Institute
Ministry of Transport
3-1-1, Nagase, Yokosuka-shi, Kanagawa-ken 239-0826
Tel: 0468-44-5030
Fax: 0468-44-0839
E-mail: iai@ipc.phri.go.jp

Dr. Toshio Iwasaki
President, Civil Engineering Research Laboratory
1-18 Kandasuda-cho
Chiyoda-ku, Tokyo 101-0041
Tel: 03-3254-9481
Fax: 03-3254-9448

Mr. Kouichi Iwase
Office for Disaster Prevention Research
Research and Development Bureau
Science and Technology Agency
Prime Minister's Office
2-2-1, Kasumigaseki, Chiyoda-ku, Tokyo 100-0013
Tel: 03-3503-8164
Fax: 03-3503-8169

Dr. Takashi Kaminosono
Associate Director for International Codes and Standards
Codes and Evaluation Research Center
Building Research Institute
Ministry of Construction
1, Tatehara, Tsukuba-shi, Ibaraki-ken 305-0802
Tel:0298-64-6665
Fax:0298-64-6774
E-mail: kamino@kenken.go.jp

Dr. Kazumasa Kato
Director, Hydraulic Engineering Division
Port and Harbour Research Institute
Ministry of Transport
3-1-1, Nagase, Yokosuka-shi, Kanagawa-ken 239-0826
Tel: 0468-44-5009
Fax: 0468-41-3888

Mr. Shirou Kato
Director, Road Disaster Prevention Section
Road Bureau
Ministry of Construction
2-1-3, Kasumigaseki, Chiyoda-ku, Tokyo 100-0013
Tel: 03-3580-4311
Fax: 03-5251-1949
E-mail: katou0zv@road.hs.moc.go.jp

Prof. Kazuhiko Kawashima
Professor, Department of Civil Engineering
Tokyo Institute of Technology
2-12-1, O-okayama, Meguro-ku, Tokyo 152-0033
Tel: 03-5734-2922
Fax: 03-3729-0728
E-mail: kawasima@cv.titech.ac.jp

Mr. Osamu Matsuo
Head, Soil Dynamics Division
Earthquake Disaster Prevention Research Center
Public Works Research Institute
Ministry of Construction
1, Asahi, Tsukuba-shi, Ibaraki-ken 305-0804
Tel: 0298-64-2933
Fax: 0298-64-2576
E-mail: matsuo@pwri.go.jp

Mr. Chikahiro Minowa
Cooperative Research Officer
National Research Institute for Earth Science and Disaster Prevention
3-1, Tennodai, Tsukuba-shi, Ibaraki-ken 305-0006
Tel: 0298-51-1611
Fax: 0298-51-5658
E-mail: minowa@geo.bosai.gov.jp

Mr. Toshitaka Miyata
Director, International Affairs Division
Economic Affairs Bureau
Ministry of Construction
2-1-3, Kasumigaseki, Chiyoda-ku, Tokyo 100-0013
Tel: 03-3580-4311
Fax: 03-3502-3955
E-mail: miyat01e@econ.hs.moc.go.jp

Dr. Takashi Nagao
Chief of Geotechnical Earthquake Engineering Laboratory
Port and Harbour Research Institute
Ministry of Transport
3-1-1, Nagase, Yokosuka-shi, Kanagawa-ken 239-0826
Tel: 0468-44-5028
Fax: 0468-44-0839
E-mail: nagao@ipc.phri.go.jp

Dr. Nobuyuki Narita
President, Japan Steel Structure Corporation
3-3-1, Marunouthi, Chiyoda-ku, Tokyo 100-0005
Tel: 03-3212-0875
Fax: 03-3212-0878

Mr. Kazuhiro Nishikawa
Head, Bridge Division
Structure and Bridge Department
Public Works Research Institute
Ministry of Construction
1, Asahi, Tsukuba-shi, Ibaraki-ken 305-0804
Tel: 0298-64-2905
Fax: 0298-64-0565
E-mail: knishikawa@pwri.go.jp

Dr. Isao Nishiyama
Head, Housing Construction Division
Production Department
Building Research Institute
Ministry of Construction
1, Tatehara, Tsukuba-shi, Ibaraki-ken 305-0802
Tel: 0298-64-2151
Fax: 0298-64-6774
E-mail: isao@kenken.go.jp

Mr. Tomiyoshi Ogawa
Director, Building Disaster Prevention Section
Housing Bureau
Ministry of Construction
2-1-3, Kasumigaseki, Chiyoda-ku, Tokyo 100-0013
Tel: 03-3580-4311
Fax: 03-3580-7050
E-mail: ogawa0a2@house.hs.moc.go.jp

Mr. Keiichi Ohtani
Director, Disaster Prevention Research Division
National Research Institute for Earth Science and Disaster Prevention
Science and Technology Agency
3-1, Tennodai, Tsukuba-shi, Ibaraki-ken 305-0006
Tel: 0298-51-1611 ex.321
Fax: 0298-52-8512
E-mail: ohtani@knetgk.k-net.bosai.go.jp

Dr. Hisashi Okada
Director, Structural Engineering Department
Building Research Institute
Ministry of Construction
1, Tatehara, Tsukuba-shi, Ibaraki-ken 305-0802
Tel: 0298-64-6641
Fax: 0298-64-6773
E-mail: okada@kenken.go.jp

Prof. Tsuneo Okada
Professor, Department of Architecture and Building Engineering
Shibaura Institute of Technology
3-9-14 Shibaura, Minato-ku, Tokyo 108-0023
Tel: 03-5476-2452
Fax: 03-5476-2446

Dr. Izuru Ohkawa
Head, Construction Techniques Division
Production Department
Building Research Institute
Ministry of Construction
1, Tatehara, Tsukuba-shi, Ibaraki-ken 305-0802
Tel: 0298-64-2151
Fax: 0298-64-6777
E-mail: okawa@kenken.go.jp

Mr. Kazuo Okayama
Director, Earthquake Disaster Countermeasure Division
Disaster Prevention Bureau
National Land Agency
1-2-2, Kasumigaseki, Chiyoda-ku, Tokyo 100-0013
Tel: 03-3593-3311
Fax: 03-3501-5199

Dr. Hiroshi Sato
Head, Structure Division
Structure and Bridge Department
Public Works Research Institute
Ministry of Construction
1, Asahi, Tsukuba-shi, Ibaraki-ken 305-0804
Tel: 0298-64-2874
Fax: 0298-64-0565
E-mail: hsato@pwri.go.jp

Dr. Takahiro Sugano
Chief, Structural Dynamics Laboratory
Structural Engineering Division
Port and Harbour Research Institute
Ministry of Transport
3-1-1, Nagase, Yokosuka-shi, Kanagawa-ken 239-0826
Tel: 0468-44-5029
Fax: 0468-44-0839
E-mail: macsuga@ipc.phri.go.jp

Dr. Hideki Sugita
Head, Earthquake Disaster Prevention Technology Division
Earthquake Disaster Prevention Research Center
Public Works Research Institute
Ministry of Construction
1, Asahi, Tsukuba-shi, Ibaraki-ken 305-0804
Tel: 0298-64-3245
Fax: 0298-64-0598
E-mail: sugita@pwri.go.jp

Mr. Hidetaka Takagi
Director, Structure Department
Civil Engineering Research Institute
Hokkaido Development Bureau
Prime Minister's Office
1-3, Hiragishi, Toyohira-ku, Sapporo-shi
Hokkaido 062-0931
Tel: 011-841-5175
Fax: 011-820-2714

Mr. Ken-ichi Takahashi
International Cooperation Coordinator, International Affairs Division,
Science and Technology Promotion Bureau
Science and Technology Agency
2-2-1, Kasumigaseki, Chiyoda-ku, Tokyo 100-0013
Tel: 03-3593-0362
Fax: 03-3501-5909
E-mail: katakaha@sta.go.jp

Mr. Syuji Takasu
Director, Dam Department
Public Works Research Institute
Ministry of Construction
1, Asahi, Tsukuba-shi, Ibaraki-ken 305-0804
Tel: 0298-64-2832
Fax: 0298-64-0164
E-mail: takasu@pwri.go.jp

Dr. Keiichi Tamura
Head, Ground Vibration Division
Earthquake Disaster Prevention Research Center
Public Works Research Institute
Ministry of Construction
1, Asahi, Tsukuba-shi, Ibaraki-ken 305-0804
Tel: 0298-64-2926
Fax: 0298-64-0598
E-mail: tamura@pwri.go.jp

Dr. Masaomi Teshigawara
Head, Structure Division
Department of Structural Engineering
Building Research Institute
Ministry of Construction
1, Tatehara, Tsukuba-shi, Ibaraki-ken 305-0802
Tel: 0298-64-6753
Fax: 0298-64-6773
E-mail: teshi@kenken.go.jp

Mr. Ken-ichi Tokida
Director, Earthquake Disaster Prevention Research Center
Public Works Research Institute
Ministry of Construction
1, Asahi, Tsukuba-shi, Ibaraki-ken 305-0804
Tel: 0298-64-2829
Fax: 0298-64-0598
E-mail: tokida@pwri.go.jp

Mr. Ken-ichi Torii
Head, Coast Division
River Department
Public Works Research Institute
Ministry of Construction
1, Asahi, Tsukuba-shi, Ibaraki-ken 305-0804
Tel: 0298-64-2211
Fax: 0298-64-1168
E-mail: torii@pwri.go.jp

Dr. Hajime Tsuchida
Executive Counselor, Nippon Steel Co., Ltd.
2-6-3, Ohte-machi, Chiyoda-ku, Tokyo 100-0004
Tel: 03-3275-5894
Fax: 03-3275-5648

Dr. Takaaki Uda
Director, River Department
Public Works Research Institute
Ministry of Construction
1, Asahi, Tsukuba-shi, Ibaraki-ken 305-0804
Tel: 0298-64-2211
E-mail: uda@pwri.go.jp

Dr. Shigeki Unjoh
Head, Earthquake Engineering Division
Earthquake Disaster Prevention Research Center
Public Works Research Institute
Ministry of Construction
1, Asahi, Tsukuba-shi, Ibaraki-ken 305-0804
Tel: 0298-64-4966
Fax: 0298-64-4424
E-mail: unjoh@pwri.go.jp

Mr. Shoin Yagi
Director, Typhoon Research Department
Meteorological Research Institute
Japan Meteorological Agency
1-1, Nagamine, Tsukuba-shi, Ibaraki-ken 305-0052
Tel: 0298-53-8663
Fax: 0298-53-8735

Dr. Yoshikazu Yamaguchi
Head, Fill-type Dam Division
Dam Department
Public Works Research Institute
Ministry of Construction
1, Asahi, Tsukuba-shi, Ibaraki-ken 305-0804
Tel: 0298-64-2413
Fax: 0298-64-0164
E-mail: yamaguti@pwri.go.jp

Dr. Hiroyuki Yamanouchi
Director, Codes and Evaluation Research Center
Building Research Institute
Ministry of Construction
1, Takehara, Tsukuba-shi, Ibaraki-ken 305-0802
Tel: 0298-64-6688
Fax: 0298-64-67701
E-mail: yamanoch@kenken.go.jp

Mr. Takashi Yokota
Senior Assistant for Disaster Prevention
Planning Division
Administration Department
Japan Meteorological Agency
1-3-4, Ohte-machi, Chiyoda-ku, Tokyo 100-0013
Tel: 03-3212-8341
Fax: 03-3212-2453

Dr. Akio Yoshida
Director, Seismology and Volcanology
Research Department
Meteorological Research Institute
Japan Meteorological Agency
1-1, Nagamine, Tsukuba-shi, Ibaraki-ken 305-0052
Tel: 0298-53-8675
Fax: 0298-53-8735

Dr. Kiyofumi Yoshino
Director, Disaster Management Division
River Bureau
Ministry of Construction
2-1-3, Kasumigaseki, Chiyoda-ku, Tokyo 100-0013
Tel: 03-3580-4311 Ext. 3431
Fax: 03-5251-1946
E-mail: yanag0an@river.hs.moc.go.jp

SECRETARIES COMMITTEE MEMBERS

Dr. Michio Okahara
Secretary-General, Japan-side Panel on Wind and Seismic Effects
Director, Structure and Bridge Department
Public Works Research Institute
Ministry of Construction
1, Asahi, Tsukuba-shi, Ibaraki-ken 305-0804
Tel: 0298-64-2211
Fax: 0298-64-0565
E-mail: okahara@pwri.go.jp

Mr. Jiro Fukui
Head, Foundation Engineering Division
Structure and Bridge Department
Public Works Research Institute
Ministry of Construction
1, Asahi, Tsukuba-shi, Ibaraki-ken 305-0804
Tel: 0298-64-2211
Fax: 0298-64-0565
E-mail: fukui@pwri.go.jp

Dr. Hisahiro Hiraishi
Director, Structural Engineering Department
Building Research Institute
Ministry of Construction
1, Tatehara, Tsukuba-shi, Ibaraki-ken 305-0802
Tel: 0298-64-6633
Fax: 0298-64-6773
E-mail: hiraishi@kenken.go.jp

Dr. Masanori Iiba
Head, Aerodynamics Division
Structural Engineering Department
Building Research Institute
Ministry of Construction
1, Tatehara, Tsukuba-shi, Ibaraki-ken 305-0802
Tel: 0298-64-6654
Fax: 0298-64-6773
E-mail: iiba@kenken.go.jp

Mr. Kenji Ikeda
Director, Structures Division
Structures Department.
Civil Engineering Research Institute
Hokkaido Development Bureau
Prime Minister's Office
1-3, Hiragishi, Toyohira-ku, Sapporo-shi
Hokkaido 062-0931
Tel: 011-841-1111
Fax: 011-820-2714
E-mail: ikedak@ceri.go.jp

Mr. Jun-ich Kaneko
Head, Planning Division
Geographic Department
Geographical Survey Institute
Ministry of Construction
1, Kitasato, Tsukuba-shi, Ibaraki-ken 305-0811
Tel: 0298-64-1111
Fax: 0298-64-1804

Mr. Osamu Matsuo
Head, Soil Dynamics Division
Earthquake Disaster Prevention Research Center
Public Works Research Institute
Ministry of Construction
1, Asahi, Tsukuba-shi, Ibaraki-ken 305-0804
Tel: 0298-64-2933
Fax: 0298-64-2576
E-mail: matsuo@pwri.go.jp

Mr. Chikahiro Minowa
Cooperative Research Officer
National Research Institute for Earth Science and Disaster Prevention
3-1, Tennodai, Tsukuba-shi, Ibaraki-ken 305-0006
Tel: 0298-51-1611
Fax: 0298-51-5658
E-mail: minowa@geo.bosai.gov.jp

Dr. Takashi Nagao
Chief of Geotechnical Earthquake Engineering Laboratory
Port and Harbour Research Institute
Ministry of Transport
3-1-1, Nagase, Yokosuka-shi, Kanagawa-ken 239-0826
Tel: 0468-44-5028
Fax: 0468-44-0839
E-mail: nagao@ipc.phri.go.jp

Mr. Ryouji Namikawa
Head, International Cooperation Division
Planning and Research Administration Department
Public Works Research Institute
Ministry of Construction
1, Asahi, Tsukuba-shi, Ibaraki-ken 305-0804
Tel: 0298-64-4412
Fax: 0298-64-4322
E-mail: namikawa@pwri.go.jp

Mr. Kazuhiro Nishikawa
Head, Bridge Division
Structure and Bridge Department
Public Works Research Institute
Ministry of Construction
1, Asahi, Tsukuba-shi, Ibaraki-ken 305-0804
Tel: 0298-64-2905
Fax: 0298-64-0565
E-mail: knishika@pwri.go.jp

Dr. Nobuyuki Ogawa
Head, Earthquake Engineering Laboratory
National Research Institute for Earth Science and Disaster Prevention
Science and Technology Agency
3-1, Tennodai, Tsukuba-shi, Ibaraki-ken 305-0006
Tel: 0298-51-1611
Fax: 0298-51-5658
E-mail: ogawa@geo.bosai.go.jp

Mr. Keiichi Ohtani
Director, Disaster Prevention Research Division
National Research Institute for Earth Science and Disaster Prevention
Science and Technology Agency
3-1, Tennodai, Tsukuba-shi, Ibaraki-ken, 305-0006
Tel: 0298-51-1611 Ext. 321
Fax: 0298-52-8512
E-mail: ohtani@knetgk.k-net.bosai.go.jp

Dr. Hisashi Okada
Director, Structural Engineering Department
Building Research Institute
Ministry of Construction
1, Tatehara, Tsukuba-shi, Ibaraki-ken 305-0802
Tel: 0298-64-6641
Fax: 0298-64-6773
E-mail: okada@kenken.go.jp

Dr. Hiroshi Sato
Head, Structure Division
Structure and Bridge Department
Public Works Research Institute
Ministry of Construction
1, Asahi, Tsukuba-shi, Ibaraki-ken 305-0804
Tel: 0298-64-2874
Fax: 0298-64-0565
E-mail: hsato@pwri.go.jp

Mr. Masaya Sato
Director, Research Planning and Coordination Section, Administration Division
Civil Engineering Research Institute
Hokkaido Development Bureau
Prime Minister's Office
1-3, Hiragishi, Toyohira-ku, Sapporo-shi
Hokkaido 062-0931
Tel: 011-841-1111
Fax: 011-820-2714

Dr. Takahiro Sugano
Chief, Structural Dynamics Laboratory
Structural Engineering Division
Port and Harbour Research Institute
Ministry of Transport
3-1-1, Nagase, Yokosuka-shi, Kanagawa-ken 239-0826
Tel: 0468-44-5029
Fax: 0468-44-0839
E-mail: macsuga@ipc.phri.go.jp

Dr. Hideki Sugita
Head, Earthquake Disaster Prevention Technology Division
Earthquake Disaster Prevention Research Center
Public Works Research Institute
Ministry of Construction
1, Asahi, Tsukuba-shi, Ibaraki-ken 305-0804
Tel: 0298-64-3245
Fax: 0298-64-0598
E-mail: sugita@pwri.go.jp

Dr. Keiichi Tamura
Head, Ground Vibration Division
Earthquake Disaster Prevention Research Center
Public Works Research Institute
Ministry of Construction
1, Asahi, Tsukuba-shi, Ibaraki-ken 305-0804
Tel: 0298-64-2926
Fax: 0298-64-0598
E-mail: tamura@pwri.go.jp

Mr. Ken-ichi Tokida
Director, Earthquake Disaster Prevention Research Center
Public Works Research Institute
Ministry of Construction
1, Asahi, Tsukuba-shi, Ibaraki-ken 305-0804
Tel: 0298-64-2829
Fax: 0298-64-0598
E-mail: tokida@pwri.go.jp

Mr. Ken-ichi Torii
Head, Coast Division
River Department
Public Works Research Institute
Ministry of Construction
1, Asahi, Tsukuba-shi, Ibaraki-ken 305-0804
Tel: 0298-64-2327
Fax: 0298-64-1168
E-mail: sato@pwri.go.jp

Dr. Shigeki Unjoh
Head, Earthquake Engineering Division
Earthquake Disaster Prevention Research Center
Public Works Research Institute
Ministry of Construction
1, Asahi, Tsukuba-shi, Ibaraki-ken 305-0804
Tel: 0298-64-4966
Fax: 0298-64-4424
E-mail: unjoh@pwri.go.jp

Dr. Yoshikazu Yamaguchi
Head, Fill-type Dam Division
Dam Department
Public Works Research Institute
Ministry of Construction
1, Asahi, Tsukuba-shi, Ibaraki-ken 305-0804
Tel: 0298-64-2413
Fax: 0298-64-0164
E-mail: yamaguti@pwri.go.jp

Mr. Toyotaro Yamauchi
Head, The First Research Laboratory
Seismology and Volcanology Research Department
Meteorological Research Institute
Japan Meteorological Agency
Ministry of Transport
1-1, Nagamine, Tsukuba-shi, Ibaraki-ken 305-0052
Tel: 0298-51-3730
Fax: 0298-53-8735

ASSOCIATE MEMBERS

Dr. Minoru Fujiwara
President, Strait Crossing Highway Research Association
1-4-13, kyobashi, chuo-ku,Tokyo 104-0031
Tel: 03-3245-9840
Fax: 03-3245-9844

Dr. Masami Fukuoka
President, Management System Assessment Center,
2-17-7, Kyoubashi, Chuo-ku, Tokyo 104-0031
Tel:03-3535-4021
Fax: 03-3535-4024

Dr. Masaya Hirosawa
Professor, Kogakuin University
1-24-2-91, Nishi-shinjuku, Shinjuku-ku, Tokyo 163-0023
Tel: 03-3342-1211
Fax: 03-3340-0149

Dr. Shiro Ibukiyama
President, Kogyokusha College of Technology
5-14-2, Nishigotanda, Shinagawa-ku, Tokyo 141-0031
Tel: 03-3493-5671
Fax: 03-3495-4071

Dr. Kaoru Ichihara
Adviser, Central Consul Tant Inc.
2-16-2, Minami-Kamata, Ohta-ku, Tokyo 144-0035
Tel:03-5703-6161
Fax:03-5703-6151

Dr. Ryuichi Iida
President, Japan Dam Engineering Center
2-4-5, Azabudai, Minato-ku, Tokyo 106-0041
Tel: 03-3433-7811
Fax: 03-3432-6204

Dr. Takashi Iijima
President, Sekisui-jushi Co., Ltd.
1-11-1, Kaigan, Minato-ku, Tokyo 105-0022
Tel: 03-5400-1801
Fax: 03-5400-1805

Mr. Yasutake Inoue
President, Fukuoka-Kitakyusyu Expressway Public Cooperation
2-7-53, Higashihama, Higashi-ku, Fukuoka-shi, Fukuoka-ken 812-0055
Tel: 092-631-3281

Dr. Toshio Iwasaki
President, Civil Engineering Research Laboratory
1-18 Kandasuda-cho,Chiyoda-ku, Tokyo
101-0041
Tel: 03-3254-9481
Fax: 03-3254-9448

Mr. Shunichiro Kamijo
President, Mitsui Construction Corporation,
1-2-3, Ohte-machi, Chiyoda-ku,
Tokyo 100-0004
Tel: 03-5223-3915
Fax: 03-5223-3920

Mr. Kenji Kawakami
Adviser, Kubota Corporation
3-1-3, Nihonbashi-muromachi, Cyuoh-ku, Tokyo 103-0022
Tel: 03-3245-3660
Fax: 03-3245-3454

Prof. Eiichi Kuribayashi
10-2-801, Nishihouwa, Yayoi-cho, Toyohashi-shi Aichi-ken 441-8122
Tel: 0532-47-0429

Dr. Tatsuro Murota
President, General Building Research Corporation of Japan
5-8-1, Fujishirodai, Suita-shi, Osaka-fu 565-0873
Tel: 06-6872-0391
Fax: 06-6872-0784

Mr. Mitsuru Nagao
President, Japan Construction Mechanization Association
3-5-8, Shibakoen, Minato-ku, Tokyo 105-0011
Tel: 03-3433-1501
Fax: 03-3432-0289

Prof. Kiyoshi Nakano
979-66, Kumada, Minaminasu-machi, Nasu-gun, Tochigi-ken
Tel: 0287-88-0022

Dr. Kazuto Nakazawa
Adviser, Public Works Research Center
1-6-4, Taito, Taito-ku, Tokyo 110-0016
Tel: 03-3835-3609
Fax: 03-3275-5648

Dr. Nobuyuki Narita
President, Japan Steel Structure Corporation
3-3-1, Marunouthi, Chiyoda-ku,
Tokyo 100-0005
Tel: 03-3212-0875
Fax: 03-3212-0878

Dr. Setuo Noda
President, Coastal Development Institute of Technology
3-16, Hayabusa-cho, Chiyoda-ku, Tokyo 102-0092
Tel: 03-3234-5861
Fax: 03-3234-5877

Dr. Shin Okamoto
Central Research Institute for Construction Technology
Japan Association of Representative General Contractors
1-6-34, Kounan, Minato-ku, Tokyo 108-0075
Tel: 03-3458-1011
Fax: 03-3458-6321

Mr. Yoshijiro Sakagami
Receive, Japan Development Construction Corporation,
4-9-9, Akasaka, Minato-ku, Tokyo 107-0052
Tel: 03-5410-5730
Fax: 03-3403-9039

Dr. Tadahiko Sakamoto
President, Japan Dam Engineering Center
2-4-5, Azabudai, Minato-ku, Tokyo 106-0041
Tel: 03-3433-7811
Fax: 03-3432-6204

Prof. Yasushi Sasaki
Professor, Department of Civil and Environmental Engineering
Hiroshima University
1-4-1, Kagamiyama, Higashihiroshima-shi, Hiroshima-ken 739-0046
Tel: 0824-24-7783
Fax: 0824-24-7783
E-mail: ysasaki@ue.ipc.hiroshima-u.ac.jp

Dr. Yukihiko Sumiyoshi
Executive Counselor, Nippon Steel Co., Ltd.
2-6-3, Ohte-machi, Chiyoda-ku,
Tokyo 100-0004
Tel: 03-3275-5868
Fax:03-3275-5636

Mr. Jiro Taguchi
President, Construction Research Institure
11-8, Ohdenma-chou, Nihonbashi, Chuo-ku,
Tokyo 103-0011
Tel: 03-3663-2411
Fax: 03-3633-2417

Dr. Hiroshi Takahashi
4-22-1, Nishihara-machi, Fuchuu-shi, Tokyo 183-0046
Tel: 0425-72-3227

Dr. Masateru Tominaga
President, Public Works Research Center
1-6-4, Taito, Taito-ku, Tokyo 110-0016
Tel: 03-3835-3609
Fax: 03-3275-5648

Dr. Hajime Tsuchida
Executive Counselor, Nippon Steel Co., Ltd.
2-6-3, Ohte-machi, Chiyoda-ku, Tokyo 100-0004
Tel: 03-3275-5894
Fax: 03-3275-5648

Mr. Seizo Tsuji
President, Japan Highway Public Corporation
3-3-2, Kasumigaseki, Chiyoda-ku, Tokyo 100-8979
Tel: 03-3506-0123
Fax: 03-3506-0396

Dr. Makoto Watabe
2-25-5, Tokiwadai, Itabashi-ku, Tokyo 174-0071
Tel: 03-3960-0374

Prof. Kouichi Yokoyama
Professor, Urban and Civil Engineering
Faculty of Engineering, Ibaraki University
4-12-1, Nakanarisawa-machi, Hitachi-shi,
Ibaraki-ken 316-8511
Tel: 0294-38-5161
Fax: 0294-35-8146

UNITED STATES-SIDE PANEL ON WIND AND SEISMIC EFFECTS
MEMBERSHIP LIST

Dr. S. Shyam Sunder
Chairman, U.S.-side Panel
Chief, Structures Division
Building and Fire Research Laboratory
National Institute of Standards and Technology
100 Bureau Drive, Stop 8611
Gaithersburg, MD 20899-8611
301-975-6061; Fax 301-869-6275
E-mail: sunder@nist.gov

Dr. John L. Gross
Secretary-General, U.S.-side Panel
Leader, Structural Systems and Design Group
Building and Fire Research Laboratory
National Institute of Standards and Technology
100 Bureau Drive, Stop 8611
Gaithersburg, MD 20899-8611
301-975-6068; Fax 301-869-6275
E-mail: john.gross@nist.gov

Mr. Stephen A. Cauffman
Research Engineer
Structural Systems and Design Group
Building and Fire Research Laboratory
National Institute of Standards and Technology
100 Bureau Drive, Stop 8611
Gaithersburg, MD 20899-8611
301-975-6051; Fax 301-869-6275
E-mail: stephen.cauffman@nist.gov

Dr. Daniel P. Abrams
Director, Mid-America Earthquake Center
Hanson Engineers Professor of Civil Engineering
University of Illinois
1241 Newmark Laboratory
205 North Matthews Avenue
Urbana, IL 61801
217-244-6302; Fax 217-333-3821
E-mail: d-abrams@uiuc.edu

Dr. Kharaiti L. Abrol
Principal Structural Engineering Consultant
Department of Veterans Affairs
810 Vermont Avenue, NW, Room 475
Washington, DC 20420
202-565-5579; Fax 202-565-5478
E-mail: abrkha@hq.med.va.gov

Dr. John Ake
Geophysicist
Seismotechtonics and Geophysics Section
Bureau of Reclamation
U.S. Department of Interior
Code D-8330
P.O. Box 25007
Denver, CO 80225
303-236-4195 x276; Fax 303-236-9127
E-mail: jake@seismo.usbr.gov

Mr. John Baals
Seismic Safety Coordinator
P.O. Box 25007 (D-8110)
Bureau of Reclamation
U.S. Department of Interior
Denver, CO 80225
303-236-3999 x534; 303-236-9099
E-mail: jbaals@do.usbr.gov

Dr. Celso S. Barrientos
Supervisory Physical Scientist
National Environmental Satellite Data Information Service – Code E/RA28
National Oceanic and Atmospheric Administration
U.S. Department of Commerce
5200 Auth Road
Camp Springs, MD 20746
301-763-8102; Fax 301-763-8020
E-mail: cbarrientos@nesdis.noaa.gov

Dr. Eddie N. Bernard
Director, Pacific Marine Environmental Laboratory
National Oceanic and Atmospheric Administration
U.S. Department of Commerce
7600 Sand Point Way, NE
BIN C15700/Building 3
Seattle, WA 98115-0070
206-526-6800; Fax 206-526-6815
Email: bernard@pmel.noaa.gov

Mr. Mike Blackford
IOC-NWS/INTERNATIONAL
Director, International Tsunami Information Center
737 Bishop Street, Suite 2200
Honolulu, HI 96813-3213
808-532-6423; Fax 808-532-5576
E-mail: Michael.Blackford@noaa.gov

Dr. David M. Boore
U.S. Geological Survey
345 Middlefield Road, MS 977
Menlo Park, CA 94025
650-329-5616; Fax 650-329-5163
E-mail: boore@samoa.wr.usgs.gov

Dr. Roger D. Borcherdt
Branch of Seismology
U.S. Geological Survey
U.S. Department of the Interior
345 Middlefield Road, MS 977
Menlo Park, CA 94025
650-329-5619; Fax 650-329-5163
E-mail: borcherdt@samoa.wr.usgs.gov

Dr. Mehmet K. Çelebi
Research Civil Engineer
Branch of Earthquake and Geomagnetic Information
U.S. Geological Survey
U.S. Department of the Interior
345 Middlefield Road, MS 977
Menlo Park, CA 94025
650-329-5623; Fax 650-329-5163
E-mail: celebi@usgs.gov

Mr. Harish Chander
U. S. Department of Energy (EH-31)
CXXI, Room 2016 (GTN)
19901 Germantown Road
Germantown, MD 20874-1290
301-903-6681; Fax 301-903-8693
E-mail: harish.chander@hq.doe.gov

Dr. Ken P.Chong
Program Director
Civil and Mechanical Systems Division
4201 Wilson Boulevard, Room 545
Arlington, VA 22230
703-292-7008; Fax 703-292-9053
E-mail: kchong@nsf.gov

Mr. James D. Cooper
Chief, Structures Division, HNR-10
Federal Highway Administration
U.S. Department of Transportation
6300 Georgetown Pike
McLean, VA 22101
202-493-3023; Fax 202-493-3442
E-mail: jim.cooper@fhwa.dot.gov

Mr. William Freeborne
Department of Housing and Urban Development
Room 8132
451 Seventh Street, SW
Washington, DC 20410
202-708-4370 x5725; Fax 202-708-5873
E-mail: william_e._freeborne@hud.gov

Mr. Peter E. Gurvin
Director, Building Design and Engineering Division
Foreign Building Operations
Building SA-6, Room 335
U.S. Department of State
Washington, DC 20520
703-875-6117; Fax 703-875-6204
E-mail: peter.e.gurvin@dos.us-state.gov

Dr. Robert L. Hall
Chief, Structural Analysis Group
U.S. Army Engineer Research and Development Center
3909 Halls Ferry Road
Vicksburg, MS 39180-6199
601-634-2567; Fax 601-634-3412
E-mail: hallr3@mail.wes.army.mil

Dr. Allen M. Hittelman
Chief, Solid Earth Geophysics Division
E/GC1, National Geophysical Data Center
NOAA, NESDIS
325 Broadway
Boulder, CO 80303-3328
303-497-6591; 303-497-6513
E-mail: allen.m.hittelman@noaa.gov

Mr. Larry C. Hultengren
Senior Structural Engineer
Office of Civil/Structural Engineering
Foreign Building Operations
U.S. Department of State
Building SA-6, Room 346
Washington, DC 20520
703-875-6194; Fax 703-875-6204
E-mail: hultengremlc@state.gov

Dr. Mary Ellen Hynes
Chief, Earthquake Engineering and Geophysics Branch
Geotechnical Laboratory
U.S. Army Engineer Research and Development Center
3909 Halls Ferry Road
Vicksburg, MS 39180
601-634-2280; 601-634-3453
E-mail: hynesm@ex1.wes.army.mil

Dr. William B. Joyner
Geophysicist
Branch of Seismology
U.S. Geological Survey
U.S. Department of the Interior
345 Middlefield Road, MS 977
Menlo Park, CA 94025
650-329-5640; Fax 650-329-5163
E-mail: joyner@samoa.wr.usgs.gov

Dr. George Lee
Director, Multidisciplinary Center for Earthquake Engineering Research (MCEER)
State University of New York at Buffalo
Red Jacket Quadrangle
Buffalo, NY 14261
716-645-3391; Fax 716-645-3399
E-mail: gclee@acsu.buffalo.edu

Dr. H. S. Lew
Structures Division
Building Fire and Research Laboratory
National Institute of Standards and Technology
100 Bureau Drive, Stop 8611
Gaithersburg, MD 20899-8611
301-975-6060; Fax 301-869-6275
E-mail: hai.lew@nist.gov

Dr. Shih-Chi Liu
Program Director
Civil and Mechanical Systems Division
National Science Foundation
4201 Wilson Boulevard, Room 545
Arlington, VA 22230
703-292-8360; Fax 703-292-9053
E-mail: sliu@nsf.gov

Dr. Josephine Malilay
Disaster Assessment and Epidemiology Section
National Center for Environmental Health
1600 Clifton Road, NE (Mailstop E-23)
Atlanta, GA 30333
404-639-2589; Fax 404-639-2565
E-mail: jym7@cdc.gov

Dr. Francis G. McLean
Value Engineering Program Manager
Code D-8170
P.O. Box 25007
Bureau of Reclamation
U.S. Department of the Interior
Denver, CO 80225
303-445-3091; Fax 303-445-6475
E-mail: FMCLEAN@do.usbr.gov

Dr. Raymond E. Meyer
Department of State
SA14/Room 1705
USAID
Washington, DC 20523-1443
202-712-1078; Fax 202-216-3707
E-mail: Rmeyer@usaid.gov

Dr. Jack Moehle
Director, Pacific Earthquake Engineering Research Center (PEER)
1301 South 46th Street
Richmond CA 94804-4698
510-231-9554; 510-231-9471
E-mail: moehle@eerc.berkeley.edu

Mr. Ugo Morelli
Policy Manager
Federal Emergency Management Agency
500 C Street, SW
Washington, DC 20472
202-646-2810; Fax 202-646-2577
E-mail: ugo.morelli@fema.gov

Mr. Howard D. Nickerson
Earthquake Engineering and Weapons Specialist
Naval Facilities Engineering Command
Washington Navy Yard
901 M Street, SE
Code 00CE9
Washington, DC 203745063
Phone: 202-443-8759
Fax: 202-433-8777
E-mail: hdnickerson@nfesc.navy.mil

Dr. Stuart Nishenko
Federal Emergency Management Agency
500 C Street NW
Washington, DC 20472
202-646-3945; Fax 202-646-4596
E-mail: stuart.nishenko@nist.gov

Mr. Tom Post
Chief, Earthquake Engineering Division
California Department of Transportation (CALTRANS)
P.O. Box 942873
Sacramento, CA 95814
916-227-8728; Fax 916-227-8898
E-mail: tpost@trmx3.dot.ca.gov

Dr. Phillip Yen
Federal Highway Administration
U.S. Department of Transportation
6300 Georgetown Pike
McLean, VA 22101
202-493-3056; Fax 202-493-3442
E-mail: wen-huei.yen@fhwa.dot.gov

ALTERNATE MEMBERS

Dr. Clifford Astill
Program Director
Civil and Mechanical Systems Division
National Science Foundation
4201 Wilson Boulevard, Room 545
Arlington, VA 22230
703-292-8360; Fax 703-292-9053
E-mail: castill@nsf.gov

Mr. Michael Changery
Chief, Global Analysis Branch
National Oceanic and Atmospheric Administration
U.S. Department of Commerce
Federal Building
Asheville, NC 28801
704-271-4765; Fax 704-271-4246
E-mail: mchangery@ncdc.noaa.gov

Dr. C. Y. Chen
Senior Civil/Geotechnical Engineer
Office of Foreign Buildings
Department of State
Code SA-6, Rm. 347
Washington, DC 20520
703-875-6207; Fax 703-875-6204
E-mail: chency@state.gov

Mr. Vincent P. Chiarito
Research Structural Engineer
Structural Mechanics Division
Structures Laboratory
U.S. Army Engineer Research and Development Center
3909 Halls Ferry Road
Vicksburg, MS 39180-6199
601-634-2714; Fax 601-634-3412
E-mail: chiariv@ex1.wes.army.mil

Mr. James Lander
Geophysicist
Cooperative Institute for Research in Environmental Sciences
University of Colorado
Campus Box 449, Room 152 RL3
3100 Marine Street
Boulder, CO 80309
303-497-6446; Fax 303-497-6513
E-mail: jlander@ngdc.noaa.gov

Mr. Michael Mahoney
Physical Scientist
Federal Emergency Management Agency
500 C Street SW
Washington, DC 20472
202-646-2794; Fax 202-646-4387
E-mail: mike.mahoney@fema.gov

Dr. Martin C. Miller
Chief, Coastal Oceanography Branch
U.S. Army Engineer Research and Development Center
Coastal and Hydraulics Laboratory
3909 Halls Ferry Road
Vicksburg, MS 39180
601-634-3999; Fax 601-634-4314
E-mail: m.miller@cerc.wes.army.mil

Dr. Erdal Safak
Research Structural Engineer
U.S. Geological Survey
Box 25046, MS 966
Denver Federal Center
Denver, CO 80225
303-273-8593; Fax 303-273-8600
E-mail: safak@usgs.gov

Dr. John B. Scalzi
Program Director
Civil and Mechanical Systems Division
National Science Foundation
4201 Wilson Boulevard, Room 545
Arlington, VA 22230
703-292-8360; Fax 703-292-9053
E-mail: jscalzi@nsf.gov

Resolutions

RESOLUTIONS OF THE THIRTY-SECOND JOINT MEETING
U.S.-JAPAN PANEL ON WIND AND SEISMIC EFFECTS (UJNR)
National Institute of Standards and Technology, Gaithersburg, MD
16-19 May 2000

The following resolutions are hereby adopted:

1. The Thirty-Second Joint Panel Meeting provided the forum to exchange valuable technical information that is beneficial to both countries. In view of the importance of cooperative programs on the subject of wind and seismic effects, the continuation of Joint Panel Meetings is considered essential. Both sides agreed to explore new ideas and areas to strengthen cooperative activities in support of the Panel's mission.

2. The following activities have been conducted since the Thirty-first Joint Meeting:

   a. Technology Exchanges. Technical experts, technical documents, and applications of electronic media have been exchanged. These exchanges have contributed to the development of new research programs and enhanced ongoing research in both countries.

   b. Task Committee Workshops. The Panel held five workshops, symposia, or committee meetings; approximately 300 specialists from both countries participated in these activities:
      1. Task Committee (C), 6th U.S.-Japan Joint Technical Coordinating Committee Meeting on Composite and Hybrid Structural Systems, 25 March 2000, Los Angeles, USA.
      2. Task Committee (C), 1st U.S.-Japan Technical Coordinating Committee Meeting on Auto-Adaptive Media (Smart Structural Systems), 6-8 January 2000, Tsukuba, Japan.
      3. Task Committee (E), 1st U.S-Japan Workshop on Design for Wind and Wind Hazard Mitigation, 24-26 May 1999, Tsukuba, Japan.
      4. Task Committee (G), 1st U.S.-Japan Workshop on Seismic Information Systems, 15-16 November 1999, Tsukuba, Japan.
      5. Task Committee (J), 15th Bridge Workshop, 9-10 November 1999, Tsukuba, Japan.

   c. Common Agenda. The Panel recognizes the importance of providing earthquake science and technology expertise to the 17 April 1996 U.S.-Japan Natural Disaster Reduction Initiative of the U.S.-Japan Framework for New Economic Partnership

(Common Agenda). Panel members organized and participated in the First High-Level U.S.-Japan Earthquake Policy Cooperation Forum, 20-22 October, 1998, Seattle, Washington, USA, and in the Second Forum, 10-12 November, 1999, Yokohama, Japan. The Panel will continue to provide, in close cooperation with the Earthquake Disaster Mitigation Partnership, technical leadership and participation in the Third High-Level Forum Meeting that will address five themes: 1. Strategies to encourage implementation of preparedness and loss prevention measures; 2. Exchange of information and experience on tsunami hazards and risk reduction; 3. Lessons learned from recent large-scale earthquakes around the world; 4. Establishing the development of a joint presentation that describes the High-Level Forum achievements and a strategy for international dissemination; 5. Plans for future cooperation. Appropriate Task Committees will respond to the Common Agenda in planning their work.

3. The Panel approved the Task Committee reports presented during the 32nd Joint Panel Meeting. Each report included objectives, scope of work, accomplishments, future plans, and other information. The Panel will continue to review the Task Committees' progress toward meeting their objectives; consolidating, eliminating, and/or creating Task Committees as desirable.

4. The Panel endorses the following five (5) proposed Task Committee Workshops or Committee Meetings during the coming year:
   a. Task Committee (A), 2nd U.S.-Japan Workshop on Soil-Structure Interaction, March, 2001, Tsukuba, Japan.
   b. Task Committee (C), 2nd U.S.-Japan Technical Coordinating Committee Meeting on Auto-Adaptive Media (Smart Structural Systems), by the end of 2000, USA.
   c. Task Committee (C), International Workshop on Performance-Based Design of Building Structures, November 13-15, 2000, Tsukuba, Japan.
   d. Task Committee (D), 3rd U.S.-Japan Workshop on Advanced Research on Earthquake Engineering for Dams, in 2001, USA.
   e. Task Committee (G), in coordination with Task Committee (A), Workshop on Seismic Information Systems, 2000, in conjunction with the 3rd High-Level Forum Meeting, USA.

      Task Committee (I), 6th Tsunami Workshop, 2001, USA.

      Task Committee (J), 16th U.S.-Japan Bridge Workshop, October 2000, Lake Tahoe, USA.

In the event that T/C co-chairs deem it essential to conduct a joint meeting or workshop

that is not included in this endorsement, the T/C co-chairs will make such a request through their respective Secretary-General for approval by the U.S. and Japan Joint Panel Chairmen.

Scheduling for the Workshops will be done by the U.S. and Japan Chairmen of the Task Committees with concurrence of the Joint Panel Chairmen. Both sides' Secretaries-General will be kept informed of the planning, conduct and results of workshops or committee meetings including resolutions and reports. Results of each activity conducted before the 33rd Joint Panel Meeting will be presented at the 33rd Joint Panel Meeting.

5. The Panel recognizes the importance of continued exchange of personnel, technical information, research results, and recorded data that lead to mitigating losses from strong winds and earthquakes. The Panel also recognizes the importance of using available large-scale testing facilities and complementary capabilities in both countries. Thus, these activities should be continued, strengthened, and expanded. Further, the Panel will study the feasibility of establishing a network for live transmission of experimental testing, including data, models, and simulation tools.

6. The Panel recognizes the significant vulnerability of residential construction to natural hazards and believes that reduction of life and property losses in the housing sector is critical for both sides and in other parts of the world. The panel affirms the need to make disaster-resistant housing a priority and to strengthen activities in support of this objective in the future.

7. The Panel recognizes the importance of continuing its joint research programs on Soil Liquefaction and Countermeasures and on Auto-Adaptive Media (Smart Structural Systems).

8. The Panel recognizes the importance to continue to seek means to contribute to the International Organization for Standardization (ISO) through participation of its members and related agencies in appropriate ISO Technical Committees. The Panel also recognizes the importance of continuing the related information exchange to contribute to the ISO.

9. The Panel will continue to transfer technical information obtained through the Panel and Task Committee activities including technology transfer on wind and seismic effects to developing countries.

10. The Panel encourages all members from both sides to use electronic media, as much as

possible, in communicating Panel findings and summaries of its activities. The Public Works Research Institute (PWRI) and the National Institute of Standards and Technology (NIST) will maintain the electric mailing list aid in the distribution of information to Panel members.

11. The Panel, in recognition of its many strengths and past successes and a desire to position itself both functionally and organizationally to address future challenges, will develop jointly a strategic Plan for the UJNR Panel on Wind and Seismic Effects. An Ad-Hoc Committee will be formed to develop the Strategic Plan that will:

    Evaluate the current organization, task committee structure, annual technical meeting and site visit program, cooperative research projects, and related operating procedures.

    Assess current and emerging technical needs and interests of government agencies in the two countries such as Performance-Based Design and Rehabilitation.

    Review options for Panel affiliations/linkages with different U.S.-Japan government-to-government cooperation mechanisms, including participation of industry and university representatives.

    Review options for streamlining and increasing the efficiency of Panel operations and for moving toward more effective operating procedures.

    Develop new proposals for Panel functional statement, organizational structure and membership, operational procedures (including procedures for requesting and approving the formation of new Task Committees and for conducting cooperative research projects and workshops), and government-to-government affiliation mechanisms.

    Additionally, the Ad-Hoc Committee will take into consideration recommendations from the report on U.S.-Japan Dialogue on the Role of Science and Technology in Society into the New Millennium in forming its recommendations. The U.S.- and Japan-side Chairs will nominate two individuals each to serve on the Ad-Hoc Committee as soon as possible. The Ad-Hoc Committee will present the Draft Strategic Plan by October 1, 2000 for joint review and approval by the U.S. and Japan-side Chairs.

12. The Panel published its seventh newsletter issue, Wind and Seismic Effects, Winter 2000. Continuation of the publication of the Panel's newsletter in accordance with the Panel Strategic Plan.

13. The Thirty-Third Joint Panel Meeting of the UJNR Panel on Wind and Seismic Effects will be organized by the successor to the Public Works Research Institute, Tsukuba, Japan, after the reorganization of the Japanese Governmental Ministries and Agencies, in May 2001. Dates, program, and itinerary will be proposed by the Japan-side with

concurrence of the U.S.-side Panel.

Papers

Theme 1

Information Technology for Land Management and Natural Disaster Prevention Countermeasures

Web-Based Geographic Information System Support to Disaster Response

William E. Roper[1]

Abstract

Natural disasters have a major impact, globally and within the United States (U.S.) causing injury and loss of life, as well as economic losses. To better address disaster response needs, a task force has been established to leverage technological capabilities to improve disaster response management. Web based geospatial analysis is one of these important capabilities. Samples of geospatial technologies applicable to disaster management are presented. These include 3-D visualization, hyperspectral imagery, LIDAR, use of spectral libraries, digital multispectral video, radar imaging systems, photogeologic analysis and geographic information systems.

Key words: Data management; Disaster management; Global Disaster Information Network; mapping; hyperspectral; web mapping; geospatial library; LIDAR; radar imaging; GIS; Global Positioning System; satellite sensors; 3-D fly through.

1. Introduction

Despite technological advance, disaster risk continues to grow. Emergency managers and others continue to be called on to make decisions during disaster events, as well as in the pre-and-post disaster phases, with incomplete information. In order to make optimal decisions to reduce the loss of life and property, stakeholders uniformly must be able to obtain the needed information in a format that is appropriate for their capabilities. (NRC 1998).

This paper is intended to stimulate the systematic consideration of the information technology and information processing requirements associated with the larger community of Disaster Management. This document has two audiences. For technologists this document is intended to provide background and overview material pertinent to the disaster community at large. For disaster stakeholders this may serve as an introduction to distributed interoperable technologies and the role of scenarios in developing appropriate solutions.

Natural disasters are a constant threat to mankind on a global scale. Global disaster costs are continuing to rise. Annual global economic costs related to disaster events average $440 billion per year (World Disaster Report, 1996) with floods being the major cause. In the U.S., the number of lives lost due to natural disasters has been decreasing over the last several deceased, largely because of advances in disaster indication and warning capabilities. In terms of damage to property, however, the trend is reversed. For the period of 1992-1996, the average cost of natural disasters in the U.S. has been $54.3 billion, with hurricanes and earthquakes

tied as the leading cause. These rising costs are the combined result of increased urbanization, particularly in high-risk coastal areas, and the increased complexity and size of our infrastructure.

The loss of life and property continues to rise in many regions of the world because of these events. One example is the Bangladesh weather event of 1970, when a tropical cyclone slammed into its delta region killing 300,000 people (Tobin and Montz, 1997). The crop losses were estimated at $63 million, and more than 280,000 cattle were drown (Burton, Kates, and White, 1993). The rich delta soil is an agricultural resource that still draws people to settle there; therefore a recurrence of this type of weather event could likely pose a similar disaster. Another more recently example was Hurricane Mitch in the fall of 1998 that resulted in over three thousand deaths and massive damage in Central

2. Data Management for Disasters

It is clear that despite excellent efforts by many groups the approach to providing information for disaster management is not effectively utilizing a wealth of data that resides, with various organizations and that existing technology could deliver to disaster mangers important information products that could save lives, reduce damage to property, and lessen the environmental impacts of disasters. The current situation is characterized by numerous shortcomings that inhibit optimal decision making for disaster management. The inability to access information and the lack of standardization, coordination, and communication are all obstacles that need to be overcome [NRC 1998].

Considerable effort has been expended throughout the Disaster Management community to articulate issues and to characterize the dynamics and the inter-relationships that need to be accommodated in a viable information management strategy. An important guide for this effort is found in the recommendations made by the Board On Natural Disasters (BOND) in their report to the National Research Council (NRC 1998). The BOND's primary goals as articulated in its cha were to:

- Improve decision making before, during, and after emergencies through better access to and quality of data and information
- Identify users and their needs
- Provide information products specifically designed to meet users' need
- Promote efficiency and cost effectiveness
- Stimulate and facilitate mitigation

2.1 Board on Natural Disaster Observations and Recommendations

The BOND responded to its charter with a series of observations and recommendations that provide significant input and guidance to the formative process needed for improved disaster management. The BOND in its report put the following observations forth.

- The need for an improved information network and its potential benefits are clear
- The foundations of an information network are already in place.

- Recent advances in technology provide the mechanism for establishing a network.
- Successful implementation of the disaster information network concept will require a commitment of resources from a broad spectrum of stakeholders.

In addition to these observations the BOND provided a set of recommendations to the community at large. These recommendations are consistent with much of the philosophy that drives this initiative. They also help to forge a realistic set of parameters and directives that can be used to focus on the disaster management community.

- The products of Disaster Information Network should be based from the outset on user's needs.
- A major of a Disaster Information Network should be on integration of various data types.
- Data and information quality and reliability are major issues that need to be addresses.
- An effective dissemination and access plan is critical to the success of any information network.
- The Global Disaster Information Network Transition Team should focus initially on establishing a national disaster information network (i.e., with a U.S. focus), but the model should be extended to a global process (Global Disaster Information Network) as soon as it can be demonstrated that a Global Disaster Information Network is technically and organizationally feasible (GDIN 1997).

In addition, to the BOND discussion of focus areas for improvement and growth there are a number of functional areas related to data and information processing. The four main areas for improvement in information management are:

- Locating information
- Assessment and evaluation of information integrity, currency and accuracy
- Assimilation and Integration of new information
- Application(s) that incorporate new information to produce customized, understandable (interpretable) domain specific (context specific) results

BOND conclusions were weighted towards developing integrative products to assist in decision support and planning. For instance, a series of recommendations that emerged from the NRC publication included:

- International, national, regional, or local maps showing how hazards and risks vary in space and time;
- Estimates of probability of occurrence of hazardous events;
- Estimates and examples of potential effects, especially for structures;
- Real-time display of what is happening during the course of a disaster;
- Systems for contingency planning; and
- Codes, standards, and construction methods for structures.

These are important components in any workable framework for comprehensive disaster management. However, the focus here is directed towards derived products, procedure and protocol. It is

important that the process develop baseline products and implement solutions that reflect the complex fabric of the disaster management community. This work is done at a lower, more formative level in the information management life cycle and in fact forms the basis for the production of the products referred to by the BOND. As noted above the assessment process will work to identify the constituent components associated with specific disaster events and scenarios. The constituent components will then become the basis for technology specifications and the delivery of capabilities that encompass the products identified by the BOND.

2.2 Disaster Data Management Considerations

This section provides assumptions based on information and conclusions that have emerged from recent studies in disaster management community itself (NAPA 1998). These assumptions certainly do not constitute and exhaustive set of parameters. Rather, they provide a point of departure and a set of "operating hypotheses" that can be used to help frame discussion and consideration of needs and requirements.

2.2.1 Information Availability

Available Information and capacity is not uniform, consistent and standardized for disaster managers. Large cities may have invested millions of dollars in their information systems, while smaller municipalities may be operating with one personal computer.

2.2.2 Multiple Boundary Problem

Disasters will constantly crosscut established boundaries. A fundamental problem in dealing with disasters is that they do not respect boundaries that include organizational, political, geographic, professional, topical, or sociological consideration.

2.2.3 Coordination & Communication Challenge

Disasters will often overwhelm mechanisms for coordination and communication. In addition, the mechanisms to bring data and information to decision makers are uncoordinated. Information is often produced from disparate sources and transmitted in whatever format the provider prefers, requiring significant effort to compile it into a form that provides a coherent picture or even thwarting integration altogether. Data standards are often inconsistent, and, even more dangerous; users are sometimes unaware of the limitations and uncertainties in data or are presented with conflicting interpretations of data without the means to assess the reliability of the sources. All of these issues reduce the efficacy of the decision-making process (NAPA 1998). The problem is compounded because information delivery systems in many cases become overloaded during crises. For instance, in 1996 a moderate (magnitude 4.7) earthquake in San Jose, California, led to more than a million attempted hits in less than one day on the U.S. Geological Survey's World Wide Web earthquake information server. Most of those attempts were unsuccessful, including those by emergency managers trying to access data and information to aid in the formulation of a response plan.

3. Disaster Management Process Issues

Disaster management is an exercise in logistics and information processing and distribution. To effectively undertake these tasks requires a good understanding of disaster information requirements and the characteristics associated with them Disaster events are not all created equally. They come indifferent sizes, have different behavior and can be categorized on the basis of their impact on natural resources, agriculture, communities etc. They can also be discriminated and classified along a number of dimensions including impact, severity, duration, geographic setting and advance warning. In order to develop an Information Technology architecture or even plausible use-case scenarios it is essential to understand the disaster event from the perspective of those responsible for assimilating the data and information and producing operational plans to deal with the disaster event and its aftermath.

For instance, it is important to appreciate the four basic phases of disaster management may actually manifest themselves in different ways depending on the nature of the disaster. The mitigation phase is essentially a continuous process of preparation, analysis of performance and subsequent modification and refinement. As a result it will likely exhibit the smallest amount of variance. However, the other phases (preparedness, response and recovery) will likely have significantly different attributes depending on the nature of the event. For example consider the difference in the preparedness phase that would be associated with major seasonal flooding along the Mississippi or the Missouri Rivers, the Chaparral fires along the Pacific Coast, a Tsunami that impacts much of the Pacific Rim and an earthquake such as Northridge or Loma Prieta (Roper 1999). In each case the geographic coverage and the amount of time for planning and staging is very different. As a result, many of the other systemic aspects of the disaster management initiative will be different as well.

An event warning which impacts the manner in which the preparedness phase is managed also has implications and consequences for the recovery phase (e.g. In the case of the Loma Prieta earthquake the emergency response resources were directed to the bay area despite the fact that Santa Cruz and Watsonville had more significant damage). Partially as a result of this California is building the Tri-Net seismic sensing network to measure shake and model damage in order to make more informed decisions regarding staging recovery resources.

4. Disaster Management Communities

The disaster management is extremely heterogeneous. In order to develop effective systemic solutions to the needs of this community any framework must address the need to effectively and efficiently share information across institutional boundaries within and between the groups that make up this community. In essence an interface must be specified at each boundary that separates levels in an agency or at the juncture between different agencies or between different sectors. These interfaces each have at least three components: 1) technical, 2) institutional

and 3) institutional administrative. The importance of these interfaces is also proportional to the difficulty of implementing them in an automated context. For instance, the lightest weight interfaces should be between levels within the same entity within a single sector. In contrast the heaviest interfaces would be those that attempt to span sectors.

A number of these communities have made significant institutional investments in the construction of foundation data products that feed modeling, analysis and decision support in a range of contexts. Not surprisingly the situation in the disaster management community in regard to data parallels spatial data issues across the federal government and throughout state and local government and the private sector.

The issue of data sharing by the disaster management community was addressed by the BOND. Their findings recognized that despite the importance of significant databases, their utility is impaired by a host of problems deriving from incompatible formats, inconsistent geographic reference systems, conflicting standards, and other human-caused factors. Many of these problems could be resolved and the value and utility of the databases for disaster decision making greatly enhanced through improved organizational and technological coordination with only an incremental increase in cost. This is clearly in the public interest to accomplish this (NRC 1998).

Disaster management scales for international agencies and governments to the individual. However, a very significant level of responsibility is vested at the local level. For instance, it is the on the ground officials, many of whom are local, that ultimately play the role of first responders (e.g. police, fire, medical and public works) and who also manage many of the recovery operations.

To be effective in this context protocols must define communications, database structure, data formatting, hardware and software requirements, networking, quality control, and other issues needed to assure the linkage will improve decision making before, during, and after emergencies through improved access to quality information. In addition, such a linkage will provide information products that are specifically designed to meet the needs of users

5. Common Characteristics of Disasters

Disaster management is not a linear process that can be documented easily in a flow chart with a readily apparent beginning and absolute end point. Rather, it is a cyclical process of approximation, response and re-calibration that involves many different actors whose roles in relation to one another are likely to change based on circumstances and the stage in the process. The one constant evident in the process is the chaos that drives the system. Another absolute is that the effective, efficient application of information technologies and products has the capacity to improve the system in a number of ways that will combine to save lives, mitigate overall damage, conserve resources and ameliorate human suffering.

To develop effective architectures and technologies that meet the needs of the disaster management community there must be a precise understanding of the disaster management life-cycle (Mitigation, Preparedness, Response and Recovery), the Information Communities that combine to define the disaster management community and the information processing requirements associated with the cycle of data development, dissemination, analysis and review. In addition, and perhaps more importantly, there must be a precise understanding of the dynamics between these components and the "interfaces" that these dynamics imply. Only with such an understanding can we effectively model the process and derive technology solutions that map well into the business model of disaster management.

6. Data and Information Processing Requirements

Data needs, the characteristics of data and the ability of data to contribute to analysis, response and recovery is well understood. The basic attributes of information that are considered most important by this community include:

- Timeliness: delivery of data and information in time to drive decision making
- Consistency: delivery of data and information in a consistent, uniform manner
- Understandability: delivery of data and information in a manner that is appropriate and understandable in the target community
- Accuracy: precision in measurement and observation
- Flexibility: adaptability to multiple situations

These information attributes have evolved over time within the disaster management community representing the viewpoint of a range of providers, users and consumers scaled from the local to national level. In this regard the communities involved transcend boundaries between recognized sectors at each of these levels (private, public, not-for-profit, NGO etc.).

7. Hurricane Scenario

Hurricanes, cyclones and tropical storms are among the most visible disasters that visit coastal areas around the world on a regular, seasonal basis. They are familiar to most everyone and like other kinds of disasters strike fear into those who have come into direct contact with them.. In the remainder of this paper a hypothetical scenario will be developed for the response to a hurricane drawing attention to the multiple actors and information communities that are involved and the potential for highly heterogeneous information and operating environments that may exist during such an event.

7.1 Hurricane Disaster Description

Hurricanes generally emerge as tropical depressions in the June to November time frame. The primary forces at work in a hurricane are high, sustained winds; coastal flooding from storm surge; inland flooding from heavy rains and battering and beach erosion from heightened wave action. There are countless secondary hazards as well including tornadoes, other severe storms and infrastructure failure (e.g. seqage treatment, power plants etc.). High

winds pose significant structural load risks as well.

Hurricanes are "ranked" on the Saffir-Simpson scale from 1 (74-95 mph sustained winds) to 5 (greater than 156 mph sustained winds). From a ranking three and higher (winds greater than 111 mph) large trees can be blown down. Structural damage will also occur, particularly for less substantial buildings. Strom surge of between 9 to 18 feet can be expected which will result in coastal flooding and damage to natural and man made structures. Waves of 18 to 25 feet will be possible and will cause significant erosion and damage to shoreline property.

7.2 Event Timeline

A hurricane event timeline is delimited in phases that correspond to the onset of the storm measured in hours. This system covers pre-storm, landfall and continues until the completion of response activities. The Federal Emergency Management Agency recognizes three primary phases.

- Awareness: 72 to 60 hours before the arrival of gale force winds (32 to 63 mph)
- Standby: 60 to 48 hours before the arrival of gale force winds. It is likely that a tropical storm watch would be issued during this period.
- Response: 48 hours before arrival of gale force winds through termination of the emergency. Hurricane watches and warnings would be issued by the National Weather Service during this period.

Preparing for an approaching hurricane, response and recovery requires incorporating meteorological data into models that predict storm track and storm surge. These predictions are then incorporated into maps showing population distribution, evacuation routes, deployment of emergency personnel and supplies, and other relevant response information. This effectively brings to bear the collective capabilities of many federal, state and Local agencies and requires the support of a number of private sector entities that maintain basic infrastructure (utilities, tax base, insurance) and communications media. In addition to federal agencies there are a number of officials at the local level that act in a "hands-on" manner throughout the emergency. In essence, many of the participants and their domains at the local level are characterized in Table 1. Many of these same types of participants would be reflected at the state level also.

The matrix in Table 1 has been annotated with the Federal Emergency Management Agency's assessment of lead agencies and departments. In some cases an agency or department will play both a lead (P for primary) and a secondary (S for secondary) role depending on the scope etc. of the event. For the purposes of this example each cell boundary in the Table 1 matrix can be thought of as a place holder for one or more interfaces that will be required in a final, fielded application for disaster management. However, once the participants are identified the relationships and dependencies between these groups must be described in precise event by event detail. When this has been accomplished the participants from many of the communities will come into play and their roles,

responsibilities and mandates must be integrated seamlessly with this matrix.

7.3 Information Needs

The information requirements associated with the disaster life cycle, hurricane scenario, are not insignificant. By rough count, a minimum of forty separate entities spread across the continuum of providers and consumers that extend from the federal to the local level and cross well established boundaries that exist between the public and the private sectors must work together in a seamless manner throughout to ensure success. These communities have diverse expectations, requirements, technical capabilities, missions, different hardware and software etc.

The process must define the requirements and expectations of each community and develop an appreciation of the input they expect and the output they produce in order to begin to conceptualize the nature and the extent of the interfaces that are required to meet the needs of this community. However, a major issue is the need for development of good schemas that have been successfully federated across these information communities. It is also clear that a range of data products (raster, vector, video, voice etc.) will need to fielded across a range of platforms and harmonized with users who require tools for analysis, decision support and mission planning.

8. Web Based Geospatial Test-Bed Demonstration of Hurricane Scenario

The Web Mapping Technology Program is a collaborative effort between military and civil agencies of the US government, international organizations, and the commercial geo-processing technology sector to develop interoperable web mapping technology solutions. The program will advance the current state of proprietary web mapping technology solutions, enabling web-based mapping to support diverse applications that require access to multiple, distributed geospatial information sources across the World Wide Web (Figure 1). Applications for this kind of interoperable technology include environmental analysis and management, disaster relief operations, emergency response and management, and military operations.

The Test-bed will identify and develop software components implementing common interfaces and protocols necessary for web-based geospatial information display and interaction services. These components will support diverse applications across the spectrum of web user environments, ranging from enterprise intranets to home users on dial-up connections. Based on the user environment and potential applications, the Test-bed design acknowledges that there will be at least three different cases of client-server distribution of web-based display and interaction services. The cases are distinguished how much actual geospatial information, symbolized map displays (i.e. gif or jpeg images), or intelligent graphics travel across the web and the client-server distribution of services necessary to support that transfer. The Test-bed design process also anticipates that the cases can also be combined. A major focus of the test-bed will be to assess the content, format, and transport mechanisms of the web communications necessary in each case. The test-bed will also explore methods to interlink standards-based, geospatial information,

allowing nonlinear discovery and integration of distributed geospatial resources by information use and content. The effectiveness of these architectures will be tested by conducting scenarios to assess the capability of interoperable web mapping to support environmental management, emergency management, disaster relief, and military humanitarian relief and stabilization operations.

Early in the Web Mapping Test-bed (WMT) project, two fictional scenarios were created to generate requirements for data discovery, access, and display, and to keep the demonstration "focused" and centered on "real world" issues. One scenario centered on the needs of a TV journalist who uses the web to access spatial data to help her create a news report about a hurricane approaching Mobile, Alabama. In the demonstration, the journalist uses a "paper thin" desktop; it merely needs to run Netscape. The other scenario focused on the needs of a team of disaster managers in a mobile disaster response control center, preparing for the same hurricane. This team has additional software, including "pre-built" queries to generate appropriate views. In both cases, online geo-data servers were registered in a Open-GIS Catalog Specification catalog that enabled a query very much like an ordinary web search engine query.

In the first scenario, the journalist using a standard web browser was presented with a "shopping basket" metaphor that allowed browsing geospatial data sources of potential interest (figure 1). The journalist selected a data source and specified a region to view. The zoomed map or image came into view on the web browser, just as one can see now with today's non-interoperable web mapping applications. The difference from today's technology became clear when the journalist selected 4 additional sources and added them to the "shopping basket." Now the standard web browser was used to access these 4 additional spatial data servers, and these servers provided data that automatically overlaid the first map (figure 2). Five layers were displayed, each a live "view" into data on separate servers around the world (figure 3). The servers were from different vendors. Some served vector data of different kinds, others raster data. Any combination of map layers could be viewed, overlaying each other in any stacking order (figure 4). Zooming on one map or image caused the various servers around the world to perform identical zooms, so that the layers would stay identically geo-referenced (figure 5). The maps and images were not stored on the servers as gif images, but they were created as requested, and delivered to the web browser as gif images.

In the second scenario, more capable clients, GISs and custom software from different vendors, were used to access some of the same servers used in the first scenario. These clients created smarter displays using previously built and stored presentation styles (figure 6). For example, as shown in figure 7 storm surge information from one source, and evacuation route information from another source could automatically be combined to highlight routes cut off by the storm using a single "pre-built button."

The relatively simple new web mapping protocols and interfaces which enable the interoperability described above depend on foundation work done earlier

in Open GIS Consortium. This includes the work underlying the Open-GIS Simple Features Specification and Open-GIS Grid Coverage Specification. New Open-GIS Specifications based on these new protocols and interfaces are now approved as Open-GIS Specifications. The Open GIS Consortium's software vendor members are expected to implement these interfaces in client and server products which will interoperate. As with all Open GIS Consortium specifications, the Web Mapping protocols will be made available free on their web site to all software developers within a few months.

There were essentially two types of applications: Web Mapping Clients, and Web Mapping Servers. The Clients created requests that conform to the Web Mapping Protocols. The main interface is the Get-Map protocol, that identifies one or more layers to be displayed, along with the various parameters needed to ensure the display is exactly the one intended. Examples of these parameters are the Spatial Reference System of the display, the center and dimensions of the display window, instructions for transparency, the order in which to display layers, and so on. Two additional interfaces are provided: Get-Capability and Get-Feature-Info. These protocols enable a client to discover the abilities of a server, and the ability to "drill down" through a display to discover the attributes of a displayed feature.

The Web Mapping Servers are able to interpret requests that conform to the Web Mapping Protocols and able to generate appropriate objects to be returned to requesting clients.

Additionally, a "Cascading Server" was used that is able to query other servers and report their capabilities as if those capabilities were its own. The Cascading Server invokes other servers whenever a cascading service is requested.

8.1 Demonstration Data Providers

A number of participating agencies and private sector organization provided data and software for this demonstration. The following providers were part of the demonstration: City of Mobile GIS Department, Raytheon ITSS (STX), FEMA, NOAA/NESDIS, NRL-Monterey, NASA-JPL, USDA-NRCS, USATEC, Alabama Coastal Hazards Assessment CD-ROM, NOAA Coastal Services Center in partnership with Region IV FEMA, Alabama Emergency Management Agency, Alabama Dept. of Economic and Community Affairs, and South Alabama Regional Planning Commission

8.2 University and Private Sector Participants

Participating university and private sector technology providers included: Autodesk (US), BBN (US), Technologies Blue Angel Technologies Cadcorp (UK), Compusult (Canada), Cubewerx (Canada), ESRI (US), Galdos Systems (Canada), Geodan IT (Netherlands), Geomatics (Canada), Hitachi (Japan), ILOG (France), Intergraph (US), Ionic Software SA (Belgium), Laser Scan (UK), Litton/TASC (US), Lockheed-Martin (US), MapInfo (US), Microsoft (US), MIT (US), Mitsubishi (Japan), NTT Data (Japan), ObjectFX (US), Oracle

Corp (US), Ordnance Survey (UK), PCI Geomatics (Canada), Penn State University (US), SICAD Geomatics (Germany), Social Change Online (Australia), Sun Microsystems (US), and Universal Systems (Canada).

9. Conclusions

The Web Mapping Test-bed is an opportunity for technology, infrastructure, and geospatial information providers and users to mutually define interface and protocols (and thus candidate interoperability specifications) in the context of a hands-on engineering experience expected to shape the future of Web mapping software development and Web data publication. The Web Mapping Technology Initiative is expected to generate a significant capability and support a long-term effort. Current and future work efforts include developing Map-Server interface specifications, XML encoding standards for geospatial information, client interactivity and discovery tools, standards for geospatial hyper-linking, and standards-based methods to encode and transport information about spatial-temporal events such as floods, earthquakes and hurricanes.

10. References

Burton, Ian, Robert W. Kates, and Gilbert F. White, The Envirnment as Hazard, 2d Edition, New York, NY: The Guilford Press, 1993

Disaster Information Task Force Report, Harnessing Information and Technology for Disaster Management, Global Disaster Information Network, 1997

NAPA Report, Geographic Information for the 21st Century: Building a Strategy for the Nation, National Academy of Public Administration Press, 1998

NRC Report, Information Infrastructure for Managing Natural Disasters, Board on Natural Disasters, National Academies Press, 1998

Roper, William, Geospatial Technology Support to the Nation's Navigation System, Transportation Research Board, National Research Council, Washington, DC, January 1999

Tobin, Graham A., and Burrell E. Montz, Natural Hazards: Explanation and Integration, New York, NY: The Guilford Press, 1997

Organization Type	Direction And Control	Comm-unications	Warning	Emergency Public Information	Evac-uation	Mass Care	Health And Medical	Resource Management
CEO	**P**							
Fire	**P/S**							
Police	**P/S**							
Health & Medical	**P/S**						**P**	
Public Works	**P/S**							
Emergency Programs								
EOC Manager								
Communic-tions Coord.		**P**						
Public Information Officer				**P**				
Evacuation Coordinator					**P**			
Mass Care Coord.						**P**		
Resource Manager								**P**
Education Dept.								
Animal Control								
Warning Coord.			**P**					
Volunteer Organizations								
Other Organizations								

Table 1: Public Sector Organizational Responsibilities in Response

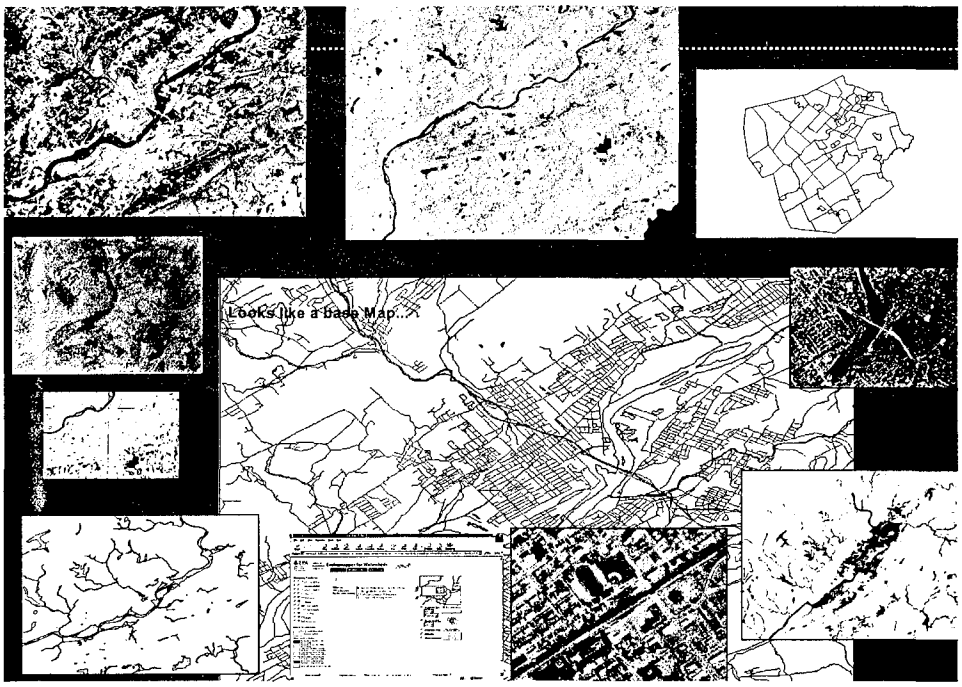

Figure 1: Examples of world wide maps, images and information sources

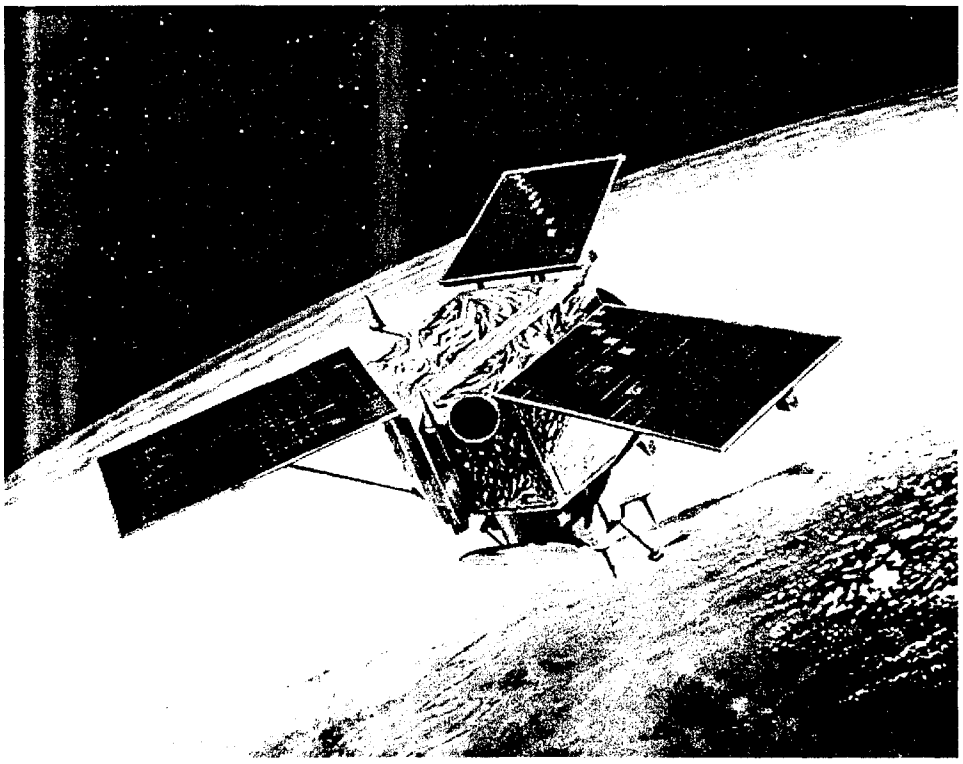

Figure 2: Geospatial spatial sources including new high resolution Ikonos commercial imagery

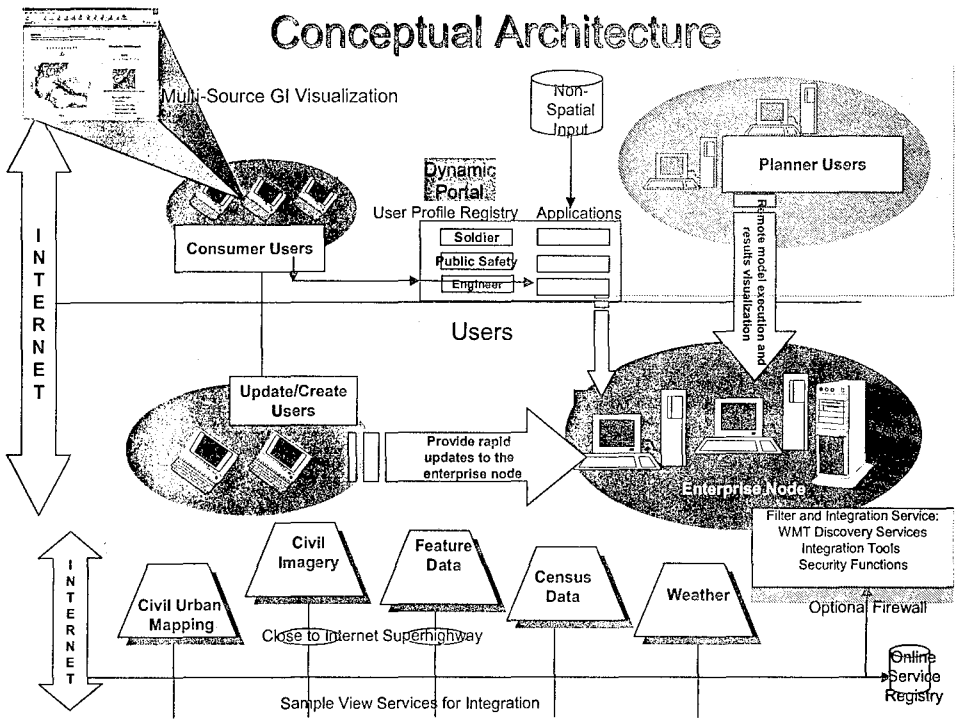

Figure 3: Web based server structure and interaction capabilities

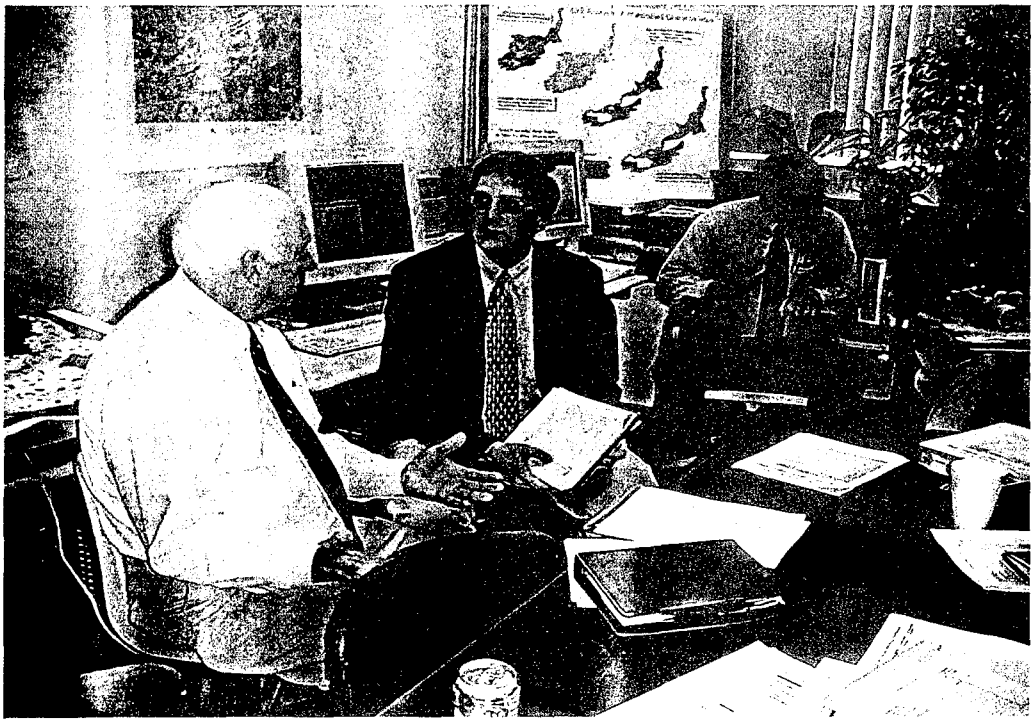

Figure 4: Interactively developed products being used by emergency decision makers

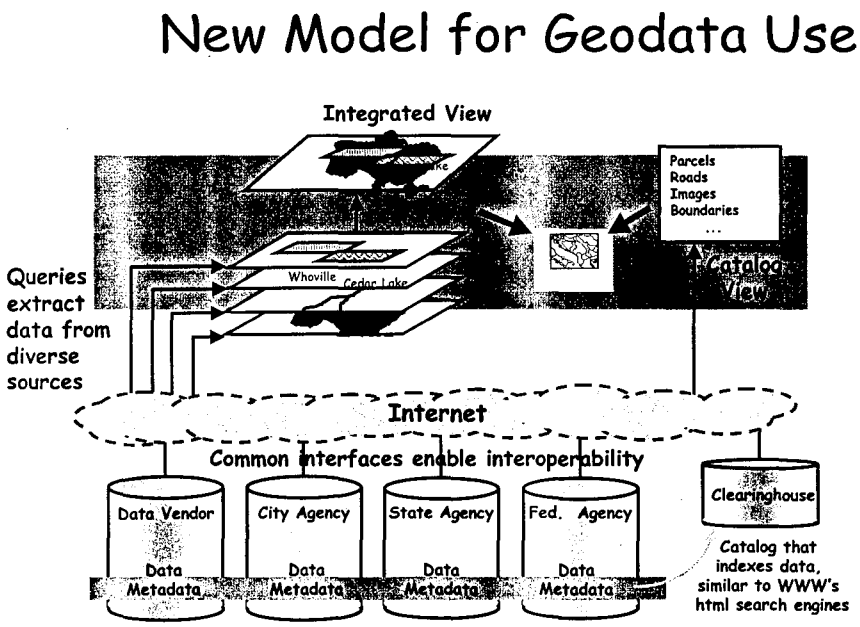

Figure 5: Multiple data inputs of different type used to create integrated products

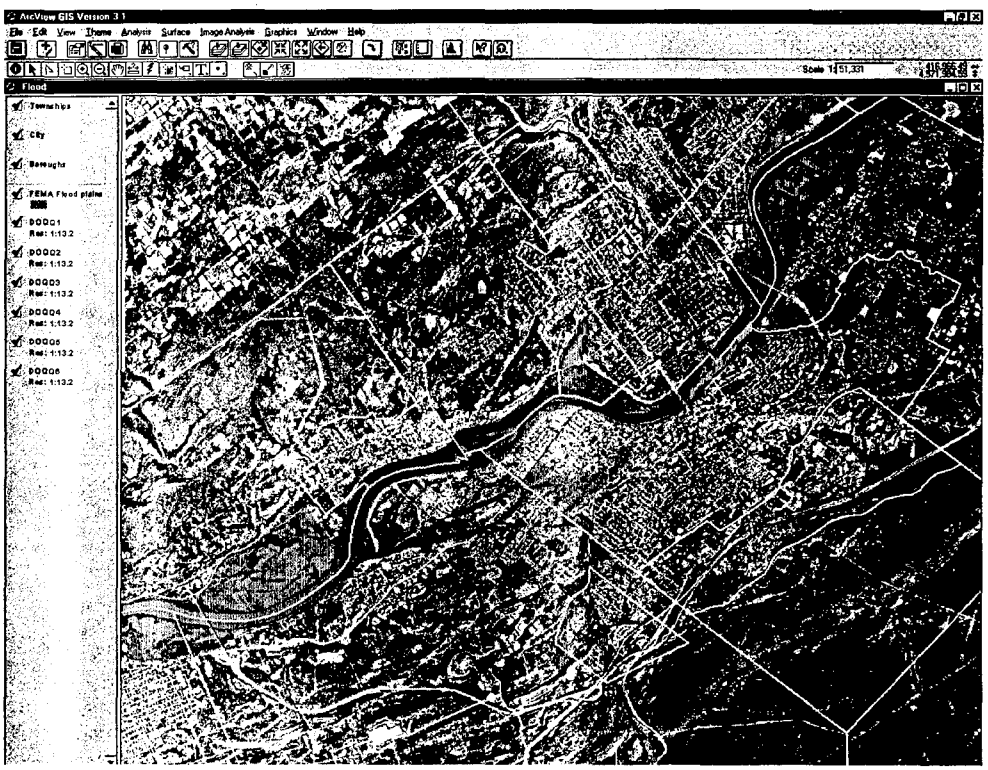

Figure 6: Integrated overlay and scale change for products from world wide data

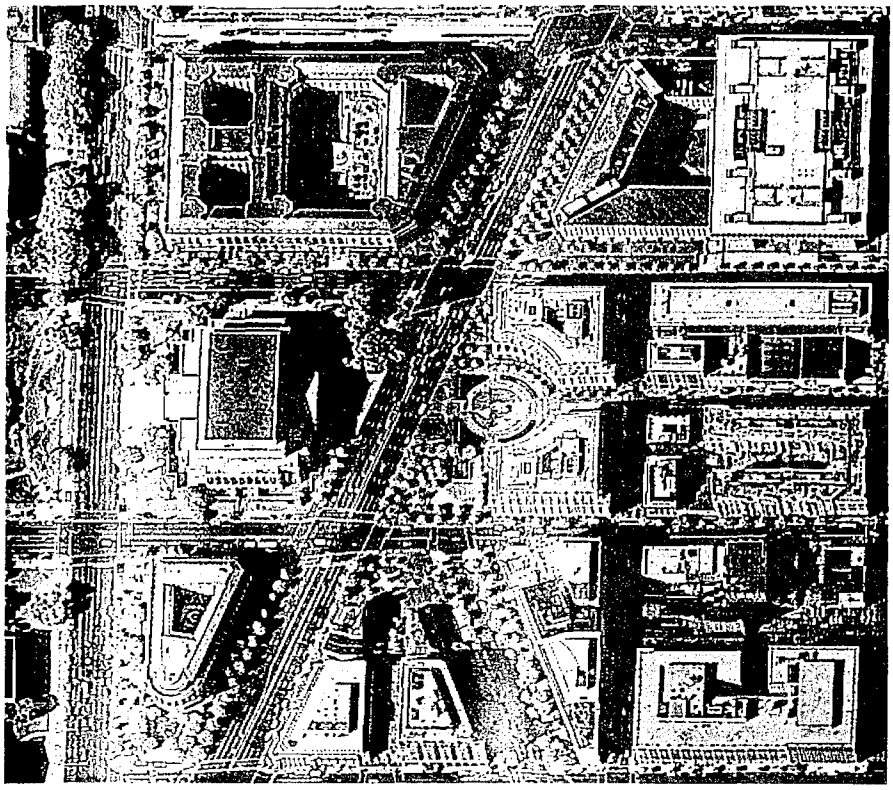

Figure 7: Application of high resolution commercial satellite imagery into products

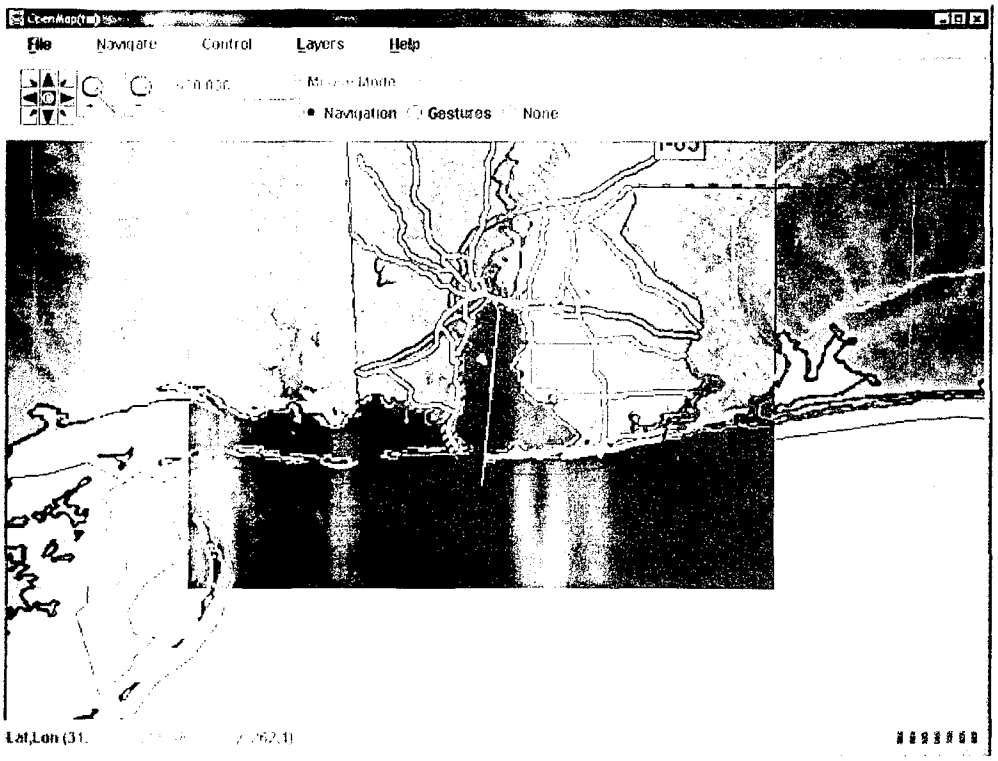

Figure 8: Hurricane in Mobile Bay product with road nets and other information

DRAFT MANUAL FOR SEISMIC INFORMATION SYSTEM DEVELOPMENT

by

Hideki SUGITA[1], Tomofumi NOZAKI[2]

ABSTRACT

This paper introduces the "Draft Manual for Seismic Information System Development" that Public Works Research Institute, Ministry of Construction recently developed. The manual was prepared to develop efficient seismic information system: SIS for civil infrastructure administrating bodies from the viewpoint of the national land management policy. This paper includes a basic concept of SIS development, requirements of SIS, element technologies for SIS, and safety/ security.

KEY WORDS: Earthquake Disaster
Information System
System Requirement
Safety, Security

1. INTRODUCTION

Recent situations such as environmental changes and severe disasters over the world require more comprehensive countermeasure than before. Such countermeasure must be an overall program including monitoring of circumstances, adequate planning and administration in addition to the construction. Especially, civil infrastructures require overall management because they have counteractions to nature and social activities.

The Ministry of Construction has initiated a five-year comprehensive research project "Application of Advanced Technologies for the National Land Management" since 1999. In the national land management (designated hereinafter as NLM) framework, four important tasks are needed to cope with the major missions (**Figure 1**) including the safety against disaster. The research project includes applications of recent advanced information technologies such as GIS, GPS and satellite images.

Among various missions included in NLM, earthquake disaster prevention for civil infrastructures is unique because;

1) Disaster mitigation requires various kinds of information, i.e. hazard distribution, disaster potential, and social activities,
2) Damage of facilities tend to be developed simultaneously in wide area,
3) Urgent works are needed to prevent the expansion of disaster influence,
4) Disaster influence is unpredictable due to the complexity of urban functions.

A seismic information system (designated hereinafter as SIS) is one of the solutions to support disaster response activities (**Figure 2**).

Although advanced technologies have been rapidly developed, their performance may not agree with the requirements of disaster response activities. For example, satellite images may not be precise to detect damage of facilities, or

1) Head, Earthquake Disaster Prevention Technology Division, PWRI, MOC
1 Asahi, Tsukuba, Ibaraki 3050804 Japan
2) Senior research engineer, ditto

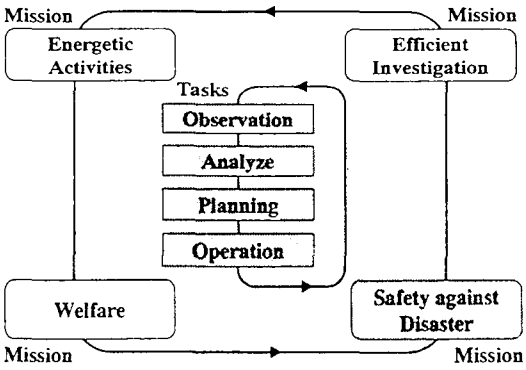

Fig.1 Framework of NLM

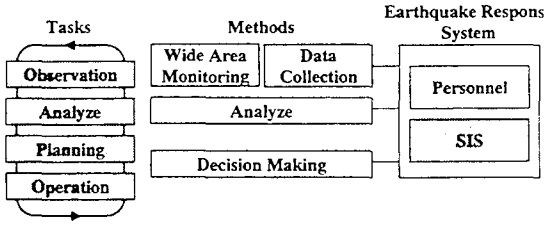

Fig.2 Earthquake Response System for NLM

maneuverability of the GIS is too complex for the emergency actions. Besides, other problems may exist due to a framework of the SIS. For example, sometimes the same kinds of data set are stored to different computer systems redundantly. In addition, once a huge system is constructed, it needs much cost to extend or revise the system. In other words, there are many possible problems and losses depending on the SIS architecture. Being aware of these issues, the PWRI has composed a draft guideline for the efficient development of the SIS. In this paper, the brief contents of the "Draft Manual for Seismic Information System Development" are introduced.

2. STRUCTURE OF MANUAL

2.1 Overview

For the efficient development of the SIS, the manual contains important topics, namely, planning and development concepts of user-oriented and flexible SIS, and a list of state-of-the-art of technologies as a reference for the system planners. Also, the system safety issue is included. The topics are arranged in corresponding chapters as shown in **Figure 3**. Note that the numbers of chapter are not of this paper but of the manual.

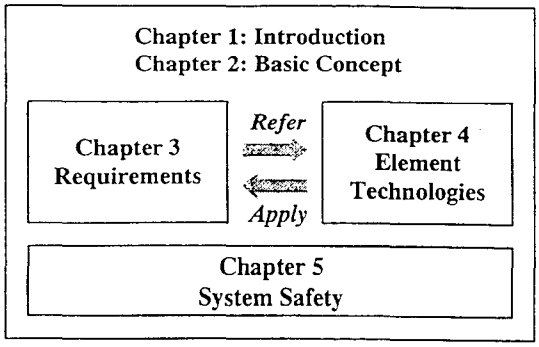

Fig.3 Structure of Manual

2.2 Key issues

Brief statements of the key topics in **Figure 3** are as follows. The detailed explanations are in the chapter three to six of this paper.

(1) Basic Concept of SIS Development

The basic concept of the SIS development includes: concept for user-oriented SIS, concept for flexible SIS, consideration of the system interface, and the application of SIS in normal state. These issues are fundamentals for the SIS that satisfies requirements for earthquake disaster response systems. While the concept mainly aims to initial development of the SIS, they can be applied to improve existing SIS with careful consideration.

(2) Activities and Requirements for SIS

Classification of the earthquake response activities, information required for the activities, and functions required for the SIS are described

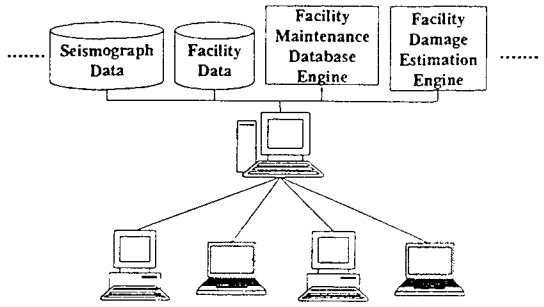

Fig.4 Data Sharing Architecture

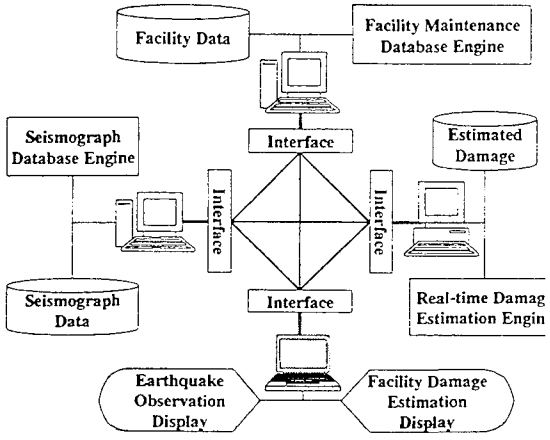

Fig.5 Distributed Data Sharing Architecture

against earthquakes. Especially, SIS must be flexible from the viewpoint of expandability because it utilizes rapidly changing advanced technologies. The better solution to cope with this problem is a distributed data sharing system (**Figure 5**). In such system, the data are stored in each server for specific function, and the data are utilized by arbitrary clients through common interfaces.

To realize the true distributed data sharing system, the structure and the format of the data dealt by SIS must be identified and clearly described. An image of data structure that can include the attributes and relationships is shown in **Figure 6**. Once the structure is defined and clarified, the information can be interpreted to any format. If

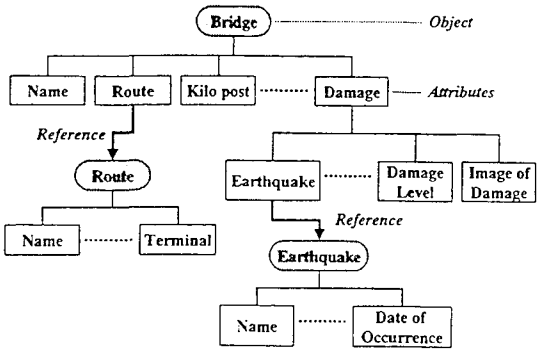

Fig.6 Data Structure

the format is well defined, arbitrarily added subsystem can access the information regardless with the types of operating systems and applications.

4. REQUIREMENTS OF SIS

4.1 General

It is essential to investigate activities of the earthquake disaster response system and the information dealt with. In the manual, an example of such investigation in which response activities are divided into four phases is shown. For each phase, activities, information needed, and functions required for SIS are clarified.

4.2 Earthquake disaster response phases

Assuming an earthquake disaster response for civil infrastructures, response phases can be classified as follows:

1) Emergency response phase: Overall rough damage inspection is performed. Temporary measures without heavy equipments are taken occasionally.
2) Temporary restoration phase: Activities include damage inspection, decision-making and activities for the temporary restoration.
3) Complete restoration phase: Similar to the temporary restoration phase, while it requires

in the chapter three of the manual.

(3) Review of Element Technologies for SIS

After requirements and structure of the SIS is determined, planners must investigate proper technologies to realize the functions of the SIS. Because the SIS requires knowledge on both advanced information technology and earthquake engineering technology, planners need their comprehensive list. The manual provides an inventory of current advanced technologies of both fields in the chapter four.

(4) Consideration of Safety of SIS

Because the SIS is supposed to be used in an emergency situation, it must be well prepared for a disastrous condition. Therefore, planners must consider safety of devices, facilities and data related to the SIS against earthquakes. Besides the safety and security must be established and maintained because the SIS is developed under network situations. The technologies and methodologies for the safety and the security are introduced in the last chapter of the manual.

3. BASIC CONCEPT

3.1 General

When one tries to develop an efficient SIS, there are several problems. First, advanced information systems are usually developed mainly from a viewpoint of information technology professionals who do not necessarily know the activities of earthquake disaster response system. As a result, sometimes personnel in the response system encounter insufficiency of system performances including the accuracy, speed and capacity while some other performances exceed their aims. Second, there can be another problems related a system architecture. Once SIS is developed as a large host-terminal system, it cannot be revised easily. Data may not be shared easily between different systems that are separately developed, or even it may be difficult to exchange data between different versions of the same applications because of frequent revision. In the first part of the manual, therefore, several suggestions are stated to develop efficient and flexible SIS that meet with the requirements of the earthquake disaster response activities.

3.2 Objective oriented concept

To develop the SIS that satisfies requirements of an earthquake disaster response system, SIS should not be thought simply as an integration of devices and application software. Rather, it is suggested that the system should be developed based on the earthquake response activities and the information dealt with in the activities. To accomplish this objective, following three steps are needed.

1) To investigate and organize disaster response activities
2) To investigate information dealt with in the activities
3) To clarify the requirements of functions to efficiently deal with the information

Charts, tables and even the analytical method such as the systems analysis are necessary to perform the tasks above.

3.3 Flexibility

SIS deals with many kinds of data of daily maintenance in addition to the emergency information after earthquakes. Therefore, it needs to be able to access almost any information regarding the facility management. One of the solution of such data sharing system is servers with highly integrated functions and clients that browse the result of servers' functions (**Figure 4**), However, it has disadvantages such as inflexibility, bottleneck and concentration of risk

more detailed inspection and complete restoration of damaged facilities.

4) Response system support phase: This phase is different from other three phases, which concerns overall response activities from the start to the end. For example, it includes ensuring safety of the personnel and management of resources to maintain the response system.

4.3 Activities, information, requirements for each phase

For each phase, response activities are itemized as shown in **Table 1**. For example the emergency response phase includes four activities, namely, setup of earthquake response system, emergency damage inspection, investigation of response planning and emergency response. Each activity requires various kinds of information for its execution, and the functions of SIS to deal with the information are listed.

The numbers in the brackets indicate the section numbers of the manual where the technologies corresponding to the functions are explained. Details of those technologies are explained in the chapter four of the manual. The chapter three exemplifies that once the planners analyzes the activities, information and the required functions, they can distinguish the appropriate technologies applicable for SIS by referring the corresponding sections.

5. ELEMENT TECHNOLOGIES

5.1 General

In the chapter four "Element Technologies for SIS" of the manual, numbers of technology

Table 1 Activities, Information and Required Functions

Emergency Response Phase

Activities	Information	System Functions
Set-up of EQ Response System	Earthquake	Earthquake Detection(4.3.1)
	Facility Damage	Damage Detection(4.3.2,4.3.3)
	Set-up Trigger	Emergency Call(4.4.1)
Emergency Damage Inspection	Inspection Strategy	Detection of Phenomena(4.3.1-4.3.5)
	Inspection Activity	Field Activity Support(4.3.4)
	Facility Damage	Field Activity Support(4.3.4)
	General Information	Remote Sensing(4.3.5)
Study of Response Planning	Related Organ's Action	Information Exchange(4.4.3)
	Construction Staffs	Information Management(4.4.2)
	Priority	Decision Making Support(4.4.1-4.4.3)
Emergency Response	Response Activity	Field Activity Support(4.3.4)

Temporary Restoration Phase

Activities	Information	System Functions
Damage Investigation	Investigation Strategy	Remote Sensing(4.3.5)
	Investigation Activity	Field Activity Support(4.3.4) Remote Sensing(4.3.5)
	Facility Damage	
	General Information	
Restoration Planning	Related Organ's Action	Information Exchange(4.4.3)
	Construction Stuffs	Information Management(4.4.2)
	Priority	Decision Making Support(4.4.1-4.4.3)
Temporary Restoration	Restoration Activity	Field Activity Support(4.3.4)

Complete Restoration Phase

Activities	Information	System Functions
Investigation	Investigation Strategy	Decision Making Support(4.6.1-4.6.3)
	Investigation Activity	Field Activity Support(4.3.4)
	Facility Damage	
	General Information	
Restoration Planning	Related Organ's Action	Information Exchange(4.4.3)
	Construction Stuffs	Information Management(4.4.2)
	Regional Restoration Plan	Information Exchange(4.4.3)
	Priority	Decision Making Support(4.4.1-4.4.3)
Complete Restoration	Restoration Activity	Field Activity Support(4.3.4)
	Construction Stuffs	Information Management(4.4.2) Information Exchange(4.4.3)

Response System Support Phase

Activities	Information	System Functions
Response System Related Information	Response System Level	Common Infrastructure(4.2)
	Response System Staffs	Information Management(4.4.2)
Disaster Prevention Base	Building Damage	Field Activity Support(4.3.4)
	Device Damage	
Activity Support Stuffs	Storage and Distribution	Information Management(4.4.2)

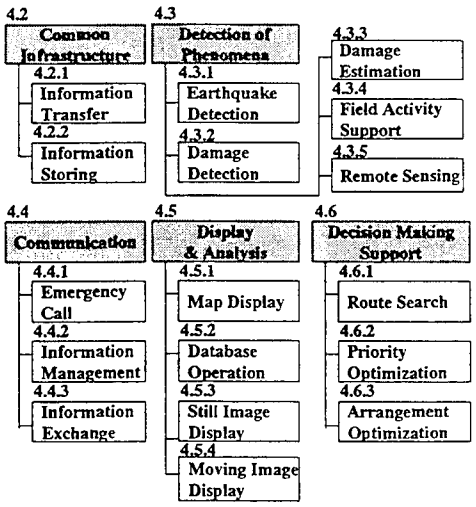

Fig. 7 Element Technologies

that can be applied to SIS are introduced. The

planners of SIS can refer them to find the technologies suitable for the function of SIS that they have investigated in the chapter four. Also, it can be referred as the handbook to know the state-of-the-art of the technologies for SIS. While the advanced technologies are often explained separately in respective specific area, this manual collects them so as to be the comprehensive reference for SIS planners. Also, it is intended that the manual be useful for the personnel who are not necessarily the professionals of the information technology to discuss about SIS with the information technicians. The technologies included in this chapter are divided into five categories. The structures of this chapter with subcategories are shown in **Figure 7**.

Table 2 Information Transfer Technologies

Technologies	Speed	Vulnerability			Cost		Service Area
		Conflict	Restrict	Damage	Initial	Run	
Telephone Line	O	X	X	Δ	OO	OO	OO
Ditto (ISDN)	O	X	X	Δ	O	OO	O
Ditto (Packet)	OO	OO	O	Δ	Δ	Δ	Δ
Cellular Phone	O	Δ	Δ	O	OO	O	OO
Wireless (Ground)	X	OO	OO	OO	----	----	----
Wireless (Satellite)	X	OO	O	OO	----	----	----

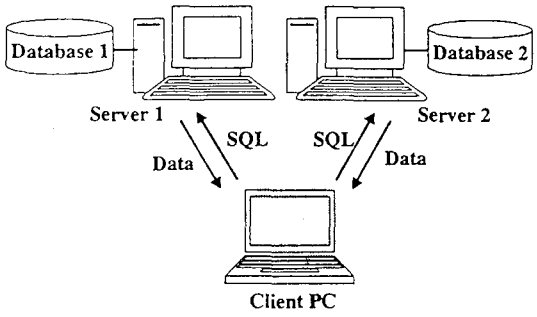

Fig.8 Data Sharing using SQL

5.2 Common infrastructure technologies

This section introduces two kinds of fundamental and important technology that are common to any SIS. The information transfer technologies are the vital for all kinds of information systems that includes wired/ wireless signal transfer technologies. In the manual, several kinds of those technologies are listed and compared each other as shown in **Table 2**.

The Information storing technology section focuses on the storage devices such as hard disk drive and magnet-optic disk. Also, this section introduces a brief concept of the relational database that is related to the distributed data sharing system. **Fig. 8** shows an image of data shared system with "Structured Query Language: SQL" that is generally used to control RDB.

5.3 Technologies to detect phenomena

Prompt detection of phenomena caused by the earthquake disaster is necessary for the efficient response. This section includes following five kinds of technologies.

1) Earthquake detection: Technology to detect the ground motion of earthquakes by accelerographs.
2) Damage detection: Technology to directly detect the damage of facilities by utilizing various types of sensors.
3) Damage estimation: Technology to estimate the damage of facilities indirectly based on the monitored ground motion data.
4) Field inspection support: Combination of technologies to support the field inspection of damage.
5) Remote-sensing: Advanced remote sensing technologies from platforms such as helicopters, airplanes and artificial satellites.

For example, sensors to detect damage should be used properly depending on the distribution of facilities and the required accuracy. While rough detection of damage in the wide area needs only simple sensors such as the wire sensor, more sophisticated sensors are necessary for accurate damage detection for important facilities. **Fig 9** illustrates an image of accurate damage detection

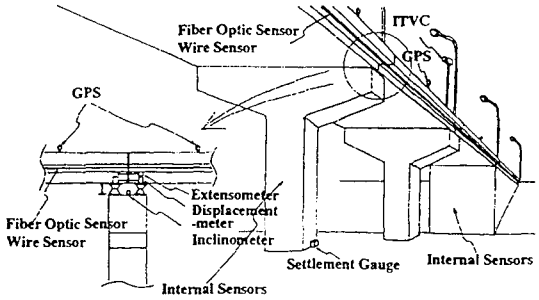

Fig.9 Damage Detection of Highway Bridge

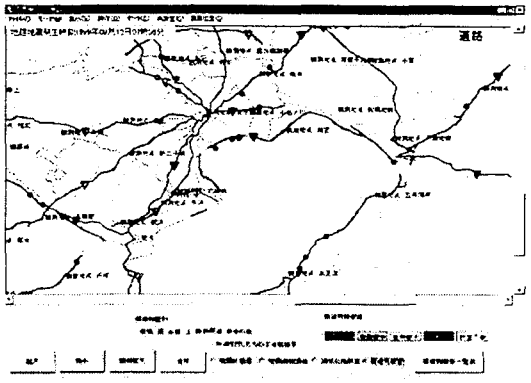

Damage of Highway Bridges

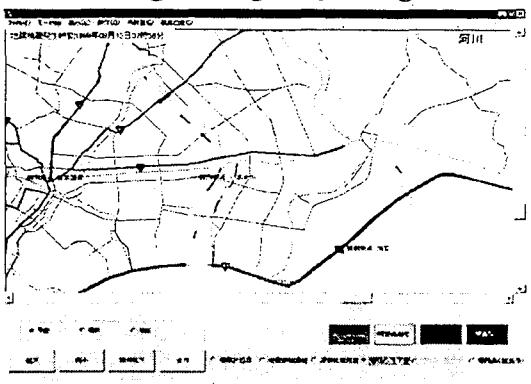

Damage of River Levees

Fig. 10 Urgent Damage Estimation System

for a highway bridge.

Figure 10 shows an urgent damage estimation system for highway bridges and river levees. The system provides rough estimation based on the monitored ground motion data and pre-stored structures database.

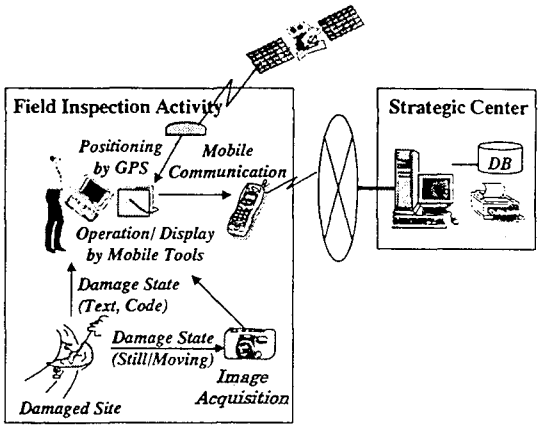

Fig. 11 Field Inspection Support Technologies

Field inspection support technology is illustrated in **Figure 11**, in which various kinds of advanced equipments are utilized. For example, personnel of inspection team can easily understand their position in the damaged area with the help of the GPS and GIS devices. The information about the damage including texts, still and moving images can be sent to the response center through the communication technology. Planners can develop such a system with exclusive devices, or they can use existing equipments in the market. Recent technology can provide the flexibility of development of the system.

Because of the extension of the earthquake damage distribution, the information in wide area needs to be collected all at once. Remote-sensing technology can be a candidate for such requirement. The remote-sensing technology consists of two parts, one is a platform and the other is a sensor. Various kinds of platform are characterized by their height, mobility and stability. As for the sensor technology, it also has various kinds such as an optical sensor, infrared sensor and laser profiler. They are characterized by the ability to detect phenomena, accuracy and

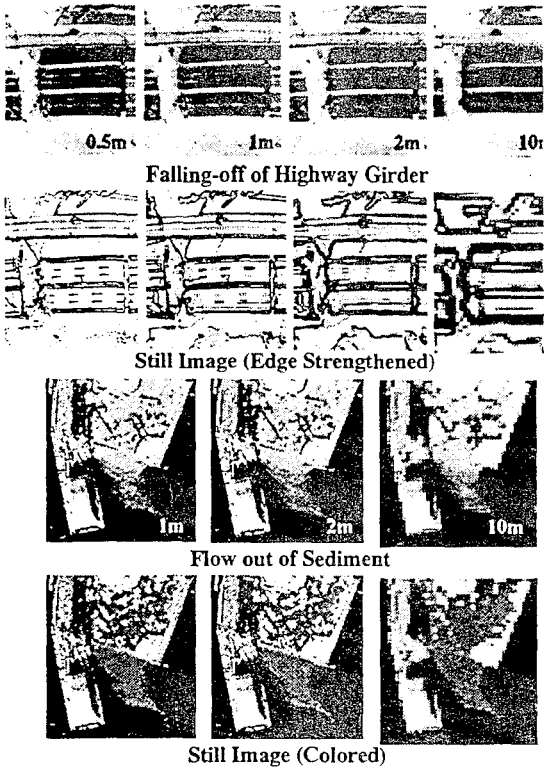

Fig. 12 Damage Detection by Remote Sensing

influence of weather such as cloud and rain. **Figure 12** shows simulated satellite images for understanding earthquake damage.

5.4 Technologies for information exchange

For the prompt and efficient earthquake response activities, organizations and the personnel need to exchange their information. This section includes following three kinds of technologies:

1) Emergency call: It is vital to note the information for the establishment of the response system to personnel all at once. Pager, voice modem and Internet technology can be used.
2) Information Management: Information collected and stored need to be appropriately managed. For example, information of stock materials for the restoration is meaningless if they are not updated timely. Information management issue is explained here although it is rather a management technique than a pure hardware/ software technology.
3) Information exchange: Technology that is applicable to exchange information between different organizations is introduced. **Figure 13** shows an image of the extranet that utilizes the Internet technology. More than one organizations exclusively exchange their information through the Internet by using extranet technology.

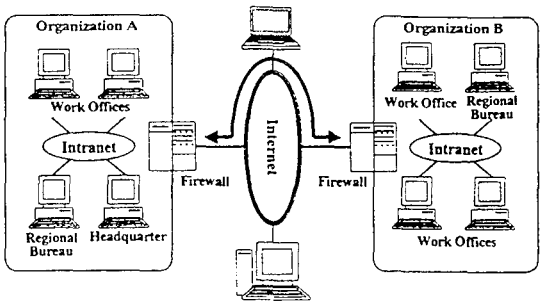

Fig.13 Data Exchange between Extranet

5.5 Technologies for display and analysis

While the information is gathered and stored, it becomes useful only when they are analyzed and displayed in proper manner. This section includes recent technologies to display maps, database and still/ moving image.

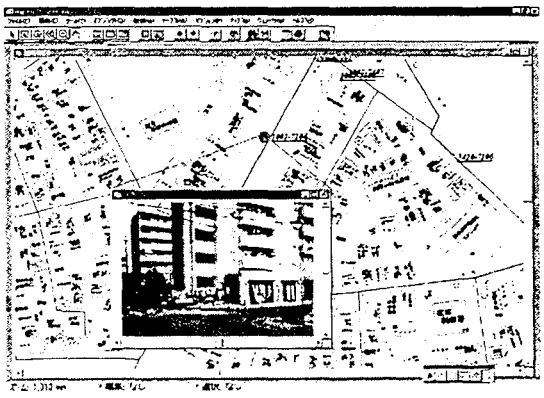

Fig. 14 Still Image Displayed in GIS

While those technologies are not only for SIS but general for any kinds of information system, their mechanisms are briefly discussed to help planners grasp rough ideas to import them into their SIS. For example, a still image linked with an object in GIS is shown in **Fig14.** In the manual the mechanism of each technology is explained conceptually.

5.6 Technologies to support decision-making

While the earthquake/ damage/ general information itself improve the response activities, it can be useful if the SIS provides more creative information to support examination on efficient response alternatives. This section introduces three kinds of examples:

1) Technology to find the shortest route
2) Technology to find priorities of emergency restoration activities
3) Technology to find optimized pattern of person/ material arrangement

Those technologies do not necessarily give the completely exact results, however, the earthquake response team can investigate the appropriate countermeasure by examining the alternatives.

6. SAFETY AND SECURITY

6.1 General

Vulnerability to disasters and security problems are the negative aspects of SIS. It may be true if the system is not constructed and maintained properly. This section introduces several measures for the reduction of these kinds of risks to realize the functionalities of SIS both in the usual and the emergency states.

6.2 Safety against earthquake disaster

SIS must be functional under the anticipated level of earthquake. On the other hand, the information system devices are weak against such conditions as shock, vibration and irregular temperature during earthquakes. This section explains following three kinds of issues to reduce and manage the risk of SIS.

1) Constructing earthquake standing SIS: Many points regarding the settings and arrangements of system devices and facilities
2) Risk control with distributed SIS: Concepts and techniques to keep the redundancy of the system, network line and data
3) Preparedness for the critical situation: Importance of consideration of contingent situation in which the response system must act without sophisticated SIS

An Example of data distribution by using Redundant Arrays of Inexpensive Disk: RAID

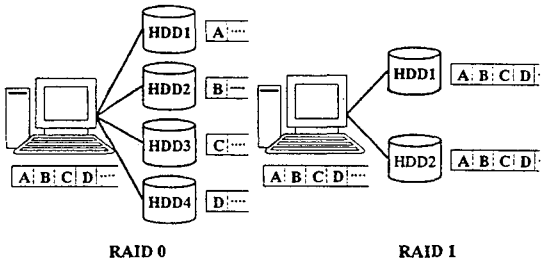

Fig.15 Data Distribution using RAID

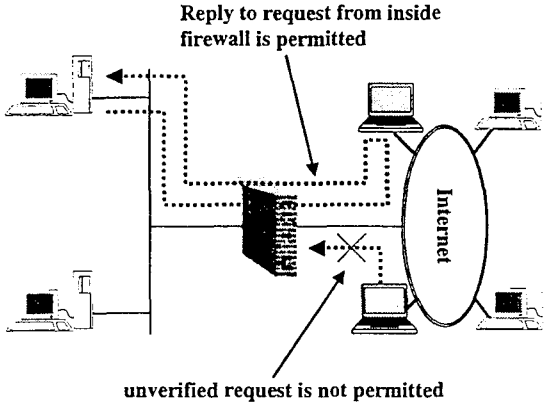

Fig. 16 Security of SIS using Firewall

technology is shown in **Figure 15**. "RAID 0" is used to improve the disk access speed and "RAID 1" is used to improve safety of data. There are other efficient and practical disk system of RAID versions, and the planners can improve the data safety by utilizing them.

6.3 Security

Although the security does not directly related to the efficiency of SIS function, it is an important issue regarding the computer network system. Because the ideal SIS deals with almost all the kinds of data of the earthquake disaster response organization, the data stored and transferred in SIS must be well secured by such technologies as firewall and encryption. **Figure 16** illustrates an idea of a firewall for a network system.

On the other hand, strong security occasionally becomes an obstruction for disaster response activities. An example is a case in which all the limited authorized personnel are not accessible to the system in a disaster. Thus, the manual suggests that both the security and its exception from the point of the earthquake disaster response need to be considered.

7. CONCLUDING REMARKS

This paper introduces the "Draft Manual for Seismic Information System Development" that PWRI recently developed. The manual was prepared to develop efficient seismic information system for civil infrastructure administrating bodies. Highlights of the manual can be summarized as follows:

1) Seismic information system is one of the most sophisticated information systems to develop. Because of the characteristics of earthquake disaster response activities, user-oriented, feasible, earthquake standing and highly secured system is required.
2) "User-oriented" seismic information system must be studied based on the information dealt with in each earthquake response phase. Assuming the response activities for infrastructure, disaster response phase can be classified as emergency response, temporary restoration, and complete restoration phase.
3) "Feasible" seismic information system must be studied to achieve data sharing, risk distribution, rational maintenance, and extensibility of the system. This concept is essential not only for the construction of SIS but also reconstruction/ upgrading occasions.
4) The manual describes element technologies suitable for the damage detection, communication, display and analysis, and decision-making support. Technologies must be carefully selected considering the cost and required performance. It is essential to study the performance including accuracy, speed and capacity from the earthquake engineering of viewpoints.

REFERENCES

1) PWRI: Guidelines for Disaster Information Systems for Important Infra-structures, 25th Joint Panel Meeting, UJNR, 1993.5
2) Sugita and Hamada: Development of Urgent Damage Estimation System for Road Facilities, 7th U.S.-Japan Lifeline Workshop, UJNR, 1998.11
3) Sugita and Nozaki: Seismic Information System for Civil Infrastructures, 30th Joint Panel Meeting, UJNR, 1999.5
4) Earthquake Disaster Prevention Div.: Draft Manual for Seismic Information System Development, Technical Memorandum, vol.3674, 1999.11

GIS and Pre- and Post-Disaster Risk Assessment

by

Stuart Nishenko[1], Claire Drury[1],
Scott Lawson[2], Thomas Durham[2], and Jawhar Bouabid[2]

ABSTRACT

In a pre-earthquake environment, loss estimates from credible scenario earthquakes demonstrate the scope of the problem and reinforce the continued need for structural and non-structural mitigation measures as a central feature in long-term initiatives to reduce seismic risk in California and the United States. Economic losses associated with building damage from magnitude 7.0 scenario earthquakes along the Hayward Fault in San Francisco are estimated to be $37 billion (2000 dollars) and $80 billion along the Newport-Englewood Fault in Los Angeles. In both cases, building related damage will contribute to between $6 and $15 billion in losses due to business interruption.

Loss estimates can also help determine the significance of seismic design and construction standards in reducing losses for certain building types in earthquakes. This information is key to understanding the role of seismic rehabilitation in reducing building losses from various levels of ground shaking. Using the above scenario examples, business interruption losses can be reduced by >65%, economic losses to wood buildings can decrease by >33%, and disruption to households and numbers of displaced people can decrease by up to 95% when the building stock is upgraded as part of Comprehensive Rehabilitation Program.

The early collection, transmission and mapping of earthquake ground motion data has numerous scientific and emergency management benefits. It provides vital information to emergency response personnel to expedite field inspections, provides quantitative data for damage and loss estimation models, and prioritizes early reconnaissance. Real-time data from the National Earthquake Information Center and TriNet were utilized by FEMA during the October 16, 1999 Mw 7.2 Hector Mine CA earthquake. Results from three simulations, based on preliminary and revised epicenter and magnitude data and TriNet /ShakeMap data, demonstrate how damage estimates are improved as better data become available with time.

KEYWORDS: Geographic Information Systems, HazardsUS, HAZUS, scenario earthquakes, seismic rehabilitation, TriNet, ShakeMap

1.0 INTRODUCTION

This report summarizes studies by the Federal Emergency Management Agency (FEMA) to describe the economic and social impact of scenario and actual earthquakes in

[1] Federal Emergency Management Agency
500 C Street SW, Washington DC 20472
[2] Durham Technologies, Inc., 4200 Northside Parkway
Building 5, Atlanta, GA 30327

California. We also address the potential reductions in direct economic and social losses from the seismic rehabilitation of buildings and the adoption of seismic design standards.

These estimates were based on an earthquake loss estimation methodology HazardsUS (HAZUS) that was developed by FEMA under a cooperative agreement with the National Institute of Building Sciences (NIBS). HAZUS was developed to provide local, state, and federal officials in seismically vulnerable regions of the United Sates with a uniform methodology for estimating losses in future earthquakes (Whitman et al., 1997; Jamieson and Milheizler, 1997). HAZUS provides loss estimates for use by state, local, and regional governments in planning for earthquake loss mitigation, emergency preparedness, and response and recovery. The methodology is based on up-to-date ground shaking projections from the United States Geological Survey (USGS) and the California Division of Mines and Geology (CDMG), extensive databases on the built environment, and state-of-the art shaking to damage functions. FEMA is currently engaged in developing similar loss estimation methodologies for wind and flood hazards (Nishenko and Drury, 1999).

2.0 PRE-EARTHQUAKE STUDIES

2.1 Scenario Earthquakes

Policy, land-use and development decisions are risk-driven and require appropriate economic and social information to evaluate different strategies and to assess the trade-offs between costs and various benefits. Loss estimates based on scenario earthquakes provide a means to evaluate the consequences of policy decisions.

2.1.1 San Francisco Bay Area

A recent United States Geological Survey (USGS) study has identified the Hayward-Rogers Creek fault system as the most hazardous in the San Francisco Bay area (USGS, 1999). FEMA (2000a) provides a summary of the losses from a magnitude 7.0 earthquake on the Hayward Fault for ten counties that touch the San Francisco Bay.

The major findings from this study include:

- Economic losses due to building damage are estimated to be nearly $37 billion (2000 dollars), with over $16 billion occurring in Alameda County.
- Building damage will cause over $6 billion in losses due to business interruption.
- When economic losses are characterized by building type, it is estimated that wood buildings will account for over 50 percent of the total building losses.

2.1.2 Los Angeles

The Los Angeles Basin is underlain by at least a half a dozen faults capable of generating earthquakes over magnitude 7.0. The Newport-Englewood fault was the site of the 1933 magnitude 6.3 Long Beach earthquake and is considered to be one of the greatest urban hazards in the nation.

FEMA (2000b) provides a summary of the estimated losses from a magnitude 7.0 earthquake on the Newport-Englewood fault using HAZUS. An earthquake of this magnitude would potentially impact a six county region in the Los Angeles Basin that has a population of over 15 million people. Over 95 percent of the damages would occur in Los Angeles and Orange counties, which have the highest densities.

The major findings from this study include:

- Economic losses due to building damage are estimated to be nearly $80 billion (2000 dollars).
- 75 percent of the total economic losses will occur in Los Angeles County.
- Building damage will cause over $15 billion in losses due to business interruption.

2.2 Seismic Rehabilitation

In the San Francisco and Los Angeles scenarios, the estimates of building damage demonstrate the scope of the problem and reinforce the continued need for structural and non-structural mitigation measures as a central feature in long-term initiatives to reduce seismic risk. This section describes how HAZUS was used to assess the impact of seismic rehabilitation measures in reducing economic and social losses from the Hayward and Newport-Englewood scenario earthquakes.

The expected seismic performance of buildings is determined by a combination of parameters, including Building Design Standards (low seismic design, moderate seismic design, high seismic design) and Building Construction Quality (code compliant construction, non-code compliant construction). By changing these parameters, HAZUS can be used to test the significance of seismic design and building practices on the level of damage to buildings.

To determine the significance of seismic rehabilitation in reducing losses from a magnitude 7.0 earthquake three 'building-related' scenarios are used:

- Existing Condition – the building inventory is assumed to be representative of the existing building composition in the San Francisco area for the Hayward Fault scenario, and in the Los Angeles area for the Newport-Englewood Fault scenario. The inventory includes a mixture of pre-code structures with no seismic rehabilitation, seismically rehabilitated structures, and structures designed for various levels of seismic resistance.
- Targeted Rehabilitation Program – the most seismically vulnerable buildings are assumed to be rehabilitated to meet a minimum level of seismic resistance (protection of life safety).
- Comprehensive Rehabilitation Program – all buildings are assumed to be either constructed or rehabilitated to the current seismic design standards of the region.

For both the San Francisco and Los Angeles scenarios,

- Business interruption losses could be reduced by over 60 percent ($6.5 billion to $2.3 billion in San Francisco and $15 billion to $5.7 billion in Los Angeles) when the building stock is upgraded as part of a Comprehensive Rehabilitation Program.
- When wood buildings are upgraded as part of a Comprehensive Rehabilitation Program, economic losses decrease by over 30 percent ($18.9 billion to $12.7 billion in San Francisco and $42.8 billion to $29 billion in Los Angeles)
- When the building stock is seismically upgraded as part of a Targeted Rehabilitation Program, major injuries and deaths drop by 65 percent.
- Seismic rehabilitation has a significant effect in reducing disruption to households caused by the earthquake. Implementation of a Comprehensive Rehabilitation Program could decrease the number of displaced people by over 90 percent.

2.3 Estimated Losses to Building – By Building Type

One of the objectives of these studies was to determine the significance of seismic design and construction in reducing losses for certain building types in a scenario magnitude 7.0 earthquake. This information is key to understanding the role of seismic rehabilitation in reducing building losses from various levels of ground shaking.

Figures 1 through 4 illustrate direct economic loss as a function of ground motion for four basic building types-

- Residential- single family home-
  wood frame construction
  masonry construction

- Commercial – office building - low-rise (< 4 stories)
  concrete frame construction
  masonry construction

The curves in Figures 1 through 4 were developed for ground shaking from a magnitude 7.0 vertical strike slip earthquake. Homes and commercial structures are assumed to be located on deep alluvium sites (NEHRP Type D soil) and are not subject to potential ground failure. Curves were developed for structures in the Los Angeles area, and results are generally applicable to the San Francisco Bay area as well.

For each building type, three loss curves were developed that reflect three levels of seismic design - No Seismic Design, Moderate Seismic Design, and High Seismic Design. For each building type, the loss curves show the estimated level of direct economic loss (measured in dollars per square foot) from ground shaking (measured by the level of peak round acceleration (PGA)). The direct economic losses include the cost to repair the damaged structure, cost to replace damaged contents, and temporary living or business interruption expenses incurred as a result of the earthquake.

All four building types dramatically illustrate the benefits that are accrued by moving from No Seismic Design to a Moderate Seismic Design standard – a factor of two difference in direct economic loss. Additional reductions in loss are realized by adopting High Seismic Design Standards.

2.4 Limitations

Uncertainties are inherent in any type of loss estimation study. They arise in part from incomplete scientific knowledge concerning the severity and distribution of shaking from earthquakes and their effect on the built environment, and in part from the approximations and simplifications necessary for analysis of all facilities in a region. The range of uncertainty in HAZUS is considered to be a factor of two to four. It is natural to compare the results in this report with the output of similar models. For such comparisons, the assumptions used for each model need to be computable i.e., the exact location and magnitude of the earthquake, the time of occurrence and the time of occurrence, and the geographic area modeled are the same. The output should represent damage and loss for the same classes and inventories of buildings and infrastructure.

3.0 POST-EARTHQUAKE STUDIES

In the immediate aftermath of a potentially damaging earthquake, HAZUS can rapidly assess losses and guide emergency response and recovery operations. HAZUS is currently being incorporated into FEMA's Response and Recovery operations to support and facilitate the Information and Planning mission of the Federal Response Plan (FEMA, 1999).

The October 16, 1999 Mw 7.2 Hector Mine, California earthquake provided an unique opportunity to exercise the capability of HAZUS in a real-time capacity.

Three scenarios were developed for loss estimates based on the availability of information immediately following the earthquake.

1. Preliminary epicenter and magnitude (Ms 7.3) information from the National Earthquake Information Center (NEIC) along with a default rupture mechanism generated by HAZUS and a default building inventory scheme for the impacted region.
2. A revised epicenter and magnitude (Ms 7.0) from NEIC and assuming the rupture at the nearest fault (Bullion Fault)
3. A TriNet-based ground shaking map (ShakeMap, see Figure 5) along with an improved building inventory for the impacted area.

Figures 6 and 7 clearly indicate how damage estimates improved as better data became available and were used. The number of heavily damaged buildings was improved by a factor of 15 while property damage losses were refined by a factor of six from the initial estimate. Casualty and shelter estimates were reduced by factors of 10 and 60, respectively.

4.0 CONCLUSIONS

The pre- and post-earthquake examples discussed in this report demonstrate the utility of the HAZUS loss estimation methodology as a decision support tool.

In a pre-earthquake environment, loss estimates from credible scenario earthquakes demonstrate the scope of the problem and reinforce the continued need for structural and non-structural mitigation measures as a central feature in long-term initiatives to reduce seismic risk in California and the United States. These study results were used to support the drafting of Federal legislation that would provide incentives to encourage individuals, as well as state, local governments and businesses to invest in mitigation and earthquake loss reduction ('The Earthquake Loss Reduction Act of 2000').

In the immediate aftermath of a damaging earthquake, HAZUS can rapidly assess losses and guide emergency response and recovery operations. Future activities to improve these capabilities include linking HAZUS to other real-time networks in California as well as future USGS Advanced National Seismic System (ANSS) stations throughout the United States.

5.0 REFERENCES

FEMA, 1999, Federal Response Plan, 9230.1-PL, Washington DC

FEMA, 2000a, Impact of a Magnitude 7.0 Earthquake on the Hayward Fault: Estimates of Socio-Economic Losses Using HAZUS (Hazards US), FEMA, Washington DC

FEMA, 2000b, Impact of a Magnitude 7.0 Earthquake on the Newport-Englewood Fault: Estimates of Socio-Economic Losses Using HAZUS (Hazards US), FEMA, Washington DC

FEMA, 2000c, Improving the Seismic Performance of Existing Buildings: Implications for Loss Reduction in the San Francisco Bay area – a HAZUS (Hazards US) Assessment, FEMA, Washington DC

FEMA, 2000d, Improving the Seismic Performance of Existing Buildings: Implications for Loss Reduction in the Los Angeles Basin – a HAZUS (Hazards US) Assessment, FEMA, Washington DC

Jamieson, G. and Milheizler, J., 1997, The use of GIS in loss estimation and risk assessment, Proc. 29th Joint Meeting of the US-Japan Panel on Wind and Seismic Effects, UJNR, May 13-16, 1997, Tsukuba, Japan.

Nishenko, S. and Drury, C., 1999, Recent FEMA activities in earthquake risk analysis and mitigation, EQ; Earthquake Quarterly, Summer, 1999, 14-17.

USGS, 1999, Earthquake Probabilities in the San Francisco Bay region: 2000-2030, USGS Open File Rpt. 99-517

Whitman, R. V., Anagnos, T., Kircher, C., Lagorio, H.J., Lawson, R. S., and Schneider, P., 1997, Development of a national earthquake loss estimation methodology, Earthquake Spectra, 13, 643-662.

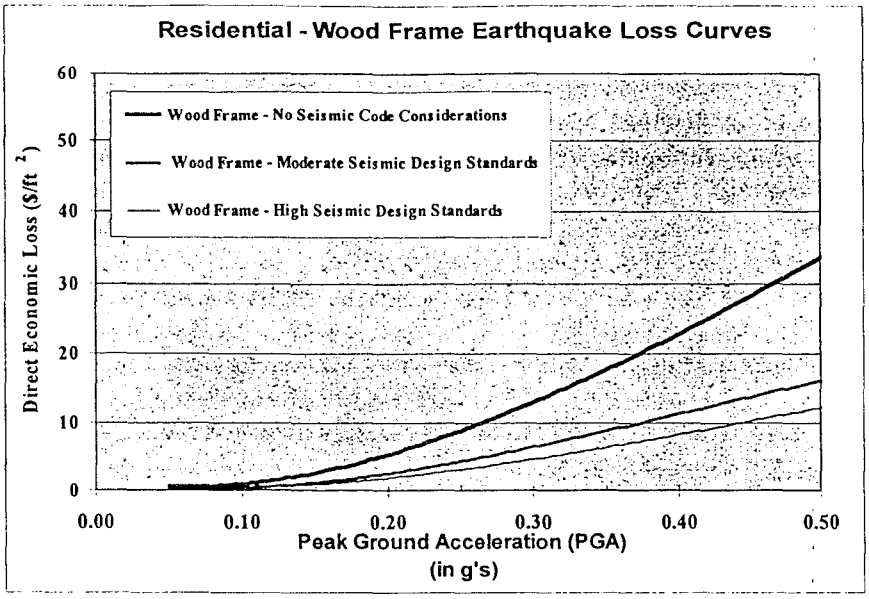

Figure 1 Potential damage to wood frame single-family residence from various levels of ground shaking intensity for three levels of seismic design. The damage is quantified in terms of the economic loss ($/ft^2) and includes the cost to repair the damaged home, the cost to replace damaged contents and any additional temporary living expenses caused by the earthquake.

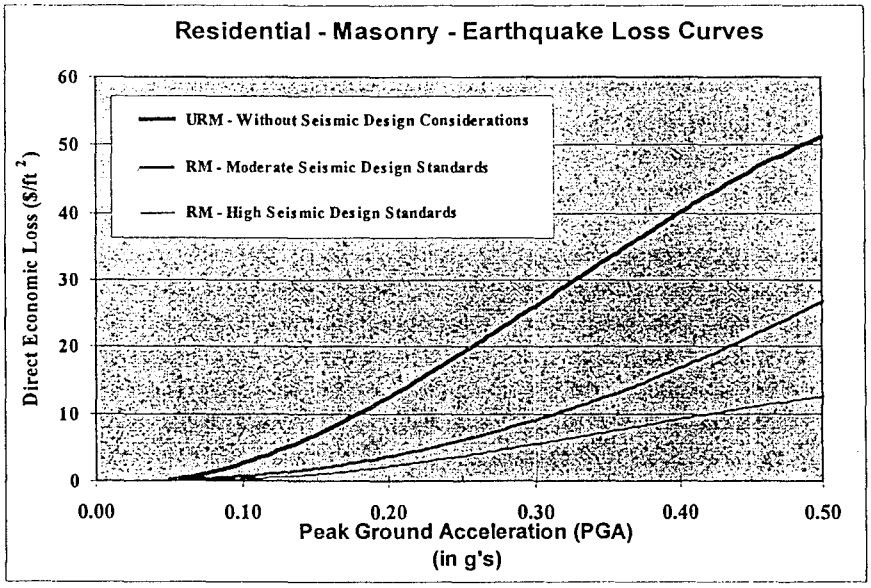

Figure 2. Potential damage to a masonry single-family residence from various levels of ground shaking intensity for three levels of seismic design. The damage is quantified in terms of the economic loss ($/ft^2) and includes the cost to repair the damaged home, the cost to replace damaged contents and any additional temporary living expenses caused by the earthquake.

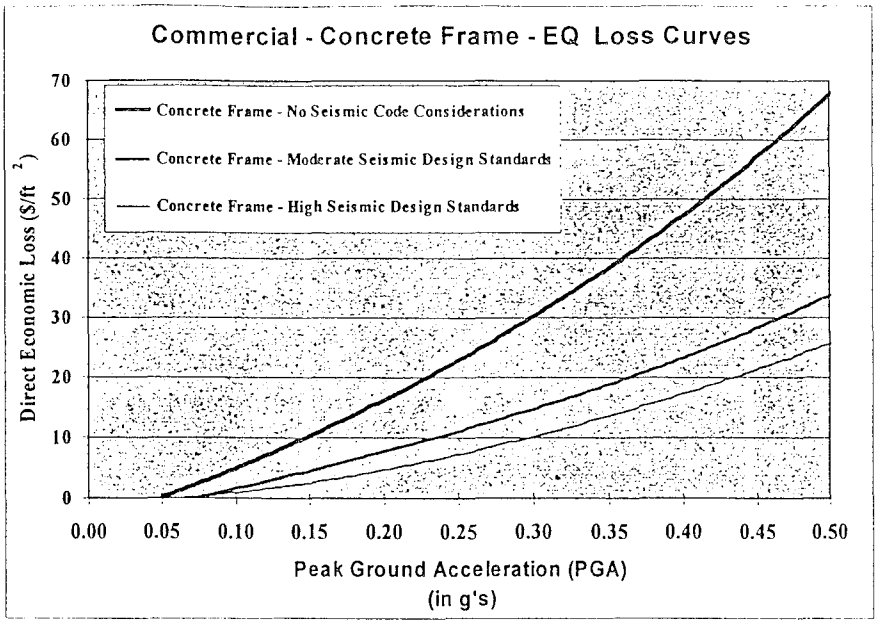

Figure 3. Potential damage to concrete frame office building from various levels of ground shaking intensity for three levels of seismic design. The damage is quantified in terms of the economic loss ($/ft^2) and includes the cost to repair the damaged structure, the cost to replace damaged contents and any additional business interruption expenses caused by the earthquake.

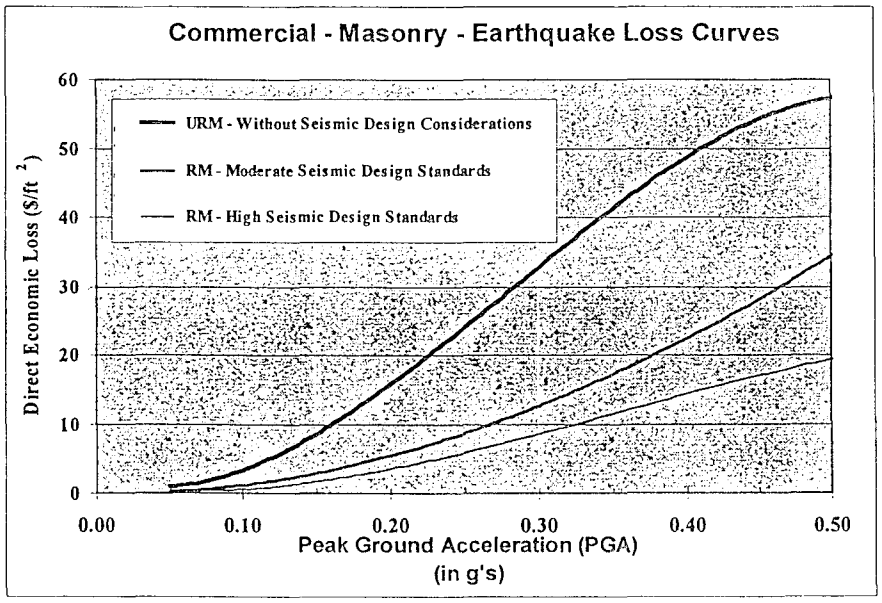

Figure 4. Potential damage to a commercial, low-rise masonry office building from various levels of ground shaking intensity for three levels of seismic design. The damage is quantified in terms of the economic loss ($/ft^2) and includes the cost to repair the damaged structure, the cost to replace damaged contents and any additional business interruption expenses caused by the earthquake.

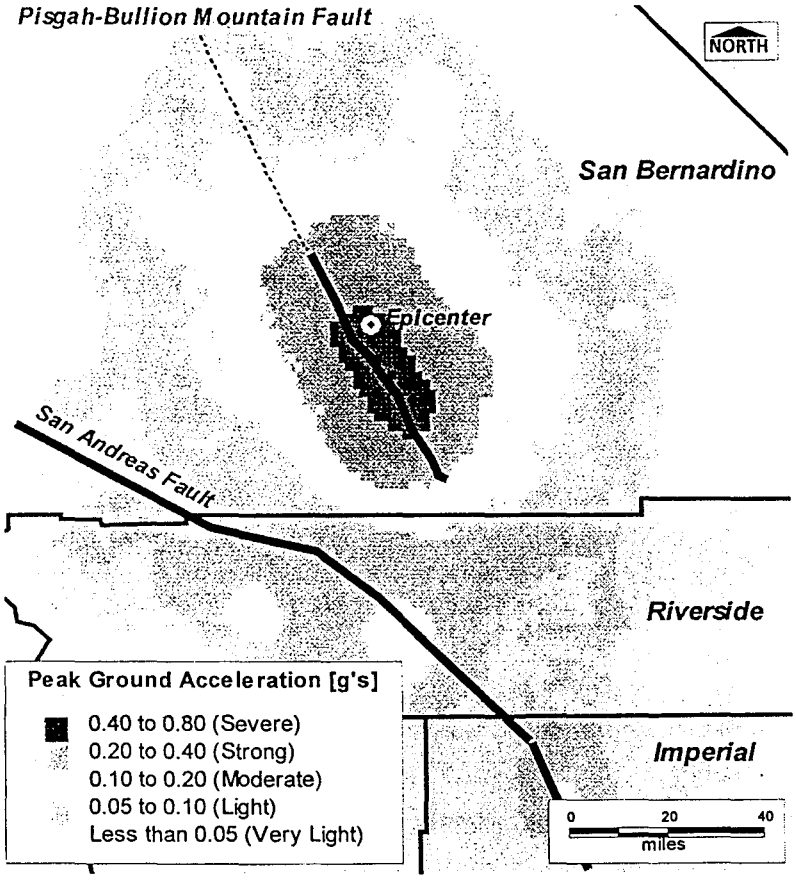

Figure 5. Peak ground acceleration map for the October 16, 1999 Mw 7.2 Hector Mine California earthquake based on real-time TriNet data.

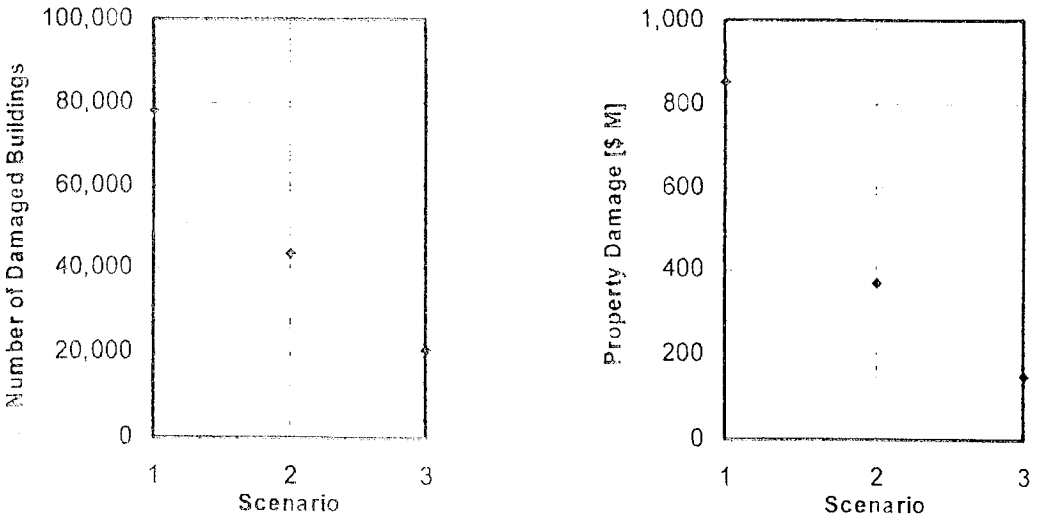

Figure 6. HAZUS-based building damages from the three Hector Mine scenarios

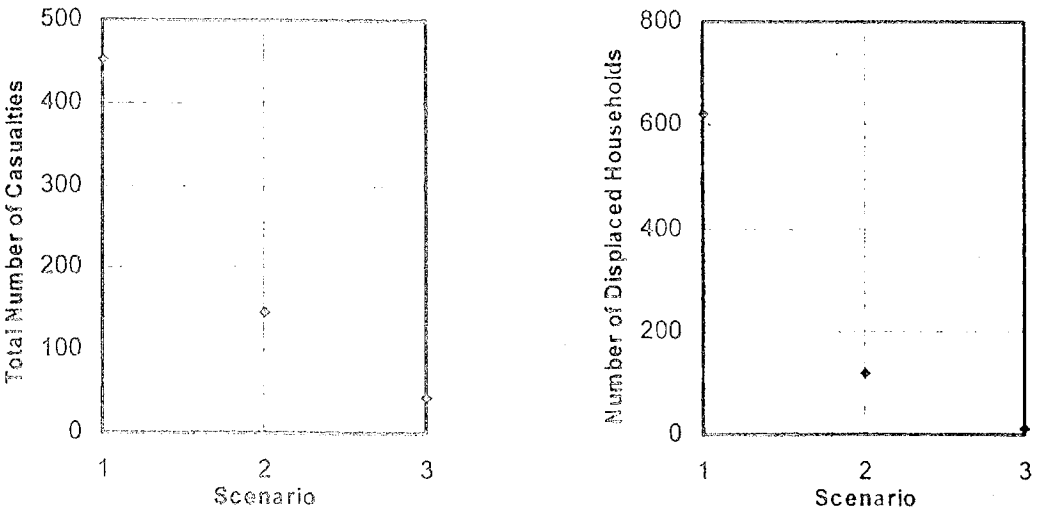

Figure 7. HAZUS-based social losses from the three Hector Mine scenarios

EARLY ESTIMATION SYSTEM FOR TSUNAMI HAZARD

KIRIYAMA Takaharu[1], OKAYAMA Kazuo[2]

ABSTRACT

The National Land Agency has created Tsunami Hazard Maps of the entire coast of Japan for the purpose of having a prior estimate of the tsunami inundation range and has developed an "Early Estimation System for Tsunami Hazard" with the ability to use the Tsunami Inudation Forecasting Database(created from the results of the calculations used to create the Tsunami Hazard Maps) to estimate the tsunami inundation range. The system searches the Tsunami Inundation Forecasting Database to find relevant locations based on the forecasting zones announced in the new tsunami forecasts of the Meteorological Agency and the specific tsunami heights expected. It then displays these locations on the screen to provide a picture of the tsunami inundation area and a rough estimate of the number of buildings and population contained there immediately after an earthquake.

KEY WORDS: Tsunami,
Hazard Map,
Database,
Tsunami Forecasting,
Early Estimation.

1. INTRODUCTION

Japan is surrounded by water and has suffered severe damage from the tsunami generated by earthquakes, making measures to counteract tsunami damage is an important issue for coastal areas. One effective means of implementing tsunami countermeasures is to envision the tsunami that are likely to occur in a given region and create a "Tsunami Hazard Map" that indicates, on a map, the areas where tsunami inundation is expected.

Like earthquakes, when tsunami strike it is vital to have a rough estimate of the damage as quickly as possible. The tsunami that accompanied the Hokkaido Southwest Offshore Earthquake of July 12, 1993 occurred at 22:17 but virtually nothing was known about the extent of the damage until the next morning because of the fact that it occurred on the remote island of Okushiri and because of the lateness of the hour.

Since fiscal 1996, the National Land Agency has been operating an "Early Estimation System for an Earthquake" that provides a seismic intensities distribution map, building damage estimate, and human damage estimate immediately after an earthquake. Tsunami estimation functions were recently added to this.

This paper describes the creation of Tsunami Hazard Maps of the entire coast of Japan for the purpose of having a prior estimate of the tsunami inundation range, and the development of the "Early Estimation System for Tsunami Hazard" with its ability to use a database (created from the results of the calculations used to create the Tsunami Hazard Maps) to estimate the tsunami inundation range.

---

[1] Deputy Director, Earthquake Disaster Countermeasures Division, Disaster Prevention Bureau, National Land Agency.

[2] Director, Earthquake Disaster Countermeasures Division, Disaster Prevention Bureau, National Land Agency

2. CREATION OF TSUNAMI HAZARD MAPS

2-1 OUTLINE

Tsunami Hazard Maps are maps that show the area that is expected to be inundated in the event of a tsunami attack. The map forms the basis for studies of tsunami countermeasures in the area. Figure 1 is an example of Tsunami Hazard Map created by the National Land Agency. It shows at 1/25,000 scale the inundation area and inundation depth for each meter when a tsunami of a certain height attacks a certain stretch of coast.

The map can be consulted to find the extent of the tsunami inundation area, its depth, and the streets, government institutions, public facilities, roadways, transportation facilities, factories and the like located therein. This provides a clear picture of the tsunami disaster prevention tasks to be addressed in the area.

2-2 METHOD OF CREATION

In the past, the creation of Tsunami Hazard Maps was to a large extent a matter of inference based on past tsunami experiences. However, experience may be inadequate for tsunami of relatively low frequency.

The National Land Agency, in cooperation with the Meteorological Agency and Fire and Disaster Management Agency, has therefore created a "Tsunami Damage Forecasting Manual" that draws on recent research into tsunami and recent advances in computer technology to formulate Tsunami Hazard Map creation methods based on seismic fault models and tsunami behavior simulations. The Tsunami Hazard Map creation method of the National Land Agency follows the method described in the Tsunami Damage Forecasting Manual. An outline is provided in Figure 2.

(1) Set calculation range

The first step is to set the range of the initial calculation. We used rectangular areas of 30-50 kilometers per side for our ranges. These ranges were adjusted to conform with the forecasting points used in the new tsunami forecasts of the Meteorological Agency (described below). We set a total of 412 ranges covering the entire coastline of Japan, including remote, populated islands.

We also set a seismic fault model that would generate the largest conceivable tsunami for the range.

(2) Study past tsunami

We gathered information on local inundation depths and seismic fault models etc. for representative tsunami of the past in order to verify the validity of the calculation results.

(3) Set calculation grid

We set the calculation grid at 100 meters. This grid was chosen as a means of balancing precision and costs.

(4) Digitalize topography

We digitalized topographic features using topographical maps and ocean floor topographical maps. For this, we considered only river areas of 200 meters or more in width and lakes with 200 meters or more contact with the ocean. We did not take into account the effect of levees or flood gates.

(5) Set tsunami waveform

We set tsunami waveforms to produce tsunami heights of 2, 4, 6, 8, and 10 meters in each area. However, for areas with a maximum tsunami height of less than 10 meters in the seismic fault model, we did not consider tsunami heights above the maximum.

(6) Set calculation conditions

We set the friction coefficient (ocean floor and land), calculation time interval, and other conditions.

(7) Run numerical calculations

We ran numerical calculations using the methods described in the Tsunami Damage Forecasting Manual.

(8) Analyze results

We analyzed results to determine if the inundation areas and depths were reasonable given the tsunami height and topography set. Where past tsunami examples were available, we compared them against calculation results to judge the validity of results.

(9) Create Tsunami Hazard Map

We expressed calculation results on a 1/25,000 map. Calculation results were in the form of data for a 100 meter grid, but we

expressed them as color-coded inundation depth lines for 1 meter intervals.

(10) Create files containing calculation results

We created files containing the calculation results for use as a database.

3. EARLY ESTIMATION SYSTEM FOR TSUNAMI HAZARD

3-1 OUTLINE

The Early Estimation System for Tsunami Hazard searches the Tsunami Inundation Forecasting Database (created from the calculation results for the creation of the Tsunami Hazard Maps) to find relevant locations based on the forecasting zones announced in the new tsunami forecast of Meteorological Agency and the specific tsunami heights expected. It then displays these locations on the screen. This gives the government a picture of the tsunami inundation area and a rough estimate of the number of buildings and population contained therein immediately after an earthquake (within about 30 minutes). It is expected that this information will help to accelerate the government's initial response.

3-2 NEW TSUNAMI FORECASTS

The new tsunami forecasts were inaugurated by the Meteorological Agency in fiscal 1999 and use the forecasting zones shown in Figure 3 to display expected tsunami heights in concrete numerical terms (eight increments: 0.5 m, 1 m, 2 m, 3 m, 4 m, 6 m, 8 m, 10+ m).

The Meteorological Agency's model envisioned approximately 4,000 epicenters in ocean waters up to about 600 kilometers off the coast of Japan and created a standard seismic fault model for earthquakes occurring at these points. The Agency then ran numerical simulations of tsunami changing the magnitude and fault depth of the earthquake to create a database of results (approximately 100,000 records). When an earthquake occurs, the system searches the database of results for a corresponding epicenter and magnitude, and displays the tsunami forecasts described above.

The Meteorological Agency database has forecast points set every 20-30 kilometers along the coastline. A single forecasting zone will contain several forecast points; the tsunami height displayed for the tsunami forecast is the maximum height for the zone.

3-3 SYSTEM FUNCTIONS

When a tsunami forecast is published, the Meteorological Agency sends the National Land Agency on-line data on the tsunami height for each forecasting zone (in the future, this will also include tsunami heights for each forecast point). The Early Estimation System for Tsunami Hazard uses this data to search for corresponding locations in the Tsunami Inundation Forecasting Database and display them on-screen.

The original Tsunami Inundation Forecasting Database utilizes a 100 meter grid, but the system converts this to 250 meter mesh data (using the maximum value for inundation depth in the mesh). This is done to simplify expression of wide-range estimates. Expressing detailed information on specific areas is not the purpose of this system.

Below is a description of the information displayed by the system.

(1) Wide-range estimates (Figure 4)

These displays are used to provide rough pictures of wide-areas of 300 kilometers or more. This shows prefectural boundaries and the maximum inundation depth on the coastline for municipal units.

(2) Middle-range estimates (Figure 5)

These displays are used to provide rough pictures medium-range areas of 100-300 kilometers. They also display information in prefectural units. This shows municipal boundaries and the maximum inundation depth on the coastline for municipal units. The points and figures in the ocean areas indicate the forecasting point and the corresponding tsunami height.

(3) Narrow-range estimates (Figure 6, Figure 7)

These displays show local conditions for areas of 100 kilometers or less, roughly in municipal units. The map indicates municipal boundaries and inundation depths at a 250 meter mesh.

(4) Record displays (Table 1)

The system displays lists of potential inundation areas in individual municipalities (inundation depth of 2 meters or greater, and less than 2 meters), and of the number of buildings and population included in these areas. The building and population data is based on the three-dimensional mesh of the National Land Numerical Data (approximately 1 kilometer square), split up by number of land-area meshes and converted to a 250 mesh.

The examples showing in Figures 4-7 and in Table 1 are models of the Nihonkai-Tyuubu Earthquake that occurred on May 26, 1983. We have estimated figures for forecast points from past inundation records, and then input those figures to search the Tsunami Inundation Forecasting Database.

4. FUTURE TASKS

The Meteorological Agency began its new tsunami forecasts in fiscal 1999. Luckily, Japan has yet to experience a tsunami that would result in the publication of tsunami forecasts, and therefore the system has no track record. Nonetheless, the fact that this system can be used to ascertain tsunami inundation levels directly after an earthquake will have a significant impact in accelerating initial government response efforts.

Currently, the Meteorological Agency provides data only on tsunami heights for forecasting zones. It would be desirable in the near future to be given tsunami heights for individual forecast points in order to increase the precision of estimates. It would also be desirable to add functions to estimate the building destruction and outflow, human damage, and other specific damage from the tsunami.

BIBLIOGRAPHY

1) National Land Agency, Meteorological Agency, Fire and Disaster Management Agency, "Tsunami Damage Forecasting Manual," (1997).

2) Meteorological Agency, "New Tsunami Forecasts" (pamphlet).

3) Watanabe Hideo, *Survey of Tsunami Damage in Japan* (University of Tokyo Press, 1985).

Table 1 Results of forecasting Tsunami damage

Prefecture	Municipal	Inundation Area (2m ～)	Inundation Area (～ 2m)	Inundated Buildings	Inundated Population
All Japan		119.4km^2	1072.6km^2	224,941	403,831
Aomori	Fukaura T.	11.4km^2	7.5km^2	2,012	3,900
	Iwasaki V.	6.8km^2	4.2km^2	771	1,244
Akita		56.0km^2	34.9km^2	17,166	32,214
	Akita C.	7.0km^2	4.6km^2	1,876	5,751
	Noshiro C.	9.5km^2	6.2km^2	2,557	5,236
	Oga C.	16.5km^2	11.3km^2	4,810	9,745
	Hatimori T.	5.2km^2	0.6km^2	1,411	1,919
	Hachiryu T.	2.3km^2	0.1km^2	258	222
	Minehama V.	2.3km^2	0.3km^2	75	219

Figure 1 Tsunami Hazard Map (tsunami height:10m)

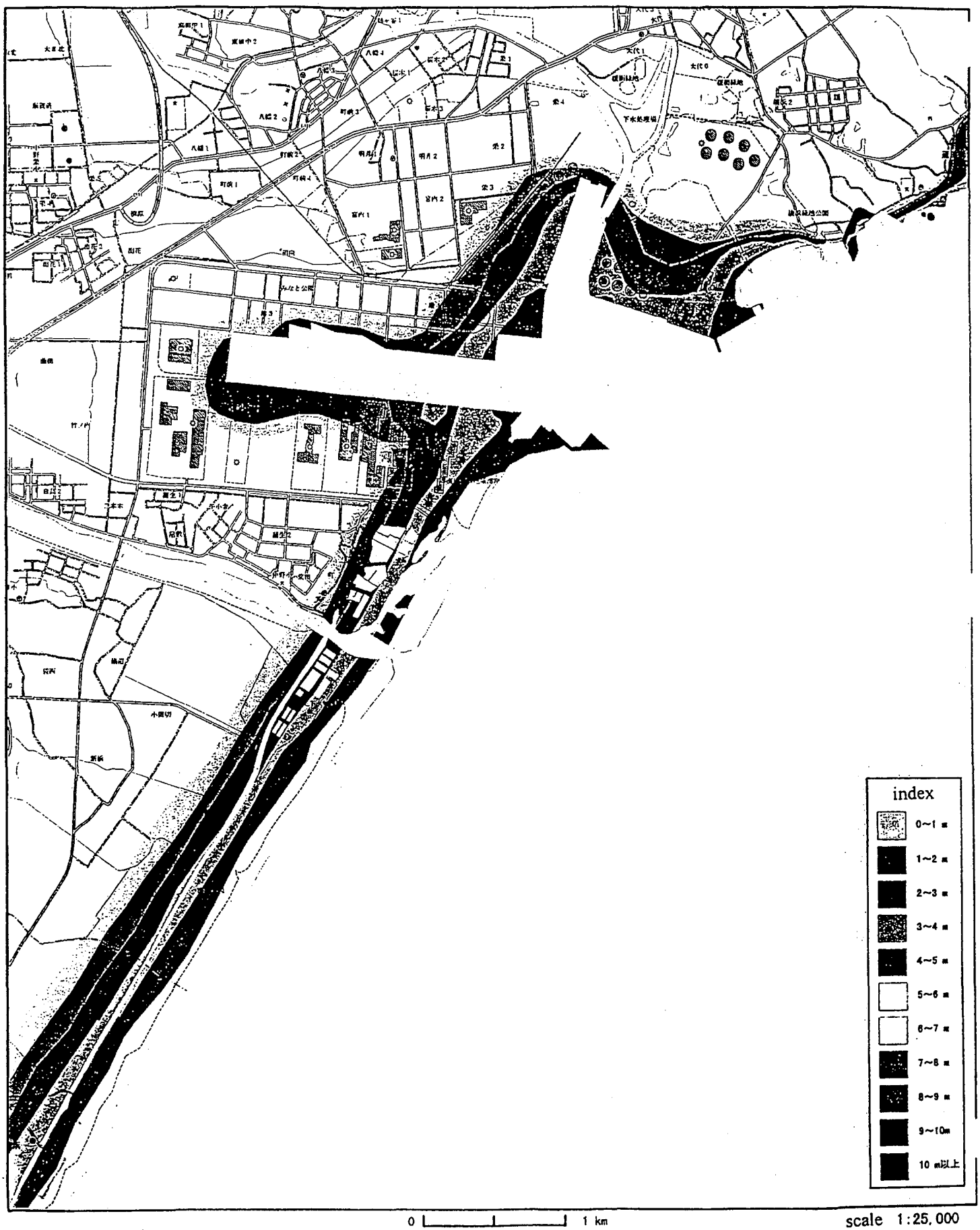

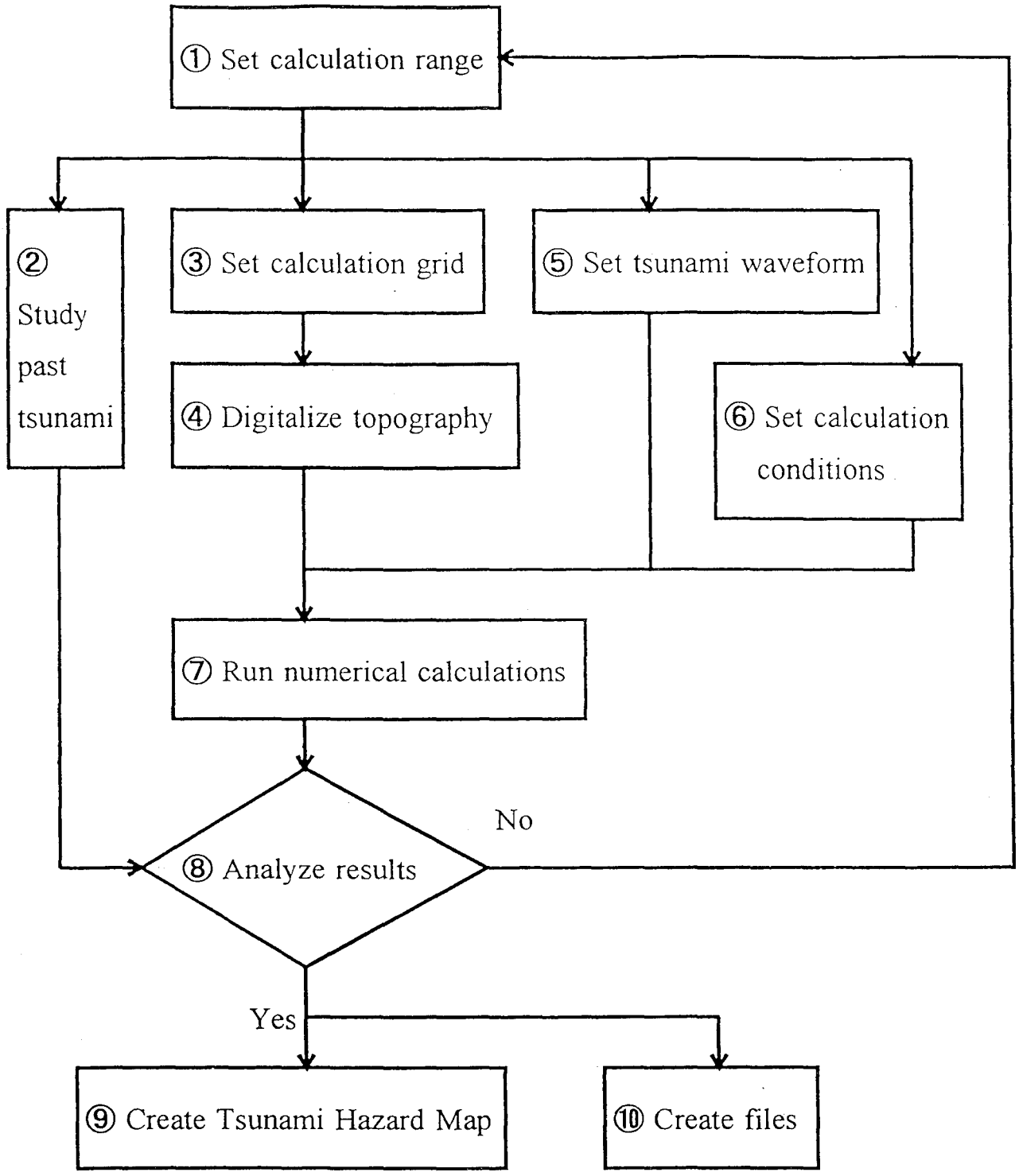

Figure 2 An outline of creating Tsunami Hazard Map

Figure 3 Tsunami Forecasting Zones

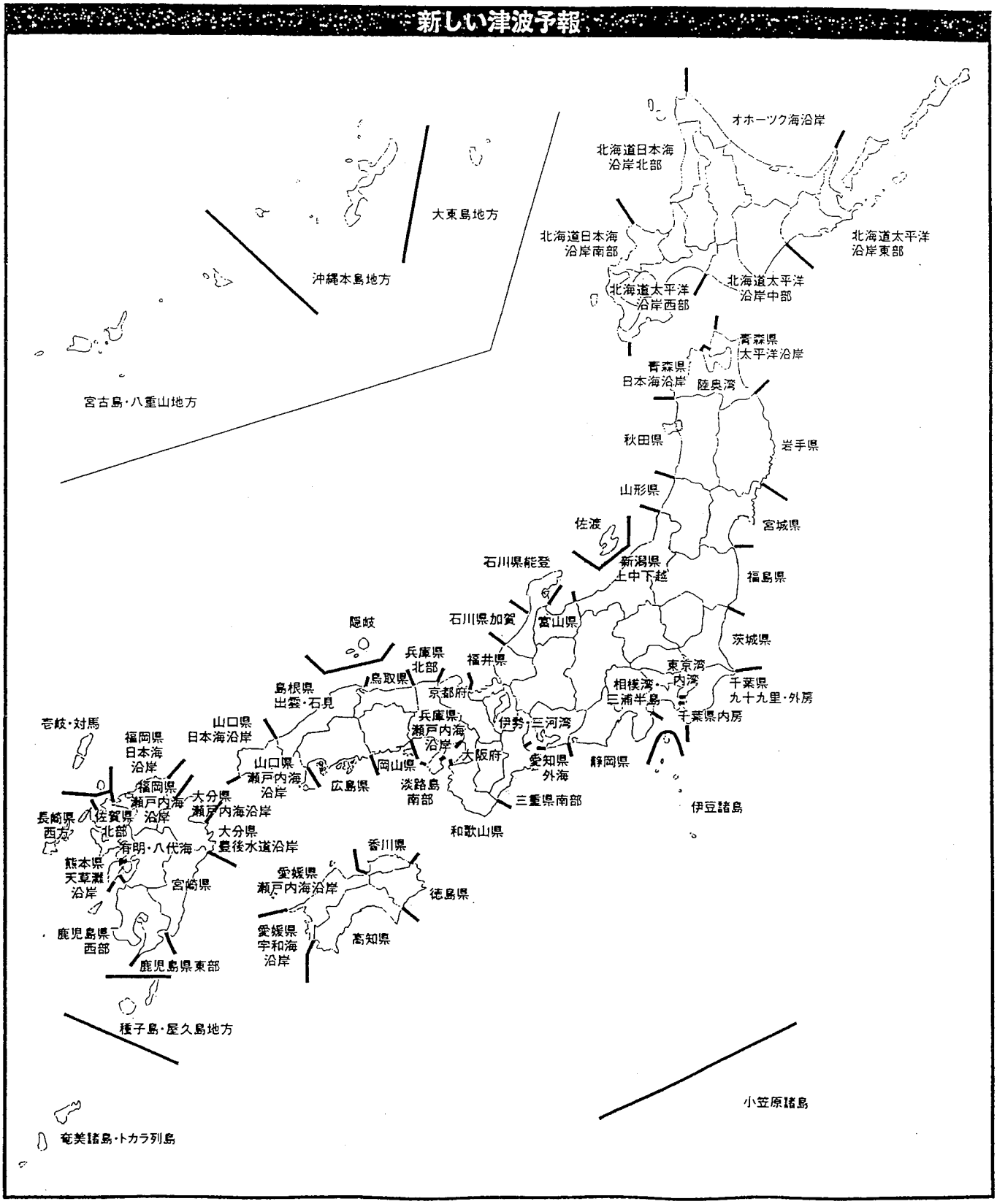

Figure 4 Wide-range Estimates

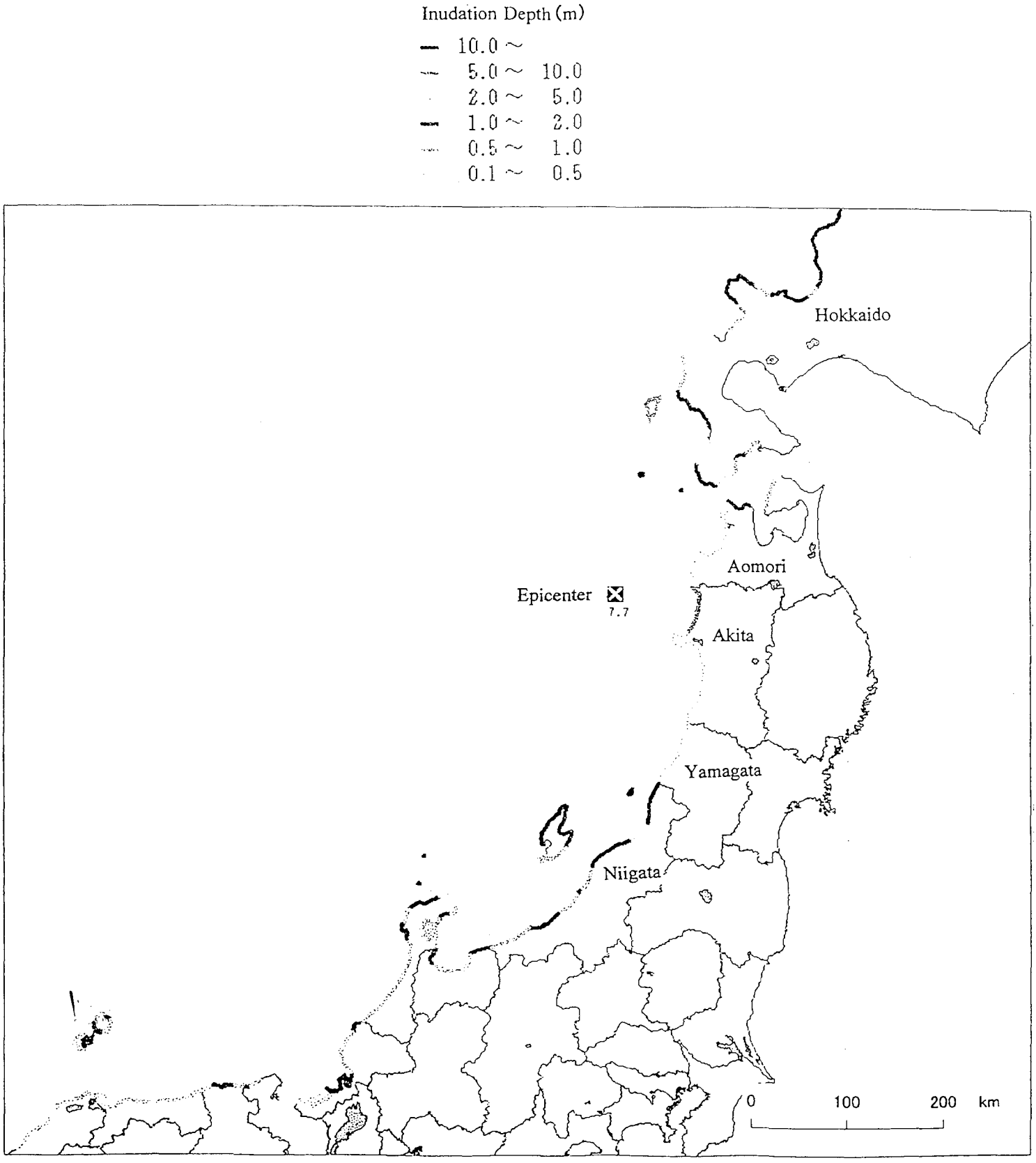

Figure 5 Middle-range Estimates

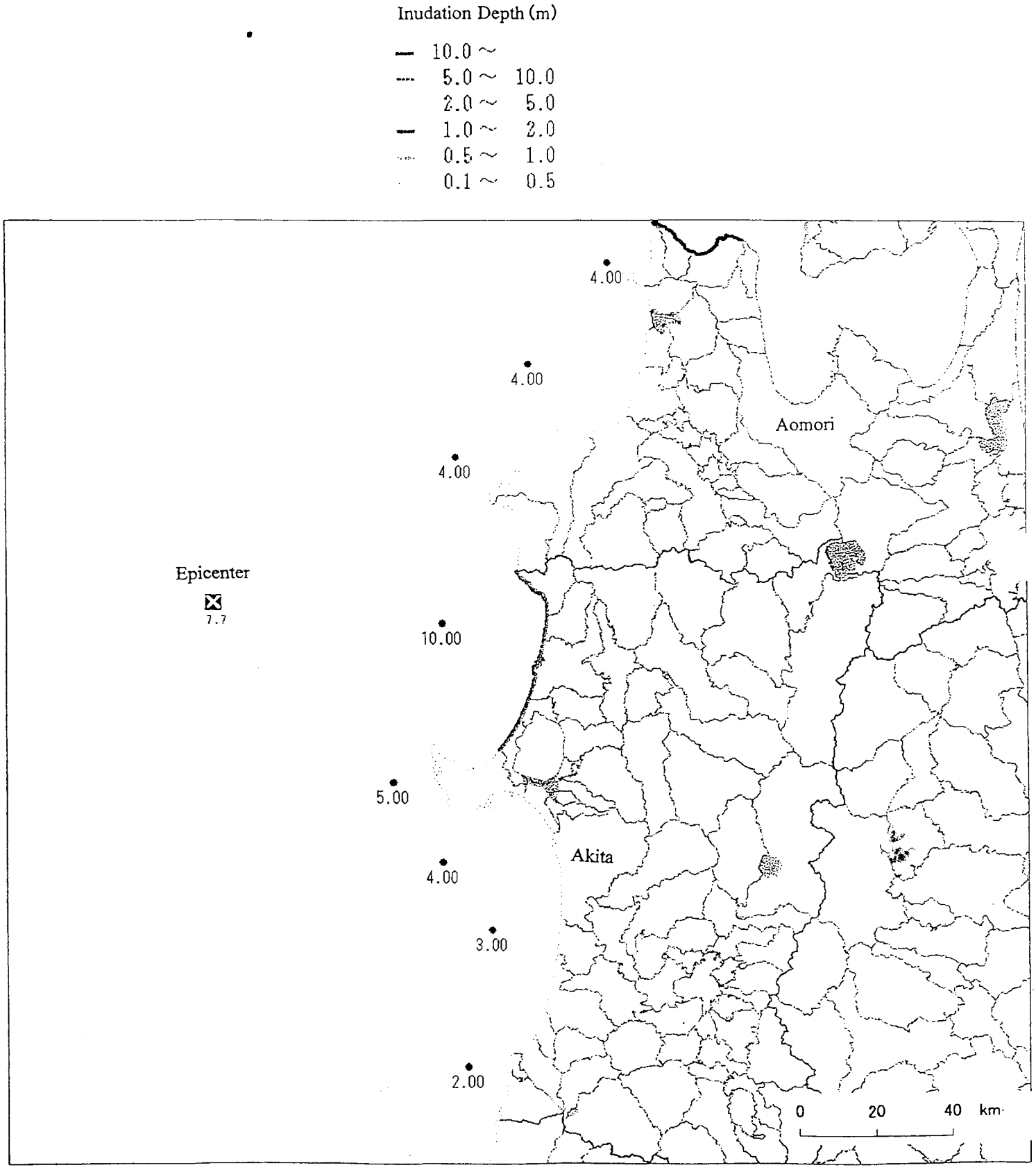

Figure 6 Narrow-range Estimates (1)

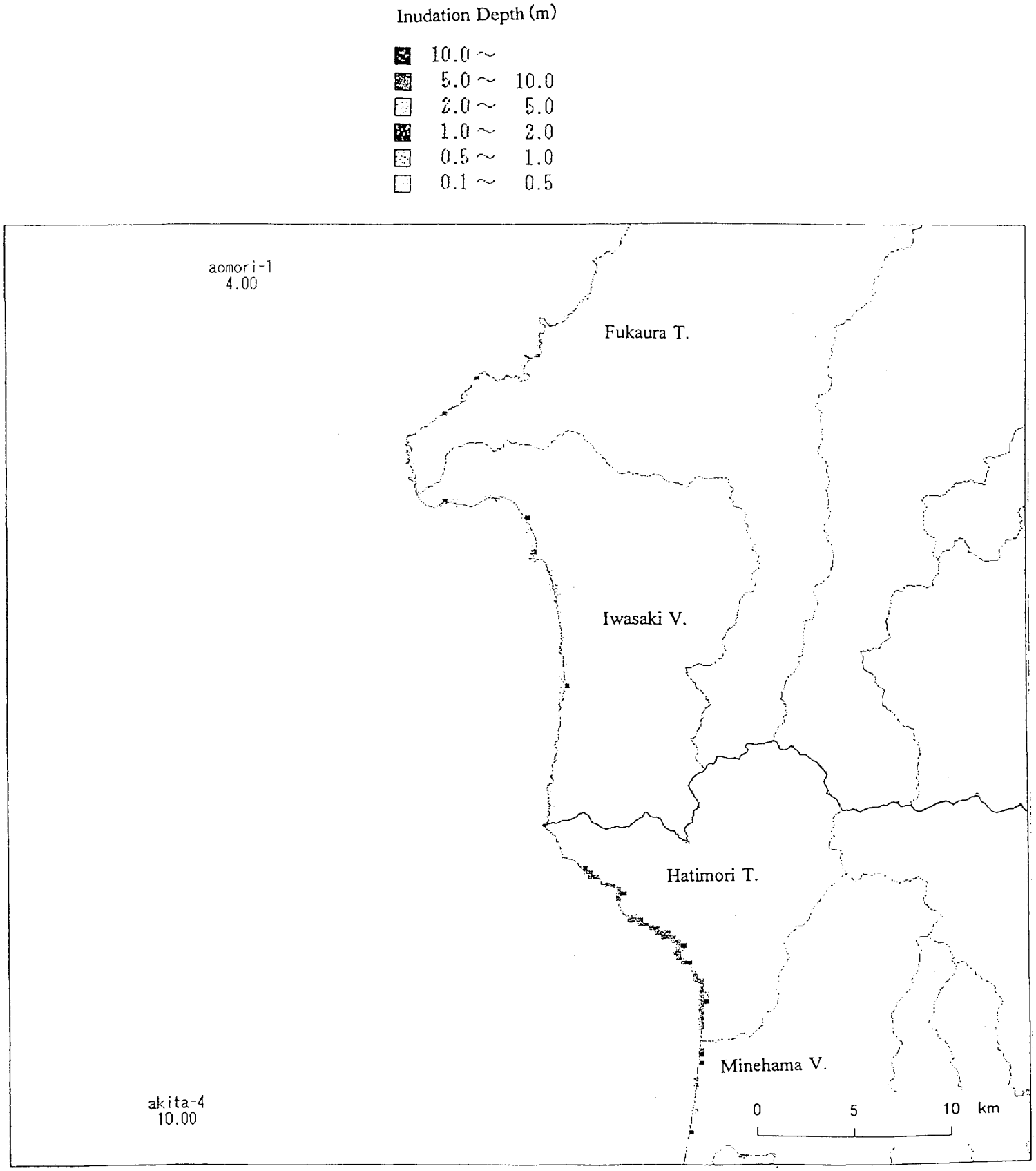

Figure 7 Narrow-range Estimates (2)

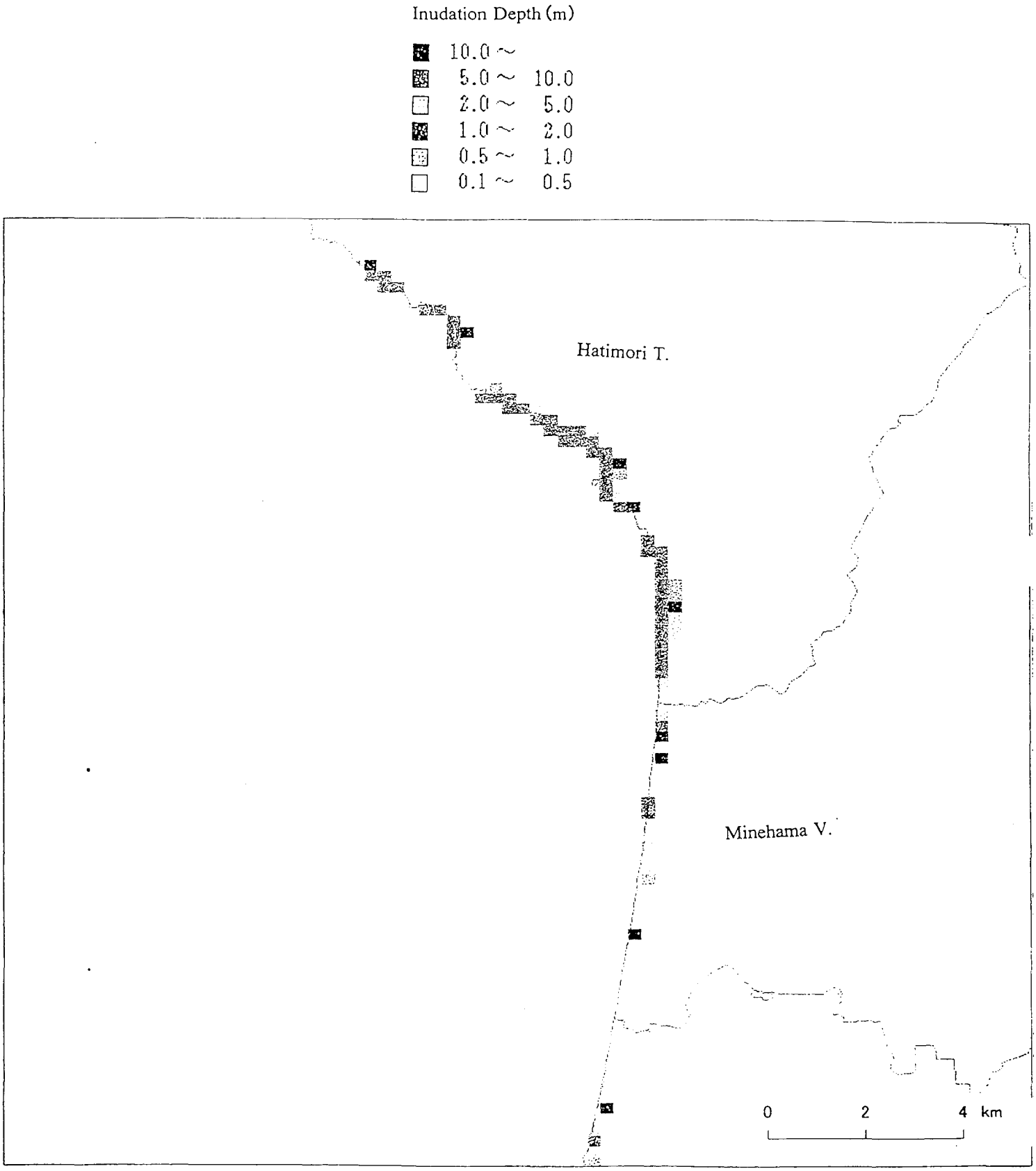

THEME 2

WIND ENGINEERING

Rain/Wind Induced Vibration of Bridge Cables in the United States

By

Harold R. Bosch[1]

ABSTRACT

The wind-induced vibration of stay cables on bridges in the United States has become a significant problem. Of the 24 cable-stayed bridges that are currently in service, 10 have exhibited some degree of cable sensitivity to wind. Several of these have suffered structural damage requiring repairs. This paper begins with a very brief introduction to the problem of cable response. Next, a review of cable-stayed bridges in the U.S. is presented. This will be followed by several examples of cable response problems and retrofit measures to alleviate them. Finally, some remarks regarding a national research study of this problem and conclusions are provided.

KEYWORDS: aerodynamics; bridges; long-span; cable-stayed; cables; wind; rain.

1. INTRODUCTION

For more than 3 decades, engineers have been aware of the potential for wind-induced vibration of cables on bridges [1-4]. In the 1970's, large vibrations were observed on the Koehlbrand and Brotonne Bridges. Mitigation measures were devised and implemented at both sites. Many other bridges around the world, especially cable-stayed bridges, have exhibited similar cable behavior in the years that have followed. With more than 600 cable-stayed bridges worldwide, there are thousands of stay cables in service representing a rather large inventory that has potential for vibration problems.

There have been many investigations to identify the origins of this problem and to develop various methods of mitigation. While most of the significant research has been conducted in Japan, there have been notable studies in other countries such as France and Germany. Despite what has been learned about the problem, large amplitude cable vibrations continue to be observed, even on relatively new structures.

2. AERODYNAMICS OF CABLES

The interaction between wind and bridge cables (stays) can result in vibrations that are often quite large. Sometimes, the presence of rain is also necessary for the vibrations to commence and the amplitudes to become significant. While research over the past 15 years has improved our general understanding of the problem, the phenomenon itself still is not fully understood.

Many factors can influence the response of bridge cables to wind loading. These include, among other things, wind speed and direction, cable inclination, presence of rain, cable properties, and structural damping. Response can be the result of **vortex shedding, galloping, rivulet formation,** buffeting, or aerodynamic excitation of the roadway [5]. Both vertical and lateral vibrations can be significant, although the vertical motions tend to predominate. Large amplitude motion has frequently been observed under the following conditions: low to moderate wind speed, quartering yaw angle, light to moderate rain, downward sloping cables (relative to wind), moderate to long cable lengths, and low cable damping.

Various mitigation measures have been developed and implemented around the world. (See Figure 1). Since structural damping is very low in the cables, one approach is to supplement it through the use of neoprene bushings, hydraulic or viscous shear dampers, and cross ties. The bushings serve a secondary purpose of

---

[1] Research Structural Engineer, FHWA Turner-Fairbank Highway Research Center, 6300 Georgetown Pike, McLean, Virginia 22101.

centering the cable in the guide pipe. The ties also serve to segment the cable span, which raises the cable's natural frequency and critical wind speed. The apparent elliptical shape of an inclined cable presents some aerodynamic stability problems, especially in the presence of water rivulet(s). To address this, a number of aerodynamic surface treatments have been used.

3. U.S. CABLE-STAYED BRIDGES

Despite their popularity elsewhere, cable-stayed bridges did not begin to appear in the U.S. until the 1970's [6]. There are currently 24 of these bridges that are in service. Nineteen of these are major highway bridges while the other 5 are low volume or pedestrian structures. In addition, there are another 6 bridges either in planning, design, or under construction. The 30 bridge sites are primarily located on our Pacific, Atlantic, and Gulf coasts or along the Mississippi and Ohio Rivers (Figure 2). The bridges are steel, concrete, or steel/concrete construction with single or dual towers and main spans ranging from 33 to 396 meters. Cable types and geometries vary with number of stays on each bridge ranging from 12 to more than 200.

4. VIBRATION OF U.S. BRIDGE CABLES

For virtually all of the 24 cable-stayed bridges currently in service, wind-induced response of the cables was not directly considered during the design. In addition, it has not been common practice to consider this issue during the routine wind tunnel testing and aerodynamic assessment which generally takes place near the end of the design phase. Formal guidelines for the aerodynamic design of cables do not currently exist in the United States. It should be noted here that most of the bridges were designed with guide pipes and neoprene bushings, while the Sitka Harbor and Luling Bridges do not have either. Only one bridge, Sunshine Skyway, was designed with some special cable treatment and it has hydraulic dampers. In contrast, most of the 6 bridges in design or under construction include some provisions to prevent large cable motions.

Approximately 10 of the in-service bridges have exhibited some degree of cable sensitivity to wind (Table 1). Three of these (Dames Point, Burlington, Hartman) were retrofit with cross ties during or shortly after construction. Cable ties on the Fred Hartman Bridge began failing in Fall 1997 and all were removed in Spring 1998 (Figure 3). Most of the guide pipes have fractured or cracked (Figure 4). Detailed inspections and measurements have been conducted on the Hartman and Cochrane bridges and are underway on Veterans Memorial. A redesigned restrainer system has been installed on Hartman as a temporary measure and prototype dampers are being evaluated at both Fred Hartman and Veterans Memorial sites. The installation of hydraulic dampers and realignment of guide pipes is planned at the Cochrane site. Measurements have been performed on the Weirton and Huntington bridges, prototype dampers have been evaluated, and installation of dampers is planned (Figure 5). Since cracks have been discovered in three guide pipes on the Talmadge Bridge, a detailed inspection and evaluation is planned (Figure 6). Reports of large cable vibrations on the Luling Bridge have been infrequent, but significant nonetheless. Bridge and cable behavior, as well as wind conditions at this site have been monitored on a long term basis using remote instrumentation (Figure 7). This monitoring will continue with greater focus on cable activity and rain conditions.

5. NATIONAL RESEARCH UNDERWAY

In September 1999, the Federal Highway Administration (FHWA) initiated a major research project to advance our understanding of this problem and to develop comprehensive guidelines for the aerodynamic design of bridge cables in the U.S. [7]. Twelve State Highway Agencies (SHA's) have joined us as research partners. (See Table 2). A contract has been awarded to HNTB Corporation and work is well underway on the information gathering phase. The research team consists of HNTB staff as well as key members from five other firms and several prominent technical advisors. (See Tables 3 and 4).

6. CONCLUDING REMARKS

There is growing concern about the wind and rain/wind induced vibration of bridge cables, especially stay cables. Large amplitude motions have been observed on a number of bridges in the U.S. and there has been structural damage requiring repairs. The interaction of wind with rain and cables is a very complex problem. Although there have been many investigations in other countries, the cable behavior and the excitation mechanisms are still not fully understood. A number of mitigation measures have been developed which primarily involve increasing the cable's structural damping or changing the cable's surface profile. Formal design guidelines, which address this issue, do not currently exist in the United States. Since there is a need to advance our understanding of this problem and to establish design guidelines, a major national study was launched in September 1999.

7. REFERENCES

[1] Langsoe, H.E., Larsen, O.D., "Generating Mechanisms for Cable Stay Oscillations at the Faro Bridges", Proceedings of the International Conference on Cable-Stayed Bridges, Bangkok, 1987.

[2] Hikami, Y., Shiraishi, N., "Rain-Wind Induced Vibrations of Cables in Cable Stayed Bridges", Journal of Wind Engineering and Industrial Aerodynamics, 1988, 409-418.

[3] Matsumoto, M., et.al., "Rain-Wind Induced Vibration of Cables of Cable-Stayed Bridges", Journal of Wind Engineering and Industrial Aerodynamics, 1992, 2011-2022.

[4] Ruscheweyh, H.P., "The Mechanism of Rain-Wind-Induced Vibration", Wind Engineering into the 21st Century, Balkema, 1999, 1041-1048.

[5] Irwin, P.A., "Wind Vibrations of Cables on Cable-Stayed Bridges", Building to Last, ASCE, 1997, 383-387.

[6] Bosch, H.R., "Wind-Induced Vibration of Bridge Cables: A National and International Overview", Proceedings of Workshop on Rain-Wind Vibrations in Cable Stayed Bridges, Atlanta, 1999.

[7] Bosch, H.R., "Wind-Induced Vibration of Bridge Cables: Future Research - A National Study", Proceedings of Workshop on Rain-Wind Vibrations in Cable Stayed Bridges, Atlanta, 1999.

Table 1. U.S. Bridges Exhibiting Cable Vibrations

Bridge	When Observed	Measurements	Damage	Action
Weirton-Steubenville	Construction	Monitor and Evaluate Prototype Spacer and Visco-Elastic Damper	No	Dampers Planned
Burlington	Construction	No	No	X-Ties Installed
Dames Point	Construction	No	No	X-Ties Installed
Fred Hartman	Construction In-Service	Monitor and Evaluate Prototype Dampers	Significant Guide Pipe Damage (Detailed Inspection)	Original X-Ties Failed Temporary X-Ties Installed
Cochrane	In-Service	Yes	Minor (Detailed Inspection)	Hydraulic Dampers Planned Realign Guide Pipes
Veterans	In-Service	In-Progress Monitor and Evaluate Prototype Dampers	No	Monitor and Evaluate
East Huntington	In-Service	Monitor and Evaluate Prototype Dampers	No	Hydraulic Dampers Planned
Talmadge	In-Service (No Visual)	No	Some Guide Pipe Damage	Inspect and Evaluate
James River	Construction	General Measurements During Construction	No	None
Luling-Destrehan	Construction In-Service Infrequent	Long Term Monitoring Spans, Tower and Stays	No	Continue to Monitor

Table 2. State Research Partners

State	Cable-Stay Bridges
Virginia	James River
Georgia	Talmadge and Sidney Lanier
Kentucky	Maysville and Owensboro
Florida	Dames Point and Sunshine Skyway
Alabama	Cochrane
Louisiana	Luling-Destrehan
Texas	Veterans Memorial and Fred Hartman
Mississippi	US82
Illinois	Quincy and Clark
Iowa	Burlington
Missouri	Cape Girardeau
South Carolina	Charleston

Table 3. Key Team Members

Firm	Area of Expertise
HNTB Corporation (HNTB)	Project management, bridge design and analysis.
Johns Hopkins University (JHU)	Flow induced vibration and wind engineering.
Buckland & Taylor (B&T)	Bridge design, analysis and testing.
Rowan Williams Davies & Irwin (RWDI)	Wind engineering, wind tunnel testing, damping systems, dynamics and meteorology.
E*Sorb Systems (E*Sorb)	Damping technology.

Table 4. Key Technical Advisors

Consultant	Affiliation
R. Scanlan	Johns Hopkins University
G. Fox	HNTB
M. Matsumoto	Kyoto University
O. Flamand	CSTB Laboratory

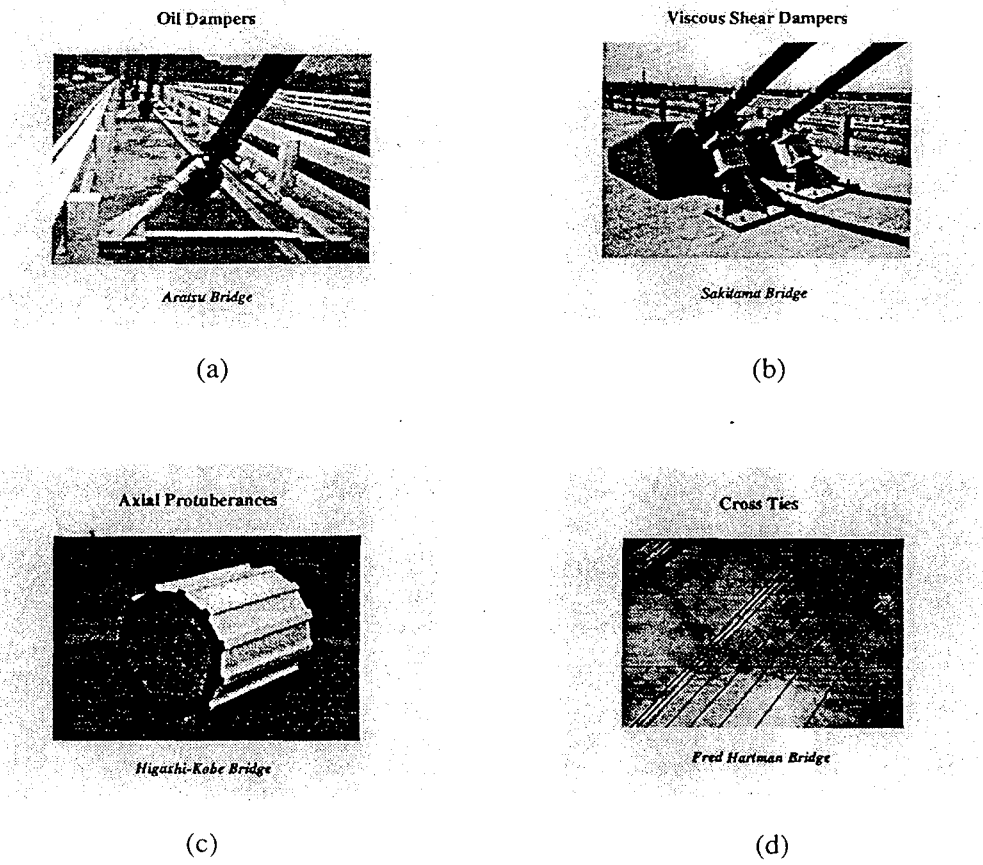

Figure 1. Common Mitigation Measures

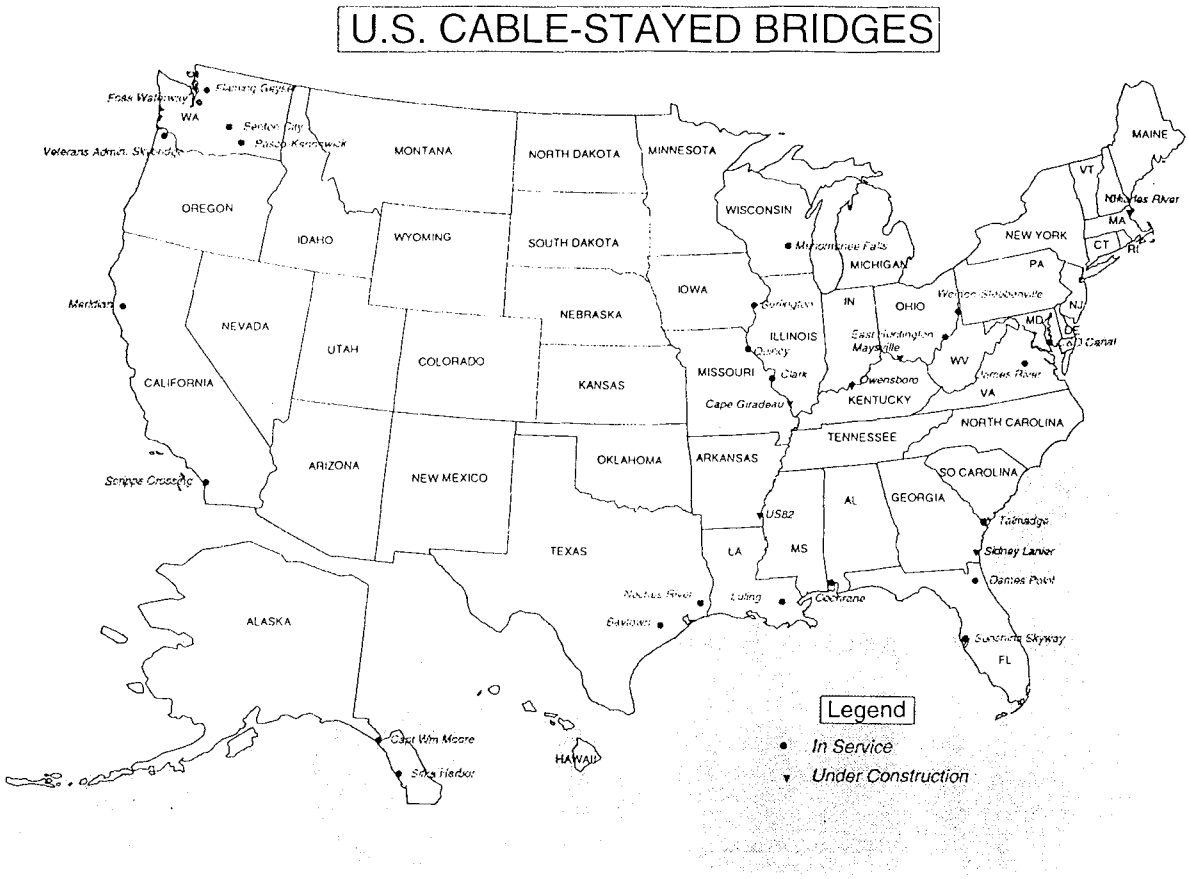

Figure 2. Cable-Stayed Bridge Sites in U.S.

(a) (b)

Figure 3. Damaged Cross Ties - Fred Hartman Bridge

Figure 4. Damaged Guide Pipes - Fred Hartman Bridge

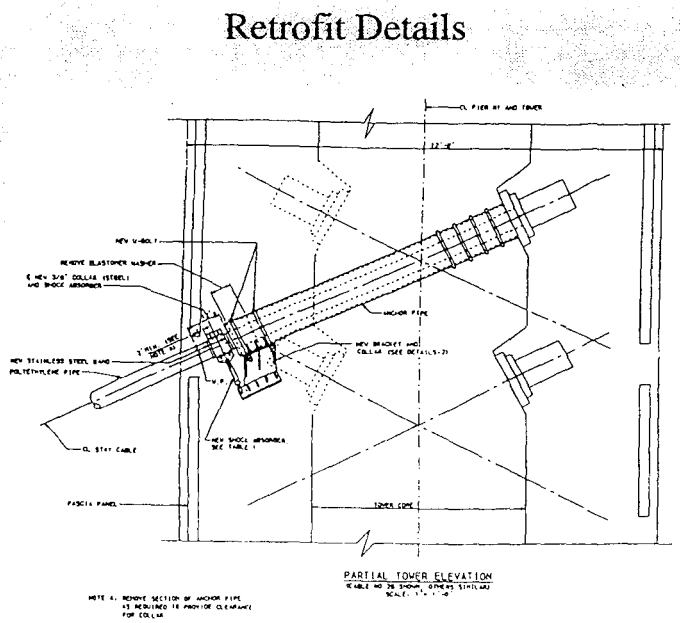

Figure 5. Hydraulic Damper Detail - East Huntington Bridge

Wind Damage - Spalling and Crack

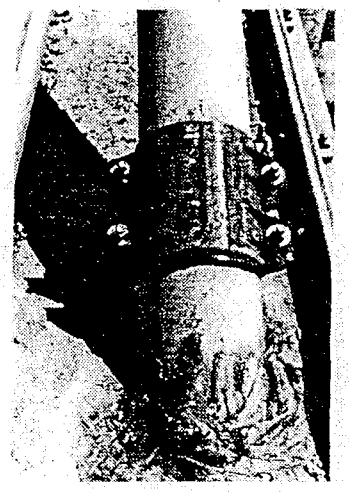

Figure 6. Guide Pipe Repairs - Talmadge Bridge

Cable Sensors

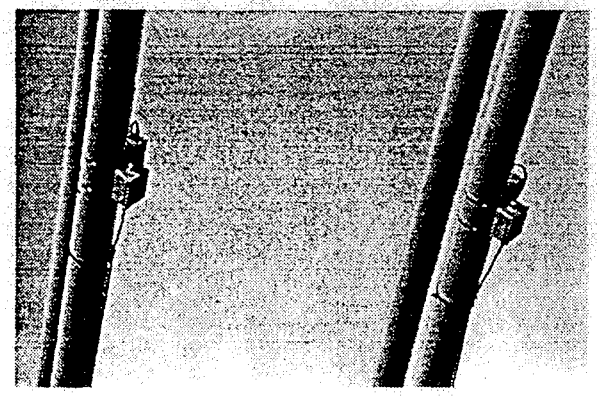

Figure 7. Cable Instrumentation - Luling Bridge

STUDY ON PERFORMANCE-BASED DESIGN METHODS FOR WIND EFFECTS ON HIGHWAY BRIDGES

by

Hiroshi Sato[1] and Ken-ichi Ogi[2]

ABSTRACT

Performance-based design methods for wind effects on highway bridges are studied based on the NKB level system. It was found that the existing wind resistant design methods for highway bridges in Japan could be easily converted to the performance-based design methods. To improve the design methods, quantitative values for required performance, such as a return period and allowable vibrational amplitude should be studied further.

1. INTRODUCTION

In Japan, the wind-resistant design of highway bridges up to the span length of 200m are conducted according to the Wind Resistant Design Manual for Highway Bridges [1], [2] (hereinafter referred to as 'the Manual'), which was published in 1991. This Manual is also applicable to the highway bridges up to the span length of 300m with minor modification of its provisions. If span length of a bridge becomes longer than 300m, the specific design specification will be established for the bridge. The basic concept of wind-resistant design of such a long-span bridge is, however, almost similar to that of the Manual.

Recently attentions have been paid to performance-based design methods. In the performance-based design methods, the performance level of structures is described clearly, and designers have more freedoms in designing structures.

In this paper, the existing wind resistant design methods for highway bridges and the NKB level system are outlined first. Then the existing wind resistant design methods are converted to the performance-based design format according to the NKB level system.

2. OUTLINE OF THE EXISTING WIND RESISTANT DESIGN METHODS FOR HIGHWAY BRIDGES IN JAPAN

The procedure of wind resistant design using the Manual is as follows (Fig. 1). The wind properties (basic wind speed, design wind speed, turbulence intensity etc.) are decided first. The design wind load is calculated, and the static design of the bridge is made.

At this stage, where major dimensions of the bridge are determined, wind-induced vibrations to be studied further are chosen considering the design wind speed, the deck width and the span length of the bridge. For a bridge with short span length, no study on wind-induced vibration is required.

For long-span bridges, wind-induced vibrations specified above should be predicted using the formulae provided in the Manual. Then the wind-induced vibrations are evaluated. The formulae were established considering past wind tunnel test results. Since the formulae are expressed by means of only a few parameters, the prediction error of the formulae is not negligibly small. Therefore, the formulae were established, so that their prediction may become safer. It means that evaluation 'good' based on the formulae is almost always 'good', however, evaluation 'no good' based on the formulae is not always 'no good' because of the safety margin of the formulae. In case that the evaluation based on the formulae turns out to be 'no good', the bridge engineer can modify the design or he can predict wind-induced vibrations more accurately by means of wind tunnel testing. The evaluation based on wind tunnel testing has priority over that based on the formulae.

---

1) Head, Structure Division, Structure and bridge Department, Public Works Research Institute, Ministry of Construction, Asahi 1, Tsukuba-shi, Ibaraki-ken, 305-0804, Japan
2) Research Engineer, ditto

3. PERFORMANCE STANDARDS AND NKB LEVEL SYSTEM

3.1 Performance Standards

There are two kinds of design standards, namely, prescriptive standards and performance standards. The prescriptive standards describe the design and constituent materials of products [3]. On the other hand, the performance standards define specific behavior of products. They define requirements without imposing restrictions on the form or materials of the solutions [3].

Therefore, a structural engineer can design and construct the structure with more freedom according to the performance standards. The latest and advanced technology can be applied to the structure if it is verified to satisfy the requirements. There may be a chance that more rational structures can be constructed according to the performance standards.

In the performance standards, however, verification of compliance with the requirements is more difficult than in the prescriptive standards. It will take some time and money to verify the performance of the structure or its elements.

3.2 NKB Level System

Nordiske komite for bygningsbestemmelser (hereinafter referred to as 'NKB') developed what is called NKB level system [4]. The NKB level system consists of five levels characterizing the purpose of building regulations. The five levels are illustrated in Fig 2. The levels are classified into three: 'Performance requirements (Level 1 – 3)', 'Verification methods (Level 4)' and 'Examples of solutions (Level 5)'.

a) Definition of the levels

The definition of each level [4] is shown below.

Level 1: Overall objectives

The overall statement of the properties of a building that must be regarded as important from the point of view of society and its individual members.

Level 2: Functional areas

The main properties specified as overall goal level are classified in functional areas and principles laid down for the realization of the specified intentions.

Level 3: Required performance

Operative requirements in order that principles laid down under level 2 within the various functional areas may be applied in the design and construction of buildings.

Level 4: Verification

Instructions or guidelines laid down for verification of compliance with the requirements.

Level 5: Solutions

Supplement to the regulations with examples of acceptable solutions, deemed to satisfy the regulations.

b) Examples of the levels

The examples of contents of the levels can be given as follows.

Level 1: Safety, serviceability, durability and so on.

Level 2: Safety of the structure or its element 'y' to the effect 'z' caused by the action 'x'.

Level 3: The intensity of the effect 'z' on the structure or its element 'y' should be 'b' or less, when the intensity of the action 'x' is 'a'.

Level 4: Analytical methods, testing methods, calculation methods and so on.

Level 5: If a structure that is designed and constructed in accordance with some specifications of prescriptive standards can be expected to achieve the required performance, the specifications can be also described here as examples of solutions.

c) Merits of the NKB level system

If structural design standards are described according to the NKB level system, the performance required for the structure will be clarified in the Levels 1-3. Therefore the standards have the merits of performance standards. The purpose of each article of the standards will become clear. To overcome some demerits of the performance standards, namely difficulties in verification, the Level 5 can be utilized. Some of

the specifications of prescriptive standards that can be assumed to satisfy the required performance can be included in the Level 5.

4. PERFORMANCE-BASED DESIGN METODS FOR WIND EFFECTS ON HIGHWAY BRIDGES

The wind resistant design methods described in the Manual are converted to the performance-based design format according to the NKB level system.

4.1 Overall Objectives (Level 1)

A highway bridge shall be planned and constructed in such a way that its safety and serviceability be obtained and maintained under the wind actions that are expected at the bridge site during the service life of the bridge.

4.2 Functional Areas (Level 2)

Wind actions that shall be considered in the design of a highway bridge are as follows:

a) wind load;
b) gust response;
c) flutter;
d) galloping;
e) vortex-induced vibration.

The wind actions may produce the following effects:

f) excessive forces, stress or deformation of the bridge or its elements;
g) repeated dynamic stress or deformation causing fatigue of the bridge or its elements;
h) aeroelastic instability;
i) excessive dynamic movements causing concern or discomfort to users of the bridge.

4.3 Required Performance (Level 3)

a) Wind load and gust response

For the wind load and gust response, the safety of the bridge shall be examined in viewpoint of the wind effects referred to in 4.2 f).

The design wind load P_d for static design may be obtained from the following formula.

$$P_d = 0.5\,\rho\,U_d^2\,C_d\,A_n\,G \quad (1)$$

where, ρ : air density, U_d: design wind speed, C_d: drag coefficient, A_n: projected area, G: gust factor.

The resultant forces, stress or deformation shall be less than the allowable values specified in the Specification for Highway Bridges.

b) Flutter and galloping

For flutter and galloping, the safety of the bridge shall be examined in viewpoint of the wind effects referred to in 4.2 h).

The following inequalities shall be satisfied,

$$U_{cf} > U_r \text{ --- Flutter} \quad (2)$$
$$U_{cg} > U_r \text{ --- Galloping} \quad (3)$$
$$U_r = U_d\,E_{r1}\,E_{r2} \quad (4)$$

where, U_{cf}: critical wind speed for flutter, U_{cg}: critical wind speed for galloping, U_r: reference wind speed for flutter and galloping, U_d: design wind speed, E_{r1}: correction factor for the effect of gust, E_{r2}: safety factor(1.2).

The design wind speed for dynamic design U_d may be obtained from the following formula.

$$U_d = U_{10}\,E_1 \quad (5)$$

where, U_{10}: basic wind speed, E_1: correction factor for altitude and terrains.

The basic wind speed U_{10} is defined as the mean wind speed over open farmland at an elevation of 10m, averaged over a period of 10 minutes. Its return period is 100-years. The probability that the annual maximum mean wind speed exceeds the basic wind speed is 40% in a 50-year period. The basic wind speeds in Japan were classified into 4 categories, namely 30m/s, 35m/s, 40m/s and 45m/s.

c) Vortex-induced vibration

For vortex-induced vibrations, the safety of the bridge shall be examined in viewpoint of the wind effects referred to in 4.2 f) and g). The serviceability of the bridge shall be examined in viewpoint of the wind effects referred to in 4.2 i).

Unless the following inequality (6) is satisfied, the maximum amplitude of the vortex-induced vibration shall be less than the

allowable amplitude shown in equations (7) and (8).

$$U_{cv} > U_d \quad (6)$$

where, U_{cv}: wind speed for the maximum amplitude of vortex-induced vibration.

$$h_a = 0.04/f_h \text{ --- bending (in m)} \quad (7)$$

$$\theta_a = 2.28/(b\, f_\theta) \text{ --- torsion (in deg.)} \quad (8)$$

where, h_a: allowable amplitude for bending vortex-induced vibration, f_h: natural frequency of the 1st bending mode, θ_a: allowable amplitude for torsional vortex-induced vibration, b: distance between the deck center and the center of outmost lane, f_θ: natural frequency of the 1st torsional mode.

4.4 Verifications (Level 4)

The wind-induced vibrations such as flutter, galloping and vortex-induced vibration may be predicted either by the formulae or by wind tunnel tests. The predicted critical wind speed or maximum amplitude shall be compared with the reference wind speed or the allowable amplitude described in 4.3.

a) Prediction of wind-induced vibrations by the formulae

The formulae to predict wind-induced vibrations are provided in the Manual. They were established by considering past wind tunnel test results.

The formula for prediction of critical wind speed of flutter is as follows:

$$U_{cf} = 2.5\, f_\theta B \quad (9)$$

where, U_{cf}: critical wind speed for flutter, f_θ: natural frequency of the 1st torsional mode, B: deck width.

Galloping may take place for solid steel deck whose deck width to depth ratio (B/d) is less than 5, and when turbulence intensity is small. The formula for prediction of critical wind speed of galloping is as follows:

$$U_{cg} = 8\, f_h B \text{ ; when angle of attack is almost 0 deg.} \quad (10)$$

$$U_{cg} = 4\, f_h B \text{ ; when angle of attack is positive.} \quad (11)$$

where, U_{cg}: critical wind speed for galloping, f_h: natural frequency of the 1st bending mode.

Vortex-induced vibrations may take place for solid deck. The formulae for prediction of critical wind speed and amplitude of vortex-induced vibrations are as follows:

$$U_{cv} = 2.0\, f_h B \text{ --- bending} \quad (12)$$

$$U_{cv} = 1.33\, f_\theta B \text{ --- torsion} \quad (13)$$

$$A_c = A_e E_{ms} E_t \quad (14)$$

$$A_e = \beta_{ds} \cdot 0.05 \cdot (d/B)/(m_r \delta_h) \text{ --- bending (in h/B)} \quad (15)$$

$$A_e = \beta_{ds} \cdot 13.2 \cdot (d/B)^3/(Ip_r \delta_\theta) \text{ --- torsion (in deg.)} \quad (16)$$

where, U_{cv}: wind speed for the maximum amplitude of vortex-induced vibration, A_c: corrected maximum amplitude of vortex-induced vibration, A_e: maximum amplitude of vortex-induced vibration for rigid model in smooth flow, E_{ms}: correction factor for vibrational mode (about $4/\pi$), E_t: correction factor for the effect of turbulence, β_{ds}: correction factor for sectional shape, m_r, Ip_r: reduced mass or reduced mass moment of inertia, δ_h, δ_θ: structural damping (logarithmic decrement).

b) Prediction of wind induced vibrations by wind tunnel tests

Wind tunnel tests increase the reliability of wind resistant design of bridges. Since the prediction of wind-induced vibrations based on the formulae may often provide safer values, there is a fair chance that wind tunnel study provides more economical design.

Wind tunnel testing methods applicable to the prediction of wind-induced vibration of highway bridges are as follows: full aeroelastic model test, taut-strip model test, and spring-mounted rigid model test.

4.5 Solutions (Level 5)

According to the types of a bridge, main span length L, deck width B and design wind speed Ud, the bridge may be assumed to satisfy the required

performance for some wind-induced vibrations. The conditions that a bridge can be assumed to satisfy the required performance for some wind-induced vibrations are shown in Table1.

4.6 Discussions

The return period for design wind speed is the most important and fundamental value for wind resistant design. The rational return period for design wind speed should be studied further by comparing with the return periods for other natural disasters, such as earthquakes.

The allowable amplitude for the vortex-induced vibration shown in equations (7) and (8) were determined by considering full-scale data of the vortex-induced vibration and bridges that countermeasures were actually applied to. The rational allowable amplitude should be studied further, especially in viewpoint of serviceability.

5. CONCLUSION

The performance-based design methods for wind effects on highway bridges were studied. The wind resistant design methods described in the Wind Resistant Design Manual for Highway Bridges were converted to the performance-based design format according to the NKB level system. It was found that the existing wind resistant design methods could be easily converted to the performance-based design methods, because the required performance and verifications are clearly described in the existing methods. Some of the quantitative values for required performance, such as a return period for design wind speed and allowable vibrational amplitude, however, should be studied further to improve the design methods.

REFERENCES

[1] K. Yokoyama and H. Sato: On the proposed wind resistant design manual for highway bridges in Japan, International Colloquium on Bluff Body Aerodynamics and its Applications, 1988, 10, (Journal of Wind Engineering and Industrial Aerodynamics, 33, 1990, pp.395-405, Elsevier Science Publishers)

[2] H. Sato and T. Mabuchi: Development of manual and expert system for wind resistant design of highway bridges, Transaction of the Jubileum Conference on Wind Effects on Buildings and Structures, Part II, 1998, 5, pp. 69-76

[3] ISO: Performance standards in building — Principles for their preparation and factors to be considered, ISO6241- 1984 (E), 1984

[4] Den nordiske komite for bygningsbestemmelser: Strokturering av Byggregler (Structure for Building Regulations), NKB report No 34, 1978

Table1 Bridges that can be assumed to satisfy the required performance for the wind actions

Type of girder	Wind actions
Truss girder for cable-stayed or suspension bridges	can be assumed to satisfy the required performance for: flutter, if L Ud/B<350; galloping; vortex-induced vibration.
Open solid girder for cable-stayed or suspension bridges	can be assumed to satisfy the required performance for: flutter, if L Ud/B<350; galloping, if L Ud/B<330, B/d>5, Iu>0.15 or if it is made of concrete; vortex-induced vibration, if L Ud/B<200 or if Iu>0.20.
Closed solid girder for cable-stayed or suspension bridges	can be assumed to satisfy the required performance for: flutter, if L Ud/B<520; galloping, if L Ud/B<330, B/d>5, Iu>0.15 or if it is made of concrete; vortex-induced vibration, if L Ud/B<200 or if Iu>0.20.
Steel girder bridges	can be assumed to satisfy the required performance for: flutter; galloping, if L Ud/B<330, B/d>5 or if Iu>0.15; vortex-induced vibration, if L Ud/B<200 or if Iu>0.20.
Bridges other than the above types	can be assumed to satisfy the required performance for: flutter; galloping; vortex-induced vibration.

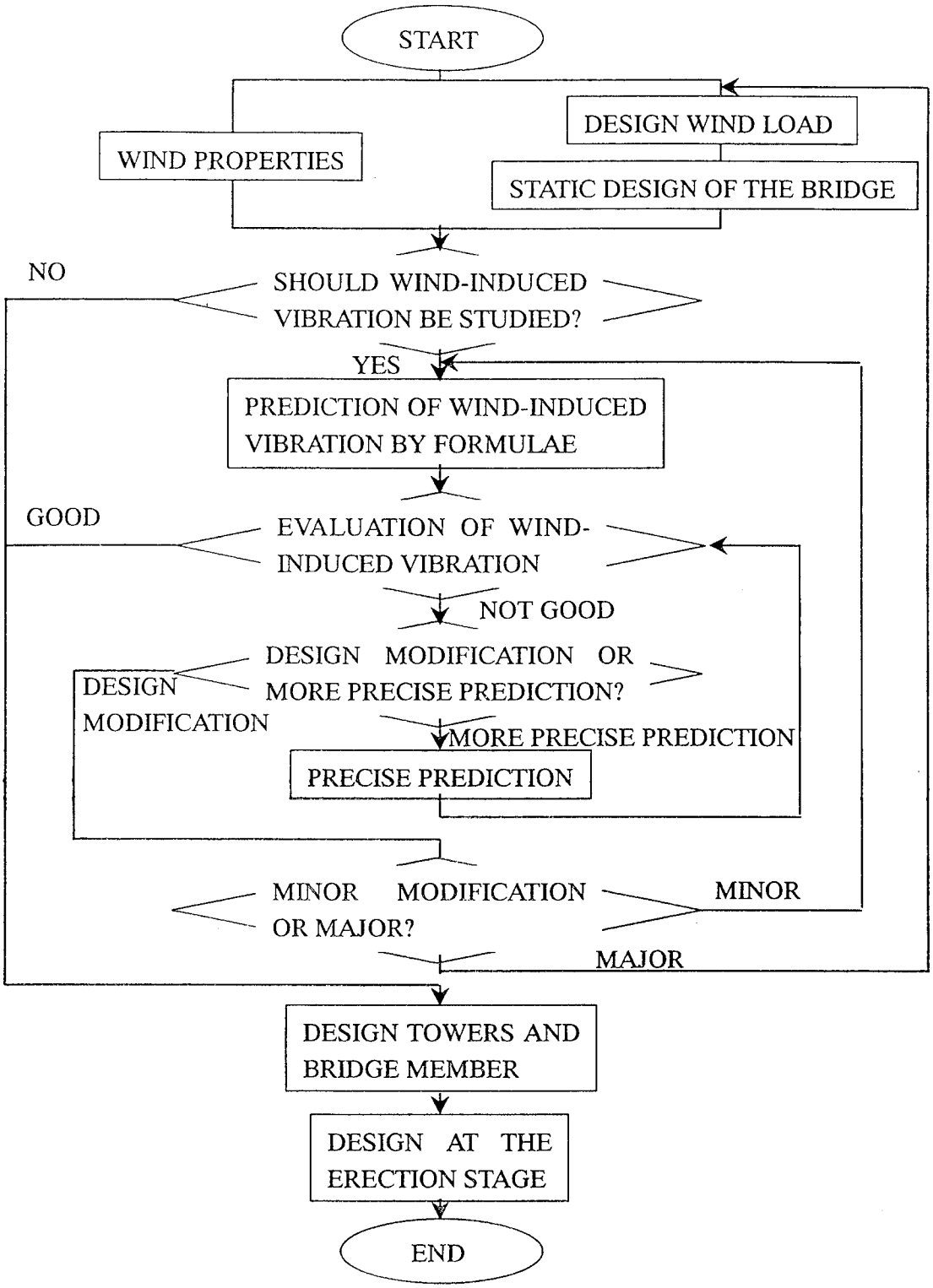

Fig. 1 Procedure of wind resistant design using the Manual

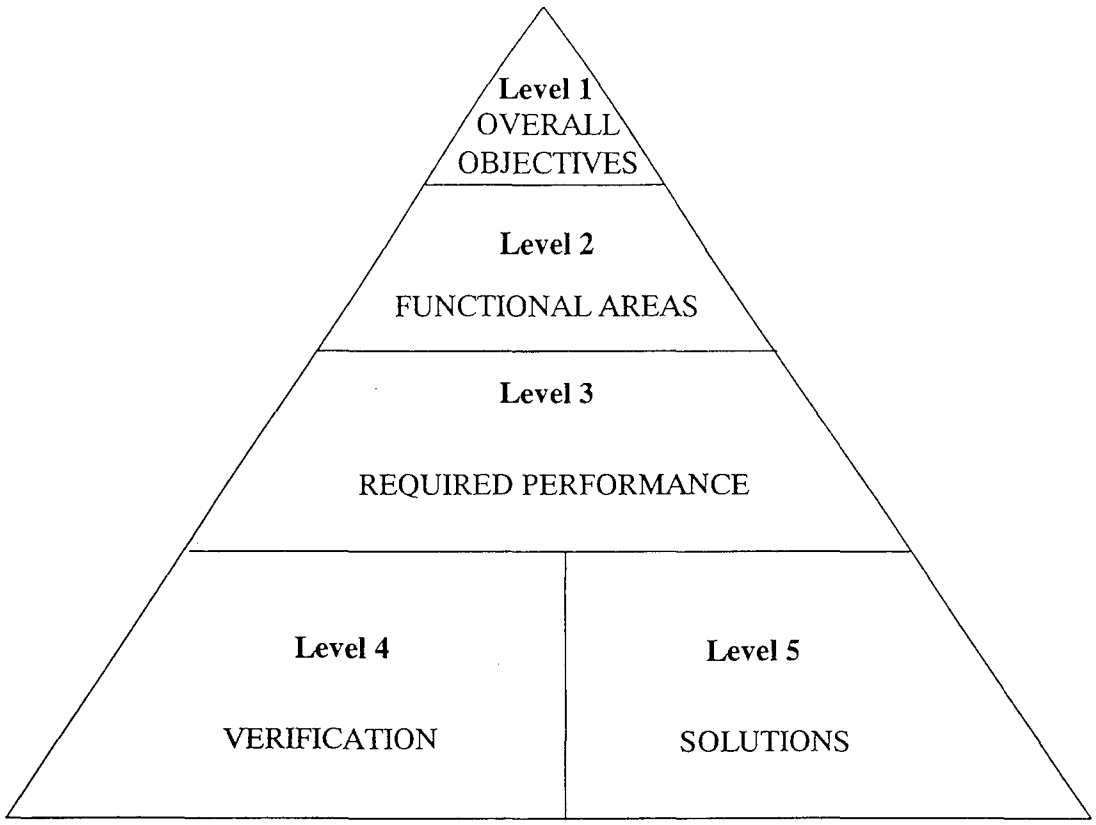

Fig.2 NKB level system

WEATHER SITUATION ON GROUND OBSERVED AT FIRE STATIONS – CASE OF TYPHOON VICKI

by

Yasuo OKUDA[1], Hirohiko ISHIKAWA[2], Takeshi FUJII[3] and Hisashi OKADA[4]

ABSTRACT

Collecting a weather observation data at fire stations located in Kinki district and Chubu district, the weather situation on the ground of typhoon Vicki was investigated. There were four severe storm areas where the instantaneous wind velocity exceeds 50m/s in Kinki district. The severe storms occurred in the two cases: at the almost same time when the daily minimum atmospheric pressures appeared and at about one hour after the daily minimum atmospheric pressures appeared. Comparing the severe storm areas with the combined radar echo chart, it was showed that the severe storms of the latter case occurred around the rain band to form in the rear of the typhoon and the direction of the severe storms was divided into the two directions; tangent and normal directions against the rotation of the typhoon. The detailed weather situation on the ground of the typhoon became clear about temperature, humidity, precipitation, and atmospheric pressure. In this way, the weather observation data at the fire stations was showed very useful in order to collect weather information on the ground of the typhoon.

KEY WORDS: Typhoon Vicki
Fire Station
Weather Situation
Combined Radar Echo

1. INTRODUCTION

Typhoon Vicki was landed at about 1 p.m. September 22nd, 1998 at the northern region of Gobo city in Wakayama prefecture, following typhoon Waldo that was landed in Wakayama prefecture previous day. Typhoon Vicki ran up through Kinki district and exerted enormous damages on each place in Kinki district, mainly in the Nara prefecture. As this typhoon passed the central region of Kinki district as well as the typhoon 7916, the weather elements of the typhoon on the ground was observed in a lot of places at the fire stations and the schools in addition to the meteorological observatories and so on.

In recent years, the number of the fire fighting headquarters is increasing where the weather data acquisition systems for the fire fighting were installed in the local governments in the whole country. The weather data acquisition system for the fire fighting observes the weather elements automatically for the prevention against disasters and the publicity work in the local area. There are tens fire fighting headquarters per each prefecture in Kinki district and Chubu district. The weather data acquisition system for the fire fighting is installed at the most of the fire fighting headquarters. Therefore, the weather observation network with this fire fighting headquarters becomes much closer than the weather observation network of the meteorological observatories that are only one or two places per prefecture. In the great city, the weather observation network with this fire fighting headquarters becomes closer than

1) Head, Department of Structural Engineering, Building Research Institute, Ministry of Construction
2) Associate Professor, Disaster Prevention Research Institute, Kyoto University
3) Professor, General Education and Research Center, Kyoto Sangyo University
4) Director, Department of Structural Engineering, Building Research Institute, Ministry of Construction

AMeDAS (Automatically Meteorological Data Acquisition System, four measured elements of precipitation, wind vector, sunshine and temperature). Moreover, this weather data acquisition system can measure the weather elements in a time series, which are indispensable to observe typhoons such as the instantaneous wind velocity, the atmospheric pressure, and the humidity, which were not measured in AMeDAS. This weather data acquisition system is expected to be ideal for the investigation of the ground weather elements of the typhoon.

Uematsu et al.(1999) made a data base about the weather observation situation at the fire stations in Aomori and Akita prefecture in Tohoku district. However, there was no report to verify the utility of this weather observation network by collecting the weather data observed with such weather data acquisition systems from the extensive area. Because the purpose of this weather data acquisition system itself seems to provide the weather information only for the purpose of the area.

Table 1 Number of fire stations

Name of prefecture	Number of fire station	Number of answer	Rate of answer (%)
Kinki district Kyoto	17	10	59
Mie	16	11	69
Shiga	11	7	64
Osaka	33	22	67
Wakayama	21	8	38
Nara	13	11	85
Chubu district Aichi	47	38	81
Gifu	24	13	54
Fukui	12	8	67
Total	194	128	66

Table 2 Total Number of measuring points

Classification of measuring points	Number
Fire station	128
Meteorological observatory	27
AMeDAS(four measured elements)	71
Power station	27
Total	253

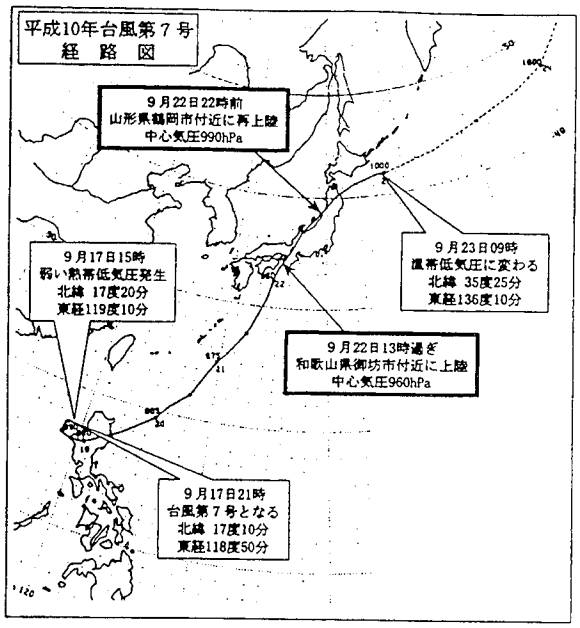

Fig.1(a) Path of Typhoon Vicki

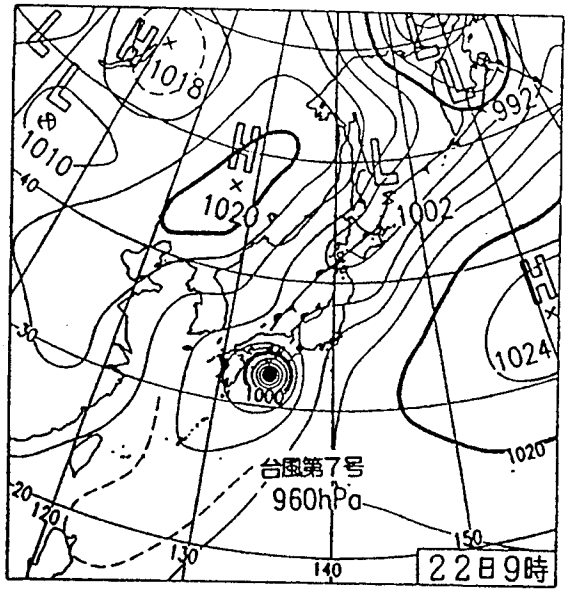

Fig.1(b) Weather chart at 9:00 on 22nd September.

Therefore, the authors requested the provision of the weather data after the passage in typhoon Vicki in the purpose to examine the ground weather situation in typhoon Vicki in detail. As a result, a lot of answers were gotten as shown in Table 1. Especially, the answer percentage of Nara and Aichi prefecture exceeded 80%. After that, it gets a similar weather data from the weather government service station (Meteorological Agency, 1998a) and the power stations in Kinki district. The weather data could be gotten from 253 observation points in all as shown in Table 2. Here, it reports the result examined about the time series change of the weather elements with the typhoon passage charts, compared with the rainfall strength figures from the combined radar echo charts Based on this result, it verifies the utility of the weather observation network observed at the fire stations.

2. WEATHER GENERAL CONDITION OF TYPHOON VICKI

The course in typhoon Vicki (Meteorological Agency, 1998b) and the weather chart at 9:00 on September 22nd (Meteorological Agency, 1998b) are shown in Figs.1(a)(b). The weak tropical depression, which occurred on the western sea of Philippine Luzon Island at 15:00 on September 17th, developed into typhoon Vicki at 21:00 on the same day. It developed gradually on the course which is shown in Fig.1(a) and hit Kii peninsula of Japan around 13:00 on September 22nd. The minimum atmospheric pressure at the center of typhoon Vicki was 960hPa at the landing. The maximum wind velocity was 35m/s around the center. The radiuses of the severe storm area where the wind velocity was over 25m/s were 190km at the southeast side and 150km at the northwest side. The radiuses of the severe storm area where the wind velocity was over 15m/s were 700km at the southeast side and 220km at the northwest side.

After the landing, it ran from the southwest to the northeast in Kinki district while weakening gradually the power of the typhoon and went through to Toyama bay. Moreover, it re-landed on Yamagata prefecture before 22:00 on the same day. The central atmospheric pressure at the

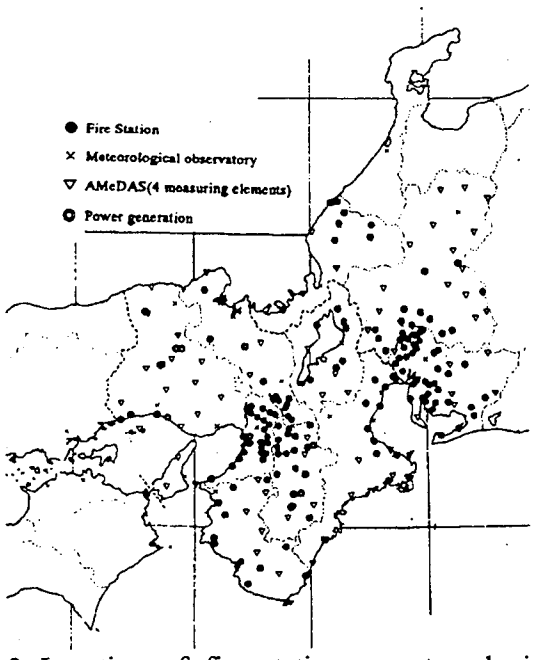

Fig.2 Location of fire stations meteorological observatories and power stations

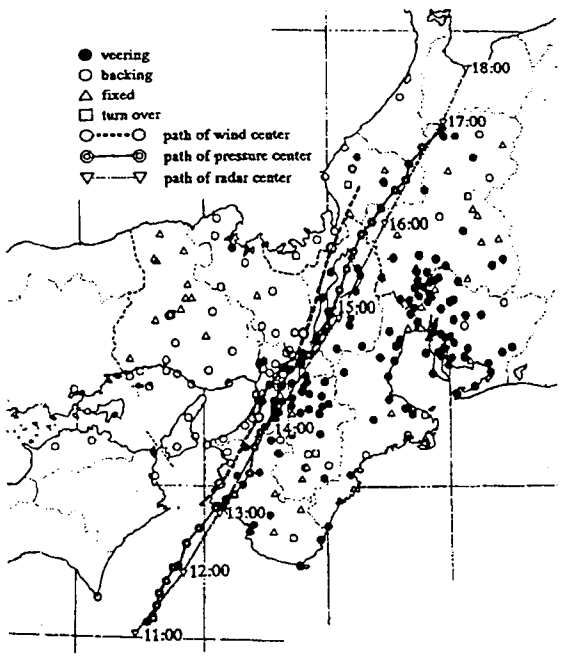

Fig.3 Path of Typhoon 9807(Vicki) on Kinki district

re-landing was 990hPa and the maximum wind velocity was 25m/s near the center. The radiuses of the severe storm area where the wind velocity was over 15m/s were 460km at the southeast side and 190km at the northwest side. Then, it went through to the Pacific Ocean and it became the extra tropical depression at 9:00 on 23rd September. This typhoon was a very ordinary typhoon at size and strength but this typhoon moved very fast and accompanied the heavy rainfall in the influence of the front. The movement speed (Meteorological Agency, 1998b) of this typhoon is about 50-55 km/hr immediately before Kii peninsula landing and after the landing it is raising speed in about 75-85 km/hr.

3. WEATHER SITUATION ON GROUND

3.1 Weather Observation Point

The position of the fire fighting headquarters, the weather government service station and the power stations, where the observation data could be got, shows in Fig.2. AMeDAS is equally arranged approximately over all the prefectures, but one or two meteorological observatories were located per prefecture. On the other hand, the observation points of the fire fighting headquarters concentrate on the urban regions of the great city such as the Osaka or Nagoya city. There are few numbers of the observation points of the fire fighting headquarters in the ravine regions. However, a lot of observation points at the power stations exist in the ravine regions and the coastal region in Kinki district. They complement an observation network in the fire fighting. In the northern region of Nara prefecture where the large damages were sustained in the typhoon Vicki, the number of the meteorological observatory was only one and the number of AMeDAS was only three. But the number of the fire fighting headquarters was 11 and more detailed weather information on the ground could be collected. This figure shows that the weather observation network at the fire stations formed the close observation network mainly in the urban region is very effective in order to grasp the damage situation of the severe storm disaster on the urban region like this typhoon.

3.2 Course of Typhoon Vicki

The wind directions at observation points changed to be clockwise at filled circle marks and anticlockwise at empty circle marks shown in Fig.3. The boundary that approximately divided Kinki district into east and west certainly existed. The thick broken line showed this boundary. This line is equivalent to the course in the wind center of the typhoon. As the times when the wind direction changed were recorded at some autograph observation points, the position of the wind center of the typhoon was shown by every hour on Fig.3. Also, the position of the atmospheric pressure center of the typhoon which was looked for every 10 minutes by the objective analysis(Fujii et al., 1999) was shown by double circle mark. Fujii et al. used atmospheric pressure records by the weather government service. The triangle mark is the position that the Meteorological Agency mainly looked for every hour. It finds that each course of the typhoon was meandering and that the course in the wind center and the atmospheric pressure center of the typhoon resembled very well each other but that the course in the wind center shifted to the direction of the progress than the course in the atmospheric pressure center with the about 10 to 20km left.

3.3 Situation of Severe Storm

The distributions of the average wind velocity value for 10 minutes (the average from 50' to 00' in every hour) and wind velocity vectors are shown by the time series from 13:00 to 16:00 in Figs.4(a)-(d). In the figure circle marks show the position of the atmospheric pressure center of the typhoon that was found at each time from the objective analysis (Fujii et al., 1999). In 14:00, when the atmospheric pressure center of the

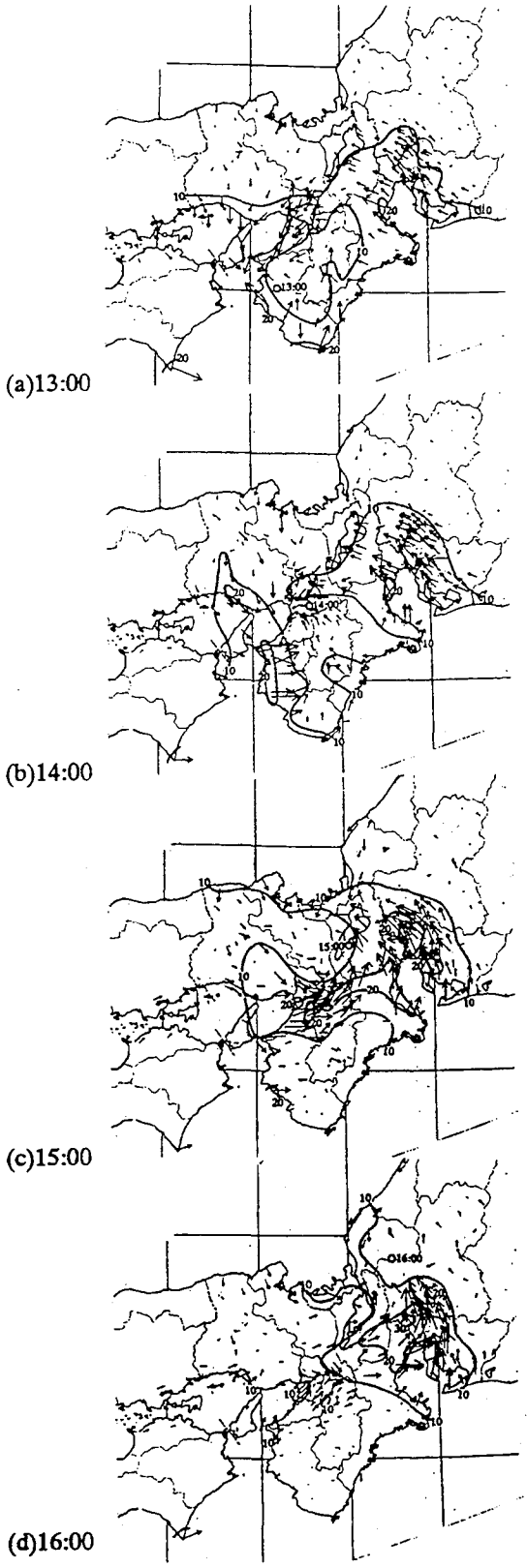

Fig.4 Distribution of mean wind vectors (m/s)
typhoon reaches the prefecture border between

Osaka and Nara prefecture, the severe storm area where the average wind velocity exceeds 20m/s appears in the rear of the typhoon in addition to the right side of the typhoon. In Wakayama city, the maximum wind velocity recorded 32.4m/s at 14:20. After that, this severe storm area passed Osaka, Nara and Mie prefecture and reached to the western region of Aichi prefecture and the southwest region of Gifu prefecture. The severe storms were recorded over 30m/s respectively, i.e.; maximum wind velocity 31.9m/s at 15:48 in Kameyama city in Mie prefecture, the same 32.7m/s at 15:57 in Kaitsu town in Gifu prefecture. As shown in the wind velocity vector of Fig.4, the wind direction in the severe storm area formed in the right of the typhoon was mainly the southeast to the south, but the wind direction in the severe storm area in the rear of the typhoon was mainly south to the west.

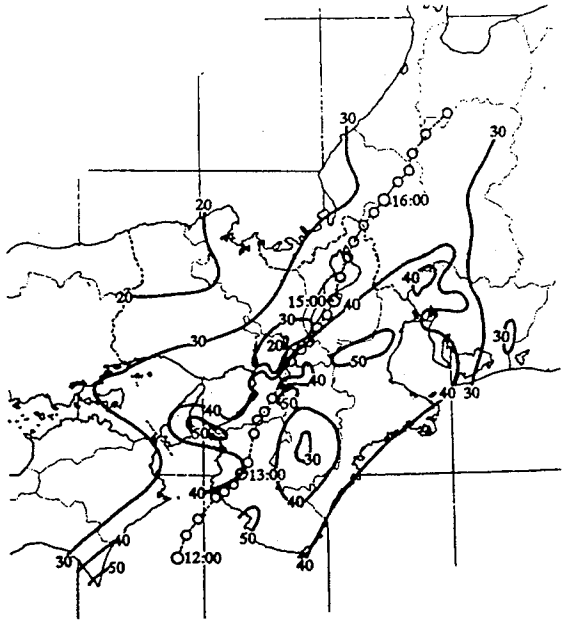

Fig.5 Distribution of daily maximum instantaneous wind velocity (m/s)

Fig.5 is the distribution of the daily maximum instantaneous wind velocity in each observation point. In Fig.5 the circle mark shows the position of the atmospheric pressure center of the typhoon looked for from the objective analysis (Fujii et al., 1999). The severe storm area, where the maximum instantaneous wind velocity exceeds 40m/s, spread from the southern region of Kinki district to the western region of Chubu district. The daily maximum instantaneous wind velocities were recorded 51.0m/s in Tanabe city at 13:13, 50.0m/s in Wakayama city at 14:13, 50.8m/s in Sumoto city at 14:07, 59.5m/s in Shinjo town at 14:59 and 56.4m/s in Ueno city at 15:14.

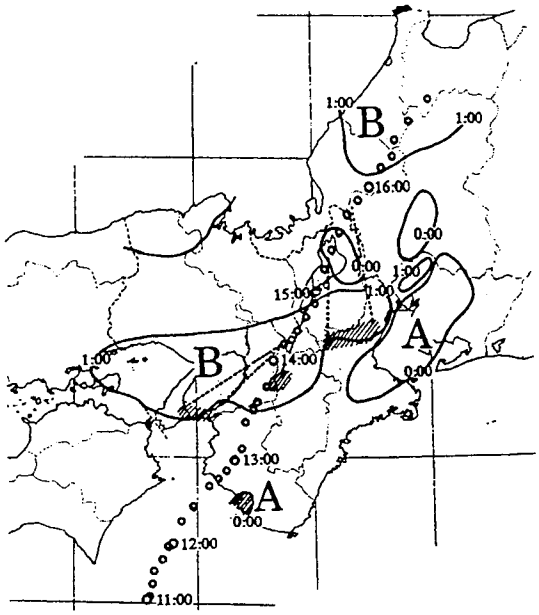

Fig.6 Difference hours between occurrence time of daily maximum instantaneous wind velocity and daily minimum atmospheric pressure

Fig. 6 shows the difference of occurrence times when the daily maximum instantaneous wind velocity and the daily minimum atmospheric pressure were recorded at each observation point. The figure is divided into the two areas; the differences of occurrence times were almost zero (A in the figure) and more than one hour(B in the figure). In Tanabe city the daily maximum instantaneous wind velocity and the daily minimum atmospheric pressure were recorded at the almost same time, but in Sumoto city, Wakayama city, Shinjo town and Ueno city, the daily maximum instantaneous wind velocity was

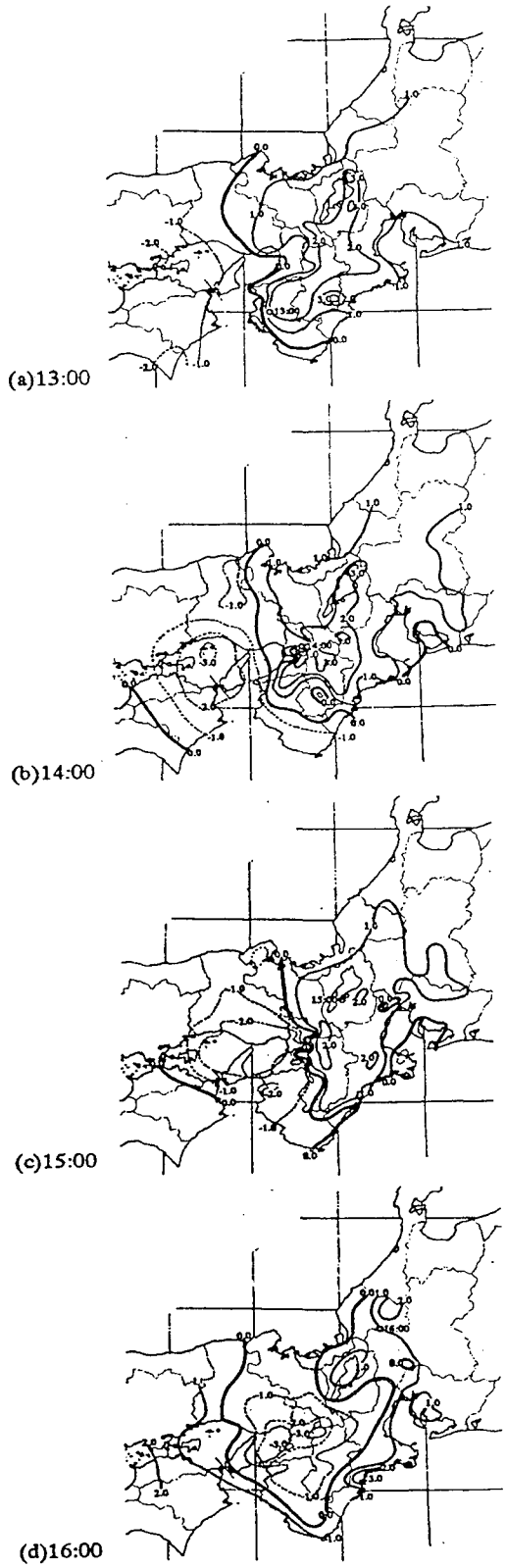

Fig.7 Distribution of temperature difference from daily mean temperature ()
recorded about one hour after the daily minimum atmospheric pressure occurred.

3.4 Situation of Temperature

The distributions of the temperature from 13:00 to 16:00 are shown in Figs.7(a)-(d). The absolute value of temperature can not be compared each other because it depended on the altitude of each observation place. The distribution of the temperature in Fig.7 is showed in the difference from the day average value at each observation point. In the figure shows the position of the atmospheric pressure center of the typhoon at the time that was found from the objective analysis (Fujii et al., 1999).

The cold area spread on the western side around the center of the typhoon when the typhoon hit. From 14:00 to 15:00, this cold area was distributed like a hook from the western side around the center of the typhoon. It can be understood that the cold air entered from the northwestern side into the center of the typhoon. At this time the interval of the isotherm became denser from the southern region of Osaka prefecture to the northern region of Nara prefecture and the temperature inclination in space became very large. In this way, the cold air from the northwestern side of the typhoon found to be brought the rapid decline of the temperature across the border between Osaka and Nara prefecture.

3.5 Situation of Precipitation and Specific Humidity

The distributions of the hourly precipitation from 13:00 to 16:00 are shown in Figs.8(a)-(d). In the figure shows the position of the atmospheric pressure center of the typhoon at the time that was found from the objective analysis (Fujii et al., 1999). As typhoon Vicki approached, the precipitation in the southern region of Kinki district was rapidly increased. From 14:00 to 15:00, the distributions of the precipitation

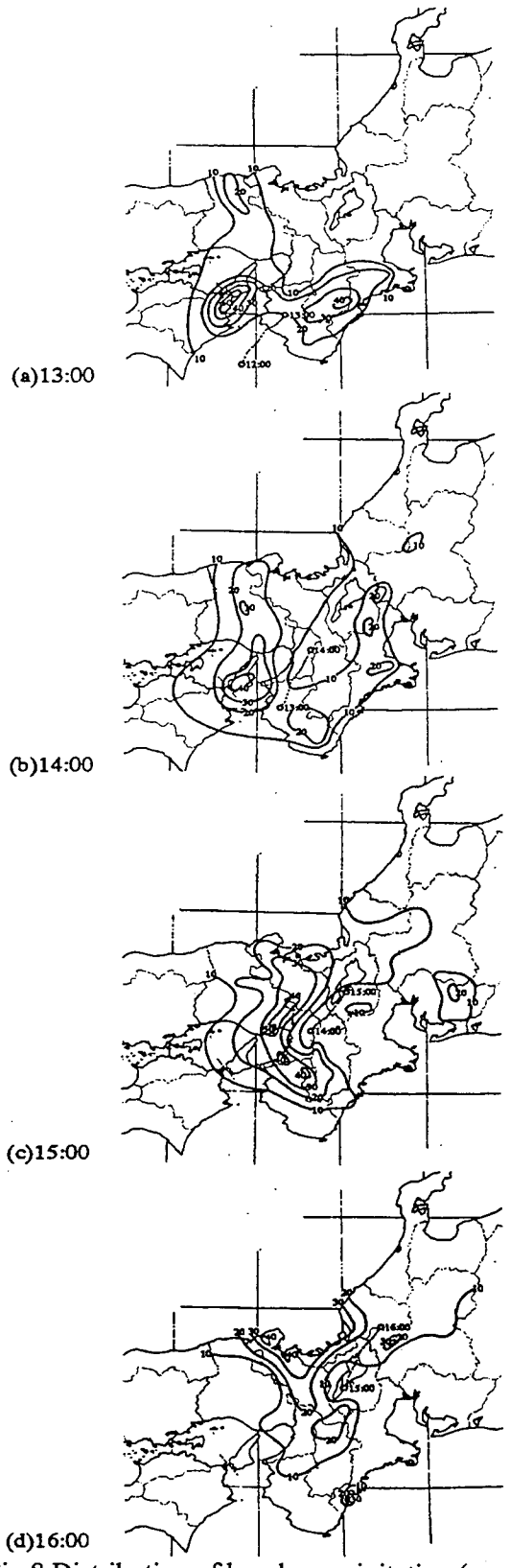

Fig.8 Distribution of hourly precipitation (mm/hr)

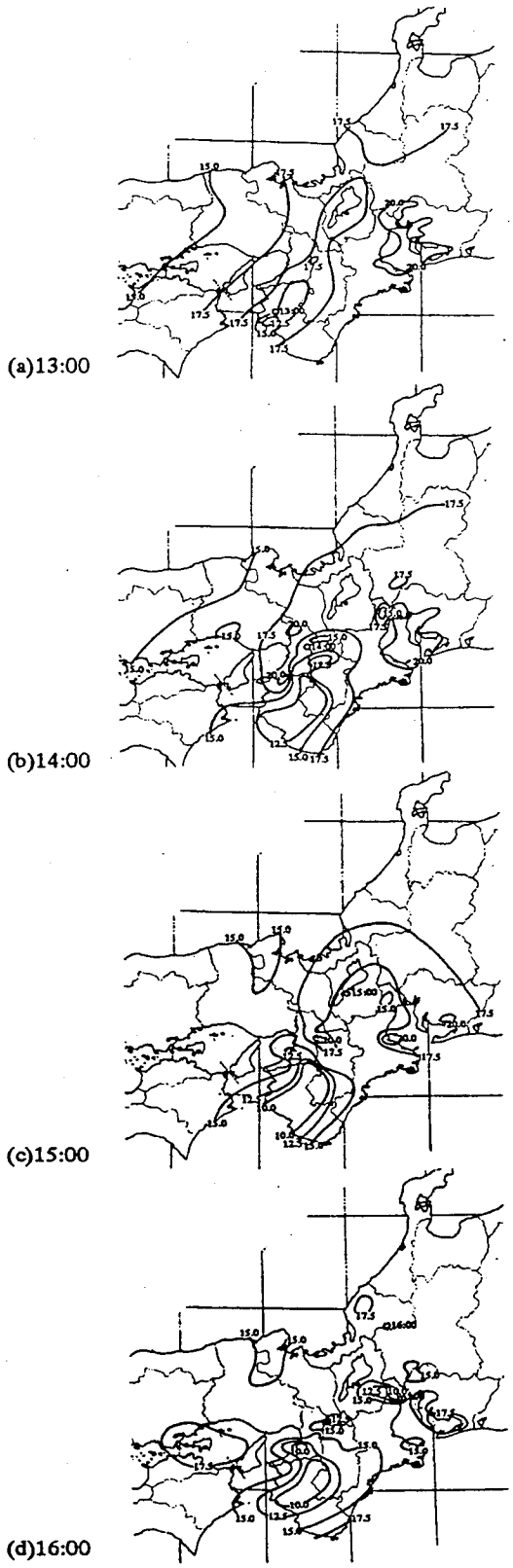

Fig.9 Distribution of specific humidity (g/kg)

became like a hook as the rainfall area surrounded the center of the typhoon from the western side of the typhoon. On the other hand, in the east side of the typhoon, the precipitation was less than several mm and there was the area where it was hardly raining. After that, the rainfall area moved to the northeastern direction with the movement of the typhoon. The distribution shape of a hook became illegible and the precipitation became 0 mm in Kinki district except the northern region.

The distributions of the specific humidity from 13:00 to 16:00 are shown in Figs.9(a)-(d). In the figure shows the position of the atmospheric pressure center of the typhoon at the time that was found from the objective analysis (Fujii et al., 1999). As typhoon Vicki hit Kinki district, the dried air entered into Kii peninsula from the southwestern direction and caught the damped air of the northeastern side and became the distribution like a swirl figure around the eye of the typhoon from 14:00 to 15:00. That the specific humidity exceeded 20g/kg in the border in Wakayama and Osaka prefecture at 14:00 seems to be brought by the rain band which was developed on the western side of the typhoon. On the other hand, the specific humidity in the east side of the typhoon became 10-15g/kg with the dried air flowing in from the southwestern direction of Kinki district.

3.6 Situation of Atmospheric Pressure

Figs.10(a)-(d) are atmospheric pressure distributions from 13:00 to 16:00. The atmospheric pressures observed at the meteorological observatories were the absolute pressures revised at the surface of the sea, but the atmospheric pressures observed at almost fire stations were not revised at the surface of the sea, and also the zero of the barometers in some fire stations was sometimes shifted because they were not given official approval of Meteorological Agency. Therefore, it expressed as the

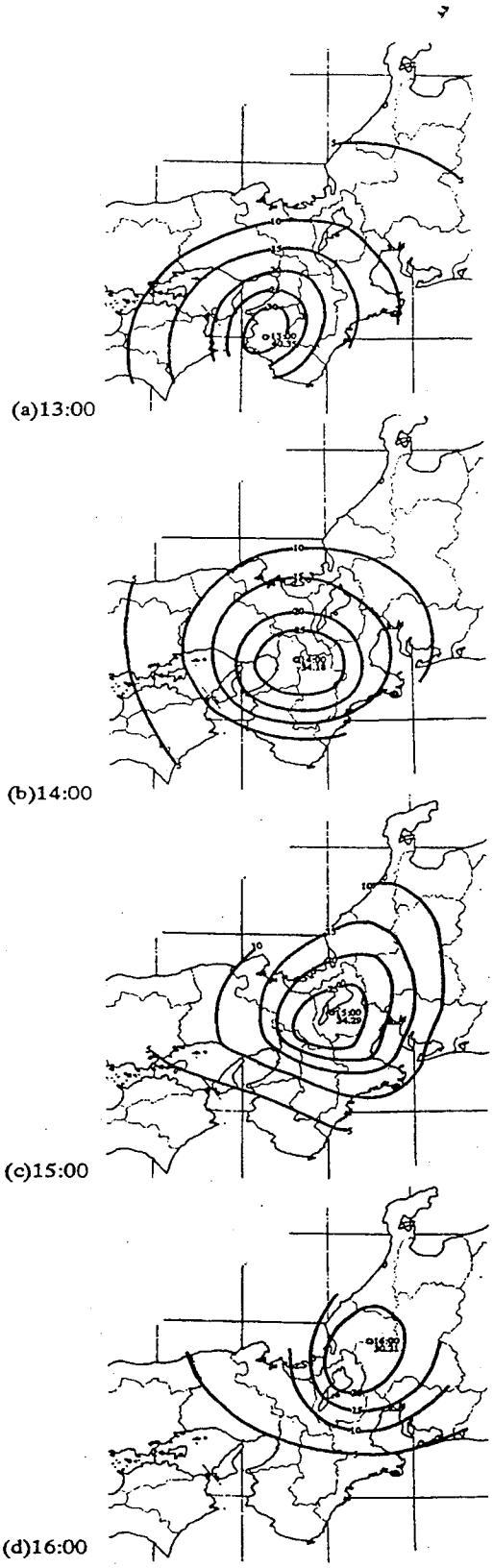

Fig.10 Distribution of differences from maximum atmospheric pressure before daily minimum atmospheric pressure (hPa)

atmospheric pressure difference between the atmospheric pressure at each time and the maximum atmospheric pressure before the passage of the typhoon. In the figure shows the position of the atmospheric pressure center of the typhoon at the time that was found from the objective analysis (Fujii et al., 1999). The shape of the distribution of the atmospheric pressure was almost a circle at 14:00 and an elliptical form at 13:00, 15:00 and16:00.

4. RELATION BETWEEN COMBINED RADAR ECHO AND SEVERE STORM IN KINKI DISTRICT

Figs.11(a)-(p) are the combined radar echo charts by every 7 minutes and 30 seconds from 14:00 to 16:00 and the daily maximum instantaneous wind velocities were displayed as vectors in these figures according to the time when the daily maximum instantaneous wind velocity was recorded in each place. The combined radar echo of 14:45 lacks data. Described in Fig.6, the severe storm area is mainly divided into two areas where the minimum atmosphere pressures and the daily maximum instantaneous wind velocities were recorded at the almost same time and the daily maximum instantaneous wind velocities were recorded about one hour after the minimum atmosphere pressures occurred. The former corresponds to the severe storm area that occurs in the right side of the typhoon whereas the latter is the severe storm area formed behind the center of the typhoon. Yamamoto et al.(1963) reported the severe storms accompanied with the cold front in their report of 2nd Muroto typhoon. This severe storm behind typhoon Vicki is supposed to have the same character as the severe storms observed in 2nd Muroto typhoon. There are some reports of observation (Nakajima et al., 1980 and Fujii et al., 1992) on this severe storm but it seems that there is not detailed observation report yet.

In the combined radar echo chart at 14:00, there is a rain band with strong rainfall on the western side of the typhoon. The severe storms occurred in the direction of the rotation of the typhoon inside the rain band at the both ends of north and south at the rain band. The severe storm in the west-northwest was observed inside the rain band in Sumoto city, Hyogo prefecture at 14:15. The south severe storm was observed by Matsuzaka city, Mie prefecture at the same time but this severe storm occurred in the right side of the typhoon. The west severe storm was also observed in the Wakayama city. This severe storm was observed 6 minutes later after at Sumoto city. These severe storms were observed at Sumoto and Wakayama city inside the same rain band. After that, the severe storm area moved to the northwestern west with the movement of this rain band. At 14:37 the severe storm area moved from the northern region of Wakayama prefecture to the western region of Nara prefecture.

The two severe storms were observed in the south direction in the Nara basin and in west-southwest direction along Yoshino River. The wind at Yoshino River had the direction of the rotation of the typhoon whereas the south wind on the Nara basin became the direction of the normal of the typhoon. The south severe storms occurred to 15:00 across Mt. Kongo located in the border between Osaka and Nara prefecture. The maximum wind velocity was observed 59.5m/s at Shinjo town in Nara prefecture. Only the wind direction at Shinjo town was south-southeast. After that, at 15:07, the almost west severe storms were observed around this rain band from the southern region of Osaka prefecture to the northern region of Nara prefecture. In this way within only 15 minutes from 14:52 to 15:07, the wind direction changed from west to south and from south to west again across Mt. Kongo. The author's field study in Nara prefecture got a lot of testimonies, that at first the south wind blew and

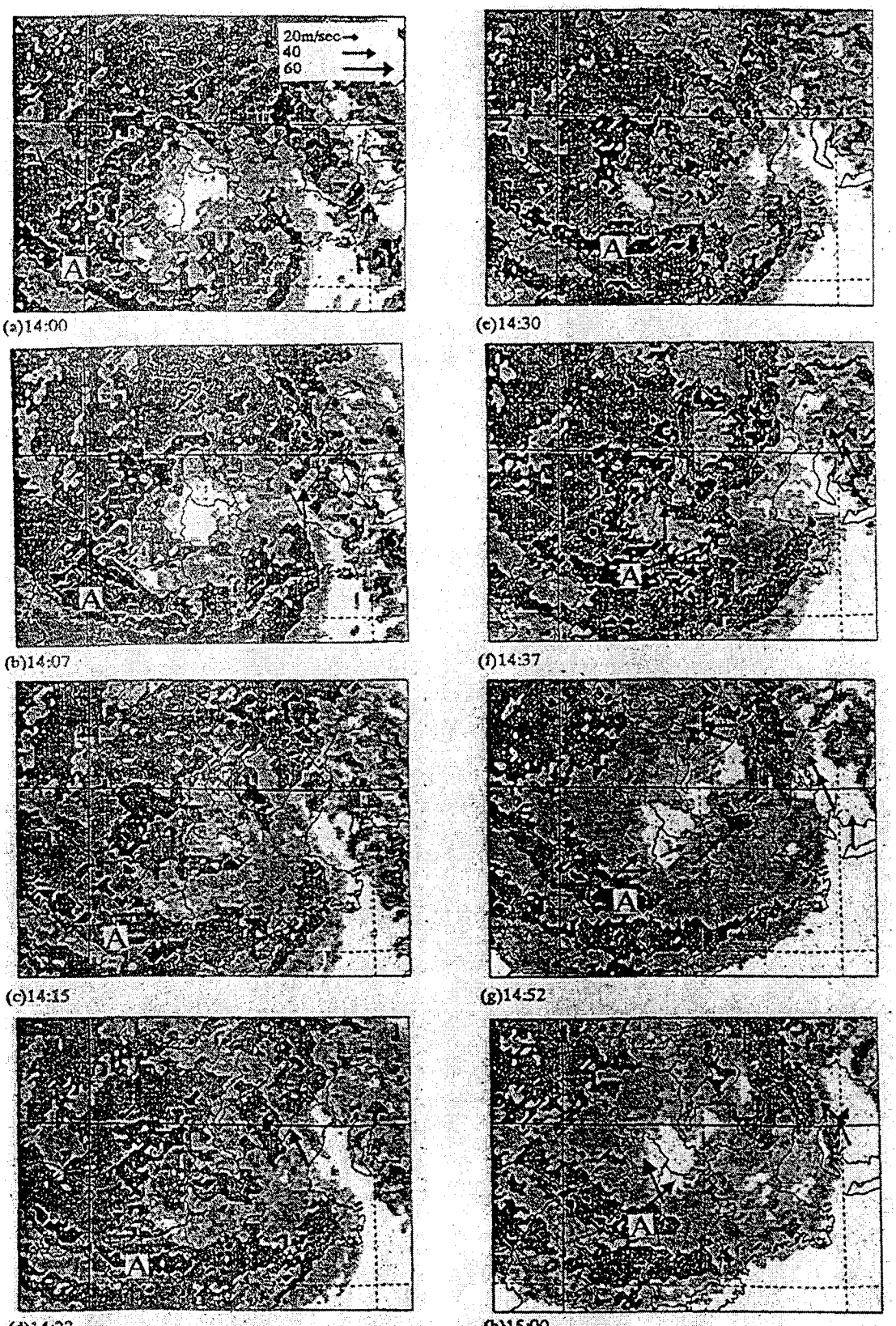

Fig.11 Combined radar echo and daily maximum instantaneous wind vectors

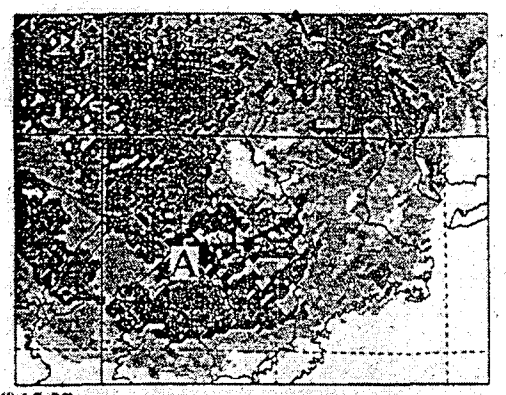

(i)15:07

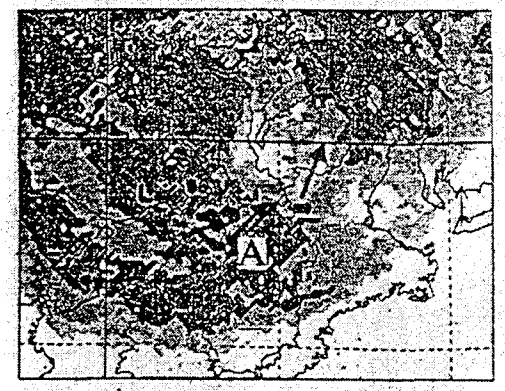

(j)15:15

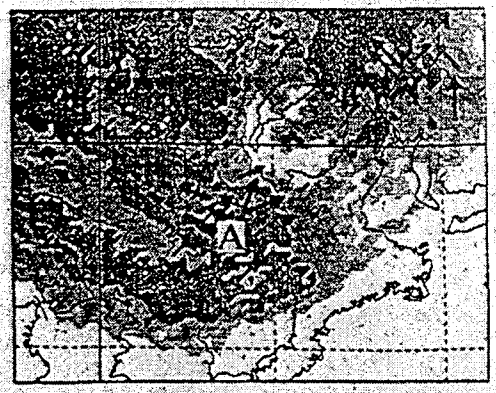

(k)15:22

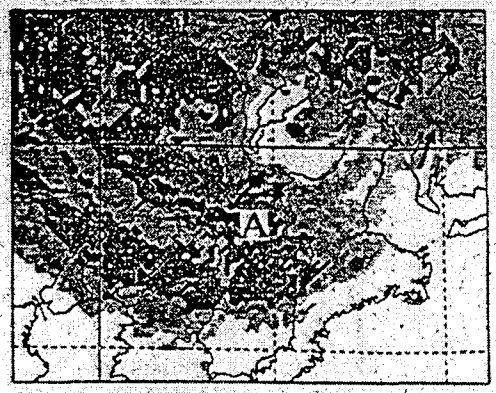

(l)15:30

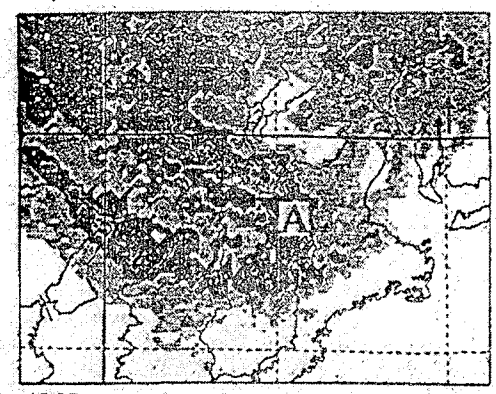

(m)15:37

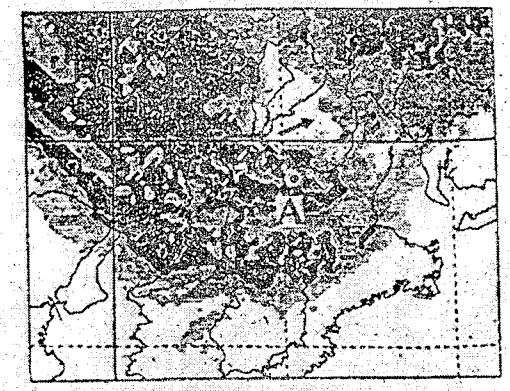

(n)15:45

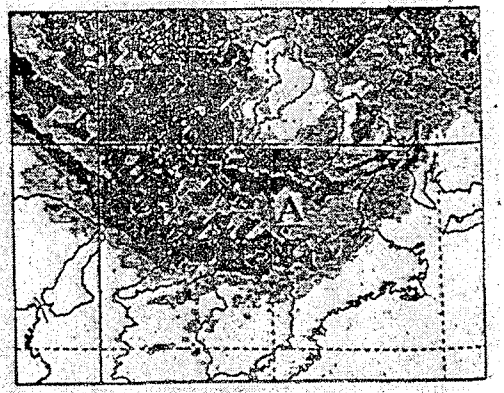

(o)15:52

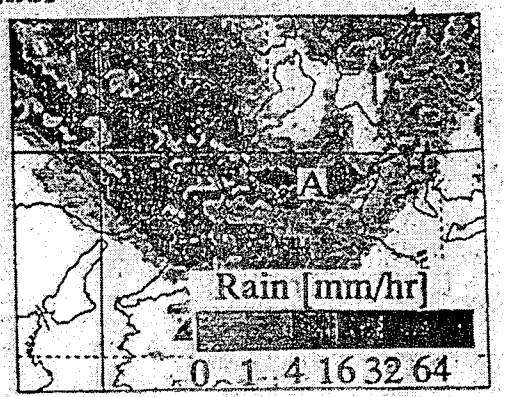

(p)16:00

Fig.11

(continued)

then changed to the west wind, and a lot of evidences of the damages with the west wind in addition to the south wind. It thinks that the severe storm with such the rapid change of the wind direction occurred. This phenomenon seems to be caused by the meteorological factors as well as the geographical features. Comparing with the temperature distributions at 14:00 and 15:00 and these combined radar echo charts, it finds that this rain band was approximately on the 0 degree isotherm on the ground. That is, the severe storm occurred in the neighborhood of the 0 degree isotherm. It thinks that the temperature distributions related to the occurrence of the severe storms.

Sakakibara et al.(1999) showed that the converging shear line existed near the rain band over Nara city from the results of the radar echo observed at Kansai international airport at 15:30. They reported that this converging shear line caused the occurrence of severe storm on the ground. Kawano et al.(1999) observed 3 components of the wind velocity in the typhoon Vicki using MU radar system in Shigaraki town, Shiga prefecture. At 15:53, their observation stopped by the blackout but they observed the strong down stream, 4-5m/s, in the space of 2-3 km high over Shigaraki town. At the same time, the rain band above-mentioned approached over Shigaraki town from the results of the combined radar echo charts. The daily maximum instantaneous wind velocity was observed 36.4m/s at 15:45, in Ritto town and 41.6m/s at 16:16 in Yoka-ichi city in Shiga prefecture. That is, it thinks that there is some causality between this down stream and the severe storm on the ground.

Using the weather observation data at the fire stations, the interesting facts were found about the severe storm behind typhoon Vicki. The weather elements in the sky of the typhoon can be observed quite detailed using the radar echo systems or the meteorological satellite named Himawari. But the weather elements on the ground have been observed only by meteorological observatories or AMeDAS and there have been few amounts of weather information on the ground. However, using the weather observation network at the fire stations in addition to the meteorological observatories and AMeDAS, it is possible to expect that the more detailed weather observation on the ground of the typhoon becomes possible.

5. CONCLUSION

Mainly using the weather observation data at fire stations, it investigated about ground weather elements in typhoon Vicki. The results as follow:

1) It found that the weather observation network at the fire stations were extremely useful because the weather observation network at the fire stations were much closer than the observation network of the meteorological observatories and AMeDAS in the urban region.
2) The three courses of typhoon Vicki on Kinki district was showed meandering. Especially, the wind center and the atmospheric pressure center resembled very well each other.
3) The severe storm area in typhoon Vicki was divided into two areas, which were formed in the right of the typhoon and in the rear of the typhoon. The severe storm of the former was observed in Wakayama prefecture and Aichi prefecture. The severe storm of the latter was observed in the central region of Kinki district and brought enormous damages to each place in Kinki district.
4) The distribution of the temperature showed that the cold air entered into the center of the typhoon from the northwestern side. It was found that the temperature gradient in space became very large near the prefecture border between Osaka and Nara prefecture at 15:00.
5) The distribution of the hourly precipitation showed the rainfall area in typhoon Vicki.
6) The distribution of specific humidity showed that the dried air from the southwestern direction and damped air from the northeastern direction the state flew into the center of the typhoon at 15:00.
7) The shape of typhoon Vicki was often an elliptical form shown by the distribution of the atmospheric pressure.

REFERENCES

Fujii T. et al.(1992): On Analysis of Typhoon 9119 and Distribution of Severe, Annuals of Disaster Prevention Research Institute, Kyoto University, No. 35 B-1, pp.183-191(in Japanese).

Fujii T. et al. (1999): Relation between Wind Velocity Calculated from Atmospheric Pressure Field and Observed Wind Velocity (Part 3)-Analysis of Typhoon Vicki, Annuals of Disaster Prevention Research Institute, Kyoto University, No. 42 B-1 (in Japanese).

Kawano N. et al.(1999): Observation of Typhoon Vicki Used a Method of MU radar, Preprint of annual scientific meetings, Meteorological Society of Japan, pp.223(in Japanese).

Meteorological Agency (1998a): Ground Weather Observation Data, Area Weather Observation Data and Upper-Air Observation Data, Meteorological Agency Monthly Report-September, (in Japanese).

Meteorological Agency (1998b): Heavy Rain and Severe storm by Typhoon No.6, No. 7, No. 8, No. 9 and front from 18th September to 2nd October, Disaster Weather Newsletter

Nakajima C. et al.(1980): On Typhoon 7916, Annuals of Disaster Prevention Research Institute, Kyoto University, No. 23 B-1, pp.87-111(in Japanese).

Sakakibara H. et al(1999): Severe Storm Caused by Typhoon Vicki, Preprint of annual scientific meetings, Meteorological Society of Japan, pp.215(in Japanese).

Shaw N.(1918): The Travel of Circular Depressions and Tornadoes, Meteorological Office, Geophysical Memoirs, No.12, pp.19-44.

Uematsu Y. et al.(1999): Wind Measurements in the Tohoku District (Part 1 Aomori and Akita prefectures), Journal of Wind Engineering, No. 78, pp.81-93 (in Japanese).

Yamamoto R. et al.(1963): On Distribution of Severe Storm of 2nd Muroto Typhoon, Annuals of Disaster Prevention Research Institute, Kyoto University, No. 6, pp.113-127(in Japanese).

Theme 3

Earthquake Engineering

Seismic Testing of a 1/20-Scale 2D Model of Koyna Dam

by

Robert L. Hall[1], Mostafiz R. Chowdhury[1], and Enrique E. Matheu[2]

ABSTRACT

A series of shaking table experiments were proposed as part of the ongoing earthquake engineering research program at the U.S. Army Engineer Research and Development Center (ERDC) as an effective way to provide realistic data for validation of numerical procedures modeling the seismic performance of concrete gravity dams. This paper describes the first experiment of the series, performed on a 1/20-scale model of Koyna Dam. The objective of this experiment was to study the dynamic response characteristics of the model when subjected to a sinusoidal horizontal base excitation acting on the upstream-downstream direction (in-plane or transversal direction). The value of the excitation frequency was selected slightly higher than the first in-plane natural frequency of the model. The amplitude of the excitation was increased for each test run until failure occurred at an excitation level of 0.16g. The model behavior was documented with acceleration, displacement, and strain measurements. The recorded data will provide valuable information for the update and calibration of linear and nonlinear numerical models predicting the seismic response of concrete gravity dams.

KEYWORDS: Concrete dams, scaled model experiments, nonlinear response.

1. INTRODUCTION

The seismic research and development in the area of concrete dams is currently focused on the generation and validation of three-dimensional time-domain analytical procedures to predict the dynamic performance of these critical structures. The main objective of the procedures under development is to capture the most important phenomenological aspects controlling the dynamic performance of the structural system, including detailed representations of the interactions between the subsystems (dam, foundation, reservoir, and sediments) and the nonlinear characteristics of the material behavior. As part of the ongoing earthquake engineering research program at the U.S. Army Engineer Research and Development Center (ERDC), a series of shaking table experiments have been formulated as an effective way to provide realistic data for validation of numerical procedures modeling the seismic performance of concrete gravity dams.

This paper describes the first experiment of the series, performed on a 1/20-scale model of the tallest nonoverflow monolith of Koyna Dam. This 103m high concrete gravity dam is one of the few concrete dams to have experienced significant damage induced by seismic ground motions. The dam is located on the Koyna River in the western side of India, and it was completed in 1963. The structure is comprised of 56 monoliths, about 15.24m wide each (Saini et al., 1972). The 1967 Koyna earthquake, with magnitude of 6.5 and epicenter in the immediate vicinity of the dam, caused significant structural damage, including horizontal cracks on the upstream and downstream faces of a number of nonoverflow monoliths around the elevation at which the slope of the downstream face changes abruptly. The overflow monoliths were not damaged. The earthquake was recorded on a strong motion accelerograph located in a gallery of the dam. Although the structure did not appear to be in danger of imminent catastrophic failure, the damage induced by the earthquake was serious enough to require permanent strengthening by adding concrete buttresses on the downstream face of the nonoverflow monoliths (Chopra, 1978).

[1] Structures Laboratory, U.S. Army Engineer Research and Development Center, Vicksburg, MS 39180 (USA).
[2] Department of Civil and Environmental Engineering, Louisiana State University, Baton Rouge, LA 70803 (USA).

The historic performance of Koyna Dam and the special characteristics of its cross section have resulted in this structure being a classical problem for experimental studies and for the validation of numerical procedures for predicting the seismic response of concrete gravity dams. Previous tests performed by the U.S. Army Corps of Engineers, the University of California at Berkeley, and the Bureau of Reclamation can be cited among the experimental studies performed in the U.S. which were based on scale models of Koyna Dam. These tests are discussed briefly in the following.

A comprehensive series of experimental tests involving a scale model of this gravity dam were performed at the University of California at Berkeley (Niwa and Clough, 1980). An extensive testing program was carried out to obtain an appropriate material mix that would allow the reduced-scale investigation of the nonlinear response and failure characteristics of concrete dams. A mix based on casting plaster, celite, sand, lead power and water was adopted for the model representing a monolith of Koyna Dam at a 1/150 scale. The lead power was added to approximate the density of the prototype material. The strength characteristics of the mix were adequate but the resulting elastic modulus was significantly higher than the assumed prototype value. The presence of the reservoir was incorporated in the model by using a rectangular tank filled with water. The first natural frequency of the model under empty conditions was determined to be about 43 Hz (3.51 Hz, prototype scale). This value is higher than the values usually obtained in numerical studies because of the increased elastic modulus. The original idea was to test the model using a scaled version of the Koyna record. However, it was determined that the dynamic characteristics of the shaking table would result in attenuation of motion components for frequencies above 16 Hz. Therefore, because of these equipment limitations, an artificial harmonic excitation was used in the dynamic tests. The amplitude of the peak table acceleration varied from 0.075g to 1.21g. During the 1.21g-level test, a crack formed at the elevation corresponding to the downstream slope change and it propagated completely through the section. After cracking, the upper part of the model subsequently engaged in a rocking motion characterized by large crest displacements.

Another series of dynamic tests were performed on a 1/60-scale model of Koyna Dam at the facilities of the U. S. Army Engineer Waterways Experiment Station (Norman, 1986). The material properties were not scaled, and the main objective of these tests was to investigate the failure characteristics of a geometric model constructed of standard low strength concrete. The presence of the reservoir was not considered in these experiments. Forced vibration tests were conducted to determine natural frequencies and mode shapes. The first two natural frequencies were identified at about 3.43 Hz and 7.55 Hz (prototype scale). The dynamic failure tests were performed by inducing the motion of the foundation block through the impact of a moving mass. The foundation block was placed on top of a smooth sliding surface, and it was connected to a reaction wall through a multi-spring system. During the base excitation test, a crack immediately formed at the elevation corresponding to the downstream slope change. Unfortunately, many of the sensors went off-range during the test, and most of the conclusions were of a qualitative nature.

The Bureau of Reclamation recently performed a series of shaking table experiments on a 1/50-scale model of Koyna Dam (Harris et al., 1999). The presence of the reservoir was not included in the modeling. A mix based on cement, bentonite, sand, gravel and water was designed to satisfy the similitude requirements. An advantage of this mix is that it did not rely on lead products to achieve the similitude requirements regarding unit weight. Two models were built and tested. The first model was cast horizontally and lifted onto the table after 28 days. This model developed a shrinkage crack along a cross section at about the middle of the height. The second model was cast upright and tested at an earlier age to avoid the cracking experienced in the first model. Both models were tested using a 14 Hz (1.98 Hz at prototype

scale) sinusoidal excitation whose amplitude was gradually increased until failure. This excitation frequency was well below the first natural frequency associated with the in-plane or transversal response of the models, which was about 24 Hz (3.39 Hz, prototype scale). The test runs performed on the first model exhibited the expected nonlinear behavior caused by the initially cracked condition. The tests on the second model showed the abrupt development of a crack pattern that eventually caused the separation of the top section of the model. It was observed that these results were influenced by the failure of the foundation of the model, which created a boundary condition difficult to represent in numerical models.

This paper describes a new series of shaking table experiments performed on a 1/20-scale model of Koyna Dam. A diverse team of engineers and scientist from different ERDC Laboratories collaborated in the completion of these experiments. The special material mix used for the model was developed at the ERDC Structures Laboratory (Vicksburg, Mississippi), which had the project lead responsibilities. The tests were carried out using the Triaxial Earthquake and Shock Simulator (TESS) at the ERDC Construction Engineering and Research Laboratory (Champaign, Illinois). A series of tests were conducted to record the natural dynamic characteristics as well as the controlled forced response of the instrumented Koyna dam model when subjected to a sinusoidal horizontal base excitation acting on the upstream-downstream direction (in-plane or transversal direction). The frequency of the sinusoidal excitation was selected slightly higher (14 Hz) than the first in-plane natural frequency of the model. Peak support accelerations were varied from 0.005 to 0.16 g, level at which failure occurred. This type of sinusoidal input was used to ensure that the model response would be dominated by motions associated with the first mode of vibration in the in-plane direction. The recorded data included the input and output motions including acceleration, strain, and linear variable differential transducer (LVDT) time-histories.

2. MODEL DESCRIPTION

The purpose of small-scale modeling is to study the response of the structural system (prototype) by reproducing its behavior using a reduced size version of the structure that satisfies the constraints imposed by the equipment available or the laboratory conditions. In order for the model to reproduce meaningfully the behavior of the prototype, it is necessary the satisfaction of a set of similitude requirements relating the physical and time scales of the model along with the corresponding material parameters. The number of these similitude constraints depends on the nature and characteristics of the problem.

Let us define a generic scaling factor as follows:

$$\lambda_\alpha = \frac{\alpha_{prototype}}{\alpha_{model}}$$

where α represents any variable of the problem. In general, if a number of "basic" scaling factors is predetermined, then the remaining scaling factors can be determined by dimensional analysis. The number of basic scaling factors corresponds to number of similitude requirements, that is, the minimum number of independent constraints that must be satisfied to guarantee the proper representation of the problem at the model scale. For this case, the scaling factors corresponding to geometry (length), modulus of elasticity and density are adopted as the basic scaling factors. They are denoted by λ_L, λ_E, and λ_ρ, respectively. The scaling factors corresponding to the remaining physical variables of the problem can be written in terms of these factors as indicated in Table 1. The table shows the particular case in which the density of the model material is kept the same as the density of the prototype material while the geometry and strength variables are subjected to the same scaling. For this case, all the scaling factors can be written in terms of the scaling factor defining the geometry. This was the scaling strategy adopted for this experiment, based on a 1/20-scale model ($\lambda_L = 20$).

Table 1. Scaling relationships

Variable	Scaling factors
	$\lambda_L = \lambda_E, \lambda_\rho = 1$
Time	$\lambda_t = \sqrt{\lambda_L}$
Frequency	$\lambda_f = \frac{1}{\sqrt{\lambda_L}}$
Force	$\lambda_F = \lambda_L^3$
Stress	$\lambda_\sigma = \lambda_L$
Strain	$\lambda_\varepsilon = 1$
Displacement	$\lambda_u = \lambda_L$
Velocity	$\lambda_{\dot{u}} = \sqrt{\lambda_L}$
Acceleration	$\lambda_{\ddot{u}} = 1$

The corresponding model at the 1/20 scale is shown in Figure 1, with a height of 5.15m. It can be noticed the abrupt change of slope on the downstream face, at an elevation of 3.32m with respect to the base level. The maximum dimension at the base of the model is 3.51m. According to the selected geometric scale, the model width should be 0.76m. However, this could have resulted in a very weak model with respect to the out-of-plane direction. Although the test was designed to investigate only the in-plane or transversal behavior of the monolith, small variations in geometry, material properties or actual test conditions could induce the undesirable excitation of the out-of-plane response of such a slender structure. Since the model was deprived of the beneficial restraining effect of the adjoining monoliths present in the real structure, there was some concern about the possibility of failure occurring in this unnatural mode. It was decided therefore to investigate the feasibility of wider models, stronger in the out-of-plane direction. Finite element analyses were performed on three-dimensional models of the monolith at a 1/20 scale. The objective of these analyses was to determine the influence of the width on the free vibration characteristics of the model. The material properties used were as follows: unit weight, 23.57 kN/m3; modulus of elasticity, 1.379 GPa; Poisson's ratio, 0.20. Figure 2 shows the variation of the first two natural frequencies as a function of the width of the model. The fundamental frequency associated with the out-of-plane response increases with the width, starting at 5.52 Hz for the 0.76-m wide model. The first natural frequency associated with in-plane response (transverse bending) is practically not affected by changes in the out-of-plane geometry, and it has a constant value of about 13.68 Hz. It is clear that the slender model shows the advantage of two well-separated natural frequencies, taking into account that the model would be tested using a sinusoidal excitation with a frequency close to that of the fundamental in-plane mode. However, there were some concerns about the inherent weakness of this thin structure. Note that if the width is increased to produce a stronger section, the separation between these two natural frequencies decrease. A compromise solution was adopted for the model width, whose value was selected to be two times the original width, i. e., 1.52 m.

3. MIX DESIGN

A material mix was developed at the ERDC Structures Laboratory to satisfy the similitude requirements. The resulting material should exhibit a density equal to that of the prototype material, while the strength and modulus should be 1/20 of the corresponding prototype values. Note that the density requirement translates into unity scaling for the unit weight. Table 2 lists the material properties assumed for the prototype material, and the corresponding target values for the model material.

Table 2. Material properties

Property	Prototype	Model
Unit weight	23.57 kN/m^3	23.57 kN/m^3
Modulus of elasticity	27.58 GPa	1.379 GPa
Compressive strength	27.58 MPa	1.379 MPa
Tensile strength	2.76 MPa	0.138 MPa
Poisson's ratio	0.20	0.20

Several trail mixes were tested in the laboratory in order to design a material mix that exhibited

reduced strength and elastic modulus while keeping the values of density and ultimate compressive strain close to those considered standard for normal concrete. The resulting mix was a very fluid paste, characterized by a water-cement ratio of 2.95, which was intended to produce a low strength material. The main aggregate of the mix was barite powder, which is a material with a high specific gravity and it was added to control the value of the unit weight. A small amount of plastic fibers was also incorporated in the mix to improve the ductility and deformation characteristics of the material. Table 3 shows the composition of the final laboratory mix.

Table 3. Mix composition

Material	Specific Gravity	Volume (1 m^3)
Cement	3.15	0.0536
Natural concrete sand	2.56	0.0833
Barite	4.25	0.3501
Plastic fibers	0.91	0.0050
Water	1.00	0.4980

The mix was commercially ordered and supplied, and the material was batched in ready-mix trucks. Standard control procedures were followed to ensure the quality of the material, and laboratory testing was performed on test cylinders and beams. The average values of the material properties corresponding to the specimens tested at an age of 28 days are shown in Table 4. The resulting material was stronger than the original laboratory mix, and it exhibited a compressive strength 1.7 times the original target value. The flexural modulus of elasticity, obtained from third-point loading testing on beam specimens, was about 2.4 times the target value. Note also that the ratio between the splitting tensile strength and the compressive strength is 0.12, which is close to the normal value for the same ratio in standard low-strength concrete.

After casting, the material showed significant settlement, and the amount of bleeding was higher than anticipated from the laboratory material tests. The significant bleeding caused the model to be slightly shorter than the original design.

Table 4. 28-day material test results

Property	28-day value
Unit weight	24.33 kN/m^3
Modulus of elasticity (flexural)	0.329 GPa
Compressive strength	2.38 MPa
Tensile strength	0.29 MPa
Modulus of rupture	0.69 MPa

Several drilled core samples were taken from the model after the completion of the dynamic tests. The cylindrical core specimens were obtained from the material near the critical section (elevation corresponding to the downstream slope change) and near the base of the model. The samples were taken from these two different locations in order to quantify the variation of material properties along the height of the model. The core specimens were tested at an age of 115 days, and the results of the corresponding tests are shown in Table 5.

Table 5. 115-day material core tests

Property	a) Base	b) Critical section
Unit weight	23.28 kN/m^3	19.56 kN/m^3
Modulus of elasticity	3.447 GPa	1.379 GPa
Compressive strength	4.60 MPa	1.07 MPa
Tensile strength	0.60 MPa	n/a

It is clear that the properties of the material were not homogeneously distributed along the height. The material near the base showed strength and elastic modulus values that were significantly higher than those predicted from the previous laboratory tests. On the other hand, the material near the critical location was characterized by reduced density and strength values. Visual inspection also confirmed the inhomogeneous characteristics of the material. In particular, the fiber content seemed to be abnormally low in those specimens taken from the region near the critical section. A possible explanation for these

results could be based on the exaggerated settlement of heavier solid particles that trapped the fibers forcing them to migrate towards the base of the model. This phenomenon could have been fueled by the fact that the barite aggregate used for the model was obtained from a different provider than the one used for the laboratory mix in the design phase.

The dam model was anchored to the shaking table by means of a reinforced concrete base beam with a height of 0.46m and with reinforcing steel that extended 0.61m inside the model. Instrumentation included accelerometers, strain gauges, and linear variable differential transducers (LVDTs) installed on the model surface for a total of 56 data channels. Accelerometers were attached to the base beam to characterize the input motions at the base of the model. Accelerometers were also installed along the height of the upstream face in a 3-column pattern, to check for any undesired torsional response. Strain gauges and LVDTs were installed near the expected location for crack initiation, at the change of slope along the downstream face.

4. SHAKING TABLE TESTS

Modal tests: Prior to conducting any tests using the shaking table to excite the model, modal tests were conducted using an electrostatic shaker attached to the upstream face of the dam model. The model response was recorded using a scanning laser vibrometer system. The vibrometer was located directly in front of the upstream face, with the laser head positioned at the average elevation of the model upstream surface. The response to the random excitation provided by the shaker was recorded by scanning the upstream face of the model according to a predetermined grid pattern. From these tests, the first two natural frequencies in the in-plane direction were measured at 13.4 and 34.4 Hz, respectively. The values of the corresponding damping ratios were identified as 5.5 and 2.5%, respectively.

Sine-sweep tests: A series of sine-sweep tests were performed using the shaking table to determine the in-plane vibration characteristics of the model. These tests began a frequency of 4 Hz and swept up to 64 Hz (4 octaves) at a rate of 5 seconds per octave, with the exception of the third test of the series that was conducted at a slower rate of 10 seconds per octave. The tests began at a low excitation level, which was gradually increased until the model was sufficiently excited to record modal parameters with good data resolution. The test at the slower sweep rate provided the cleanest signals and it was used to estimate the model natural frequencies. A transfer function was computed between the horizontal components of table acceleration and model crest acceleration. Figure 3 shows the resulting transfer function. The natural frequencies corresponding to the first and second in-plane vibration modes can be estimated from the magnitude peaks as 12.7 and 37.0 Hz, respectively.

Koyna time-history test: Before the sinusoidal tests, the Koyna model was tested using as input a scaled version of the transversal component of the 1967 earthquake. The peak acceleration corresponding to the original record was about 0.38g. To avoid inducing any damage to the model, the amplitude of the acceleration record was scaled down to 0.027g. Figure 4 shows the resulting input motion. The variation of the peak values of absolute acceleration response along the upstream face is summarized in Table 6, in which the elevation of each sensor is defined in terms of the total height H of the model. The accelerometer A9x, located along the upstream-face centerline, did not work properly, and therefore the acceleration at the corresponding elevation is reported in terms of A14x, located at the same elevation but close to a lateral face.

Table 6. Peak absolute acceleration values

Sensor	Elevation	Koyna	Sine5
A7x	1.5% H	0.027g	0.136g
A8x	25.7% H	0.049g	0.214g
A14x	65.4% H	0.073g	0.568g
A10x	98.5% H	0.204g	1.131g

Sinusoidal tests: The model was tested to failure with sinusoidal motions with a frequency of 14 Hz. This value was selected slightly above the fundamental in-plane natural frequency. This was done to avoid the possibility of a complete resonant condition arising from a shift of the fundamental frequency induced by damage. Each of the sinusoidal support motions ramped up to the maximum amplitude level in 1 second, maintained this level for 5 seconds, and then ramped down to zero in 1 second, for a total duration of 7 seconds. The series of sinusoidal tests began at very low amplitude levels (0.005 g for the first test in the series). Test levels were gradually increased, and the response of the model remained essentially linear up through the fifth test in the series (Sine5), with maximum amplitude of 0.12g. Figure 5 shows the time history of the base-beam horizontal acceleration corresponding to this test. Figure 6 shows the time history of the acceleration at the top of the model, measured on the upstream face. Figure 7 shows a particular strain time history near the critical location, recorded by a strain gauge located 2.5 cm above the change of slope along the downstream face. The peak acceleration profile is summarized in the last column of Table 6.

The last test in the series (Sine6), with maximum amplitude of 0.16g, induced the first nonlinear response and led to the ultimate failure of the model. Figure 8 shows the time history of the crest acceleration. Figure 9 depicts the strain history at the critical downstream location, indicating the initiation of tensile cracking at approximately 1.27 seconds. According to the other measurements near the critical location, the crack affected completely the downstream face during the next two response cycles (at 1.41 seconds). This primary crack propagated to the upstream face at 1.52 seconds, at an inclined angle, consistent with previous experimental observations. Figure 10 shows detailed views of the damaged area.

5. CONCLUSIONS

A systematic validation and updating of an analytical finite-element model using benchmark experimental data is essential for the development of representative, reliable, and credible virtual tools predicting the response of physical structures. In spite of considerable research efforts towards modeling the dynamic response of large concrete dams, only a limited number of well-documented correlation studies using experimental data are available.

This study was based on a large 1/20-scale model that was developed to minimize the modeling distortions usually associated with small-scale models. A new concrete mix consisting of cement, plastic fibers, barite, sand, and water was designed based on the governing scaling relationships. The dynamic behavior of the model was extensively documented. The model failed exactly as predicted by the field observations, with a crack beginning at the change in slope on its downstream face. The recorded data will provide valuable information for the calibration of numerical models predicting the seismic response of concrete gravity dams.

6. ACKNOWLEDGEMENTS

This work was sponsored by the Direct–Allotted Civil Works Earthquake Engineering Research Program of the U.S. Army Engineer Research and Development Center in Vicksburg, Mississippi. The authors appreciate the cooperation of the authorities at the U.S. Army Engineer Research and Development Center, which permitted the presentation and presentation of this study. Permission to publish this paper was granted by the Chief of Engineers, U.S. Army Corps of Engineers.

7. REFERENCES

Saini, S. S., Krishna, J., and Chandrasekaran, A. R. (1972). "Behavior of Koyna Dam – Dec. 11, 1967 Earthquake," Journal of the Structural Division, ASCE, Vol. 98, No. 7.

Chopra, A. K. and Chakrabarti, P. (1971). "The Koyna Earthquake of December 11, 1967 and the Performance of Koyna Dam," Report No. EERC 71-1, Earthquake Engineering Research

Center, University of California at Berkeley, CA.

Chopra, A. K. and Chakrabarti, P. (1973). "The Koyna Earthquake and the Damage to Koyna Dam," Bulletin of the Seismological Society of America, Vol. 63, No. 2, pp. 381-397.

Chopra, A. K. (1978). "Earthquake Resistant Design of Concrete Gravity Dams," Journal of the Structural Division, ASCE, Vol. 104, No. ST6, pp. 953-971.

Hall, J. F. (1988). "The Dynamic and Earthquake Behavior of Concrete Dams: Review of Experimental Behavior and Observational Evidence," Soil Dynamics and Earthquake Engineering, Vol. 7, No. 2, pp. 58-121.

Norman, C. D. (1986). "Dynamic Failure Tests and Analysis of a Model Concrete Dam," Technical Report SL-86-33, Structures Laboratory, USAE Waterways Experiment Station, Vicksburg, MS.

Harris, D. W., Snorteland, N., Dolen T., and Travers, F. (1999). "Shaking Table 2-D Models of a Concrete Gravity Dam for Computer Code Validation," Report DSO-98-13, Bureau of Reclamation, Dam Safety Office, Denver, CO.

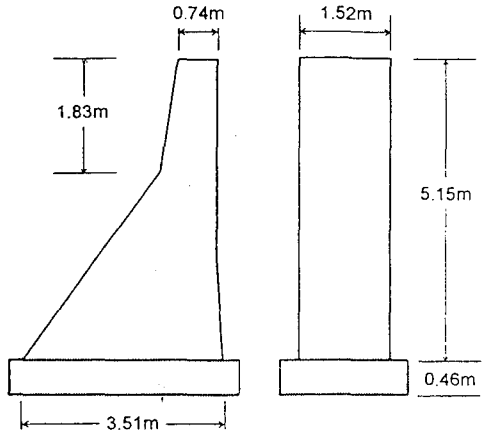

Figure 1. Model

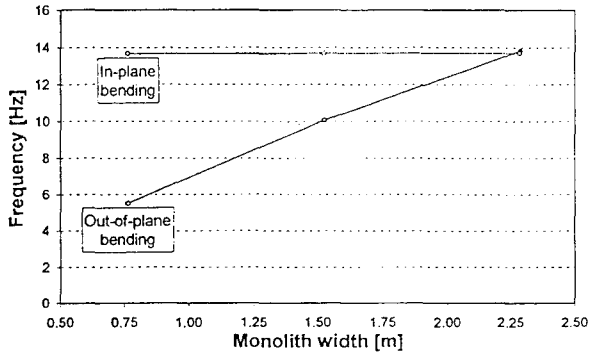

Figure 2. Variation of model frequencies

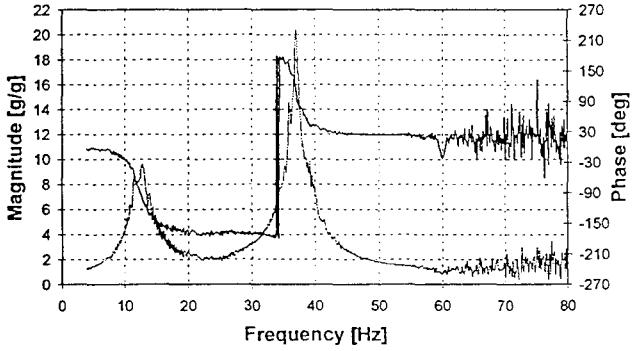

Figure 3. Transfer function

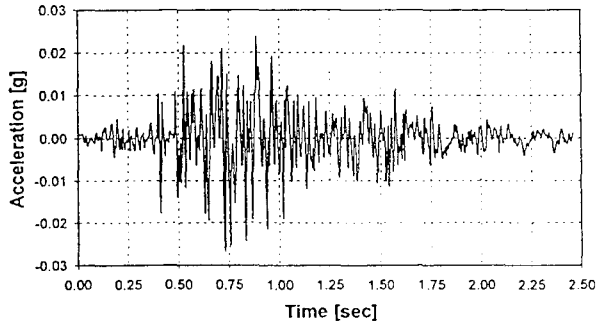

Figure 4. Koyna scaled record

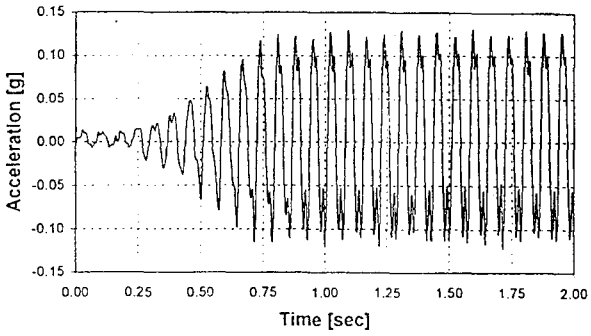

Figure 5. Base beam acceleration (Sine5)

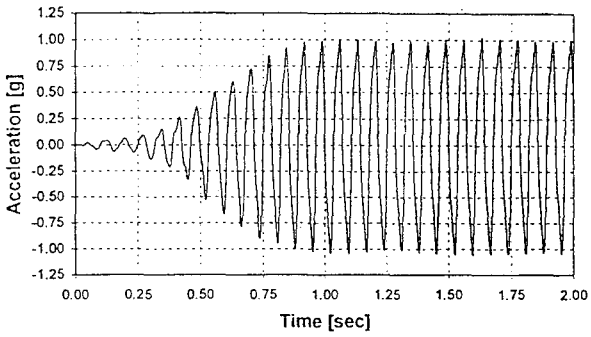

Figure 6. Crest acceleration (Sine5)

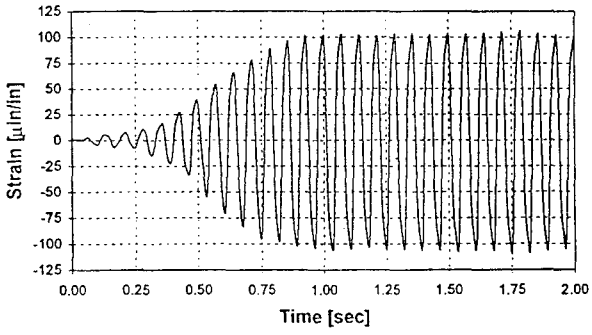

Figure 7. Critical strain (Sine5)

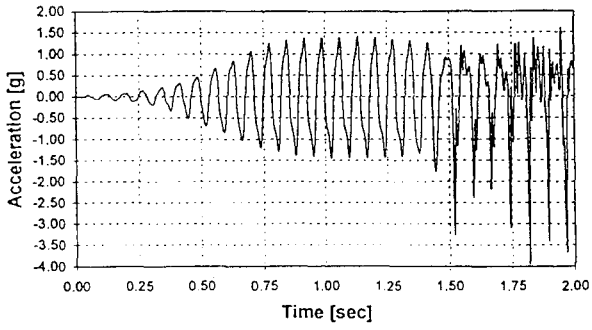

Figure 8. Crest acceleration (Sine6)

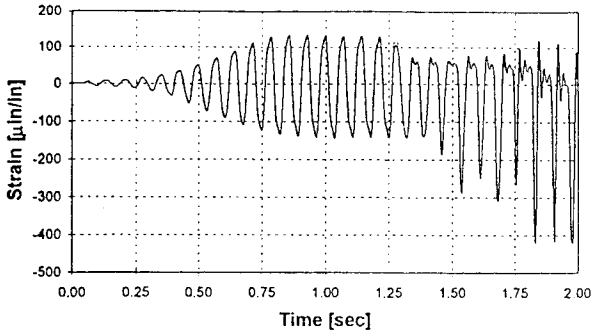

Figure 9. Critical strain (Sine6)

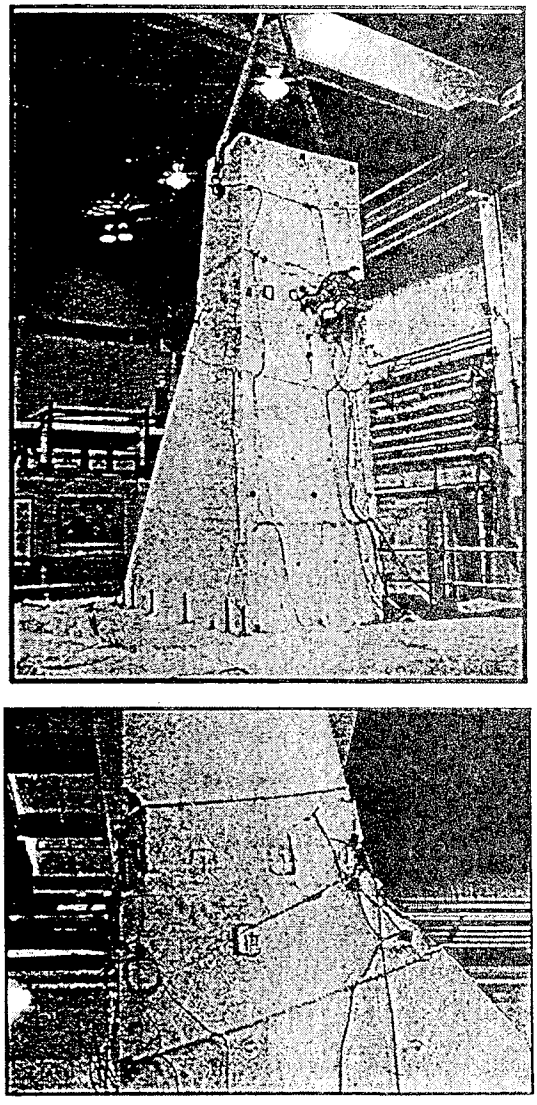

Figure 10. Damage after failure (Sine6)

Development of Smart Systems for Building Structures

by

Shunsuke OTANI [a], Hisahiro HIRAISHI [b], Mitumasa MIDORIKAWA [b],

Masaomi TESHIGAWARA [b], Hideo FUJITANI [b], Taiki SAITO [b]

ABSTRACT

Building Research Institute, Japanese Ministry of Construction, initiated a 5-year research and development project of "Smart Materials and Structural Systems" in 1998 as a part of U.S.-Japan cooperative research efforts. The U.S. Counterpart is the National Science Foundation. Smart Structural Systems (also called as Autoadaptive Media) are defined as systems that can automatically adjust structural characteristics, in response to the change in external disturbance and environments, toward structural safety and serviceability as well as the extension of structural service life. The research and development of (1) concept and performance evaluation of smart structure system, (2) sensing of structure performance, and (3) development and evaluation of structural elements using smart materials will be conducted.

Keywords: Smart Materials, Smart Structural Systems, Autoadaptive Media, Sensing Technology

1. INTRODUCTION

A conventional structural system is designed to achieve a set of intended functions under pre-selected loads and forces. Such a conventional system can not successfully develop its ability against unexpected loads and forces unless a large safety factor is provided for safety limit states to take into account various uncertainties in load and force amplitudes and structural response. Furthermore, since seismic design requirements have been improved after each lessons learned through past earthquake disasters, the safety level of old buildings are always inferior to new buildings as evidenced in many past earthquake disasters, e.g., the 1995 the Great Hanshin-Awaji earthquake disaster. Strengthening or removal of those old buildings becomes necessary to protect societal welfare.

Smart Structural Systems are defined as structural systems with a certain-level of autonomy relying on the embedded functions of sensors, actuators and processors, that can automatically adjust structural characteristics, in response to the change in external disturbance and environments, toward structural safety and serviceability as well as the extension of structural service life.

The Building Research Institute (BRI), Ministry of Construction, Japan and the U.S. National Science Foundation (NSF) initiated the U.S.-Japan Cooperative Research Program on Autoadaptive Media (Smart Structural Systems) in 1998, under the aegis of the U.S.-Japan Panel on Wind and Seismic Effects of the U.S.-Japan Cooperative Program in Natural Resources. The First Joint Technical Coordinating Committee (JTCC) Meeting was held in Tsukuba, Japan, from January 6 through 8, 2000. At the meeting, research items and plans are discussed in detail corresponding to three research thrusts: (1) structural systems, (2) sensing and monitoring technology, and (3) effector technology.

This paper described the research items and plans of the research program in Japan based on the recommendations summarized at the JTCC meeting. To achieve research objectives, following three sub-committees have been formed under Technical Coordinating

[a] Department of Architecture, University of Tokyo, Tokyo, Japan

[b] Building Research Institute, Ministry of Construction, Tsukuba 305-0802, Japan

Committee of the project, chaired by Prof. S. Otani, University of Tokyo:

"Sub-committee on structural systems" chaired by Prof. A. Wada, Tokyo Institute of Technology,

"Sub-committee on sensing and monitoring technology" chaired by Prof. Y. Kitagawa, Hiroshima University,

"Sub-committee on effector technology" chaired by Prof. T. Fujita, Institute of Industrial Science, University of Tokyo.

2. CONCEPT OF SMART STRUCTURAL SYSTEMS FOR BUILDINGS

The concept of smart structural system was initially proposed in the field of aerospace engineering, however, structural systems for building engineering have different features from those for aerospace engineering as shown in Table 1. The value of a building should be determined not only by structural safety but also taking into account non-engineering points of view such as "beauty", "economy", and "function." Therefore, in the first stage of research project, the objectives and needs of smart structural systems for building engineering should be clarified. Table 2 summarizes the research needs of a smart structural system for buildings.

Based on the conceptual study of smart structural systems for buildings, the following items are selected as research targets for the sub-committee on structural systems (chaired by Prof. A. Wada, Tokyo Institute of Technology).

(a) Autoadaptive structural systems

Proposal of feasible structural systems with autoadaptive features

Integration of smart materials or devices / members to achieve target performance of structural systems

Investigation of the proposed structural systems by computer or experimental simulations

Establishment of performance evaluation guidelines for structural systems with autoadaptive features

(b) Reinforced Concrete (RC) structural systems with damage fuses

Examination of performance based design/ assessment methods

Selection of damage-control devices and damage-sensor systems

Development of performance based design/ assessment methods

Development of repairing/ replacing techniques for damage-control devices and damage-sensor systems

(c) Innovative life safety systems

Survey of causes of collapse of traditional light construction

Proposal of innovative life safety systems for traditional light construction

Investigation of proposed systems* by computer and experimental simulations

Establishment of performance guidelines for life safety systems in traditional light construction

* such as using aluminum alloy window frames, reinforced sliding doors, the air-bag system and support frame systems.

3. SENSING AND MONITORING TECHNOLOGIES

3.1. Objectives

The purpose is to identify research needs for developing new sensing systems, which consist of advanced sensors and procedures for data collection, management, and interpretation. Research is needed to develop new types of sensors and obtain information about the long-term viability of the sensors. The sensor is one part of smart building structures, which include sensors, effectors, and processors.

Highly-reliable monitoring systems which combine various advanced sensors with system identification and damage diagnosis techniques are required. The monitoring systems must be able to pinpoint the location and determine the extent of the damage for different types of structural systems.

3.2. Research Items

Items of research and development on the issue of sensing and monitoring technologies are described below.

1) Sensor technology

New sensors should be wireless, portable, self contained, capable of discriminating among different types of data, and subjected to environmental testing.

New sensors are needed to detect cracks, to monitor stress, strain, corrosion potential, and temperature.

Innovative technologies, such as MEMS, should be considered for new sensing devices.

2) Monitoring and Damage Assessment

Monitoring technologies that integrate the output from global and local sensors are needed to identify damage in real time.

New algorithms are needed to quantify the extent of damage from ambient vibration measurements and external excitation.

Software for efficient signal processing and integration of data from various sensors must be developed.

Evaluation strategy of structural performance for incorporation into smart structural systems is also required.

3) Networking

Integration of network systems to evaluate data from multiple structures throughout a city is required.

Because the life of the sensors is expected to be longer than the life of current computer systems or software, the interface between sensors and monitoring systems must be flexible.

3.3. Current Activities

Ongoing research plan in the sub-committee on sensing and monitoring technology (chaired by Prof. Y. Kitagawa, Hiroshima University) are classified into two subjects. One is defined as structural health monitoring system. The other is networking systems integrated with sensors. Current activities of two subjects are shown below.

1) Experimental test for structural health monitoring systems

The main target of health monitoring systems is to detect damage parts and evaluate present structural performance. A five-story steel frame with approximately one-third scale (as shown in Figure 2) was built to examine various damage detection methods. Structural damage is simulated by removing members or changing member properties in localized region. In addition to the conventional sensors to measure floor displacements and accelerations, optical fiber sensors are put on the surface of members to detect local deformations. Using these sensing data, several damage detection methods such as the method using vibration mode shapes are applied to evaluate the simulated damage and the limitation and improving points of the methods are examined.

2) Concept of sensor networking systems

It is recognized that integration of network systems to evaluate damage data of structures throughout a city is essential to identify damage regions and make necessary countermeasures. The networking systems can be classified into three scales; a system for a single building, a system to cover several buildings in a block, and a system to cover all buildings in a city. The sensor network system should be equipped with database of structural information such as design drawings. Also, the system should utilize effectively the up-to-date information

technologies such as wireless data transportation using mobile phones and satellite image, virtual reality techniques to visualize damage situation, high speed internet for data transfer, etc.

4. EFFECTOR TECHNOLOGIES

4.1. Objectives

The purposes are to develop smart materials and smart devices, and to verify that they can effectively control responses of structures and increase the safety and serviceability of structural systems, and disaster recovery. At the first stage, characteristics of smart materials and devices will be investigated. By relating these characteristics to their applications, methods of implementing this technology will be evaluated, e.g. suitable placement, required capacity, effective use, etc. , so that engineers can design more damage tolerant structural systems.

4.2. Research Items

Items of research and development on the issue of effector technologies are described below.

1) Smart materials and devices

The following smart materials and devices are mainly considered.

Shape memory alloys

Controllable fluids (e.g. electro-rheological and magneto-rheological fluids)

Electro-strictive elements (e.g. piezo-ceramics) and magneto-strictive elements

High-performance cementitious composites (HPCC)

2) Assessment of the applicability and efficacy of smart materials to structural systems

Large scale prototype and components for auto-adaptive devices and smartma t erial components should be developed and evaluated. This process should entail large scale testing on devices, on shaking table systems, and with pseudo-dynamic methods.

The result of this testing should be used to determine dynamic mechanical properties of auto adaptive devices and smart structural components, and of the overall structural performance of complete auto adaptive systems.

Corresponding to the listed four smart materials, four different working groups were formulated under the sub-committee on effector technology (chaired by Prof. T. Fujita, Institute of Industrial Science, University of Tokyo).

4.3. Current Activities

4.3.1. Shape memory alloys (SMA)

Shape Memory Alloy (SMA) shows three different characteristics depending on the temperature; shape memory effect, pseudo elasticity and partial pseudo elasticity. The objectives of this study are to utilize SMA for the smart structural members in order to realize the smart structural system in buildings. Some SMA devices will be developed for these purposes, and the guidelines on SMA for structural design will also be summarized. The current activities of the SMA working group (chaired by Prof. Y. Kitagawa, Hiroshima University) are described below.

1) Survey on properties and current application to buildings

General properties of SMA compounded of nickel and titanium were surveyed using references; shape memory effect and pseudo elasticity, transformation temperature, general stress-strain relation and its strain rate were quantitatively grasped. Especially, it was found to be important to apply the SMA to structural members of buildings that the stress-strain relation depends on the transition temperature, number and amplitude of cyclic loading, strain rate, and surrounding temperature. At present, it is very difficult to weld SMA with other metals,

but it is possible to use mechanical joints because SMA can be drilled, cut and sliced. Table 3 summarized some examples of application of SMA in Japan.

2) Test of SMA specimens

The required specification of SMA specimens was selected to be a wire and a bar with pseudo elasticity under room temperature (around zero to 30 degree centigrade). The casting variables are reduction ratio at the cold forming and heat temperature for shape-memory. Some specimens were produced under the combination of these variables and examined to compare their stress-strain relation in tension. A part of test results is shown in the Figures 3 and 4. A wire with 30% of reduction ratio shows good pseudo elasticity under room temperature. Especially the treatment under 550 degree centigrade heat and quench was found to give a fine pseudo-elasticity to the wire specimen. Bars with 16.5mm of diameter will be shaped without cold form process and be memorized with controlling heat and quench because of the production lines.

3) Cutting and shaping of SMA bars

The various conditions of cutting external threads and shaping SMA bars were examined. The bits for normal carbon steel such as SS400 of JIS (Japan Industrial Standard) were found to be unsuitable for SMA bars. Now, the bits for hard metals are tested to cut and shape the SMA bars.

4.3.2. Controllable fluids (e.g. electro-rheological and magneto-rheological fluids (ER/MR))

Electro/Magneto Rheological (ER/MR) Fluids have essential characteristics that change from free-flowing, linear viscous fluid, to a semisolid with a controllable yield strength in milliseconds when exposed to an electric and magnetic field. These fluids are effective materials for development of controllable devices. It is intended to develop a structure that changes its stiffness and damping characteristic to behave adaptively against earthquake or wind forces and achieve safety and functions by using ER/MR devices with less energy. The research items of the ER/MR working group (chaired by Prof. S. Soda, Waseda University) are described below.

1) Quantification of mechanical characteristics and material properties of ER/MR fluid

The mechanical characteristics are investigated using MR fluids developed and the required performance of new MR fluids is discussed.

2) Performance evaluation and development of ER/MR devices

The mechanical characteristics of ER/MR devices are investigated by experimental tests of ER/MR devices which are available on the market and the performance evaluation method and the required performance of ER/MR devices are discussed.

3) Development of adaptive structures using ER/MR devices

Ideas of adaptive structures using ER/MR devices are summarized and their effectiveness will be verified by numerical simulations and real-scale experimental tests. The evaluation method and design method of adaptive structures will be discussed. Examples of application of ER/MR devices are presented in Figures 5 and 6.

4.3.3. Electro-strictive and magneto-strictive elements

Electro/magneto-strictive elements (induced strain actuator (ISA)) can change their own shapes according to external electric/magnetic fields, and vice versa. Recently these materials have been widely used for the small/precision machines because of some advantages from viewpoint of small sizes, rapid reaction, high power, high accuracy etc. The objectives in this study are to develop smart members for building and to realize the smart, comfortable and safe structures. Designing guidelines of ISA materials/devices are also discussed. The research items of the ISA working group

(chaired by Prof. T. Fujita, Institute of Industrial Science, University of Tokyo) are described below.

1) Development of smart structural members using ISA devices

ISA materials are very suitable for structural control. We try to integrate these materials into normal structural members such as columns, beams etc. to realize smart structural systems. Example images are shown as Figures 7 and 8.

2) Using ISA as sensor materials

ISA materials can act as sensors because they cause change of electric or magnetic fields under deformation (see Figure 9). As schematically shown in Figure 10, PVDF (Polyvinylidene fluoride) sensors are suitable for membrane structures.

3) Improvement of Acoustic Environment

Polymers based ISA films or distributed ISA devices can control vibration mode of plane members. Applications to music halls or dwelling partition walls are expected. Experimental study of noise control is now planning.

4.3.4. High-performance cementitious composites (HPCC)

HPCC is chopped fiber reinforced mortar/concrete micro-structurally designed using micro-mechanical principles. HPCC exhibits strain-hardening with superior strain capacity, shear ductility, and extreme damage tolerant mechanical behavior. The ultra ductile behavior of HPCC, combined with its flexible processing requirements, isotropic properties, and moderate fiber volume fraction (typically less than 2% depending on fiber type and interface and matrix characteristics) make it especially suitable for critical elements in seismic applications where high performance such as energy absorption, steel/concrete deformation compatibility, spall resistance and damage tolerance are required. Applications to both new structures and in retrofitting of existing reinforced concrete structures to withstand future earthquakes are considered.

HPCC elements are expected to decrease the response and damage of building structures under external disturbances to achieve a high level of building performance requirements. Those requirements are not only structural safety but also reparability, serviceability, and durability of buildings after external disturbances. Stiffness, strength and ductility of the HPCC elements can be controlled easily by its dimensions and types of HPCC materials used. Then it is expected to develop the suitable energy dissipation and damage tolerant elements for concrete structures with higher stiffness than the other types of structures. Since the HPCC elements will be able to dissipate the input energy by external disturbances even in the small deflection state of the buildings, response and damage of building will be decreased. Experiments and studies on HPCC elements are carried out by the HPCC working group (chaired by Prof. Y. Matsuzaki, Science University of Tokyo).

5. CONCLUTIONS

The Building Research Institute, Ministry of Construction, Japan initiated a research program on smart materials and structural systems in 1998 as a part of U.S.-Japan cooperative research efforts. This paper described the research items and plans of the research program in Japan which have three research thrusts, (1) structural systems, (2) sensing and monitoring technology, and (3) effector technology. Although these three thrusts are common for the activities planned to take place in Japan and in the U.S.A, the activities in Japan will have a primary emphasis on system applications and proof-of-concept demonstrations while the activities in the U.S.A. will focus on enabling concepts and fundamental aspects of the technological elements. For the success of the joint program, the exchange of researchers and coordination and integration of cooperative research are essential.

ACKNOLEDGEMENT

This work has been carried out under the US-Japan cooperative structural research project on Smart Structure Systems (Chairperson of Japanese side: Prof. S. Otani, University of Tokyo, Chairperson of U.S. side: Prof. M. A. Sozen, Purdue University). We would like to acknowledge the hard work and contribution of structural systems, Prof. Y. Kitagawa, chairperson of sub-committee on sensing and monitoring technology, Prof. T. Fujita, chairperson of sub-committee on effector technology, and all members of the project for their useful advice and suggestions.

the U.S. participants at the JTCC meeting in Tsukuba, 6 - 8 January, 2000. The outcome of discussion at the meeting is fundamental to this paper. The authors also would like acknowledge Prof. A. Wada, chairperson of sub-committee on

Table 1 Smart Structural Systems for Aerospace Engineering and Building Engineering

	Aerospace Engineering	Building Engineering
Characteristics of structure	Airplane is originally active and adaptive.	Building is not required to be active or adaptive.
	Airplane has a simple usage and works as a single unit.	A group of buildings form a social unit having multiple usage.
External disturbance and objective safety	Structure must be safe in daily usage and disturbance.	Structure must be safe in rare events, such as strong winds or an earthquake.
	Constant maintenance is required.	Free-maintenance is desirable.
Research needs	Integrate smart functions into a structure to achieve light-weight and high-performance.	Put smart functions to a structure to achieve objective performance such as minimum life cycle cost.
Typical example	Active control system	Health monitoring system

Table 2 Research Needs in Building Engineering

Category	Research needs
Function	Effective control of noise and vibration Creation of large open space without column and wall Design of highly irregular buildings Flexibility in building usage Extension of building life
Disaster prevention	Prevention of building or ground collapse Rehabilitation of old structures Damage detection of hidden structural elements Human safety at ultimate stage Repair of building damage Evaluation of seismic safety in urban environment Public education toward disaster mitigation
Environment	Protection of nature Control of environmental pollution Control of industrial waste Reduction of dust and noise during construction
Production	Countermeasures against shortage of expert builders Improvement of construction quality High speed construction Development of new material

Table 3 Examples of application of SMA in Japan

Properties of SMA	Examples of application
Shape memory effect	Control of room temperature using SMA sensors and actuators Door unlock system for earthquakes using SMA actuators Deflection control of structure using SMA wires Stress control of pre-cast concrete members using SMA springs Demolition of a part of concrete structures using SMA devices Joints of steel pipes using SMA tubes Framework of reinforced concrete curved membranes using SMA supports
Pseudo elasticity	RC members with longitudinal bars of SMA Isolation system of containers for vibration Base isolation device with the combination of SMA, rubber and lead Seismic energy absorbing device for historic structures or bridges

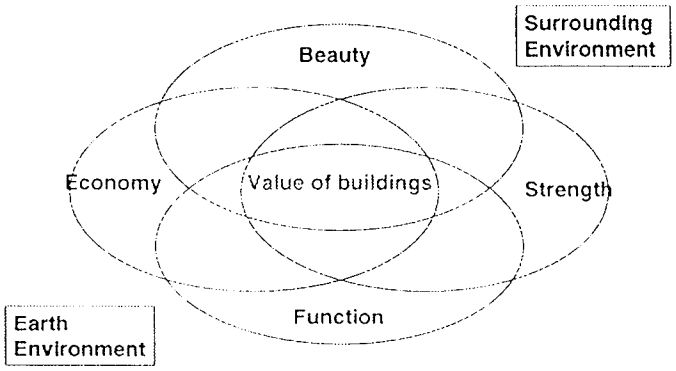

Figure 1 Evaluation Elements of Building

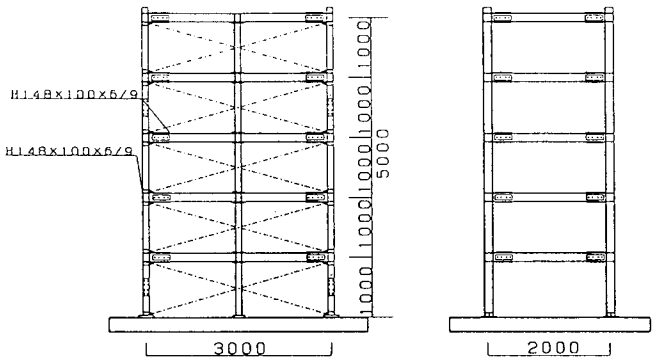

Figure 2 A five-story steel frame model (unit:mm)

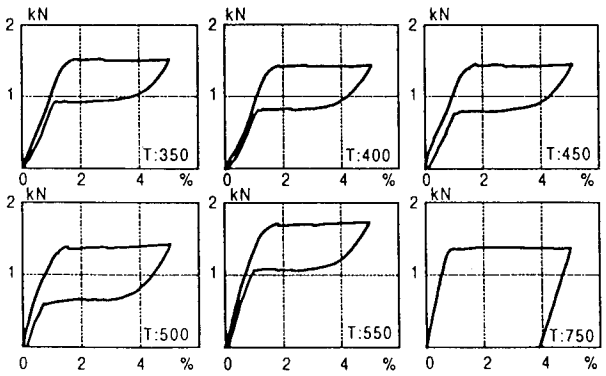

Fig. 3 Stress-strain relations of specimens under deferent temperatures at shape memory treatment (cf. test condition : in room temperature)

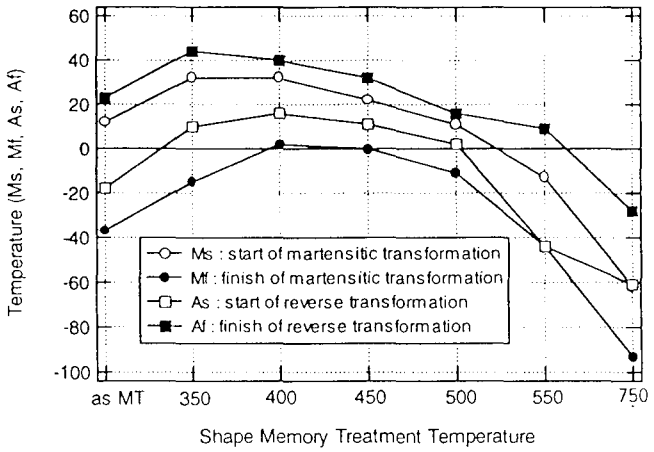

Fig. 4 Transformation temperature vs. shape memory treatment temperature of SMA

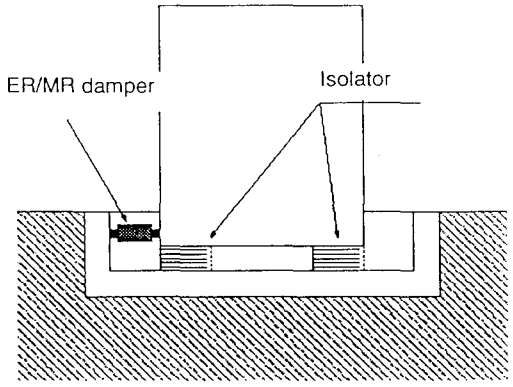

Fig. 5 Base-isolated structure controlled by ER/MR devices

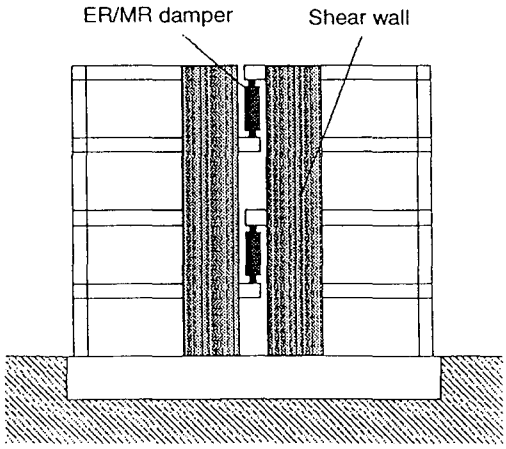

Fig. 6 Control of flexural behavior by ER/MR devices

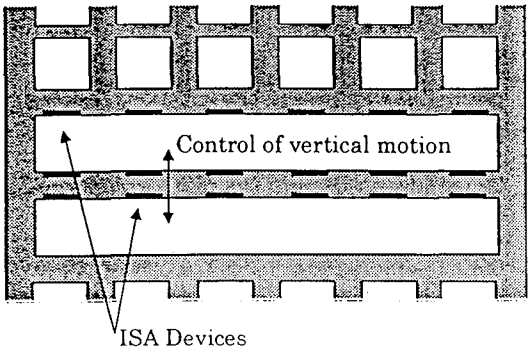

Fig. 7 Active control of floor

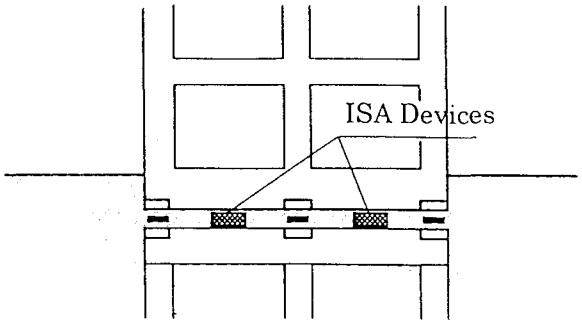

Fig. 8 Friction control for base isolation

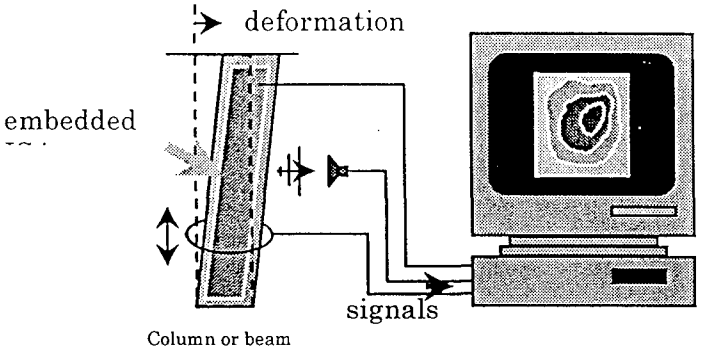

Fig. 9 Sensing system with or without cabling

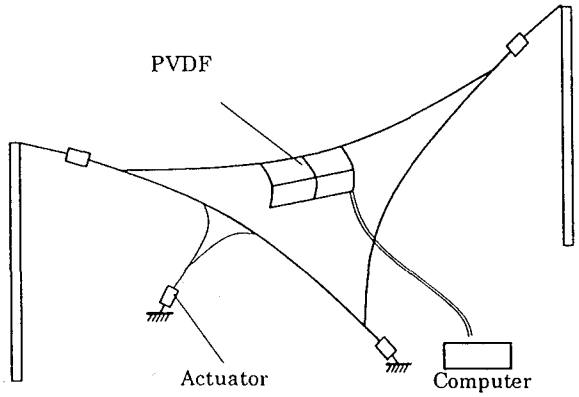

Fig. 10 PVDF sensors for membrane

高知能建築構造システムの開発

小谷俊介[1)]、平石久廣[2)]、緑川光正[2)]、勅使川原正臣[2)]、藤谷秀雄[2)]、斎藤大樹[2)]

建設省建築研究所は１９９８年度に日米共同研究の一環として、５カ年計画の高知能建築構造システムの開発を開始した。高知能建築構造システムは（別称自己適応型構造）建築の構造体それ自身が外部から受ける影響に適応して安全性や使用性などの構造性能を自動的に調整するシステムである。本研究開発は、（１）高知能建築構造システムの概念と性能評価、（２）建築構造性能の検知、（３）高知能材料を用いた建築構造要素の開発と評価を中心に行う。

１．研究実施体制と全体研究計画の概要

国内に技術調整委員会（TCC，委員長：小谷俊介　東京大学教授）を組織し、高知能建築構造システムに関する全体的な研究の検討を行っている。研究期間の後半では、具体的な高知能構造システムの開発と大型実験による性能検証を行うとともに、高知能構造システムの性能評価ガイドラインや材料・部材の利用ガイドラインを作成する。

２．各部会の開発研究項目

(1)システム部会（主査：和田　章　東京工業大学教授）

システム部会では、高知能建築構造システムの実現に向けて以下の検討を行う。

・高知能建築構造システムの概念構築
・高知能建築構造システムの実現に必要な要素技術の検討
・高知能建築構造システムの提案
・高知能建築構造システムの性能評価指針の作成

(2)センサー部会（主査：北川　良和　慶応大学教授）

センサー部会では、建築物の損傷を検知するセンサー技術の開発および損傷部位、損傷程度を特定するための技術開発を行う。

・建築構造物のヘルスモニタリング技術の開発
・建築構造物の性能検査技術の開発
・センサーネットワーク技術の検討

(3) エフェクタ-部会（主査：藤田　隆史　東京大学生産技術研究所教授）

エフェクタ-部会では、高知能材料を用いた構造部材の開発と利用ガイドラインの作成を行う。以下の高知能材料を開発目標とする。

・形状記憶合金
・電気・磁気粘性流体
・圧電磁歪素子
・セメント系複合材料

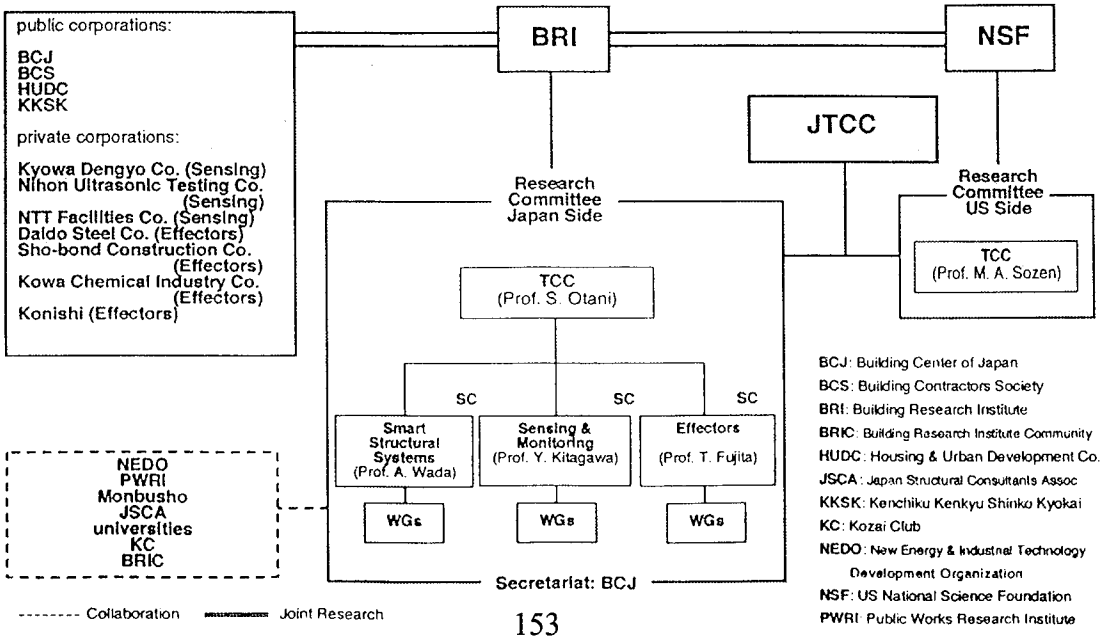

研究実施体制

Nonlinear Rock Mechanics Analysis of Gravity Dams under Combined Flood and Earthquake Loading

by

Luis A. de Béjar[1] and Robert L. Hall[1]

ABSTRACT

The two-dimensional nonlinear incremental response of a gravity dam subjected to earthquake loading is outlined. The dam is assumed to stand on jointed rock and to be impounding a full-reservoir upstream water level. The material constitutive relations for rock discontinuity are expressed in terms of an incremental plasticity model that fully represents the coupling between joint normal and shear deformations due to dilatancy. The model also accounts for stiffness degradation of joints upon wear and shear distortion, and for the bulking/seating effects of separated rock debris. The instantaneous center of rigidity and the associated principal directions of rigidity for the dam-rock system are located analytically for each step of the load history, and the displacement and force responses of the rock joint elements are obtained incrementally. Results are compared to those from corresponding finite-element analyses.

KEYWORDS: Bottom-absorption hydrodynamic force spectra; finite-element modeling; flood; nonlinear earthquake analysis; rock mechanics.

1. INTRODUCTION

In order to build the model in this investigation, several recent studies dealing with the behavior of rock discontinuities under shear and normal loading were examined. Saeb and Amadei (1992) developed a tangent formulation for the deformability of a rock joint that fully accounts for the coupling between joint normal and shear responses due to dilatancy. Plesha (1987) and Qiu et al. (1993) have developed a macroscopic constitutive law for initially closely mated joints undergoing small displacements that includes dilatancy, damage of surface roughness, and cyclic sliding behavior in the light of the theory of plasticity. This theoretical model was experimentally verified for simple laboratory experiments on both natural and artificial rock joints (Huang et al. 1993). Mroz and Giambanco (1996) developed an interface constitutive model accounting for slip and sliding effects. The microslip effects were described by considering the interaction between asperities modeled as spheres in contact by appealing to the generation of progressive or reverse slip zones.

The constitutive law for rock discontinuities applied in this investigation mirrors Plesha's model (See de Béjar, L.A. & S. Garner 1998). Associated-flow plasticity was adopted because it results in symmetric stiffness matrices that dramatically simplify the ensuing numerical analysis procedures. Joint asperities are modeled as harmonic elements in regular array, starting from the fresh-joint perfectly mating configuration. Degradation is modeled in terms of an exponential decay of inclination with respect to the initial overall joint plane, as a function of the cumulative plastic work on the asperities. Bulking/seating effects are built into the normality rule and subsequently into the consistency condition of the theory. Bulking effects may be disregarded for monotonically increasing load but must be included in the formulation for problems involving reversal of frictional shear in the case

[1] U.S. Army Engineer Research and Development Center
3909 Halls Ferry Road, Vicksburg, MS 39180-6199
www.wes.army.mil

of earthquake loading.

2. MODELING THE DAM-FOUNDATION ROCK SYSTEM

The dam-parent rock system is idealized as a rigid body standing on a set of elasto-plastic rock discontinuities (Figure 1). The surface of contact of the rock discontinuities is idealized as sinusoidal (Figure 2). This assumption allows easy calculation of the displaced configuration as mating blocks friction slide and climb on each other during dynamic response. Each discontinuity resists normal and tangential forces through stiffnesses that evolve as the exciting load fluctuates in magnitude (Figure 3). The instantaneous center of rigidity and the associated principal directions of rigidity for the dam-rock system are located analytically for each step of the load history (Ayre 1938, de Béjar 1985). The model includes the hydrodynamic pressure field on the upstream face of the dam, effective upon bottom absorption of seismic energy in the reservoir. The model also includes the effects of a downstream pool and the resultant uplift forces exerted by the pore water pressure field within the rock joints on the upper discontinuity surfaces. This last effect varies continuously as the dam-foundation rock system translates and rotates during the response history.

3. ELASTO-PLASTIC CONSTITUTIVE LAW FOR ROCK DISCONTINUITIES

In this model, stresses are assumed uniformly distributed over each segmental rock joint; however, there is no limit as to the number of joints to be considered in a given problem. The Coulomb dry friction slip criterion is taken as the slip surface to signal the onset of plastic flow in rock discontinuities, and is given by (Qiu et al. 1993):

$$F(\{f\},\alpha) = |f_t \cdot \cos\alpha + f_n \cdot \sin\alpha| + \mu \cdot (-f_t \cdot \sin\alpha + f_n \cdot \cos\alpha) = 0 \qquad (1)$$

where $\{f\} = \langle f_t \; f_n \rangle^T$ = vector of internal forces on the rock joint, α = the instantaneous tangential inclination of the point of contact between lower and upper faces of a joint asperity, and μ = static coefficient of dry friction for the rock joint. The same function $F(\{f\}, \alpha)$ is specified as the plastic deformation potential leading to associated flow. The formulation of the theory of plasticity leads to an explicit relation between the increment of displacement and the corresponding increment of internal force, which may be written as:

$$\{df\} = \begin{cases} [E]\cdot\{dg\} & , F<0 \text{ or } dF<0 \\ [E^*]\cdot\{dg\} & , F=0 \text{ and } dF=0 \end{cases} \qquad (2)$$

where [E] = Elastic stiffness matrix (diagonal) for the rock discontinuity, and
[E*] = Elasto-plastic stiffness matrix (fully populated and symmetrical).

4. NUMERICAL ANALYSIS

The two-dimensional response of the gravity dam standing on jointed rock is calculated incrementally. At each step in the analysis, the incremental displacement response of the system is obtained after adjusting the material state (elastic/plastic) of all joints for consistency with their corresponding states at the end of the step. If, during the analysis for a given step, lack of consistency is detected between the initial and the final states of any joint in the set, the analysis is repeated altogether for the step, using half the current value of the time step.

The incremental response for a given step is obtained as the summation of partial contributions obtained from successive attempts to restore dynamic equilibrium under the effective earthquake forces, which include both the inertial and structural damping components. At each attempt, the partial response of the system is obtained using its current stiffness matrix at the beginning of the step and the principal rigidity properties for the system, obtained from the elements as if their normal and tangential actions were uncoupled. This process is graphically illustrated by the

flow diagram in Figure 4 (for the one-dimensional case), in which ($\{f\},\{\delta\}$) and ($\{F\},\{\Delta\}$) are the effective earthquake force and displacement response pairs for the joints and the system, respectively (Quantities for the system are referred to the principal rigidity coordinates attached to the center of rigidity).

As a simple example of application, Figure 5 shows an idealized dam-rock system under a comprehensive representation of the equilibrating forces during earthquake response. The hydrodynamic pressure field D in this representation is effective, after bottom-absorption effects have been estimated from previous studies (de Béjar, L.A. 2000).

Figure 6 shows a typical set of hydrodynamic force spectra normalized with respect to the corresponding scaled hydrostatic resultant force on the upstream face of the dam, for various degrees of elasticity of the underlying supporting rock (represented by the coefficient of reflection α), and developed for the San Fernando earthquake of Feb. 9, 1971. Figure 7 shows the distribution of the shell major principal stresses of the system standing on nonlinear gap elements simulating the rock discontinuities. An extreme-load scenario of simultaneous flood-earthquake excitation has been assumed to emphasize the detrimental effects on the system under such conditions. The results of the analysis using the rigid-body engineering model are contrasted with those from the finite-element formulation for comparison.

5. SUMMARY

An engineering model for the nonlinear behavior of rock discontinuities under concrete gravity dams subjected simultaneously to flood and earthquake has been outlined. The material representation for rock joints had been previously verified in closely controlled laboratory experiments. The resulting computer capability is intended to examine effectively the progression of damage associated with specific states for concrete gravity dams during earthquake response. In particular, the model will assist in the definition of limit states and the construction of fragility curves for comprehensive risk analyses (de Béjar, L.A. 1999).

6. ACKNOWLEDGMENTS

This investigation was conducted at the U.S. Army Engineer Research and Development Center, Waterways Experiment Station through the Earthquake Engineering and the Risk Analysis for Dam Safety Research Programs, both sponsored by Headquarters, U.S. Army Corps of Engineers. The authors gratefully acknowledge permission from the Chief of Engineers to publish the information in this paper.

7. REFERENCES

1. Ayre, R.S. 1938. Interconnection of translational and torsional vibrations in buildings. *Bull. Seismol. Soc. Amer. #2.* 28:89-130.

2. de Béjar, L.A. 1985. Linear and nonlinear analyses of building systems subjected to multicomponent earthquake excitations. *Ph.D. Thesis at Cornell University.* Ithaca, NY.

3. de Béjar, L.A. & S. Garner 1998. Nonlinear rock mechanics analysis of gravity dams under flood loading. *Proceedings Int. Symp. New Trends and Guidelines on Dam Safety.* Barcelona, Spain.

4. de Béjar, L.A. 1999. Fragility analysis for concrete gravity dam safety under flood. *Proceedings of ASDSO Dam Safety Conference. St. Louis, MO.*

5. de Béjar, L.A. 2000. Reservoir-bottom effects on hydrodynamic loads for concrete gravity dams subjected to earthquake. *Proceedings of ASCE 14th Engineering Mechanics Conference.* Austin, TX.

6. Huang, X., B.C. Haimson, M.E. Plesha & X. Qiu 1993. An investigation of the mechanics of rock joints—Part I. Laboratory investigation. *Int. J. Rock Mech. Min. Sci. & Geomech. Abstr.* 30(3):257-269.

7. Mroz, Z. & G. Giambanco 1996. An

interface model for analysis of deformation behavior of discontinuities. *Int. J. Numer. Anal. Methods Geomech.* 20:1-33.

8. Plesha, M.E. 1987. Constitutive models for rock discontinuities with dilatancy and surface degradation. *Int. J. Numer. Anal. Methods Geomech.* 11:345-362.

9. Saeb, S. & B. Amadei 1992. Modeling rock joints under shear and normal loading. *Int. J. Rock Mech. Min.Sci. & Geomech. Abstr* 29(3):267-278.

10. Qiu, X., M.E. Plesha, X. Huang & B.C. Haimson 1993. An investigation of the mechanics of rock joints—Part II. Analytical investigation. *Int. J. Rock Mech. Min. Sci. & Geomech. Abstr.* 30(3):271-287.

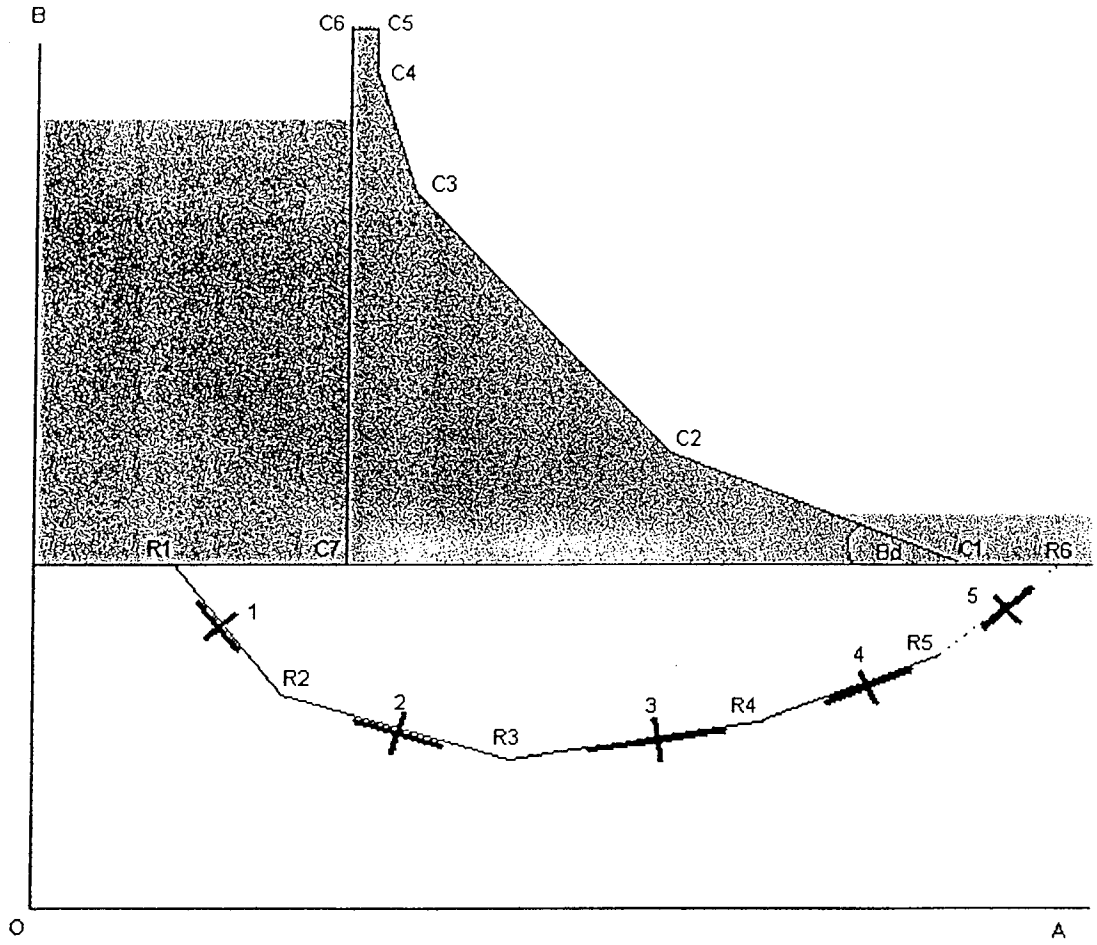

FIGURE 1. Analytical model for dam-rock-discontinuities system

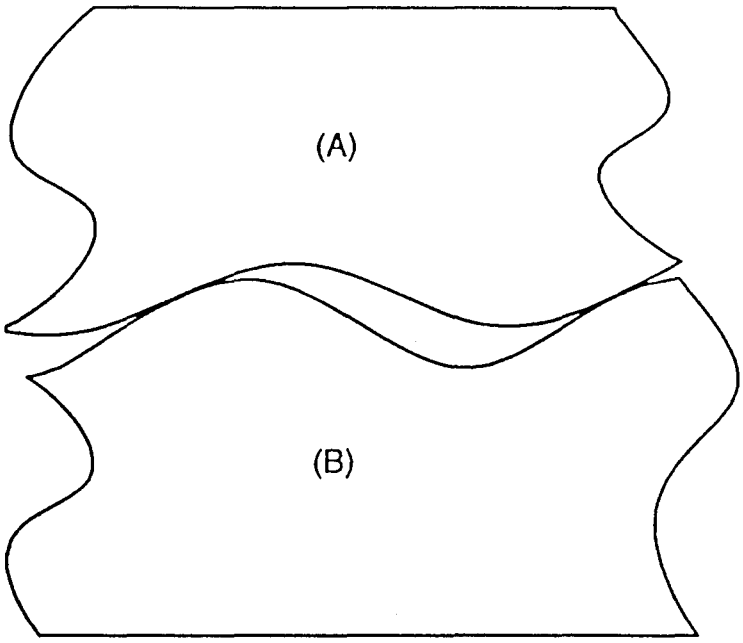

FIGURE 2. Idealization of asperity contact in rock discontinuity friction sliding

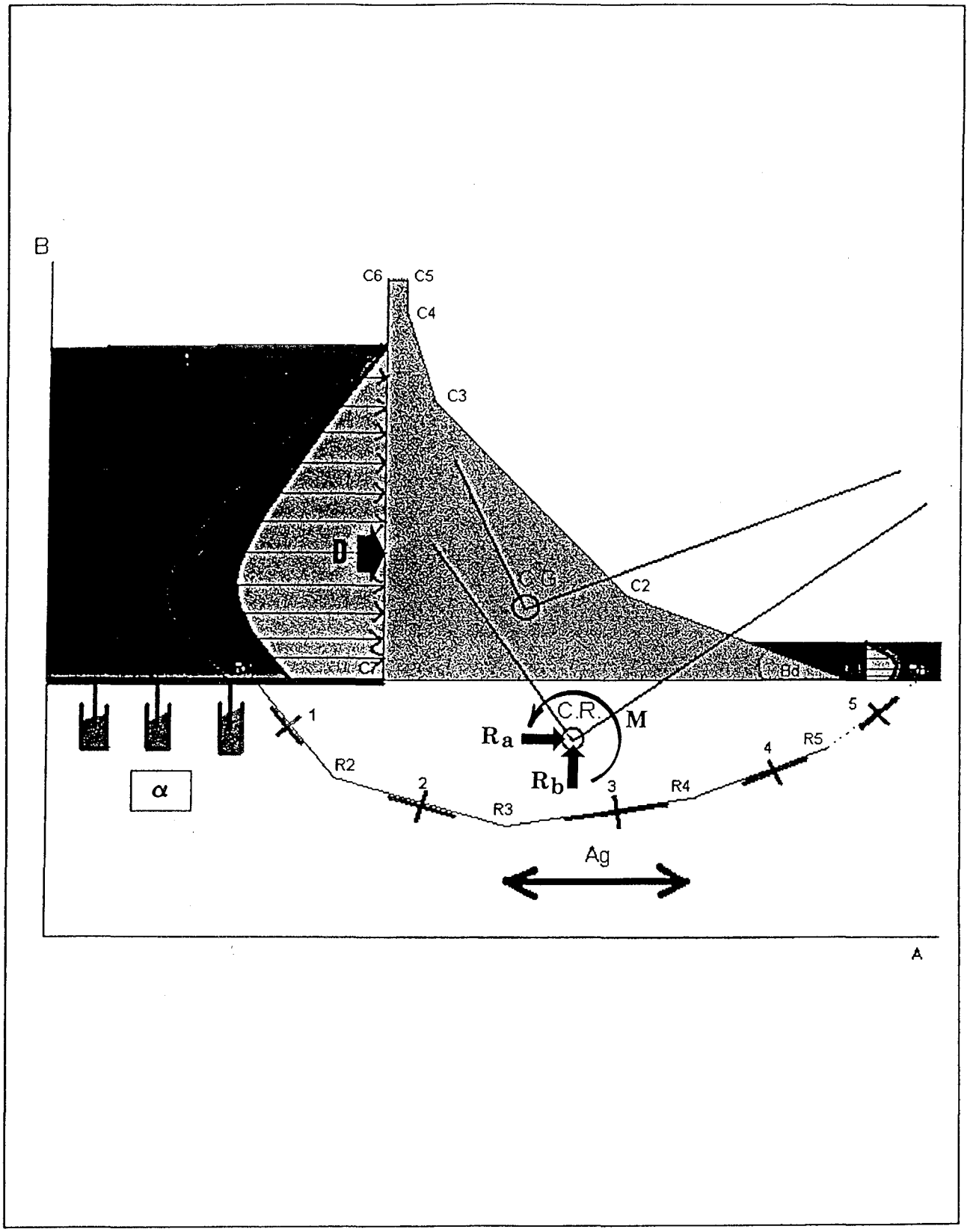

FIGURE 3. Analytical model for the dam-system components under earthquake

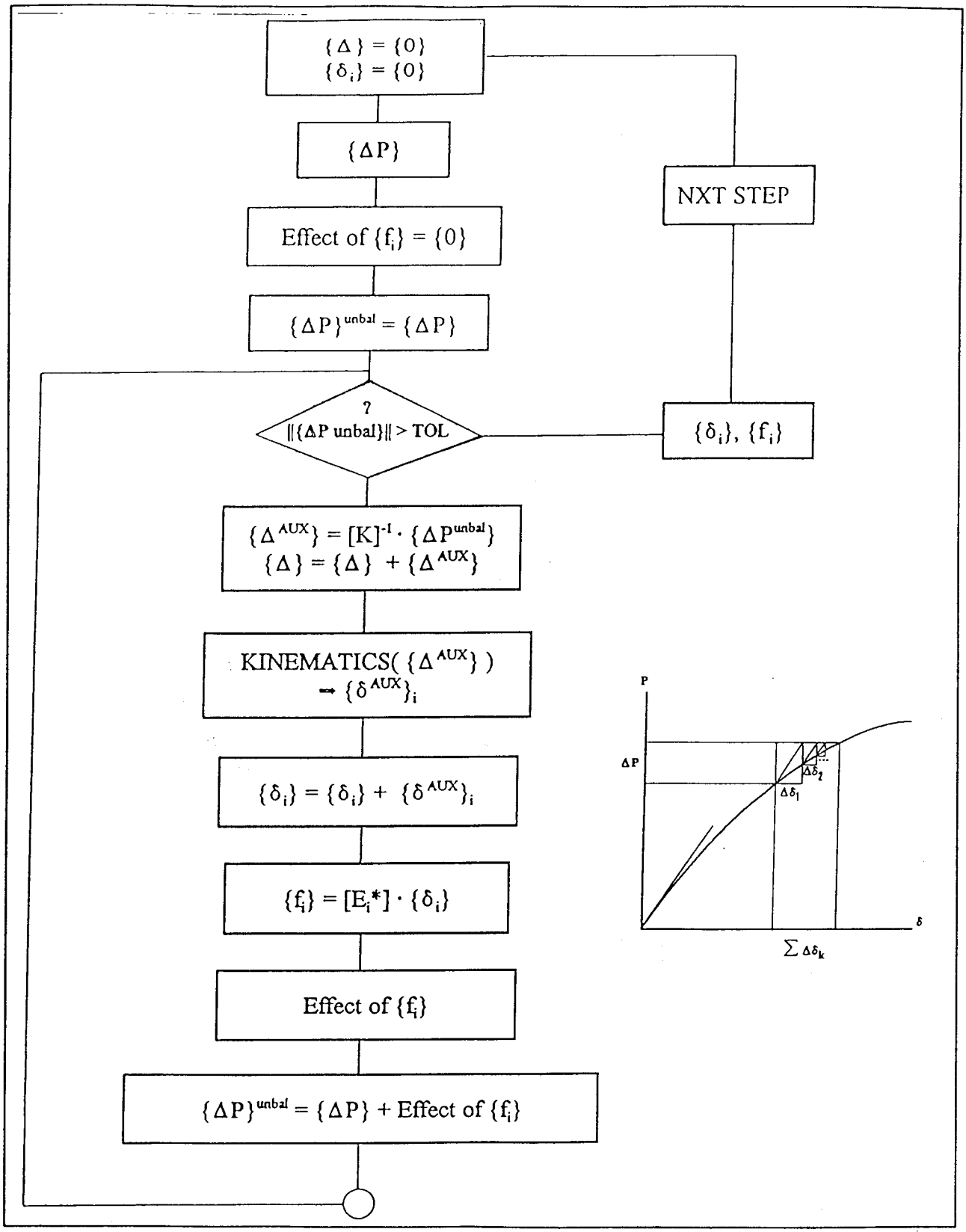

FIGURE 4. Global flow of numerical iterations within a given load step

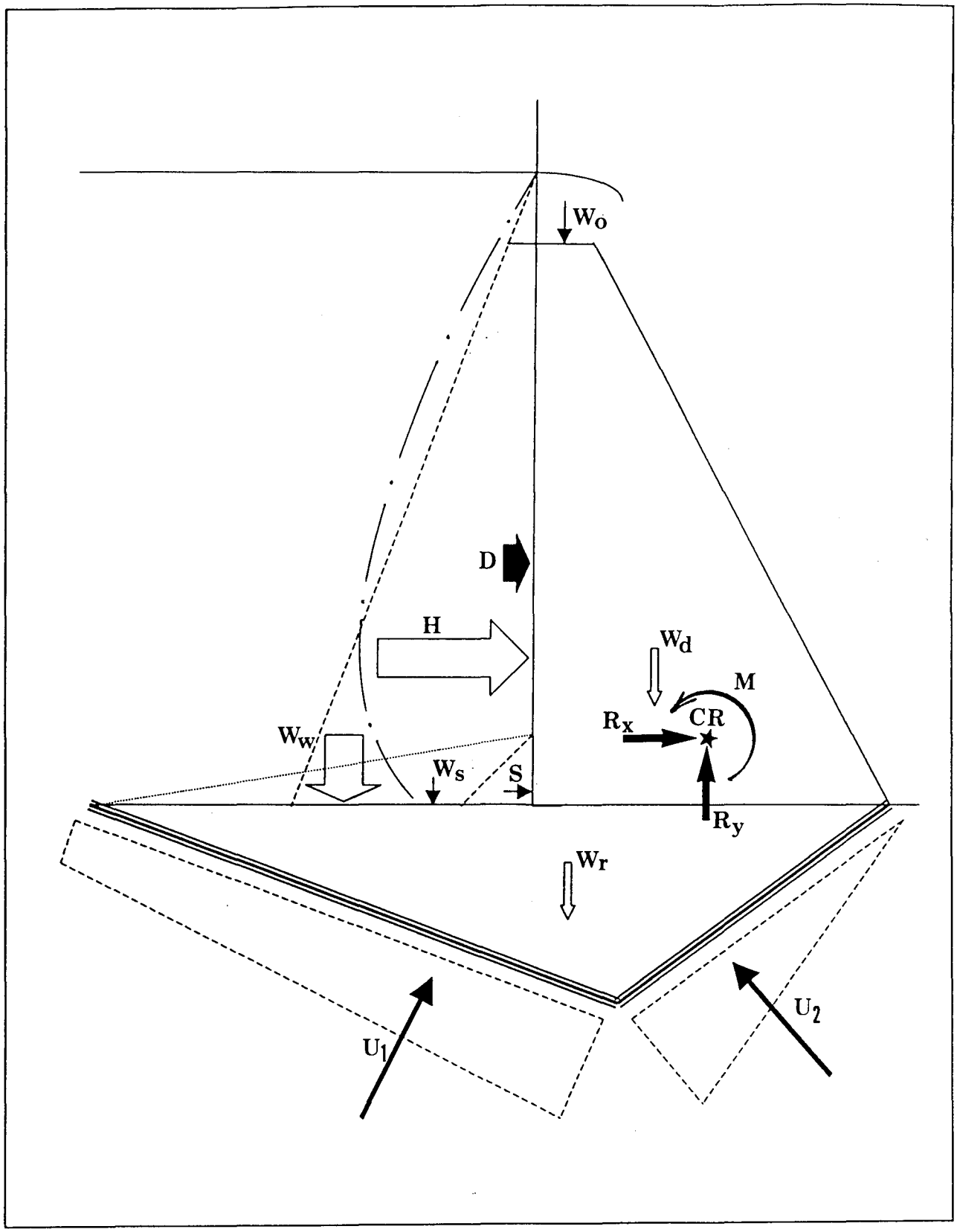

FIGURE 5. Two-dimensional system of simultaneous gravity, hydraulic, and seismic forces on dam-rock-discontinuities system

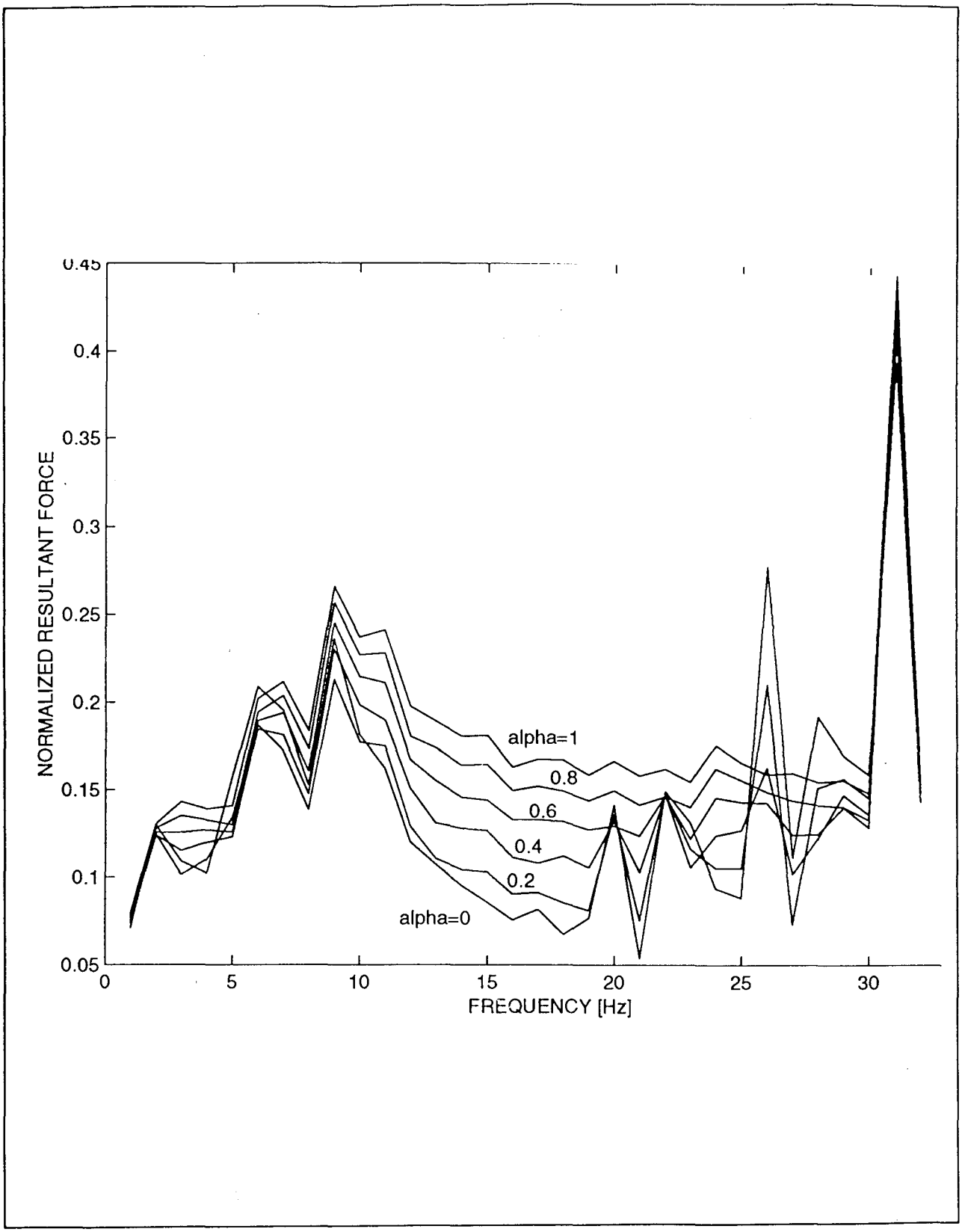

FIGURE 6. Hydrodynamic force spectrum for the San Fernando earthquake as recorded at Whittier Narrows Dam, 1971 (S53W component)

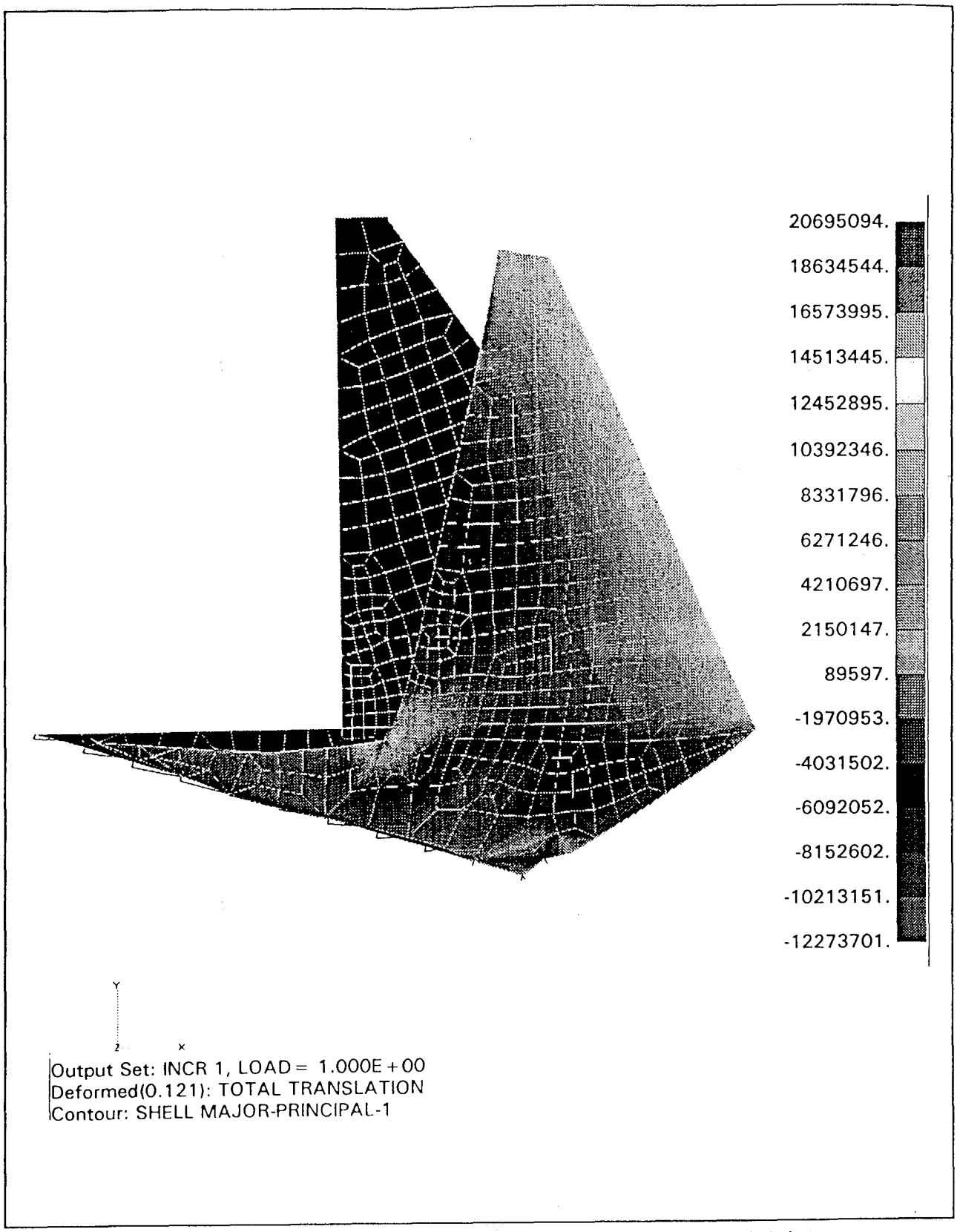

FIGURE 7. Typical 2-D dam-rock system standing on nonlinear rock joints.
Loading: Gravity + 5m overtopping + earthquake + uplift + sediments

OUTLINE AND PRE-ANALYTICAL STUDY ON DAMAGE DETECTION TESTS OF FIVE-STORY STEEL FRAME WITH SIMULATED DAMAGES

by

TESHIGAWARA Masaomi[1)], KAMINOSONO Takashi[1)], INUKAI Mizuo[1)], ISODA Hiroshi[1)], MORITA Koichi[1)] and NOGUCHI Kazuya[1)]

ABSTRACT

This paper presents outline and pre-analytical study on damage detection tests of five-story steel frame with simulated damages. Fiber brag grating (FBG) sensors, accelerometers and strain gauges will be installed in this frame. From the results of pre-analytical study, we can estimate which story is damaged from the change of natural period or mode shape to some extent. Damage identification method using modal analysis is shown here. Damage detection methods from local information will be also examined, and various identification methods will be also applied.

KEY WORDS : Smart Structure
Health Monitoring
Damage Detection
Identification Techniques

1.INTRODUCTION

If we need to reduce life cycle costs of a building from construction to maintenance, it is very effective to monitor structural health of a building. However, the research on health monitoring of buildings is rare, and health monitoring technique of a building is not still establishing. We have a plan of damage detection tests using smart sensors, as fiber optics, and this is a part of US-Japan cooperative research project on smart structural systems. We show here outline of tests and results of pre-analysis.

2.OUTLINE OF TEST FRAME AND EXPERIMENTS

Test frame is five-story steel structure shown as figure 1. Floor height is 1m, total height is 5m and floor plan is 2m*3m. The cross section of members is following.
column : H148*100*6/9(SS400)
beam : H148*100*6/9(SS400)
stud : H100*50*5/7(SS400)
We put a weight of 2 ton on each story.
There are two test cases, tests with studs shown as figure 1.1) and tests without stud shown as figure 1.2). Braces can be installed, when studs are removed. Natural periods are almost 0.3 – 0.4 seconds.
Test frame will be set up on shaking table, and excitation tests using a vibration exciter will be also carried out, if we need to excite higher modes. Sensors will be put on each floor and installed at beam edges. Fiber brag grating (FBG) sensors, accelerometers and strain gauges will be installed. In addition, ultrasonic measurements will be carried out. Settings of simulated damages are as fellow.
+Studs or braces will be extracted only from one story.
+Part of flanges of beams or columns will be cut off. (See figure 2)
+Bolts of beams or columns will be loosened.
Etc.
The following tests from i) to vii) will be carried out in order to the number.
i) Normal sound test structure with studs
ii) Removing studs from only one story
iii) Normal sound test structure without studs
iv) Loosening bolts of beams of test structure without studs
v) Exchanging sound beam for damaged beam
vi) Extracting braces from only one story
vii) Cutting of part of column

1) Building Research Institute, Ministry of Construction, Tsukuba-shi, Ibaraki-ken, 305-0802, Japan

3.PRE-ANALYSIS

(1)Change of modal property by setting damage

We examine how natural periods and modal shapes change when damages are set at part of beams or columns. Some cases are examined, and all results tend to be same. Here, only the case in which damages are set at beam edge of test structure without stud is explained. Damages at beam are assumed as pin in analysis.

Table 1 shows that natural periods of test structure, in which damages at beam edge are assumed, are compared. First natural periods greatly change, when damages at lower story are assumed. Higher (third) natural periods greatly change, when damages at upper story are assumed. Figure 3 shows similar results of mode shapes. First mode shape also greatly changes, when damages are assumed at lower story. Higher (third) mode shapes also greatly change, when damages are assumed at upper story. From these results, it is effective to examine higher mode when there seem to be damages at upper story. We can estimate which story is damaged from the change of natural period or mode shape to some extent.

(2)Damage Identification by use of change of modal property

We make simulation waves calculated as results of same models used in (1) with white noise for input. Identification technique [1] using the change of flexibility is applied to this simulation waves. Damaged location is estimated by comparison of sound modal properties and damaged modal properties. We show here results of the case setting damage at beam edge of 1, 3, 5 story in figure 4 – 6. Each figure shows the flame in case of figure 1 2). Y direction is height direction and dark line shows that damage index is large. That is to say, if the color of lines is dark, there should be damage. In figure 4 (assumed damages at lower story), the color of lower story is dark. In figure 5 (assumed damages at intermediate story), the color of intermediate story is dark. In figure 6 (assumed damages at upper story), the color of upper story is dark. From these figures, damage identification seem to be difficult when damage at upper story is assumed. And we can estimate which story is damaged when damages exist at lower story.

4. Conclusions

Outline of damage detection tests and results of pre-analysis are reported. Damage identification method using modal analysis is shown here. Damage detection methods from local information will be also examined, and various identification methods will be also applied.

[Reference]
[1] "Damage Identification and Health Monitoring of Structural and Mechanical Systems from Changes in Their Vibration Characteristics" : A Literature Review, Los Alamos National Laboratory Report, LA-13070-MS, 1996.

Table 1 : Comparison of Natural Periods [sec]

	1st	2nd	3rd
Sound structure	0.366	0.120	0.0710
Damaged beam at 5th story	0.371	0.131	0.0786
Damaged beam at 4th story	0.385	0.141	0.0745
Damaged beam at 3rd story	0.409	0.132	0.0729
Damaged beam at 2nd story	0.431	0.120	0.0768
Damaged beam at 1st story	0.437	0.129	0.0716

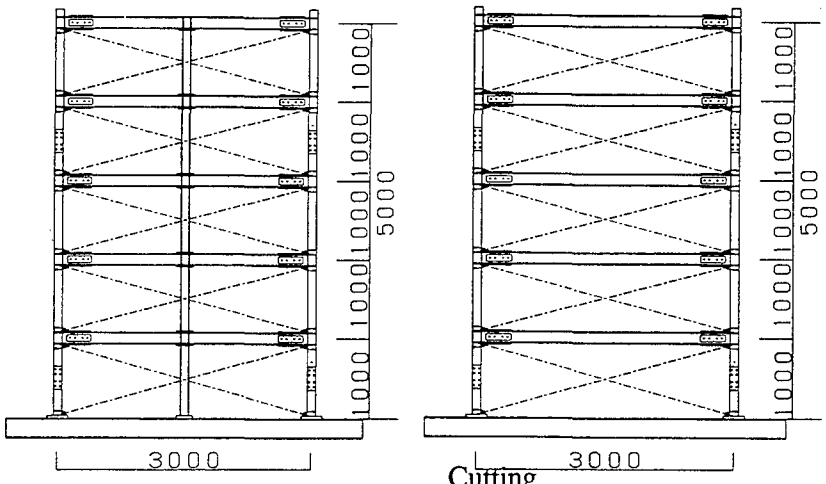

Cutting

Fi

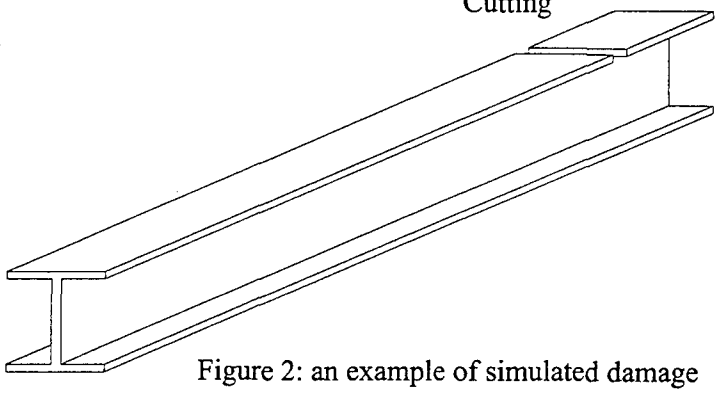

Figure 2: an example of simulated damage

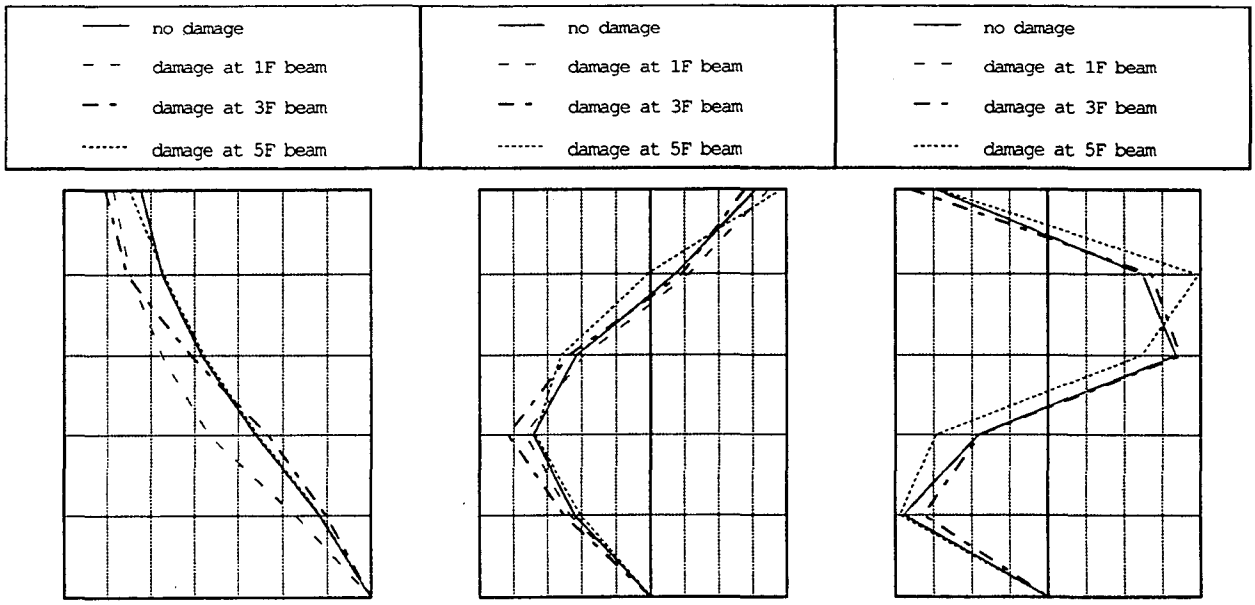

Figure 3 : Comparison of Mode Shape without damages and Mode Shapes with damages

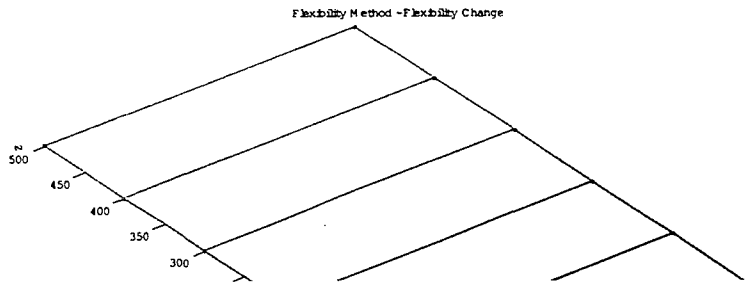

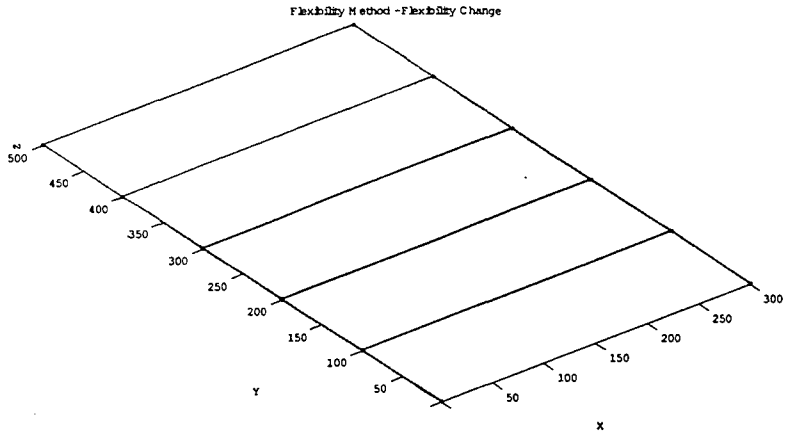

Figure5 : In Case of Setting Damages at 3rd Story

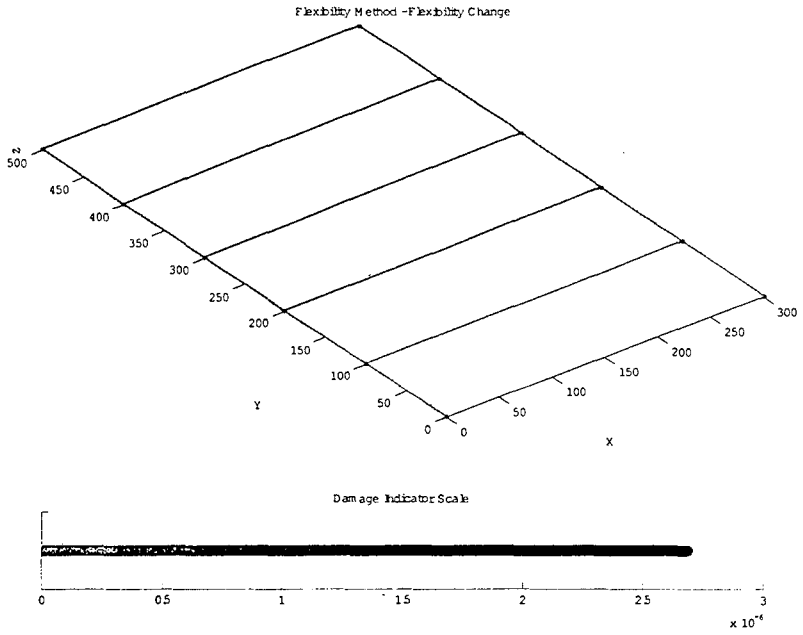

Figure6 : In Case of Setting Damages at 5th Story

The influence of high confining stress on the cyclic behavior of saturated sand

by

R. Scott Steedman[1], Richard H. Ledbetter[2] and Mary E. Hynes[2]

ABSTRACT

This paper describes the findings of an experimental study supported by the U.S. Army Centrifuge Research Center and Engineer Earthquake Engineering Research Program (EQEN) into the behavior of saturated sands under high initial effective confining stresses subjected to strong ground shaking. The research was conducted using the Army Centrifuge at the U.S. Army Engineering Research and Development Center (ERDC), located in Vicksburg MS, formerly known as the Waterways Experiment Station (WES). The centrifuge studies have shown that the generation of excess pore pressure is capped at a level below 100 percent for vertical effective confining stresses exceeding around 3 atmospheres (atm, or 300 KPa). This limit reduces at higher confining stresses. If verified, the potential benefits from this finding for the design of remediation works for large earth dams could be substantial. The paper describes the equipment used for the experiments, the research program, and presents the initial results, contrasting the development of excess pore pressure at low confining stress with that at high confining stress. Possible consequences for a hypothetical dam are discussed.

KEYWORDS: centrifuge; dams; ERDC; liquefaction; modeling; remediation

1.0 INTRODUCTION

The current state-of-practice for the evaluation of liquefaction potential and for remediation design and analysis depends on empirical correlations of in-situ measurements of strength versus field experience of liquefaction at shallow depth and laboratory data of the behavior of confined elements under cyclic loading. (Liquefaction is defined here to mean the development of pore pressure equal to 100% of the initial vertical effective stress.) This approach is known as the "simplified procedure". Opinions vary as to the maximum depth in the field at which liquefaction has been observed, but there is no established field evidence from historic earthquakes of liquefaction at depths greater than a few tens of meters. The NCEER Workshop in 1996 on the Evaluation of Liquefaction Resistance of Soils noted that the simplified procedure was developed from evaluations of field observations and field and laboratory test data, Youd and Idriss (1997). The report notes, "These data were collected mostly from sites ... at shallow depths (less than 15m). The original procedure was verified for and is applicable only to these site conditions".

Hence, in design practice the assessment of liquefaction under high initial effective confining stress, such as might relate to the foundations of large earth dams, is based on the extrapolation of observed behavior and correlations at shallow depths. In practice, the behavior of saturated soil under these conditions is not well understood. Based on the results of laboratory tests, researchers have postulated that there is a reduction in the liquefaction resistance of such soil compared to shallow depths. This reduction is accounted for in standard approaches by a ratio known as K_σ, a "correction factor" developed by Seed (1983) in the simplified procedure. This strength ratio is postulated to reduce with increasing initial effective confining stress, which has potentially

[1] Steedman & Associates Ltd, 25 Eldon Square, Reading RG1 4DP, UK, Robert.S.Steedman@erdc.usace.army.mil
[2] US Army ERDC Waterways Experiment Station, Vicksburg, MS 39180, Mary.E.Hynes@erdc.usace.army.mil

large impact on the extent and method (hence cost) of remedial construction required to assure adequate seismic performance of large dams. For example, it may reduce the cyclic shear stress ratio predicted to cause liquefaction in a soil layer under a typical large dam (of the order of 30m high) to about 50% of its value in the absence of the dam. The predicted deformations and resistance and the remedial strength required are a direct function of the reduced shear strength. The effects of the K_σ strength reduction is driving the majority of seismic dam safety concerns and needs for remediation, which may result in costs in the billions of dollars in North America alone in the coming years.

The factor K_σ quantifies the curvature in the cyclic shear strength envelope (cyclic shear stress required to cause liquefaction versus confining stress) for a soil as observed in laboratory tests on discrete specimens. Although some curvature may be expected, such large reductions in cyclic shear strength ratios are counter-intuitive. It is generally accepted that increased confining stress should broadly improve the capacity of a soil to resist applied loads, not reduce it. Clearly the volume of soil which is required to be treated and the difficulty and expense of that treatment are highly dependent on an accurate assessment of the potential for and consequences of liquefaction.

There is therefore strong motivation for owners of large dams to investigate the behavior of saturated sands subject to strong ground shaking under high initial effective confining stresses. In the absence of field data, the use of a centrifuge was considered to be the only practical option to realistically represent a deep soil deposit subjected to earthquake shaking. The studies to date have focused on level ground initial stress conditions in a two-layer (dense over loose) deposit of clean, fine Nevada sand. Examination of more complex stratigraphy and sloping ground stress conditions is planned for future studies.

2.0 THE ERDC CENTRIFUGE, EARTHQUAKE ACTUATOR AND ESB SPECIMEN CONTAINER

The design specification for the ERDC centrifuge followed a review of the Army's research needs and a study of the available academic facilities, Ledbetter (1991). Many of the field problems with which the U.S. Army Corps of Engineers is concerned are physically large, such as earth dams, locks and river control structures, environmental problems and military research. It was determined that a new facility with a high payload capacity and high g capability was required to meet future Army needs. A large beam centrifuge was commissioned, termed the Acutronic 684, based on the French designed Acutronic 661, 665 and 680 series of geotechnical centrifuges, Ledbetter et al. (1994a). The capacity of the ERDC centrifuge is a payload of 8 tonnes at up to 143 g, reducing to 2 tonnes at 350 g, with a platform area of 1.3m square. This high capacity enables field problems of the order of up to 300m in breadth, 300m in depth, and 1000m in length to be simulated under a wide variety of loading conditions. The facility is now fully operational, and is equipped with a large range of equipment and appurtenances, Figure 1.

The research approach for this high confining stress liquefaction study uses the large capacity of the WES centrifuge to investigate the generation of excess pore pressure and liquefaction under conditions which much more closely resemble those at depth in the field, Ledbetter et al. (1999). To do this required the design and construction of a large dynamic actuator.

2.1 Shaker design

A mechanical design was adopted for the earthquake actuator for the ERDC centrifuge, based closely on a smaller version designed for Cambridge University, England. Complex servo-hydraulic shaking systems have been developed and are operational on several centrifuges around the world, but these are limited in the g level to which they may operate,

and are considerably more expensive to build. The research by ERDC into the basic behavior of liquefying soils and comparison with present design methods required a base motion comprising a series of uniform cycles of base shaking, of variable duration and uniform frequency. A rotating mechanical system is ideally suited for this purpose. The large carrying capacity of the centrifuge meant that the shaker itself could act as the reaction mass for the specimen, minimizing the vibrations which would be otherwise transmitted to the centrifuge itself, and the model container could be much deeper and longer than usual.

The principle of the operation of the Mk I shaker was based on the use of stored energy to drive the specimen back and forth. Flywheels are incorporated in the shaker mechanism to store the energy in advance of the shaking event in the form of stored angular momentum. A system of linkages and eccentrics transferred the stored energy of the fly wheels to the shaking platform and thence into the soil specimen, Figure 2. A hydraulic or electrical motor drove the flywheels up to full speed, and then, on a signal, a high speed clutch grabbed the oscillating shaft and transferred energy into the model until another signal released it again. Clearly the frequency of the oscillation was directly proportional to the speed of the motor (and flywheels). The amplitude was controlled by the arrangement of the eccentrics; three displacement amplitudes for the platform were available (+/- 0.49mm, +/- 1.47mm and +/-4.41mm).

The shaker was designed (structurally) for operation up to 150g, at which the maximum load capacity of the shaking platform is reached (75 tonnes). The design maximum lateral force which the mechanism could exert on the shaking platform was 30 tonnes, and the maximum frequency at which the shaker could be safely operated was 150 Hz (eg. 1Hz prototype at 150g, or 3Hz prototype at 50g). (The Mk I shaker has recently been upgraded.)

2.2 Model containment

The specimen is built within a hollow rectangular model container, termed an equivalent shear beam (ESB) container, comprising a series of eleven aluminium alloy rings stacked one above the other, and separated by an elastic medium, Figure 3. Several of these chambers have been constructed, and extensive dynamic analysis and testing has been carried out to determine their dynamic response characteristics, Butler (1999). The model container has internal dimensions of 627mm deep by 315mm wide by 796mm long. Each of the eleven aluminium alloy rings is 50mm high. The rings are not stiff enough along their long dimension to support the outward pressure from the soil inside under high g, but they are supported by the massive reaction walls of the shaker unit itself. A rubber sheet separates the rings from the steel walls on either side. This concept has the added advantage of raising the center of gravity of the reaction mass in line with the center of gravity of the specimen, thus minimizing eccentric forces that may lead to rocking.

Thin metal sheets, termed shear sheets, are positioned on the interior end walls of the chamber and fixed securely to its base. The shear sheets accommodate the complementary shear force generated by the horizontal shaking within the specimen and transmit that force to the base of the container, Figure 4. This improves the uniformity of the stress field at each elevation along the model, reducing the tendency for the chamber to 'rock'.

The ESB concept is to create an equivalent shear beam with an average stiffness comparable to the stiffness of the soil specimen. Expressed rigorously, the concept is more accurately defined as achieving a dynamic response that does not significantly influence the behavior of the soil specimen inside. In certain classes of experiment, where the zone of interest is limited to the central region of the chamber, it may be expected that the stiffness of the soil (at least near the end walls) would not reduce significantly during shaking due to excess pore pressure rise. In this case the stiffness of the chamber may be designed accordingly, perhaps considering a shear modulus appropriate to the level of dynamic strain expected in the soil free-field at mid-depth. For other experiments

involving the liquefaction of large volumes of soil inside the container, the stiffness changes (and hence dynamic response) will change dramatically throughout the base shaking. A stiff chamber may lead to undesirable effects, as noted by Peiris (1999) who observed that liquefaction in a loose saturated sand model did not occur near the stiff end walls of the chamber. A chamber with no stiffness simply adds mass to the soil specimen, again changing its dynamic response. This poses a particular challenge for the design of an ESB container.

The ERDC ESB used in these experiments was assembled using a urethane adhesive sealant (commonly used as a windshield sealant for cars) between the aluminum alloy rings. This material has good elastic properties (exhibiting only minimal hysteresis under cyclic loading) and bonded well to the metal and to itself. The ESB has a relatively low shear stiffness of 441 KN/m^2 (shear stiffness of the full stacked ring assembly) and mass of 229 kg, with a first mode at 16Hz, and second, third, and fourth modes at 46, 87, and 116Hz respectively (Butler 1999). A typical saturated specimen at 50g in the ERDC ESB will have a theoretical natural frequency of around 84Hz, based on an average small strain shear modulus of 96 MN/m^2.

2.3 Dynamic response of the model container and specimen

In his doctoral thesis, Butler (1999) completed a thorough theoretical and experimental analysis of the dynamic response of the coupled soil-container system. At high g the soil and container act as a coupled system, where the lower stiffness of the container reduces the natural frequency (slightly) of the combined system compared to the soil column alone. However, provided the driving frequency is low relative to the natural frequency of the coupled system, Butler (1999) demonstrates that the displacement response of the system is unaffected compared to the soil acting independently, an ideal situation.

For higher driving frequencies, Butler (1999) concludes that it would be necessary to reconsider the elastic stiffness of the ESB container, and to tune the container to ensure that even with the expected level of degradation in the soil specimen, the coupled system did not deviate significantly from the condition of the soil column alone. This may be possible by adding mass to the rings of an initially stiffer ESB to reduce its first mode to the desired level, Butler (1999).

The liquefaction of a level sand bed has previously been the subject of other research. Experiments were conducted at many centrifuge centers under the VELACS project, Arulanandan and Scott (1994). The objective of the ERDC study is to investigate the onset of liquefaction under much higher initial effective overburden stresses.

3.0 RESEARCH PROGRAM

Table 1 summarises the experiments conducted during 1998 and 1999. The models are grouped in series, where each series corresponds to a different target range of vertical effective overburden stress in the loose layer. In all cases, the bottom 160mm of the specimen was around 50% Relative Density (RD) and the upper portion was around 75% RD. All models were shaken at 50g. Some models were overconsolidated by a factor of 2.5 prior to shaking (achieved by running the centrifuge up to 125g). A large series of experiments have been conducted with a range of overburden depths to provide repeatability and redundancy in the instrumentation and data records. All the models were built using Nevada sand and tested at 50 g. The experiments are summarized in Table 2.

The Nevada sand used in the models was characterized by standard laboratory tests to determine parameters such as dry density and gradation. Table 3 presents key material parameters for this sand.

The pore fluid comprised a mixture of glycerine and water, 80% by weight for experiments conducted at 50g. Measurements of the viscosity of glycerine-water mixes at a range of temperatures and proportions show that the viscosity is sensitive to both parameters.

The density of a glycerine-water mix was calculated from:

$$\rho_m = \rho_g(m_g + m_w)/(m_g + \rho_g m_w)$$

where ρ_m is the density of the mix, ρ_g is the density of glycerine, m_g is the mass of glycerine, and m_w is the mass of water. Table 4. summarizes the properties of the glycerine-water solution used as the pore fluid.

The models were poured dry from a hopper and saturated under vacuum, or slowly under gravity. Instrumentation was placed in the model as it was being constructed.

The typical arrangement of the model specimens for the different test series is shown in Figure 5. Instrumentation was positioned through the depth of the models, and comprised pore pressure transducers and accelerometers. The location of the instrumentation for Model 5b is shown in Figure 6.

4.0 AMPLIFICATION OF BASE INPUT MOTION

As the base input motion propagates through the height of the specimen, it may be amplified or attenuated depending on the dynamic properties of the soil column and the frequency content of the input motion. This is similar to conditions in the field, where elastic wave energy is modulated as it passes through different soil deposits. Examination of the time histories of acceleration at different depths in a deep soil column such as Model 5b, Figure 6, shows that in the absence of significant degradation caused by large strains or excess pore pressures, the amplification factor is around 1, Figure 7. A similar response was also found for shallow specimens. In specimens where large excess pore pressures started to develop through the soil column, however, the characteristics of the motion propagating upwards tended to change dramatically. In the extreme, the lateral accelerations of the surface becomes isolated from the base input, as may be seen in Figure 8 which shows the acceleration at different depths in Model 2f.

5.0 DEVELOPMENT OF EXCESS PORE PRESSURES AND LIQUEFACTION AT SHALLOW DEPTHS

The target initial effective vertical stress in Model 2f was 1 tsf (100 KPa) at mid-depth in the loose layer (Table 2). The specimen was overconsolidated by accelerating the centrifuge to 125g prior to subjecting it to shaking motion at 50g. Figure 9 shows how the excess pore pressures at different depths developed with time. It is clear that within a few cycles of shaking, the loose sand layer has fully liquefied.

Comparison between the acceleration time histories in Figure 8 and the excess pore pressures in Figure 9 for the loose and dense layers shows the correlation between transmitted motion and level of excess pore pressure. The upper section (near surface) of the dense layer liquefies within 0.2 seconds (0.2 x 50 = 10 seconds field equivalent). The percentage of excess pore pressure is calculated by dividing the measured fluid pressure by the calculated initial overburden stress. The actual overburden stress may vary over time due to small movements of the transducer in the liquefied ground; this has a larger effect on the accuracy of measurement at shallower locations, such as PPT 38.

It is interesting to note that despite the difference in relative density between the dense and loose layers, the soil column behaves more like a single unit than as two layers. This is because each increment of excess pore pressure at depth immediately causes a fluid pressure, which affects the whole column through the volumetric compressibility of the pore fluid. This is considerably lower than the shear compressibility of the soil skeleton, which is determining the speed of transmission of the elastic shear wave upwards.

6.0 GENERATION OF EXCESS PORE PRESSURES AT HIGH CONFINING STRESS

At high initial effective confining stress pore pressures are also observed to rise strongly

during the initial cycles of shaking. After some time, this steady rise is arrested, and then excess pore pressure is capped at a value less than the full 100% of the initial vertical effective stress seen in shallow soil columns. Figure 10 shows a set of data from Model 4d, a deep soil specimen with an initial effective vertical stress of around 500 KPa (4.7 tsf) at mid-depth in the loose layer.

A similar picture was found at even higher initial vertical effective stress. Figure 11 shows the development of excess pore pressure under a vertical effective stress in the middle of the loose layer of 1037 KPa (9.7 tsf). In this figure, the actual fluid pressure has been plotted in KPa, to be compared with the initial vertical effective stress. The time history of base shaking is shown below the pore pressure record in two forms. The first trace shows the measured record, which includes a degree of high frequency noise. In the second, lower trace, this signal has been processed with a Butterworth band pass filter, 250 and 10 Hz, to extract the main shaking frequency. From this record, it is clear that the amplitude of the shaking motion is almost constant throughout the record, and particularly that the amplitude remains at or near its peak level throughout the second half of the shaking episode, when the excess pore pressure has been capped (after about 0.8 seconds of shaking, or 40 seconds field equivalent). In this case, the excess pore pressure is capped at around 50% of the value required to reach 'initial liquefaction'.

The amplitude of cyclic shaking was easily sufficient to generate excess pore pressures at a strong rate during the first half of the event, and this can be seen in the top trace of Figure 11. Indeed, after around 0.4 seconds of shaking the rate of excess pore pressure build-up increases, and this may be related to a moderate increase in the amplitude of base shaking at the same time. Between around 0.4 seconds and 0.7 seconds of shaking the rate of increase of excess pore pressure is around 350/0.3 ~ 1000 KPa/second (or 20 KPa/second field equivalent). The driving frequency of input motion is around 50 Hz (1 Hz field equivalent). During the same period, the amplitude of shaking is around +/- 15% g, which corresponds to a cyclic displacement of +/- 0.76 mm (38 mm field equivalent) at that depth.

This pattern of behavior was found in all specimens at initial vertical effective confining stresses of around 250 KPa or greater. Although not a rigorous comparison, as there are a number of variables (including amplitude) between the different experiments, Figure 12 shows the normalised results from a range of initial conditions. There is a general trend with increasing initial vertical effective stress, towards the capping of excess pore pressure at a level lower than the expected 100%.

All of the records of excess pore pressure from all the model specimens were re-examined to determine the residual pore pressure at the level of capping. Although the amplitudes of shaking and the densities of the sand varied (the data-set includes both 'dense' and 'loose' sand layers as described above) a clear correlation was found between the maximum level of excess pore pressure and the initial vertical effective stress, as shown in Figure 13. This figure includes 125 data points from first and succeeding earthquakes, normally and overconsolidated specimens, and dense and loose layers.

Figure 14 shows the data from first earthquakes only, broken out by normally consolidated and overconsolidated (including dense and loose results). Again, there is a strong correlation between the maximum level of excess pore pressure generated during the shaking and the initial vertical effective stress. In this case, the overconsolidated data is seen to lie to the left of the normally consolidated data, indicating that the level of excess pore pressure may reduce for increased overconsolidation. This is consistent with experience.

On the right hand side of Figures 13 and 14, an approximate depth scale has been given for guidance, expressed in feet. Clearly the calculation of equivalent field depth depends on many assumptions, but it is worth noting that the data appear to show that whilst liquefaction may readily occur within the upper 40 feet or so of a saturated sand deposit, it becomes increasingly

unlikely at greater depths. This is consistent with field observation.

Research work is continuing with a view to full verification of these findings and the preparation of design guidance. Further experiments will address the effects of amplitude of shaking, sloping ground and density.

7.0 CONSEQUENCES FOR A HYPOTHETICAL LARGE EARTH DAM

To illustrate the potentially highly significant consequences of capped pore pressures decreasing with depth, a hypothetical earth dam of the form outlined in Figure 15 is assessed. The estimated deformation response is calculated for earthquake induced potential pore pressures based on standard approaches, Seed and Harder (1990), Youd and Idriss (1997), and on limiting pore pressure generation. Deformations are estimated following the procedures of Ledbetter and Finn (1993), Finn et. al. (1995), and Ledbetter et. al. (1994b), with the use of the non-linear dynamic effective stress analysis program TARA, Finn el. al. (1986), and Finn and Yogendrakumar (1989).

The dam is located across stream channel deposits with assumed profile, Figure 15, as: (a) foundation older stiffer alluvium below elevations 151 m (u/s) - 163 m (d/s), (b) younger less stiff alluvium above the older alluvium, and (c) roller compacted zoned earth dam founded on the young alluvium. Crest level and Pool level are 211m and 199m respectively. Standard Penetration $(N_1)_{60}$ values range from 5 to 15 and shear-wave-velocity (V_s) from 180-450 m/s in the young alluvium freefield upstream and downstream. Beneath the dam, the young alluvium downstream $(N_1)_{60}$ values range from 30 – 40 and V_s from 425-700 m/s and upstream $(N_1)_{60}$ values range from 6-20 with V_s from 150-350 m/s. Ground motions are assumed to be from a magnitude 7.75 earthquake occurring at a distance from the dam about 50 miles with a peak acceleration of 0.22g at the dam.

7.1 Maximum potential residual excess pore pressure

Seed's simplified procedures (Seed and Harder, 1990) were coupled with non-linear dynamic effective stress finite element analysis to yield "field observation and laboratory based" estimates for earthquake induced pore pressures. These pore pressures are considered the "maximum potential residual excess pore pressures" that that could be generated by the design earthquake, based on historic field earthquake response. Unless the soils have low permeability and/or are bounded by low permeability layers that prevent the dissipation of excess porewater pressures, earthquake-generated porewater pressures should be less than the maximum potential.

For this example dam, Figure 15 shows the maximum potential residual excess porewater pressures (shaded zones) that can be generated by the design earthquake. The young alluvium can generate pore pressures (a) downstream of the downstream toe but nothing of significance beneath the downstream shell and (b) upstream of the upstream toe and beneath the upstream shell. The lighter shaded upstream zone extends completely beneath the darker shaded zone. Pore pressures in these lighter shaded zones are between 80 – 100 % of the initial vertical effective stress with the majority between 90 and 100 %.

The research findings expressed in this paper are for level ground conditions. Continuing research will be addressing the effects of residual shear stresses such as induced by the geometry of a dam. Until the geometry effects are known, this example applies the pore pressures trend shown in Figure 14 for the normally consolidated case as the cap or limitation. In this example, the zone of soil that will be effected and have reduced pore pressure potential is the darker shaded zone beneath the upstream shell; quite naturally, this is a high confining stress zone and where K_σ leads to a strength reduction due to the high confinement. This zone is exactly where strength increase or less strength degradation is of prime importance

to the dam behavior under earthquake loading. The pore pressure potential in the darker shaded zone is reduced from 80 – 100 % to 50 –75% of the vertical effective stress.

7.2 Deformation response of the dam

Figures 16 and 17 illustrate the effects or differences in earthquake induced deformations and strains caused by the applied pore pressure limits. For the deformation stage shown in the figures, the only elements that appear shaded are those significantly straining and participating. Figure 16 shows the deformations at effective strength reduction to 72 % of the initial caused by pore pressure increase. The dam will continue to deform as pore pressure builds to the maximum potentials and residual strength is reached beneath the dam in the foundation, which is around 90 % reduction of initial strength. Unless remediated, severe earthquake damage to the dam is possible accompanied by overtopping and piping through the core resulting in complete failure.

Figure 17 illustrates the benefits achieved by applying the limiting pore pressure with depth trend. The deformation stage in Figure 17 is the same as that in Figure 16. As shown strains, deformations and the active elements are significantly reduced. The dam continues to deform as pore pressures increase to their maximum potentials and residual strengths; however, the final stages of deformation are considerably less than those under the conditions in Figure 16.

Immediately obvious from comparison of Figures 16 and 17 is that more strength is available to resist deformation movements and to buttress and assist remedial treatments. The availability of more strength translates to smaller and less remediation and lower costs. The stage of progressive strength reduction illustrated in both Figures 16 and 17 was chosen to best exemplify the impact of limiting pore pressure criteria on dams with liquefiable soils in high initial effective confining stress fields.

The implication of the present study is that although soil at depth may soften and degrade under earthquake induced excess pore pressure behavior, the reduction in strength is limited and liquefaction under high confining stresses may not be the hazard that it is presently assumed to be.

8.0 CONCLUSIONS

1. A large data-set of the behavior of loose saturated sands under high initial effective confining stresses and subject to earthquake-like shaking has been collected during an extensive experimental program on the ERDC Centrifuge, Vicksburg MS.

2. This data has shown that, at moderate amplitudes of excitation, the maximum level of excess pore pressure development is capped at high initial effective confining stress and does not reach a level sufficient to cause 'initial liquefaction' (defined as 100% of the initial vertical effective stress).

3. These findings are currently being verified and will then be used to develop appropriate design guidance.

4. High pore pressures and the potential for liquefaction beneath dams may not be the hazard that it is currently perceived to be.

5. The implication for the assessment of liquefaction hazard and requirements for remediation works under large earth dams is potentially very significant.

9.0 ACKNOWLEDGEMENTS

The ERDC Centrifuge Research Center and the Army Civil Works Earthquake Engineering Research Program of the U.S. Army Corps of Engineers sponsored this research. The members of the ERDC centrifuge team who helped conduct this work were Richard Burrows, Lee Miller, Dr Gary Butler, Rodgers Coffing, Wipawi Vanadit-Ellis, and Dr Mike Sharp. The ERDC machinists contributed greatly to the project. Drs William Marcuson and Michel

O'Connor were Directors of the Geotechnical Laboratory. Permission to publish this paper by the Chief of Engineers is gratefully acknowledged.

10.0 REFERENCES

Arulanandan, A. and Scott, R.F. (1994) editors, Proc. Int. Conf. on Verification of Numerical Procedures for the Analysis of Soil Liquefaction Problems, at U.C. Davis; Volumes 1 & 2; Balkema.

Butler, G.D. (1999). A dynamic analysis of the stored energy angular momentum actuator used with the equivalent shear beam container, PhD thesis, Cambridge University (in preparation).

Finn, W.D.L. and Yogendrakumar, M., Yoshida, N. and Yoshida, H., (1986), "TARA-3: A Program to Compute the Response of 2-D Embankments and Soil-Structure Interaction Systems to Seismic Loadings", Department of Civil Engineering University of British Columbia, Canada.

Finn, W.D.L., Ledbetter, R.H., and Marcuson, W.F. III (1995). "Seismic Deformations in Embankments and Slopes", Symposium on Developments in Geotechnical Engineering - From Harvard to New Delhi, 1936-1994, Bangkok, Thailand, A.A. Balkema, Rotterdam.

Finn, W.D.L. and Yogendrakumar, M., (1989) "TARA-3FL; Program for Analysis of Liquefaction Induced Flow Deformations", Department of Civil Engineering, University of British Columbia, Vancouver, Canada.

Ledbetter, R.H. (ed) (1991) Large centrifuge: a critical Army capability for the future, Misc. Paper GL-91-12, Dept. of the Army, Waterways Experiment Station, Vicksburg, MS, May.

Ledbetter, R.H., and Finn, W.D.L. (1993). "Development and Evaluation of Remediation Strategies by Deformation Analysis", ASCE Specialty Conference on Geotechnical Practice In Dam Rehabilitation, Raleigh, North Carolina, April, pp 386 - 401.

Ledbetter, R.H., Steedman, R.S., Schofield, A.N., Corte J.F., Perdriat J., Nicholas-Font J. and Voss H.M. (1994a) US Army's engineering centrifuge: Design, Proc. Centrifuge 94, pp63-68, Singapore, 31 Aug – 2 Sept, Balkema.

Ledbetter, R.H., Finn, W.D.L., Hynes, M.E., Nickell, J.S., Allen, M.G., and Stevens, M.G. (1994b). "Seismic Safety Improvement of Mormon Island Auxiliary Dam", 18th International Congress on Large Dams, Durban, South Africa.

Ledbetter, R.H., Steedman, R.S. and Butler, G.D. (1999) Investigations on the behavior of liquefying soils, Proc Int Workshop on Physics and Mechancs of Soil Liquefaction, Baltimore MD, Lade P.V. and Yamamuro J.A. (eds), 10-11 Sept 1998, Balkema, pp 295-306.

Peiris, L.M.N. (1999) Seismic modelling of rockfill embankments on deep loose saturated sand deposits, PhD Thesis, Cambridge University.

Seed H.B. (1983) Earthquake-Resistant Design of Earth Dams, Proceedings of Symposium on Seismic Design of Embankments and Caverns, May, ASCE pp 41-64.

Seed R.B. and Harder L.F. (1990) SPT-Based analysis of cyclic pore pressure generation and undrained residual strength, Proc. H Bolton Seed Memorial Symposium, Vol. 2, pp 351 - 376, BiTech Publishers Ltd, Vancouver.

Youd, L. and Idriss, I., Eds (1997) Workshop on Evaluation of Liquefaction Resistance of Soils, Proceedings, Salt Lake City, Technical Report NCEER-97-0022, sponsored by FHWA, NSF and WES, published by NCEER.

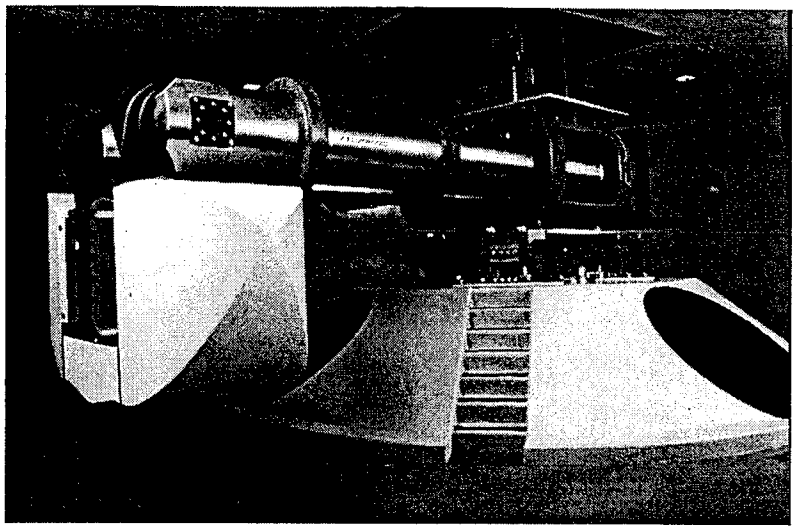

Figure 1. The WES centrifuge

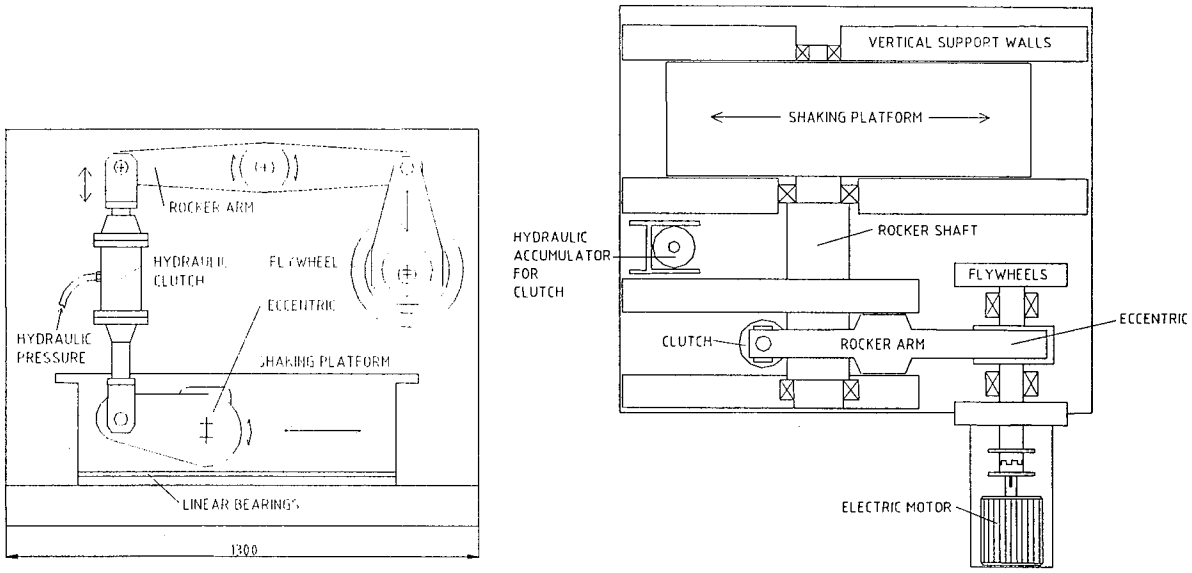

Figure 2. The ERDC Mk I earthquake actuator

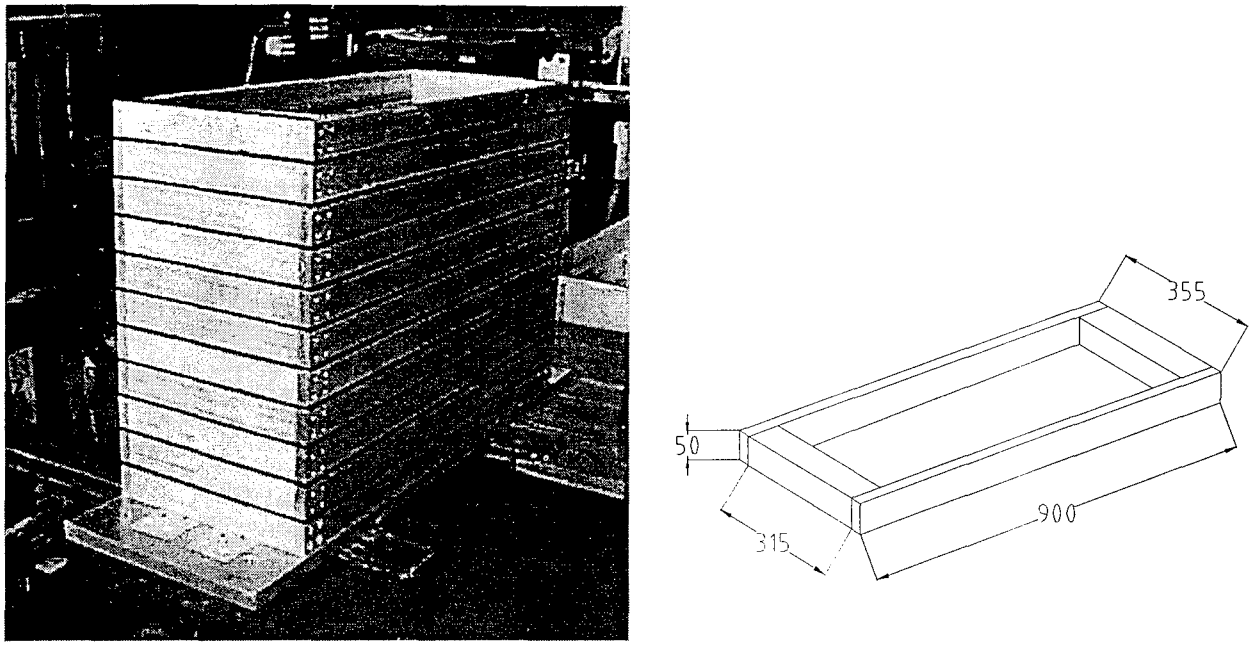

Figure 3. Typical Equivalent Shear Beam specimen container

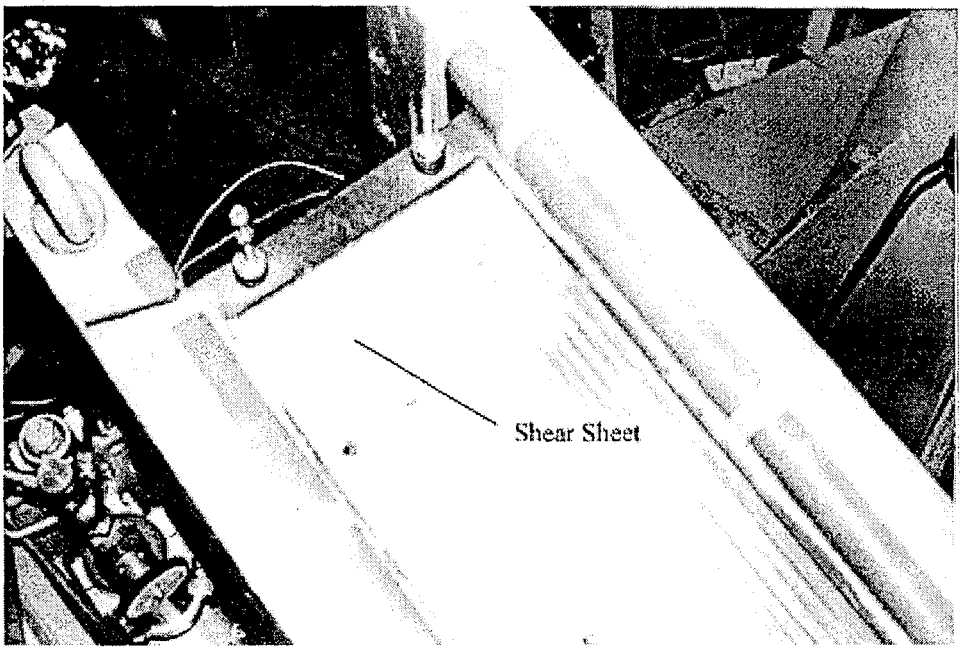

Figure 4. Shear sheets form the boundaries on the end walls of the ESB

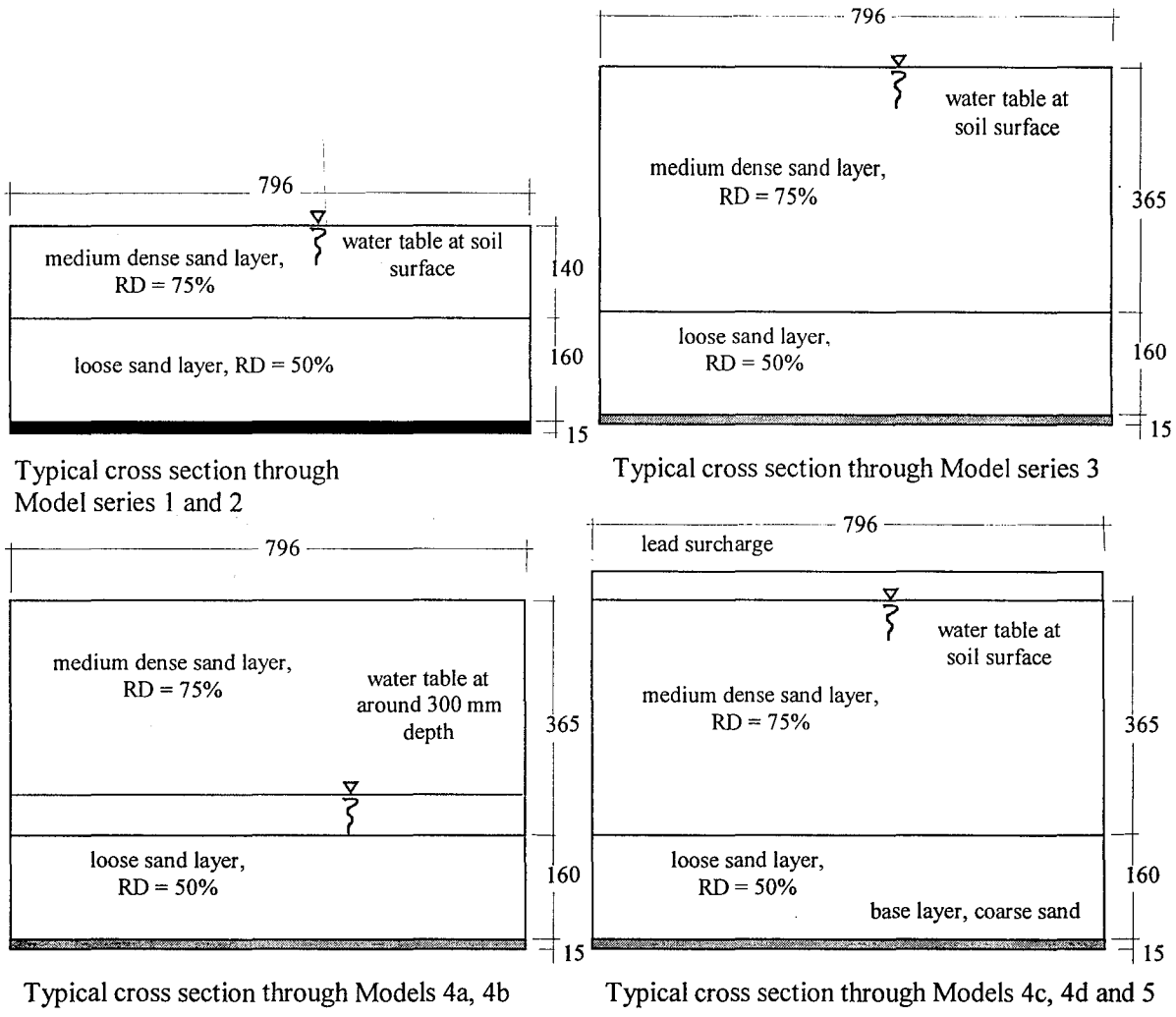

Typical cross section through Model series 1 and 2

Typical cross section through Model series 3

Typical cross section through Models 4a, 4b

Typical cross section through Models 4c, 4d and 5

Figure 5. Cross sections through the different model configurations

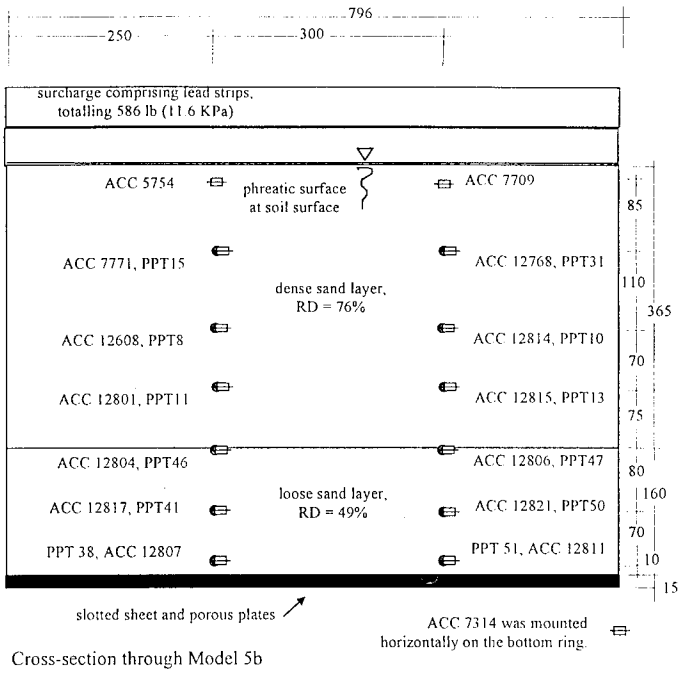

Figure 6. Instrumentation for Model 5b

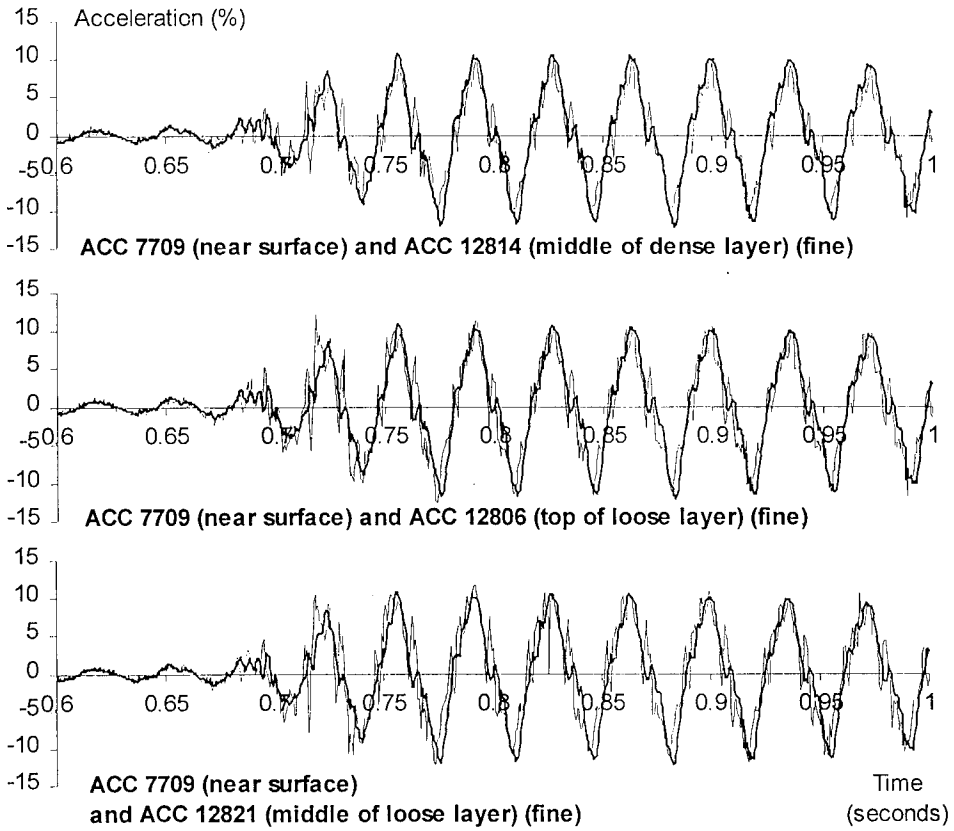

Figure 7. Comparison of the measured surface acceleration with the acceleration at different depths, Model 5b

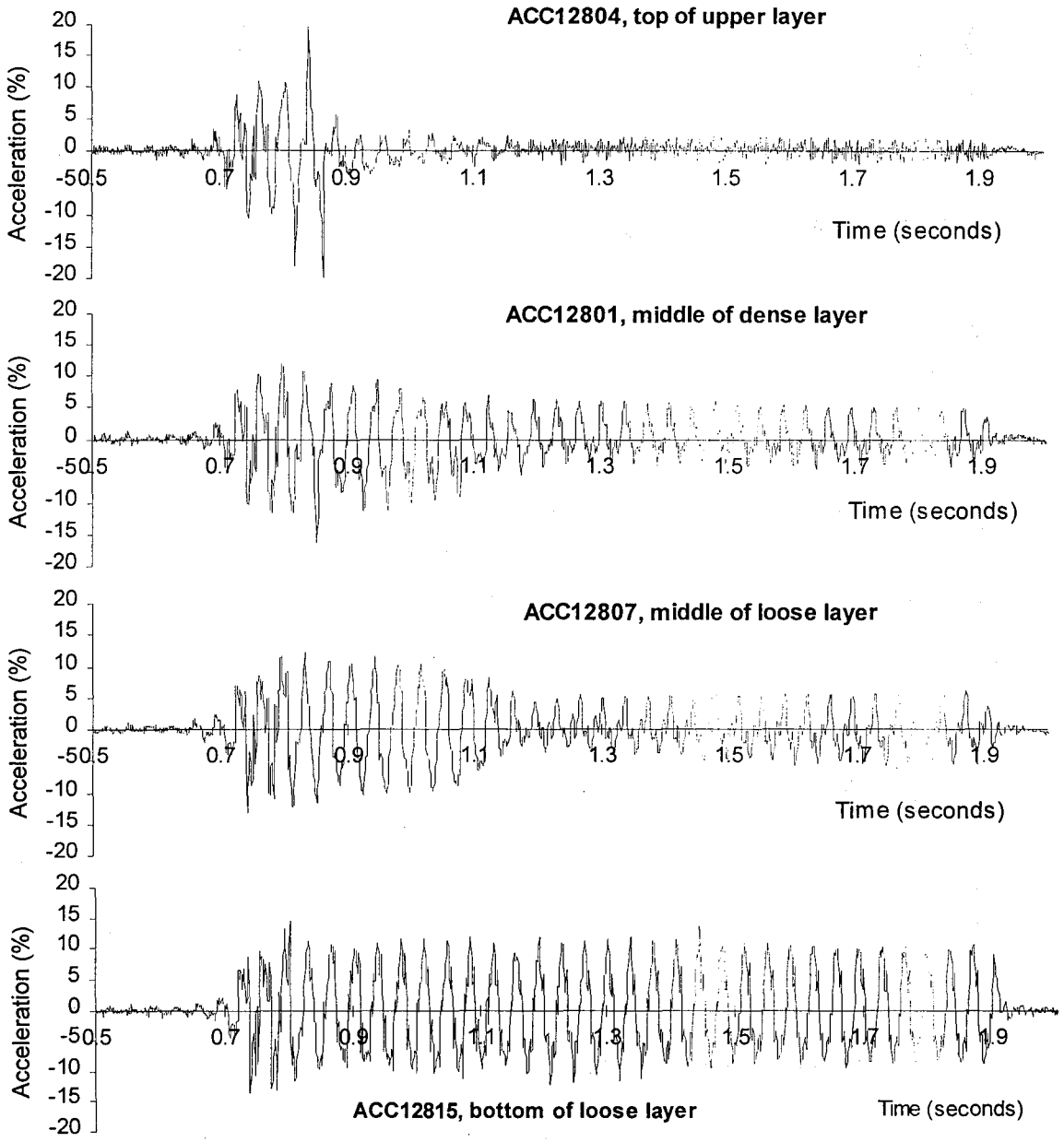

Figure 8. Comparison of measured accelerations at different depths, Model 2f

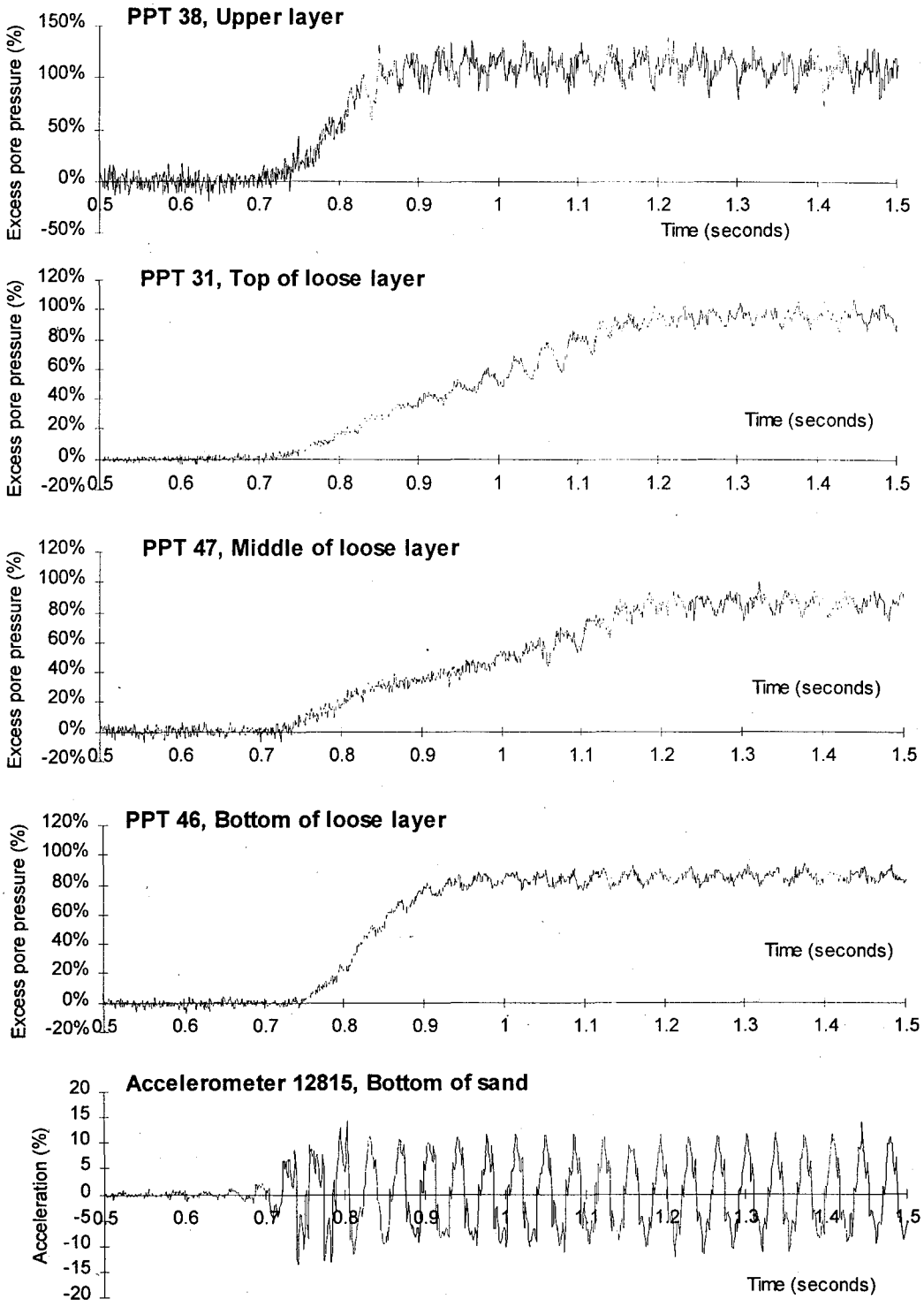

Figure 9. Development of excess pore pressure in a shallow bed, Model 2f

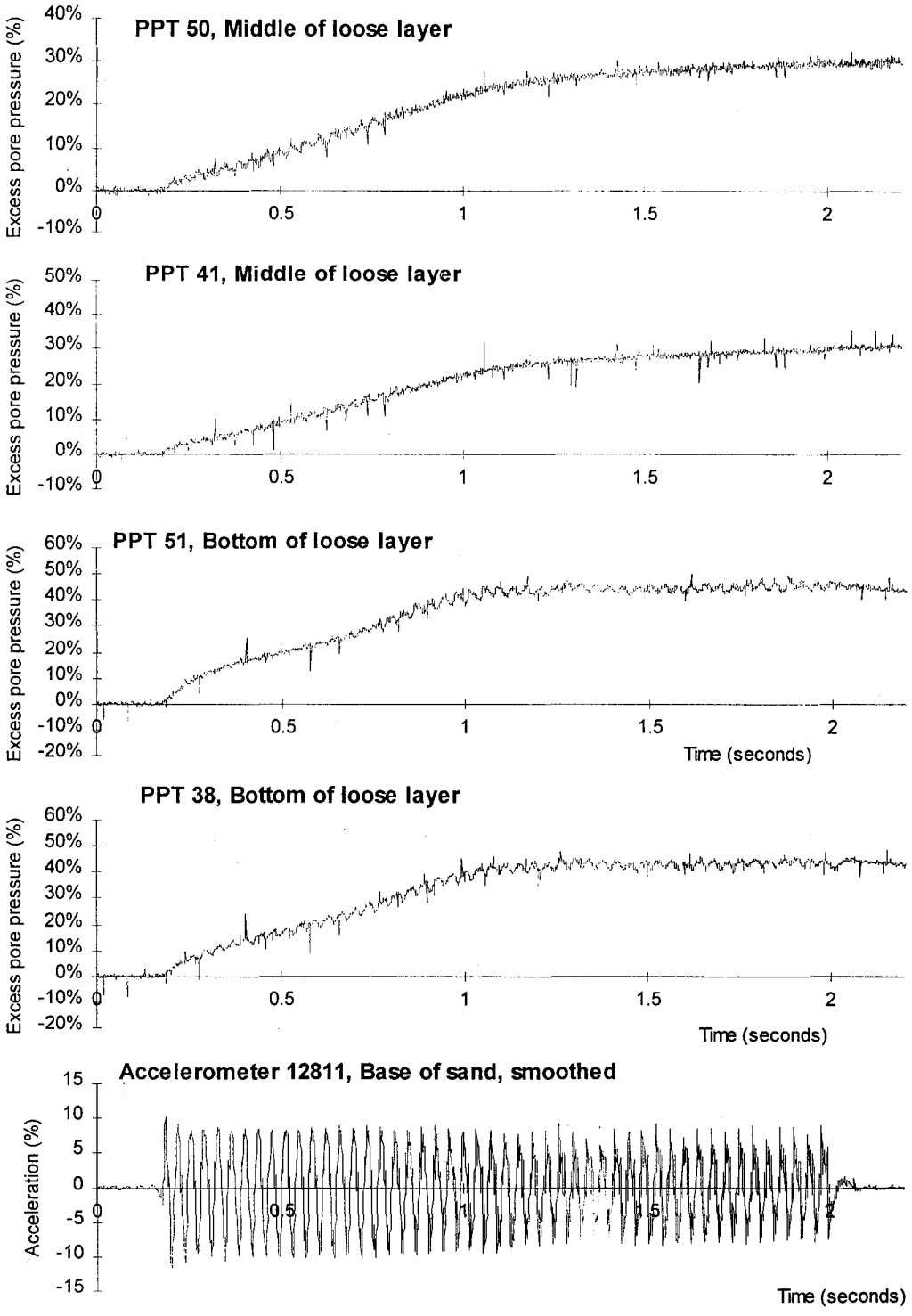

Figure 10. Development of excess pore pressure at over 500 KPa, Model 4d

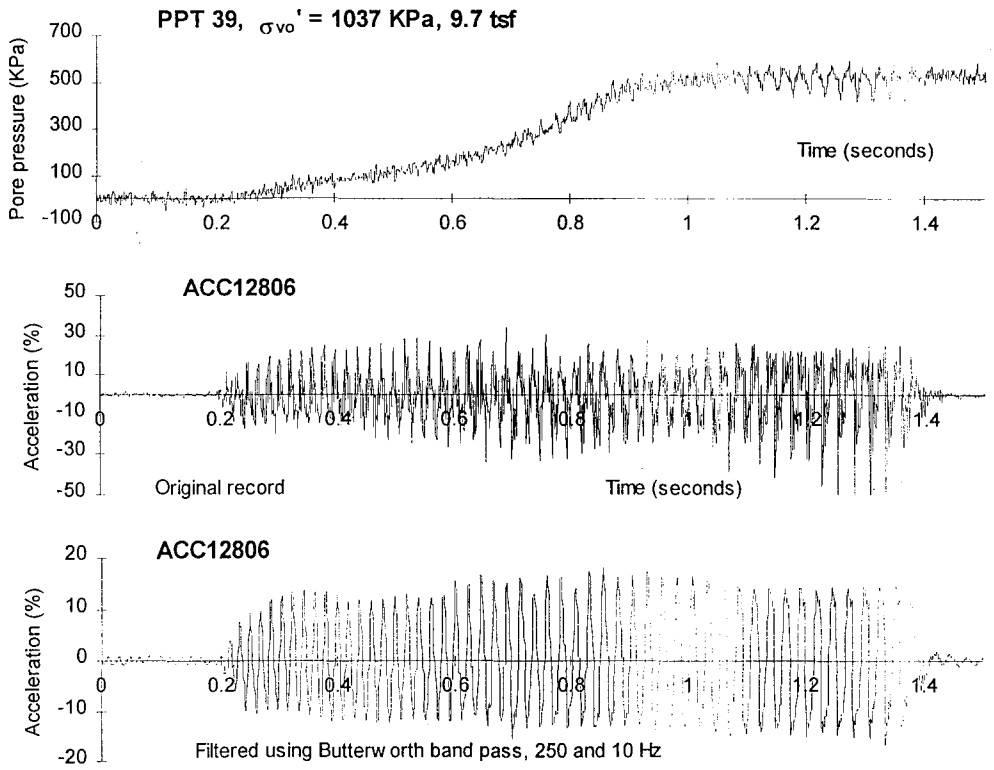

Figure 11. Development of excess pore pressure at initial vertical effective stresses of up to 1000 KPa (10 tsf), Model 5d

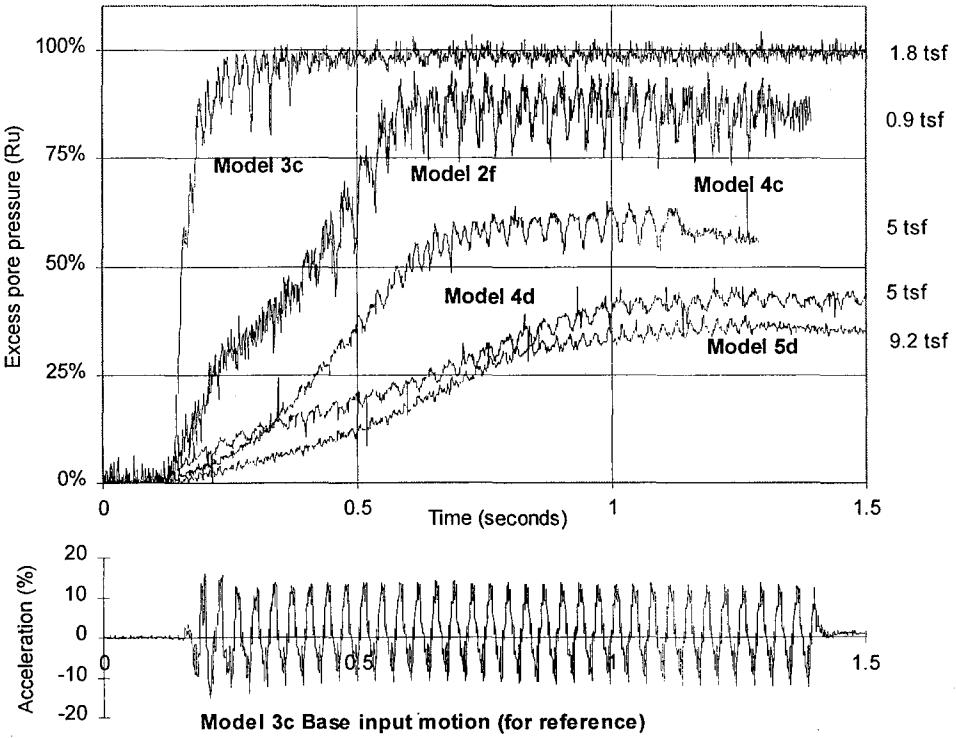

Figure 12. Comparison between excess pore pressure development at different initial vertical effective stresses

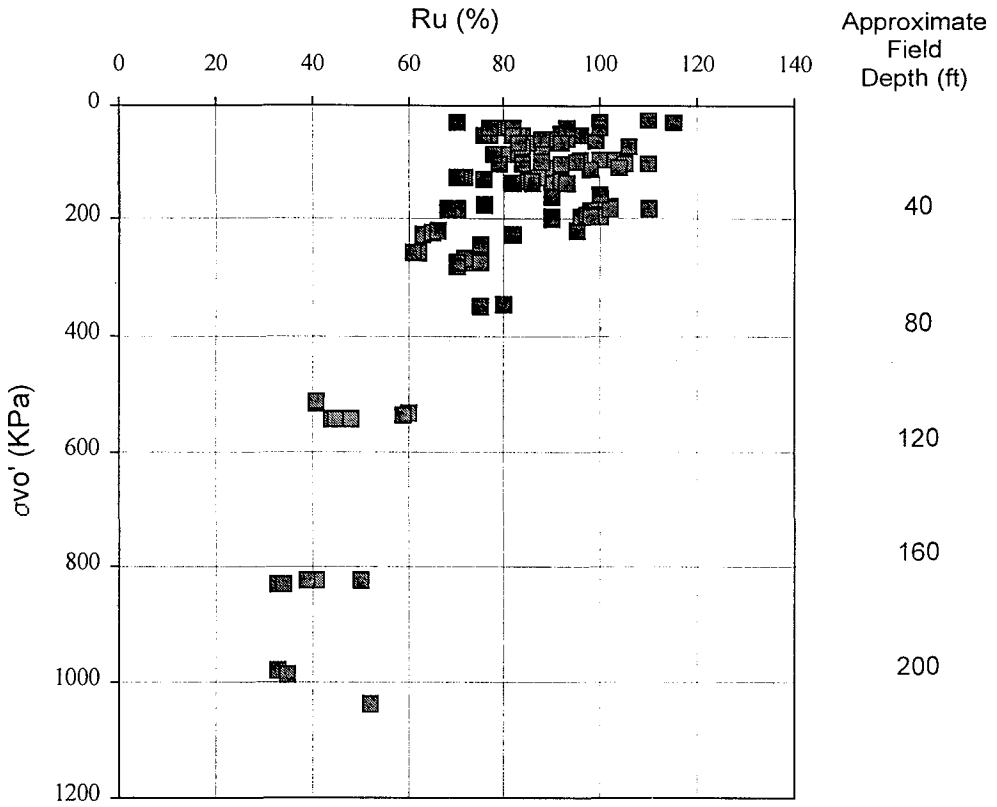

Figure 13. Comparison between maximum residual excess pore pressure and initial vertical effective stress, all data

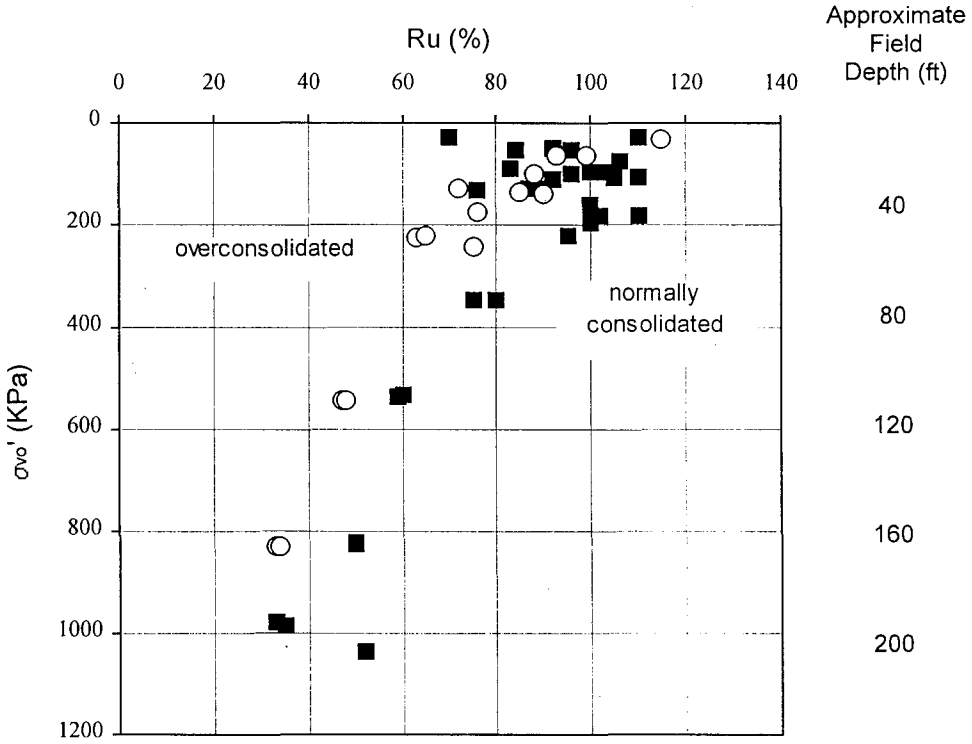

Figure 14. Comparison between overconsolidated and normally consolidated data, all data

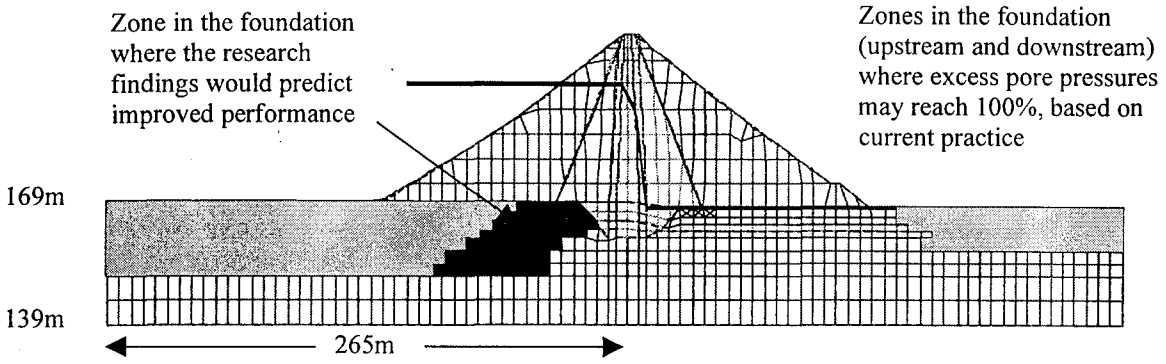

Figure 15. Comparison of affected zones in the foundation

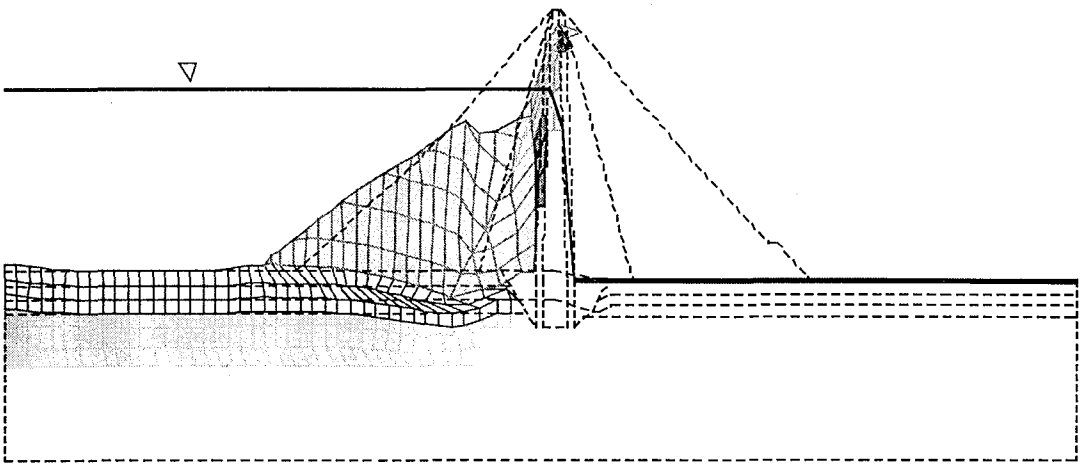

Figure 16. Deformations calculated using current analyses

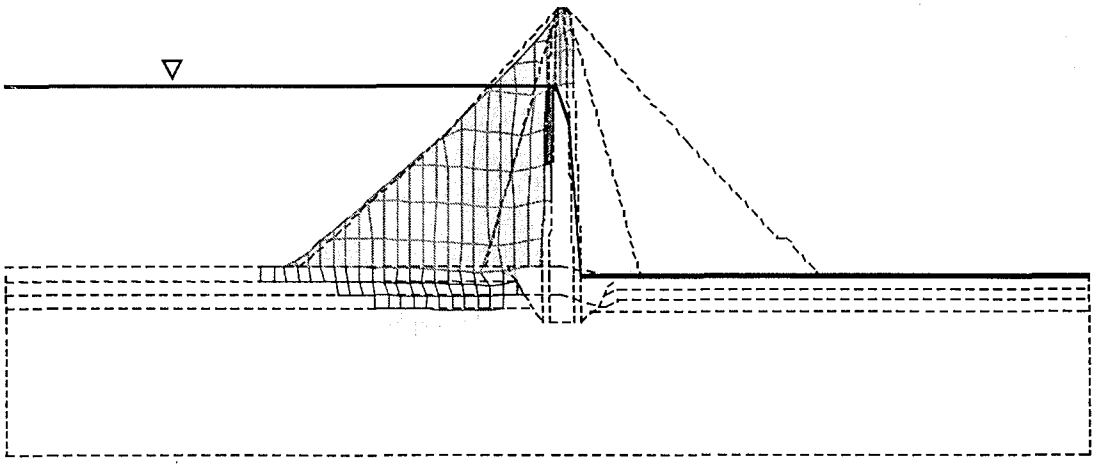

Figure 17. Deformations predicted using pore pressure limits and improved soil strength

Model series	Models in series	Effective overburden stress in loose layer	Depth of prototype (approx)	Depth of specimen	Notes
2	a, b, c, d, e, f	1 tsf	15 m	300 mm	Nevada sand
3	a, b, c, d, e	2 tsf	26 m	525 mm	Nevada sand
4	a, b, c, d	3 – 5 tsf	26 – 40 m	525 mm	Nevada sand with lowered w.t. or surcharge
5	a, b, c, d	7 – 10 tsf	54 – 63 m	525 mm	Nevada sand with lead surcharge

Table 1. Summary of model tests

Model Code	Overall depth (mm)	Relative Density	σ_v' at mid-depth in loose layer (tsf)	OCR	Number of earth-quakes	Comments
2a	300	44% loose 83% dense	1	1	3	Saturated to ground surface.
2b	300	50% loose 75% dense	1	1	2	Saturated to ground surface.
2c	300	49% loose 74% dense	1	1	5	Saturated to ground surface.
2d	300	50% loose 75% dense	1	1	4	Saturated to ground surface.
2e	300	49% loose 73% dense	1	2.5	4	Saturated to ground surface.
2f	300	50% loose 75% dense	1	2.5	4	Saturated to ground surface.
3a	525	34% loose 73% dense	2	1	2	Saturated to ground surface.
3b	525	49% loose 77% dense	2	1	3	Saturated to ground surface.
3c	525	49% loose 79% dense	2	1	3	Saturated to ground surface.
3d	525	54% loose 80% dense	2	2.5	4	Saturated to ground surface.

Table 2a. Detailed summary of experiments, Models 2a – 3d

4a	525	49% loose 80% dense	3	1	4	Saturated to top of loose layer only.
4b	525	56% loose 74% dense	3	2.5	4	Saturated to top of loose layer only.
4c	525	50% loose 75% dense	4.7	1	4	Saturated to ground surface. Lead surcharge.
4d	525	50% loose 68% dense	4.7	2.5	4	Saturated to ground surface. Lead surcharge.
5a	525	51% loose 72% dense	7.4	1	4	Saturated to ground surface. Lead surcharge.
5b	525	49% loose 76% dense	7.4	2.5	4	Saturated to ground surface. Lead surcharge.
5c	525	52% loose 75% dense	9.2	1	3	Saturated to ground surface. Lead surcharge.
5d	525	57% loose 80% dense	9.2	1	1	Saturated to ground surface. Lead surcharge.

Table 2b. Detailed summary of experiments, Models 4a – 5d

Specific gravity	2.64
Maximum void ratio	0.757 (density 93.8 pcf)
Minimum void ratio	0.516 (density 108.7 pcf)
D_{50}	0.18 mm (approx)
D_{10}	0.11 mm (approx)

Table 3. Nevada Sand (parameters as measured)

Density	1200 kg/m^3
Viscosity	50 cs
Specific Gravity	1.26
Composition	80% glycerine-water mix (by weight)

Table 4. Parameters for pore fluid (as measured)

SOIL AMPLIFICATION FACTOR FOR SEISMIC DESIGN OF BUILDINGS

By

Izuru OKAWA[1], Masanori IIBA[2], Mitsumasa MIDORIKAWA[3],
Shin KOYAMA[4], and Kenji MIURA[5]

ABSTRACT

In this paper, a method for evaluating the amplification property of earthquake motions due to the surface soil.
In the current Japanese building code, the site response effect is represented by three kinds of soil classification, hard, intermediate and soft. This classification is simple enough to specify the design seismic force for the soil conditions. However, when soil investigation is conducted and one may get numbers of information on soil properties and can evaluate some properties consistent with the soil condition, it is extremely rough to use only three categories. Therefore, we bear it in mind to evaluate the necessary property with given data specific to the site as much as possible. This might be conformed to the performance-based design method.
The basic concept of our proposal for seismic design spectra for major earthquake motions is 1) Basic design spectra defined at the engineering bedrock, and 2) evaluation of site response for geotechnical data of surface soil layers. Meanwhile, it is not recommended for general structures to be verified its seismic safety and/or performance through the analyses using time history of design ground motions.

This paper proposes a method for evaluating nonlinear amplification due to surface soil overlying engineering bedrock (EBR) using design response spectrum. The proposed method follows the procedures below.

(1) Represent the response characteristics of surface soil on EBR by a multi-lumped mass model with shear springs and damping coefficients.
(2) Calculate a period T_1, a mode shape $\{U_1\}$ and a modal damping factor h_1 for the first vibration mode.
(3) Evaluate the equivalent shear wave velocity Vs_e of surface soil
(4) Evaluate the amplification factor R_1 of the surface to EBR at T_1 using an equivalent surface single layer
(5) Evaluate the displacements in surface soil from $R_1\{U_1\}$, and hence evaluate the shear strains.
(6) With given nonlinear relations between shear modulus (G), damping factors (ξ) and shear strains, replace soil constants G and h by those corresponding to strains.
(7) Return to step (1) with revised G and ξ Iterate these procedures until T_1 converges.
(8) After T_1 is converged, calculate the response distributions in surface soil. The results obtained by the proposed method are compared with those by "SHAKE" in terms of the response spectrum at the surface as well as distributions of displacement, shear wave velocity and damping factor in the surface soil. The applicability of the proposed method for evaluating the nonlinear amplification is confirmed through the comparative studies.

KEY WORDS : Amplification factor, Seismic design, Engineering bedrock, SHAKE

1) Head, Construction Techniques Division, Production Engineering Division, Building Research Institute, Ministry of Construction
2) Head, Evaluation System Division, Codes and Evaluation Research Center, BRI
3) Director, International Institute of Seismology and Earthquake Engineering, BRI
4) Senior Engineering Staff, IISEE, BRI
5) Director, Kobori Research Complex, Kajima Corporation

1. INTRODUCTION

It is commonly adopted in seismic design of structures to incorporate the dynamic property of surface ground. The currently enforced Japanese Building Standard Law specifies concept of soil classification to differentiate its effect to seismic load. However, the classification is made so simply that the actual property of the surface soil may not be necessarily reflected with the geotechnical data of the site, even if it is available. It is important for engineers to design structures based on the field investigation result. Therefore, the design code should facilitate such option to utilize site specific property.

2. BASIC RESPONSE SPECTRUM AT ENGINEERING BEDROCK

In our proposal, the earthquake load for seismic evaluation is specified with earthquake ground motion not with seismic force given in the current Building Standard Law of Japan. The evaluation of earthquake motion is represented with the acceleration response spectrum in the following formula.

$$S_A(T) = ZG_s(T)S_0(T) \qquad (1)$$

Where, $S_A(T)$: acceleration response spectrum for evaluation, Z: seismic zoning factor, $G_s(T)$: soil amplification factor, and $S_0(T)$: basic acceleration response spectrum at exposed (outcrop) engineering bedrock.

The engineering bedrock is defined as a layer with more than approximately 400 m/s in shear wave velocity. The basic response spectrum for major earthquakes is illustrated in Figure 1.

3. EVALUATION PROCEDURE OF ACCELERATION RESPONSE SPECTRUM AT GROUND SURFACE

We can compute the amplification factor (transfer function) for one layer system supported by flexible bedrock. Using the vertical shear wave propagation and the hysteretic damping assumption, the amplification factor at the first natural frequency is,

$$H(\omega_1) = \frac{1}{(\pi/2)\xi + \alpha} \cong \frac{1}{1.57\xi + \alpha}$$

Similarly, for the second natural frequency ω_2,

$$H(\omega_2) = \frac{1}{(3\pi/2)\xi + \alpha} \cong \frac{1}{4.71\xi + \alpha}$$

where,

$H(\omega)$: The amplification ratio between surface and outcrop flexible base layer

$$\alpha = \frac{\rho V_s}{\rho_b V_{sb}}$$

ρ : mass density of the layer

ρ_b : mass density of the bedrock

V_s : shear wave velocity of the layer

V_{sb} : shear wave velocity of the bedrock

ξ : damping factor of the layer

The amplification to be determined here is the ratio of response spectra. Therefore, the function $H(\omega)$ is different from the $G_s(\omega = 2\pi/T)$.

It is easily supposed, however, that these two values are related and take similar values. We will not evaluate $G_s(T)$ theoretically but estimate in an approximate manner employing the expression of $H(\omega)$. The followings are the method we discuss here. First of all, to evaluate the acceleration response spectrum at the ground surface, the amplification of surface soil deposits on the engineering bedrock is estimated. An evaluation procedure by using the equivalent linearization technique considering nonlinear soil properties is expressed in the followings. The simplified analytical method in this procedure is proposed and examined in detail elsewhere [Miura et al., 2000].

(1) *Transformation of response spectrum defined at outcrop engineering bedrock*: The earthquake motion defined at the outcrop engineering bedrock is given as an acceleration response spectrum with 5% damping ratio, $S_A(T, \xi = 0.05)$.

$S_A(T, \xi = 0.00)$, A velocity response spectrum, $S_V(T, \xi = 0.00)$, and a Fourier spectrum of acceleration, $F_A(T)$, have the approximate relations as follows.

$$F_A(T) \approx S_V(T, \xi = 0) \approx \frac{T}{2\pi} S_A(T, \xi = 0) \quad (2)$$

(2) *Eigen value analysis of soil profile*:

Subdividing the soil profile, a shear model of n degrees of freedom is formed. The natural period, T_i, the vibration mode, U_i (normalized by the value at the surface), and the modal damping ratio, ξ_i, are obtained through the Eigen value analysis.

(3) *Equivalent shear wave velocity and impedance*: The surface soil layers are replaced to a uniform stratum with an equivalent shear wave velocity, V_{se}, and an equivalent mass density, ρ_e, and an equivalent damping ratio, ξ_e, which are calculated from the properties of each soil layer.

$$V_{se} = \frac{1}{H}\sum_{i=1}^{n-1} V_{si} d_i \quad (3)$$

$$\rho_e = \frac{1}{H}\sum_{i=1}^{n-1} \rho_i d_i \quad (4)$$

Where, $V_{si} = \sqrt{G_i / \rho_i}$, H: the total thickness of the surface soil layers, and, G_i, ρ_i, and d_i are shear modulus, mass density, layer height, and damping ratio at the i-th layer from the surface, respectively. The impedance of a wave motion, α, between the equivalent surface soil layer and the engineering bedrock is expressed as follows.

$$\alpha = \frac{\rho_e V_{se}}{\rho_b V_{sb}} \quad (5)$$

where, ρ_b: mass density at the engineering bedrock, V_{sb}: shear wave velocity at the engineering bedrock.

(4) *Amplification by surface soil*: The amplification of the uniform surface soil layer to the outcrop engineering bedrock is obtained by using the one-dimensional wave propagation in frequency domain. The transfer function of the surface soil layer and the engineering bedrock to the outcrop one are expressed as follows: a) surface/outcrop engineering bedrock; $G_s(T, \xi_e, \alpha)$, and b) engineering bedrock /outcrop engineering bedrock; $G_b(T, \xi_e, \alpha)$. An equivalent shear modulus, G_{ei}, and an equivalent damping ratio, ξ_{ei}, of each soil layer are calculated through the $G-\gamma$, $\xi-\gamma$ relationships of soil properties considering the nonlinear characteristics of the surface soil layers.

(5) *Acceleration response spectra at ground surface and engineering bedrock*: They are evaluated as follows.

$$S_A(T, \xi = 0) \approx F_A(T) G_s(T, \xi_e, \alpha) / (\frac{T}{2\pi}) \quad (6)$$

$$S_{Ab}(T, \xi = 0) \approx F_A(T) G_b(T, \xi_e, \alpha) / (\frac{T}{2\pi}) \quad (7)$$

(6) *Modification of acceleration response spectrum at ground surface*: To estimate the acceleration response spectrum conservatively at the ground surface, the spectrum is modified by connecting the two peak points, by a straight line, of the acceleration response spectrum corresponding to the first and second modes of the surface soil layer, in order to avoid excessive reduction between these peaks.

The computations of amplification factors are summarized as follows.

$$\begin{aligned} Gs(T) &= Gs_2 \frac{T}{0.8T_2} && T \le 0.8T_2 \\ &= cT + d && 0.8T_2 < T \le 0.8T_1 \\ &= Gs_1 && 0.8T_1 < T \le 1.2T_1 \\ &= \frac{e}{T} + f && 1.2T_1 < T \le 10 \end{aligned} \quad (8)$$

where,

$$\begin{aligned} c &= \frac{Gs_1 - Gs_2}{0.8(T_1 - T_2)} \\ d &= Gs_2 - 0.8cT_2 \\ e &= \{Gs_1 - 1.0\} / \{1/1.2T_1 - 0.1\} \\ f &= Gs_1 - \frac{e}{1.2T_1} \end{aligned} \quad (9)$$

H_i: thickness of the i-th layer

ρ_i: mass density of the i-th layer

Vs_i: Shear wave velocity of the i-th layer

G_{0i}: Shear modulus of the i-th layer ($G_{0i} = \rho_i V_{si}^2$)

T_1, T_2 can be computed with the following equations.

$$T_1 = \frac{4(\sum H_i)^2}{\sum \sqrt{\frac{G_i}{\rho_i}} H_i} \quad (10)$$

$$T_2 = \frac{T_1}{3}$$

T_1 : The first dominant period of the soil deposit corresponding to the ground motion level.
T_2 : The first dominant period of the soil deposit corresponding to the ground motion level.
G_i : The shear modulus of the i-th layer as reduced with the given table corresponding to the induced shear strain.

Gs_1 , Gs_2 , and G_b are given as follows.

$$Gs_1 = \frac{1}{\alpha\left\{\left(1-\frac{1}{-0.24\alpha^2+1.27\alpha+0.03}\right)\xi_e^2+\frac{\xi_e}{-0.04\alpha^2+0.61\alpha}+1\right\}}$$

$$Gs_2 = \frac{1}{\alpha\left\{\frac{1}{-0.13\alpha^2+0.22\alpha+0.03}\xi_e^2+\frac{\xi_e}{-0.02\alpha^2+0.21\alpha}+1\right\}}$$

$$G_b = \frac{1}{\alpha\left\{\left(1-\frac{1}{-0.34\alpha^2+0.79\alpha+0.03}\right)\xi_e^2+\frac{\xi_e}{0.61\alpha}+1\right\}}$$

where,
α : Wave impedance ratio computed with the following equation

$$\alpha = \frac{\sum(\sqrt{G_i/\rho_i}H_i)\sum(\rho_i H_i)}{\left(\sum H_i\right)^2}\frac{1}{\rho_b V_b}$$

where,
ρ_B : mass density of the engineering bedrock
V_B : shear wave velocity of the engineering bedrock
h : damping factor computed with the following equation

$$\xi_e = \frac{\sum \xi_i w_i}{\sum w_i}$$

where,
ξ_i : Damping factor of the i-th layer as modified with the given table corresponding to the induced shear strain.
w_i : Strain energy in the i-th layer computed with the following equation.

$$w_i = \frac{G_i}{2H_i}(u_i - u_{i-1})^2$$

u_i : the deformation of the i-th layer top to the engineering bedrock

In some cases, the amplification factor $Gs(T)$ at shorter period will be excessively decreased. Therefore, for design, conservative values might be assigned for $Gs(T)$, for example, greater than 1.0 or larger.

The deforamtion and its shape of the soil deposit can be roughly evaluated as follows.

4. EXAMPLES OF EVALUATION OF ACCELERATION RESPONSE SPECTRUM AT GROUND SURFACE

Figure 2 shows shear wave velocities, V_s, in several soil deposits to be evaluated. The shear wave velocities are measured by the PS logging method. The soil layer of V_s of more than approximately 400 m/s is selected as the engineering bedrock. The nonlinear characteristics of the surface soil layers are modeled according to the other publication [Ohsaki et al., 1978]. The mass density of the soils is around 1.6 to 2.0.

The amplification factors (transfer functions) of the ground surface to the outcrop engineering bedrock are shown in Figure 3. The figure includes the results from three analytical methods in the following.
1) Transfer functions in case of multi-layers with V_s by the linear analysis (indicated by "Linear"),
2) Ratios of acceleration response spectrum at the ground surface to that at the outcrop engineering bedrock, that are calculated by the computer program SHAKE [Schnabel et al., 1972] (indicated by "Equivalent"), and
3) Transfer functions obtained by the proposed method (indicated by "Proposed").
The predominant periods of the surface soil layers subjected to severe earthquake motions are longer by 1.3 to 2.0 times than those to moderate earthquake motions because of the nonlinear behavior of soils. There are some differences between the predominant periods of the proposed method and Shake at Sites 3 and 4. The amplification factors at Sites 3 and 4 by the proposed method are a little less than those by Shake. Figure 4 shows the acceleration response spectra at the surface, which are obtained by the proposed method and Shake. "Modified $C_0 \cdot R_t$"

also indicates the acceleration response spectrum converted from the base shear coefficient of buildings for medium soil deposits prescribed in the Building Standard Law of Japan. The response spectra by the proposed method have good agreement with those by Shake.

5. CONCLUSIONS

A response spectrum method is proposed for evaluating the nonlinear amplification of surface strata overlying the engineering bedrock, and its applicability is examined. Concluding remarks are as follows.

(1) The proposed method does not require acceleration waveforms, as do the rigorous methods.
(2) The responses and the nonlinear characteristics of the subsoil can be evaluated by the proposed method when the design earthquake input motion is prescribed only in the form of a response spectrum instead of a time history. No significant differences are observed between the results obtained by the proposed method and by the rigorous method.
(3) The acceleration response spectrum on the ground surface can be accurately evaluated by the proposed method. However, when the soil constants change rapidly, such as at Site-4, the acceleration response spectra obtained by the proposed method are less than those obtained by SHAKE in the range of the whole periods.
(4) The applicability of the proposed method is confirmed from the viewpoint of practical seismic design, if attention is paid to the peculiarity of the proposed method described in the above term 3.

6. REFERENCES

(1) Hiraishi, H. and et al. (1999), "Seismic evaluation of buildings by acceleration spectrum at engineering bedrock (Part 1-Part 13)", Structures II, *Summaries of Technical Papers of Annual Meeting*, AIJ (in Japanese).
(2) Hiraishi, H., Midorikawa, M., Teshigawara, M., Gojo, W. and Okawa, I. (2000), "Development of performance-based building code of Japan -framework of seismic and structural provisions-", *Proceedings 12th World Conference on Earthquake Engineering.*
(3) Miura, K., Koyamada, K. and Iiba, M. (2000), "Response spectrum method for evaluating nonlinear amplification of surface strata", *Proceedings 12th World Conference on Earthquake Engineering.*
(4) Ohsaki, Y., Hara, A. and Kiyota, Y. (1978), "Stress-strain model of soils for seismic analysis", *Proceedings 5th Japanese Earthquake Engineering Symposium*, pp. 679-704 (in Japanese).
(5) Schnabel, P. B., Lysmer, J. and Seed, H. B. (1972), "SHAKE: A computer program for earthquake response analysis of horizontally layered sites", *Report No. UCB/EERC-72/12*, Univ. of California, Berkeley, Calif.

Figure 1: Basic response spectrum at engineering bedrock
Figure 2: Shear wave velocity distribution at example sites
Figure 3: Transfer functions of ground surface to engineering bedrock
Figure 4: Acceleration response spectra at ground surface (h = 5%)

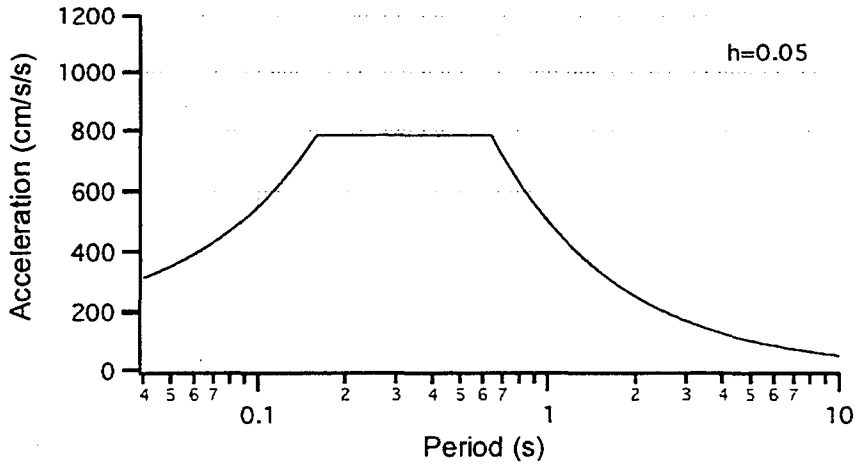

Figure 1 Basic response spectrum at engineering bedrock

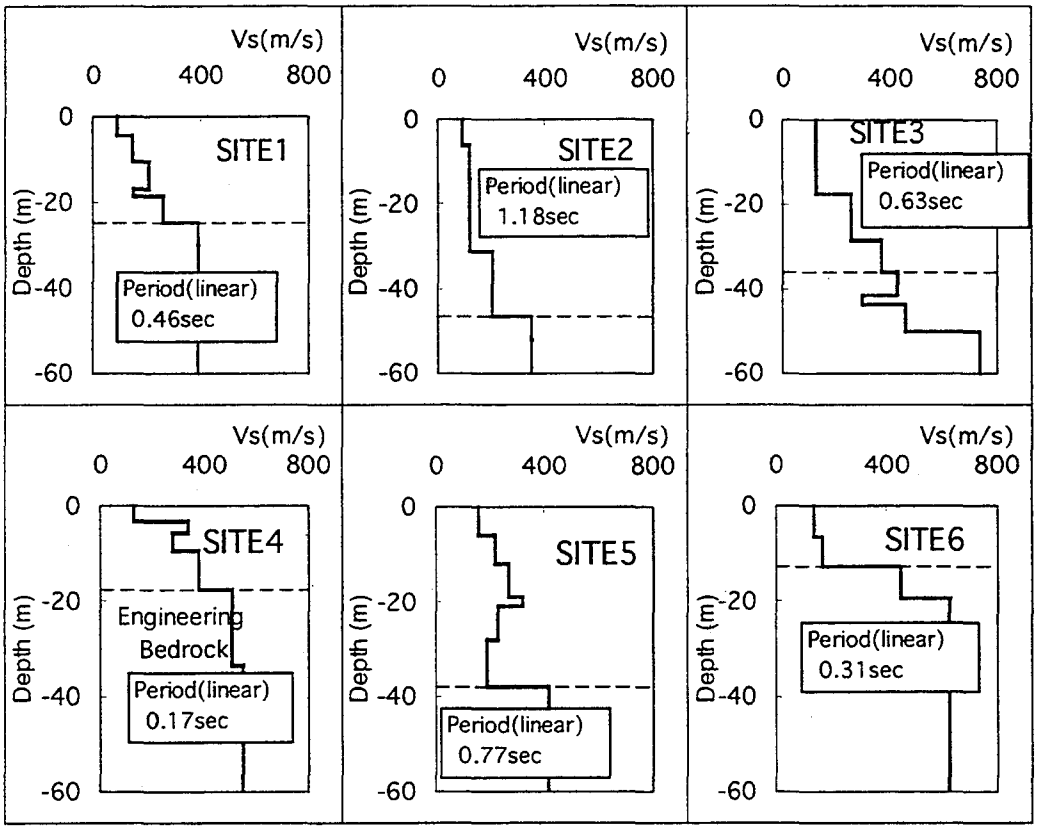

Figure 2 Shear wave velocity distribution at example sites

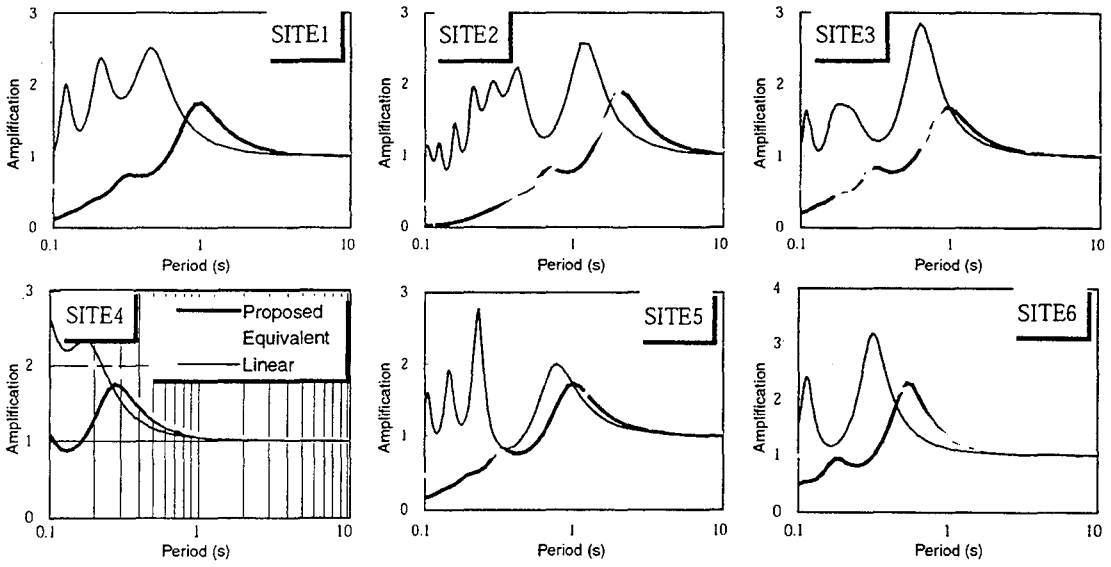

Figure.3 Transfer function of the ground surface above the engineerig bedrock

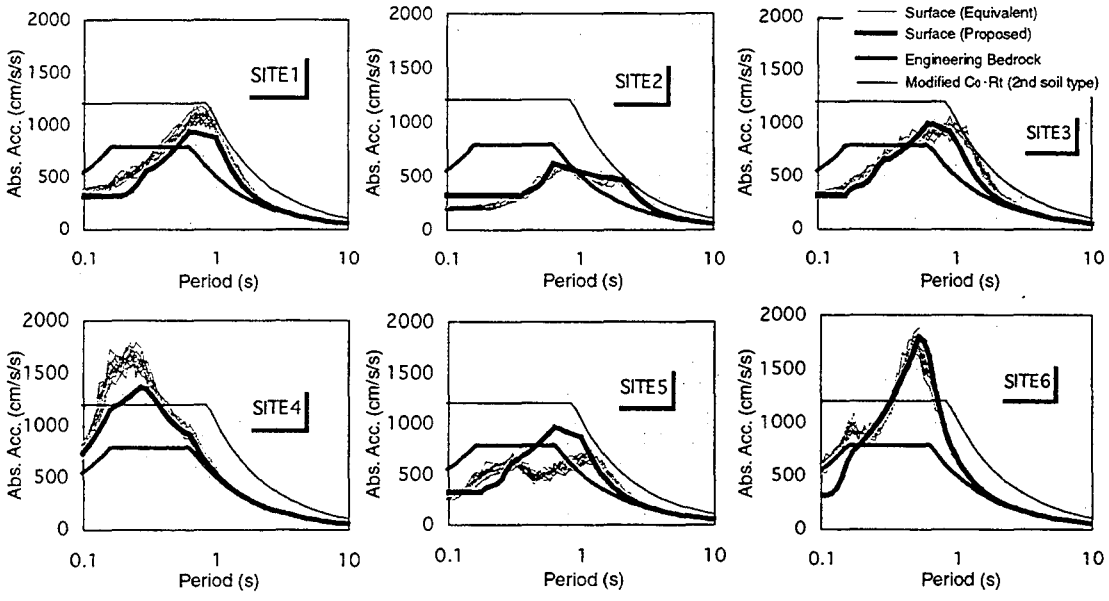

Figure 4 Acceleration response spectra at ground surface ($\xi = 0.05$)

CONSTRUCTION OF A BASE-ISOLATED HOUSE FOR OBSERVATION OF ISOLATION EFFECTS DURING EARTHQUAKE AND WIND

by

Masanori IIBA[1], Mitsumasa MIDORIKAWA[2], Yasuyuki YAMANOUCHI[3], Masayoshi IKENAGA[4] and Kenichi MACHIDA[5]

ABSTRACT

Base isolation is very effective on keeping safety during earthquakes. In case of houses, it is difficult to elongate enough period of buildings by laminated rubber bearing isolators because of light weight. In addition to rubber bearings, sliding and rolling devices are needed to be developed or applied. Recently base-isolated buildings have been constructed for considering seismic safety. The number of base-isolated houses is little. Because of cost for isolation such as isolators, reinforcement of 1st floor and foundation. In order to confirm the effectiveness of base isolation during earthquakes and influence on habitability during winds, a base-isolated house has constructed in Building Research Institute. It is very important to accumulate the observed date of the base-isolated house.

KEY WORDS: Base Isolation for Houses
Construction
Isolator Characteristics
Superstructure Characteristics

1.INTRODUCTION

Many structures suffered from the 1995 Hyogoken-Nanbu Earthquake. Some of buildings have collapse at 1st or intermediate stories[1]. Since the earthquake occurred in the gray dawn (5:45am), there were many persons which were dead and injured at their houses.

Two buildings with base isolation were constructed in Kobe City. The observed earthquake motion records in the buildings showed the effect of base isolation on reduction of acceleration response[2]. After the earthquake, many low- and medium-rise buildings with isolators have been designed and constructed. But the base isolation for houses has not become popular[3)-6)].

Base isolation is very effective on keeping safety during earthquake (response reduction of acceleration and inter-story drifts, and protection from overturning of furniture, etc.). Laminated rubber bearings have been used much for isolated buildings.

In case of houses, it is difficult to elongate a period of buildings by laminated rubber isolators because of the light weight of houses. In addition to the rubber bearing devices, sliding- and rolling-type devices are needed to be developed or applied[7)-8)].

In order to accumulate the observed date of

1) Head, Structural Dynamics Division, Building Research Institute, Ministry of Construction, Tsukuba-shi, Ibaraki-ken, 305-0802, Japan

2) Director, International Institute of Seismology & Earthquake Engineering, Building Research Institute, Ministry of Construction, Tsukuba-shi, Ibaraki-ken, 305-0802, Japan

3) Deputy Director General, Building Research Institute, Ministry of Construction, Tsukuba-shi, Ibaraki-ken, 305-0802, Japan

4) Oiles Corporation, Hakari-cho, Ashikaga-shi, Tochigi-ken, 326-0327, Japan

5) Sumitomo Forestry Co., Ltd., Midorigahara, Tsukuba-shi, Ibaraki-ken, 300-2646, Japan

the base-isolated house, a base-isolated house has constructed in Building Research Institute. Purposes to construction of the base-isolated house are as follows;

a) to clarify issues in the design and construction of base-isolated houses,

b) to observe effects of isolation on response of houses during earthquake, and

c) to obtain behavior of the base-isolated house during strong wind.

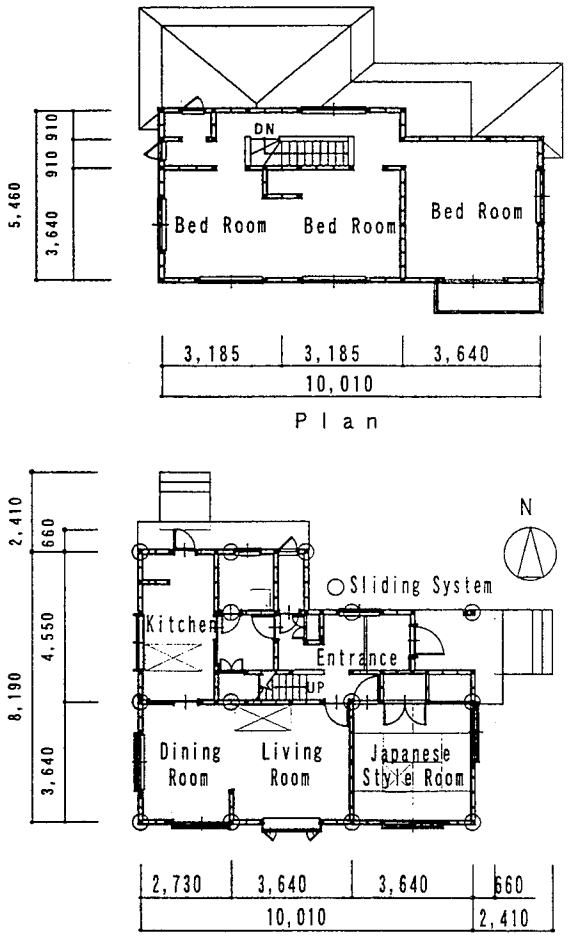

Fig.1 Plan of Base Isolated house

2.OUTLINE OF BESE-ISOLATED HOUSE

A plan of the base-isolated house, which has been constructed at Building Research Institute, in Tsukuba, is drawn in Fig.1.

A superstructure was built through a conventional construction method in Japan (posts and beams of glued laminated timbers). The outline of the house is as follows;

Building use	Residence
Number of stories	2
Floor height(m)	1F 2.925
	2F 2.785
Eaves height(m)	6.82
Floor Area(m^2)	1F 69.56
	2F 51.34
Total Area(m^2)	120.90

The house is a standard size in Japan, and its foundation is a mat one. To considering stable bearing capacity to prevent from non-equal settlement for a long term, a soil improvement was made.

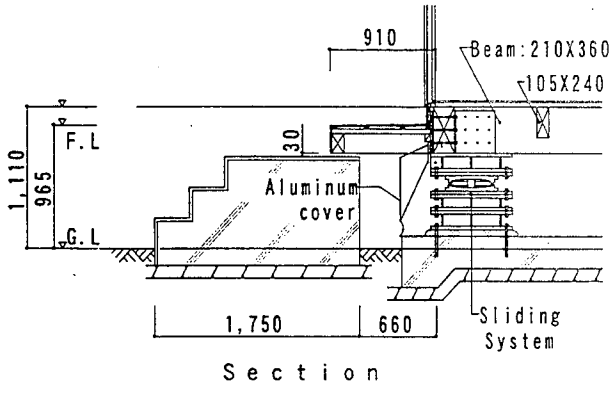

Fig.2 Section of Base Isolated House

A section of the base-isolated house is shown in Fig.2. Beams for supporting a weight of 1st floor are made of glued laminated timbers with a large cross section of 210mm in width and 360mm in height. The floors, which are made of plywood with 35mm in

thickness are attached to beams to improve the in-plane stiffness of floors. Isolators are set between 1st floor and foundation (isolated layer). The isolators with a friction system so called the friction pendulum system (FPS) as shown in Fig.3 are used in the house. The isolator is consisted of double spherical plates, and a sliding cylinder made of Teflon material. The 14 isolators are installed. A relationship between horizontal force and displacement is drawn in Fig.4. A coefficient of friction is about 0.02, and a period from length of the pendulum is 3.2 sec. The allowable displacement is 340mm in one side.

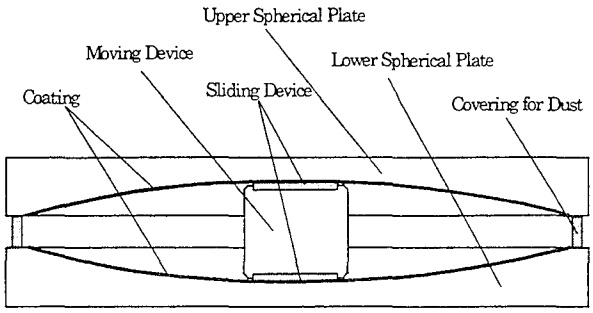

Fig.3 Section of Isolator

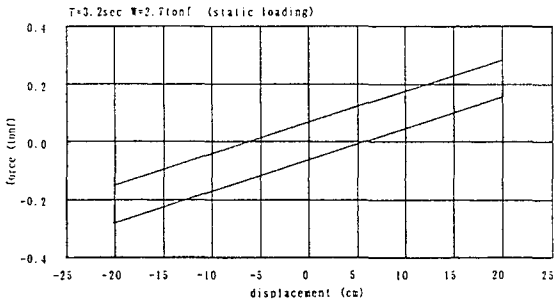

Fig.4 Characteristics of Isolator

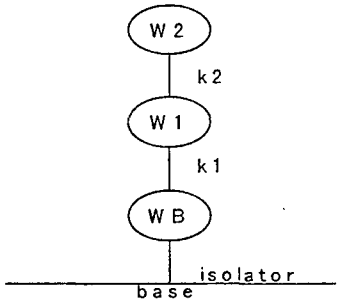

Fig.5 Analytical Model

Table 1 Fundamental properties

direction		X axis	Y axis
stiffness kgf/cm	K1	9500	10000
	K2	6700	5700
weight	WB	13547	13547
	W1	16310	16310
	W2	8679	8679
natural period	1st	0.361	0.362
	2nd	0.166	0.175

Fig. 5 presents an analytical model to simulate seismic response of the house. The house is modeled to three degree of freedom with shear deformation. The superstructure and isolator are assumed to be linear and the

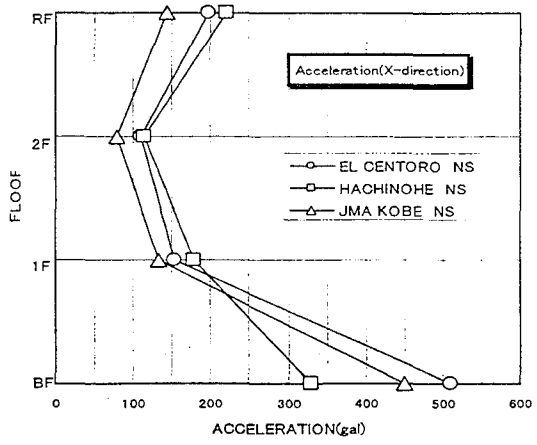

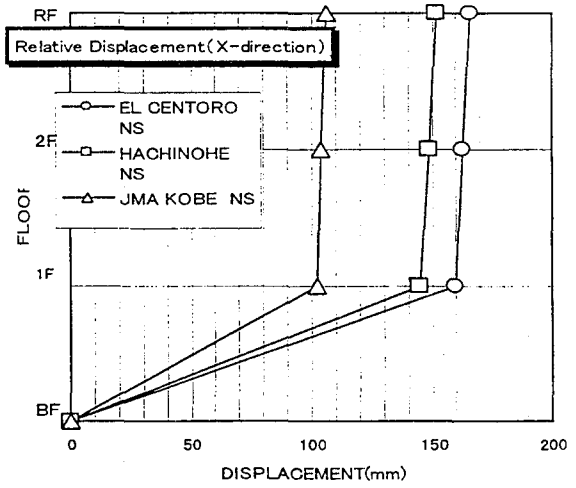

Fig.6 Acceleration and Displacement Response During Earthquake

NS Earthquake ground motions are 1940 El Centro, 1968 Hachinohe Harbor NS and 1995 Japan Meteorological Agency at Kobe NS records which amplitudes are adjusted to 50 cm/s. The maximum accelerations of 1st floor are about one third of the maximum ones of input motions. The displacements of isolators are 100 to 160 mm and angles of each story drift are less than 1/700.

3.CONSTRUCTION OF BASE-ISOLATED HOUSE

The construction period of the base-isolated house is June to September in 1998. It took around one week to setting isolators, beams of 1st floor and coverage around isolated layer. The period related to works for isolation was not so much long. The construction flow is shown in the following.

Subsoil exploration
↓
Soil improving(Photo. 1)
↓
Bar arrangement
↓
Isolator(Photo. 2)
↓
Beem Establishment(Photo. 3)
↓
Upper structure
↓
Entrance・approach
↓
Equipment piping
↓
Gutter
↓
Complete view(Photo. 4)

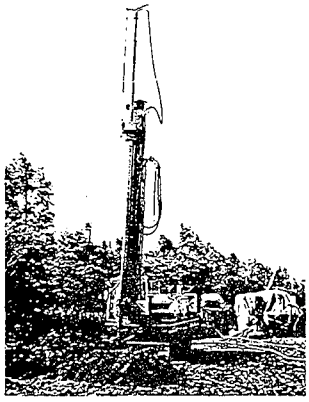

Photo.1 Soil Improvement

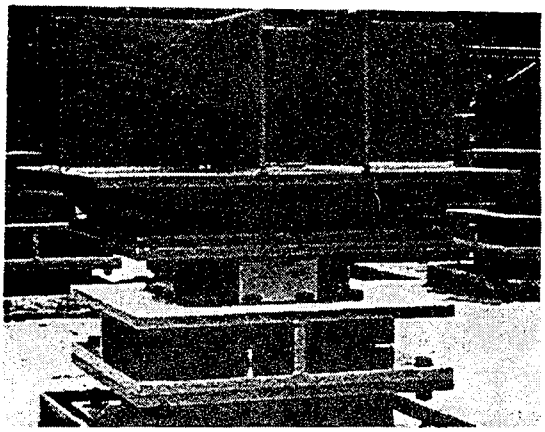

Photo.2 Isolators

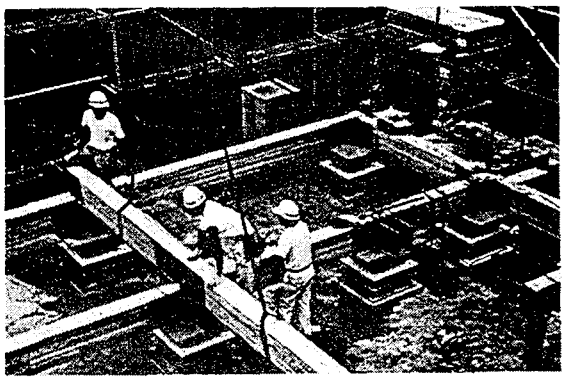

Photo.3 Girders for 1st floor

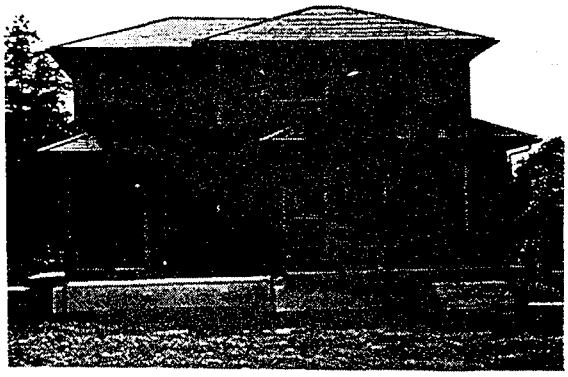

Photo.4 Overall view of Base Isolated House

4.CHARACTERISTICS OF ISOLAOTR

In order to clarify characteristics of isolated layer, a static loading test was carried out. Two static oil jacks were set between the 1st floor and a reaction wall, as illustrated in Fig. 7. Horizontal forces were exerted to the isolated house and horizontal displacements were measured in each isolator. The relationship between force and displacement in X-direction is drawn in Fig. 8. In the figure, the relationship with several coefficients of friction. Much horizontal force is need to starting slippage at the beginning of stage because of static friction. In the region of small displacement, the friction force is larger than that of coefficient of 0.02. The reason is as follows. There is a rubber coverage around isolators protecting from dust entering inside. The friction force between the isolator and rubber coverage is negligible and the coefficient of friction tends to be large. As the displacement will be large, the influence of the friction force by rubber becomes little. To investigate the effect of the rubber coverage, the results without it is shown in Fig. 9. Though there is the static friction at the beginning stage, the static friction changes to the dynamical one after starting sliding.

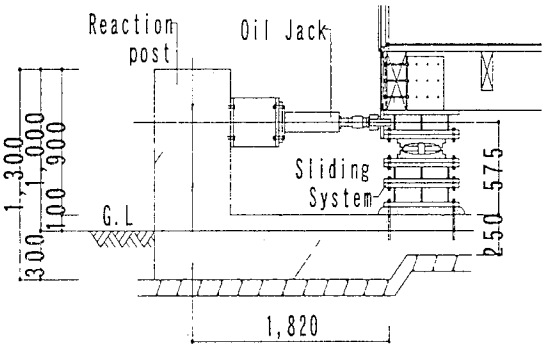

Fig.7 Setup for Loading Test

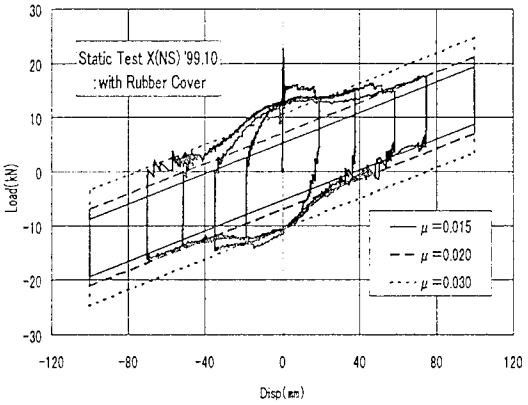

Fig.8 Load vs. Displacement (with Coverage of Rubber)

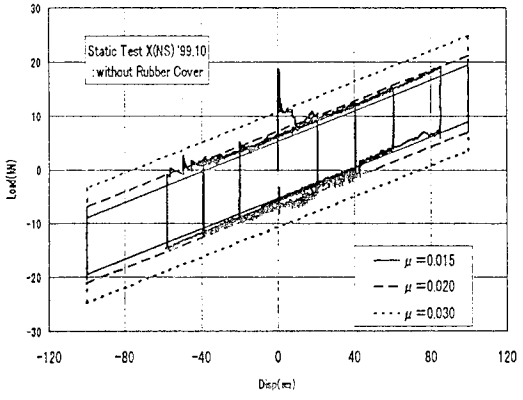

Fig.9 Load vs. Displacement (with Coverage of Rubber)

5.CHARACTERISTICS OF SUPER-STRUCTURE

To clarify characteristics of a superstructure of the base isolated house, microtremor and oscillator tests on the base isolated house were carried out. Since amplitudes of external force on these tests are not so large, the isolators does not move and the superstructure is assumed to be fixed at the base.

Resonant curves of the superstructure in the X(NS) and Y(EW) directions by the oscillator test are drawn in Fig.10 and 11, respectively. In the figures, amplitudes of displacements at each level which are normalized by the force due to the oscillator,

and phase lags at each level to the oscillator force are presented. The oscillator was set on the center of the roof frame. The moving weight is 36 kgf. The superstructure was excited by sweep vibration, that is, variable frequency with 3 to 12 Hz. The resonant frequencies of the superstructure in X and Y directions are 6.0 and 6.5 Hz, respectively. Damping factors are 6.4 and 8.4%, which are calculated through the one by the square root method. From the oscillator test, the damping factors are lager than those which are expected.

6.OBSERVATION SYSTEM FOR ISOLATED HOUSE DURING EARTHQUAKE AND WIND

To investigate the characteristics of the base isolated house during earthquake and strong winds, the observation system was installed. A sensor list is presented in Table 2. Accelerometers are set on the each floor (to see in Photo. 5) and displacement transducers are set several isolators (to see in Photo. 6).

Table 2 Sensor Lists for Observation

Channel no.	Trigger	Position	Sensor	Direction	Sensitivity
1		1st floor	Acc.	NS	2000gal/10V
2				EW	
3				UD	
4		2nd floor	Acc.	NS	2000gal/10V
5				EW	
6				UD	
7		Roof	Acc.	NS	2000gal/10V
8				EW	
9	1gal	Base floor	Acc.	NS	2000gal/10V
10			Vel.		200kine/10V
11			Vel.		5kine/10V
12	1gal	Base floor	Acc.	EW	2000gal/10V
13			Vel.		200kine/10V
14			Vel.		5kine/10V
15	1gal	Base floor	Acc.	UD	2000gal/10V
16			Vel.		200kine/10V
17		Base floor	Disp.	NS	500mm/10V
18				EW	
19				NS	
20				EW	
21		Pole	Wind direction	-	540° /V
22	9m/s		Wind velocity	-	60m/V
23		1st floor	Pressure	NS	1g/cm²/1V
24		2nd floor	Pressure		

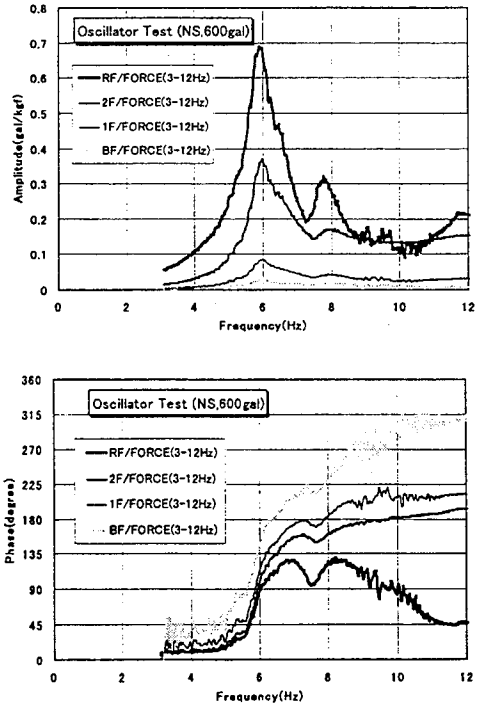

Fig.10 Resonant Curve (X-direction)

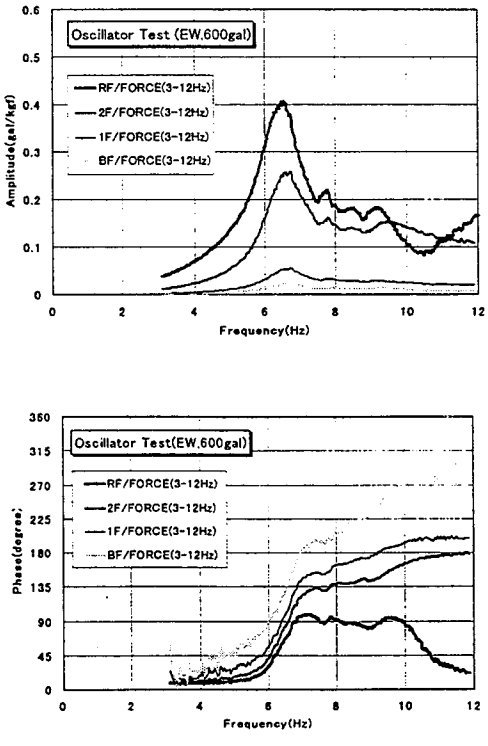

Fig.11 Resonant Curve (Y-direction)

Against the strong wind, a wind velocity and direction will be measured in the system.
The earthquake observation wave records are drawn in Fig. 12. The earthquake with JMA magnitude of 5.1 occurred at 26th of March in 1999. The epicenter of the earthquake was the north in Ibaraki-ken. The distance is about 100 km and the depth id about 50 km.
In Fig.12, the acceleration records at each floor, shear force calculated from the accelerations and the displacement of the isolator in the X-direction. The amplitude of acceleration on the foundation and 1st floor are 41.7 and 46.8 gals, respectively. Though the isolator shows the movement with the displacement of 1.22 mm, there is no remarkable effect of base isolation to the response of the superstructure.

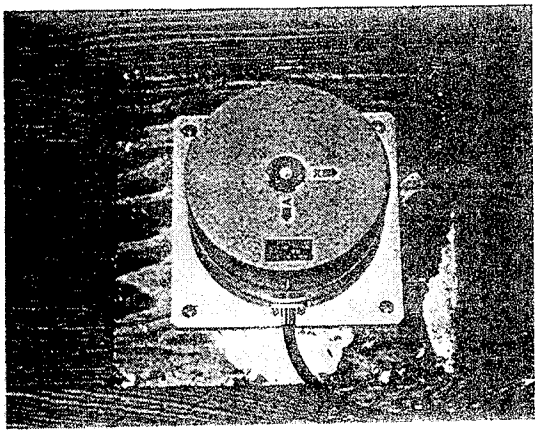
Photo.5 Accelerometer

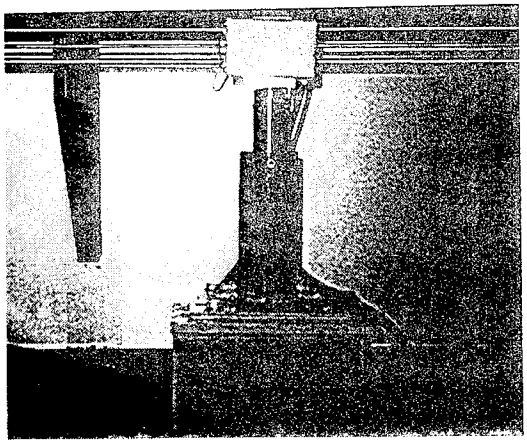
Photo 6 Displacement Transducer

7.CONCLUSIONS

There are several issues to spread the construction of base isolated houses. The issues are to considering the effect of strong winds to isolators and to decrease costs to construction of base isolated houses. In case of light and/or low story houses, the dynamic characteristics of houses against earthquakes and strong winds are dependent on those of isolators. To investigate the dynamic behaviors of base isolated houses, it is necessary to accumulate the practical data though the observation during earthquakes and strong winds.

8.ACKNOWLEGDEMENT

The shaking table tests and date analysis were conducted under the committee on the cooperative research "Development of seismic isolated houses(chairman is Mr. Shoichi Yamaguchi, president of Tokyo-Kenchiku Structural Engineers). The authors express our sincere thanks to the members of the committee.

9.REFERENCES

1. Building Research Institute : A Survey Report for Building Damages due to the 1995. Hyogo-ken Nanbu Earthquake, 1996 March
2. The Building Center of Japan : Base isolated Buildings -Technical development and Earthquake Motion Observation Records Part 2-, 1995 June (in Japanese)
3. Yamanouchi H., M. Midorikawa and M. Iiba (Editor): Research and Development on

Base Isolation Technology for House - Survey of Knowledge and Shaking Table Test on House Model, for Evaluation of Performance on Base isolated House-, Building Research Data, No. 89, 1997 March (in Japanese)

4. Hiroyuki Harada et al.: Studies on Response Control Technologies for Building Structures Part 11., Summaries of Technical Papers of Annual Meeting, 1996 Sep., pp.735-736 (in Japanese), Research committee on Development of Seismically Isolated Houses: Research and Development on Seismic Isolation Technology for Houses -Design Guidelines for Seismic Isolation Houses (Draft)- Building Research Data, No.94, 2000 March (in Japanese)

5. Building Center of Japan : Sheet of outlines for base isolated buildings, The Building Letter 1996 June, pp.57-58 (in Japanese)

6. Iiba, M., Yamanouchi, H., Midorikawa, M., Yamaguchi, S., Ohashi, Y.and Takayama, M.: Research on Performance of Base Isolated House, Proceedings of the Second World Conference on Structural Control (2WCSE), Kyoto, Japan, 1998, 2, pp.1119-1126

7. Iiba, M., Midorikawa, M., Kawai, M., Kawazoe, Y., Ikenaga, M. and Morikawa S.: Shaking Table Tests on Seismic Behavior of Isolators for Houses, Proceedings of the 10th Japan Earthquake Engineering Symposium, Yokohama, Japan, 1988, pp.2653-2658

8. Iiba, M., Midorikawa, M., Yamanouchi, H., Yamaguchi, S., Ohashi, Y. and Takayama, M: Shaking Table Tests on Performance of Isolators for Houses Subjected to Three Dimensional Earthquake Motions, Proceedings of the Twelfth World Conference on Earthquake Engineering (12WCEE), Auckland, New Zealand, No.1765/6/A, 2000 Jan.

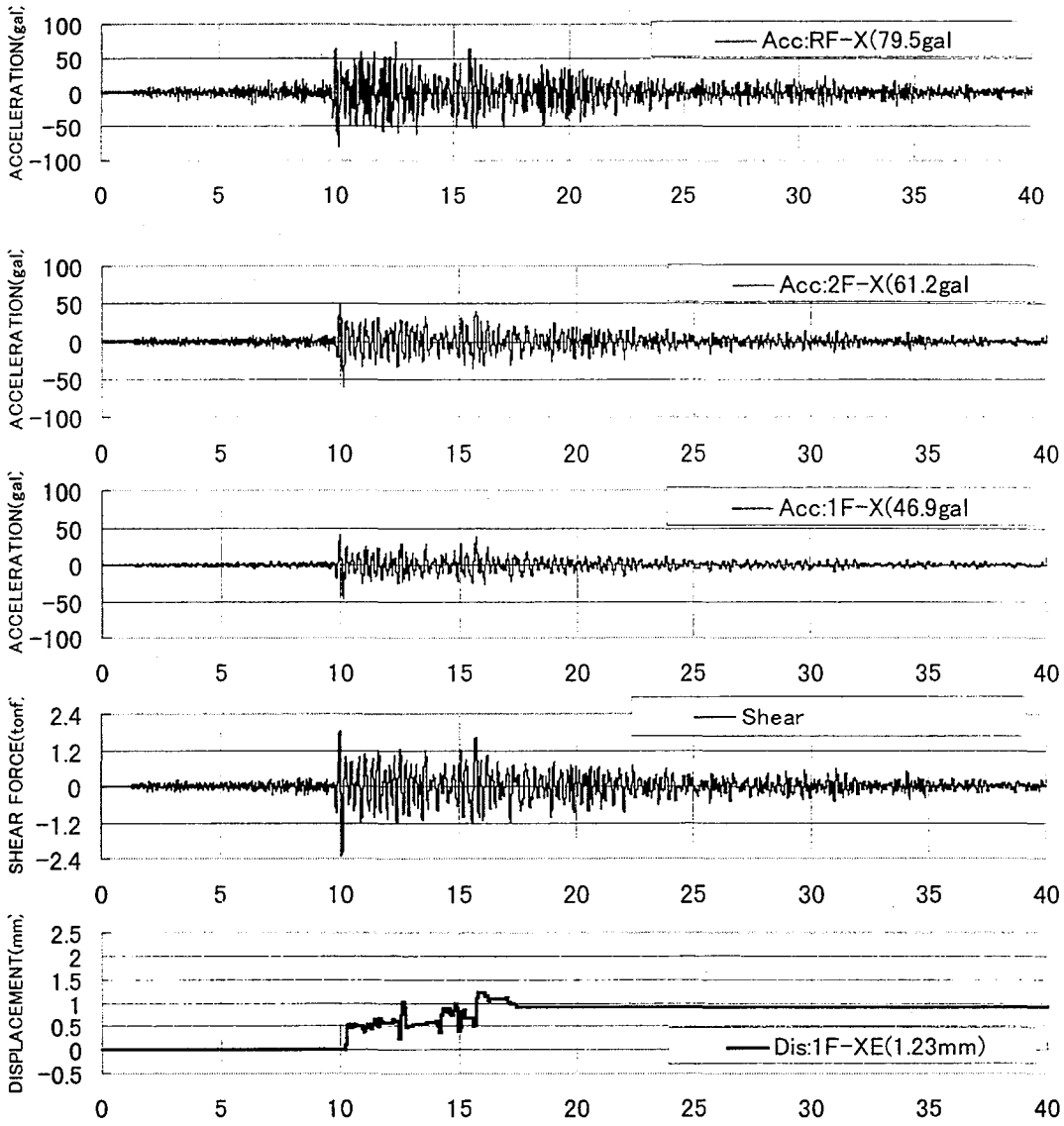

Fig.12 Observed wave forms in 1999.3.26 earthquakes

Design Procedures for Structures with Supplemental Dampers

by

Fahim Sadek[1] and Michael A. Riley[2]

ABSTRACT

Passive energy dissipation devices are used to reduce the damage from earthquakes by absorbing a portion of the earthquake-induced energy in structures. Wide acceptance of these devices in structures will depend on the availability of simplified methods for their analysis and design. This study is concerned with: 1) investigating the effect of increased viscous damping on the seismic response of structures; 2) assessing the accuracy of the linear static and dynamic procedures recommended in the NEHRP Guidelines for the Seismic Rehabilitation of Buildings (FEMA 273) for the design of structures with velocity-dependent dampers; and 3) proposing modifications to the current procedures to improve their accuracy. Based on the analysis of several single-degree-of-freedom structures subjected to a large number of earthquake records, the study identifies two limitations of the FEMA 273 procedures: 1) the use of a constant reduction factor for the displacement response of short-period structures; 2) the assumption of a harmonic response to compute the peak velocity and the story and base shears. In most cases, these assumptions result in nonconservative estimates of the peak response and design forces. Comparisons of the methods proposed in this study and in FEMA 273 indicate that the former produces more accurate results.

KEYWORDS: design codes; passive energy dissipation devices; seismic codes; supplemental damping; structural control; viscous dampers.

1 INTRODUCTION

Supplemental dampers, also known as passive energy dissipation devices, can absorb a portion of earthquake-induced energy in the structure and reduce the energy demand on the primary structural members. The NEHRP Guidelines for the Seismic Rehabilitation of Buildings (FEMA 273) categorize these devices according to their mechanical behavior as: 1) displacement-dependent devices, which have force-displacement response characteristics that are primarily a function of the relative displacement; 2) velocity-dependent devices, which have force-displacement response characteristics that are primarily a function of the relative velocity or the frequency of motion; and 3) other devices, which cannot be classified as either displacement- or velocity-dependent.

FEMA 273 guidelines present simplified linear static and dynamic procedures, as well as the more sophisticated nonlinear static and dynamic procedures, for the analysis of rehabilitated structures incorporating these devices. This study is concerned with investigating the influence of velocity-dependent supplemental dampers on the seismic response of structures, evaluating the accuracy of the linear static and dynamic procedures presented in FEMA 273, and proposing modifications to these procedures for the analysis of structures with velocity-dependent dampers.

The paper includes a brief review of studies on the influence of supplemental viscous damping on the seismic response of structures, as well as the analysis procedures presented in FEMA 273. Analyses of several single-degree-of-freedom

[1] Research Associate, Southern Methodist University, Dallas, TX 75275; on Assignment, National Institute of Standards and Technology, 100 Bureau Dr., Stop 8611, Gaithersburg, MD 20899-8611

[2] Research Structural Engineer, National Institute of Standards and Technology, 100 Bureau Dr., Stop 8611, Gaithersburg, MD 20899-8611

(SDOF) structures with different damping ratios under a large number of earthquake excitations were carried out. The results of the statistical analysis were used in developing linear static and dynamic procedures for the design of structures with linearly elastic behavior and velocity-dependent dampers. The method proposed in this study is compared with that recommended in FEMA 273 and with time history analyses to illustrate the accuracy of the proposed method.

2 PREVIOUS RESEARCH AND SEISMIC PROVISIONS

The influence of increased viscous damping on the seismic response of structures has been studied by a number of investigators. Newmark and Hall (1982) presented the effect of damping ratio, β, in the range of 0.5 to 20 % on the median acceleration, velocity, and displacement amplifications used to construct design spectra. Their results indicated reduced amplifications for increased damping. The effect of inherent and supplemental damping on the earthquake spectral displacement, SD, has been studied by Ashour and Hanson (1987), who used damped SDOF structures with natural periods, T, ranging from 0.5 s to 3.0 s. The computed spectral displacement for each period was normalized to those for zero and 5 % damping ratios for each record. Their statistical analysis led to the introduction of a reduction factor that reflects the decaying pattern of the spectral displacement with the increase in the damping ratio. Wu and Hanson (1989) studied the elastic-plastic response of SDOF systems with large damping and different ductilities. The study indicated that the effect of damping on the inelastic response is similar to its effect on the elastic response.

The above studies indicate similar conclusions regarding the reductions in earthquake spectral displacements with an increase in viscous damping. No consideration, however, was given to the influence of increased damping on the absolute acceleration response which, as discussed later, is the key parameter for computing the seismic forces and base shears in structures with passive energy dissipation devices.

The NEHRP Guidelines for the Seismic Rehabilitation of Buildings (FEMA 273) present a method for constructing design spectra for a given damping from the 5 % damped spectra. The procedure is to divide the spectral ordinates in the constant acceleration and constant velocity regions by factors, B_S and B_1, respectively, corresponding to the specified damping ratio. These factors are based on the recommendations of Newmark and Hall (1982). FEMA 273 also presents the first comprehensive method of analysis and design for structures with passive energy dissipation devices. The guidelines recommend the use of a simplified linear static procedure (LSP) or a linear dynamic procedure (LDP) for structures with linear behavior and with displacement- and velocity-dependent dampers. In addition, for structures with nonlinear behavior, the guidelines recommend a nonlinear static or a nonlinear dynamic procedure.

The main assumptions of the LSP and LDP can be summarized as follows: 1) use factors B_S or B_1 to reduce the base shear (if LSP is used) or spectral acceleration (if LDP is used) for 5 % damping; 2) assuming a harmonic response, compute the velocity between the damper ends by multiplying the displacements by the fundamental frequency (LSP) or the modal displacements by the modal frequencies (LDP); and 3) compute design shears as the maximum of the following stages of deformation: at maximum drift, at maximum velocity and zero drift where only the viscous forces in the dampers are applied to the structure, and at maximum floor acceleration where the shear forces are computed as the sum of the forces at maximum drift multiplied by CF_1 and the forces at maximum velocity multiplied by CF_2. The expressions for CF_1 and CF_2 as a function of the effective damping ratio, β_{eff}, are given assuming a harmonic motion as:

$$CF_1 = cos[tan^{-1}(2\beta_{eff})]$$
$$CF_2 = sin[tan^{-1}(2\beta_{eff})] \quad (1)$$

3 ANALYSIS

The reduction factors presented by Newmark and Hall (1982), Ashour and Hanson (1987), and Wu and Hanson (1989) can be used to modify the displacement or drifts of structures with supplemental dampers. They cannot, however, be used to compute the design base shears. The reason is explained in the following:

For a conventional structure modeled as a SDOF with mass m, damping c, and stiffness k subjected to an earthquake excitation, the equation of motion is given by:

$$m\ddot{x}_t(t) + c\dot{x}(t) + kx(t) = 0 \qquad (2)$$

where $\ddot{x}_t(t)$ is the absolute acceleration which is equal to $\ddot{x}(t) + \ddot{x}_g(t)$; $x(t)$, $\dot{x}(t)$, and $\ddot{x}(t)$ are the relative displacement, velocity, and acceleration, respectively; and $\ddot{x}_g(t)$ is the ground acceleration. For design purposes, the base shear, V, is typically computed as the peak force in the spring, which is equal to:

$$V = k|x(t)|_{max} = m\omega^2 SD = m\,PSA \qquad (3)$$

where ω is the natural frequency and PSA is the pseudo-acceleration $=\omega^2 SD$. When the SDOF structure is equipped with a supplemental damper, the base shear is computed from the sum of the forces in the spring and damper. Therefore,

$$V = |kx(t) + c\dot{x}(t)|_{max} = |m\ddot{x}_t(t)|_{max} = m\,SA \qquad (4)$$

Here c represents the sum of the inherent and supplemental damping coefficients. For this case, the base shear is equal to the mass times the peak absolute acceleration, SA, rather than the pseudo-acceleration PSA. Note that for zero damping, PSA is equal to SA and for small damping ratios (up to 10 %), the two are approximately equal and may be used interchangeably. For larger damping ratios, however, the difference between PSA and SA is significant and the pseudo-acceleration cannot replace the absolute acceleration for computing base shears.

To investigate the effect of the damping ratio on the relative displacement and absolute acceleration response of structures, linear SDOF systems with periods ranging from 0.1 s to 4.0 s with increments of 0.1 s and damping ratios of 2, 5, 10, 15, 20, 30, 40, 50, and 60 % were considered in this study. The structures were subjected to a set of 72 horizontal components of accelerograms from 36 stations in the western Unites States. Refer to Sadek et al. (1999) for a complete list of these records. For each damping, the relative displacement and absolute acceleration response ratios are computed as the ratio of the peak responses of the structure to their counterparts with a damping ratio of 5 %. The mean displacement and acceleration ratios for the 72 records are presented in Figures 1 and 2, respectively. The figures show that increasing the supplemental damping results in a further reduction in the displacement response. The effect of damping is more pronounced in the velocity region (structures with mid-range periods). While larger damping ratios (greater than approximately 40 %) provide further reductions in the displacement response, the additional reductions are not that significant and the increased damping adversely affects the absolute acceleration response and consequently, the shear forces, for long-period structures. For short-period structures (T < 1 s), however, the figure indicates that increased damping results in smaller absolute accelerations and consequently smaller shear forces.

Since the force in a viscous damper depends on the relative velocity, it is important to study the effect of increased damping on the relative velocity response of structures. Therefore, for each record, the spectral velocity, SV, was computed for different periods and damping ratios and divided by the pseudo-velocity, $PSV = \omega\,SD$. From the mean values of SV / PSV for the 72 accelerograms, Figure 3, it may be concluded that assuming the spectral velocity to be equal to the pseudo-velocity (harmonic response) is valid only for periods in the neighborhood of 0.5 s. For periods shorter than 0.5 s, the peak velocity is smaller than the pseudo-velocity while for periods longer than 0.5 s, the peak velocity is larger and increases as the period and damping ratio increase. A regres-

sion analysis was used to establish the following relationship between the spectral velocity and pseudo-velocity responses:

$$SV = \alpha_v \, PSV = \alpha_v \, \omega \, SD \tag{5}$$

where

$$\begin{aligned} \alpha_v &= a_v T^{b_v} \\ a_v &= 1.095 + 0.647\beta - 0.382\beta^2 \\ b_v &= 0.193 + 0.838\beta - 0.621\beta^2 \end{aligned} \tag{6}$$

Figure 4 presents the mean ratio of the spectral to pseudo-acceleration response (*SA/PSA*). The figure confirms the discrepancy between *SA* and *PSA* especially for structures with long-periods and large damping. The relationship between *SA* and *PSA* can be obtained using regression analysis as:

$$\begin{aligned} SA &= (1 + a_a \, T^{b_a}) \, PSA \\ a_a &= 2.436\beta^{1.895} \\ b_a &= 0.628 + 0.205\beta \end{aligned} \tag{7}$$

4 PROPOSED PROCEDURES

Based on the analysis presented in the previous section, improved linear static and dynamic procedures for analysis of structures with velocity-dependent dampers were developed. In the proposed procedures, three damping factors are introduced: a displacement damping factor, α_d, that can be used to reduce displacements and drifts; a velocity damping factor, α_v, that can be used to compute relative velocities; and a force damping factor, α_a, that can be used to amplify or reduce story and base shears. The factor α_d, which is based on Figure 1, is presented in tabular form in Sadek et al. (1999). α_v is given by Equation (6) while α_a can be derived as follows assuming that $SA \cong PSA$ for β =5 %:

$$\begin{aligned} \alpha_a &= \frac{SA(\beta)}{SA(5\%)} = \frac{SA(\beta)}{PSA(\beta)} \frac{PSA(\beta)}{SA(5\%)} = \\ &(1 + a_a T^{b_a}) \frac{\omega^2 SD(\beta)}{\omega^2 SD(5\%)} = (1 + a_a T^{b_a}) \alpha_d \end{aligned} \tag{8}$$

The three damping factors may be used in design as follows: for the structure without supplemental dampers, compute the base shear (if using LSP) or the spectral acceleration (if using LDP) from the 5 % damped design spectrum, and compute the floor displacements, inter-story drifts, and story shears as usual. Multiply the displacements and drifts by the displacement factor α_d to determine the actual deformations, multiply the story shears by the force factor α_a to compute the actual shear forces, and compute the damper forces as the damping coefficient times the relative velocities, which are computed as the product of the relative displacement, natural frequency, and velocity factor α_v. Although simple, this method does not explicitly include the contribution of the damper forces in the computation of design shears. Therefore, erroneous results may be obtained for multi-story frames with a non-uniform distribution of dampers. Consequently, another method is presented in this study. This method is similar to the one in FEMA 273 which includes the influence of the damper forces on the computed design shears directly; thereby, accounting for the distribution of the dampers along the height of the building.

The method assumes that the velocity-displacement response in the quadrant with the peak displacement, *SD*, and peak velocity, *SV*, can be approximated by an ellipse. The accuracy of this assumption has been verified using four structures subjected to two earthquake records (see Sadek et al., 1999). The velocity-displacement relationship, thus, can be expressed as:

$$\left(\frac{x(t)}{SD}\right)^2 + \left(\frac{\dot{x}(t)}{SV}\right)^2 = 1 \tag{9}$$

Maximizing the design force $F(t) = kx(t) + c\dot{x}(t)$ subject to the constraint of Equation (9) will result in the peak forces corresponding to the maximum acceleration given as:

$$V = C_1 \, k \, SD + C_2 \, c \, SV = C_1 \, F_d + C_2 \, F_v \tag{10}$$

where F_d and F_v are the shear forces corresponding to the maximum drift and velocity, respectively, and C_1 and C_2 are given by:

$$C_1 = \frac{F_d}{\sqrt{F_d^2 + F_v^2}} \quad \text{and} \quad C_2 = \frac{F_v}{\sqrt{F_d^2 + F_v^2}} \qquad (11)$$

The accuracy of the proposed method of computing the design shears has been verified using a comparison with time history analysis. Refer to Sadek et al. (1999) for details.

As Equation (10) indicates, the design shears will include the contributions of the peak restoring forces and peak damping forces. Figure 5 shows the percent contribution of each to the total design forces for damping ratios of 10, 20, 30, and 40 %. The figure indicates that for damping ratios up to 10 %, at least 90 % of the design forces are due to restoring forces, while for larger damping ratios, the contribution of damping forces is more significant. This is especially true for long-period structures, due to the effect of increased velocities as indicated by Figure 3.

Based on the above analyses and discussions, the proposed method for the linear static (LSP) and linear dynamic (LDP) procedures can be summarized in the following steps:

1. Compute the fundamental frequency using any of the methods presented in FEMA 273 (LSP) or perform a modal analysis to determine the natural frequencies and mode shapes of the structure (LDP). Assume an effective damping ratio, β_{eff}, in the fundamental mode (LSP) or in each mode (LDP) and determine the displacement, velocity, and force damping factors (α_d, α_v, and α_a, respectively) using α_d table (Sadek et al., 1999) and Equations 6, 7, and 8.

2. Compute the base shear as the product of the 5 % damped base shear and α_d and distribute the forces, F_d, along the height of the structure using the method presented in FEMA 273 for conventional structures (LSP) or multiply the 5 % damped spectral acceleration by α_d for each mode (LDP), and compute the design displacements and inter-story drifts.

3. Calculate the effective damping ratio, β_{eff}, using the method outlined in FEMA 273 and iterate on steps 1 through 3 until the desired accuracy is achieved.

4. Compute the relative velocity between the damper ends as the product of inter-story drift, fundamental frequency, and α_v (for each mode if using LDP). Calculate the damper forces as the product of the damping coefficient and the relative velocity. Estimate the forces acting on the structure corresponding to the maximum velocity, F_v, due to the damper forces.

5. Compute the design shears corresponding to the maximum floor accelerations from Equations (10) and (11). Coefficients C_1 and C_2 should be computed for each story (and for each mode if using LDP) rather than for the complete structure. The final design shears will be selected as the larger of the forces computed at maximum acceleration or at maximum drift (step 2) multiplied by α_a / α_d or $1 + a_a T^{b_a}$. This insures that the computed design shears are not less than those for 5 % damping multiplied by α_a, as recommended in the previous section.

The iterative procedure suggested in step 3 is used since the effective damping ratio, β_{eff}, depends on the displacement in the structures as recommended by FEMA 273. It should be noted that FEMA 273 also presents an expression for estimating β_{eff} (see Section 9.3.4.1 of FEMA 273). If using LDP, the modal displacements, velocities, and story shears should be combined using an appropriate method such as the square root of the sum of squares (SRSS) or the complete quadrature combination (CQC).

5 COMPARISONS

To verify the analysis procedure proposed in this study, it was compared with that presented in FEMA 273, using several SDOF structures. Both procedures are compared with the average

results of time history analyses using the 72 accelerograms to assess their accuracy. For a SDOF structure with period T, effective weight W, and no supplemental damping, the design base shear is given as (FEMA 273):

$$V_{uncontrolled} = \overline{C}_1 \overline{C}_2 \overline{C}_3 S_a W = aW \qquad (12)$$

where $a = \overline{C}_1 \overline{C}_2 \overline{C}_3 S_a$; S_a is the spectral acceleration at the fundamental period; and $\overline{C}_1$, $\overline{C}_2$, and $\overline{C}_3$ are modification factors that can be found in Section 3.3.1.3 of FEMA 273. When the structure is equipped with supplemental dampers, the three key design parameters are the displacement, velocity, and base shear. For the derivations of those three parameters using the procedures presented in FEMA 273 and in this study, refer to Sadek et al. (1999).

Figures 6 - 8 present comparisons between the methods proposed herein and in FEMA 273 for the design displacement, velocity, and base shear, respectively, for effective damping ratios of 10, 20, and 30 %. The figures also show the results from the time-history analyses. For the FEMA 273 procedure, the plots are presented for ground motion at rock or hard rock sites with spectral response acceleration of 1.0g at short periods and 0.4g at one-second period. The three figures show the difference between the two procedures (FEMA 273 and this study), especially for larger damping ratios, and indicate that the proposed method tends to be more accurate than that in FEMA 273.

Figure 6 shows that the two methods give displacements that are close to each other for long periods. For shorter periods, however, the method presented in FEMA 273 significantly underestimates the displacements. This study shows that for periods less than 0.5 s, the reduction factors vary substantially and are larger for shorter periods. Figure 7 shows that the two methods yield velocities close to each other for periods less than 1.0 s. For periods longer than 1.0 s, the FEMA 273 method gives velocities and consequently, damper forces that are much smaller than those predicted by a time history analysis. Figure 8 shows that the method presented in FEMA 273 does not reflect the increase in design base shears for structures with long-periods and large damping ratios.

6 CONCLUSIONS

The overall objectives of this study were: 1) to investigate the effect of increased viscous damping on the seismic response of structures, 2) to assess the accuracy of the linear static (LSP) and linear dynamic (LDP) procedures recommended by FEMA 273 for designing structures with velocity-dependent passive energy dissipation devices, and 3) to propose modifications to the current design procedures to achieve better accuracy and reliability. The findings of the study can be summarized as follows:

- Increasing damping in structures allows more input seismic energy to be dissipated, which generally reduces the response of structures. The reduction, however, depends on the structural period and the amount of supplemental damping. For example, the effect of damping on the displacement response is more pronounced in the velocity region (structures with periods in the range of 0.3 s to 0.5 s). For long-period structures, an increase in damping further decreases the displacement response, but increases the absolute acceleration response and consequently seismic forces.

- Design forces should include the contributions of the peak restoring forces and peak damping forces. The study indicates that for small damping ratios, approximately 90 % of the design forces are due to the restoring forces, while for larger damping ratios, the contribution of damping forces is more significant. This is especially true for long-period structures, due to the effect of increased velocities.

- The LSP and LDP recommended by FEMA 273 have the following limitations: 1) they use a constant reduction factor for the displacement response in the acceleration region of the spectrum. This assumption can result in a non-conservative design in short-period structures, 2) they assume a harmonic response to compute the peak velocity, i.e.,

the peak velocity is equal to the pseudo-velocity. This assumption results in accurate velocities, and consequently damper forces, only for structures with periods close to 0.5 s. This study, however, shows that for structures with other periods, the pseudo-velocity should be multiplied by a factor that depends on the structural period and the damping ratio, and 3) they assume that the structure undergoes a harmonic motion with an amplitude equal to the peak displacement and a frequency equal to that of the fundamental (or a given) mode. Consequently, the same coefficients are used in each story to compute the design forces. This study shows that assuming an elliptical peak displacement-velocity response and using different coefficients for each story to compute the design forces is more accurate.

Based on the analysis of SDOF structures subjected to 72 earthquake records, modifications to the LSP and LDP presented in FEMA 273 are recommended. Comparisons between the methods proposed in this study and in FEMA 273 show that the method presented herein is more accurate when compared with the time-history analysis of several structures.

7 REFERENCES

Ashour, S. A., and Hanson, R. D. (1987). "Elastic seismic response of buildings with supplemental damping." *Report UMCE 87-1*, Dept. of Civil Engrg., The University of Michigan, Ann Arbor, Michigan.

FEMA 273 (1997). "NEHRP guidelines for the seismic rehabilitation of buildings." Building Seismic Safety Council, Washington, D.C.

Newmark, N. M., and Hall, W. J. (1982). "Earthquake spectra and design." *Monograph Series*, Earthquake Engrg. Res. Inst., Oakland, California.

Sadek, F., Mohraz, B., and Riley, M. A. (1999). "Linear static and dynamic procedures for structures with velocity-dependent supplemental dampers," *Technical Report NISTIR 6329*, National Institute of Standards and Technology, Gaithersburg, MD.

Wu, J., and Hanson, R. D. (1989). "Study of inelastic spectra with high damping." *J. Struct. Engrg.*, ASCE, Vol. 115(6), pp. 1412-1431.

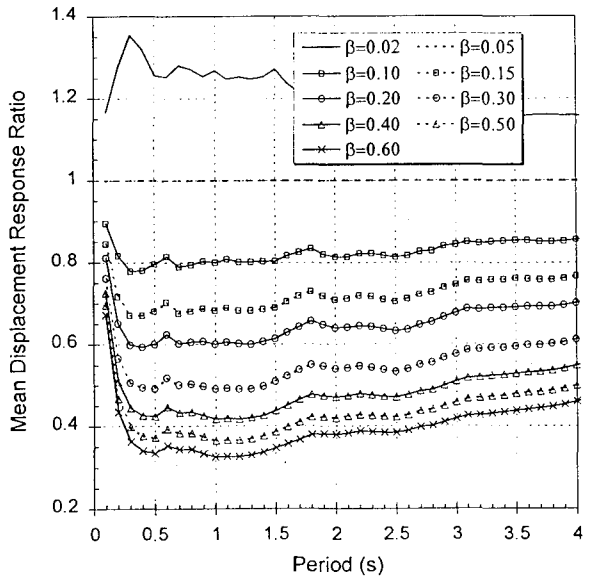

Figure 1. Mean Displacement Response Ratios

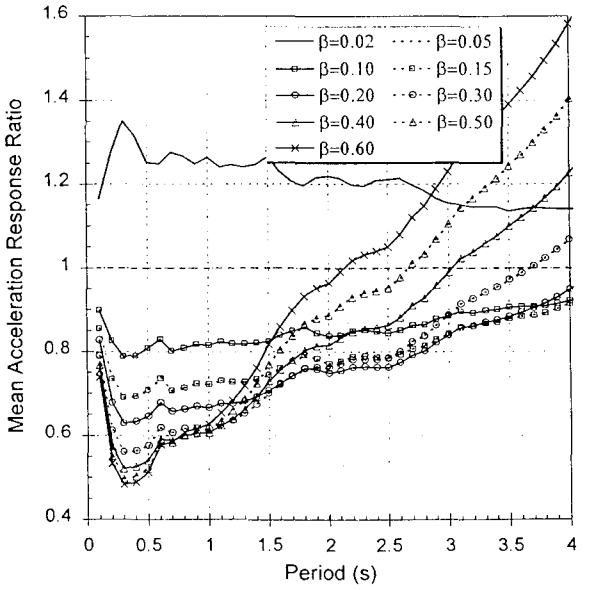

Figure 2. Mean Acceleration Response Ratios

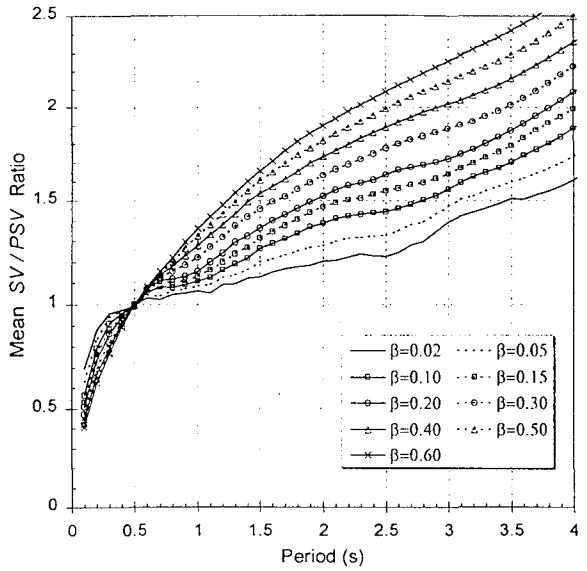

Figure 3. Mean Spectral to Pseudo Velocity Ratios

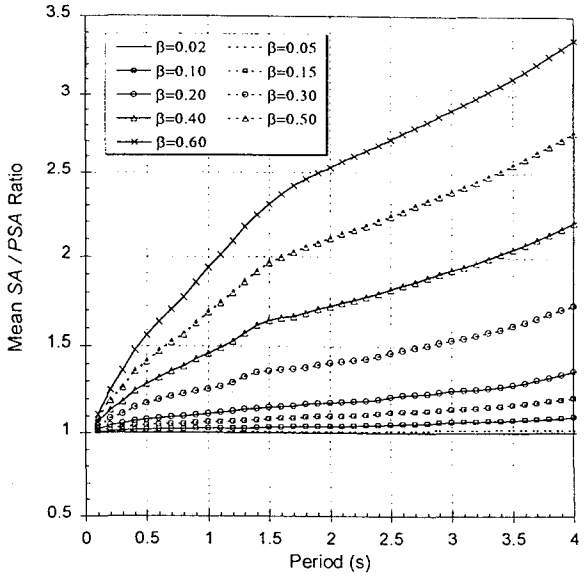

Figure 4. Mean Spectral to Pseudo Acceleration Ratios

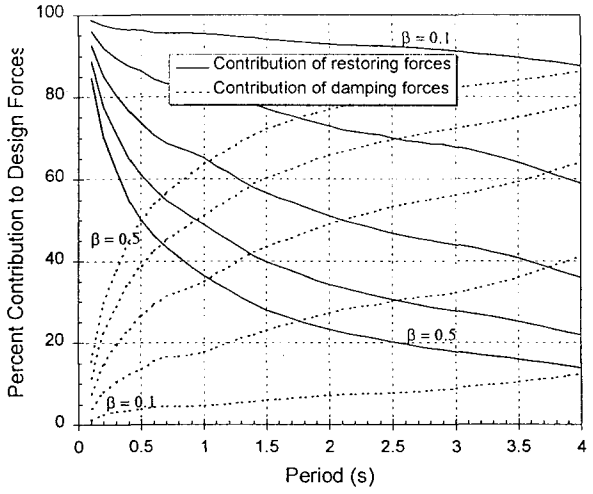

Figure 5. Contribution of Restoring and Damping Forces to Total Design Forces

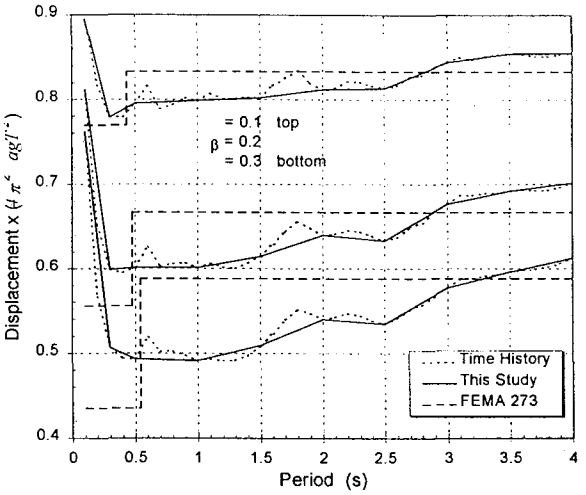

Figure 6. Design Displacement for SDOF Structures

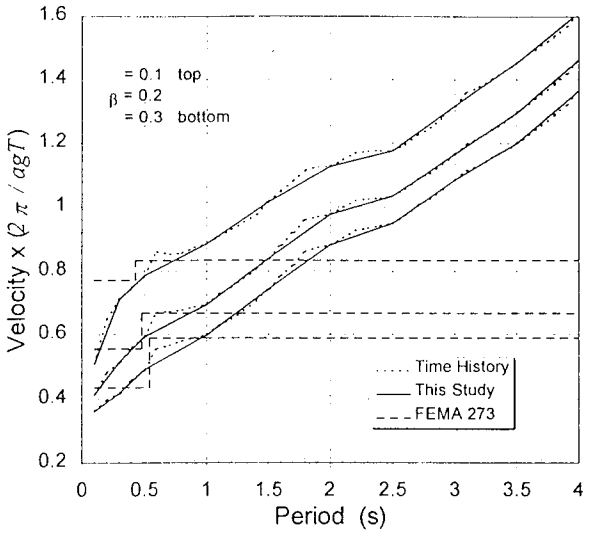

Figure 7. Design Velocity for SDOF Structures

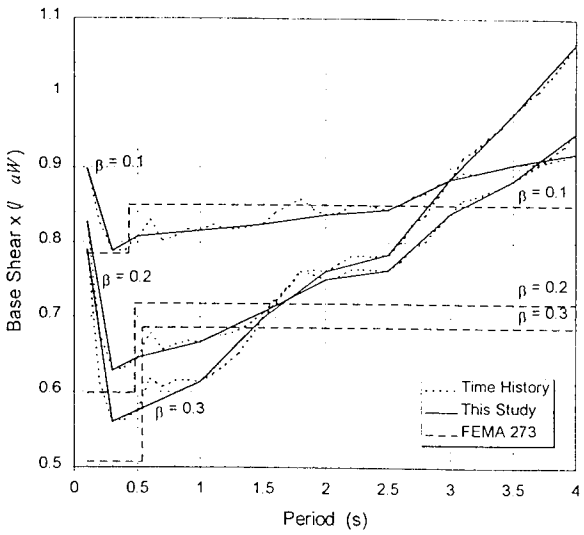

Figure 8. Design Base Shear for SDOF Structures

SEISMIC DESIGN GROUND MOTIONS FOR STRAIT-CROSSING PROJECTS IN JAPAN

by

Masahiko Yasuda[1], Keiichi Tamura[2], Shojiro Kataoka[3] and Yoshihiro Nakao[3]

ABSTRACT

In order to establish rational seismic design for strait-crossing projects in Japan, it is most essential to appropriately consider the effects of near field ground motions of large earthquakes. For this purpose, we study the applicability of semi-empirical and stochastic Green's function techniques to estimate near field ground motions, by synthesizing ground motion for the large-scale scenario earthquakes, in which earthquake source parameters are systematically changed. Based on the results of analysis, variation of ground motion resulting from uncertainty of source parameters is discussed.

Key words: strait-crossing project, seismic design, ground motion, Green's function, earthquake source parameter

INTRODUCTION

Feasibility of super long-span bridges crossing straits is being studied in Japan to meet the goal of constructing a multi-nuclei nation as set forth in the Comprehensive National Development Plan (National Land Agency, 1998). Some of these bridges will be located over or nearby the fault planes of past large earthquakes. For instance, the 1923 Kanto Earthquake (M_J=7.9, M_J is the Japan Meteorological Agency Magnitude) and 1944 Tonankai Earthquake (M_J=7.9) occurred in Tokyo Bay and Ise Bay regions, respectively, and two highway routes are being planned to cross the mouths of these two bays.

For establishing seismic design ground motions of large structures, seismic risk analysis and attenuation relation of ground motion have been widely used in Japan including the Trans-Tokyo Bay Highway Bridge (Public Works Research Institute, 1991) and Akashi Kaikyo Bridge (Honshu-Shikoku Bridge Authority, 1988). In the seismic risk analysis, an attenuation equation is usually incorporated to estimate ground motion intensity from an expected earthquake magnitude and distance. Although an attenuation equation is a simple and effective tool of engineering practice to predict ground motion, it should be noted that the applicability of this technique to the near field of large earthquake is limited, because it is an empirical formula and does not usually contain strong motion data obtained in the near fields of large earthquakes. Appling attenuation relation to the near field by substituting small value for distance may yield excessive ground motion for seismic design of structures.

The semi-empirical ground motion synthesizing method (e.g., Hartzell, 1978; Irikura, 1983), in which ground motion record from a small event is used as Green's function, has recently been applied to earthquake engineering. This technique can incorporate complicated earthquake source mechanism into calculation,

1) Formerly, Director, Earthquake Disaster Prevention Research Center, Public Works Research Institute, Ministry of Construction, Tsukuba-shi, Ibaraki-ken 305-0804 Japan
2) Head, Ground Vibration Division, ditto
3) Research Engineer, Ground Vibration Division, ditto

and has an advantage of estimating near field motions. On the other hand, this method requires various source parameters, and most of them are difficult to be determined accurately, especially for a future earthquake.

In addition to those facts, the semi-empirical method requires an actual small event record, however, it is obvious that an appropriate record is not always available. To make up this disadvantage, stochastic synthetic method has been proposed (e.g., Kamae, et al., 1991), in which stochastically simulated small event motion is used as a Green's function.

To establish rational seismic design ground motions for strait-crossing projects, we are studying the applicability of semi-empirical and stochastic Green's function techniques at the Public Works Research Institute. In this paper we simulate ground motion at Tokyo Bay region, assuming the Kanto Earthquake, which will be most influential over this area. We employ geometric parameters of the 1923 Kanto Earthquake and change dynamic source parameters variously, and examine influence of uncertainty of source parameters on the synthesized ground motion, as a basis of developing design ground motions for strait-crossing projects.

GROUND MOTION SIMULATION USING SEMI-EMPIRICAL GREEN'S FUNCTION TECHNIQUE

To simulate ground motions from a large event, ground motion record from a small event such as foreshock or aftershock that occurred within the fault area of large event is used as Green's function. The fault plane of the target event is divided into sub-faults so that their sizes coincide with the fault area of small event. The Green's functions are superimposed considering time delay due to fault rupture from the hypocenter to a sub-fault and wave traveling from each sub-fault to the estimation point. An advantage of using small event record as Green's function exists in that complicated path and site effects are incorporated automatically into ground motion estimation, which has large influence over the accuracy of simulating short period ground motions.

Temporal and spatial variations of dislocation are considered here by introducing $T_{mn}(\omega)$ and ω_{mn}, respectively, and the Fourier transform of displacement from a large event $u(\omega)$ is expressed as:

$$u(\omega)=\sum_{m=1}^{N}\sum_{n=1}^{N} T_{mn}(\omega)\omega_{mn}u_0(\omega)\exp(-i\omega\tau_{mn}) \tag{1}$$

where,

T_{mn} : Function representing the difference in source time function between small and large events (Irikura, 1986)

$$T_{mn}(\omega)=1+(N-1)\frac{\dfrac{\sin\dfrac{\omega\tau}{2}}{\dfrac{\omega\tau}{2}}}{\dfrac{\sin\dfrac{\omega\tau}{2(N-1)N_1}}{\dfrac{\omega\tau}{2(N-1)N_1}}}\cdot\exp\left[-i\left(\frac{\omega\tau}{2}-\frac{\omega\tau}{2(N-1)N_1}\right)\right] \tag{2}$$

ω_{mn} : Weight function representing spatial variation of dislocation

u_0 : Frequency component of ground motion from small event

τ_{mn} : Time delay due to fault rupture from hypocenter to sub-fault and wave

traveling from sub-fault to estimation point.

N: Number of sub-faults

τ: Rise time

N_1: Coefficient to avoid the synthetically generated periodicity

The source time function after Irikura (1986) is used in the present study, which is shown in Figure 1.

VARIATION OF EARTHQUAKE SOURCE PARAMETERS

Target Event and Basic Source Parameters

We employ a source model of the 1923 Kanto Earthquake proposed by Wald and Somerville (1995). The major parameters of this model are listed in Table 1. Ground motion at Kannonzaki is synthesized in this study. We use a strong motion data from the 1987 Chiba-ken Toho-oki Earthquake (M_J=6.7) as a small event record, which was obtained on the siltstone at Kannonzaki. The fault plane of 1923 Kanto Earthquake, and locations of epicenters of the Kanto and Chiba-ken Toho-oki Earthquakes and Kannonzaki are presented in Figure 2. Figures 3 and 4 show acceleration waveform and acceleration response spectrum (damping ratio h=0.05) of Kannonzaki record, respectively.

Since the seismic moment of the Chiba-ken Toho-oki Earthquake is calculated as 7.05×10^{25} [dyne·cm] after Harvard University (1999), the fault plane of Kanto Earthquake is divided into 5×5 sub-faults in the following analysis, according to the seismic moment ratio between two earthquakes.

Source Parameters Changed

We systematically change fault rupture mode and location of asperity to examine their influence on the synthesized ground motion (Tamura et al., 1999). We assume lateral rupture and radial rupture as illustrated in Figure 5, i.e., 5 cases for lateral rupture and 15 cases for radial rupture. According to Somerville et al. (1999), the area of asperity that has twice as large as average slip is 22% of total fault plane area, and we assign asperity for 6 sub-faults out of 25 sub-faults. Note that their result was derived from analysis of 15 crustal earthquakes, and further study may be necessary to apply it directly to the inter-plate Kanto Earthquake. We employ 2×3 and 3×2 asperities as shown in Figure 6. For each asperity shape, we assume 9 patterns of asperity distribution. Consequently, we set up (5+15)×(9+9)=360 cases for numerical simulation at this stage.

In addition to the above-mentioned asperity models, we also employ the variable-slip rupture model of the 1923 Kanto Earthquake proposed by Wald and Somerville (1995) for reference. Note that the slip vector is determined for each sub-fault in this model, however we use the slip amplitude and ignore slip angle in the present study. When we use this model, we assume bilateral rupture from the hypocenter that is indicated by a star in Figure 7, and other source parameters are set as the same as shown in Table 1.

Since the ground motion estimation point (Kannonzaki) is located over almost the center of fault plane as shown in Figure 2, some of assumed simulation cases yield similar results when symmetric rupture mode and location of asperity is assigned. Besides this, in the previous study (Tamura et al., 1999), we confirmed that the horizontal location of 2×3 asperity and vertical location of 3×2 asperity do not affect much calculation result, respectively. Considering those facts, we reassign rupture

mode and asperity locations as indicated in Figures 8 and 9. Then, numerical simulation cases are reduced to 124 cases (Table 2).

VARIATION OF GROUND MOTION DUE TO UNCERTAINTY OF SOURCE PARAMETERS

Acceleration response spectra of the 124 cases are overlaid in Figure 10, where damping ratio is taken as h=0.05. Variation of spectral amplitude depends on natural period, and it ranges from 3 to 6 times. We should be attentive that this variation is inevitable when we infer ground motion for a future earthquake that has uncertain source parameters. Figure 11 shows acceleration response spectrum using the variable-slip rupture model that is shown in Figure 7. Comparing those two figures, result from the variable-slip rupture model gives almost upper bound of variation of synthesized ground motion.

GROUND MOTION SIMULATION USING STOCHASTIC GREEN'S FUNCTION TECHNIQUE

Procedure of Ground Motion Simulation

Here, the ground motion due to each sub-fault is simulated stochastically and employed as a Green's function to synthesize ground motion of a large event. The ground motions on the seismic bedrock at Kannonzaki generated from sub-faults are produced to match observed ground motions in a stochastic sense and superimposed considering time delay due to the fault rupture process and the wave propagation. The superimposed motion multiplied by the transfer function of the ground structure between the ground surface and the seismic bedrock makes the synthetic motion on the ground surface at Kannonzaki. Table 3 and Figure 12 show the ground structure model and the transfer function at Kannonzaki used in the following simulation.

Boore (1983) modeled the acceleration spectrum $A(f)$ of shear waves at a site of which distance R from a source with seismic moment M_0 as:

$$A(f) = \frac{F}{4\pi\rho\beta^3} M_0 \cdot \frac{(2\pi f)^2}{1+(f/f_c)^2} \cdot \frac{1}{\sqrt{1+(f/f_{max})^s}} \cdot \frac{1}{R} \exp\left(-\frac{\pi f R}{Q(f)\beta}\right) \cdot \sqrt{\frac{\rho\beta}{\rho_b\beta_b}} \quad (3)$$

where,

- F : Radiation pattern coefficient
- ρ : Density at the source fault
- β : Shear velocity at the source fault
- f_c : Corner frequency
- f_{max} : Cut-off frequency
- s : Decay rate at high frequencies
- $Q(f)$: Quality factor
- ρ_b : Density at the site
- β_b : Shear velocity at the site

Equation (3) was formed following the theories of source spectrum and the parameters f_c, f_{max}, and s are chosen to match ground motion records. The last term of the right-hand side of Equation (3) is added to consider the amplification due to the ground structure between the source and the site (Dan et al., 2000).

We employ the shaping window by Jennings et al. (1968) to obtain the phase spectrum and generate a transient accelerogram whose amplitude spectrum matches Equation (3). The shaping window consists of three parts: amplifying part (quadratic curve), strong motion part (constant), and attenuating part (exponential curve) as shown in Figure 13.

VARIATION OF GROUND MOTION DUE TO UNCERTAINTY OF SOURCE PARAMETERS

The effects of the locations of hypocenter and asperities on the simulated ground motions are examined by changing them systematically on the fault plane.

Variation of Ground Motion due to Location of Hypocenter

The ground motions are simulated using 15 locations of hypocenter shown as solid circles in Figure 14. The slip of each sub-fault is assigned following the variable-slip model of the 1923 Kanto Earthquake (Wald and Somerville, 1995) shown in Figure 7.

Figure 15 shows the acceleration response spectra (h=0.05) of the simulated ground motions. We see the acceleration response varies about 3 times due to the location of hypocenter and the variation in long natural period range is somewhat larger than in short period range. The result from the simulation in which the location of hypocenter of the 1923 Kanto Earthquake shows the acceleration response close to the upper bound of the variation in short period range and mean of the variation in long period range.

Identification and Simplification of Asperities

Somerville et al. (1999) proposed a procedure to identify rectangle asperities from a variable-slip model and applied it to 15 crustal earthquakes. Figure 15 shows the rectangle asperities identified from the variable-slip model of the 1923 Kanto Earthquake by the procedure. Since two asperities were identified here, we call the larger one "Asp#1" and the smaller "Asp#2". The average slip over Asp#1 and Asp#2 become 2.00 times and 2.09 times of the average slip over the entire fault, i.e., 2.40[m]. Those values are very close to the value, 2.01, which Somerville et al. (1999) found as the average of the 15 crustal earthquakes.

Therefore, we simplify Asp#1 and Asp#2 to have uniform slip 4.80[m], just 2 times of the average slip over the entire fault. The rest of the entire fault is set to have uniform slip 1.57[m] to maintain the average slip over the entire fault. Here we call the simplified slip model "rectangle asperity model".

Figure 16 compares the simulated ground motions and their acceleration response spectra due to the rectangle asperity and variable-slip models. The location of hypocenter of the 1923 Kanto Earthquake is used here. Since the results show a fairly good agreement, we can use the rectangle asperity model and change the locations of Asp#1 and Asp#2 to examine the effects of variation of the slip distribution on the ground motion.

Variation of Ground Motion due to Location of Asperities

According to the result of a preliminary analysis, it was found that the effects of changing the location of Asp#1 in the dip direction on the ground motion are negligible. Thus, as shown in Figure 17, the locations of Asp#1 and Asp#2 are changed systematically with the location of Asp#1 in the dip direction is fixed. The location of hypocenter of the 1923 Kanto Earthquake is used here.

Figure 18 compares the acceleration response spectra (h=0.05) from the 18 rectangle asperity models shown in Figure 17. Figure 18 also shows the acceleration response spectrum from the variable-slip model of the 1923 Kanto

Earthquake, which is almost upper bound of the variation of the other 18 cases. This means the sub-faults that have large slips were concentrated around Kannonzaki as we can see in Figure 14. We see the acceleration response varies about 3 times and the variation in short period range is somewhat larger than in long period range, which is inverse of the effects of the location of hypocenter.

CONCLUSIONS

Ground motion at the mouth of Tokyo Bay from the large-scale scenario earthquakes were synthesized by semi-empirical and stochastic Green's function techniques. The geometric source parameters of the 1923 Kanto Earthquake were incorporated into the simulation, while the dynamic parameters, such as fault rupture mode, locations of hypocenter and asperities were systematically changed to study their influence on the synthesized ground motion. The following conclusions may be deduced from the present study.

1) The peak amplitude of 5% damped acceleration response spectrum calculated from the synthesized ground motion for the Kanto Earthquake is generally about 3000 cm/s^2.

2) Variation of fault rupture mode and asperity affects synthesized ground motion over wide period range, and the spectral amplitude of resultant ground motion synthesized by the semi-empirical Green's function technique changes 3 to 6 times due to this variation.

3) Acceleration response spectrum estimated by the stochastic Green's function technique also varies about 3 times over the natural period range under consideration.

4) The variable-slip rupture model yields almost upper bound of synthesized ground motions within the scope of present study. This is attributed to a fact that the sub-faults with large slips were concentrated beneath the ground motion estimation point.

REFERENCES

Boore, D. M. (1983). "Stochastic Simulation of High-frequency Ground Motions based on Seismological Models of the Radiated Spectra", *Bulletin of Seismological Society of America*, Vol.73, No.6.

Dan, K. et al. (2000). "Isoseismal Map of Strong Motions for the 1923 Kanto Earthquake (M_{JMA} 7.9) by Stochastic Green's Function Method", *Journal of Structural and Construction Engineering*, Architectural Institute of Japan (in Japanese, Submitting).

Hartzell, S. (1978). "Earthquake Aftershocks as Green's Functions", *Geophysical Research Letters*, Vol.5, No.1.

Harvard University (1999). *The Harvard CMT Catalog.*

Honshu-Shikoku Bridge Authority (1988). *Seismic Design Guideline of Akashi Kaikyo Bridge (Draft)* (in Japanese).

Irikura, K. (1983). "Semi-Empirical Estimation of Strong Ground Motions during Large Earthquakes", *Bulletin of Disaster Prevention Research Institute*, Kyoto University, Vol.33, No.298.

Irikura, K. (1986). "Prediction of Strong Acceleration Motions Using Empirical Green's Function", *Proc. of 7th Japan Earthquake Engineering Symposium.*

Jennings, P. C. et al. (1968). "Simulated Earthquake Motions", *Report of Earthquake Engineering Research Laboratory*, California Institute of Technology.

Kamae, K. et al. (1991). "Prediction of Strong Ground Motion Based on Scaling Law of

Earthquakes by Stochastic Synthesis Method", *Journal of Structural and Construction Engineering*, Architectural Institute of Japan, No.430 (in Japanese).

National Land Agency (1998). *The Grand Design for National Development in the 21st Century* (in Japanese).

Public Works Research Institute (1991). "Study on Structural Design of Trans-Tokyo Bay Highway", *Report of PWRI*, Vol.184 (in Japanese).

Somerville, P. et al. (1999). "Characterizing Crustal Earthquake Slip Models for the Prediction of Strong Ground Motion", *Seismological Research Letters*, Vol.70, No.1.

Tamura, K. et al. (1999). "Developing Seismic Design Ground Motions for Super Long-span Bridges", *Proc. of 15th U.S.-Japan Bridge Engineering Workshop*, U.S.-Japan Panel on Wind and Seismic Effects, UJNR.

Wald, D. and Somerville, P. (1995). "Variable-Slip Model of the Great 1923 Kanto, Japan Earthquake: Geodetic and Body-Waveform Analysis", *Bulletin of Seismological Society of America*, Vol.85, No.1.

Table 1 Source Parameters of the 1923 Kanto Earthquake

Fault Length	130 [km]
Fault Width	70 [km]
Strike	290 [deg]
Dip	25 [deg]
Seismic Moment	7.8×10^{27} [dyne·cm]
Rupture Velocity	3.0 [km/s]
Rise Time	5 [s]

Table 2 Number of Reassigned Simulation Cases

Rupture starts from the center	(1+3) ×(3+4)=28 cases
Rupture does not start from the center	(2+6) ×(6+6)=96 cases
Total	124 cases

Table 3 Ground Structure Model at Kannonzaki

	Depth [m]	Density [t/m^3]	S Wave Velocity [km/s]
ground surface	0 ~ 31	1.9	0.42
	31 ~ 45	1.9	0.40
	45 ~ 57	1.9	0.50
	57 ~ 77	1.9	0.61
	77 ~ 94	1.9	0.70
	94 ~ 120	1.9	0.84
	120 ~ 1005	2.0	1.15
	1005 ~ 1405	2.0	1.20
	1405 ~ 2605	2.1	1.30
	2605 ~ 3005	2.3	1.40
seismic bedrock	3005 ~	2.5	2.72

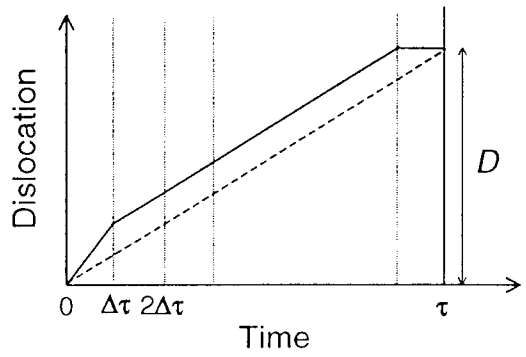

Figure 1 Source Time Function (Irikura, 1986)

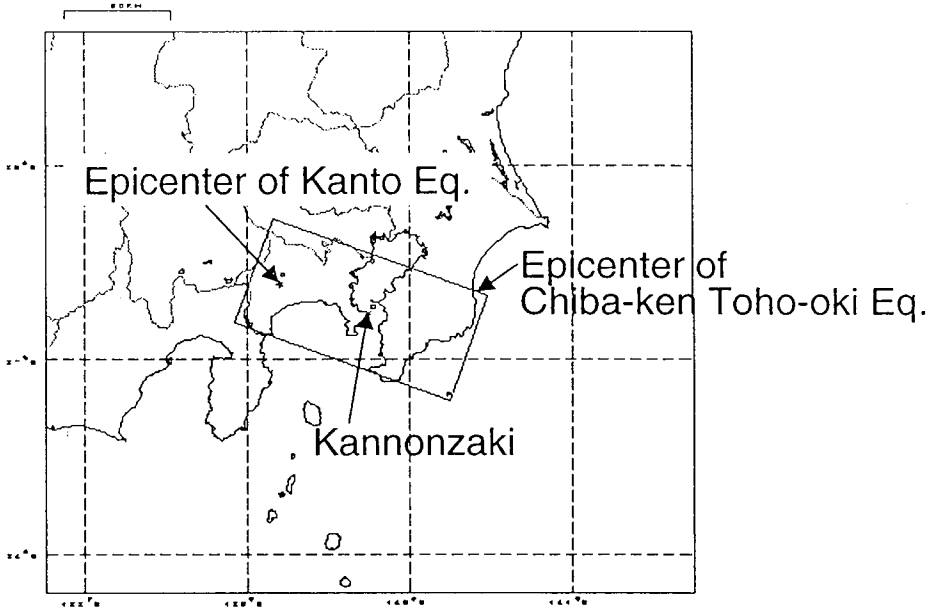

Figure 2 Fault Plane, and Locations of Epicenters and Kannonzaki

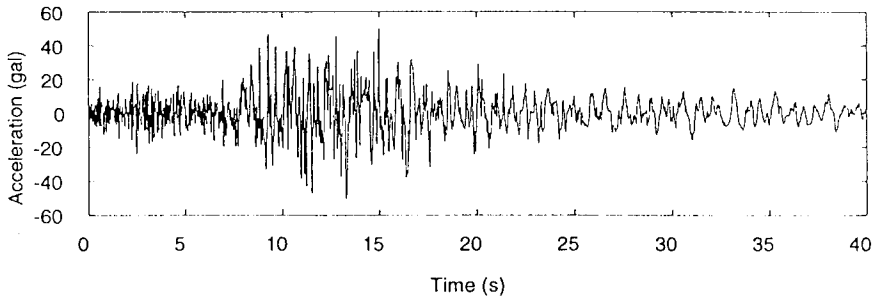

Figure 3 Kannonzaki Record from the 1987 Chiba-ken Toho-oki Earthquake (N-S Component)

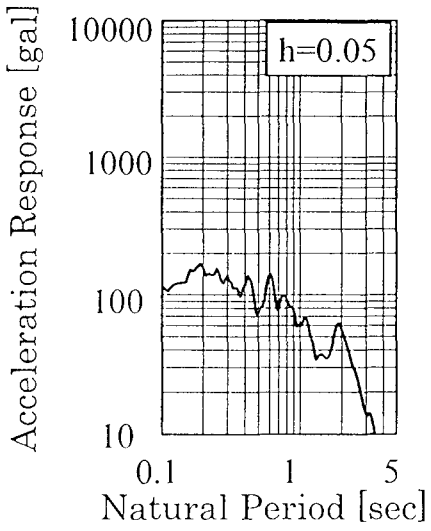

Figure 4 Acceleration Response Spectrum of Kannonzaki Record (h=0.05)

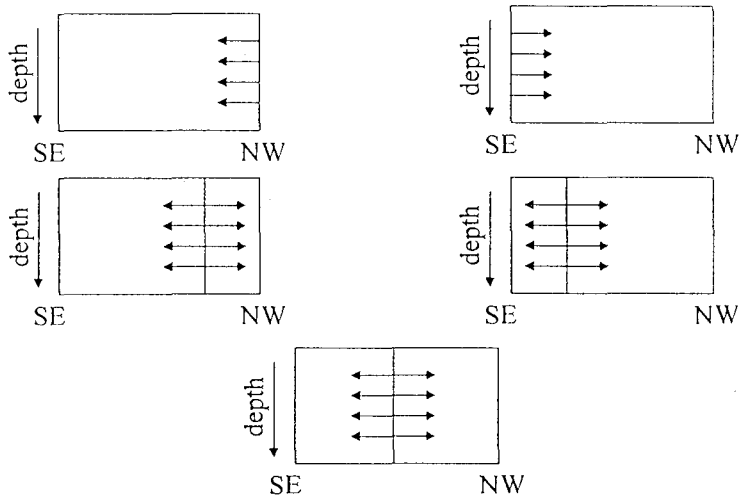

(a) Unilateral and Bilateral Rupture

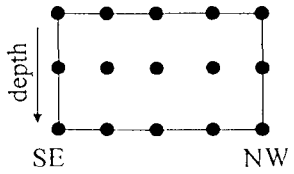

(b) Hypocenters of Radial Rupture

Figure 5 Rupture Modes and Hypocenters of Radial Rupture

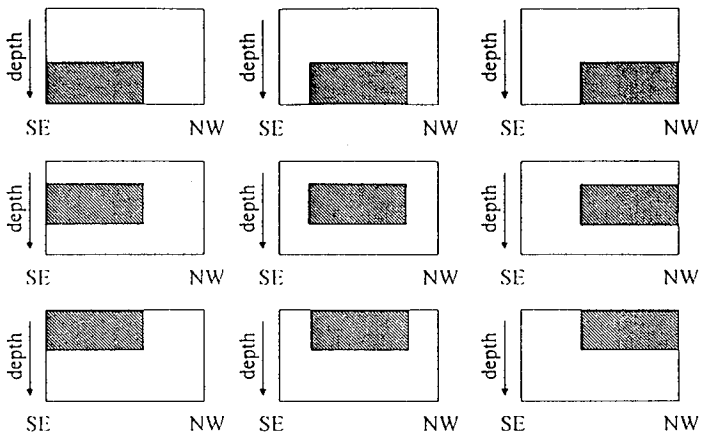

(a) 2×3 Asperity

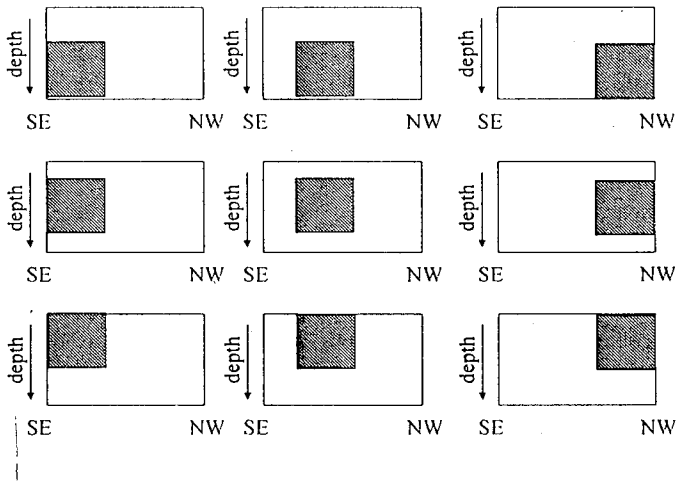

(b) 3×2 Asperity

Figure 6 Asperity Shape and Locations

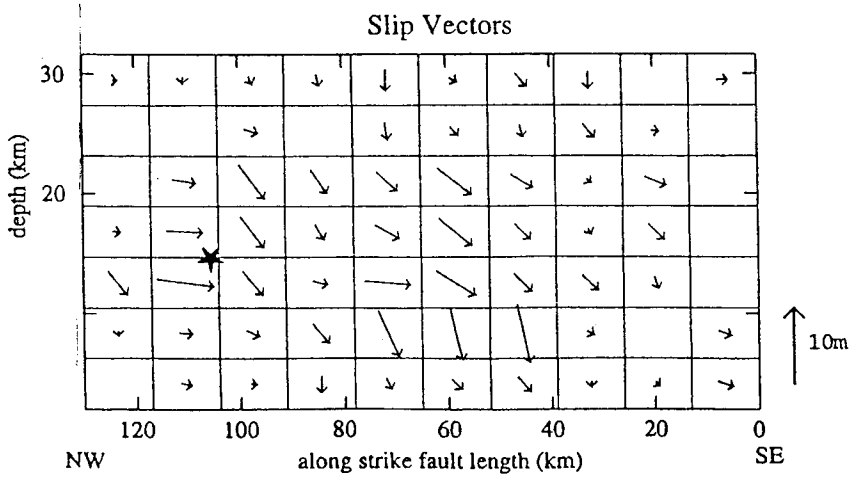

Figure 7 Variable-Slip Rupture Model of the 1923 Kanto Earthquake (Wald and Somerville, 1995)

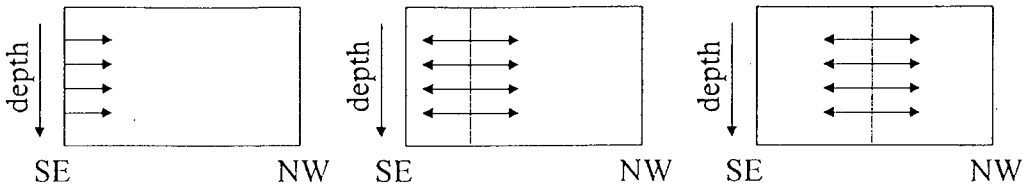

(a) Unilateral and Bilateral Rupture

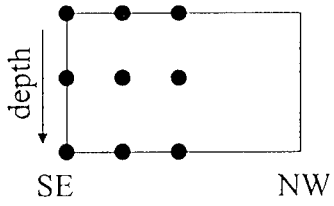

(b) Hypocenters of Radial Rupture

Figure 8 Reassigned Rupture Modes and Hypocenters of Radial Rupture

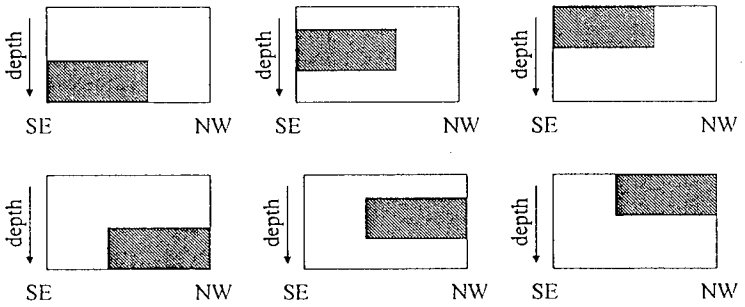

(a) 2×3 Asperity

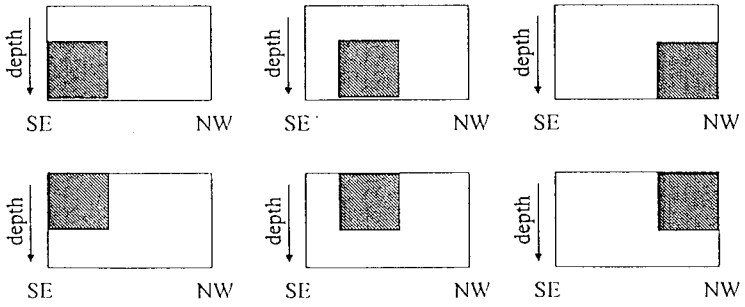

(b) 3×2 Asperity

Figure 9 Reassigned Asperity Shape and Locations

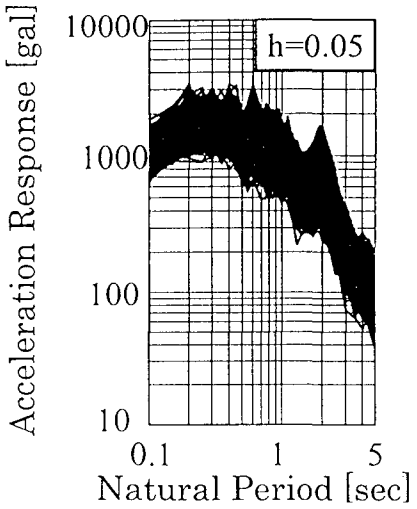

Figure 10 Acceleration Response Spectra of Synthesized Ground Motion

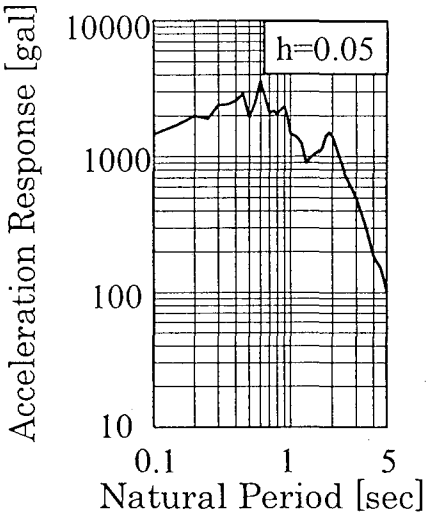

Figure 11 Acceleration Response Spectrum using the Variable-Slip Rupture Model

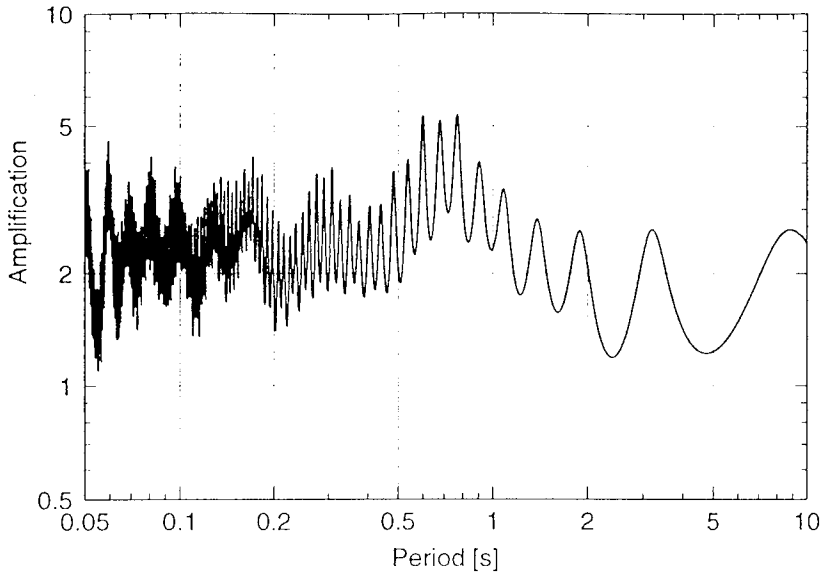

Figure 12 Transfer Function of the Ground Structure between the Ground Surface and the Seismic Bedrock at Kannonzaki

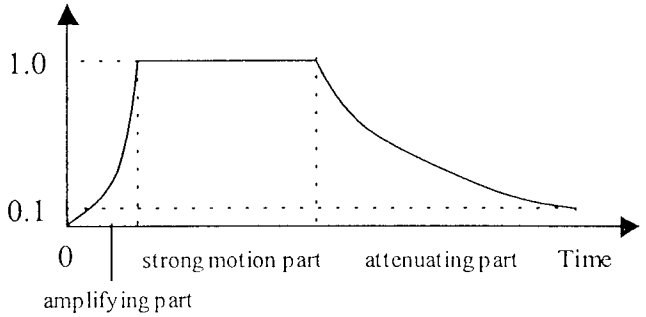

Figure 13 Shaping Window (Jennings et al., 1968)

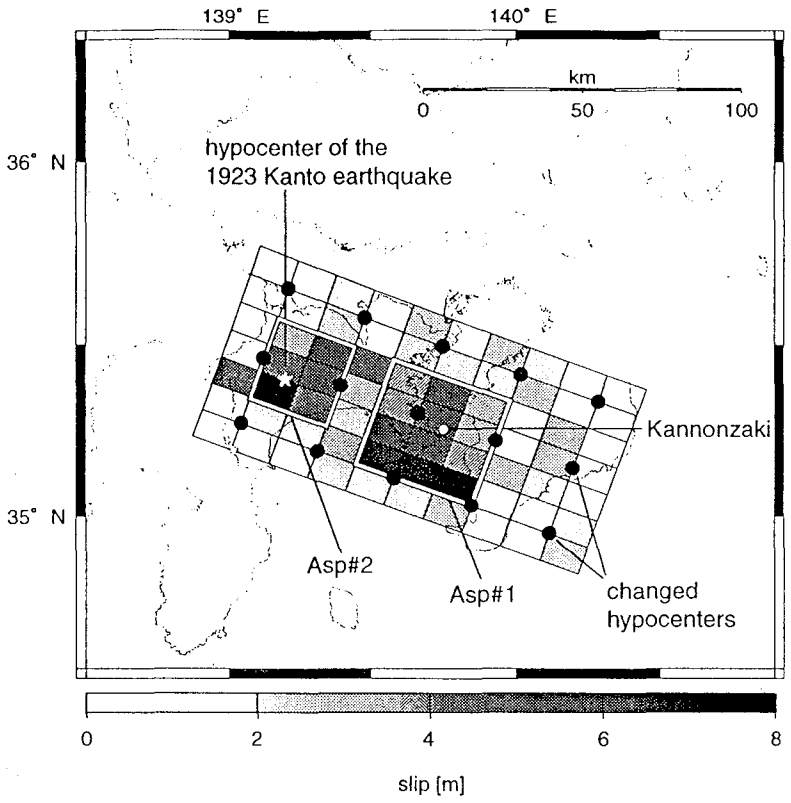

Figure 14 Rectangle Asperities Identified from the Variable-Slip Model of the 1923 Kanto Earthquake and the Locations of Hypocenters used in the Simulation

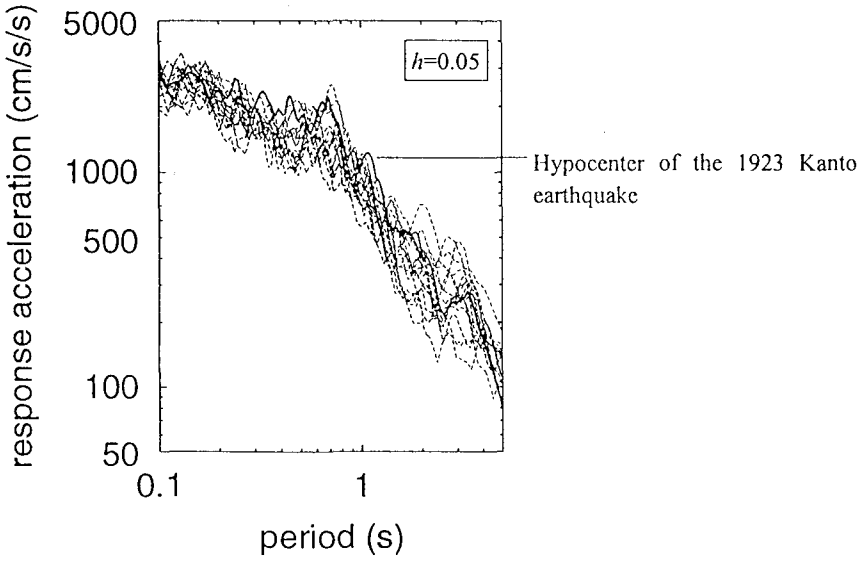

Figure 15 Variation of Ground Motion due to Location of Hypocenter

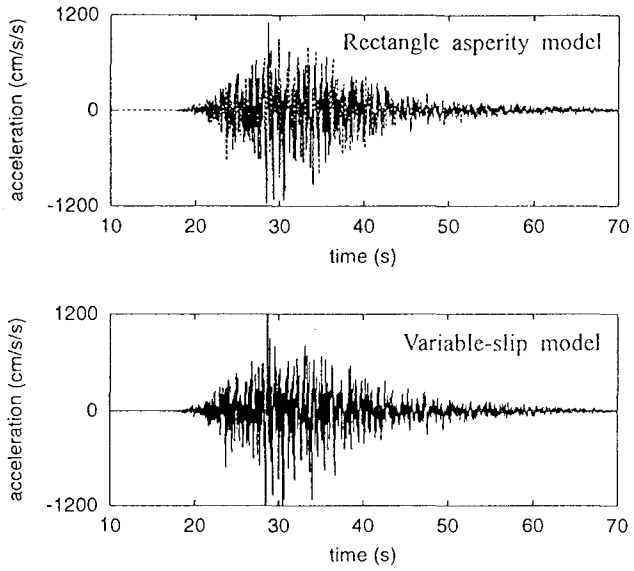

(a) Waveforms

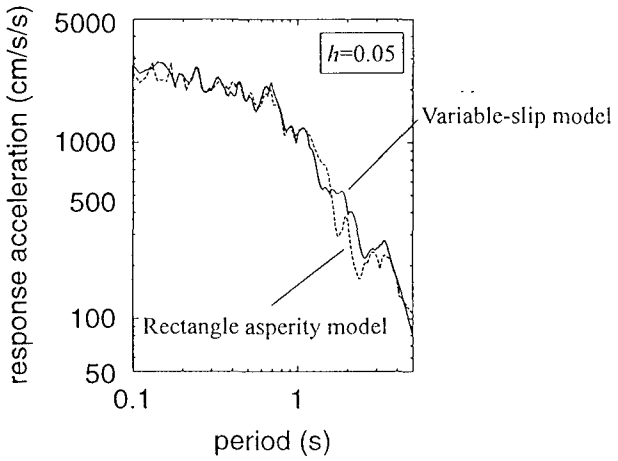

(b) Acceleration Response Spectra

Figure 16 Comparison between the Simulated Ground Motions due to the Rectangle Asperity and Variable-slip Models

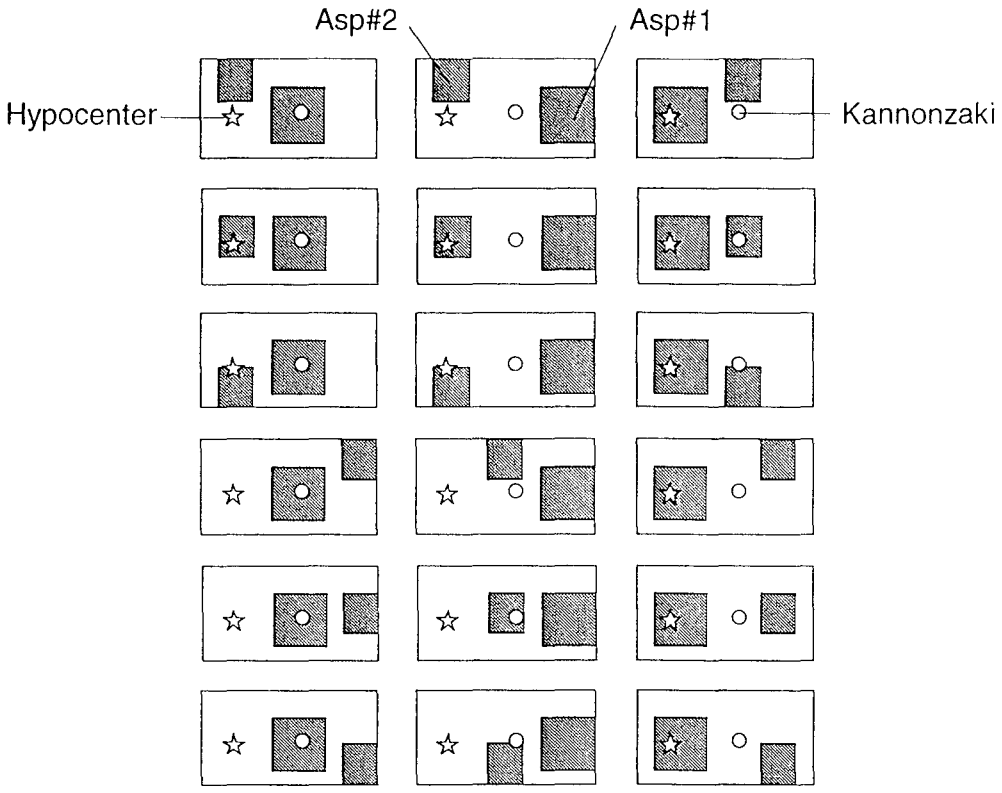

Figure 17 Rectangular Asperity Models with Variety of Locations of Asp#1 and Asp#2 The locations of hypocenter and Kannonzaki are also shown.

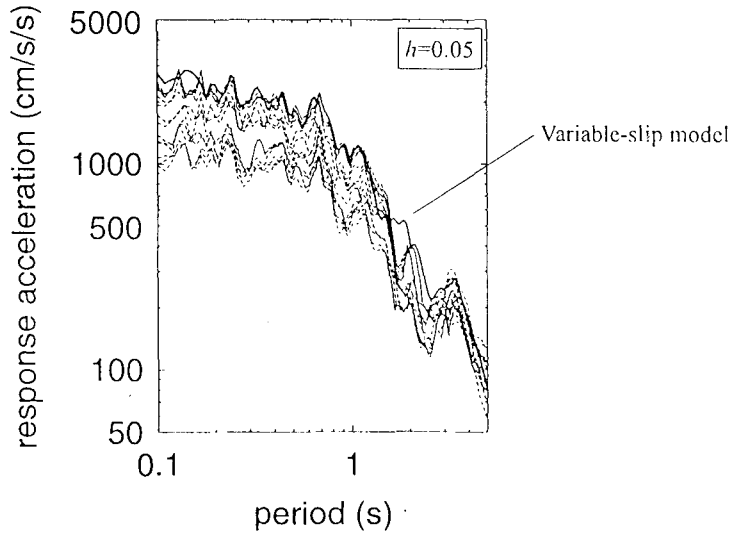

Figure 18 Variation of Ground Motion due to Location of Asperities

DEVELOPMENT OF SEISMIC ISOLATION TECHNOLOGY FOR UNDERGROUND STRUCTURES AND THE APPLICATION

by

Shigeki UNJOH[1], Junichi HOSHIKUMA[2], Kazuhiro NAGAYA[3] and Takeyasu SUZUKI[4]

ABSTRACT

The seismic isolation for underground structures is the system in which a tunnel body is covered by a thin isolation layer consisting of elastic materials with low shear modulus. The isolation layer absorbs the strain transmitted from the surrounding soils during large earthquakes so that the seismic performance of underground structures be improved. The Public Works Research Institute has developed this new seismic isolation technology with the Public Works Research Center and 17 private companies from 1995-1998. Then the seismic isolation technology is applied for a practical constrction at the connection of vertical shaft and tunnel of common utility ducts firstly in the world. This paper presents the outline of the seismic isolation technology and the practical application.

KEY WORDS: Seismic Isolation
Underground Structures
Seismic Performance
Common Utility Ducts

1. INTRODUCTION

The Hyogo-ken Nanbu Earthquake of January 1995 damaged underground structures and some underground structures such as the collapse of the Daikai Station on the Kobe Rapid Transit Railway were heavily damaged. It is essential to guarantee the operation of communication, electricity, gas, water, and other lifelines in regions struck by powerful earthquakes. To achieve this goal, the safety from strong earthquakes of utility tunnels that are typical underground structures provided to concentrate these lifeline services is required to be preserved. And while the earthquake resistance of underground structures must be improved, the public is demanding that the cost of their construction be reduced.

To meet these needs, the Public Works Research Institute of the Ministry of Construction, the Public Works Research Center and 17 private companies have taken part in joint research to develop seismic isolation technology for underground structures as a new technology that can improve the earthquake resistance of underground structures over that provided by conventional technologies at the same time as it lowers construction costs [1)-3)].

The seismic isolation structure that was developed for underground structures is a structure that can sharply reduce the effects of earthquakes by forming a flexible seismic isolation layer around the outer periphery of an underground structure to insulate the underground structure from deformation of the surrounding ground.

This paper describes an outline of seismic isolation technology for underground structures and a practical application for the starting vertical shaft of the Nakagawa Utility Tunnel. An outline of the test construction of the seismic isolation structure as well as the field test to verify the seismic isolation functions are presented.

---

1) Head, Earthquake Engineering Division, Earthquake Disaster Prevention Research Center, Public Works Research Institute, Ministry of Construction, Tsukuba-shi, Ibaraki-ken, 305-0804, Japan
2) Senior Research Engineer, ditto
3) Research Engineer, ditto
4) Deputy Director, Techical Institute of Kumagai-gumi Corp., Tsukuba-shi, Ibarakli-ken, 300-2651, Japan (Underground Structure Seismic Isolation Technology Promotion Committee)

2. R&D OF SEISMIC ISOLATION TECHNOLOGY

Fig.1 shows a conceptual diagram of the seismic isolation structure. Seismic isolation mechanisms for underground structures are categorized under the following four items.

1) Blocking the transmission of strain during earthquakes from the surrounding ground to a tunnel structure

2) Smoothing the tunnel strain in the seismic-isolated structure (longitudinal direction)

3) Dispersing the stress resultant concentrated at the corners of rectangular section tunnels (lateral direction)

4) Insulating the vertical shaft body from the tunnel at the tunnel entrance and smoothing the tunnel strain in the seismic isolated section (at vertical shaft connection points)

The performance required by a seismic isolation layer capable of providing these mechanisms was studied from the perspective of its mechanical properties and construction properties, then the seismic isolation material was developed based on the results of the study. The development process included testing to corroborate the mechanical properties, durability, etc. of the seismic isolation material, testing to verify its construction properties by trial manufacturing a seismic isolation material injection system, and corroborative material injection trials in an actual tunnel. And to develop a seismic isolation structure construction method for shield tunnels, in addition to a seismic isolation structure for use at points where ground conditions change abruptly, a seismic isolation structure for vertical shaft connections that are points of abrupt change in the structure and a method of constructing such a seismic isolation structure have been proposed. A design method and construction method for seismic isolation structures for underground structures that has been established as a result of this joint research were published in September 1998 as the Underground Structure Seismic Isolation Design Method Manual (Draft) [3].

The joint research has clearly shown that the seismic isolation structure can be effectively applied in 1) the longitudinal direction at points of abrupt change in ground conditions, 2) where the lateral section of a rectangular tunnel changes abruptly, and 3) in the longitudinal direction at connections with vertical shafts, but the results of a cost-effect analysis show that the most promising application of this seismic isolation structure is at the connections with vertical shafts of a shield tunnel.

The conventional method of providing seismic protection at connection with vertical shafts of a shield tunnel has been the application of a flexible segment. A flexible segment is a single special segment ring constructed so that it concentrates and absorbs strain generated in the surrounding tunnel. A flexible segment can absorb tunnel strain that is locally concentrated at the location where it is installed, but its effects are generally limited to a small range. But if a vertical shaft is isolated from a segment by a seismic isolation layer at the same time as a seismic isolation layer is installed within the range where the ground strain is most concentrated for about 10 m from the shaft, it is possible to provide isolation from both a point of abrupt change in the structure and from concentrated ground strain. In this way, the tunnel stress resultant can be reduced in a short seismic isolation section [4].

3. PRACTICAL APPLICATION OF DEVELOPED SEISMIC ISOLATION TECHNOLOGY

3.1 Outline

The seismic isolation structure for underground structures has progressed to the research and development stage, but because it has still not reached the stage where it is a practical design and execution technology, an actual structure must be designed and a trial execution of this design performed.

In 1997, initial seismic design for L1 earthquake motion was performed for the vertical shaft connection point of the No. 1 Nakagawa Utility Tunnel (below referred to as "Nakagawa Utility Tunnel"), and a flexible segment was chosen for the start side and a flexible joint for the arrival side of the connection point. The Nagoya

National Highway Construction Office of the Chubu Regional Construction Bureau of the Ministry of Construction applied the field trial system, the connection was redesigned to provide seismic resistance capable of withstanding L2 earthquake motion one rank higher than the previous design, and to confirm the applicability of the new system in actual tunnels and execution costs, this seismic isolation technology was selected for execution on the No. 1 Nakagawa Tunnel in 1997. This was the first attempt to use this seismic isolation structure anywhere in the world.

3.2 Seismic Isolation Design of Vertical Shaft Connection

(1) Structure Conditions

Fig.2 shows the surface ground structure at the start side of the vertical shaft and the locational relationship of the vertical shaft and tunnel. The bottom plate of the vertical shaft is in a diluvial clay layer, and the SMW wall diaphragm that surrounds it extends for about 40m down to a diluvial sandy soil layer. The earthquake wave input bedrook and the bedrock of the axisymmetric finite element method model for this design were assumed to be the top of the diluvial sandy soil layer Ds_3 (V_s = 320m/s) at a depth of 30.9m in the figure. The figure also shows the mechanical physical properties during slight strain of the surface ground.

The vertical shaft is a reinforced concrete structure with external width of 14m and depth of 10.8m and the plane shape shown at the top of **Fig.2**. Its wall thickness varies somewhat according to the depth and it has partition walls, but because the overall shear stiffness is not effected by accounting for these, it was assumed to be a box-shaped structure with a constant wall thickness of 14m for this study. The modeling of the vertical shaft by an axisymmetric finite element method model included the modeling of not only the vertical shaft body, but also the wall diaphragm constructed by SMW as part of the vertical shaft.

The tunnel studied was a shield tunnel with an exterior diameter of 5,050mm made of reinforced concrete segments with a thickness of 250mm, it was constructed by the slurry shield method (external diameter of the shield machine: 5,190mm), and its segment ring joints were connected with long bolts. The tension stiffness of the shield tunnel was modeled using equivalent tension stiffness calculated from the spring of the segments and from the serial spring of the spring of the ring joints. The compression stiffness used was the compression stiffness of the concrete of the segments.

Because the external diameter of the shield machine was 5,190mm, the thickness of the isolation layer was set at 7cm that equals the thickness of the tail void.

The verification of safety during an earthquake of the shield tunnel was performed based on two factors the allowed aperture of the ring joint (2mm) and the yield stress of the joint bolts ($940N/mm^2$) during tension deformation, and based on the allowed compression stress ($24N/mm^2$) of the segments during compression deformation.

(2) Input Earthquake Motion

The input earthquake motions for L2 earthquake motion were chosen from among standard waves used for seismic design of highway bridges. Waves obtained by performing amplitude compensation of the component at right angles to the bridge axis of the Kaihoku Bridge during the Miyagi Prefecture Offshore Earthquake of 1978 were used as Type-1 earthquake motion for category I ground. Waves obtained by performing amplitude compensation of the NS component recorded at the Kobe Marine Meteorological Observation Station during the Hyogo-ken Nanbu Earthquake of 1995 were used as the Type-2 earthquake motion. **Fig.3(1)** shows the Type-1 earthquake motion and **Fig.3(2)** shows the Type-2 earthquake motion. The one-dimensional seismic response analysis of the surface ground was performed by the substitute structure approach: considering these input earthquake motions to be waves observed at the outcrop of free rock, reducing the amplitude by 50%, and inputting the resulting waves from the top of the bedrock layer D_{s3}. The strain dependency of the ground used for the analysis was obtained from a mean strain dependency evaluation equation for typical ground [5) 6)].

The ground inertial force applied by the axisymmetric finite element method model was calculated by the ground response seismic coefficient method[7] that uses the ground acceleration at the time when the maximum value of the total of the shear strain of the ground from the bed rock to the surface is generated based on seismic response analysis.

(3) Design Results

Fig.4 shows the results of a parametric study of deformation during tension subject to strict design conditions that was conducted to determine the shear modulus of rigidity of the seismic isolation layer and the length of the seismic isolation section. The variables for the parametric study were shear modulus of rigidity of the isolation layer of 0.3 and 0.5N/mm^2 and the length of the seismic isolation section from the exterior wall of the vertical shaft that were 10, 15, and 20m. The shearing modulus was set considering silicon seismic isolation material (SISMO-003 or SISMO-005) that is isolation layer material with superior durability and workability. Analysis results have revealed that within a seismically isolated section length between 10m and 20m, there is little variation in the tension axial force of the tunnel and that even if the shearing modulus of the seismic isolation layer is reduced from 0.5N/mm^2 to 0.3N/mm^2, the tension axial force of the tunnel declines very little. The shearing modulus of the seismic isolation layer was, therefore, set at 0.5N/mm^2 and the seismically isolated section length was set at 10m from the exterior wall of the SMW.

Fig.5 shows an example of the results of an analysis of the joint aperture during tension deformation caused by Type-1 earthquake motion. In addition to showing the results for a seismic isolation structure case, the figure presents the results of an analysis of a rigid connection case and of a case hypothesizing a flexible segment with a Young's modulus of 0.1N/mm^2 at a point 1 m from the external wall of the vertical shaft. If a seismic isolation structure is adopted in this way, the ring joint aperture will be within the allowed value (2mm), but in the cases hypothesizing the adoption of a rigid connection and a flexible segment, the aperture exceeded the allowed value. The tension stress of the joint bolts was within the range of the allowed values for all cases.

Fig.6 shows the results of an analysis during compressive deformation. This figure shows that under both types of earthquake motion, the compressive stress of the segment was within the allowed value (940N/m^2) for all cases. It also reveals that adopting the seismic isolation structure lowers the compressive axial force on the segment to about half that obtained with the rigid connection method, which is larger than the reduction to 2/3 possible with a flexible segment.

Fig.7 is a schematic diagram of the seismic isolation structure at the start vertical shaft established by the above seismic isolation design process. The design calculations modeled the SMW and the vertical shaft body as a vertical shaft. The seismic isolation section that was analyzed extended for 10m from the external wall of the vertical shaft, but for execution reasons including the fact that the segment length is 1.2m, the seismic isolation layer was formed in the tail void for 10 rings from the tunnel entrance. This means that the seismic isolation section extended 9.6m from the external wall of the SMW and 10. 5m from the external wall of the vertical shaft body. On the ground side of the SMW wall, the seismic isolation layer was 7cm thick that is the same as the tail void, but it was thicker at the entrance. And to provide the tunnel entrance with waterproof properties and to insulate the vertical shaft body from the segment, a natural rubber ring with a wedge-shaped section, covered on three sides by water-absorbing rubber, and with a shearing modulus of 0.6N/mm^2 (tunnel entrance insulation layer) was installed at the tunnel entrance and integrated with the tunnel entrance concrete.

The adoption of a seismic isolation structure as described above, provides an existing structure with the ability to withstand Type L2 earthquake motion. And the waterproofing function of the silicon seismic isolation material guarantees waterproofing even if an unpredictable joint aperture occurs.

3.3 Practical Construction

(1) Isolation Material

The seismic isolation material used for the trial execution was silicon seismic isolation material SISMO-005 with its shearing modulus G adjusted to 0.5N/mm^2 or less. Silicon type seismic isolation material is a rubber elastic body hardened at normal temperatures by the condensation reaction caused by mixing and agitating fluid A that is a mixture of silicon polymer + finely powdered silica and fly ash with fluid B that consists primarily of a hardener and plasticity adjustment agent at a mix ratio by weight of 10:1. A cross linking agent is added uniformly to fluid A and a catalysis is added to fluid B. It is, therefore, possible to control only the hardening time without altering the hardness of the rubber that is the seismic isolation material by adjusting the quantity of the catalyst in fluid B. The seismic isolation material is an inorganic material based on silica and is both non-polluting and durable. **Fig.8** shows the strain dependency of the shearing modulus of the seismic isolation material obtained by cyclic hollow cylindrical cyclic shear testing performed at a loading frequency of 1Hz. This test shows that the seismic isolation material has stable dynamic physical properties regardless of the shearing strain. The material has no constraining pressure (depth) dependency and it is an elastic material with a damping factor less than 3%[8].

Fluid A is supplied to the agitator (capacity 1.8m^3) of the plant from a hopper located above the ground, then it is pressure fed from the agitator at a fixed rate by a mono-pump. Fluid B is supplied to the fluid B agitator (capacity 0.2m^3) of the plant from a drum, then it is pressure fed from the agitator at a constant rate by a mono-pump. The tip of the injector is a rubber injector used for backfill injection. After the two fluids have been mixed, a quarrying column mixer is passed through a 2-inch steel pipe for a total of 80 cm and its pressure loss is utilized to completely mix the fluids. Because this mixer is long and it is difficult to work with, the injector unit and mixer are connected by a flexible rubber tube.

The specific gravity of the seismic isolation material is 1.36, and its elongation is 100%. As stated above, the mix proportion was designed to lower the shearing modulus to less than 0.5 N/mm^2. Therefore, when the seismic isolation material is shipped from the factory, it provides JIS hardness of 32 degrees and a shearing modulus of 0.44N/mm^2 and satisfies the required physical properties after it has been blended indoors based on the stipulated mix proportion and is cured for one week at a temperature of 20 Centi-Degree.

(2) Construction

The level difference between the injection pump and injection outlet was minimized, care was taken to obtain a stable blend of fluid A and fluid B, and the seismic isolation material plant was installed in an intermediate level of the vertical shaft. **Fig.9** is a schematic diagram of the seismic isolation structure at the start side of the vertical shaft. As shown in the figure, the seismic isolation material was, in principle, injected during excavation from injection holes in the segments into the tail void produced as the shield excavator advanced in the same way as immediate backfilling injection is performed. It was feared that during the seismic isolation material injection work, seismic isolation material might flow into the blades where it would get into the chamber. To prevent this from occurring, as the shield excavator advanced, void filling clay (clay shock) was injected into the void between its steel shell and the natural ground from an injection outlet installed near the articulation of the shield excavator to block the gap between the tail void and the blade. Because the clay shock was pressure injected into small voids on the excavated natural ground, it also prevented the seismic isolation material from leaking into the natural ground.

At locations in the fluid A and fluid B pressurized feed hoses just before their respective injection and mixing locations, bypasses were installed to cycle the two fluids through agitators prior to injection in order to prevent separation of their materials and a decline in their viscosity. To form a seismic isolation layer of uniform thickness around the segments, it was vital to exercise strict control of the excavation. It was necessary to guarantee

that the seismic isolation work would not conflict with the basic principles of shield work that require the immediate filling of the tail void to prevent the collapse of the natural ground and to keep out ground water and mud. To guarantee this, before the work began, the segments were equipped with injection holes at three locations in the tunnel axis direction that differs for each segment piece, and injection was begun from the injection hole closest to the void, to permit the restarting of excavation after it was stopped because of trouble with the work.

That part of the work to form the seismic isolation structure at the vertical shaft connection that was most important and had to be done with the greatest care was the work at the entrance: the first stage in the execution. Because a large void is formed behind the segment at the entrance as shown in **Fig.9**, it was first stabilized by filling it with high density mud. After excavation to the third ring, clay shock was injected to fill the void behind the steel shell of the shield excavator to prevent the seismic isolation material from flowing into the blades, then the injection of the seismic isolation material at the entrance was performed.

(3) Quality Control

To control the quality of the seismic isolation material, the hardness of a hardened sample of the seismic isolation material made at the time it was shipped from the factory and the hardness of hardened samples made before, during, and after injection were measured by the JIS-K6301-A method. The flow rates of the seismic isolation fluid A and fluid B were controlled by installing Coriolis flow meters, and the quantities of fluid A and fluid B remaining in their respective tanks after the injection work were measured to confirm that the fluids were completely injected.

While the mean hardness of the seismic isolation material when it was shipped from the factory was 32, the hardness of samples of seismic isolation material obtained at the tip of the injector immediately before, during, and after injection and cured for 1 week ranged from 26 to 33 and the mean value was 29. Converting this to the shearing modulus obtained a result of 0.39N/mm^2, which is a little lower than the results of the measurements at the factory (hardness of 32, shearing modulus 0.45N/mm^2). The mean hardness of the seismic isolation material after 1 month passed, was 31 (G = 0.42N/mm^2), a result that fully satisfied the design value of G = 0.5N/mm^2 or less.

(4) Field Test for Effectivenes Verification

To verify the seismic isolation performance of the seismic isolation structure formed at the vertical shaft connection by this trial execution, a field experiment was carried out to measure the shear reaction force in the tunnel axis direction of the seismic isolation layer. When a seismically isolated shield tunnel surrounded by a seismic isolation layer is forcefully deformed in the tunnel axis direction, shear resistance proportional to the shear reaction of the periphery of the tunnel is obtained. Because this shear reaction force is the shear resistance of the seismic isolation layer and the ground around it, it is possible to evaluate it based on their series spring system. If the shearing modulus of the seismic isolation layer is more than 2 orders smaller than that of the ground, it is possible to approximate the shear reaction force of the seismic isolation layer body that treats the ground as a rigid body. Consequently, using the reaction force of the wall of the vertical shaft, the tunnel was moved towards the cutting face along with the shield excavator by a hydraulic jack, and the shear spring constant of the seismic isolation layer was estimated from the relationship of the tunnel axial direction deformation with the thrust of the hydraulic jack.

The shear spring constant of the seismic isolation layer can be obtained theoretically by Eq.2 from the relationship between the force and the displacement produced by treating the periphery of the seismic isolation layer as a constant condition and forcefully deforming the external surface of the tunnel in the tunnel axial direction.

$$K_m = 2\pi * G_m / \ln(R_m/R_t) * L \qquad (1)$$

Where:

- K_m: shear spring constant of the seismic isolation layer
- G_m: shear modulus of the seismic isolation layer
- L: length of the seismic isolation layer

R_m: 1/2 of the external diameter of the seismic isolation layer
R_t: 1/2 of the external diameter of the tunnel

Because it was necessary to complete the injection of the seismic isolation layer at the starting vertical shaft connection to form the seismic isolation then perform this test before the backfill injection that accompanies normal shield excavation, the test was performed four days after the final day of the seismic isolation material injection work.

Fig.10 is a schematic diagram of the seismic isolation layer reaction force measurement test. The reaction receiver installed on the vertical shaft body wall was a mobile structure that allowed the removal of the bolts to cause the temporary segment reaction frame to slide towards the tunnel. The reaction receiver was equipped with a pedestal to be used to install eight hydraulic jacks. By removing its bolts and installing jacks on the pedestal, the reaction receiver becomes a loading device structurally equipped with a movable reaction frame. As stated above, the periphery of the shield excavator is filled with clay shock and it is assumed that the shear resistance of the periphery of the shield excavator is low. It was, therefore, possible to move the segment in the direction of the cutting face along with the shield excavator to the location where the shear reaction force of the seismic isolation layer and the jack thrust were in balance, by advancing the hydraulic jacks installed on the reaction receiver and at the same time, adjusting the cutting face slurry pressure downwards to prevent the action of the jacks from increasing this pressure to maintain it at a constant level.

The jacking pressure was increased at steps of 50kN steps per jack for a total of 400kN per step. The jacking pressure was increased again after the tunnel deformation caused by the previous increase in thrust had stabilized. The loading was concluded when the tunnel had been deformed 10mm towards the cutting face. The unloading was performed in the same way as the loading: reducing the pressure applied by the jacks by 400kN, waiting for the tunnel deformation to stabilize, then lowering the pressure by another 400kN step. When the hydraulic jack pressure was down to zero, the residual displacement of the tunnel was measured. The jacks were operated from an intermediate level in the vertical shaft at a location where the operator could see the loading device equipped with the movable reaction frame.

The cutting face slurry pressure was automatically regulated so that it remained at a constant level of 0.15MPa (reaction of 3,200kN to by the slurry pressure) throughout all loading and unloading steps. But during the loading steps, the cutting face slurry pressure temporarily rose to a maximum of 0.17MPa and it took time to lower it to its stable value. But during unloading, the cutting face slurry pressure remained stable at almost exactly 0.15MPa, with the result that the pulling phase of the loading operation did not take as long as the pushing phase.

The measurements were performed by monitoring the pressure and stroke of the 8 hydraulic jacks, the relative axial direction displacement of the segment and the vertical shaft body on the left and right sides of the vertical shaft entrance, and the cutting face slurry pressure in the central control room, and by measuring the distance between the vertical shaft and the ring 1 joint of the segment closest to the cutting face using a light measure system fixed at the vertical shaft portal. The data obtained from these measurements was displayed to the operator in the intermediate level of the vertical shaft and used to make jack operating decisions. It was also monitored and recorded in a measurement vehicle located at ground level.

(4) Test Results

Fig.11 summarizes the results of the test in terms of the relationship of the relative axial direction displacement of the tunnel and the vertical shaft body wall at the entrance with the total thrust P_t of the 8 jacks installed on the reaction frame. The hysteresis in this figure is categorized as 5 loading states from I to V to explain the process of determining the shear spring constant of the seismic isolation layer. While the behavior varied according to the

loading stage as shown in **Fig.11**, the tunnel stopped at location F with residual displacement of approximately 1.57mm without being restored to its original position even after the jack pressure was finally reduced to zero at the end of the unloading steps.

With the residual displacement of the tunnel at location F represented by δ cm, the shear spring constant of the seismic isolation layer by K_m (kN/cm), the maximum static friction force of the temporary segment and the pedestal by P_{static}, and the cutting face pressure produced by the cutting face slurry pressure by P_{mud}, and assuming that the cutting face slurry pressure can be ignored because in static state, it is balanced with the slurry pressure, the following equation of equilibrium can be established for the point in time where the tunnel has stopped at the final stage.

$$K_m = \delta + P_{mud} = P_{static} \quad (2)$$

It can be concluded that because the residual displacement δ = 0.157cm, the maximum static friction force is in balance with (reaction force P_{mud} produced by the cutting face slurry pressure = 3,200kN) + (reaction force of the seismic isolation layer equivalent to the shear deformation of 0.157mm). Next, if it is assumed that the point A in **Fig.11** corresponds to the time when the temporary segment began to slide on the top of the pedestal, the maximum static friction force P_{static} = 4,570kN, and if these values are substituted in equation (2), K_m (kN/cm) is as shown below.

$$K_m = 4{,}570 \quad 3{,}200/0.157 = 8{,}730 \quad (3)$$

The thick dark line in **Fig.11** shows the results of assuming that P_{static} = 4,750kN and K_m = 8,730kN/cm to estimate the hysteresis relationship of the jack thrust with the axial displacement of the tunnel when the reaction force at the cutting face is assumed to be constant. The hysteresis that was estimated shows a separation from actual behavior caused by instability of the cutting face soil pressure at loading stage III [15], but the fact that both conform closely at loading stage II and at V that was the final stage of the unloading and an almost linear load displacement relationship was obtained during unloading reveals that a seismic isolation layer with reliable resilient behavior was formed around the periphery of the tunnel and its spring constant K_m = 8,730kN/cm.

Because the mean injection rate of the seismic isolation material was approximately 120%, the seismic isolation layer corresponding to this injection rate is 8cm, and the theoretical value of the shear spring constant of the seismic isolation layer with a shear modulus G = 0.5N/mm^2 is 11,380kN/cm^2 based on Eq.(1). Because the measured shear spring constant of the seismic isolation layer is 8,730kN/cm, the shear modulus of the seismic isolation layer is 0.383N/mm^2, which conforms almost perfectly with the mean value of 0.39N/mm^2 of the seismic isolation material injected as described above following 1 week of aging. The shear spring constant and the shearing modulus of the seismic isolation layer are, therefore, appropriate values.

Because as described above, elastic behavior capable of restoring the tunnel to its original position during unloading in a linear relationship with the jack thrust was obtained and because the shearing modulus of the seismic isolation layer is an appropriate value, it has been verified that a seismic isolation layer with the intended functions was constructed.

4. CONCLUDING REMARKS

This paper has summarized the design and execution of a seismic isolation structure for underground structures that has been made at the start vertical shaft connection of an actual shield tunnel.

(1) The trial execution of the seismic isolation structure verified the execution properties of the silicon seismic isolation material injection system.

(2) The mean injection rate of the seismic isolation material is 120%, which is a rate lower than the injection rate of normal backfill.

(3) In-situ testing conducted to measure the reaction force of the seismic isolation layer verified the functions of the seismic isolation structure by demonstrating that elastic behavior capable of restoring the tunnel to its original position during unloading in a linear relationship with the jack thrust could be obtained and that

the shearing modulus of the seismic isolation layer obtained by the test conforms with measured values.
(4) The above results have shown that this seismic isolation structure for underground structures is a technology that can be applied to the design and execution of actual underground structures.

ACKNOWLEDGEMENTS

The construction of the seismic isolation structure was performed with the generous assistance and cooperation of the staff of the Nakagawa Shield Tunnel Construction Office, Hazama-Sato Joint Venture under the contract of Nagoya Construction Office of Ministrry of Construction. The authors wish to conclude by expressing their sincere gratitude to them for their contribution to this project. The members of the Underground Structure Seismic Isolation Technology Promotion Committee provided technical advice regarding the planning and the design of the trial execution. The authors wish to also thank them for their assistance.

REFERENCES

1) Public Works Research Institute, et. al.: Report on Joint Research on the Development of Seismic Isolation Materials for Use in the Seismic Isolation Design of Underground Structures (Part 1), Joint Research Reports, Reference No. 154, Nov. 1996 (in Japanese)
2) Public Works Research Institute, et. al.: Report on Joint Research on the Development of Seismic Isolation Materials for Use in the Seismic Isolation Design of Underground Structures (Part 2), Joint Research Reports, Reference No. 192, Dec. 1997 (in Japanese)
3) Public Works Research Institute, et. al.: Report on Joint Research on the Development of Seismic Isolation Materials for Use in the Seismic Isolation Design of Underground Structures (Part 3), Underground Structure Seismic Isolation Design Manual, Joint Research Reports, Reference No. 211, Sept. 1998 (in Japanese)
4) Shigeki Unjoh, et. al.: Seismic Isolation Structures and Seismic Isolation Design of Underground Structures, Proceedings of the Sixth Tunnel Engineering Research Conference, Vol. 8, pp. 31-38, 1998 (in Japanese)
5) Public Works Research Institute: Numerical Analysis of Response Properties of Ground During Earthquakes, - DESTRA -, PWR Document No. 1778, February 1982 (in Japanese)
6) Yasuda, Yamaguchi: Dynamic Deformation Properties of Various Categories of Undisturbed Soil, Twentieth Soil Engineering Research Conference, pp.539-542, June 1985 (in Japanese)
7) Katayama Ikuo et. al.: Proposal of the "Response Seismic Coefficient Method" a Practical Quasi-dynamic Analysis Method for Structures Buried Underground, Fortieth Annual Technical Conference of the Japan Society of Civil Engineers, Part 1, pp.737-738, 1998 (in Japanese)
8) Takeyasu Suzuki et. al. Dynamic Properties of Silicon Seismic Isolation Material for Tunnel Seismic Isolation Work, Proceedings of the Thirty-second Conference on Ground Engineering, pp.2095-2096, 1997 (in Japanese)
9) Takeyasu Suzuki, et. al.: Experimental Study of Silicon Material for Urban Tunnel Seismic Isolation Structures, Collected Reports of the Japan Society of Civil Engineers, No. 534/VI-30, pp.69-76, 1996 (in Japanese)
10 Shigeki Unjoh, et. al.: Function Verification Testing of Seismic Isolation Structures for Use at Vertical Shaft Connections, Collected Papers and Reports on Tunnel Engineering Research, Vol. 9, 1999 (in Japanese)
11) Shigeki Unjoh, et. al.: Draft Manual for Seismic Isolation Design for Underground Strucutres, Proceedings of the 30th Joint Meeting on Wind and Seismic Effects, UJNR, NIST SP931, August 1998

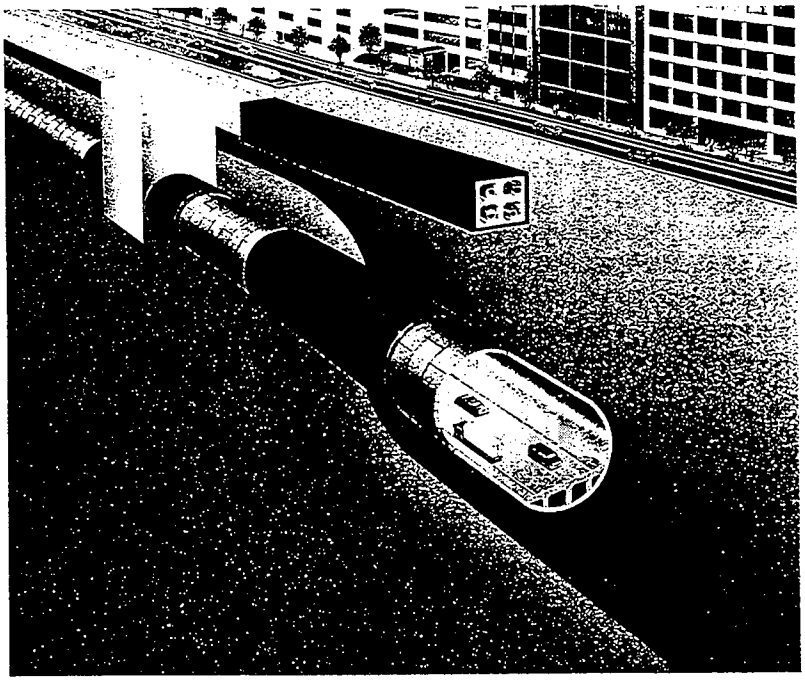

Fig.1 Seismic Isolation Technology for Underground Structures

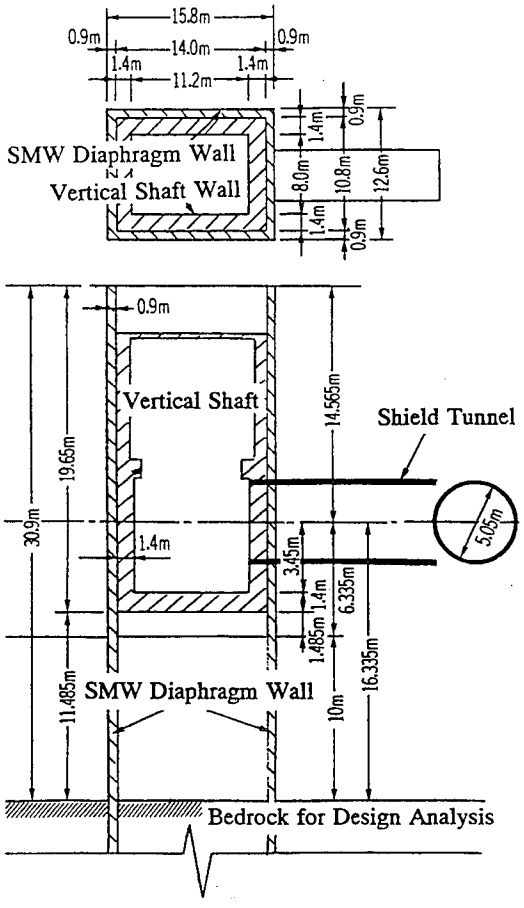

Fig.2 Layout of the Vertical Shaft and Tunnel

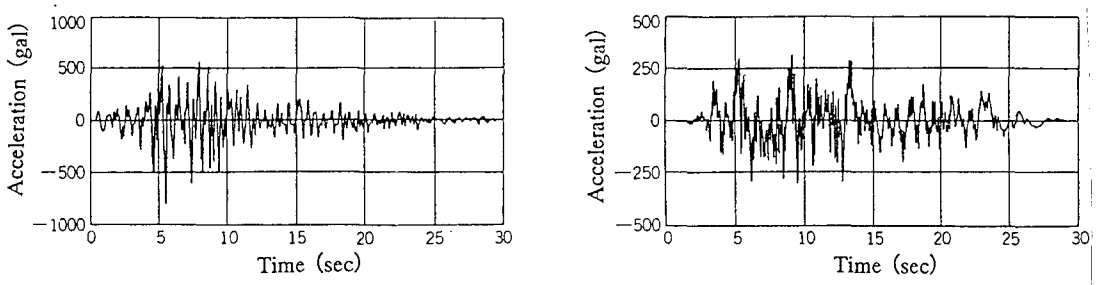

(1) Type-1 (2) Type-2

Fig.3 Input Earthquake Motion

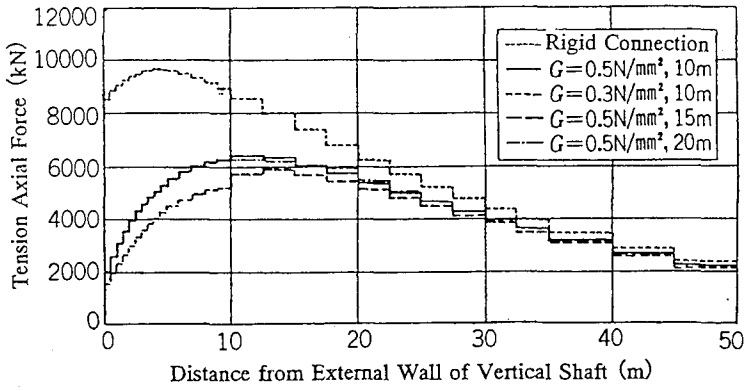

Fig.4 Effect of Shear Modulus and Length of Seismic Isolation Layer

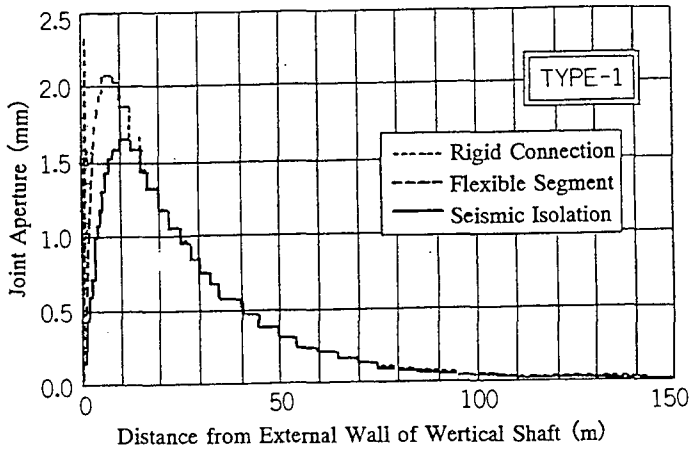

Fig.5 Analysis of Ring Joint Aperture

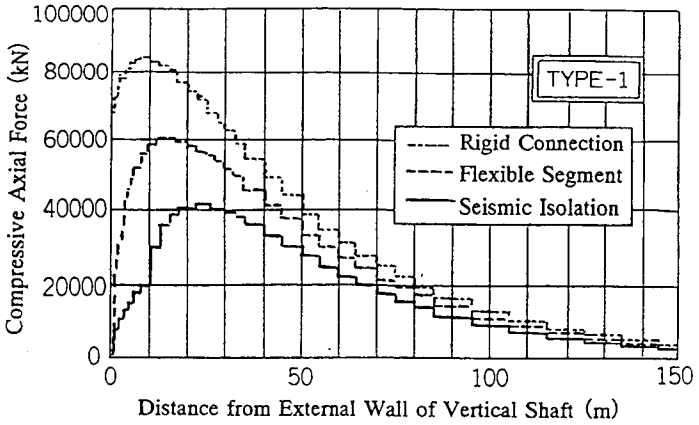

Fig.6 Analysis of Compressive Axial Force of Segments

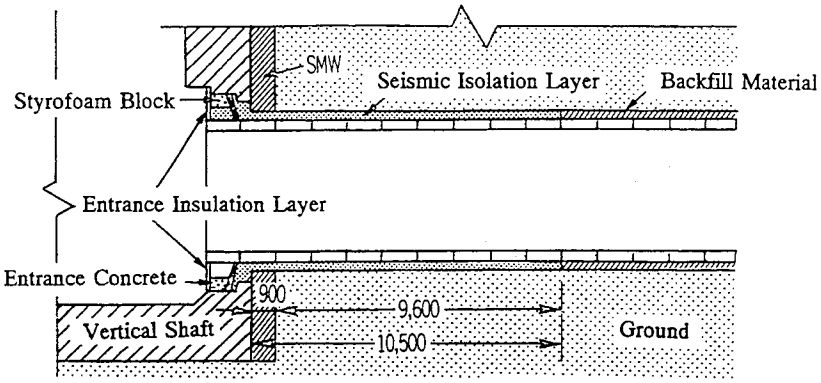

Fig.7 Seismic Isolation Structure at Start Vertical Shaft

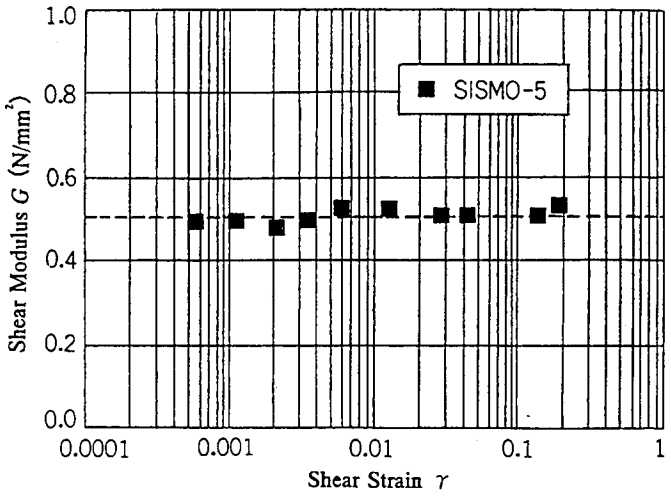

Fig.8 Strain Dependency of Shear Modulus of Silicon Seismic Isolation Material

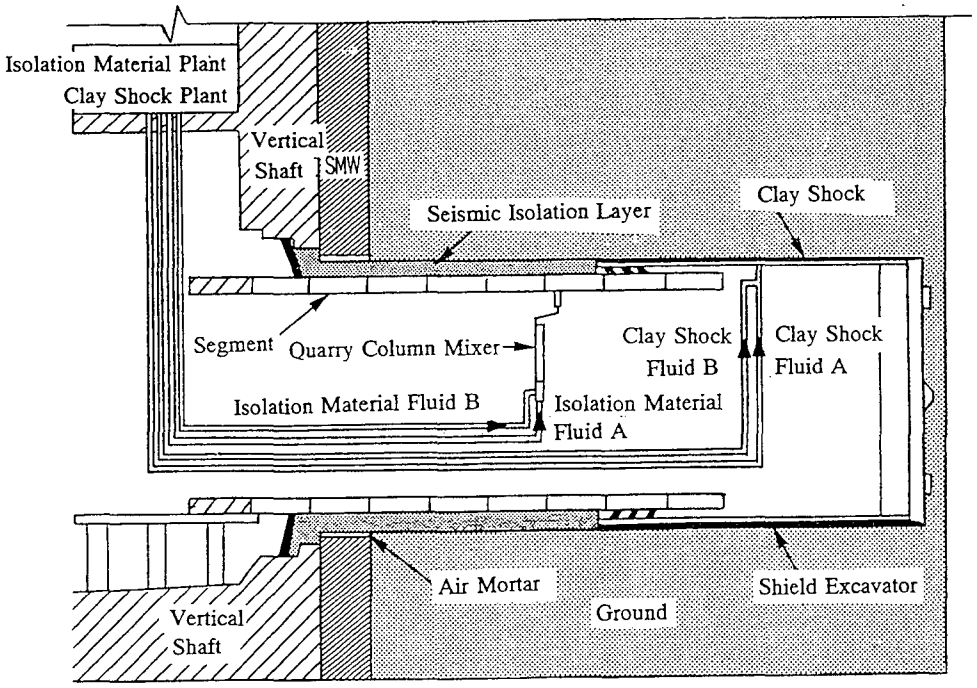

Fig.9 Silicon Seismic Isolation Material Injection

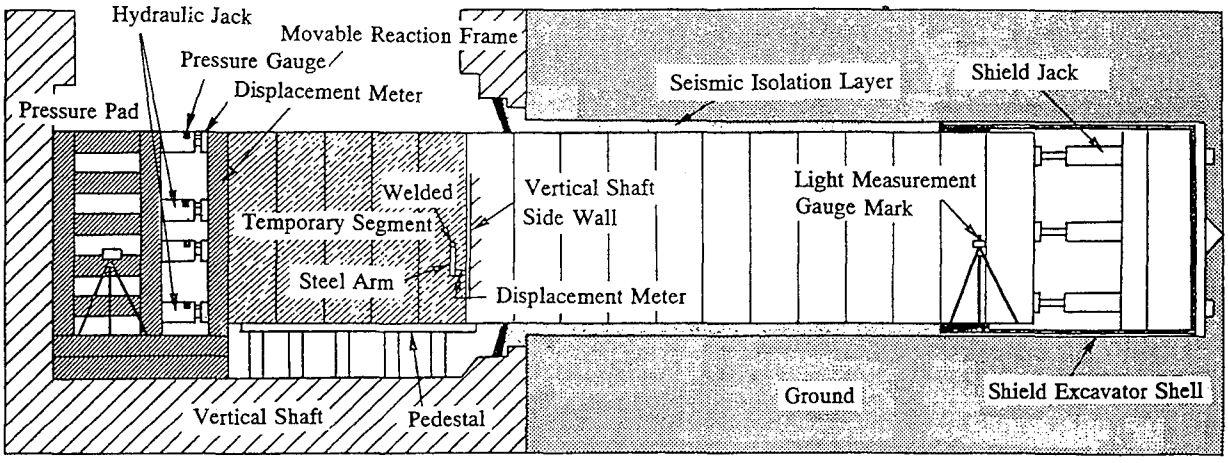

Fig.10 Schematic of Field Measurement Test

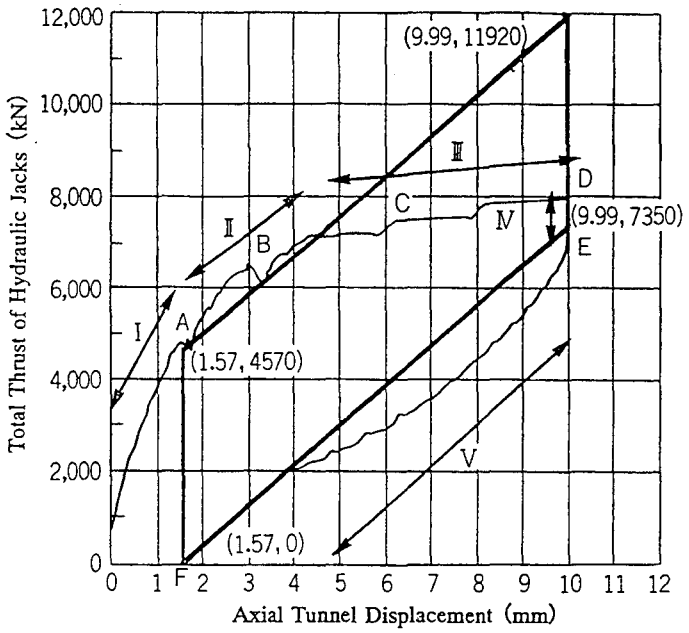

Fig.11 Jack Thrust and Axial Tunnel Displacement Relationship

EARTHQUAKE MOTIONS AT AN EMBANKMENT DAM BASE AND AN ESTIMATION METHOD OF INCIDENT SEISMIC WAVES USING THE OBSERVATIONS

Yoshikazu Yamaguchi[1] & Tomoya Iwashita[2]

ABSTRACT

Many earthquake motions have been observed at the bedrock of embankment dams. The observed waves are affected by the dynamic interaction between the dam and its foundation. The effects of the frequency contents of the input waves and the impedance ratio on the dynamic interaction at the dam base were evaluated using FEM analyses. The change of the dynamic interaction on the footprint of dams was represented analytically. The analytical results agreed with the earthquake observations and the microtremor measurements at the dam sites. Moreover, a simplified analytical procedure to estimate incident seismic wave on the basement layer from the within motion observed at the base of an embankment dam was proposed. The procedure was applied to the estimation of the incident wave at a rockfill dam site during the Kobe Earthquake.

KEYWORDS: Dam, FEM, Earthquake Record, Dynamic Interaction, Incident Wave

1. INTRODUCTION

Earthquake observations at the bedrock of dam sites are precious data of earthquake motions at the hard rock site condition, for which the S-wave velocity is over about 800 m/s. There are few earthquake observational stations situated at hard rock sites in Japan, other than dams and nuclear power plants. In most dams in Japan, in particular, seismographs have been installed in the inspection gallery at the base of embankment dams or at the bottom of concrete dams for the purpose of safety control against earthquakes. Most dams in Japan, except for small earth dams, are constructed directly on the excavated bedrock of riverbeds and abutments. The lower part of a massive dam is, roughly considered to behave in the same way as its bedrock and rock abutment during earthquakes. However, the earthquake response of a dam is affected by the dynamic interaction of the dam-foundation-reservoir system. The earthquake waves observed at the dam base or at the dam bottom are interacted especially with its foundation. In other words, the earthquake waves at the dam base are the combination of the incident waves through the foundation and the radiation waves through the dam body. They are, therefore, different from the waves at the free-field, i.e. outcrop. In order to make practical use of the observations at the dam base of the many dams where seismometers have already been installed, it is necessary to evaluate the quantitative difference of the earthquake wave at the dam base with that at the free-field.

The effects of the dynamic interaction between a dam and its foundation are evaluated by wave energy dissipation through the dam to the foundation or by radiation damping. Analytical approaches of radiation damping of embankment dams have been performed (Chopra & Perumalswami 1969, Ohmachi 1980, Yanagisawa 1982, Hirata 1989, Tohei & Ohmachi 1990). In these evaluations, analytical procedures were mainly used and few comparative evaluations with actual dam observations were conducted.

In this paper, we evaluate the effects of frequency contents of input waves and the impedance ratio on

1) Head, Fill Dam Division, Public Works Research Institute, Ministry of Construction, Tsukuba, Japan
2) Senior Research Engineer, ditto

the dynamic interaction between an embankment dam and its foundation. The little effect of a reservoir on an embankment is not considered. The evaluations are performed using both FEM numerical analysis and the earthquake observations at an existing dam. Moreover, we propose a simplified analytical procedure that estimates the incident seismic wave on the basement layer without the dynamic interaction effects from the observations at the base of an embankment dam.

2. DYNAMIC INTERACTION AT BASE OF AN EMBANKMENT DAM

(1) Analytical Method and Cases

We analyzed the two-dimensional FE model of the Miho Dam in Japan, a 95.0 m-high rockfill dam with a central core, shown in Figure 1. The physical and dynamic properties of the dam were determined from in-situ tests and laboratory tests using the fill materials of this dam. We used the complex dynamic response analysis program DINAS, which employs equivalent linear dynamic soil modeling.

We performed analyses on the five cases shown in Table 1. Where, ρ_D is the density of the dam body of 2.3 t/m^3 , ρ_F is the density of the foundation of 2.575 t/m^3 , Vs_D is the S-wave velocity for the dam body of 600m/s , Vs_F is the S-wave velocity for the foundation. In Cases 1A and 1B, the effect of the frequency contents of the input wave on the dynamic interaction was evaluated. In Case 1A, the acceleration wave which has a maximum value of 138.2gal, is shown in Figure 2, and was observed at the downstream toe of the Miho Dam during the event of March 6, 1996 (JMA magnitude of 5.8) was used as input. In Case 1B, the same wave as in Case 1A, with the time axis stretched by a factor of two (that is, with twice calculation period) was used as input. The predominant frequency of the input wave of Case 1B was consistent with the natural frequency of the dam body. In Cases 1B, 2-4, the effects of the impedance ratio between the dam body and its foundation were evaluated by changing the shear stiffness of the foundation.

Table 1 Analytical cases

Case Name	S-wave Velocity for Foundation V_{SF}(m/s)	Impedance Ratio α	Calculation Period Δt(s)	Items Investigated
CASE 1A	1950	0.29	0.01	Frequency contents of input waves
CASE 1B	1950	0.29	0.02	Frequency contents of input waves
CASE 2	1380	0.41	0.02	Impedance ratio $\alpha = \frac{\rho_D \cdot V_{SD}}{\rho_F \cdot V_{SF}}$
CASE 3	975	0.57	0.02	Impedance ratio $\alpha = \frac{\rho_D \cdot V_{SD}}{\rho_F \cdot V_{SF}}$
CASE 4	690	0.81	0.02	Impedance ratio $\alpha = \frac{\rho_D \cdot V_{SD}}{\rho_F \cdot V_{SF}}$

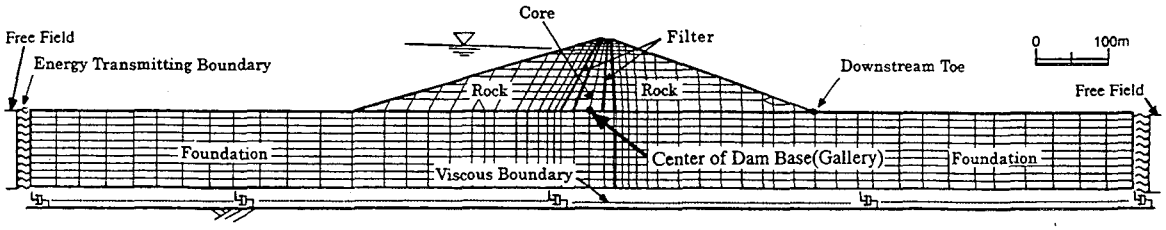

Fig.1 Finite element model of the Miho Dam

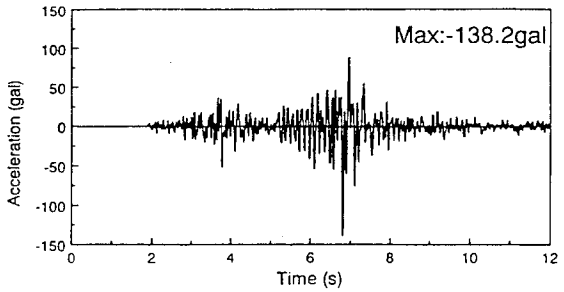

Fig.2(a) Input acceleration-time history for Case 1A

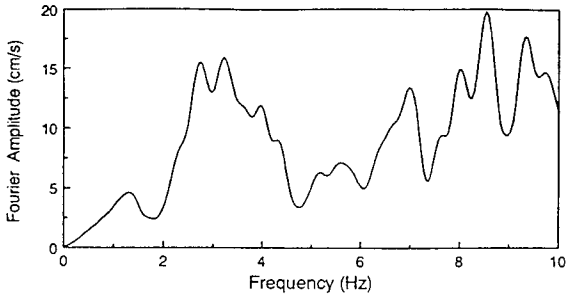

Fig2(b) Fourier amplitude spectrum of input acceleration for Case 1A

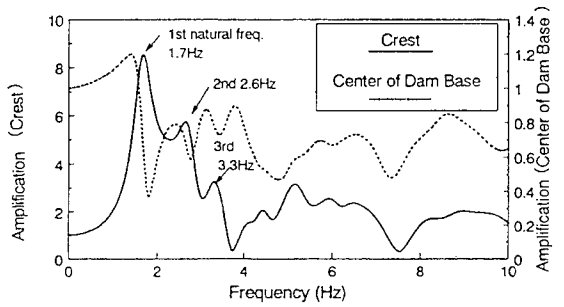

Fig.3 Amplification spectra for Case 1A

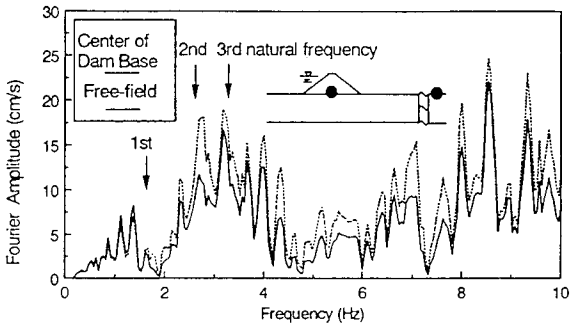

Fig.4 Fourier amplitude spectra of acceleration at dam base and at free-field(Case 1A)

(2) Results of the Analysis

a) Effects of frequency contents of input waves

The amplification spectra of the response waves at the crest and at the center of the dam base against the input wave for Case 1A are shown in Figure 3. The amplification spectrum for the dam base dips at a slightly higher frequency than the natural frequency that is indicated as the predominant frequency of the amplification spectrum at the crest. The amplification spectrum for the dam base in Figure 3 shows that the seismic wave at the dam base reduces the seismic power at the frequency range of the natural frequencies of the dam considerably.

Figure 4 shows the Fourier amplitude spectra of the acceleration at the center of the dam base and at the free-field for Case 1A. The amplitude spectrum for the dam base is smaller than that for the free-field for the second and third natural frequencies of the dam (around 3 Hz). This is because the spectrum of the input wave has large amplitudes around the second and third natural frequencies of the dam. The Fourier

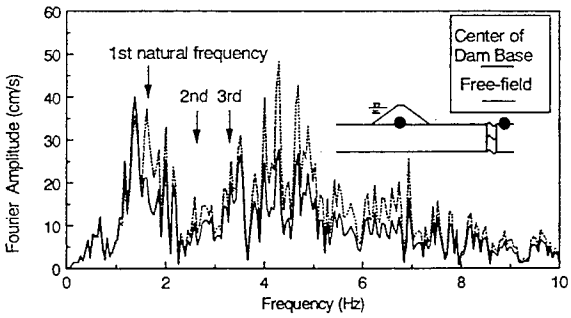

Fig.5 Fourier amplitude spectra of acceleration at dam base and at free-field(Case 1B)

amplitude spectra for Case 1B are shown in Figure 5. The amplitude spectrum for the dam base is considerably smaller than that for the free-field around the first natural frequency of 1.7Hz. When an incident wave that has large energy power around the natural frequency of a dam is input, dynamic interaction between the dam and its foundation makes the spectral amplitude of the response acceleration at the dam base decrease around this frequency.

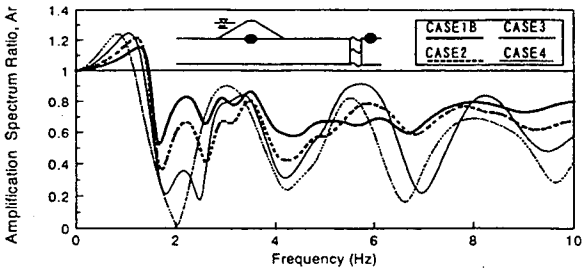

Fig.6 Amplification spectrum ratio for dam base

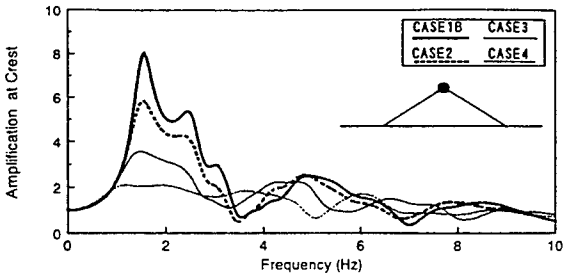

Fig.7 Amplification spectrum for crest

b) Effects of impedance ratio

The amplification spectrum ratio Ar was calculated by dividing the amplification spectrum for the dam base by the one for the free-field. The amplification spectrum ratio Ar shows the difference between the seismic response at the dam base and that at the free-field. Figure 6 shows the amplification spectrum ratios for the central part of the dam base for Cases 1B, 2 to 4. Figure 7 shows the amplification spectrum for the crest. Figure 8 shows the relationship between the frequency where the amplification spectrum ratio for the dam base sinks in Figure 6 and the predominant frequency of the amplification spectrum for the crest in Figure 7. Figure 8 shows that each sinking frequency for the dam base is slightly higher than the corresponding predominant frequency for the crest. Figure 6 shows that the larger the impedance ratio, the larger the dip in the amplification spectrum ratio. In other words, the larger the impedance ratio, the larger the effect of dynamic interaction. Figure 7 shows that as the impedance ratio decreases, so the response magnification of the dam increases. This indicates that the smaller the impedance ratio, the larger the non-linearity of the dam body and the lower its natural frequency. It is, therefore, suggested that the sinking frequency for each amplification spectrum ratio shown in Figure 6 becomes higher as the impedance ratio increases.

Figure 9 shows the distribution of maximum acceleration, which is normalized by dividing by the maximum acceleration at a free-field, along the dam base and on the downstream ground surface for each of the analytical cases. The maximum accelerations are smallest at the center of the dam base and recover as you move toward the downstream toe. The maximum accelerations at the downstream toe are only about ten percent less than the maximum accelerations at the free-field. The larger the impedance ratio, the more the drop of the maximum accelerations at the dam base becomes and the larger the dynamic interaction between the dam and the foundation becomes.

The residual of the amplification spectrum ratio was integrated from 0.5f1 to 2.5f1, where f1 is the first natural frequency. The mean residual e shown in equation (1) represents the ratio of the energy loss at the dam base due to the dynamic interaction.

$$e = \frac{1}{2f_1}\int_{0.5f_1}^{2.5f_1}(1 - Ar(f))df \qquad (1)$$

Figure 10 shows the distribution of the mean residual e along the dam base (footprint) and on the downstream ground surface for each of the analytical cases. The mean residual e is large around the center of the dam base and becomes smaller as you move toward the downstream toe. Furthermore, the larger the impedance ratio, the larger the mean residual, i.e. the larger the energy loss due to dynamic interaction. The values of the mean residual e are only about 0.1 around the downstream toe for all the cases.

Figures 9 and 10 indicate that the effect of dynamic interaction on earthquake response is low around the downstream toe, regardless of the impedance ratio. There is negligible effect of dynamic interaction due to the dam on the seismic response at the point about half a dam's width away from the downstream toe.

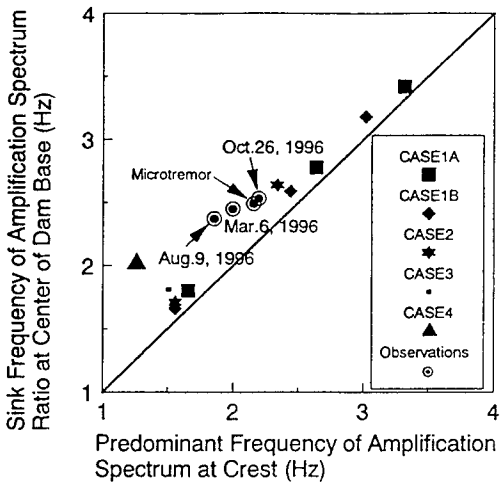

Fig.8 Comparison between sinking frequency of tansfer function ratio for dam base and predominant frequency of transfer function for crest

(3) Verification of Analytical Results Using Observations

The characteristics of the earthquake motions at the dam base obtained from the analytical procedures in part 2.(2) above were verified using the earthquake observations during three events shown in Table 2 and the data of microtremor measurements at the Miho Dam. We calculated the ratio of the Fourier amplitude spectrum of the waves observed at the crest to that at the outcrop. We also calculated the ratio of the Fourier amplitude spectrum of the waves observed at the center of the dam base to that at the outcrop. The relationships between the sinking frequency of the Fourier amplitude spectrum ratio for the center of the dam base and the predominant

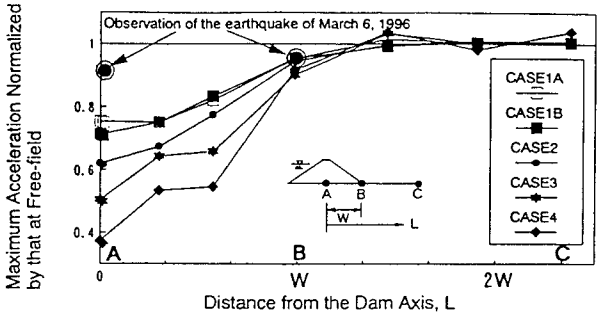

Fig.9 Distribution of maximum acceleration at dam base and downstream ground surface

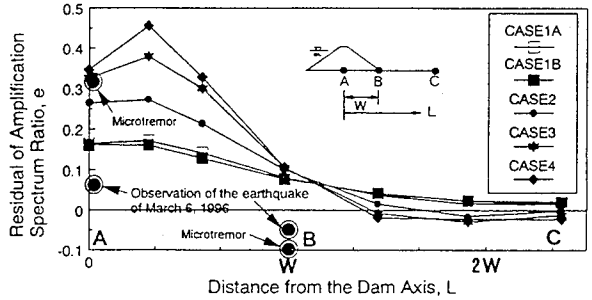

Fig.10 Distribution of mean residual of amplification spectrum ratio for dam base and downstream ground surface

frequency for the crest obtained from the observations and the microtremor data have been added to Figure 8. The points appear slightly above the 45-degree line that represents the case where the sinking frequency for the dam base is equal to the predominant frequency for the crest. In other words, the sinking frequency for the dam base is slightly higher than the corresponding predominant frequency for the crest, which agrees well with the analytical results in part 2.(2) above.

Table 2 Earthquake records at the Miho Dam

Date	Maximum Acceleration (gal)			Epicentral Distance	JMA Magnitude
	Crest	Gallary	Downstream Toe	(km)	
March 6,1996	243.9	84.4	138.2	13	5.8
August 9, 1996	62.3	13.8	21.8	17	4.7
October 26, 1996	15.9	3.4	5.4	11	4.0

The normalized maximum acceleration and the mean residual of the amplification spectrum ratio from the earthquake observations during the event of March 6, 1996 and the microtremor data measured at the center of the dam base and the downstream toe have been added to Figures 9 and 10 respectively. The waves observed at the outcrop were used as the reference wave records. The maximum acceleration at the center of the dam base is smaller than that at the downstream toe. The mean residual e at the center of the dam base is larger than that at the downstream toe. These trends agree with those seen in the analytical results.

3. ESTIMATION OF SEISMIC WAVE INCIDENT ON BASEMENT LAYER

(1) Estimation Procedure

As stated in the previous section, earthquake waves observed at the dam base are interacted with the dam body. Hence, we propose a simplified procedure for estimating the wave incident on the basement layer from observations at the base of an embankment dam analytically. Ohmachi & Kataoka (1995) estimated the incident seismic waves from the observations at the base of a concrete dam using the procedure that involved dividing the frequency characteristics of the observations at the dam base by the transfer function. However, an earth structure such as an embankment dam has the high earthquake-induced non-linearity of the soil and rockfill materials. This is the major difference between an embankment dam and a concrete dam with regard to the estimation of the incident wave for earth structure. For this reason, we performed dynamic equivalent linear pre-analysis on the model of an embankment dam with a rigid foundation. A rigid foundation model is analyzed because the wave observed at the dam base must be input. This dynamic pre-analysis gives the shear modulus of the dam reached in the inelastic region during shaking. Furthermore, a comparison between the analytical response results and other observations at the dam enables the accuracy of the dam model to be verified.

The estimation procedure is illustrated in Figure 11 and described as follows:

STEP 1. The dynamic pre-analysis of the embankment dam model with a rigid foundation is performed using the equivalent linear soil modeling method. The distribution of the shear modulus of the dam in the final iterative calculation step is obtained.
STEP 2. The transfer function for the dam base is calculated using the above shear modulus of the dam.
STEP 3. The Fourier spectrum, which involves the characteristics of both amplitude and phase, of the wave incident on the basement layer is obtained by dividing the Fourier spectrum of the wave observed at the dam base by the above transfer function.
STEP 4. The Fourier inverse transform of the Fourier spectrum calculated above gives the seismic wave incident on the basement layer.

An observed wave consists of the coupled response of horizontal and vertical vibrations. In this simplified procedure, however, we consider only the horizontal transfer function for the horizontal input motion and only the vertical transfer function for the vertical input motion.

(2) Dam Analyzed and its Model

We applied this procedure to the earthquake observations at the Minoogawa Dam during the Kobe Earthquake of 1995. The Minoogawa Dam, a 47.0 m-high rockfill dam, was located about ten kilometers northeast of the earthquake fault. The seismometers installed in the inspection gallery at the base of the dam and at the dam crest recorded acceleration waves during the excitation. Their maximum horizontal accelerations perpendicular to the dam axis were 135 gal in the gallery and 242 gal at the crest. The dam foundation is hard bedrock that has an elastic wave velocity of about 4 km/s. The impedance ratio between the dam and the foundation is about 0.3.

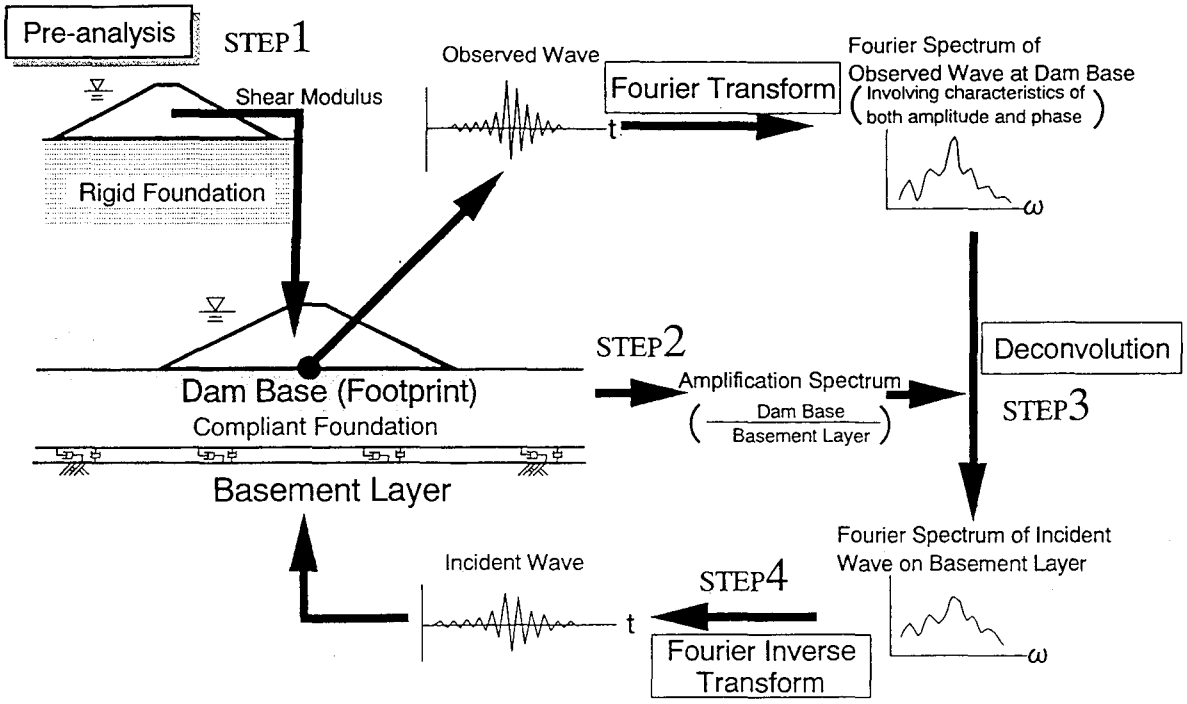

Fig.11 Illustration of the procedure to estimate incident waves

We prepared the 2-D FE model of the cross section of the Minoogawa Dam as shown in Figure 12. The properties of the dam materials were determined from the results of execution control tests in the time of the construction and the laboratory tests using the fill materials of this dam. We verified the accuracy of the vibration characteristics of the model by comparing the natural frequency of the model with that from earthquake observations and microtremor measurements (Iwashita & Yoshida 1997). In the pre-analysis of the rigid foundation model, the effects of energy dissipation by dynamic interaction were assumed to be represented by the equivalent radiation damping ratio that was added to the hysteresis damping ratio of the dam materials.

(3) Calculation of an Incident Wave

First, we analyzed the rigid foundation model and obtained the shear modulus of the dam during excitation. Figure 13 shows comparisons of the observed response acceleration at the crest with that obtained through the dynamic pre-analysis. Looking at the acceleration-time history, during the first half of the principal motion (t = 4 - 6 sec) the analytical results agree well with the observations, but during the second half (over 6 sec) the analytical results are smaller than the observed values. With regard to the Fourier amplitude spectrum, the analytical results in the low frequency range less than 2 Hz agree well with the observations, but the analytical results are

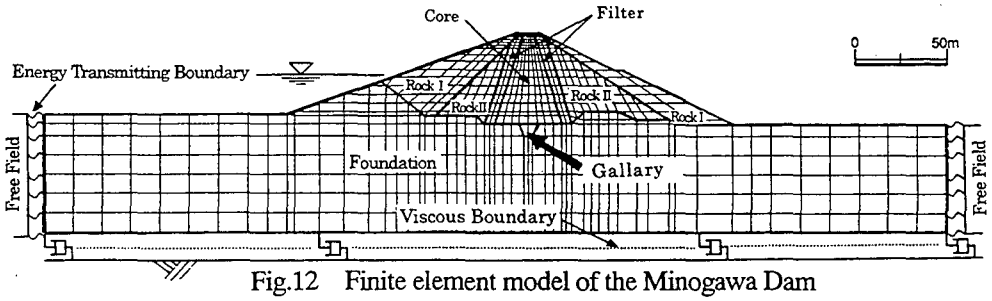

Fig.12 Finite element model of the Minogawa Dam

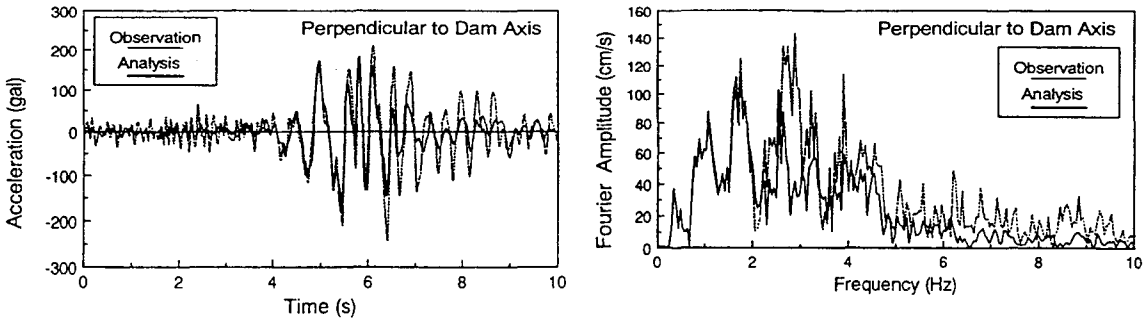

Fig.13 Comparison between observed acceleration at crest with analytical results (pre-analysis of the Minogawa Dam model with a rigid foundation)

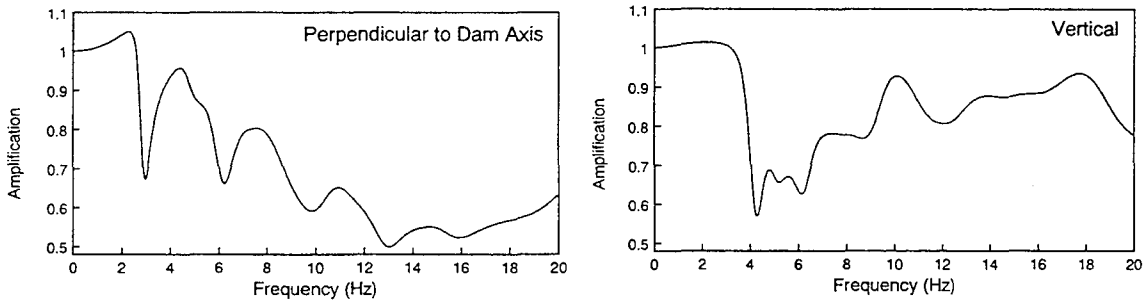

Fig.14 Amplification spectra for the center of the dam base of the Minogawa Dam model

smaller than the observed values around the natural frequency during shaking of 3 Hz. In spite of the rigid foundation model analysis, the analytical results give relatively good agreement with the observations. This confirms that the model describes the non-linearity of the dam during the earthquake quite well.

Secondly, the transfer functions for the dam base were calculated using the shear modulus of the dam, which is the output from the above pre-analysis on the rigid foundation model. The amplification spectra shown in Figure 14 have significant sinking at 3 Hz for the direction perpendicular to the dam axis and at about 4Hz for the vertical direction.

Finally, we estimated the wave incident on the basement layer of the Minoogawa Dam site using steps 3 and 4 of the above-mentioned procedure, with the earthquake observations in the inspection gallery built on the dam base and its transfer functions.

Figure 15 shows that the estimated incident wave time history and Fourier amplitude spectrum. The wave observed at the inspection gallery is also shown in the figures for the shake of comparison. The horizontal maximum accelerations of the incident wave and the wave observed in the gallery are 137 gal and 135 gal respectively; the vertical maximum accelerations are 89 gal and 80 gal respectively. The amplitude spectrum of the incident wave is larger than that for the wave observed at the gallery at the natural frequencies (the range around 3 Hz for the horizontal direction and 4 to 5 Hz for the vertical direction) because of the dynamic interaction effects described in section 2.

(4) Verification of the Estimated Incident Wave

We performed dynamic analysis on the Minoogawa Dam model with a compliance foundation. The incident wave estimated in the previous section was input under the basement boundary of the

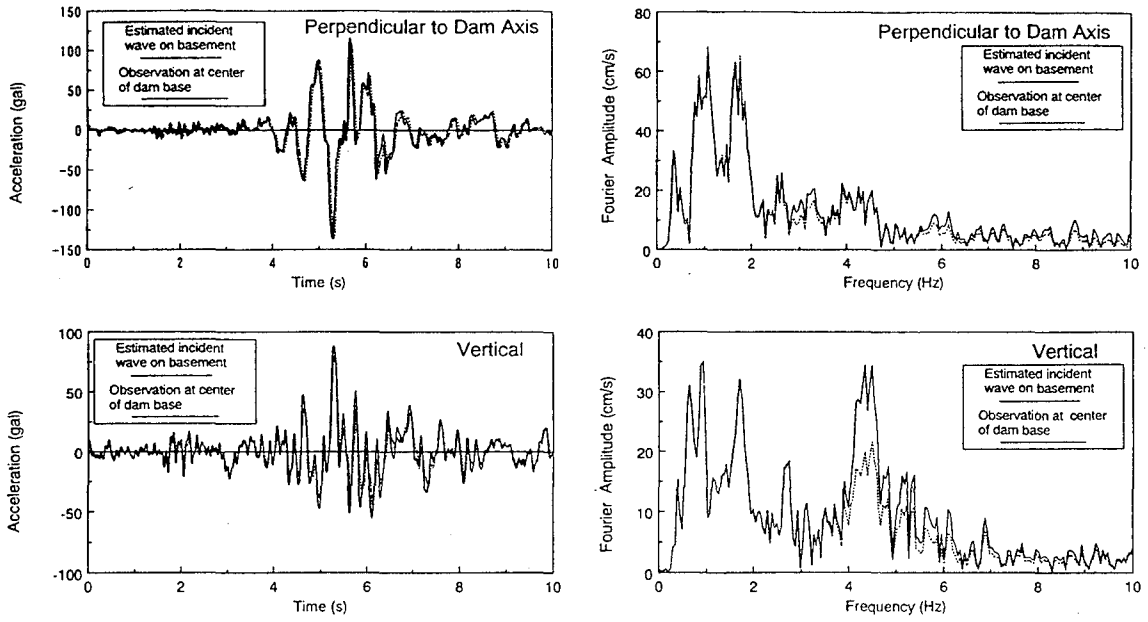

Fig.15 Estimated incident acceleration on basement layer and observed acceleration at dam base

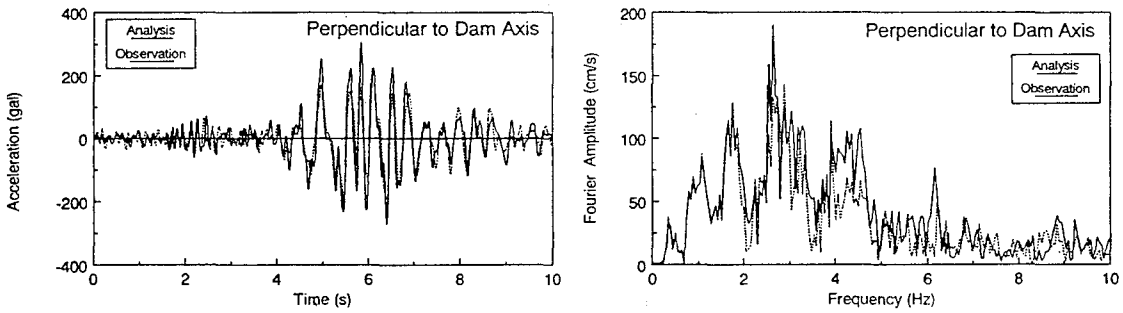

Fig.16 Comparison of observed acceleration at crest with analytical results (analysis on the Minogawa Dam model with a compliant foundation ,on which the estimated incident wave was input)

compliance foundation model. Figure 16 shows the comparisons of the acceleration-time histories and Fourier amplitude spectra of the analytical response horizontal acceleration at the crest with those of the observed acceleration at the crest. The results of the analysis agree with the observations for both the time history and the Fourier spectrum. Of particular note is the good agreement of the time histories even for the second half of the principal motion and of the Fourier amplitudes at around 3 Hz. In the above range, the results from the simulation of the rigid foundation model analysis did not agree with the observations, as shown in Figure13.

4. CONCLUSIONS

(1) Due to the dynamic interaction between an embankment dam and its foundation, the Fourier amplitude of the seismic waves at the dam base at the natural frequency is smaller than that at the free-field. It was demonstrated from FEM analysis and observations at an existing dam that the sinking frequency is slightly higher than the corresponding predominant frequencies for the response wave at the crest.

(2) The larger the Fourier amplitude of the incident seismic wave for the natural frequency of the

dam and the larger the impedance ratio of the dam and its foundation, the larger the dynamic interaction effects become.

(3) Dynamic interaction effects such as reductions in maximum acceleration and wave energy are the largest at the center of the dam base and decrease as you move towards the downstream toe. These interaction effects are fairly small by time you reach the toe. The effects at a point about half a dam's width from the downstream toe are about the same as those at a free-field.

(4) A simplified procedure for estimating the incident wave from the observations at the dam base was proposed. This procedure was demonstrated by estimating the waves incident on the basement layer at the Minoogawa Dam site during the Kobe Earthquake.

REFERENCES

Chopra, A.K. & P.R. Perumalswami (1969): Dam-foundation interaction during earthquakes, *Proc. 4th World Conference on Earthquake Engineering*, pp.37-52.

Hirata, K. (1989): Estimation of radiation damping in dynamic analysis of fill dams, *Report of Central Research Institute of Electric Power Industry*. U88061, CRIEPI.

Iwashita, T. & H. Yoshida (1997): Earthquake response analysis and seismic stability of a rockfill dam –Behavior of the Minoogawa Dam during the Kobe Earthquake–, *Engineering for Dams*. No.126, pp.27-35, Japan Dam Engineering Center.

Ohmachi, T. (1980): A fundamental study on dynamic interactions with a rockfill dam and the foundation deposit, *Tsuchi-to-Kiso*, No.1191, pp.31-36, Japanese Society odf Soil Mechanics and Foundation Engineering.

Ohmachi, T. & S. Kataoka (1995): Evaluation of dynamic interaction effects of 2-D dam-foundation-reservoir systems, *Proc. of the Japan Society of Civil Engineers*, No.519: pp.199-209, Japan Society of Civil Engineers.

Tohei, M. & T. Ohmachi (1990): Model analysis procedure using a FE-BE method in time domain and its application to a dam-foundation system, *Proc. of the Japan Society of Civil Engineers*, 416, pp.429-438, Japan Society of Civil Engineers.

Yanagisawa, E. (1982): Effect of ground condition on vibrational characteristics of earth structure, *Proc. of the Japan Society of Civil Engineers*, No.317, pp.101-110, Japan Society of Civil Engineers.

REPRODUCTION OF LARGE-SCALE 1G TEST ON DRY SAND DEPOSITS AND PILE FOUNDATIONS USING CENTRIFUGE MODELING (Step-2)

Chikahiro MINOWA[1], Masayoshi SATO[1], Yukiko SAITO[2], Takaaki KAGAWA[3] and Akio ABE[4]

ABSTRACT

The two centrifuge tests, the SC-centrifuge test and the PW-centrifuge test, were executed to reproduce the dynamic behavior of pile foundation structures and dry sand deposits in an NIED-1g large-scale test. The following conclusions may be obtained from a comparison of the three tests, (1) the PW-centrifuge test showed a good correspondence with the NIED-1g test regard to the input acceleration wave, (2) the PW-centrifuge can virtually reproduce the NIED-1g test in terms of the structure response acceleration and the bending strains of the pile, (3) centrifuge studies could confirm the composition of similitude requirements and the effectiveness as a preliminary study method for large-scale tests.

KEY WORDS : Large-scale shaking test,
Centrifuge dynamic testing, Dry sand,
Ground response, Soil-pile interaction

1. INTRODUCTION

Dynamic centrifuge model test technology has recently attracted considerable attention in the field of geotechnical earthquake engineering, mainly because it has the obvious advantage in being able to reproduce the dynamic response of actual soil ground under the conditions of satisfying the similitude requirements concerning confined stress of soil. However, when soil models are prepared for centrifuge tests, they may not always be perfectly consistent with the actual soil ground. It is important to establish test procedures and techniques for reproducing the behavior of actual soil-structure systems during earthquakes. Recently, there are many plans to execute large-scale shaking table tests. We cannot perform the large-scale tests for many cases, since they generally require considerable funds and long periods to execute. Among the numerous potential case scenarios, it is very difficult to decide which cases are important. Accordingly, there is considerable validity in selecting reasonable experimental cases of the large-scale test from the execution of centrifuge tests with many parameters. The purposes of the centrifuge studies are to check similitude requirements and to establish a preliminary study method for large-scale tests.

In the past, a dynamic centrifuge test using Shimizu Corporation centrifuge apparatus (SC-centrifuge) satisfying the similitude requirements was conducted in reference to a large-scale test with laminar containers. The centrifuge test could not reproduce the response of the large-scale test result, therefore could not reproduce the input wave. In this paper, a test was executed using Public Works Research Institute centrifuge apparatus (PW-centrifuge) that are capable of sufficiently reproducing input waves, so the comparison of the three tests results, NIED-1g large-scale test, SC and PWRI centrifuge tests, are reported in respect to the dynamic behavior of pile foundation structures and dry sand deposits.

2. SHAKING TABLE TEST APPARATUS

(1) Test apparatus

A large-scale shaking table test using a large laminar con-

Table 1 Specifications of the three test apparatus

	Unit	NIED-1g	SC-centrifuge	PW-centrifuge
Table size	m	15x14.5	0.65x0.95	1.0x1.7
Maximum loading capacity	t	500	0.3	4
Excitation direction		1	1	1
Maximum acceleration	gal	500	9,800	39,200
Maximum displacement	mm	230	±1	±5
Frequency range	Hz	DC～50	50～350	10～400
Radius of rotation	mm	—	3.1	6.6
Centrifuge acceleration	g	—	50	100

1) National Research Institute for Earth Science and Disaster Prevention, 3-1 Tennoudai, Tsukuba-shi, 305-0006, Japan.
2) Public Works Research Institute, Ministry of Construction, Tsukuba-shi, 305-0804, Japan.
3) Wayne State University, Michigan, 48202, USA.
4) Tokyo Soil Research Co., Tsukuba-shi, 305-0045, Japan.

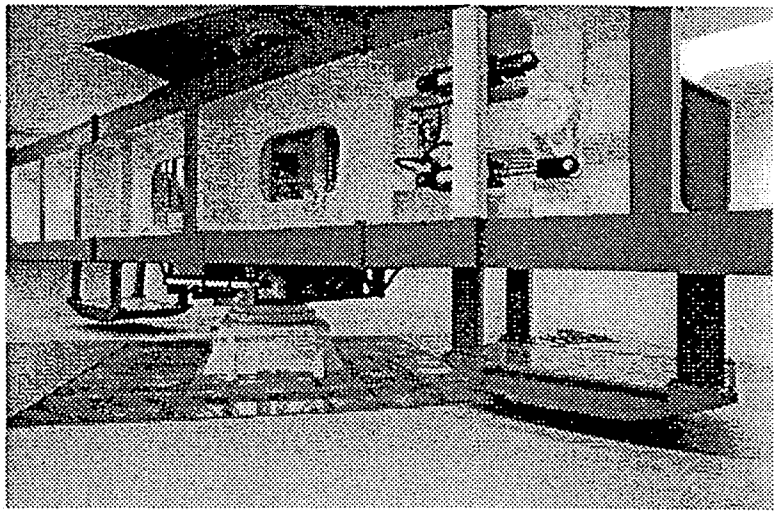

Fig.1 Centrifuge apparatus of Public Works Research Institute (PWRI)

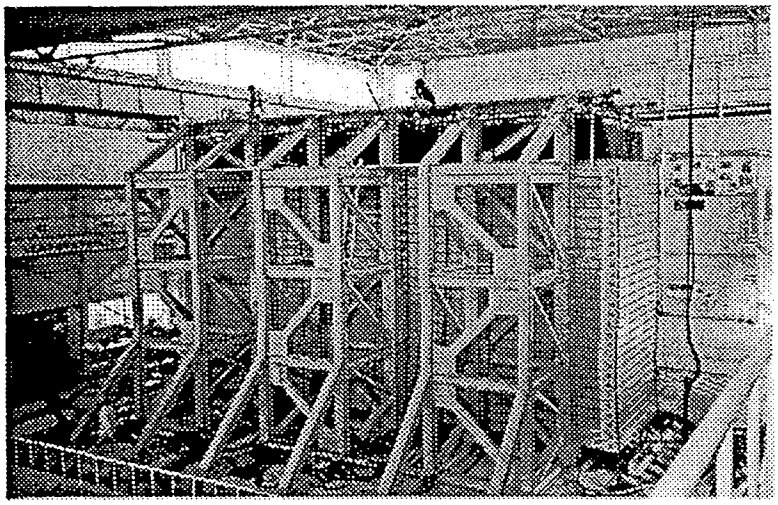

Fig.2 Laminar container of 1g Large-scale table test at the National Research Institute for Earth Science and Disaster Prevention (NIED)

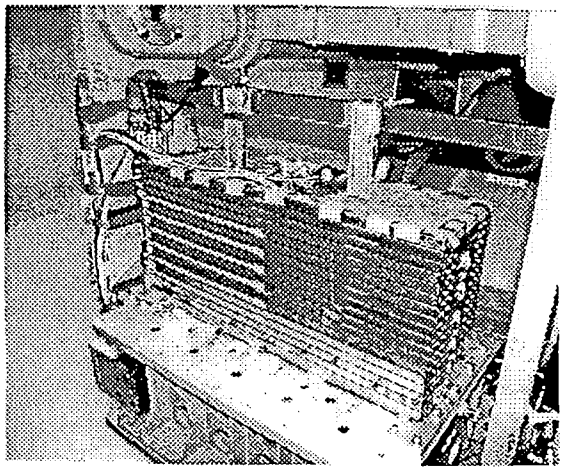

Fig.3 Laminar container of centrifuge test at Shimizu Corporation

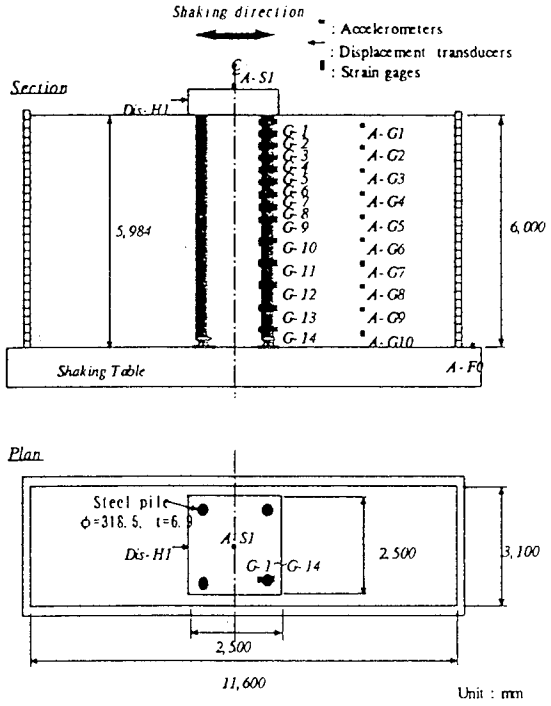

Fig. 4 A large-scale shaking test model and locations of transducers

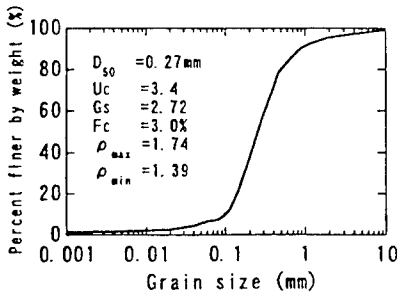

Fig. 5 Grain-size accumulation curve and physical properties

tainer was conducted at the National Research Institute for Earth Science and Disaster Prevention (NIED). The table is 15.0 m x 14.5 m in size and its maximum payload is 500 t.

The first centrifuge model tests were performed at the Institute of Technology, Shimizu Corporation (SC) [1]. The specifications have been described in detail by Sato [2]. Additional dynamic centrifuge model tests were performed at the Public Works Research Institute (PWRI). The PWRI centrifuge apparatus is shown in Fig. 1. The specifications have been described in detail by Matsuo et al. [3]. The specifications of the three test apparatuses are shown in Table 1.

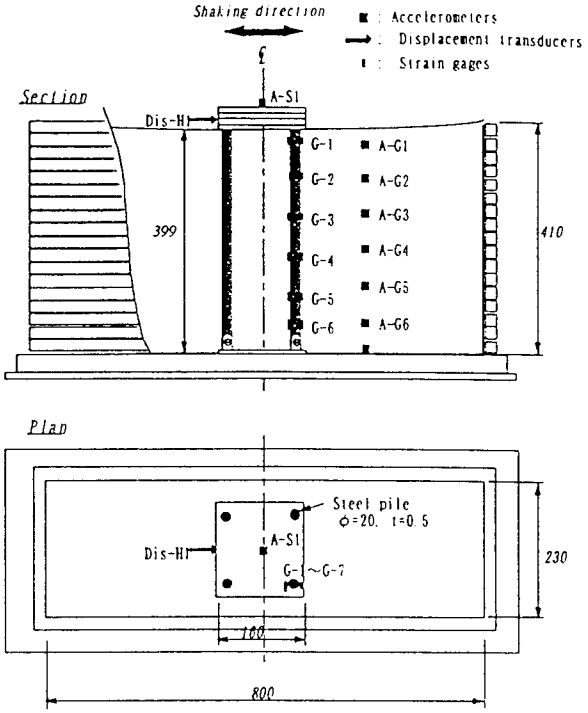

Fig. 6 A the centrifuge shaking test model and locations of transducers

(2) Large-scale laminar container

The NIED-1g large-scale laminar container is shown in Fig. 2. The container has inner dimensions of 11.6 m L x 6.0 m H x 3.1 m W. The container consists of 29 rectangular frames made of H-shaped steel members (200 mm x 200 mm).

(3) Centrifuge laminar container

The same laminar container was employed for both the SC-centrifuge test and the PW-centrifuge test. The centrifuge laminar container is shown in Fig. 3. The laminar container, which is geometrically similar to the one used in the large-scale shaking test, has inner dimensions of 80 cm L x 41 cm H x 23 cm W.

3. LARGE-SCALE SHAKING TEST

(1) Preparation ground

A NIED-1g large-scale test model and the locations of transducers are shown in Fig. 4. The test sand was poured through a funnel from a height of 1 m. The sand deposit had an average density of ρ t=1.69t/m3 and a water content of w = 11% at the beginning of the test. The grain-size

Table 2 Similitude requirements used in the experiment

		Symbol	Scale ratio	Unit	1g	Centrifuge
Sand Stratum	Thickness	H_s	$1/\lambda$	m	5.984	0.399
	Density	ρ_s	1	g/cm³	1.69	1.69
Pile	Length of pile	L	$1/\lambda$	m	6.0	0.4
	Diameter	D	$1/\lambda$	mm	318.5	20 (21.4)
	Thickness	t	$1/\lambda$	mm	6.9	0.5 (0.46)
	Young's modulus	E	1	MN/m²	206.000	206.000
	Geometrical moment of inertia	I	$1/\lambda^4$	cm⁴	8,200	0.162
	Bending stiffness	E·I	$1/\lambda^4$	MNm²	16.9	0.000300 (0.000334)
	Area	A	$1/\lambda^2$	cm²	67.55	0.300
	Normal stiffness	E·A	$1/\lambda^2$	MN	1.392	6.18
Structure	Mass	m_t	$1/\lambda^3$	kg	15,600	4.62
	Length	L_t	$1/\lambda$	m	2.5	0.167
Exciting acceleration		α	λ	g	0.6	9.0

1) Model/Prototype = $1/\lambda = 1/15$

accumulation curve and physical properties of the materials are shown in Fig. 5.

(2) Pile foundation structure

The foundation is a rigid structure, consisting of stacked rectangular steel plates, with a length of 3.0 m, a width of 2.5 m, a height of 0.26 m, and weighting 15.6 t. Four (2x2) actual steel piles with an outer diameter of 318.5 mm were used with a center-to-center spacing 6 times the diameter. The top of each pile was firmly fixed to the structure, and the bottom of each pile was pin-connected to the container base.

(3) Excitation

Excitation cases of the NIED-1g large-scale tests are described in reference [4]. In this paper, the test result of the conditions is reported: a structure weight of 15.6 t, a sinusoidal wave with incremental acceleration, an excitation frequency of 3 Hz, and a maximum acceleration of 600 gal.

4. CENTRIFUGE SHAKING TABLE TESTS

(1) Similitude requirements

The similitude requirement used in the centrifuge test is summarized in Table 2. The ratio of the centrifuge test and the large-scale test is 1/15. In the time history and strain diagrams shown in this paper, the values of the centrifuge test were translated to actual size based on the similitude requirements.

(2) Preparation of model ground

The soil density, the natural frequency of the ground, the specifications of the pile foundation, and the input wave of the large-scale test were known, as necessary data for the execution of centrifuge experiment reproducing the large-scale test results were obtained in advance.

The centrifuge shaking test model and locations of transducers are shown in Fig. 6. The same sand as that used in the large-scale test was utilized , and a model with the same preparation method employed. The natural frequency of the model ground in the centrifuge test was made equal to that in the large-scale test.

(3) Pile foundation structure

The same model of the pile foundation structure was employed in both the SC-centrifuge and the PW-centrifuge test. Model iron piles satisfying the similitude requirements in respect to bending stiffness were adopted. Each pile has a diameter of 20 mm, a wall thickness of 0.5 mm, and a length of 40 cm. The same conditions as those in the large-scale test were adopted regarding the number of piles, pile arrangement, and the fixed method of the pile top and bottom.

(4) Excitation

The input wave was reduced to the time scale of that used in the large-scale test to 1/15 respectively in the SC-centrifuge and the PW-centrifuge test.

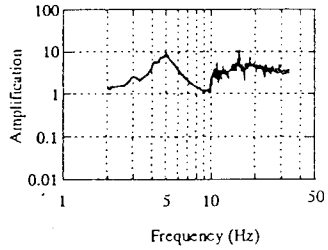

(a) SC-centrifuge test

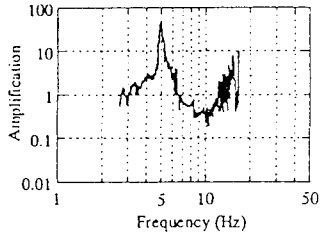

(b) PW-centrifuge test

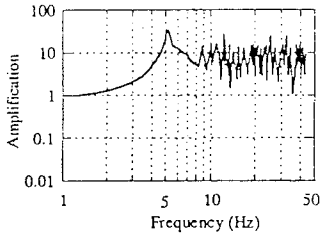

(c) the NIED-1g large-scale test

Fig. 7 Comparison of the frequency transfer function for the large-scale shaking test and the two centrifuge tests

5. COMPARISON OF EXPERIMENTAL RESULTS

(1) Natural frequency of sand deposits

Microtremors were measured to investigate the characteristics of the sand deposit before the start of the large-scale test, and the natural frequency was found to be 5 Hz as shown in Fig. 7 (c).

Due to the fact that microtremors could not be measured in the centrifuge tests, a vibration test with a very small acceleration level of excitation was conducted. The natural frequencies of the three test results are in good agreement. Accordingly, it can be estimated that the three sand deposits have almost identified dynamic response characteristics in terms of the initial shear modulus.

(2) Comparison of input waves

The time histories of the input waves for the NIED-1g large-scale test and the two centrifuge tests are shown in Fig.8. The input acceleration in the SC-centrifuge test is lower than the NIED-1g test, but the PW-centrifuge test shows good agreement.

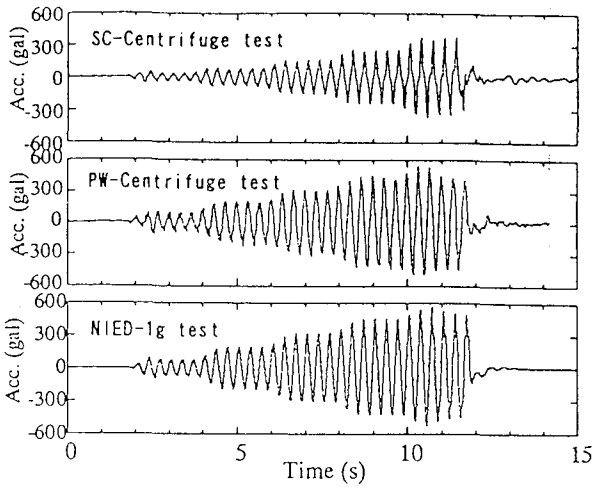

Fig. 8 Comparison of time history of the input acceleration for the large-scale shaking test and the two centrifuge tests

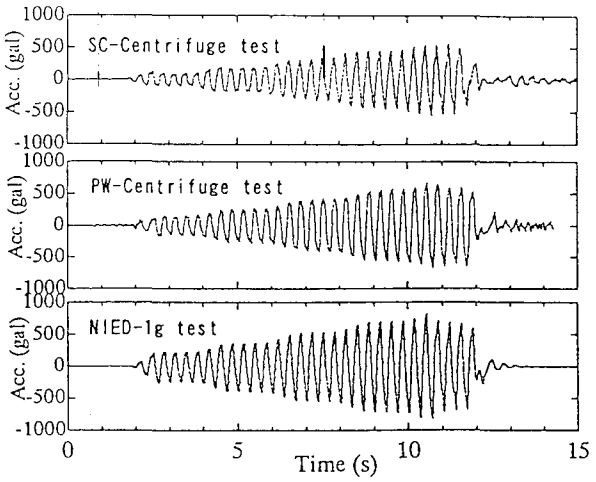

Fig. 9 Comparison of the time history of the structure acceleration for the large-scale shaking test (A-S1) and the two centrifuge tests (A-S1)

(3) Acceleration responses of the pile foundations and the sand deposits

The comparison of the time history of the three test results in terms of the structure acceleration (A-S1) is shown in Fig. 9. Both response accelerations of the SC-centrifuge and the PW-centrifuge are lower than those for the NIED-

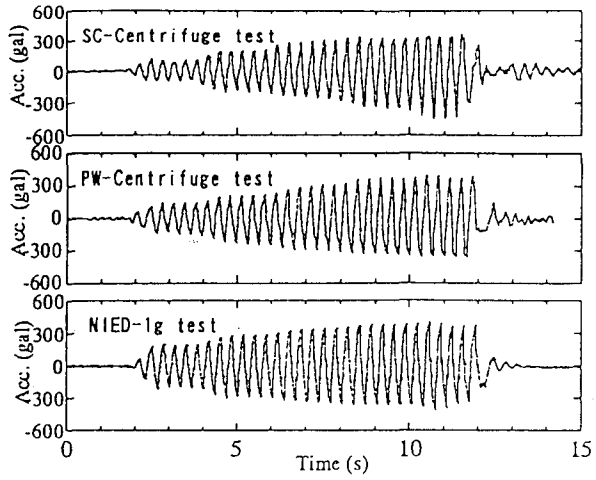

Fig. 10 Comparison of the time history of the soil surface acceleration for the large-scale shaking test (A-G1) and the two centrifuge tests (A-G1)

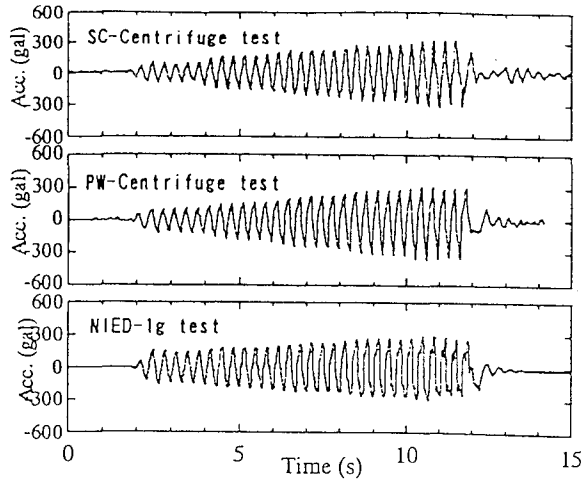

Fig. 11 Comparison of the time history of the soil midle-part acceleration for the large-scale shaking test (A-G4) and the two centrifuge tests (A-G3)

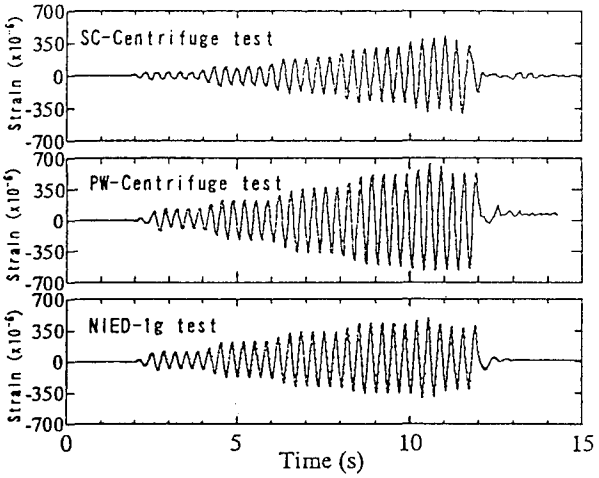

Fig. 12 Comparison of the time history of the bending strain of piles for the large-scale shaking test (G-1) and the two centrifuge tests (G-1)

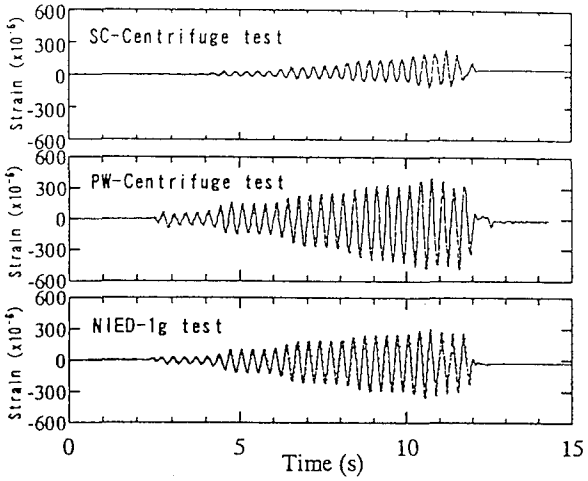

Fig. 13 Comparison of the time history of the bending strain of piles for the large-scale shaking test (G-10) and the two centrifuge tests (G-3)

1g test at the top of structure. But the test result of the PW-centrifuge corresponds to that of SC-centrifuge.

The comparison of the time history of the three test results in terms of the ground surface acceleration (A-G1) is shown in Fig. 10 and for ground acceleration in Fig.11. The three tests resulted in similar soil surface response accelerations. The disturbed shape of response acceleration wave after 9 seconds can be interpreted as degradation of soil stiffness in the intermediate depth of the NIED-1g test. In the next study, we intend to confirm the phenomenon using the nonlinear response analysis method.

(4) Bending strain of piles

The comparison of the time history of the three test results in terms of the pile top bending strains (G-1) is shown in Fig. 12 and that in the middle depth in Fig.13. The distributions of bending strain for the three tests when large values were observed for the piles are shown in Fig. 14. Incidentally, the relationship of bending strain and bending moment is described in reference [1].

The bending strain in the PW-centrifuge test at the top of the pile and the intermediate height were slightly larger than those in the NIED-1g test in terms of the time histories

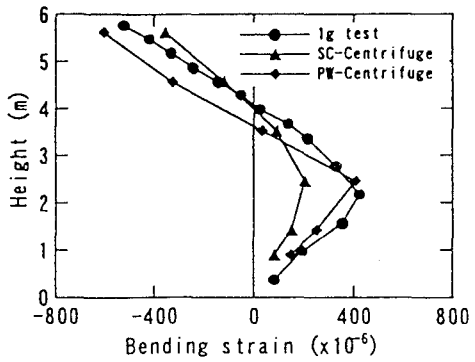

Fig. 14 Comparison of the distribution of the bending strain of piles for the large-scale shaking test and the wo centrifuge tests

and distribution, and the SC-centrifuge test results were smaller than the NIED-1g test overall. It can be concluded that the PW-centrifuge test virtually reproduced the NIED-1g large-scale test.

6. CONCLUSION

The two centrifuge tests, the SC-centrifuge test and the PW-centrifuge test were executed to reproduce the dynamic behavior of pile foundation structures and dry sand deposits in an NIED-1g large-scale test. The following conclusions may be obtained from a comparison of the three tests.

(1) The PW-centrifuge test was in good agreement with the NIED-1g test in terms of the input acceleration wave.

(2) The PW-centrifuge test can virtually reproduce the NIED-1g test in terms of the response acceleration of the structure and the bending strains of the pile.

(3) Centrifuge studies could confirm the composition of similitude requirement and the effectiveness as a preliminary study method for large-scale tests.

REFERENCE

1) Sato, M., T. Kagawa and C. Minowa (2000): "Reproduction of Large-scale Test on Unsaturated Sand Deposit and Pile Foundation using Centrifuge Modeling", Proceedings of The 12th World Conference on Earthquake Engineering, Paper No.2093 (CD-Rom), Newziland

2) Sato, M. (1994): "A new dynamic geotechnical centrifuge and performance of shaking table tests", Proceedings of The International Conference Centrifuge 94, Singapore, pp.157-162, Balkema.

3) Matsuo, O., T. Tsutsumi K. Kondoh and S. Tamoto (1998) : "The dynamic geotechnical centrifuge at PWRI", Proceedings of The International Conference Centrifuge 98, Tokyo, pp.25-30, Balkema.

4) Naganawa, T., Y. Muruno, H. Wang, A. Nishimura, and C. Minowa, (1998) : "Large-scale Shaking Table Tests for Foundations and Buried Structures (Part-7) Vibration Tests on Steel Pile Foundations in Sand Deposits", Proceedings of 33th Japan National Conference on Geotechnical Engineering, Vol.1, pp.1059-1060 (in Japanese).

An experimental study for the critical state of Footing loaded moment and shear by tension

by

Shoichi SAEKI [1], Jiro FUKUI [2], Masahiro SHIRATO [2], Shin-ichiro FURUSHO [2]

Abstract

In footings, tensile fiber stress results from bending caused by tensile forces from pull-out piles during earthquakes. However, a reasonable calculation method has not been established for the bending and shear capacity of footings in such condition yet. In this paper, we describe the result of a loading test using model footings supported piles to investigate the failure behavior of the footings whose top is tense. The loading test consists of the following four cases; two cases are to investigate bending failure behavior and the others are to investigate shear one. The experimental result shows that the footings resist with their almost full width at and after maximum strength and with a tied arch mechanism especially for shear even when their reinforcement bar at the top is the main reinforcement bar.

Key words: footing, highway bridge, moment, shear, and ultimate strength

1. Introduction

After the Hyogo-ken Nanbu Earthquake, the ductility design method was specified for not only piers introduced already but also foundations newly in the Specifications for Highway Bridges in Japan. For the design of footings and top slabs, the allowable stress design was changed into the ultimate strength design due to a substantial increase of seismic force accomplishing the introduction of the ductility design method.

When a bridge is subjected to horizontal seismic force, we can imagine two design situations for the footings of pile foundations or the top slabs of caisson foundations. One is tension fiber stress occurs at the bottom of them and another is at the top of them. In the former case, many loading tests of RC deep beams and deep slabs were performed in the past and the failure mechanisms were clarified well in moment and shear by compressive force. Based on these studies, the specification prescribes that the full footing width is effective in resisting moment and shear, and also the increase of the shear strength with respect to a RC slender beam according to shear span ratio by taken the arch action into account.

On the other hand, in the latter case where the top becomes tense, we have to design the footings and the slabs for the tension forces from the columns and piles. However the strength for those tension forces was not usual design factor in the design of the footings with extremely large dead load like bridges when the design

1) Public Works Research Center, 1-6- 4 Taito Taito-ku Tokyo Japan
2) Public Works Research Institute, 1 Asahi Tukuba-shi Ibaraki-ken Japan

seismic force was small like before the Hyogo-ken Nanbu Earthquake, almost no loading experiments assuming such condition have been performed and the failure mechanism in this condition is not clarified to date. Consequently, Specifications for Highway Bridges recommends that, in the case of that tensile fiber stress occurs at the top of the footings, the effective width 'b' in the calculation of bending strength is still b = tc + d as the same manner in the allowable design method. Where 'tc' is the column pier width, 'd' is the effective depth of the footing. And also it requires that the shear strength should be estimated as a slender beam assuming the full width to be effective. This means that even if the design seismic force increased, the design ultimate strength does not increase. As a result, the area of cross section and the volume of the reinforcement bar of the footings tend to enlarge in spite that the footings have never experienced severe damage in the past.

In this paper, we will introduce the result of a loading test using model column-footings supported piles, to study the collapse mechanism of the footings placing the top in tension. The horizontal force is applied near the top of the column to model a seismic response. We made four specimens. Two models were designed in order to undergo bending failure. The dimensions and the volume of reinforcement bars are constant in these two models, however the diameters and the spacing of the reinforcement bar were varied. Other two specimens were designed to collapse by shear. These specimens have the different shear span, namely the distance from the front surface of the column to the pull-out pile is different, but the other dimensions keep the same. Based on the experimental result obtained here, we analyze the strain distribution of the reinforcement bars at the top of the footings and the state of cracks on the top surface of the footing at each stages of horizontal force. And we carry out a trial design to clarify the bearing mechanism for the moment and shear of the footings whose fiber stress becomes tense at the top.

2. Experimental Specimens

This experiment was performed to confirm the bending and shear strength of footings, when the top of the footing of a pile foundation was in a state of tension. Table 1 shows the experimental cases and Figure 1 shows the dimensions of the specimens. The specimens are whole models of column-footing-pile foundation. The scale of these models is about 1/5 of actual bridge piers. Case 1-1 and Case 1-2 was carried out to confirm the bending failure. As shown in Figure 2 and Figure 3, while the amount of footing reinforcement bars was maintained at almost constant, the spacing and the diameter of the reinforcement bars were varied between Case 1-1 and Case 1-2, to confirm how these differences influence the stress transmission mechanism. Case 2 and Case 3 were executed to investigate the shear failure. The shear span of the tension side was varied to investigate influence of the shear span on the shear strength.

The loading apparatus is shown in Figure 4. To support the specimens, acrylic plates were installed under the footing corresponding to the each pile respectively.

These acrylic plates have almost the same vertical rigidity as actual piles under the assumed similar ratio. High strength steel bars modeling tension piles were anchored to the footing through the acrylic plates.

In all cases, only the horizontal force was loaded. No axial force was loaded on the column in order that the top of the footing became tense. All experiment was performed under the static loading condition. One-way multi-cycle loading was performed in the Case 1-1 and Case 1-2. The horizontal displacement when a reinforcement of the footing yielded was defined as 1 δ, and the displacement was increased in steps of 1 δ. For the Case 2 and Case 3, one-way monotonic loading was performed until the maximum load.

3. Results of the Bending failure Experiments

(1) General Observations for the Test

Figure 5 shows the load displacement curves at the loading point for Case 1-1 and Case 1-2. Those maximum loads were almost same. The failure states were similar, the bending cracking on the top surface of the footing was the dominant damage, and the failure type was bending failure with yielding of the top reinforcement.

Figure 6 is a schematic diagram of the crack patterns of the footing top surface. In Case 1-1, a crack first initiated at the base of the column at a horizontal load level of 78.5 kN. Then, at 157.0 kN, cracks ① occurred on the side of the footing. New Cracks② appeared at 215.8 kN and some reinforcement bars arranged at the top of footing yielded at the side of the column at the horizontal loading level of 279 kN, the horizontal displacement of 4.88 mm, 1 δ, and δ/H = 0.244%. And the cracks③ extended at the maximum horizontal load of 306 kN. Later at 1.3 δ, cracks ④ developed and the cracks evolved on the top and side surfaces. Then cracks⑤ were observed at 1.6 δ. During the loading, however, no abrupt decrease of the load was observed, finally, loading continued until 269.8 kN, 26 δ (126.8 mm), and δ/H = 6.34%. In Case 1-2, similar damage to Case 1-1 occurred, the horizontal displacement when the top surface reinforcement bar yielded was 14.69 mm, δ/H = 0.734%, and the maximum load at 294.3 kN. Loading continued until 10 δ, 147,2 mm, and δ/H = 7.36%. Photograph 1 exhibits the state of the failure in Case 1-1.

Figure 7 shows the strain distribution in the loading direction at cross-section A-A' in Figure 2.3. The yield strain of the steel reinforcement bars was approximately 2000 μ in the material test. At 1 δ in Case 1-1, the strains in reinforcement bars far away from column were larger than that close to the column. In Case 1-2, the strains at poison close to the edge of the footing were smaller than the strains around the column. But the difference between the two cases was small and, the reinforcement bars yielded across the full width at maximum horizontal load in both cases. These indicate that there is no effect of the reinforcement spacing. If the strain distribution at 1 δin Case 1-1 is converted to a rectangular distribution, the effective width b_e becomes t_c + 1.5d. The reinforcement bar yields across full width after 1 δin both cases. As a result, we can conclude that the bending is resisted by the reinforcement in the full width of

footing.

(2) Comparison of the Experimental Results and Calculated Results

The yield bending moments were calculated for each of the following effective widths and the results compared with the experimental results. The effective widths were set in the 3 ways shown below (see Figure 8).

① $b = t_c + d$ (recommended in the present design specification)
② $b = t_c + 2d$
③ Overall width of the footing
Where:
b: footing effective width
t_c: column width
d: effective footing depth

The actual strength of the concrete and the reinforcement bars obtained from material tests were used to calculate the yield bending moment. Figure 9 compares the calculated yield moment M_{cy} with the experimental result M_{eu} for the moment at critical footing section at the maximum horizontal load. The results are almost the identical value in Case 1-1 and Case 1-2. Assuming to be the effective width b was t_c + d, the calculated value was about 60% of the experimental result and a certain safety factor was involved. In case that $b = t_c + 2d$, the calculated result was lower than the experimental results. But when it was the full width, almost the same results were obtained. In the specimens used for this experiment, the footing width was relatively narrow in transverse direction. Therefore, in these results, there was almost no notable difference between the effective width of $b = t_c + 2d$ and the full width. If the footing width is larger compared with the column depth than these experimental specimens, cracks were expected to initiate from the side of footing. Considering these things, we can expect that the effective width will also be greater than $b = t_c + 2d$.

Figure 10 presents a comparison of the bending moment at critical footing section for Case 1-1 under the horizontal displacement level at 1 δ. Here, M_{cy} represents the computed yield moment for each effective width and M_{ey} represents the experimental value. According to this, when the effective width b was $t_c + 2d$ or the full width, the calculated results were estimated greater than the experimental results and it was in danger.

4 Results of Shear Failure Experiments

(1) General Observations for the Test

Figure 11 shows the load – displacement curves at the loading point in Case 2 and Case 3. Photograph 2 shows crack patterns of footing at maximum load time in Case 2. In both cases, the maximum load was reached before the tensile reinforcement yielded. Thus it was considered that the footing failed in shear. It confirms that in all cases, after maximum load, the load declined gradually and even after the strength declined, a certain degree of deformation performance was maintained.

Figure 12 shows the state of crack in Case 2. There were two kinds of crack on the side surface of the footing: an arch-shaped cracks from the top of the footing of the pull-out pile towards the compressive edge of the column ① and to the bottom edge of the footing on the push-out pile ②, and the

ultimate failure was caused by the latter ②. This indicates shear is being carried by tied arch mechanism from pull out pile to the compressive side of column through the bottom of footing under the column. The figure also confirms that the cracks extended beyond the critical section B-B and reach the footing of the portion under the column. This indicated that the shear span in the case of the top surface tension is longer than that of the bottom surface tension.

(2) Effect of the Shear Span Ratio on the Shear Strength

We will discuss the effect of the shear span ratio on the shear capacity of footing based on these results and experimental results in the past.

Figure 13 shows the relation between the shear span ratio and Sc / Se, where Sc is the shear strength assuming a RC slender beam. Se is the experimental result of the maximum shear force at critical footing section. Here we would like to define the shear span, the distance from the center of the pile to the tensile surface of the column. The experimental data we conducted in the past using cantilever beams were also shown in Figure 13. It elucidates that even in the case that top is loaded tensile stress, the shear strength rises as the shear span ratio decreases.

5. Conclusion

The bending failure experiments have confirmed that, at the maximum strength, bending is bore with the almost full width of the footing even if in the tension side. These experimental results suggest that we can design under following method. If we may permit the advance of cracking to a certain degree, design is based on bending strength, the effective width b may be equal to or greater than $t_c + 2d$. If harmful damage in footing isn't permitted, allowable stress verification may be performed under effective width $b = t_c + d$.

Judging from the shear failure experiments, when the top side is in tension, it is possible to adopt the design method that the shear strength increases according to the decrease of shear span ratio, as in the case of bottom side tension. But we need to define the longer shear span than that of compressive side based on observing shear cracks. We conclude that footing can develop a tied-arch action from the crack pattern like an arch shape observed in Figure 12 and the analysis in Figure 13. And substantial shear force can be transmitted by compression force through the arch rib formed from the top of the footing at the pull-out pile to the bottom of the column.

We will conduct further experiments to propose a practical design method for footing shear strength in the case of top side tension.

Table 1

Case	case1-1	case1-2	case2	case3
Foundation type	Pile foundation (4 piles)			
Failure mode	Bending		Shear	
Footing shape	Symmetrical model		Asymmetrical model	
Shear span a(mm)	375		600	
Effective height d(mm)	450			
Shear span ratio a/d	0.833		1.333	
Footing reinforcement (top)	D10ctc75	D13ctc150	D29ctc75	D29ctc75
Footing reinforcement (bottom)	D22ctc75	D22ctc75	D22ctc75	D22ctc75
Steel ratio (%) (top)	0.18	0.17	1.62	1.62
Steel ratio (%) (bottom)	0.98	0.98	0.98	0.98

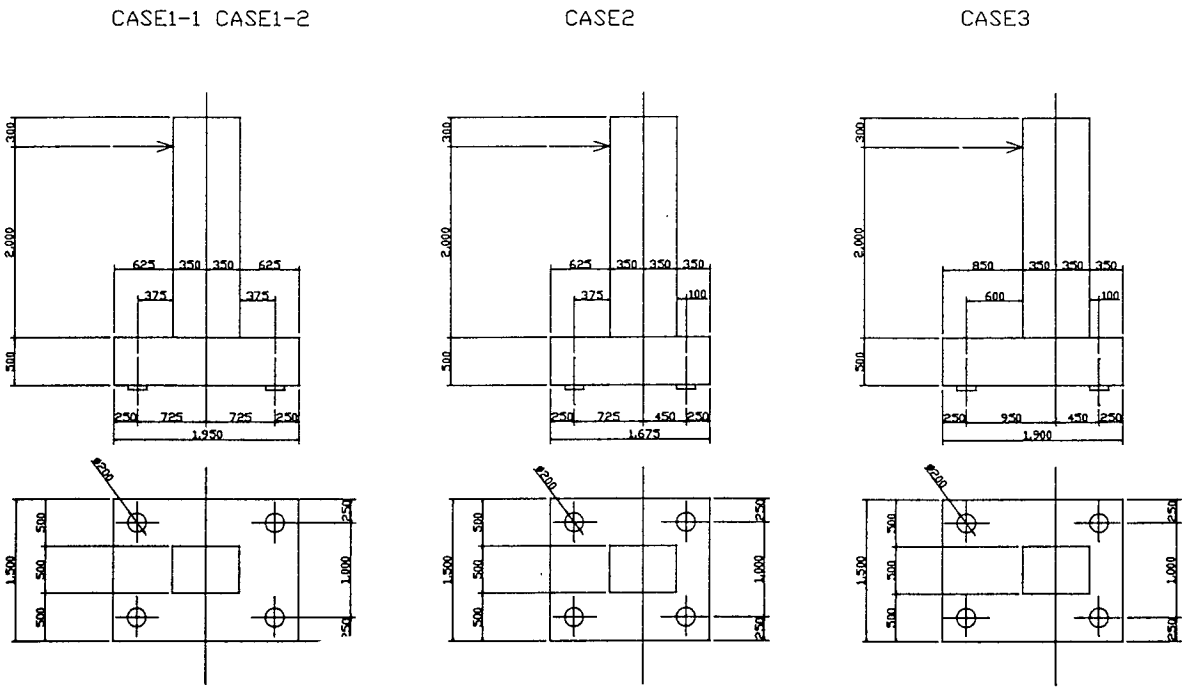

Figure 1. Dimensions of Specimens

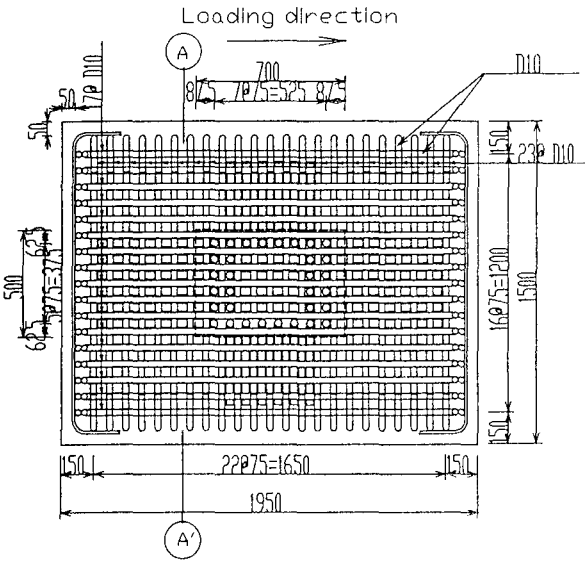

Figure 2. Case 1-1 Reinforcement

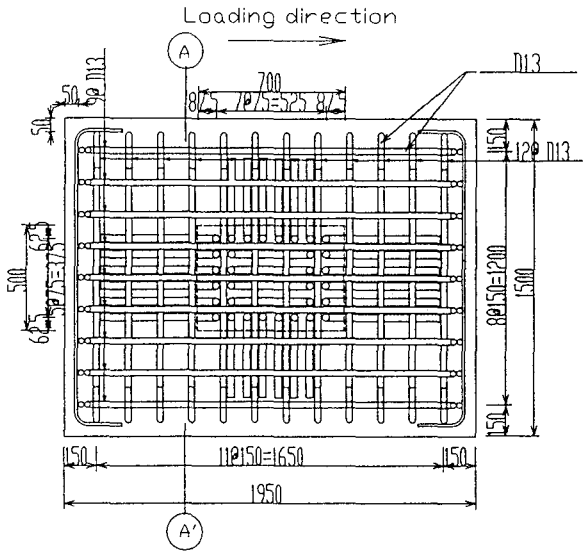

Figure 3. Case 1-2 Reinforcement

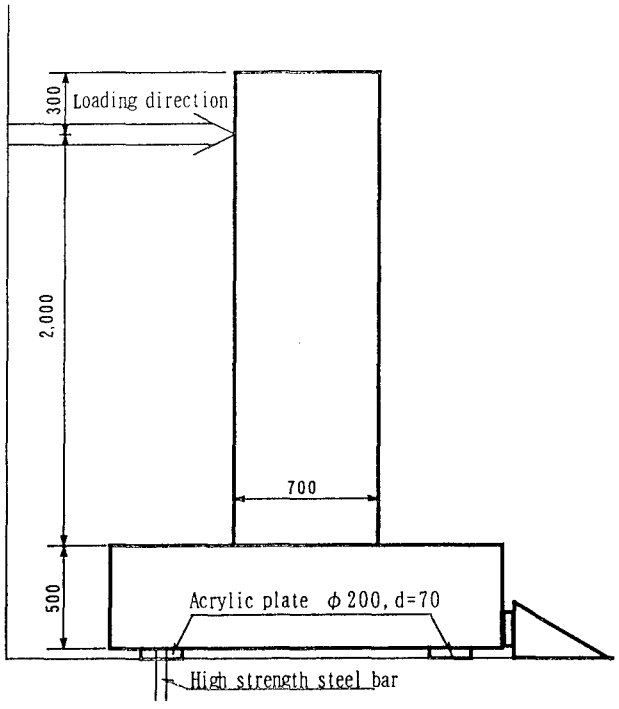

Figure 4. Test Setup

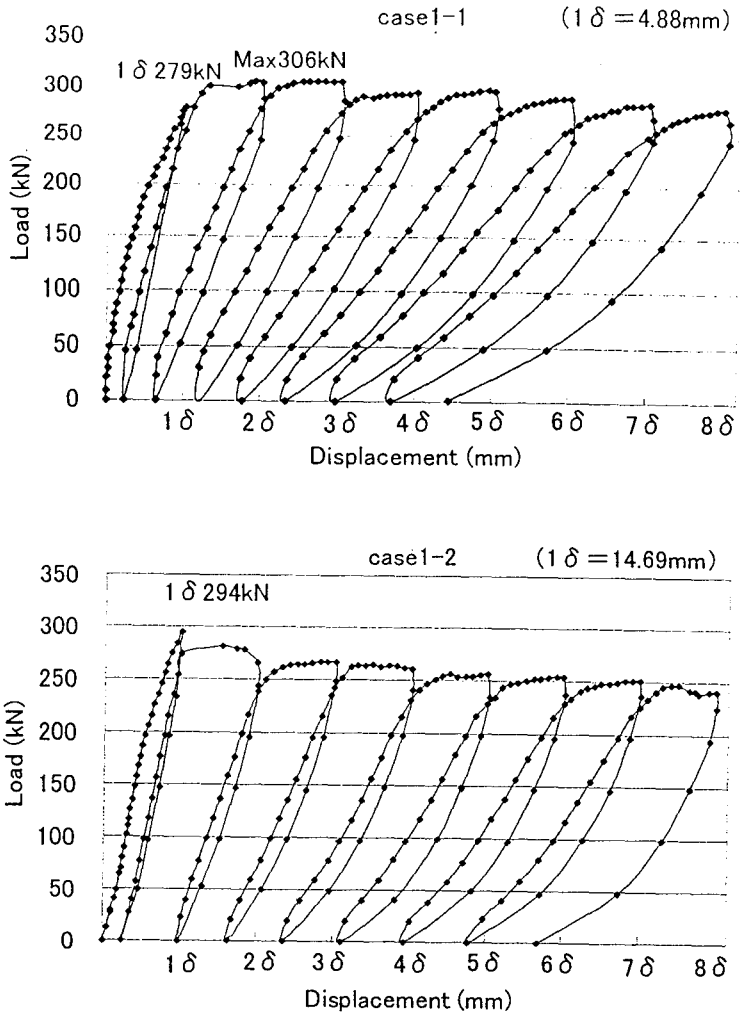

Figure 5. Load−Displacement Curve

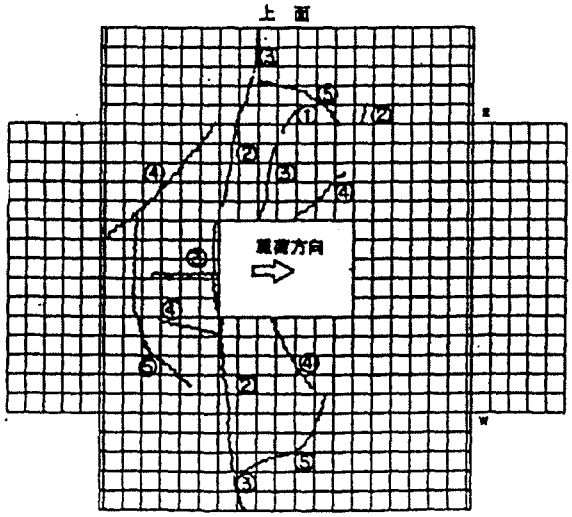

Figure 6. Crack Pattern (Case 1-1)

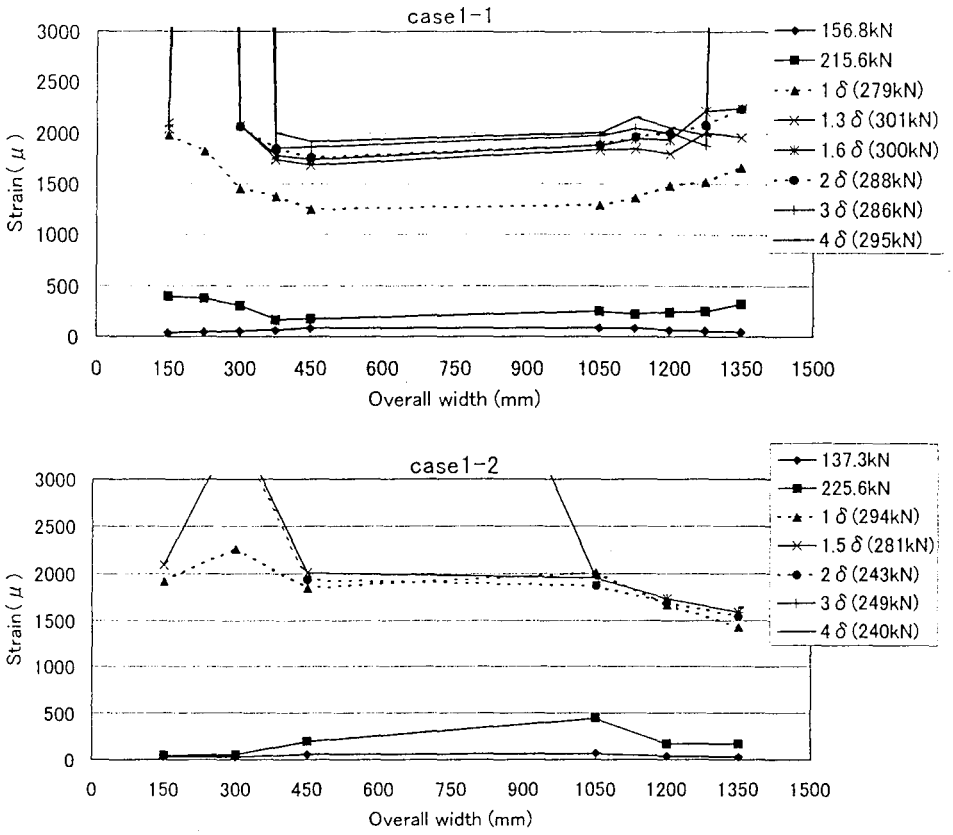

Figure 7. Strain Distribution at A-A' section in Figure 2,3 (Case 1-1 and Case 1-2)

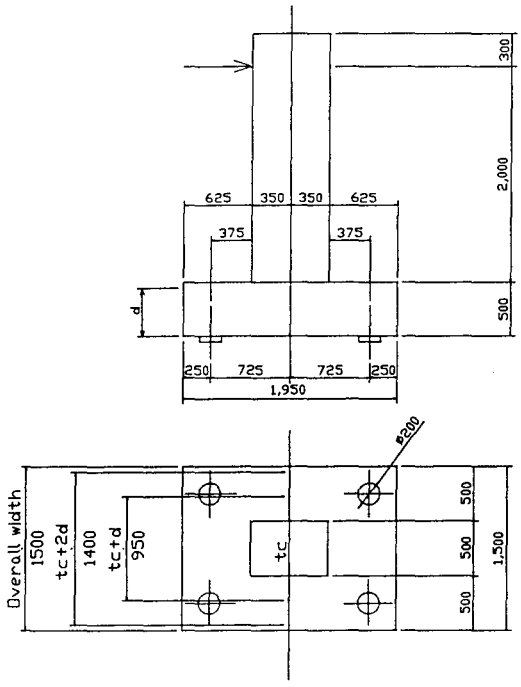

Figure 8. Obtaining the Effective Width

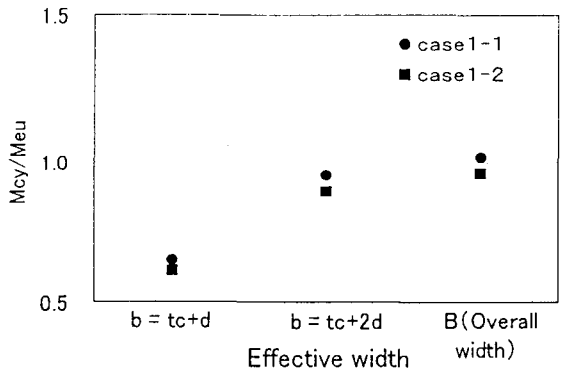

Figure 9. M_{cy} / M_{eu} (Maximum Loading)

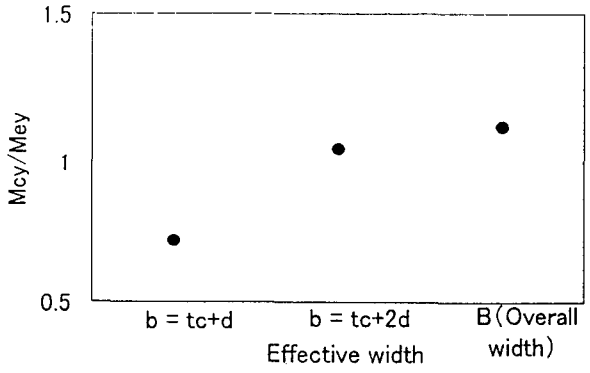

Figure 10. M_{cy} / M_{ey} (1 δCase 1-1)

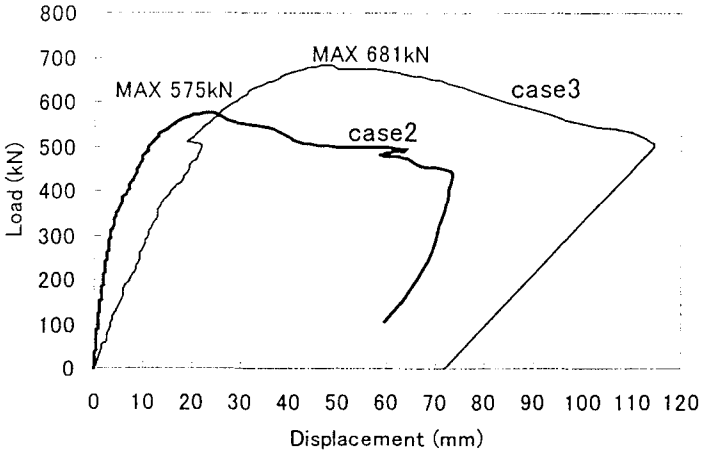

Figure 11. Load – Displacement Curve

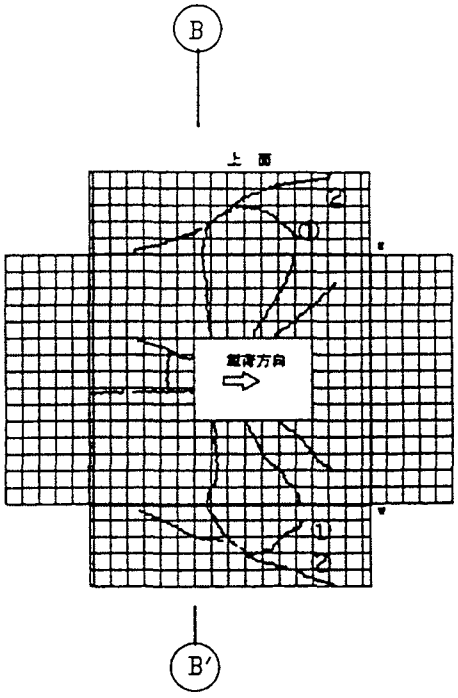

Figure 12. Crack Pattern (Case 2)

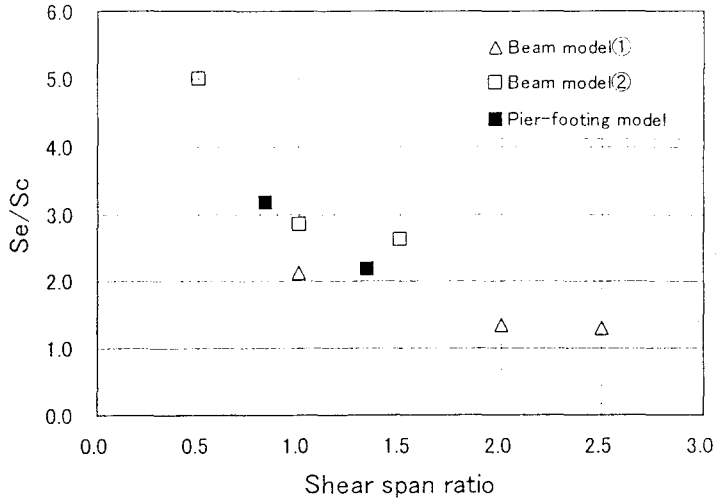

Figure 13. Se / Sc – Shear Span Ratio

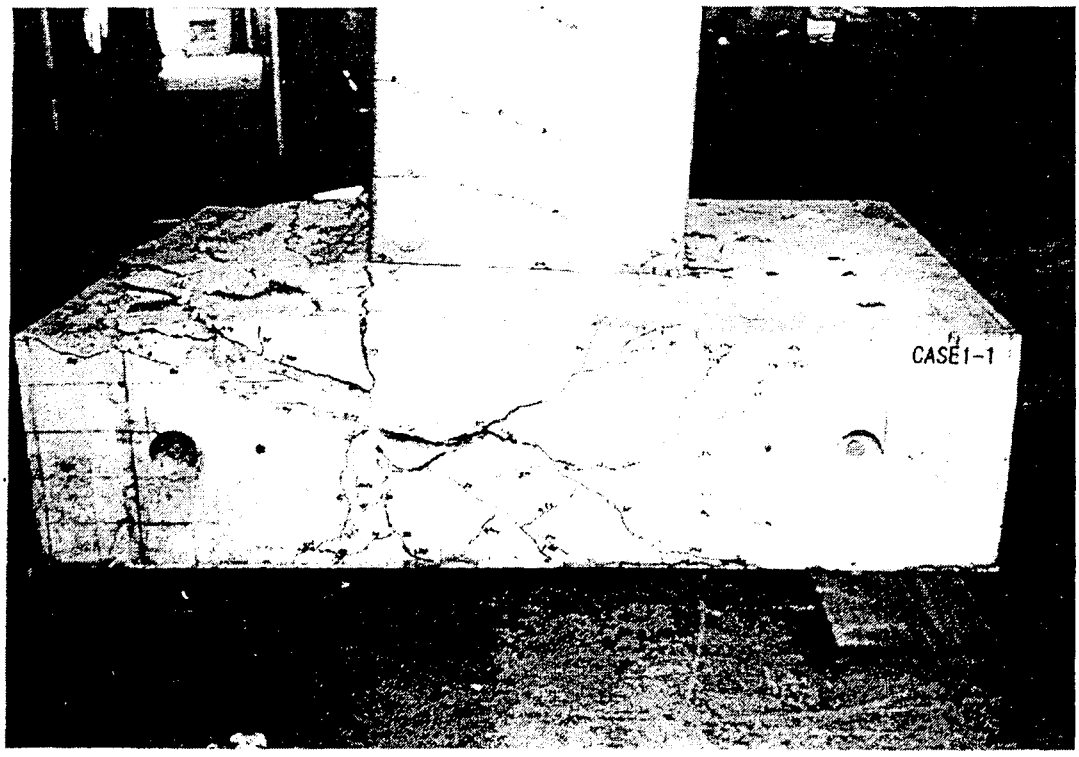

Photograph 1 State of the Failure (Case 1-1)

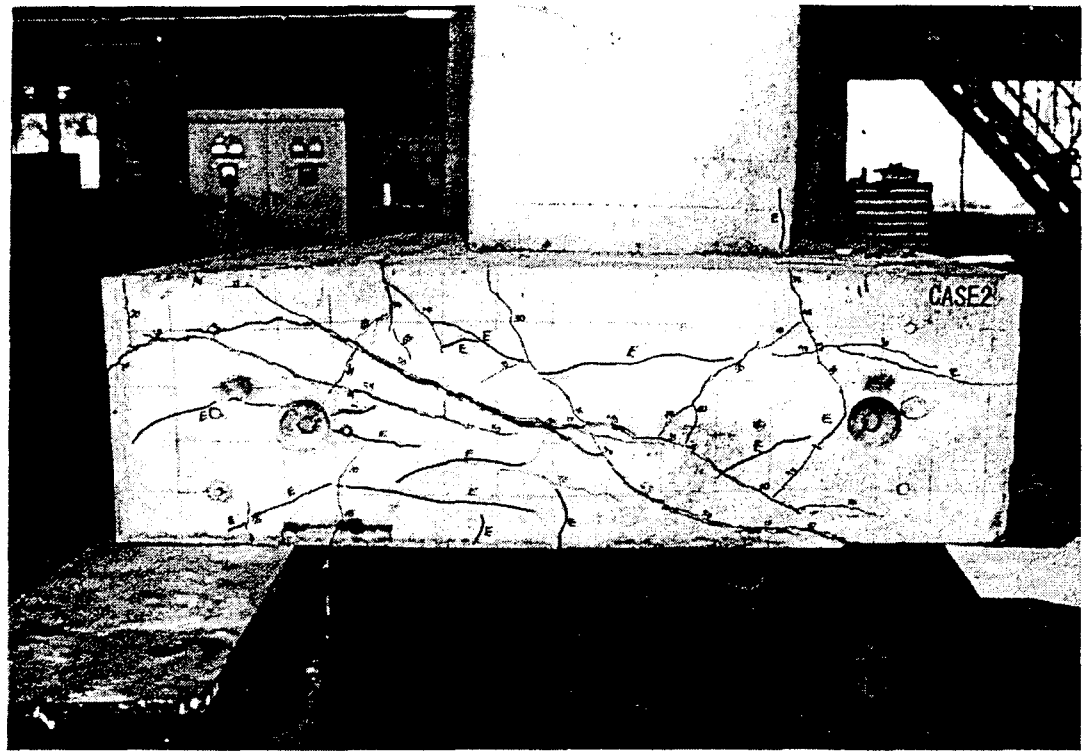

Photograph 2 State of the Failure (Case 2)

DYNAMIC CHARACTERISTICS OF MAGNETO-RHEOLOGICAL DAMPER

by

Hideo FUJITANI[1], Katsuaki SUNAKODA[2], Hiroshi SODEYAMA[2], Norio IWATA[3] and Satsuya SODA[3]

ABSTRACT

Two kinds of magneto-rheological fluid damper (MR damper) have been designed and manufactured. One has a nominal capacity of 2kN and the other 20kN. A bypass flow system is adopted for both dampers and each has the same capacity of electromagnet attached to the bypass portion. The effective fluid orifice is the rectangular space and the magnetic field is applied from the outside.

A test was performed by applying different magnetic fields to the orifice portion of the rectangular space. The damping force and the force-displacement loop were evaluated.

The test results yielded the following : 1) Two type's of dampers functioned by using one unit of the electromagnet under an appropriate electrical current control. 2) The magnitude of the damping force depends on the input magnetic field, but it has an upper limit. 3) Without an applied magnetic field, the MRF damper exhibits viscous-like behavior, while with a magnetic field it shows friction-like behavior.

A mechanical model of the damper is estimated by taking account of the force-displacement loop.

It is clarified that MRF dampers provide a technology that enables effective semi-active control in real building structures.

Keywords: Damping characteristic
Magneto-rheological fluids
MR dampers

1. INTRODUCTION

Vibration control systems are mainly divided into three types: passive, active, and semi-active. The semi-active type attracts a great deal of attention because of it's the following superior properties: 1) It is basically stable in contrast to the active type. 2) Its control effect is more flexible than the passive type. 3) Its external energy requirements are orders of magnitude smaller than those of typical active types.

Until now, various kinds of semi-active control devices have been developed. One fundamental device for semi-active control systems is the capacity adjustable viscous damper. Its viscosity is adjustable in accordance with the opening rate of the flow control valve inside the damper. A series of studies with this type of damper has been carried out and they were found to have good characteristics and efficient control system properties [1), 2)] However, magneto-rheological (MR) and electro-rheological (ER) fluid dampers attracted significant attention. The damping properties of these types of dampers are changed by changing the magnetic/electrical field applied to each fluid [3)-11)]

Research on semi-active control of building structures using controllable fluid dampers is being conducted in the U.S.-Japan cooperative research and development project of "Smart Materials and Structural Systems." launched in 1998 by NSF and Building Research Institute, Japan Ministry of Construction [12)] . This paper outlines the results of experimental tests and simulations of magneto-rehological fluid dampers conducted as one of the research items of this cooperative research on the Japan side.

Two kinds of Magneto-rheological fluid damper (MRF damper) have been designed and manufactured. One has a nominal capacity of 2kN and the other 20kN. A test was performed by applying different magnetic fields to the orifice portion of the rectangular space. The damping force and the force-displacement loop were evaluated.

1) Head, Performance System Division, Codes and Evaluation Research Center, Building Research Institute, Ministry of Construction, Tsukuba-shi, Ibaraki-ken, 305-0802, Japan
2) Sanwa Tekki Corp., Shinagawa-ku, Tokyo, 140-8669, Japan
3) Department of Architecture, Waseda University, Shinjuku-ku, Tokyo, 169-8555, Japan

Furthermore, an analytical model is proposed to simulate the behavior of the MR dampers, and simulation and experimental results are compared.

2. DESIGN OF MRF DAMPER

The bypass flow type MRF damper has been developed in this study. Fig.1 shows its hydraulic circuit. The bypass flow portion is a passage for MR fluids connecting two pressure chambers. The bypass flow is at the outside of the cylinder. In bypass type hydraulic dampers such as this, a cylinder is divided to two airtight pressure chambers by a piston with rubber O-rings. The MR fluid flows from a high-pressure chamber to a low-pressure chamber through the bypass flow portion. The bypass flow portion has an orifice and the MR fluid flow is narrowed rapidly at the orifice. Moreover, intense magnetic fields are

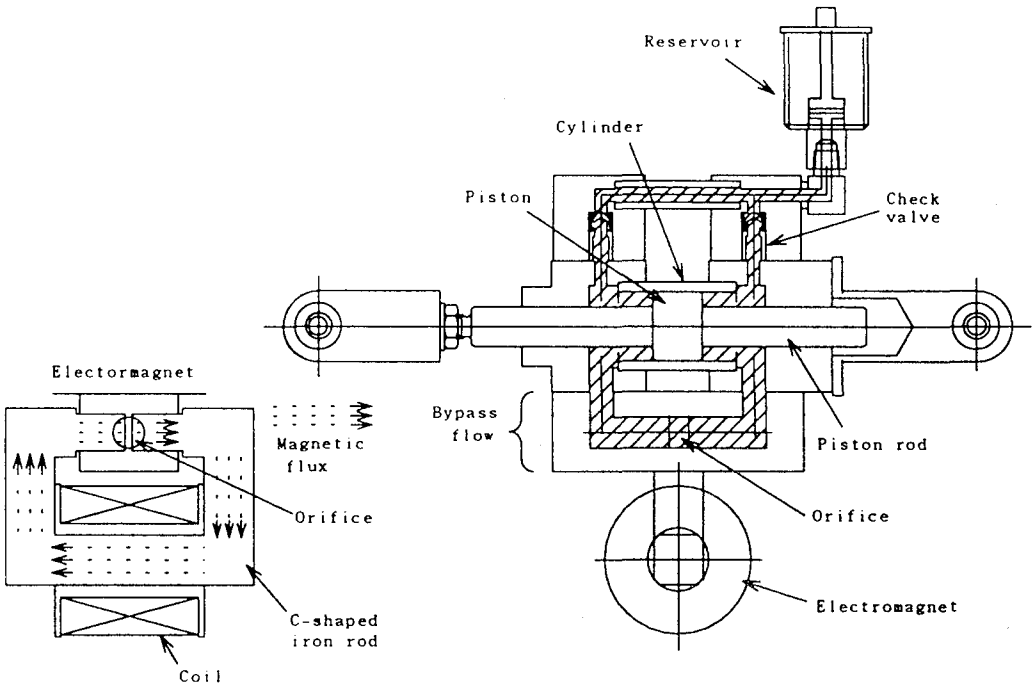

Figure 1 Hydraulic Circuit of Bypass Type MRF Damper

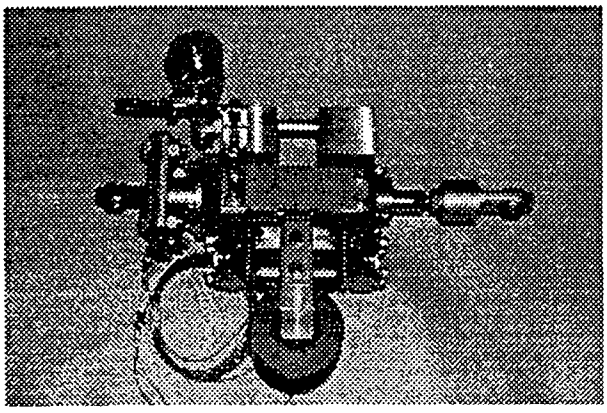

Figure 2 MRF Damper - 2kN

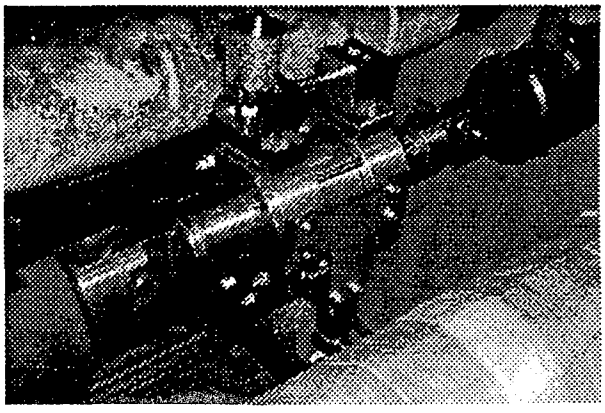

Figure 3 MRF Damper - 20kN

applied to the MR fluid at the orifice by electromagnets. To simplify the analysis of the MR fluid flow state in the magnetic field, a rectangular cross section is selected as the orifice shape. The magnetic fields are applied perpendicularly to the MR fluid flow at the orifice. The electromagnet is formed by copper wire wound around a C-shaped iron rod. The air gap between the ends of the C-shaped iron rod forms the rectangular cross section of the orifice. Thus, the length of the air gap of the electromagnet is equivalent to the thickness of the orifice that is penetrated by the magnetic flux. This method of magnetizing MR fluids has the advantages that the MR fluid is rarely affected by the heat generated on the electromagnet.

Two different capacities of MRF dampers have been designed and built. Fig.2 and Fig.3 show photographs of them. Fig.2 shows the one whose the nominal maximum damping force is 2kN, and Fig.3 shows the one whose the nominal maximum damping force is 20kN. Table1 shows their design specifications. These two dampers have the same basic mechanism. In particular, their electromagnets are identical. The electromagnet's design is based on the larger dampers. It is therefore used under the small input electric currents for the 2kN MRF damper. The basic specifications of the electromagnet are also shown in Table1-1. Very low carbon steel is used for the C-shaped iron rod to obtain a high level of magnetic saturation and low residual magnetization. The 2kN MRF damper's orifice is 0.6 x 16mm in cross section and 10mm long. The 20kN damper's orifice is 2 x 20mm in cross section and 20mm long. When designing the orifice size, the Reynolds number of the fluid flow at the orifice was considered to be less than the critical Reynolds number.

As shown in Fig. 1, these MRF dampers have two check valves on the passages to the reservoir. These check valves are open under the non-vibration condition. Therefore, the thermal expansion due to the temperature rise of the MR fluid is absorbed by the reservoir. However, the check valves are shut during vibrations, and the flow of MR fluid occurs only through the bypass portion.

Two different kinds of MR fluids were tested on the 2kN MRF damper, in order to find the most suitable commercial MR fluid for the bypass type MRF damper. One was LORD MRF-132LD and the other was LORD MRF-128NB. Based on the experimental results of these 2kN dampers, MRF-132LD was selected as the fluid for the 20kN MRF damper.

Table 1 Design Specifications of MRF Dampers

	MRF damper - 2kN	MRF damper - 20kN
Max. Force (nominal)	2 kN	20 kN
Stroke	±10 mm	±35 mm
Cylinder bore	35 mm	95 mm
Orifice size	0.6 mm×16 mm	2 mm×20 mm
Orifice length	10 mm	20 mm
MR fluid	① MRF-132LD ② MRF-128NB	MRF-132LD
Coil	ϕ 0.5 mm 3800 turns	
Inductance	1.5 henries	
Coil resistance	60 ohms	
Max. current	0.08 A	0.16 A

3. EXPERIMENT

Various tests have been carried out using of the vibration-testing machine to verify the damping characteristics of the developed MRF dampers. Fig.4 shows a schematic diagram of the experimental setup for the MRF dampers. The actuator of the vibration-testing machine has a maximum dynamic load of 2000kN and a maximum velocity of 40cm/s. Various sinusoidal displacements are applied to the dampers and the generated damping forces are measured by a load-cell on the opposite side of the actuator. The input electric current to the electromagnet is selected as the one of the test parameters and is maintained to a constant value during the dynamic loading test.

Fig.5-1, Fig.5-2 and Fig.5-3 show the measured force-displacement loops for the 2kN MRF dampers under maximum input velocities of 5cm/s, 9cm/s and 20cm/s sinusoidal waveform movement, respectively. The right hand side loops of every figure show the test results for the MRF damper using the MR fluid, MRF-132LD, and the left hand side loops show the results for the MRF-128 damper. The dynamic loading tests were performed under input electric currents of 0A, 0.016A, 0.032A, 0.048A, 0.064A and 0.08A.

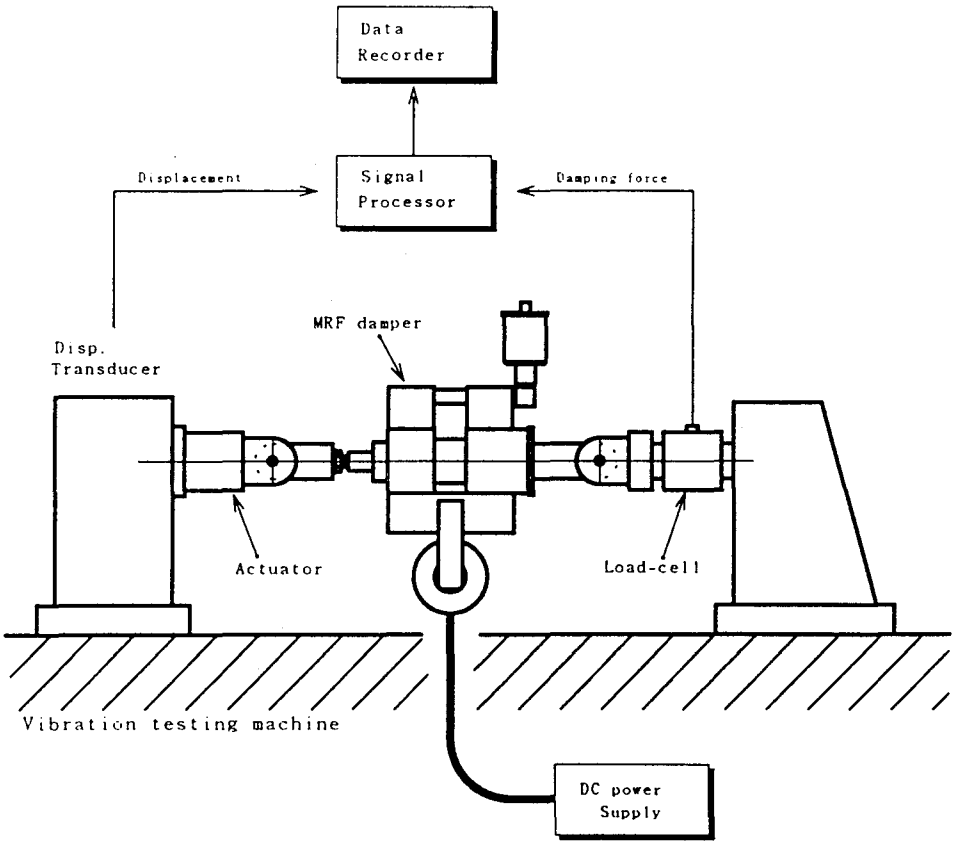

Figure 4 Experimental Setup for MRF Damper

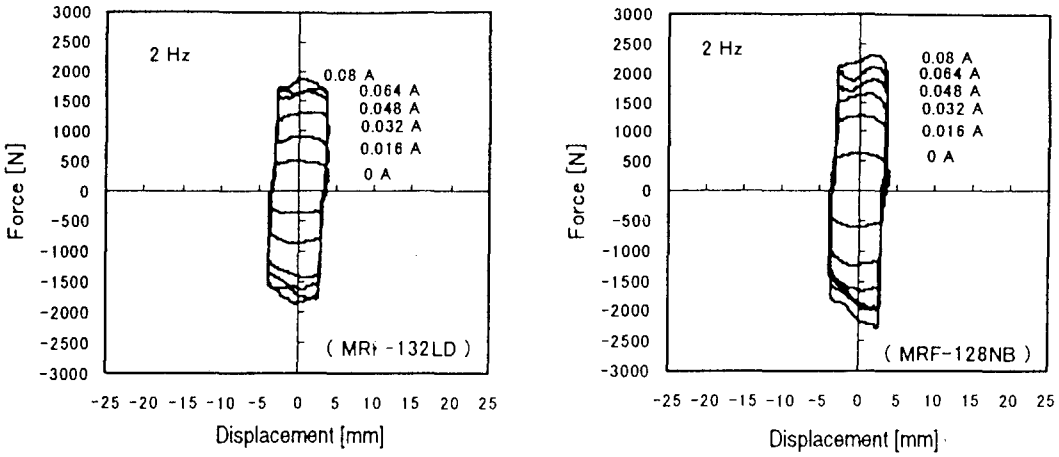

Figure 5-1 Force-displacement Loops at 5cm/s

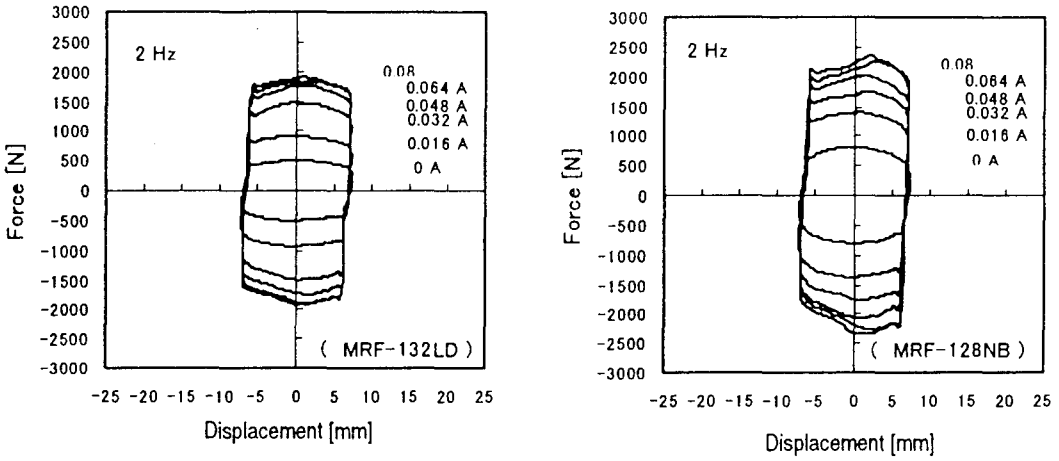

Figure 5-2 Force-displacement Loops at 9cm/s

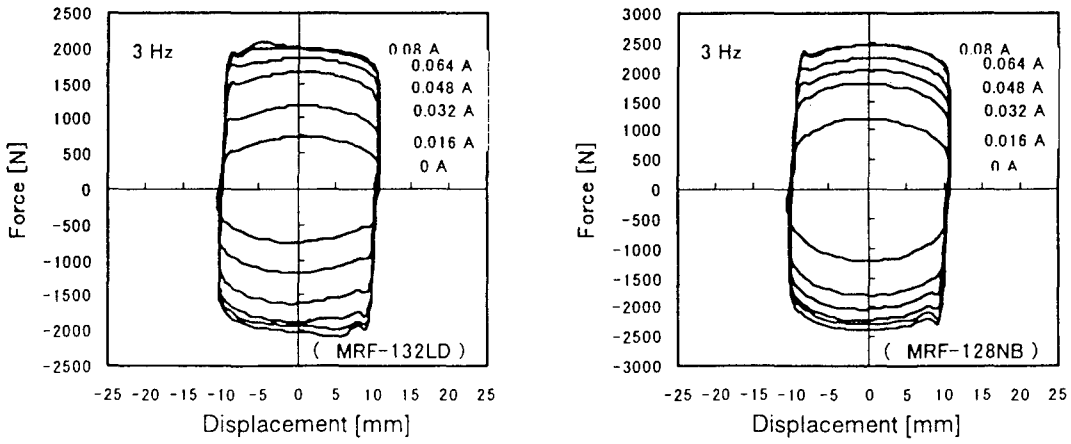

Figure 5-3 Force-displacement Loops at 20cm/s

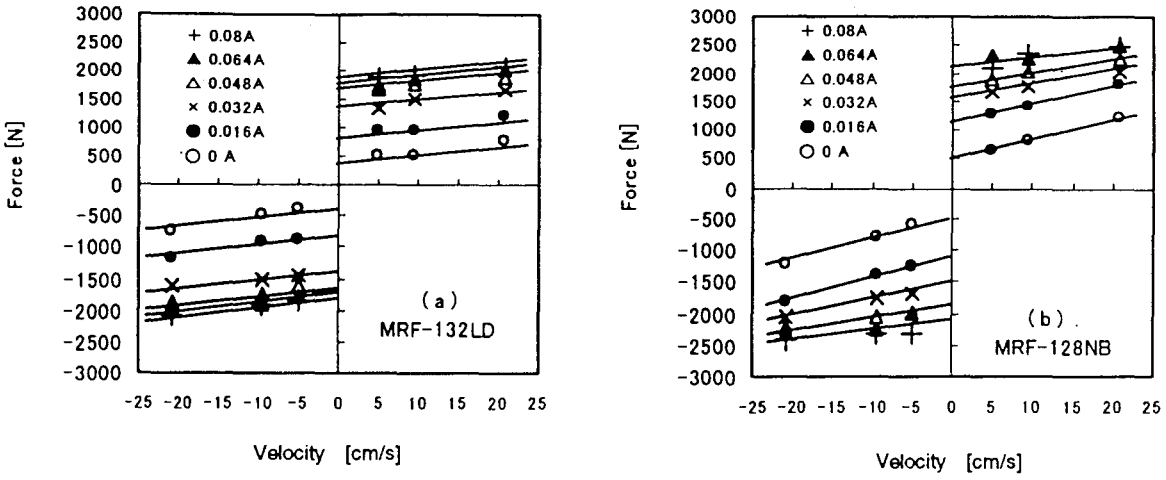

Figure 6 Force-velocity Relationship for 2 kN MRF Damper

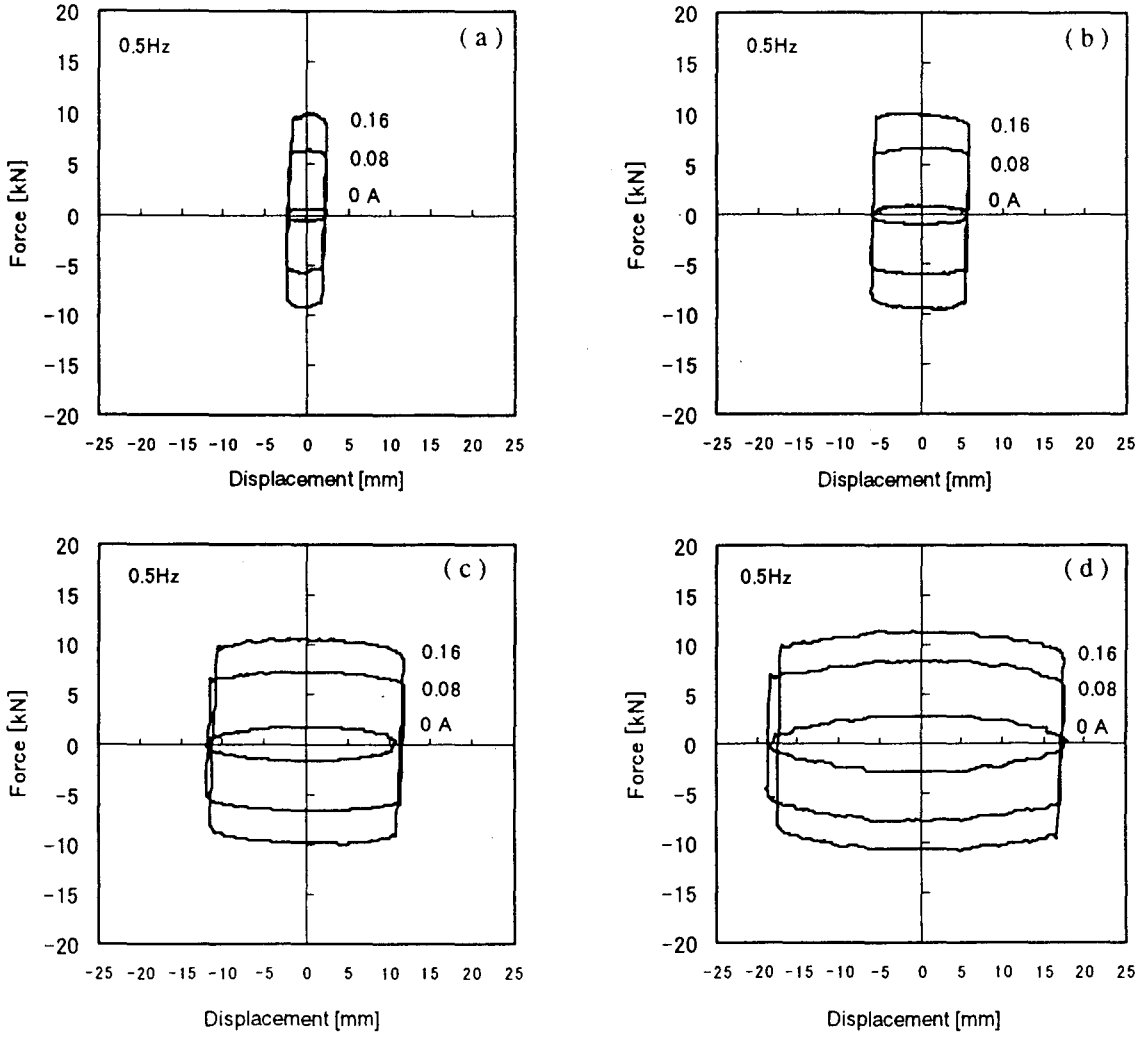

Figure 7 Force-displacement Loops for 20kN MRF Damper

It was verified that the maximum damping force was controllable by adjusting the magnetic field. Furthermore, an upper limit of the controllable damping force was observed. The magnetic field of the electromagnet can be increased linearly to approximately 0.16A. Therefore, it is understood that this phenomenon is due to the magnetic saturation of the MR fluid. The force-displacement loop under no magnetic field exhibits the behavior of a viscous damper, especially in the high velocity range of around 20cm/s. The friction force of the sealing or the damping force due to the residual magnetization is dominant for the total damping force in the low velocity range.

Fig.6(a) and Fig.6(b) show the force-velocity relationships. Although the absolute values of the maximum damping forces of the two dampers are similar, the increase rate of the damping force of the MRF damper using the MRF-128NB is higher than that of the damper using the MRF-132LD. The dynamic range of the damper using the MRF-128NB is smaller in the high velocity range. These results mean that the MRF-132LD is more suitable for the developed bypass type MRF dampers. The MRF-132LD was used for the 20kN MRF damper

Fig.7 shows the force-displacement loops for the 20kN MRF damper under 0.5Hz sinusoidal waveform. Fig.8 shows the relationship between the maximum input velocity and the measured maximum damping force. It was verified that the electrical currents applied to the electromagnet controlled the damping force of the 20kN MRF damper. The characteristics of the damping forces at the low velocity level, less than 5cm/s, were also investigated through these tests. It was confirmed from the Fig.7(a) and Fig.8 that the MRF damper functioned under a comparatively low velocity and over a small displacement range.

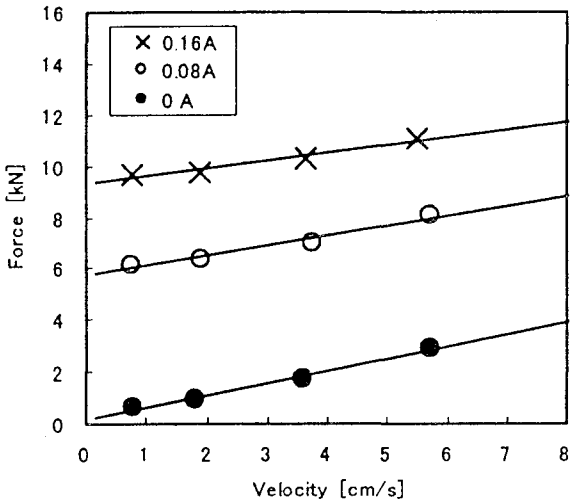

Figure 8 Max.force-max.velocity Relationship for 20kN MRF Damper

4. ANALYTICAL MODEL FORMULATION

This section proposes the analytical model for simulating the behavior of the MRF dampers, and compares the simulation and experimental results. Until now, some types of mechanical models for MR(ER) fluid dampers have been proposed. The simplest one is the Bingham viscoplastic model, in which a couple comprising a dashpot and a friction slider are connected in parallel. Gavin used the mechanical model proposed by Gamota to simulate the behavior of ER fluid dampers, in which the Zener element shows frequency dependent behavior over a wide range of the frequencies [Gavin et al. (1998)] [3] . The model proposed by Spencer consists of two springs, two dashpots and the Bou-Wen model, which can exactly simulate the behavior of both the displacement-force and velocity-force relationships of MRF dampers [Spencer et al. (1997)] [6] .

In this paper, the involution model is used to simulate the behavior of MRF dampers. In this model, the velocity-force relationship is expressed by:

$$F=CV^{\alpha} \qquad (1)$$

where F is the damping force, C is a constant independent of the frequency; V is the velocity of the piston and α is an exponent such that $0.0 < \alpha \leq 1.0$. This expression has often been used to simulate viscous fluid dampers, and is available to simulate the behavior of MRF(ERF) dampers because the damping force remains within the specified bound under the condition that α is close to zero. In addition, since there are only two parameters in this expression(C and α), they are easier to estimate than the elements in the mechanical models mentioned above.

Fig.9 and Fig.10 shows the simulation results of the 2kN damper obtained from Expression (1). Both parameters(C and α) are assumed to be independent of the amplitude and the frequency. Values of C and α, shown in Table2, were determined to minimize the square of the errors between the experimental force and the analytical one. Good agreement with experimental results is confirmed for each applied current.

The experimental results of the 20kN damper were simulated by following the same procedure as for the 2kN damper. In this case, though, ideal sine waves were used as input displacement because some noises were included in observed displacement. The results are shown in Fig.11. Values of C and α are identified as shown in Table3. As well as the case of the 2KN damper, it is found that the analytical model can exactly predict the behavior of the experimental results.

Through a series of simulations, it is confirmed that the behavior of MRF dampers is exactly predicted by the velocity-force relationship expressed in (1) over a wide range of applied current, amplitude, and frequency. However, it should be noted that this analytical model can be applied only to simulate the dynamic behavior of MRF dampers, because the intrinsic property of the term "CV^{α}" can not simulate the static behavior.

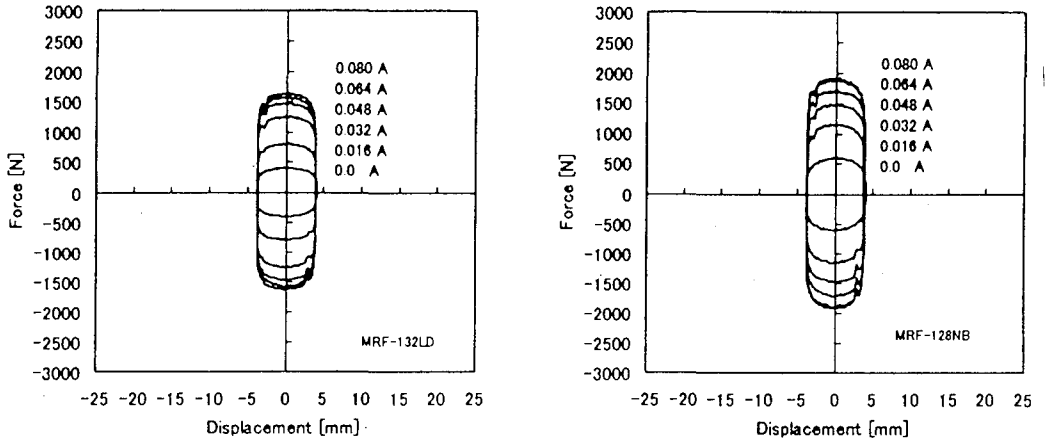

(a) MRF-132LD (b) MRF-128NB

Figure 9 Simulation Results (2kN Damper, Frequency=2.0Hz)

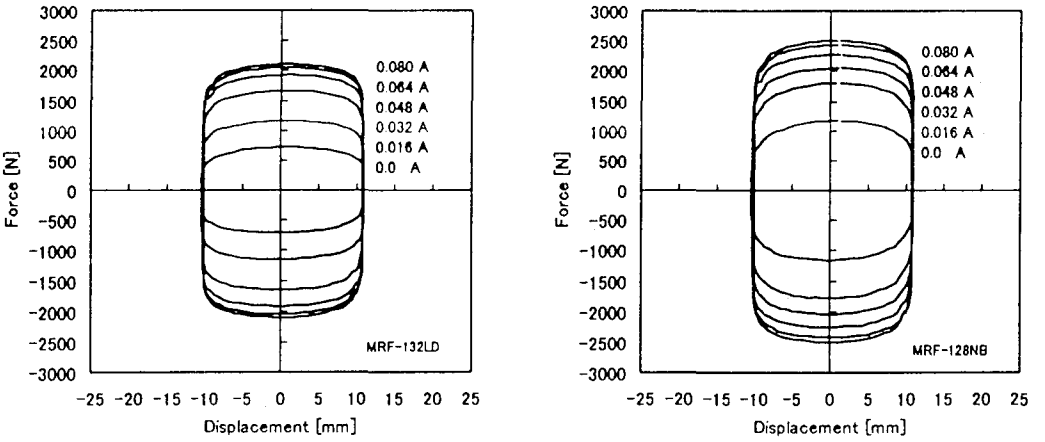

(a) MRF-132LD (b) MRF-128NB

Figure 10 Simulation Results (2kN Damper, Frequency=3.0Hz)

Table 2 Values of Analytical Model ($F=C\,V^{\alpha}$) for 2kN Dampers

Current[A]	MRF-128NB		MRF-132LD	
	C[N$(mm/s)^{-\alpha}$]	α	C[N$(mm/s)^{-\alpha}$]	α
0.000	97.4	0.47	85.6	0.40
0.016	349	0.31	292	0.26
0.032	608	0.23	576	0.20
0.048	788	0.20	704	0.19
0.064	940	0.18	752	0.19
0.080	920	0.19	812	0.18

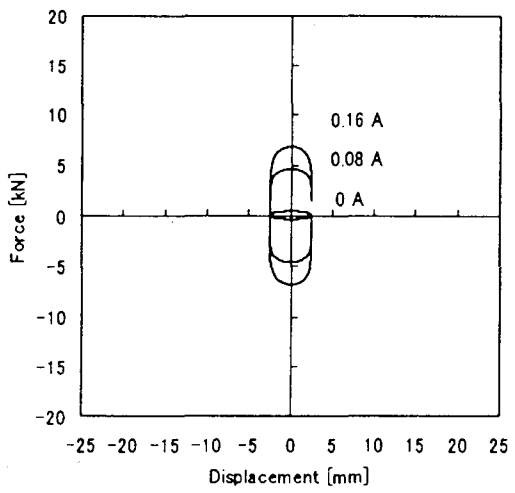

(a) Amplitude=2.5[mm]

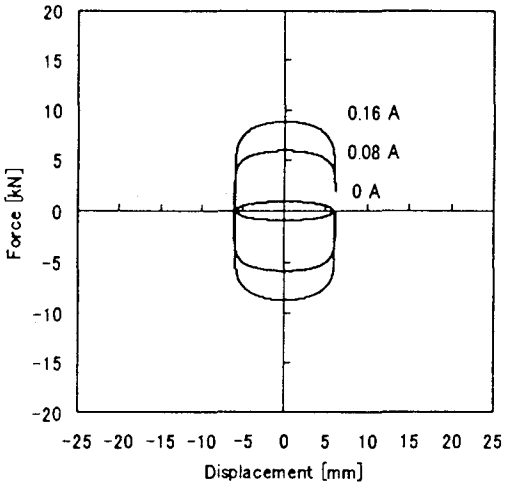

(b) Amplitude=5[mm]

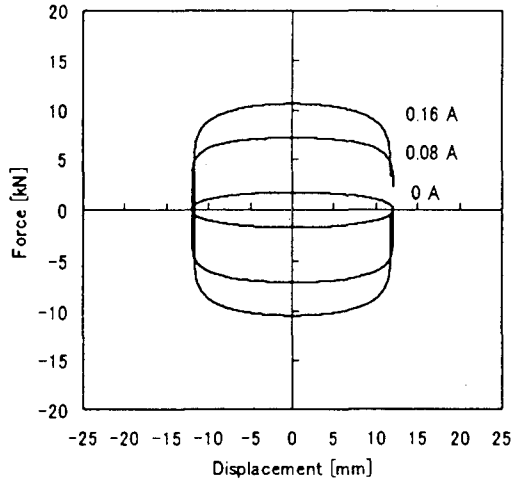

(c) Amplitude=12.5[mm]

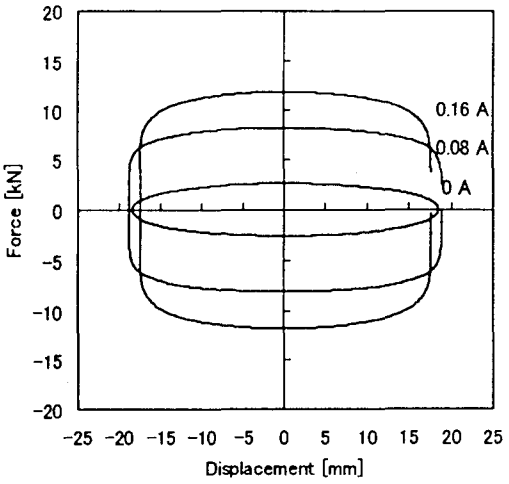

(d) Amplitude=20[mm]

Figure 11 Simulation Results (20kN Damper, Frequency=0.5[Hz])

Table 3 Values of Analytical Model ($F=C\,V^{\alpha}$) for 20kN Damper

Current[A]	C[KN(mm/s)]	α
0.00	0.065	0.91
0.08	2.59	0.28
0.16	3.84	0.28

5. CONCLUSIONS

Various tests have been carried out using a vibration-testing machine to verify the damping characteristics of developed MRF dampers. The following test results were obtained: (1) Two types of dampers functioned by using one unit of the electromagnet under an appropriate electrical current control. (2) The magnitude of the damping force depends on the input magnetic field, but it has an upper limit. (3) In the absence of an applied magnetic field, an MRF damper exhibits viscous-like behavior, while it shows friction-like behavior in a magnetic field.

Through a series of simulations, it is confirmed that the behavior of the MRF dampers is fairly predicted by the velocity-force relationship expressed in equation (1) over a wide range of applied current, amplitude, and frequency.

It is clarified that the MRF dampers provide a technology that enables effective semi-active control in real building structures.

ACKNOWLEDGMENTS

The authors would like to express their appreciation to the members of ER/MR working group in the Effector section of the Japan side of the project, "Smart Materials and Structural Systems" for their fruitful discussions.

REFERENCES

1. Niwa, N., Kobori, T., Takahashi, M., Matsunaga, Y., Kurata, N. and Mizuno, T. (1998). Application of Semi-active Damper System to an Actual Building. Proc., 2nd World Conference on Structural Control, pp.815-824.
2. Kurita, N., Kobori, T., Takahashi, M. and Niwa, N. (1998). Semi-Active Damper System in Large Earthquakes. Proc., 2nd World Conference on Structural Control, pp.359-366.
3. Kawashima, K., Otsuka H., Unjoh S. and Mukai, H. (1995). Development of Hybrid Seismic Response Control of Bridges. Proc., 27th Joint Meeting of UJNR, pp.295-316.
4. Gavin., H.P. and Hanson, D. (1998). Seismic Protection using ER Damping Walls, Proc., 2nd World Conference on Structural Control, pp.1183-1190.
5. Hidaka, S., Ahn, Y.K. and Morishita, S. (1998). Structural Control by Damping-Variable Dynamic Damper using ER Fluid. Proc., 2nd World Conference on Structural Control, pp.451-460.
6. Fukukita, A., Tamura, K., Hayashi, S. and Shiba, K. (1995). Semi-active control of rotational variable damper using elctro-rehological fluid. Journal of Structural Engineering, Vol.41B, pp.23-32. (in Japnese)
7. Spencer Jr., B.F., Dyke, S.J., Sain, M.K., and Carlson, J.D. (1997). Phenomenological Model for Magnetorheological Dampers. J. of Engineering Mechanics, ASCE, Vol. 123, No.3, pp.230-238
8. Johnson, E., Ramallo, J.C., Spencer Jr., B.F. and Sain, M.K. (1998). Intelligent Base Isolation Systems. Proc., 2nd World Conference on Structural Control, pp.367-376.
9. Carlson, J.D. and Spencer Jr., B.F. (1996). Magneto-Rheological Fluid Dampers for Semi-Active Seismic Control. Proc., 3rd Int. Conf. on Motion and Vib. Control, Vol.3, pp.35-40.
10. Spencer Jr., B.F., Yang, G., Carlson, J.D. and Sain, M.K. (1998). "Smart" dampers for Seismic Protection of Structures: A Full-Scale Study. Proc., 2nd World Conference on Structural Control, pp.417-426.
11. Jolly, M.R., Bender, J.W. and Carlson, J.D. (1998). Properties and Applications of Commercial Magnetorheological Fluids. Proc., SPIE's 5th Annual International Symposium on Smart Structures and Materials.
12. Otani, S., Hiraishi, H., Midorikawa, M., Teshigawara, M., Saito, T and Fujitani, H. (2000). Development of Smart Systems for Building Structures. Proc., SPIE's 7th Annual International Symposium on Smart Structures and Materials.

Theme 4

Performance-Based Design Methods

COMPARISON OF PERFORMANCE REQUIRED BY BRIDGE DESIGN CODES IN VARIOUS COUNTRIES

by

Michio OKAHARA [1], Jiro FUKUI [2], Masahiro NISHITANI [3] and Kenji MATSUI [4]

ABSTRACT

The authors carried out a comparative analysis of the regulations for bridge design codes in various countries, as for required performance and seismic performance etc. In Japan, the revision of the Design Specifications of Highway Bridges to performance based design is now under study. This comparison analysis will make a significant contribution to the revision of the Specifications. The end of this report concludes with a summary of principal contents and an outline of future issues.

KEY WORDS: Bridge Design
Performance Based Design
Required Performance
Seismic Performance

1. INTRODUCTION

Around the world, the adoption of performance based codes is being debated by many organizations in architectural field and has been partially completed. In Japan, new Building Standard Law, that is performance based standard, will be enforced the beginning in 2000 and a trial of performance based ordering of paving work is being carried out. Performance based design clarifies the performance that structures require, and a number of suitable verification methods to be used to verify their performance have been proposed.

In Japan, the revision of the Design Specifications of Highway Bridges to performance based code is now under study. A comparative analysis of the performance required by bridges under codes in various countries will make a significant contribution to this study.

To study the requirements for performance based design in bridge design codes, the authors performed a comparative analysis of the regulations for general bridge design, required performance and seismic performance in present bridge design codes in various countries. Excluding the articles specifying seismic design in the codes of various countries, there are no complete codes that can be defined as performance based codes. Consequently, the authors focused and arranged at terminology such as "philosophy" and "requirements" in various countries' codes.

The study dealt with the following codes.

---

1) Director, Structure and Bridge Department, Public Works Research Institute, Ministry of Construction, Tsukuba-shi, Ibaraki-ken, 305-0804, JAPAN
2) Head, Foundation Engineering Division, ditto
3) Senior Research Engineer, ditto
4) Chief Engineer of R&D Headquarters, CTI Engineering Co., Ltd., Chuo-ku, Fukuoka-shi, 810-0041

Regulations and required performance for general bridge design compared were those stipulated in the LRFD version of the AASHTO, Eurocode, Caltrans and the revised edition of the Design Specifications of Highway Bridges (Japan, now under study). And the seismic design in the LRFD version of the AASHTO, Eurocode, Transit Bridge Manual (New Zealand) and Design Specifications of Highway Bridges were compared.

(1) United States of America;
- AASHTO LRFD Bridge Design Specifications (1998, 2nd Edition)[1] [AASHTO]
(2) European Union;
- Draft prEN1990: Basis of Design (1999)[2]
- Preliminary Draft EN1997-1: Geotechnical Design, Part 1 General Rules (1999)[3]
[Draft EN]
- ENV1998: Design provisions for earthquake resistance of structures (1994)[4] [ENV1998]
(3) State of California, U.S.;
- Memo to Designers 20-1/Seismic Design Methodology (1999)[5]
- Caltrans Bridge Design Specifications (1990)[6]
- Seismic Design Criteria, version 1.1(1999)[7] [Caltrans]
(4) New Zealand;
- TNZ Bridge Manual for Design and Evaluation (1995)[8] [TNZ]
(5) Japan;
- Revised edition of the Design Specifications of Highway Bridges (200X)[9),10)] [Draft JRA]

2. OVERVIEW OF PERFORMANCE BASED DESIGN

The term of performance based design is interpreted in various ways. A broad categorization of codes that are called performance based design places the following two classes.

In one case, following the arrival of the age of mega-competition as a consequence of the appearance of a single world market after the collapse of the Soviet Union that ended the cold war, the international community needed common rules. And they adopted "performance" as a key word accepted by all nations. The architectural field has past provided many performance elements including seismic, safety, fire resistance and human-friendly performance. And constraints applied by regulations and laws by governments on these various performance elements are obstacles to international trade. In the Nordic countries, a movement to establish "performance" as a key word that would destroy these obstacles began in the early 1970s. This movement spread to England in the 1980s, to Australia and New Zealand in the 1990s, and in recent years has been reflected in the revision of the Building Standard Law of Japan. So based on the hierarchical character of regulations (or required performance), the degree to which they are endowed with legally constraining is debated. Figure 1 presents a hierarchy of regulations based on the Nordic 5 level system[11]. The only legal objection is generally whether or not a building's performance is guaranteed and designers are given greater freedom to decide on the method to verify their performance. In this case, performance based design can be interpreted as synonymous with free design method.

In the second case, the need for developed seismic technology has been pointed out and great progress has been achieved based on the lessons learned from a series of earthquake disasters beginning with the Loma Prieta (1989), Northridge (1994) and Hyogo-ken

Nanbu Earthquake (1995). Because, partly as a result of its technological difficulty, the limits to the capacity of structures against a large earthquake were not adequately explained to owners (or users) who were not professionals, they fell into the illusion that most buildings could withstand any conditions. Awareness of this problem triggered a movement to clarify performance as a design index that can gain the mutual approval of owners and designers. Vision 2000[12] that the Structural Engineers Association of California (SEAOC) rushed to codify performance that structures require in the form of a performance matrix. Figure 2 shows an example of a performance matrix. The horizontal axis is called performance level, that is corresponding to performance (equal to limit states), and the vertical axis is called hazard level.

These movements appeared first in the architectural field, and it can be stated that at this time, codes incorporating these approaches have not been established in bridge design field anywhere in the world. Since the Northridge and Hyogo-ken Nanbu Earthquake, performance requirements related to seismic performance has been carried out based on the results of technology development, but nothing has been done outside of the seismic design field. Therefore, a comparison of required performance for bridge design had been carried out by focusing and arranging design philosophies or requirements in various codes.

3. COMPARISON OF PERFORMANCE REQUIRED AND OTHERS BY BRIDGES

Table 1 presents required performance, foundation design, etc. that are stipulated in codes for four regions, countries, or states. The followings are special mentions.

- Because the characteristics of the codes differ, required performance of bridges is stipulated from their respective perspectives.
- Because the AASHTO and Draft JRA deal directly with bridges, the required performance is specific.
- Eurocode is not classified by structural form; rather by each material used in civil engineering and architectural fields. Consequently, the Draft EN does not directly specify required performance for bridges.
- Caltrans stipulates the basis of seismic design on the premise that it will be applied to "normal or standard bridges." The regulations excluding seismic provisions of the Caltrans are fundamentally correspondent to the AASHTO.
- Draft JRA is based on a proposed revision that is now under study. Consequently, as in the case of the Draft EN, finally its configurations and contents may change.

(1) Required Performance

As for the Draft EN, the strict required performance can not be described, because a structure has not been specified on the character of the code. Therefore, in the Draft EN, the general limit states are stipulated, substituting with the concrete required performance. In the Draft EN, ultimate limit state and service limit state has been set. The former limit state also contains not only structural safety but also human safety, and appearance is also included in the latter limit state.

The required performance of the Caltrans for large earthquakes for bridges is simple and concrete, and only collapse limit state of a structure, this is a kind of ultimate limit state, is included. In the AASHTO, economical efficiency, beauty and landscape are

emphasized in addition to safety and serviceability of structures. To ensure the safety of bridges, ductility, redundancy and importance are considered in the code. And, the performance of serviceability is used for the wide meaning, including durability, inspectability, maintenanceability, amenity and deformability, etc.

In the Draft JRA, it would be specified almost equal required performance of the AASHTO. As an examination of economical efficiency, it would be epoch-making to recommend the evaluation of life cycle cost of a bridge. Still, in the design of substructures and seismic design of the Draft JRA, performance I~III and seismic performance I~ III would concretely be set as required performance for the safety of bridges.

The design of bridges which harmonize with beauty, landscape and environment would be emphasized, as shown in Table 1.

(2) Basis of Design

Ductility, redundancy and importance have been taken up as the basis of bridge design. In all codes, ductility in seismic design has been evaluated. In the AASHTO and Draft EN, redundancy as a bridge structure has been noticed, and in the Caltrans and Draft JRA, redundancy as a road network after earthquake has been noticed. Importance has been applied to seismic design for all codes.

(3) Design Service Life

A life is distinguished by service life and design life. Service life is correspondent to what is called design service life. Design life is correspondent to reference period of ISO2394(1998)[13], and design life is a period as a base for calculating fluctuating loads.

In the Draft EN and Draft JRA, the design service life of bridges is shown as 100 years. On the other hand, in the AASHTO, service life has been not specified, generally it has been understood with 100 years. Still, design life has been specified as 75 years.

(4) Life Cycle Cost

In the AASHTO, life cycle cost has been not described. In the U.S., the Life Cycle Design and Performance (1997)[14] that has been prepared by the U.S. Army Corps of Engineers is the regulation that stipulates the basic framework for performance based design applied to public works projects. It stipulates that engineering decisions should not do simply minimize initial costs or maximize reliability that ignores costs, and demands that designers perform evaluations based on life cycle cost of an entire project.

The design of highway bridges in the U.K. is based on BS5400 (Code of Practice for Bridges, BSI) and conforms with many Government Departmental Standards in the Design Manual for Roads and Bridges (DMRB). The code BD36 in the DMRB provides the method of comparing life cycle cost (the design service life in the U.K. is 120 years premised on appropriate maintenance).

The Draft JRA is the first code to clearly stipulate the concept of evaluating the optimum proposal based on total cost during service life.

(5) Limit States

Limit States are engineering indices for checking whether structures satisfy their required performance. In the AASHTO, service limit state, fatigue limit state, strength limit state and extreme event limit state are set. Each limit state means the following;

- Service limit state: under usual service conditions, stress, deformation and crack are

limited.
- Fatigue limit state: stress width by repetition traffic loads is limited.
- Strength limit state: for load combinations which encounter during design life, the strength and stability of the local and whole of a structure are compensated for. Though damages are received, the whole structural system is maintained.
- Extreme event limit state: for a large earthquake, flood and the collision of a ship, the residual capacity of a bridge is guaranteed.

The basis of seismic design of the Caltrans is based on the deformation. The purpose of seismic design is to check the deformation occurring by a large earthquake, and in the Caltrans, only collapse limit state is specified. Collapse limit state of a structure is defined as a state not resisting to its dead weight, by generating large deformation.

In the Draft JRA, limit states are not stipulated, because of using an allowable stress design (WSD) method.

(6) Basis of Verification Method
The verification equation of a limit state in the AASHTO is basically provided as the following.

$$\Sigma \eta_i \gamma_i Q_i \leqq \phi R_n = R_r$$

Where:

$\eta_i = \eta_D \eta_R \eta_I \geqq 0.95$, or $\eta_i = 1/(\eta_D \eta_R \eta_I) \leqq 1.0$

γ_i: load factor

Q_i: load effects

ϕ : resistant factor (factor that is multiplied by nominal resistant force)

R_n: nominal resistant force

R_r: resistant force multiplied by resistant factor (design resistant force)

Here, the factor η_D for ductility and the factor η_R for redundancy are used to verify strength limit state, and the factor η_I for importance is used to verify extreme event limit state. As the AASHTO, in future bridge design, the effects of ductility and redundancy must be represented by a factor in some way in codes. The design method of the Caltrans converted from conventional force based design method to displacement based design method. In seismic design, it seems to introduce by and by this design method.

(7) Load
As shown in Table 1, the classification of loads is different by each code at present. The classification of the Draft EN is fundamentally similar to the regulations of ISO2394. Hereafter, it is required to match the ISO code.

In the Draft JRA, the effect of salt attack, effect of corrosion, fatigue by the repetition of live loads would be newly considered as other actions and effects.

(8) Foundation Design
In the AASHTO, three limit states except for fatigue limit state have been checked. In the calculation of resistance force (design vertical bearing capacity), resistant factor $\phi \lambda_v$ is considered. Here, ϕ is the factor which depends on the estimation method of bearing capacity, and λ_v is the factor which depends on construction management and estimating system of bearing capacity. In the Eurocode, such resistant factor is not given. The desired value of the safety index β in calculating this resistant factor is 2.0 ~ 3.0, according to Appendix A[16] of Barker et al (1991).

The foundation design of the Draft EN has been specified at EN1997-1(Geotechnical design). The MFA (Material Factor Approach) and RFA (Resistance Factor Approach) have been proposed as partial design formats of

ground resistant in Draft EN. The design resistant force R_d based on each approach is represented by the following equations.

Approach of MFA: $R_d = R(X_R/\gamma_M, a_{nor})$

Approach of RFA: $R_d = R(X_R, a_{nor})/\gamma_R/\xi$

Where:

X_R: characteristic value of ground materials

γ_M: material factor

γ_R: resistant factor

a_{nor}: nominal value of geometric quantity

ξ : correlation ratio

In the MFA approach, the partial factor γ_M, as shown in Table 1, is directly considered in ground parameters. The RFA approach is used for the design of piles, and it is similar to the LRFD approach. The correlation ratio ξ is a factor considering the frequency of in-situ loading tests.

In the Caltrans, both of SLD (Service Load Design) and LFD (Load Factor Design) method are ever used as design methods. The resistant factor ϕ has been applied to the latter method. Here, the ϕ is divided in every Groups (combination of loads), and in the Group VII (present SDC) including an earthquake action, factor of 1.0 is applied, and in other Groups, factor of 0.75 is applied. There is no relation between ground parameters and estimation methods of bearing capacity.

In the present JRA, because the reliability of bearing capacity of a pile by in-situ loading tests is higher than that of empirical estimation method, the correction factor γ is applied to estimate bearing capacity to reflect the effect it. And, the introduction of the factor which represents quality and quantity of ground parameters has been also examining as future problem.

4. COMPARISON OF SEISMIC PERFORMANCE

Table 2 shows the comparison of seismic regulations in various codes. Many studies such as that by Backle (1996)[17] or NCEER (1997)[18], have compared and considered regulations in seismic design codes in various countries. This report adds considerations from the perspective of international harmonization and locality of codes. The New Zealand's TNZ Bridge Manual (1994) instead of the Caltrans is shown in Table 2.

(1) Basis of Seismic Design

The AASHTO clarifies seismic performance for two levels: medium earthquakes and large earthquakes. The ENV1998 and TNZ mention to traffic functions after an earthquake. The present JRA on the other hand treats differences in seismic performance required according to the importance of a bridge as basis of seismic design.

(2) Seismic Performance

Because in the AASHTO, the effects of earthquakes consider only extreme event limit state as stated in Table 1, the seismic performance required has been interpreted as only this limit state. As shown in 1) of Table 2, the AASHTO has adopted a two-level design seismic force, but it is not clear to the authors whether or not, in practice, this extreme event limit state is verified for both medium and large earthquakes. The limit states in the Eurocode are basically service limit state and ultimate limit state. In conformity with this concept, the ENV1998 applies these two limit states to post-earthquake service and post-earthquake safety respectively, with the former verified based on displacement and the latter verified based on strength of a structure. In the TNZ, it stipulates, not clarified in the Bridge Manual, that an earthquake equivalent to an

ultimate limit state with return period of 450 years be considered[19]. Based on the earthquake motion hypothesized by this level of earthquake, the seismic performance is specified for small and large cases. The present JRA combines three limit states, post-earthquake service, post-earthquake restoration and post-earthquake safety with bridge importance A and B. Judging from bridge importance, two seismic performances, post-earthquake service and post-earthquake restoration (for a case of class B bridges), and post-earthquake service and post-earthquake safety (for a case of class A bridges) are combined with level 1 and level 2 earthquake motion respectively.

(3) Importance

Although definitions of bridge importance differ, they are categorized in two or three classes in all codes. Categorizations based on importance are, in the case of the AAHSTO, reflected in the factor for importance η_i in the calculation equation for the design load Q. Importance in the ENV1998 and TNZ is related to adjusting the return period of design earthquake motion for a normal bridge, but for practical design procedures, the design earthquake force of a normal bridge is increased or lowered. In the case of the present JRA on the other hand, it is reflected in differences in the required seismic performance indicated in h) and in differences in the safety factor used to decide an allowable ductility factor. Considered from this perspective, in contrast to the AASHTO, ENV1998 and TNZ, the specifications of the JRA are detailed.

(4) Zone Classification

The AASHTO has set the value A for a construction site based on the hazard map of return period of 475 years (10% probability of exceedance during service life of 50 years). The seismic zone has been set as class 1 to class 4 according to the value of A. This zone factor has been used to establish differences in required analysis methods, detailed of bridge piers, and bridge abutments and foundations design method. The ENV1998 has not set specific zone factors, but the design ground acceleration ag reflects the degree of earthquake risk in each nation. The TNZ has provided the contour map from 0.4 to 0.8 as its zone factor Z. In New Zealand, instead of the present deterministic hazard map, the distribution map of maximum ground acceleration based on a probabilistic risk analysis would be used as the zone factor (Figure 3).

(5) Design Earthquake Motion

The AASHTO has set two design earthquake levels. For a medium earthquake, it is based on the value of A for return period of 475 years (10% probability of exceedance during design service life of 50 years). For a large earthquake, the maximum credible earthquake (MCE) is considered to be an earthquake with return period longer than the design earthquake: an earthquake with return period of 2,500 years for example. The ENV1998 defines a large earthquake as an earthquake with return period of 475 years, but regarding a medium earthquake, it simply stipulates: "earthquake activity with an appropriate return period shall be evaluated." In the provisions of the TNZ, one level earthquake motion of return period of 450 years is considered. The present JRA defines a medium and large design earthquake motion as earthquake motion with a high probability of occurring during the service life of a bridge and strong one with a low probability of occurring respectively, but does not stipulate specific return periods.

(6) Elastic Response Spectrum

The part m) of Table 2 presents the basic equation for the elastic response spectrum in each code. Here, only the TNZ uses non-linear spectrum (yield seismic intensity). New railway seismic codes issued in 1999, in Japan, use non-linear response spectrum[20].

(7) Load Reduction Factor

The AAHSTO and ENV1998 establish reduction factors R or q based on the importance of a bridge and the type of a substructure as ways to reduce the elastic seismic force accounting for the non-linear response of ductile members. The TNZ on the other hand, has not set a load reduction factor because it has used non-linear response spectrum for allowable ductility factor μ (= 1 to 6). The present JRA differs from the other codes in that it applies the law of energy conservation to evaluate the load reduction as the reduction of design lateral force.

(8) Over strength Factor in Capacity Design

A designer must guarantee appropriate differences in the safety (hierarchy of strength) of non-linear members and ductile members in order to count on non-linear behavior of ductile members that the designer intends. In the design of a foundation, the design lateral force that a factor is multiplied by the ultimate lateral capacity of the pier is used. The factor is an over strength factor. The over strength factor is quantitatively related to the value of q in the ENV1998. The TNZ only refers to the capacity design principles in the NZS4203:1992; it does not specify a specific factor value. Because the present JRA provisions regarding the evaluation of the design lateral force used for the design of a foundation specifies that it must be 1.1 times the ultimate lateral capacity of the pier, it is generally understood that capacity design is introduced under present conditions.

6. SUMMARY AND FUTURE ISSUES

The authors have been studying the performance regulations to compare specifications for general bridge design and specifications for seismic design in codes in various countries. This report concludes with a summary of principal items and an outline of future issues.

(1) The design methods adopted by the codes surveyed include LRFD, LSD and WSD method. They should be unified in order to clarify the safety of a structure. The ISO code concerning design methods for structures is ISO2394, and the goal is the LSD or LRFD method of partial factors format that is stipulated in ISO2394.

(2) Under present conditions, stipulated contents that define the required performance for bridge design varies between the codes. The stipulated contents and required performance are hierarchical, and it is necessary to accompany debates concerning the extent to which they provide legal constraining by unifying them based on the triangle structure shown in Figure 1.

(3) As in the case of the AASHTO, it is important that in codes the effects of ductility and redundancy are represented by factors in some way in future bridge design.

(4) The code that refers to life cycle cost is only the Draft JRA. This concept is indispensable for codes that advocates performance based design. Design service life is clearly defined by the Draft EN. It is, therefore, necessary to clarify the grounds for setting the service life 100 years for bridges.

(5) The load categorization in the Draft EN differs from that in the other codes. In the Draft EN that is based on ISO2394 (1998) and is internationally unified. Future load categorization and combinations applied in bridge design should comply with the ISO code.

(6) As for foundation design, only the MFA approach of the Draft EN has considered partial factors for ground parameters. The relation between the estimation method of bearing capacity and resistant factor is detailed in the AASHTO. In the Draft EN (RFA approach) and present JRA, the bearing capacity with in-situ loading tests has been estimated, accounting for a resistant factor.

(7) The basis of seismic design is, in many cases, focussed on serviceability, safety and inspectability after earthquakes. As pointed out by Buckle (1996)[17], the future issues are to quantitatively represent this using engineering indices.

(8) Regarding importance categorization, the JRA reflects importance in differences in seismic performance, but in the other codes, it is linked to differences in the value of design seismic forces.

(9) Except for the TNZ, the other codes set two levels of earthquake motion. The JRA actually provides for the performance of two design levels while the other codes stipulate verifications against a large earthquake and practically eliminate verifications against a middle earthquake. A two-level design method is more rational than one-level. It is necessary to study the matter to determine whether it is necessary for practical designs accounting for the importance of bridges.

(10) Excluding the JRA, the others evaluate earthquake motion probabilistically in the sense that they all account for return period. ISO/CD3010 (1999)[21], going one step further, the uncertainty of earthquake motion based on probabilistic theory has been accounted as load factors. Because internationally, research has progressed from conventional MCE based deterministic risk analysis to probability analysis, the movement to introduce probability theory to the evaluation of design earthquake motion has gained momentum.

(11) At this time, only the TNZ has accounted for non-linearity in response spectrum. This method has been adopted in railway bridge codes in Japan. After the earthquakes in Turkey and Taiwan, the evaluation of active faults has become an important research theme. The Caltrans has stipulated that the spectrum be increased by a maximum of 20 % depending on the distance from a fault.

(12) The AASHTO and Draft EN have used load reduction factors (R value or q value) to reduce an elastic response value. A particular characteristics of the latter code is that an over strength factor used for capacity design has been represented as a function of the q value. The introduction of LSD method to seismic design is counted on to provide for the evaluation of load factors and evaluation method of rational over strength factors.

In conclusion, the authors wish to express their opinion regarding precautions that should be considered during revision of the present JRA. As stated at the beginning of this report, performance based regulations in future codes is essentially international trends. It is also necessary to achieve harmonization with international rules, and ISO2394 and ISO3010 codes must be considered as closely as possible. In this sense, an LSD method based

on partial factors format (or an LRFD method) including seismic design specifications should be introduced to the future JRA. On the other hand, differences in the safety level of structures and natural environments, and regional and national differences in the stock of design and construction technology, and the level of engineers are the matters that must be recognized as localities, and which differ from items that should be unified. The revision of the present JRA must be carried out to achieve performance based design and to consider international harmony and locality.

REFERENCES

1) AASHTO: AASHTO LRFD Bridge Design Specifications (2nd Edition), 1998.

2) CEN: Draft prEN1990: Basis of Design, 1999.12.

3) CEN: Preliminary Draft EN1997-1: Geotechnical Design, Part 1 General Rules, 1999.4.

4) CEN: ENV1998: Design provisions for earthquake resistance of structures, 1994

5) Caltrans: Memo to Designers 20-1/ Seismic Design Methodology, 1999.1.

6) Caltrans: Caltrans Bridge Design Specifications, 1995-.

7) Caltrans: Seismic Design Criteria (Version1.1), 1999.7.

8) Transit New Zealand: TNZ Bridge Manual for Design and Evaluation, 1995.

9) Japan Road Association: Draft of Specifications for Highway Bridges, Part 1: Common Rules, 200X.

10) Japan Road Association: Specifications for Highway Bridges, Part V: Seismic Design, 1996.

11) NKB: Structure for Building Regulations, NKB report No.34, 1978, 11.

12) PBSE Ad Hoc Committee: Force-Displacement Approach for Performance-based Seismic Engineering - Preliminary Guidelines -, SEAOC Blue Book Appendix I-PBSE Guidelines: Part 2, 1999.

13) ISO: ISO2394: 1998 General principles on reliability for structures, 1998.

14) U. S. Army Corps of Engineers, Department of the Army: Engineering and Design LIFE CYCLE DESIGN AND PERFORMANCE, CECW- ED Engineer Regulation 1110-2-8159, 1997.

15) AASHTO : Standard Specifications for Highway Bridges, 16th Edition, 1996.

16) NCHRP: Load Factor Design Criteria for Highway Structure Foundations- final report, NCHRP 24-4, 1991.

17) I. G. Buckle: Overview of Seismic Design Methods for Bridges in Different Countries and Future Directions, Proceedings of 11WCEE, 1996.

18) C. Rojahn et al.: Seismic Design Criteria for Bridges and Other Highway Structures, Technical Report NCEER -97-0002, 1997.

19) R. Park: New Zealand Perspectives on Seismic Design of Bridges, Proceedings of 11WCEE, 1996.

20) M. W. Stirling et al: Development of a New Seismic Hazard Model for New Zealand, bulletin of NZNSEE, 1999.

21) Railway Transportation Research Institute: Seismic Design for Railway Structures, 1999.

22) ISO: ISO/CD3010: 1999 Bases for design of structures- Seismic actions on structures, 1999.

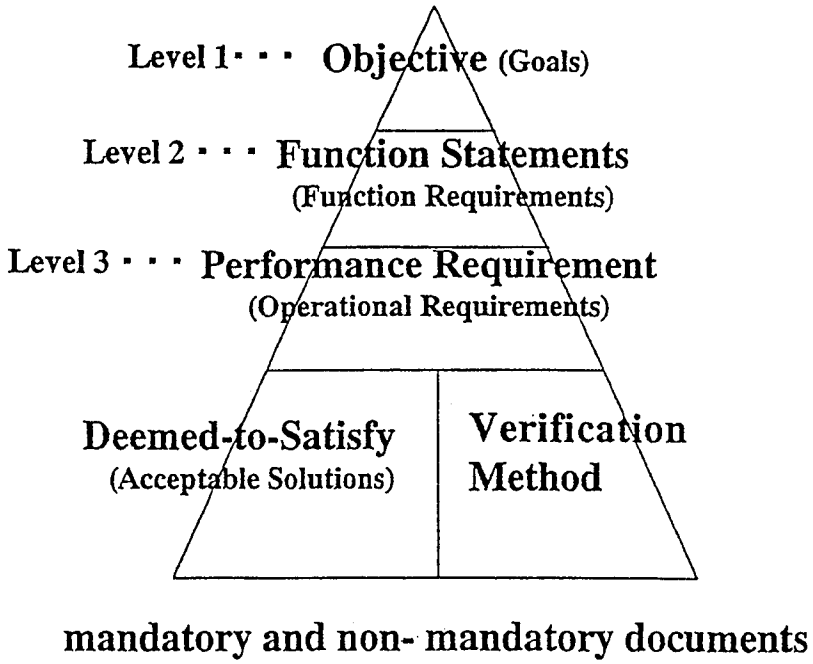

Figure 1 Nordic Five Level System

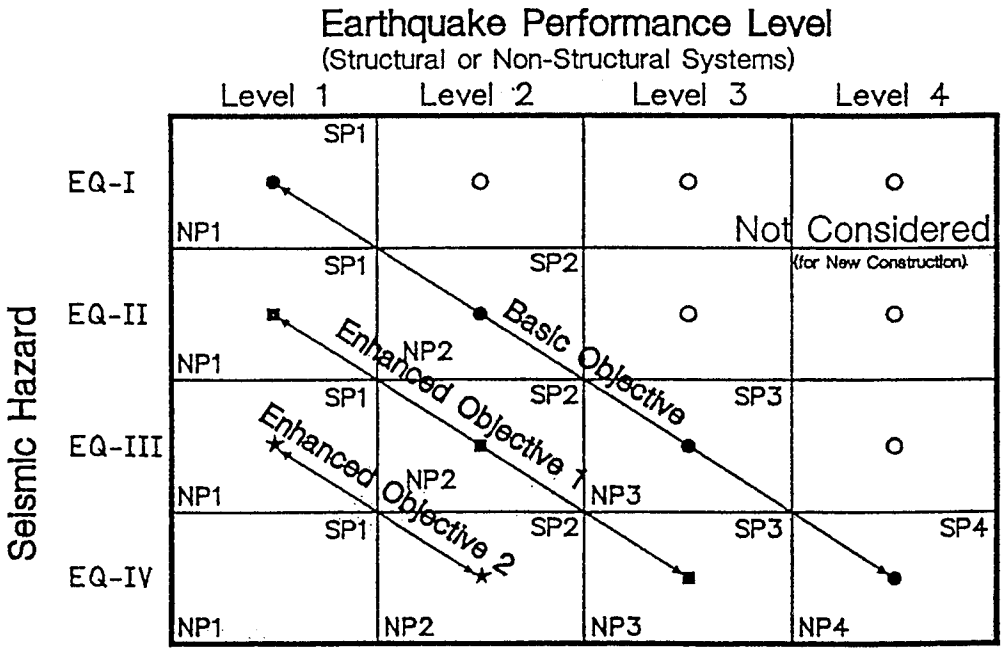

Figure 2 Typical Seismic Performance Objective for Buildings

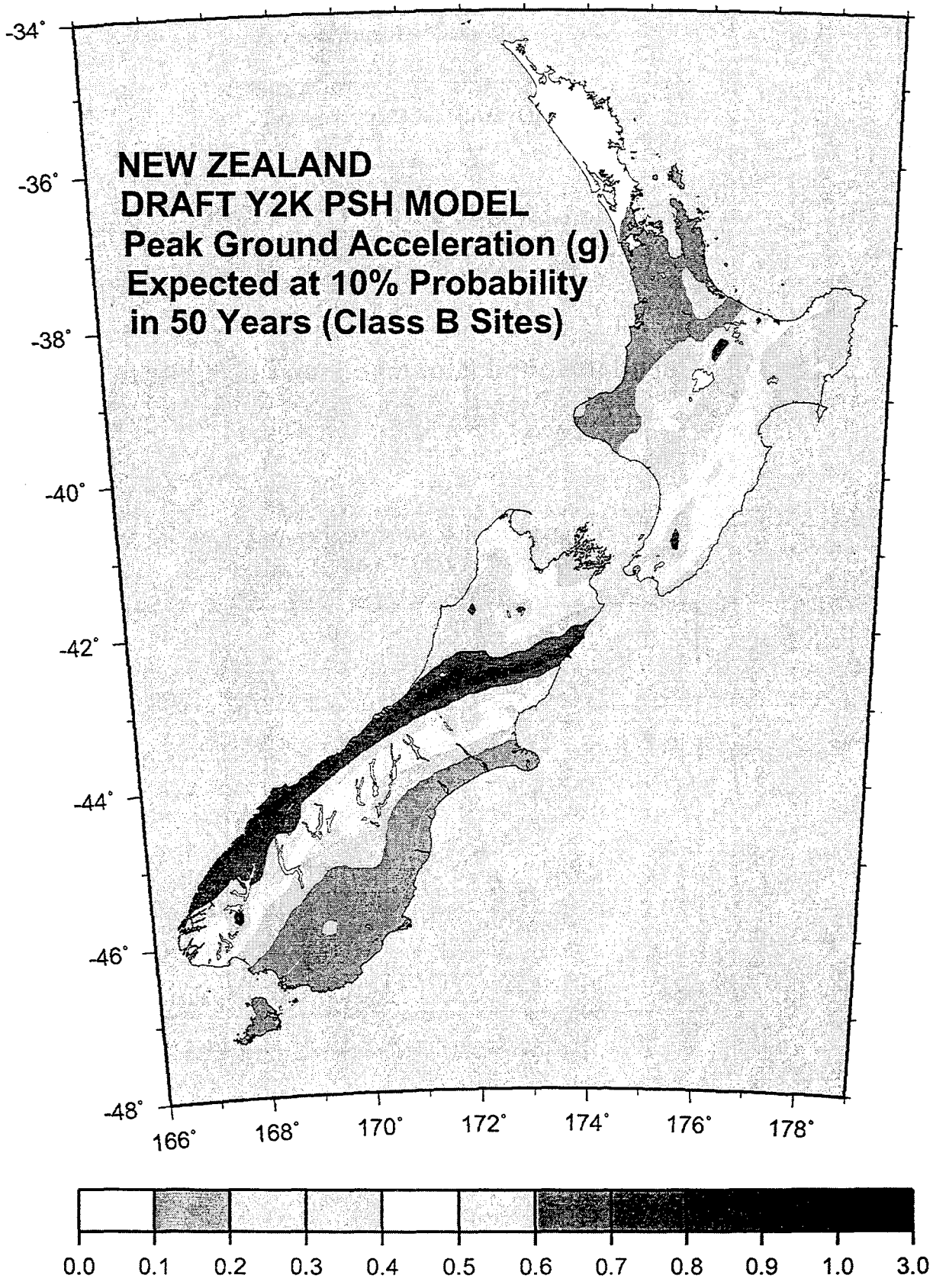

Figure 3 Distribution Map of Maximum Ground Acceleration
Based on Probabilistic Risk Analysis

Table 1 Comparison of Required Performance for Bridges in Various Countries

Region/Country	United States of America	European Union	State of California	Japan
a) Code	AASHTO LRFD Bridge Design Specifications (1998, 2nd Edition)[1] [AASHTO]	Draft prEN1990: Basis of Design (1999)[2] Preliminary Draft EN1997-1: Geotechnical Design, Part 1 General Rules (1999)[3] ENV1998: Design provisions for earthquake resistance of structures (1994)[4] [Draft EN]	Memo to Designers 20-1/ Seismic Design Methodology (1999)[5] Caltrans Bridge Design Specifications (1990)[6] Seismic Design Criteria, version1.1 (1999)[7] [Caltrans]	Design Specifications of Highway Bridges (200X) A: Common rules B: Seismic Design [Draft JRA]
b) Organization	American Association of State Highways and Transportation Officials	CEN (European Committee for Standardization)	State of California, Department of Transportation (Caltrans)	Ministry of Construction
c) Code Category	Optional domestic standard	Regional standard	Compulsory state standards	Compulsory domestic standard
d) Structure Category	Expressway Bridges	Civil engineering and building engineering	Highway bridges (B; applied to normal or standard bridges)	Highway bridges
e) Region	North America (United States, Canada)	Europe	State of California	Japan
f) Design Method	LRFD : Load Resistance Factor Design	LSD: Limit State Design	Service Load Design+Load Factor Design	Allowable stress design method
g) Required Performance	● Safety ● Serviceability ● Economy ● Bridge Aesthetics	The following two limit states are set. a) Ultimate limit state - Safety of a structure and its parts - Safety of people b) Service limit state - It must fulfill the roles of a structure (or part of a structure). - Comfort from perspective of people - External appearance	All bridges must be designed so that they can withstand deformation generated by design earthquakes. Structural members must be designed to guarantee adequate strength and ductility to avoid failure under MCE.	It must satisfy the following during the design service life: [1] Safety of a structure [2] Harmony with purpose of use [3] Economic effects [4] Harmony with the environment
h) Basis of Design (ductility)	Confirmation of ductility is important for a bridge structural system. The factor η_D is considered at strength limit state.	Structural systems that could possibly fail unexpectedly shall be avoided as much as possible.	The benefits of ductility and post-elastic strength are considered in design in order to satisfy performance with a small investment.	Ductility of a member is considered at the verification against a large earthquake.
(redundancy)	A multi-load path and continuous bridge structure should be used. The factor η_R is considered at strength limit state.	A structural form or design method that provides for resisting to accidental loss of its constituent elements or accidental damage to its parts shall be selected.	If practical, the entire bridge system must be provided with redundancy in the form of alternate routes for loads.	It is important to enhance the redundancy of a highway network.
(importance)	Bridges are classified as critical, essential or other for seismic design. The factor η_I is considered at strength limit state.	Importance is classified three classes in seismic design; upper of medium, medium, lower of medium.	By desired seismic performance level, two classes are set. ● Ordinary bridges (ordinary or not ordinary) ● Important bridges Still, the Caltrans is applied to ordinary bridges.	According to road category and bridge functions and structures, bridges are categorized two classes in seismic design. ・ bridges of standard importance (Class A bridge) ・ bridges of specially high importance (Class B bridge)
i) design service life	Not mentioned. Generally, considered at 100 years.	Example for design service life; ● general structures: 50 years ● bridges: 100 years	Same as the AASHTO.	An adequately long and appropriate design service life shall be established. The standard design service life may be 100 years.
j) life cycle cost	Not mentioned.	Not mentioned.	Same as the AASHTO.	The study of economic effects should be performed to determine structural form and materials, accounting for not only initial costs, but also approximate life cycle cost.
k) limit states	● Service Limit State ● Fatigue and Fracture Limit State ● Strength Limit State ● Extreme Event Limit State	● Ultimate Limit State ● Service Limit State	Collapse Limit State	Not mentioned.

l) basis of verification	$\Sigma \eta_i \gamma_i Q_i \leqq \phi R_n = R_f$ Where, $\eta_i = \eta_D \eta_R \eta_I \geqq 0.95$, or $\eta_i = 1/(\eta_D \eta_R \eta_I) \leqq 1.0$, γ_i : load factor, Q_i : load effects, ϕ : resistant factor, R_n : nominal resistant force, R_f : design resistant force	Ultimate limit state : Ed≦Rd Service limit state : Ed≦Cd Where, Ed : design value of load effects, Rd : design value of resistant force, Cd : limit value	$\Delta_D < \Delta_C$ Where: Δ_D: larger of the two displacements generated by an analysis of an independent system or of an overall system. Δ_C: displacement of the frame at the time that the first plastic hinge of a structure reaches the performance limit.	Verification of strength: Ed≦Rd Verification of displacement: Ed≦Cd Where, Ed : design value of load effects, Rd : design value of resistant force or strength, Cd : limit of deformation
m) load (classification)	● Permanent load ● Temporary load	● Permanent load ● Fluctuating load ● Accidental load ● Earthquake load	Same as the AASHTO.	● Primarily load (P) ● Secondly load (S) ● Special load corresponding to primarily load (PP) ● Special load (PA) ● Others
(live load)	Total weight (tf) : 18.1, 32.6, 13.6, 24.5	Not mentioned.	Same as the AASHTO.	Design vehicle load is 245 kN.
(wind load)	Design basic wind speed : 160km/h (=44m/s) Wind load : 0.0036Mpa (=360kgf/m^2· Columns and Arches), 0.0024Mpa (=240kgf/m^2· Girders)	Not mentioned.	Not mentioned.	Design basic wind speed : 40m/s (40 % exceedance of probability of 50 years) Wind load (kgf/m^2) : 150 (circle · ellipse), 300 (square)
(load combination and load factor)	It stipulates combinations of loads and load factors of 11 kinds for each of the following 4 limit states. a) Service Limit State I to III b) Fatigue and Fracture Limit State c) Strength Limit State I to V d) Extreme Event Limit State I to II	For ultimate limit state, ● Permanent design state (under service) ● Temporary design state (under construction and restoration) ● Accidental design state (under fire, explosion and collision) ● Earthquake design state (under earthquake)	18 of load combinations and load factors are set, under the following conditions. ● SLD(Service Load Design) (8 cases) ● LFD(Load Factor Design) (10 cases)	Main load combinations for superstructures: ● Primarily load ● Wind load Main load combinations for substructures: ● Primarily Load (excluding live load and impact) +earthquake
n) materials (concrete and metal)	Concrete mix characteristics by class and minimum mechanical properties of metal are stipulated.	Characteristic value of materials strength is defined as 5 % of material parameter fluctuating or 95 % of fractile value.	Same as the AASHTO.	As for concrete, minimum design basic strength is specified, to confirm durability of concrete.
(ground materials)	Not mentioned.	Characteristic value is selected as careful estimation of ground parameter at limit states.	Same as the AASHTO.	Characteristic value of ground parameters is mean value, excluding unusual data.
0) foundation design (verification method)	$Q_R = \phi \cdot Q_{ult}$ (pile foundation) Where, Q_R : design bearing capacity, ϕ : resistant factor, Q_{ult} : ultimate bearing capacity Still, ϕ is applied at strength limit state. At other limit states, ϕ = 1.0.	● MFA approach : $R_d = R(X_R/\gamma_M, a_{nor})$ ● RFA approach : $R_d = R(X_R, a_{nor})/\gamma_R/\xi$ Where, R_d : design resistant force, X_R : characteristic value of ground parameter, γ_M : material factor, γ_R : resistant factor, a_{nor} : nominal value, ξ : correlation ratio	$Q_R = \phi \cdot Q_{ult}$ Where, Q_R : design bearing capacity, ϕ : reduction factor, Q_{ult} : ultimate bearing capcity Still, ϕ is applied to load factor design.	$Ra = \gamma \cdot Ru/n$ (pile foundation) Where, Ra : allowable bearing capacity, γ : correction factor of safety factor, difference from estimation method of ultimate bearing capacity, Ru : ultimate bearing capacity, n : safety factor
(partial factor of ground parameter)	Not mentioned.	Partial factor: γ_M ● For tan ϕ, c': 1.25 ● For cu, qu, 1.40	Not mentioned.	Not mentioned.
(estimation method of bearing capacity and partial factor; for example driven pile)	Resistant factor $\phi \cdot \lambda_V$ ● Empirical estimation method : ϕ =0.45～ 0.70 ● In-situ loading test : ϕ =0.80 ● Analysis of wave motion : ϕ =0.65 Where, λ_V : factor of construction management and evaluation method of bearing capacity (=0.8～1.0)	Resistant factor γ_R : 1.30 Still, correlation ratio varies 1.4 ～ 1.0 according to the frequency of in-situ loading tests.	ϕ : reduction factor (LFD) ● Group 1～6 (not including earthquake) : 0.75 ● Group7 (earthquake) : 1.00	Correction factor of safety factor γ (To account for difference from estimation method of ultimate bearing capacity) ● Case of empirical method : 1.0 ● Case of in-situ loading tests : 1.2
(flood)	Risk of flood : return period of 100 years Pressure of flow : P(MPa)=5.14*10^{-4}C$_D$V^2 Factor : 5.14*10^{-4}C$_D$(tf · s/m^3)=0.04 (circle), 0.07 (square)	Not mentioned.	Not mentioned.	Risk of flood : return period of 100～200 years Pressure of flow : p(f/m^2)=P/A=K · V^2 Resistant factor K=0.04 (circle), 0.07 (square)

Table 2 Comparison of Seismic Performance for Bridges in Various Countries

Region/Country	United States of America	European Union	New Zealand	Japan
a) Code	AASHTO LRFD Bridge Design Specifications (1998, 2nd Edition)[1] [AASHTO]	ENV1998: Design provisions for earthquake resistance of structures (1994)[4] Part1-1: General rules Part2: Bridges [ENV1998]	TNZ Bridge Manual for Design and Evaluation (1995)[8] [TNZ]	Design Specifications of Highway Bridges (200X) Seismic Design [Draft JRA]
b) Organization	American Association of State Highways and Transportation Officials	CEN (European Committee for Standardization)	Transit New Zealand	Ministry of Construction
c) Code Category	Optional domestic standard	Regional standard	Compulsory domestic standards	Compulsory domestic standard
d) Structure Category	Expressway Bridges	Civil engineering and building engineering	Highway bridges	Highway bridges
e) Region	North America (United States, Canada)	Europe	New Zealand	Japan
f) Design Method	LRFD : Load Resistance Factor Design	LSD: Limit State Design	Service Load Design+Load Factor Design	Allowable stress design method
g) Basis of Seismic Design	For medium earthquakes: it shall remain undamaged by resisting within the elastic range of members. For large earthquakes: all or parts of a bridge shall not fail. Locations forecast to be damaged shall be ones whose damage can be detected, can be easily approached, and can be easily inspected and repaired.	The design philosophy requires general requirements that emergency vehicles can drive on the bridge with stipulated reliability after design earthquake.	It must be guaranteed that bridges can safely hold its traffic functions after an earthquake. To permit this, bridges are classified according to their importance, and the risk factor related to the earthquake return period (value of R) are assigned to a bridge.	According to road category, bridge functions and structures, bridges are categorized as bridges of standard importance (Class A bridge) and bridges of specially high importance (Class B bridge), and the goal is to guarantee the seismic performance required for each class.
h) Seismic performance (limit states)	Extreme event limit state: The survival of the structure of a bridge shall be guaranteed against earthquake, flood, or impact by a ship.	[1] Minimization of damage = Service limit state (evaluated by displacement) [2] Unseating prevention provisions = Ultimate limit state (evaluated by bearing capacity and ductility)	[1] Emergency vehicles can cross a bridge even if it is damaged by an earthquake. [2] After an earthquake smaller than the earthquake hypothesized by design, it must only be slightly damaged and not obstruct traffic. [3] After an earthquake larger than the earthquake hypothesized by design, the failure of a bridge must be prevented even if the damage is widespread. And emergency vehicles must be enabled to cross a bridge after emergency measures and long term measures must be possible.	[1] Service limit state after an earthquake. To be sound (Class A and B bridges) [2] Restoration limit state after an earthqua To permit limited damage (Class B bridge) [3] Safety limit state after an earthquake To prevent fatal damage (Class A bridge)
i) Importance	Bridges are classified as critical, essential or other for seismic design. It is treated as one of the factors that is part of the load conversion constant ηi in the equation used to calculate the design load Q ($Q = \Sigma \eta i \gamma i Qi$), and the factor ηi for the importance is stipulated at (= 0.95 to 1.05)	Three kinds of importance factor γi is the following. [1] Greater than average (γi= 1.30) [2] Average (γi= 1.00) [3] Less than average (γi=0.70) γi is multiplied by design seismic load AED.	Bridges are categorized in 3 R-values, according to their importance that is determined by traffic volume, road functions, and availability of an alternate route. The following are return period indicated by the R-values. R = 1.3: return period of 1,000 years R = 1.15; return period of 700 years R = 1.0: return period of 450 years	There are Class A bridges and Class B bridges Differences in importance of bridges must be reflected in differences in the seismic performance and in differences in the safety factor for type I and type II earthquake motion of each bridge.
j) Ground Classification	The soil types are categorized as four types: to set a site constant (S) at I, II, III and IV.	There are 3 subsoil classes: A, B, and C.	Three categories are set: Site subsoil category (a) ~ (c). This site category reflects the three yield seismic spectra in part n) in this Table (parameter: displacement ductility factor μ).	Three categories: I, II, and III
k) Zone Classification	It is categorized in four categories from 1 to 4 according to the A-value (acceleration coefficient).	Design ground accelerations ag for each nation are set in the NAD (National application document) of each nation.	It is set from 0.6 to 1.2 as zone factor Z.	The modification factor Cz is provided at values of 1.0, 0.85, and 0.7 according to the 3 zone categories.

l) Design Seismic Force	Medium earthquake (design earthquake): Earthquake with return period of 475 years (design service life: 50 years, exceedance probability 10%) Large earthquake: Earthquake longer than the return period of the design earthquake. An earthquake with return period of approximately 2,500 years is called the maximum probable earthquake.	Medium earthquake: Earthquake motion during appropriate return period is evaluated. Large earthquake: Return period of 475 years.	Return period of 450 years.	[1] Earthquake motion with a high probability of occurring during a bridge's service life. [2] Large earthquake motion with a low probability of occurring during a bridge's service life. (Type I and Type II) Type I earthquake hypothesizes a plate boundary earthquake such as the Kanto Earthquake of 1923. Type II earthquake hypothesizes an inland intraplate earthquake such as the Hyogo-ken Nanbu Earthquake of 1995. There is no concept of return period.
m) Elastic Response Spectrum	CSM = 1.2 AS/Tm$^{2/3}$ ≦2.5A Where: C_{SM}: elastic response spectrum A: A-value S: site factor Tm: natural period of the mth mode (sec)	Se(T) = (ag, S, T, η, β0, k1, k2) Where: Se(T): elastic response spectrum ag: design ground acceleration accounting for reference return period S: ground parameter T: natural period of a single degree of freedom system η: modification factor for damping β0: response multiplier of a structure k1, k2: correction factor of spectrum curve	Maximum lateral force V: V = CμZRSpW ≧ 0.05 W Where: Cμ: basic value of acceleration coefficient Z: zone factor (0.6 to 1.2) R: risk factor (1.0 to 1.3) Sp: structural performance coefficient (0.67 to 0.9) W: dead load	[1] Earthquake motion with a high probability of occurring during a bridge's service life. Kh = Czkho [2] Large earthquake motion with a low probability of occurring during a bridge's service life. (Type I and Type II) Khc = Czkhco
n) Load Reduction Factor	The R-value (response modification factor) (1.5 to 5.0) is selected, according to a substructure type and a bridge's importance.	The q-value (behavior factor) (1.0 to 3.5) is selected, according to a substructure type and required ductility of members.	The value of displacement ductility factor μ that is the basis for the basic value (Cμ) of the non-linear response spectrum shown in part m) in this Table is set from 1 to 6.	The design lateral force coefficient khc is reduced as the equivalent lateral force coefficient khe according to the allowable ductility factor μa of a bridge pier. khe = khc /[2μa-1]$^{1/2}$
o) Over Strength Factor	Concrete members: 1.3 times nominal bearing capacity Steel members: 1.25 times nominal bearing capacity	Plastic moment factor (yo): yo = 0.7 + 0.2 q (when q = 3.5, yo = 1.4) Where: q: behavior factor	It is based on Capacity Design Principles in NZS4203.	In the case of foundation design, the design lateral force is set as 1.1 times the ultimate lateral capacity of the pier that a foundation supports.

Recommended Changes to the AASHTO Specifications for the Seismic Design of Highway Bridges (NCHRP Project 12-49)

by

Ian M. Friedland, P.E.[1] and Ronald L. Mayes[2]

ABSTRACT

Under the AASHTO-sponsored National Cooperative Highway Research Program, the ATC/MCEER Joint Venture is conducting a project to develop new specifications for the seismic design of highway bridges. These new specifications will be recommended for incorporation into the AASHTO *LRFD Bridge Design Specifications*, most likely in early 2001. They are expected to be performance-based and will address state-of-the-art aspects of highway bridge seismic design, including the representation of seismic hazard, design and performance criteria, analysis methods, steel and concrete superstructure and substructure design and detailing, and foundation design. This paper presents an overview of some of the major philosophical and technical changes being incorporated into the new provisions.

KEYWORDS: analysis; bridge design; detailing; performance criteria; specifications

1.0 INTRODUCTION

In August of 1998, a joint venture of the Applied Technology Council (ATC) and the Multidisciplinary Center for Earthquake Engineering Research (MCEER) initiated work on a project to develop the next generation of seismic design specifications for highway bridges in the United States. The project is sponsored by the American Association of State Highway and Transportation Officials (AASHTO) and is being conducted by the National Cooperative Highway Research Program (NCHRP) of the Transportation Research Board. NCHRP Project 12-49, "Comprehensive Specifications for the Seismic Design of Bridges," will result in the development of specifications and commentary which are expected to be incorporated into the AASHTO *LRFD Bridge Design Specifications*. These will be supplemented by a series of design examples demonstrating the application of key features of the new specifications.

The target date for completion of the project is February 2001, at which time the recommended specifications and commentary will be assessed by the AASHTO Highway Subcommittee on Bridges and Structures, with a decision regarding adoption of these provisions to be made in May of 2001. During the course of the project, three drafts of specifications and commentary will be produced and reviewed, prior to completion and submission of the final draft to AASHTO.

The new specifications are expected to incorporate all current and state-of-the-art practices in bridge seismic design, and will be performance-based. They will address the representation of seismic hazard, design and performance criteria, analysis methods, steel and concrete superstructure and substructure design and detailing, foundation design, and soil behavior and properties. The specifications are also intended to address the differences in seismic hazard, soils, and bridge construction types found throughout the United States, and therefore are to be national in scope.

These new specifications will be a marked departure from the design philosophy, approach, and requirements currently in use in the United States. This paper provides a brief overview and discussion of some of these new approaches and procedures.

[1] Applied Technology Council, Washington, D.C. 20004, ifriedland@atcouncil.org
[2] Bridge Engineering Consultant, Moraga, California 94556, ronald.mayes@worldnet.att.net

2.0 PERFORMANCE CRITERIA

A performance-based design criteria will be included in the new specifications and commentary. Specifically, the project will recommend adoption of a dual-level performance criteria, and two levels of performance objectives. The current criteria are described in Table 1.

The recommended performance objective is now totally performance based and each State determines the desired performance objective for any particular bridge. This is a change from current AASHTO definitions of "other," "critical" and "essential" bridges for defining performance levels. The R-Factors are approximate at this time and are provided to indicate their order of magnitude and relativity. Note that in the final specification, the R-Factors will be removed from this table.

The upper level earthquake considered in these provisions is designated the Maximum Considered Earthquake or MCE. In general, the MCE ground motions have a probability of exceedance of 3% in 75 years, which is an approximate return period of 2500 years. However, MCE ground motions are bounded deterministically to values lower than 2500 year ground motions adjacent to highly active faults.

The current AASHTO specifications have a 500 ft span length limitation. The new specifications will proposed that this be removed, and a review conducted to determine what, if any, limitations should be imposed on the use of the criteria once its development is more complete.

3.0 SERVICE AND DAMAGE LEVELS

3.1 Service Levels

Two definitions of service levels have been included in the first draft of the new specifications:

Service Level – Immediate (R = 0.67 to 2) – Full access to normal traffic should be expected following the earthquake; an inspection of the bridge should be conducted as soon as possible to ensure that there is no significant damage.

Service Level – Significant Disruption (R = 6 to 8) – Limited access (reduced lanes, light emergency traffic) may be possible after shoring, however the bridge may eventually need to be replaced.

An R-Factor of 0.80 is approximately first yield of reinforcement in a reinforced concrete column whereas an R-Factor of 1.0 is when the ultimate moment capacity is achieved and occurs when all the tensile reinforcement is at yield in a reinforced concrete column or the full section has reached yield in a steel column.

It is also recommended that all single- and multi-column bents use the same R-Factor; this is a significant departure from the current AASHTO provisions which specify different R-Factors for single- and multi-column bent.

3.2 Damage Levels

The current draft of the specifications also contain three damage level definitions:

No Damage – Evidence of movement may be present but there is no notable damage.

Minimal Damage – Some visible signs of damage. Minor inelastic response may occur, but post-earthquake damage is limited to narrow flexural cracking in concrete. Permanent deformations are not apparent, and any repairs could be made under non-emergency conditions with the exception of deck joints. Specific criteria for geometric and structural constraints are provided.

Significant (Major) Damage – Considerable to total loss of operations. Although there is no collapse, permanent offsets may occur and damage consisting of cracking, reinforcement yield, and major spalling of concrete may require closure to repair. Partial or complete replacement may be required in some cases. Again, specific criteria for geometric and structural constraints at various service levels are provided.

An attempt at providing more specific criteria for concrete columns is also being made, as shown in Table 2. These results are then used in conjunction with a pushover analysis to determine displacement (drift) limit states. In columns (2) to (4) of the table, nominal strain limits are given. From these values normalized plastic curvatures ($\phi_p D$) are computed and presented in column (5). In providing these values, it is assumed that the code specified detailing provisions for transverse reinforcement are used. Then, by assuming the equivalent (rectangular) plastic hinge length is 45% of the member diameter/width, it is possible to calculate a nominal plastic hinge rotational capacity as given in column (6). From this, dependable (conservative) values are set for code specified rotational limits in column (7). These specified values may be used in lieu of a more precise analysis.

Alternately, a moment-curvature analysis based on strain compatibility and nonlinear stress-strain relations can be used to determine plastic limit states. From this, a rational analysis is used to establish the rotational capacity of plastic hinges.

4.0 GEOMETRIC AND STRUCTURAL CONSTRAINTS

In the initial phases of this project, an attempt was made to develop a set of geotechnical performance objectives that would be similar to those being developed for concrete columns. A two-day workshop was held to review initial draft proposals and to refine recommended criteria and approaches. The consensus of the workshop was that the amount of acceptable foundation and abutment movement should be related to geometric and structural constraints by bridge type, rather than explicit values on foundation movements. As a result, the first draft specification proposes constraints that would implicitly provide foundation design limits for seismic loads to meet the various performance objectives. Since this is the first time an attempt has been made at developing these constraints, preliminary specified values have been considered, but should only be considered as approximate or order of magnitude. Additional work will be required to refine and finalize these constraints.

Geometric constraints generally relate to the usability of the bridge by traffic passing on or under it. Therefore, such constraints will usually apply to permanent displacements that occur as a result of the earthquake. The ability to repair (or the desire not to be required to repair) such displacements should be considered when establishing displacement capacities. When immediate service is desired, permanent displacements should be small or non-existent, and should be at levels that are within accepted tolerances for normal highway operations. When limited service is acceptable, the geometric constraints may be relaxed. These may be governed by the geometry or types of vehicles that will be using the bridge after an earthquake, and by the ability of these vehicles to pass through the geometric obstruction. Alternately, a jurisdiction may simply wish to limit displacements to a multiple of those allowed for immediate service. In the case of a significant disruption, post-earthquake use of the bridge is not guaranteed and therefore no geometric constraints would be required to achieve these goals. However, because life safety is at the heart of this performance level, jurisdictions should consider establishing some geometric displacement limits.

Structural constraints on displacements can be based on the requirements of a number of structural elements and can result from either transient displacements due to ground shaking or permanent displacements resulting from ground movement due to faulting, seismically induced settlements, lateral spreading, and so forth. Structural damage to foundation elements is limited primarily to piles since footings and pile caps are usually capacity protected. Although pile damage can often be avoided at a reasonable cost when piles are capacity protected, requiring this for all piles could lead to overly conservative, and thus expensive, foundation designs. Therefore, it may be desirable to establish some lateral displacement limits for piles based on a limited amount of structural

damage that is unlikely to compromise the structural integrity of the bridge. These limits will be based on the type and size of the piling, and the nature of the soil near the head of the pile. Caltrans has attempted to establish such limits for its standard piling based on physical testing. Other jurisdictions may attempt to do the same, or they may perform more complex analytical studies to establish similar displacement, capacity, and stiffness limits.

5.0 DESIGN-EVENT RETURN PERIODS

Current AASHTO specifications considered a single-level earthquake hazard design event, based on a 500-year return period. At the time this event was incorporated into the AASHTO specifications, it was the only event readily available as a design value for seismic hazard representation in the United States.

For this project, it has been recommended that a 2,500-year return period, which provides an equivalent 3% probability of exceedance in 75 years, be used as the upper level design event. A lower level event with an approximate 100-year return period, which would be based on a 50% probability of exceedence in 75 years, has also been recommended. In brief, the reasons for these recommended return periods include:

- For a frequent or expected earthquake (50% probability of exceedance in 75 years), this is the design level under which the bridge should remain essentially elastic (R = 1.0). This will result in a performance that is equivalent to an elastic (no damage) design for a 100 year flood, and is less conservative but similar to an elastic design for a 100 mph base wind design.

- For a rare earthquake (3% probability of exceedance in 75 years), this design level is recommended in order to assure that a "no collapse" performance criteria for a Maximum Considered Earthquake (MCE) is satisfied. Since seismic loads increase so significantly compared to wind and flood loads as the return period increases, earthquake design needs to consider longer return period design events.

A critical earthquake design issue in preventing collapse of a bridge is to ensure that deck displacements and hence seat widths for the girders can accommodate displacements from events that have occurred and can be realistically expected to reoccur. A return period of 500 years does not come close to capturing the force and displacement levels that may have occurred during earthquakes in the New Madrid region (1811-1812) and Charleston, South Carolina (1886). A return period of the order of 2500 years is required to obtain realistic displacement levels that may have occurred during these earthquakes.

It is noted that the MCE ground motion maps incorporate deterministic bounds on the ground motions adjacent to highly active faults. These bounds are currently applicable in California, along a portion of the California-Nevada border, in coastal Oregon and Washington, and in parts of Alaska and Hawaii. These deterministic bounds are applied so that the ground motions do not become unreasonably large in comparison to the ground motions that could be produced by maximum magnitude earthquake on the faults. Deterministic bounds are defined as 150% of the median estimates of ground motions calculated using appropriate attenuation relationships, and assuming the occurrence of a maximum magnitude earthquake on the fault. However, they are limited to not less than 1.5 g for the short-period spectral acceleration plateau and 0.6g for 1.0-second spectral accelerations.

6.0 SHAPE AND CONSTRUCTION OF THE DESIGN RESPONSE SPECTRA

The long period portion of the current AASHTO acceleration response spectra is governed by the spectrum shape and the soil factor, and it decays as 1/T2/3. There was considerable "massaging" of the factors that affect the long period portion of the current AASHTO spectra in order to produce a level of approximately 50% conservatism in the design spectra when compared to the ground motion response spectra beyond 1 second period. The reasons given for this level of conservatism included:

(a) The fundamental period of a bridge increases as (1) the column height increases, (2) the span length increases, and (3) the number of columns per bent decreases. Hence, the longer the period, the more likely that high ductility requirements will be concentrated in a few columns.

(b) Instability of a bridge is more of a problem as the period increases.

Analysis of ground motion data indicates that the acceleration spectra generally decreases with period in the long period range as 1/T or more rapidly. The shape of the long period portion of the recommended response spectra is less conservative than the current spectral shape and it is recommended that the shape of the spectra decay as 1/T.

For periods longer than about 3 seconds, depending on the seismic environment, use of the 1/T relationship for spectral acceleration may be conservative because the ground motions may be approaching the constant spectral displacement region for which spectral accelerations decay as 1/T2. Either the 1/T relationship may be conservatively used or a site-specific study conducted to determine an appropriate long-period spectral decay.

The U.S. Geological Survey (USGS) has prepared MCE ground motion maps for spectral accelerations at 0.2 and 1.0 second periods. In addition, the 0.2-second and 1.0 second spectral accelerations can be obtained at other probability levels from a CD-ROM published by the USGS. Response spectra can be constructed using the spectral accelerations at these two periods and the spectrum construction method illustrated in the following figure. This spectrum construction is denoted herein as the "two-point" method because it involves intersecting the constant spectral acceleration plateau passing through 0.2 second, with the long-period branch of the spectrum that declines as 1/T and passes through 1.0-second spectral acceleration. This is also the spectrum construction method that has been adopted in the 1997 NEHRP Provisions, will continue in the 2000 NEHRP Provisions, and is proposed for the 2000 International Building Code.

7.0 DESIGN PROCEDURES AND RESPONSE-MODIFICATION FACTORS

The current draft of the specifications provide for three levels of design and analysis procedures in the moderate to high-seismic zones. This is in addition to the current no seismic or low-level minimum requirements, which are defined as Level 0:

Level 0 – These are the current AASHTO Zone 1 provisions, which require minimum seat widths and specified design forces for fixed bearings of 10% dead load for Zone 1A and 25% dead load for Zone 1B.

Level 1 – These requires no formal seismic analysis but requires the use of capacity design principles and minimum design details.

Level 2A – This is a one-step design procedure based on a new analysis method referred to as the "capacity spectrum method" and is applicable to very regular bridges. This method has been incorporated in some of the retrofit guidelines for buildings and provides the designer with the ability to assess whether or not a bridge designed for all non-seismic loads has sufficient strength and displacement capacity to resist the seismic loads.

Level 2B – This is a one-step design procedure based on an elastic (cracked section properties) analysis using either the Uniform Load or Multimode method of analysis. The analysis is performed for the governing design spectra (either 100 year or 2500 year event) and the use of a conservative response modification factor (R-factor) (i.e. 5 rather than 8 for 2500 year event for columns). The

analysis will determine the moment demand at all plastic hinge locations in the column. Capacity design principles govern foundation and column shear design. If sacrificial elements are part of the design (i.e. shear keys) they must be sized to resist the 100 year forces and the bridge must be capable of resisting the 2500 year forces without the sacrificial elements (i.e. two analyses are required if sacrificial elements exist in a bridge).

Level 3 – This is a two-step design procedure using an elastic (cracked section properties) analysis with the multimode method of analysis for the governing design spectra (100 year/1.0 or 2500 year/8) to perform preliminary sizing of the moment capacity of the columns. Capacity design principles govern foundation and column shear design. A pushover analysis is then performed. The designer can change the design forces in the columns provided they are not lowered below those required by the 100 year event and they satisfy the displacement demand.

The attempt in this project is to make the Level 1 approach applicable to as wide a range of bridges as possible. Level 2A will be applicable to very regular bridges that can be idealized as Single-Degree-of-Freedom systems, until more development work is done to extend the method. It is also recommended that for Levels 2B and 3, a quick assessment as to which of the two earthquake levels govern column flexural moment capacity is quick and easy to perform and is worthwhile.

The recommendation is to have both a one-step, two-level (Level 2) design/analysis procedure, and a two-step, two-level design/analysis procedure (Level 3). The one-step Level 2B procedure would be consistent with the current design requirements but would have more conservative R-factors than the two-step procedure (e.g. 4 vs. 6 or 5 vs. 8). It also would use the more conservative design values resulting from the 100 year or 2500 year events. The Level 2B procedure, which is the same as current AASHTO requirements, in summary would be as follows:

a) Perform an analysis using the appropriate 100 year or 2500 year design spectra. Two analyses may be necessary if sacrificial elements such as shear keys are part of the design.

b) Divide by specified (conservative) R-factors and design the components using capacity design principles.

The Level 3 procedure would include a) and b) but the R-Factors would be approximately 150% higher than the one-step (Level 2) procedure. The second essential step in Level 3 is to perform a "pushover analysis." The objective of the pushover analysis would be to ensure that the maximum plastic rotation and drift limits for the various materials and components are satisfied, and that the displacement capacity of each column exceeds the displacement demand by a factor of approximately 1.5. It is anticipated that an upper and lower bound pushover analysis would be performed using upper and lower bound soil properties. Furthermore a designer could change column design forces as part of this process provided they were never less than those required by the 100 year event.

Since the response spectra for the various return periods (2500 year and 100 year) are quickly and easily available from the USGS on the Internet, it will be relatively easy to determine which one would give the highest forces for determining the column flexural strength

It is also proposed to use the same R-factors for both single and multi-column bents. This is contrary to the current AASHTO specifications and arises from studies performed during the development of recommendations for Caltrans. Initial research conducted for Caltrans actually recommended higher R-factors for single-column bents than for multi-column bents,

which is the opposite of current AASHTO requirements. These recommendations arose out of the relative displacement ductilities that could be achieved from each system, given constant curvature ductilities in the plastic hinge zones. This is true because the displacement at first yield in a multi-column system with "pinned" column bases comprises a larger percentage of the ultimate displacement than does first yield displacement in a single column system. Therefore, the single column system should be more ductile.

The order of magnitude of R-factors being considered is given in Table 3. These will be further refined and evaluated in subsequent work on the project. The numbers provided show the relativity between the one-step (Level 2) and two-step (Level 3) procedures and between the critical and regular bridges. It should be noted that the impact of the R-ractors on the design of a column is not as important as the minimum longitudinal steel requirements and the P-Δ limits, and that R-factors higher than 6 virtually never govern. It is therefore likely that the R-factor for single and multi-column bents will not exceed 6.

8.0 LEVEL 1, NO SEISMIC ANALYSIS DESIGN REQUIREMENTS

The "no seismic analysis" design procedures are an extremely important part of the recommendations because they will apply as widely as possible in Zone 2. The purpose of the provisions is to provide the bridge designer the ability to design structures without the need to undertake dynamic analyses. The bridge elements are designed in accordance with the usual provisions, but the primary seismic resisting elements are detailed for seismic resistance.

There are capacity design requirements for shear reinforcement and confining reinforcement at the plastic hinge locations in columns. There are also capacity design requirements for detailing the connection to pile and column caps. There are no additional design requirements for the abutments or foundations with one exception – integral abutments need to be designed for passive pressure. The premise for this is based on the parameter study which demonstrated that a foundation designed using a factor of safety of 3 will perform well in these lower zones assuming the column connection to the pile cap is based on capacity design principles. These procedures will also be permitted for use in sites with liquefaction potential, will but require some additional considerations if the predominant moment magnitude, M_B , for the site exceeds 6.

The limitations on the applicability of the provisions initiated with the definition of a "regular bridge" as contained in the current AASHTO seismic design provisions. Additional limits were added based on engineering judgment, and these need to be evaluated in future studies. The limits as they currently exist consider (a) regularity, (b) axial load limits, (c) load path and force sharing, and (d) continuity. Table 4 provides the current definition of a "regular" bridge.

Span-to-span continuity must be provided by one or more of the following means:

- A superstructure that is monolithic with the substructure
- A superstructure seated on bearings that has transverse restraint
- Simply supported girders seated on bearings must be fixed at one support end, and transversely restrained at the other
- A superstructure supported on isolation bearings that act in all directions that accommodate displacements

9.0 OTHER ISSUES

9.1 Foundations

Provisions for spread footings, driven piles, drilled shafts (or cast-in-drilled-hole piles), and abutments are being significantly improved over similar provisions in current AASHTO specifications. These are, in large part, based on a number of advances made through research programs sponsored recently by the Federal

Highway Administration, Caltrans, and others. For abutments, explicit recognition of sacrificial elements is being provided, including knock-off back walls and other similar fuse elements.

9.2 Steel Superstructures

The current AASHTO specifications have minimal requirements for steel bridges. As a result, a substantial effort is being made in this project to develop appropriate provisions for steel bridges. A first draft of such provisions has been prepared, and will be reviewed during a workshop to be held in the summer of 2000 by an invited select group of consulting engineers, transportation agency staff, and researchers, all experts in seismic design and steel bridges. It is anticipated that this workshop will provide the necessary framework to resolve outstanding issues, and that a consensus will be reached regarding the appropriate scope of provisions for the seismic design of steel bridges.

9.3 Special Considerations Regarding Seismic and Geotechnical Hazards

A number of special provisions are being included to address important considerations in seismic hazard. Included in these are specifications related to vertical accelerations and their impacts on bridge performance, and near fault (and so-called "fling") effects. A significant amount of work is also being done to address the issues of soil liquefaction and lateral spreading, especially as this relates to the infrequent but potentially large upper-level 2500-year event.

10. CONCLUSIONS

The new specifications for the seismic design of highway bridges being developed under NCHRP Project 12-49 will be a significant departure from the current procedures and requirements found in AASHTO specifications. Work on NCHRP Project 12-49 is expected to be completed in the spring of 2001, and the AASHTO Highway Subcommittee on Bridges and Structures will then review the provisions resulting from the project, with possible adoption by AASHTO in late 2001.

Table 1 – Performance Objectives

		Performance Objective	
Probability of Exceedance (Approximate Return Period) For Design Ground Motions		**Life Safety**	**Operational**
Rare Earthquake 3% in 75 years (approx. 2500 Year)	**Service** *R Factor* *Damage*	**Significant Disruption** *R = 6 to 8* *Significant*	**Immediate** *R = 2* *Minimal*
Frequent Earthquake 50% in 75 Years (approx. 100 Year)	**Service** *R Factor* *Damage*	**Immediate** *R = 1.0* *Minimal*	**Immediate** *R = 0.8* *None*

Table 2 – Example of Qualitative Specified Column Performance Requirements

Service Level	**Concrete Strains**		**Steel Strain**	**Plastic Curvature** $\phi_p D$	**Plastic Hinge Rotations** θ_p **(rad)**	
	Cover	**Core**			**Nominal Capacity**	**Dependable (Code) Capacity**
(1)	(2)	(3)	(4)	(5)	(6)	(7)
Fully functional	.003	0.002	0.002	-	-	-
Life safety	spalled	0.045	0.045*	0.09*	0.04*	0.03*

* May be governed by low cycle fatigue of the longitudinal reinforcement

Table 3 – Typical Base Response Modification Factors

Substructure Element	Importance Category				
	Other		Essential		Critical
	One Step Design	Two Step Design	One Step Design	Two Step Design	Two Step Design
Wall Piers-larger dimension	2	3	1.5	2	1.5
Columns – Single and Multiple Ductile Detailing	4 to 5	6 to 8	2	3	2
Columns – Singe and Multiple Minimum Detailing (see Comments below)	3	4	1.5	2	1.5
Pile Bents and Drilled Shafts – Vertical Piles – above ground	4	6	2	3	2
Pile Bents and Drilled Shafts – in ground	2	3	1.0	1.5	1.0
Pile Bents – Batter Piles	3	5	1.5	2	1.5
All Elements – 150 year EQ	NA	1.5 (1 for wall piers)	NA	1	.75

Table 4 – Parameter Definitions for "Regular" Bridges

Parameter	Value				
Number of Spans	2	3	4	5	6
Maximum subtended angle for curved bridge	45	45	45	45	45
Maximum span length ratio, from span to span	3	2	2	1.5	1.5
Maximum bent/pier stiffness ratio from span to span excluding abutments	-	4	4	3	2

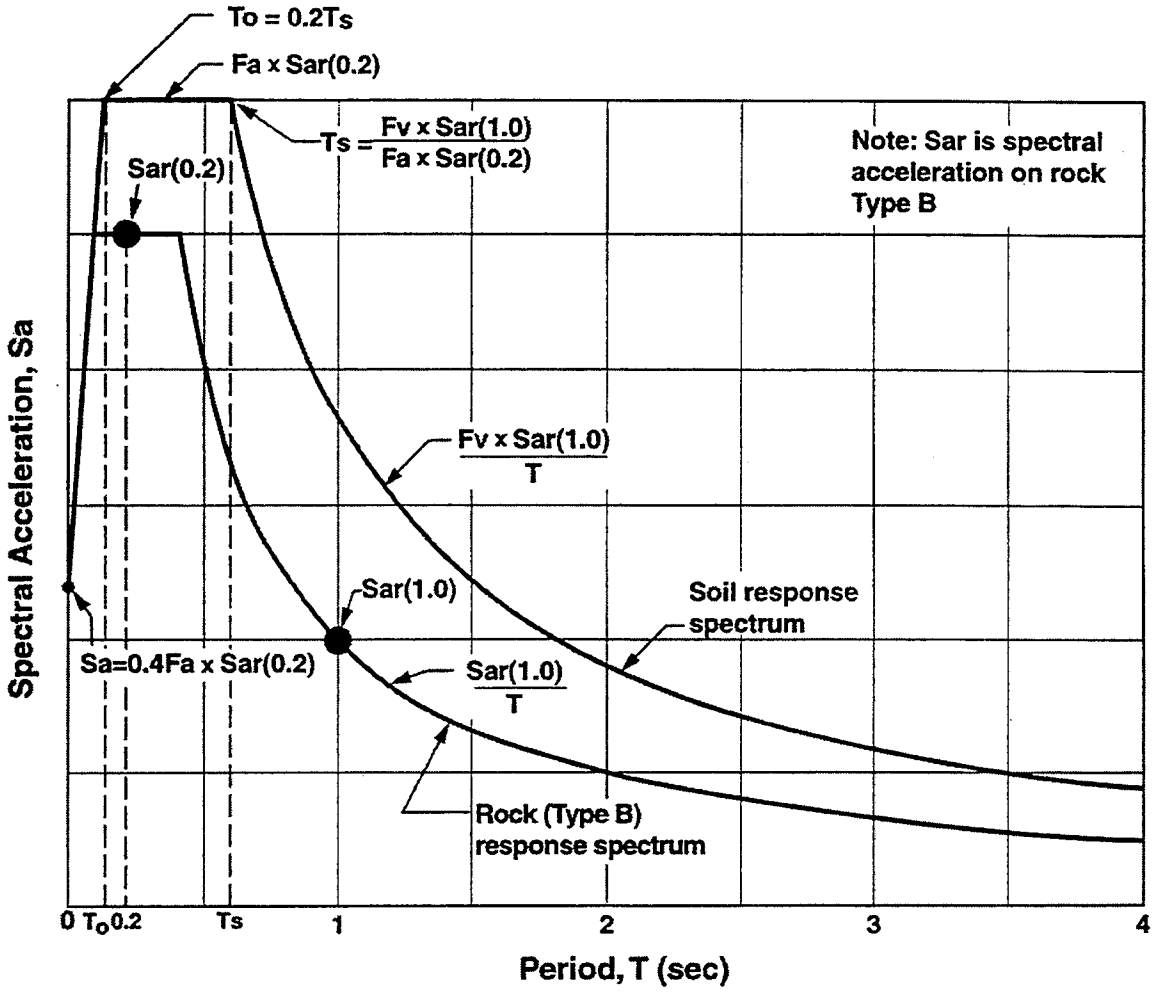

Figure 1 – Response Spectrum Construction

EARTHQUAKE RESISTANT DESIGN OF PORT FACILITIES

by

Takashi NAGAO[1], Atsushi NOZU[2]

ABSTRACT

This paper presents the earthquake resistant design way of port facilities in Japan. Technical Standard of Port and Harbour Facilities was first established in 1973, and has been revised 3 times so far. Having experienced the 1995 Hyogoken-Nambu earthquake, significant revision has been made on the outcome of the recent research.

KEY WORDS : Earthquake Resistant Design
Port Facility
Design Code

1. HISTRY OF REVISIONS OF DESIGN CODES

Having been established in 1951, the Port and Harbour Law in Japan has been revised many times so far. The important revision in view of the design of port and harbour facilities was made in 1974, in which it was noticed that the port and harbour facilities must be constructed, maintained and rehabilitated in accordance with the Technical Standard of Port and Harbour Facilities. In 1975 the engineering requirement was established as the Ordinance of the Ministry of Transport and it was prescribed in the ordinance that the facilities in ports and harbours must be stable against the loads such as earthquake loads, dead weights, wave forces, impacts due to ships and so on.

The Technical Standard of Port and Harbour Facilities was established in 1973 as the order of the Director General of Bureau of the Ports and Harbours, Ministry of Transport, in which the details on earthquake resistant design, such as design procedures, factor of safety and allowable stresses, were specified.

In 1979 the Technical Standard of Port and Harbour Facilities and its Commentary was compiled under the supervision of the Bureau of the Ports and Harbours, Ministry of Transport, and has been revised in every ten years after the 1979 edition.

Seismic stability of the port and harbour structures was to be examined only by the pseudo-static method in the 1979 edition and 1989 edition of the Technical Standards. The pseudo-static method is called the seismic coefficient method, and the earthquake load is obtained by the multiplication of the design seismic coefficient and the vertical load. The design seismic coefficient is obtained by the multiplication of the regional seismic coefficient, the factor for subsoil condition, and the importance factor. Those three factors were classified into three groups respectively, with the regional seismic coefficient ranging from 0.05 to 0.15, the factor for subsoil condition ranging from 0.8 to 1.2, and the importance factor ranging from 0.5 to 1.5. The resultant value, the design seismic coefficient, was rounded off to the nearest 0.05 or 0.00. As to the design of the reinforced concrete structures, allowable stress method was applied.

1) Chief, Geotechnical Earthquake Engineering Laboratory, Structural Engineering Division, Port and Harbour Research Institute, Ministry of Transport
2) Senior Research Engineer, Structural Engineering Division, Port and Harbour Research Institute, Ministry of Transport

Significant modification had not been made as to the earthquake resistant design procedures ever since the first edition thus far, however, the procedure of assessing the liquefaction potential was not stated in the 1973 edition, and was firstly stated in the 1979 edition.

In 1999, the order of the Director General of Bureau of the Ports and Harbours was repealed for variety of reasons, and the Ministry of Transport notified the new detailed Technical Standard. In the new Technical Standard, some significant revisions have been made based on the outcome of the recent research after the 1995 Hyogoken-Nambu earthquake. Those are summarized as follows :

(1) Principles of design

The concept of performance-based design has been introduced. The principles are:

① All the structures must be stable against the level 1 earthquake motions whose return periods are about 75 years.

②High seismic resistant facilities should keep the required performance against the level 2 earthquake motions whose return periods are over some hundred years.

(2) Seismic coefficient method

① The regional seismic coefficient and the importance factor have been modified, while the factor for subsoil condition has remained as it was. The number of regional groups for the regional seismic coefficient has come up to five, coefficient ranging from 0.08 to 0.15. Range of the importance factor has become from 0.8 to 1.5. In addition, the resultant value has been considered down to three decimal places.

② The equation for the apparent seismic coefficient, which is the seismic coefficient used for the calculation of earth pressure below groundwater level, has been modified.

③ Consideration of the dynamic water pressures acting at the front of vertical walls has been stated.

(3) Assess of earthquake-resistant performance

Assessing way of the earthquake-resistant performance in view of level 2 earthquake motions has been introduced.

(4) Assess of liquefaction potential

Assessing way of liquefaction potential has been modified.

(5) Design method of open piled piers

Modified pseudo-static design method, which is called the modified seismic coefficient method, has been introduced for the design of open piled piers.

(6) Design method of reinforced concrete structures

Limit state design method has been introduced, and safety factors for the design have been established.

The history of revisions of design codes is summarized in Table 1.

Table.1 Summary of history of revisions of design codes

	1973	1979	1989	1999
Earthquake design level	One level			Two levels
Seismic coefficient method	○			○ modified
Performance-based design principles	—			○
Assess of liquefaction potential	—	○		○ modified
Design of open piled piers	Seismic coefficient method			Modified seismic coefficient method
Design of reinforced concrete structure	Allowable stress method			Limit state design method

2. SUMMARY OF THE UP-TO-DATE DESIGN CODE

(1) Evaluation of Seismic Performance

(a) General

In the design of port facilities, the effect of earthquakes should be taken into account so that they possess appropriate amount of seismic resistance.

Explanation

At Kobe Port, the type of structures were quite uniform during the 1995 Hyogoken-Nanbu earthquake. This is why almost all of the structures suffered similar damage. If the type of structures had been more diverse, the amount of damage for each structure should not have been uniform because their response characteristics should have been different. Based on this experience, in the choice of the structural type of port facilities, it is recommended to adopt various type of structures as long as possible.

(b) Seismic performance requirement for port facilities.

(1) Port facilities should sustain their structural stability and maintain their functions for a level-1 ground motion, which by definition occurs with high probability during the facility's duration.
(2) High seismic resistant facilities, which are especially important and require high seismic resistance, are allowed to suffer only slight damage for a level-2 ground motion, which by definition occurs with relatively low probability during the facility's duration but which is very intense. In other words, high seismic resistant facilities should be prepared for rapid restoration to sustain their intended functions after a level-2 ground motion.

Explanation

In the seismic design of port structures, a level 1 ground motion, which has a return period of 75 years and a level 2 ground motion, which is a ground motion due to intra-plate earthquake with a return period of more than several hundred years or a ground motion due to a subduction zone earthquake, should be taken into account.

High seismic resistant facilities include high seismic resistant quay walls, which are specially designed for the transportation of emergency cargo or for the maintenance of economic or social activity just after the earthquake, and the revetments of the disaster prevention base, which is intended to keep the safety of the citizen just after the earthquake.

While 'to maintain their functions' means to sustain their structural stability, 'to sustain intended functions' means to suffer only a slight damage and to be prepared for a immediate restoration.

(c) Pseudo-static method

(1) In principle, seismic load for port structures with relatively short natural period and relatively high damping factor should be designated as a design seismic coefficient for pseudo-static approach. In this case, the design seismic coefficient should be used. Seismic inertia force should be the larger of the following (a) and (b) and should be assumed to act on the gravity center of the structure.
 (a) (Seismic force)=
 (Self weight) × (Seismic coefficient)
 (b) (Seismic force)=(Self weight + Surcharge) × (Seismic coefficient)
(2) For structures for which pseudo-static method is not applied, seismic load should be designated in an appropriate manner, taking into account the characteristics of the structure.

Explanation

(1) For quay walls and other similar port structures, pseudo-static method is applied as for other wide range of structures. Because natural periods of these structures are generally shorter than predominant periods of ground motions, the response of these structures during earthquake are similar to those of rigid bodies on a rigid table.

(2) Because the seismic load is assumed to act as a static load in the pseudo-static method, it is necessary to take into account the difference between the real phenomena and the assumptions in the method. To appreciate this difference, the safety factor and the allowable stress for dynamic loads are different from those for static load.

(3) It is preferable to examine the seismic resistance of those structures which has a longer natural period compared to predominant periods of ground motion or for which the distribution of acceleration is not uniform along the height.

(d) Earthquake response analysis

If the facility is especially important or the type of structure is rare and there is no similar conventional structure, it is recommended that it's seismic resistance should be examined by using earthquake response analysis together with conventional pseudo-static method or seismic deformation method.

Explanation

Recently, new type of port facilities or extremely large port facilities have been designed and constructed. On the other hand, it is sometimes required to construct port structures at a site with a poor subsoil conditions. Furthermore, it is requested to examine whether a high seismic resistant facility will maintain their functions after a near-source ground motion such as the ground motion at Kobe Port during the 1995 Hyogoken-Nanbu earthquake. It is recommended to examine earthquake resistance of structures by conducting earthquake response analysis to understand the performance of structures during earthquake more precisely if the type of structure is new or if the structure is especially important.

(e) Seismic deformation method

Because the deformation of line structures etc. buried in the soil during earthquake is controlled by surrounding soil, it is preferable that such structures should be designed by using seismic deformation method.

(2) Earthquake Load

(a) Design Seismic coefficient

(1) For pseudo-static design of port structures, horizontal design seismic coefficient should be determined with following equation.

Seismic coefficient =Regional seismic coefficient × Factor for subsoil condition × Importance factor (1)

Horizontal design seismic coefficient should be rounded to obtain two places of decimals. Standard values for regional seismic coefficient are:

Region A: 0.15

Nemuro, Kushiro, Tokachi and Hidaka districts of Hokkaido, Saitama, Chiba, Tokyo (Except for Hachijo and Ogasawara Islands), Kanagawa, Yamanashi, Shizuoka, Aichi, Gifu, Fukui, Shiga, Mie, Nara, Wakayama, Osaka and Hyogo.

Region B: 0.13

Pacific side of Aomori, Iwate, Miyagi, Fukushima, Ibaragi, Tochigi, Gunma, Nagano, Kyoto, Kochi and Tokushima.

Region C: 0.12

Iburi, Oshima and Hiyama districts of Hokkaido, Aomori (except for Pacific side), Akita, Yamagata, Niigata, Toyama, Ishikawa, Tottori, Hiroshima, Ehime, Oita, Miyazaki, Amami Islands of Kagoshima and Kumamoto.

Region D: 0.11

Abashiri, Goshi, Ishikari, Sorachi, Rumoi and Kamikawa districts of Hokkaido, Okayama, Tottori, Kagawa, Nagasaki (except for Goto, Iki and Tsushima Islands), Saga, Kagoshima (except for Amami Islands) and Okinawa (except for Daito Islands).

Region E: 0.08

Sorachi district of Hokkaido, Hachijo and Ogasawara Islands of Tokyo, Yamaguchi, Fukuoka, Goto, Iki and Tsushima Islands of Nagasaki and Daito Islands of Okinawa.

Factor for subsoil condition should be determined as shown in Table 2 and 3.

Table 2 Factor for subsoil condition

Classification	1st kind	2nd kind	3rd kind
Factor	0.8	1.0	1.2

Table 3 Classification of subsoil

Thickness of Quaternary Deposit	Gravel	Sand or clay	Soft ground
less than 5m	1st	1st	2nd
5-25m	1st	2nd	3rd
more than 25m	2nd	3rd	3rd

Importance factor should be determined according to Table 4.

Table 4 Importance factor

Category	Special	A	B	C
Factor	1.5	1.2	1.0	0.8

Category Special: The structure has significant characteristics described by items (1)-(4) of category A.
Category A: (1) If the structure is damaged by an earthquake, a large number of human life and property will possibly be lost. (2) If the structure is damaged by an earthquake, economic or social activity of the region will be severely suffered. (3) The structure will perform an important role in the reconstruction work of the region after the earthquake. (4) The structure handles a hazardous or a dangerous object and it is anticipated that the damage of the structure will cause a great loss of human life or property. (5) If the structure is damaged, it is supposed that the repair work is considerably difficult.
Category B: The structure does not belong to categories Special, A nor C.
Category C: The structure does not belong category Special nor A and is easy to repair or, even if the structure is damaged by an earthquake, the effect on economic or social activity is small.

(2) If vertical seismic coefficient is required in the pseudo-static design, the vertical seismic coefficient should be determined appropriately, taking into account the characteristics of structure and subsoil.

Explanation

(1) To determine importance factor of the structure, it is necessary to consider not only the purpose, type or size of the structure but also social or economic aspects of the structure. Following factors also should be taken into account.
a) The extent of damage in the future earthquake, the difficulty of restoration work or the residual strength after the earthquake.
b) The cargo-handling capacity of the other facilities of the same port.
Therefore, it is possible to use different importance factors for the structures for the same cargo in the same port when desired.

(2) For structures other than high seismic resistant quay walls, the upper limit of design seismic coefficient should be 0.25 for several reasons. First, in the past, the upper limit of design seismic coefficient was 0.25. Second, there has been no port structures with design seismic coefficient of 0.25 that suffered significant damage. Thirdly, high seismic resistant quay wall has been constructed in many ports.

(3) Seismic Design of High Seismic Resistant Quaywalls

(a) Evaluation of seismic performance of high seismic resistant facilities

(1) In the design process of high seismic resistant facilities, it is requested that their seismic performance should be evaluated for a level-2 ground motion to assure that their seismic resistance is satisfactory.
(2) Seismic performance should be evaluated by appropriately modeling the soil and the structure of the facility, with a method which is appropriate for the particular type of the structure.

Ground motion which is used for the evaluation of seismic performance should be determined with response analysis of the ground in principle.

Explanation

(1) Evaluation of the residual deformation of high seismic resistant facilities, which is based on a earthquake response analysis, is required for the purpose of verifying that they will sustain their intended functions after a level-2 ground motion. The reason is that, for the examination of the stability of the structure or the soil for a large ground motion such as a level-2 ground motion, conventional pseudo-static method is not sufficient.
(2) The judgement whether the high seismic resistant facilities will sustain their intended functions based on the results of earthquake response analysis should be based on the combined considerations on the stability of the structure after the earthquake, the functions and the difficulty of restoration work. Although the allowable residual deformation should be defined for this judgement, it is not easy to specify the allowable deformation at the present state of knowledge. In the case of the 1995 Hyogoken-Nanbu earthquake, some of the caisson quaywalls with a normalized deformation (lateral residual displacement / height of the quaywall) of over 10-20% was temporary repaired and offered for immediate use just after the earthquake.

(b) Design Seismic coefficient of high seismic resistance facilities

(1) When pseudo-static design is applied to high seismic resistant quaywalls, the design seismic coefficient should be determined by a global judgement base on the seismic coefficient determined by Eq.(1) with importance factor 1.5, by following equations for which peak ground acceleration should be calculated with ground response analysis for level-2 ground motion, and by other appropriate methods.

1. If α is smaller than or equal to 200Gal,
$K_h = \alpha / g$ (2)
2. If α is larger than 200Gal,
$K_h = (1/3) \times (\alpha / g)^{(1/3)}$ (3)

Here, K_h is horizontal seismic coefficient, α is peak ground acceleration at free surface and g is the acceleration of gravity.

Explanations

(1) When the design seismic coefficient can be accurately determined by investigating regional seismic activity, characteristics of ground motion, site response, etc., it is preferable to use this design seismic coefficient instead of the value designated here. For example, when the design ground motion is determined based on the information regarding regional seismic activities or based on strong ground motion observations or when seismic response analysis of the structure is conducted, design seismic coefficient can be determined based on these results.

(2) In the design of high seismic resistant facilities, target earthquake has to be selected from earthquakes including hypothetical earthquake in the disaster prevention plan set by local government.

(3) One way of calculating peak ground acceleration at free surface is to use multiple reflection model for the response analysis of the ground.

(4) From the experience of significant damage at Kobe Port during the 1995 Hyogoken-Nanbu earthquake, minimum design seismic coefficient for high seismic resistant facilities should be 0.25 if the site is in a near-source region.

(5) When it is desired, seismic resistant qua walls should be designed for level-2 ground motion with a method other than pseudo-static method such as earthquake response analysis. In this case, it is necessary to make sure that seismic resistant facilities will sustain their structural stability for level-1 ground motion.

NIST Research on Structural Performance of Housing Systems

by

Fahim Sadek[1] and Michael A. Riley[2]

ABSTRACT

An outline of NIST research in the area of structural performance of housing systems is presented in this paper. The performance of wood-frame houses in past earthquakes and hurricanes is summarized, and the state-of-the-art in experimental and analytical research conducted on wood-frame components and systems is presented. While significant progress has been made in analytical modeling and testing of shear walls and diaphragms, only limited progress has been made on the testing and modeling of complete houses and inter-component connections. Ongoing and future research efforts at NIST are introduced, and the program objective and technical approach are presented. Finally, a brief discussion of current experimental work, along with some initial results, is presented and discussed.

KEYWORDS: Housing systems; Inter-component connections, Nailed connections; Roof trusses; Shear walls; Wood-frame construction.

1 INTRODUCTION

The majority of residential construction in the United States is wood-frame buildings. These buildings perform well under gravity loads, but considerable damage has been observed in such structures after significant earthquakes and major hurricanes. To enhance the resistance of houses to natural disasters and to reduce the risk to life and property, the behavior of wood-frame buildings subjected to such loads needs to be understood.

Wood-frame buildings are constructed from several diaphragms such as walls, floors, and roofs; joined by inter-component connections such as nails, anchor bolts, metal plates, and other propriety connectors. The performance of these buildings is influenced by the behavior of their individual components and connections. Therefore, an understanding of the behavior of the different structural components and connections is essential to accurately predict the performance of a housing unit under different types of loading.

Structural performance parameters can be reliably predicted by using accurate analytical tools to model the behavior of a complete structure. Multiple simulations can be used to study the influence of different parameters on the structural performance, and they will be more cost-effective than experimental testing. Experiments, however, are still required to validate and refine the analytical tools. The result promises improved design standards that enable construction of buildings that resist earthquake and wind loads without significant damage or collapse.

Analysis of the structural response of wood-frame building components subjected to lateral loads is a difficult task due to several sources of nonlinearity, the complex nature of the connections, and the wide variability in material properties and construction techniques. Since shear walls are the most important elements for resisting lateral loads, they have been experimentally and analytically studied since the early 1970s. Simplified methods of wall analysis and finite element models have been developed to predict the behavior of the walls under static and dynamic lateral loading. The development of tools for analyzing complete wood-frame houses

[1] Research Associate, Southern Methodist University, Dallas, TX 75275; on Assignment, National Institute of Standards and Technology, 100 Bureau Dr., Stop 8611, Gaithersburg, MD 20899-8611

[2] Research Structural Engineer, National Institute of Standards and Technology, 100 Bureau Dr., Stop 8611, Gaithersburg, MD 20899-8611

started in the mid-eighties. Few investigators attempted to analyze the different structural components and the inter-component connections in an assembled model.

The scope of NIST research will include developing experimentally validated, three-dimensional, analytical models to predict the performance of housing units during natural disasters. This model will be used to establish performance characteristics of conventional and innovative housing systems. Testing will be conducted on components for which modeling and performance data are lacking, such as inter-component connections.

The following sections summarize the structural performance of wood-frame houses in past earthquakes and hurricanes, and present the state-of-the-art in experimental and analytical research conducted on wood-frame components and systems. A summary of the NIST research is presented, followed by a description of ongoing experimental work on the performance of inter-component connections.

2 PERFORMANCE OF HOUSES IN PAST EARTHQUAKES AND HURRICANES

Although recent earthquakes and hurricanes in the United States have resulted in few casualties, they have caused substantial damage, significant economic loss, and disruption of social and commercial activities. The performance of residential housing during such events has shown that wood-frame construction generally meets the life safety objective. Many houses, however, have experienced structural and nonstructural damage that prevented immediate occupancy, and resulted in expensive repairs.

Post-earthquake investigations have indicated that much of the seismic damage can be attributed to construction flaws or inadequate quality assurance, including missing fasteners, overdriving of nails, improper placement of anchor bolts, and misplaced nails. The preference for more open interior spaces, hillside homes, soft stories due to garage openings, and more irregularly shaped structures may also be contributing factors. Poor soil conditions (liquefaction, excessive settlement) or location (building on a hillside) has been also cited as a cause of damage. Houses built in accordance with seismic codes were generally found to perform well.

In general, poor seismic performance of wood-frame houses has been observed when the house did not respond as a unit, due to discontinuous load paths. Common practices which resulted in the lack of integrity included:

- Insufficient or poorly detailed inter-component connections (anchorage to foundation, wall-to-wall connections, wall-to-roof/floor connections).
- Inadequate bracing (cripple walls, total absence of shear walls, large wall openings, inadequate let-in bracing).
- Component separation (masonry fireplaces and chimneys, masonry veneers, porch roofs and other overhangs, different house sections).
- Non-uniform or irregular distribution of stiffness, due to irregular plans and elevations (split level house, setbacks), which leads to torsional movements.
- Poor detailing or quality of construction.
- Lack of continuous load path from roof to foundation.

In past hurricanes, the main cause of severe damage to wood-frame houses has been roof damage, due to inadequate anchorage of the roof framing to the wall, damage to the roof covering, and loss of roof sheathing. Foundation failure and inadequate anchorage of the structure to the foundation have also caused failures. Similar to earthquake performance, issues such as continuous load path and structural integrity are crucial for hurricane resistance, particularly because water damage from roof failures is a major contributor toward the economic losses. In addition to water damage, the internal pressure in a house is increased due to breaches in the building envelope from missiles, thereby contributing to roof failures. Properly installed plywood boards over windows or storm shutters, doors, and garage doors can alleviate this problem, but improperly installed boards and shutters can

contribute to the damage from wind-borne debris.

3 SUMMARY OF PAST EXPERIMENTAL AND ANALYTICAL STUDIES

NIST has published a comprehensive state-of-the-art report on the structural performance of single-family, wood-frame housing (Yancey et al., 1998), which includes a detailed literature review of experimental and analytical studies conducted on complete houses, in addition to wood subassemblies, such as shear wall diaphragms, and various connections. The following presents a summary of such experimental and analytical studies. Additional details may be found in the NIST report (Yancey et al., 1998).

3.1 Experimental Studies

Shear wall behavior under lateral loads has been the focus of a significant amount of studies. Tests have been conducted under monotonic, cyclic, and dynamic loads to investigate the response characteristics of the walls. Several additional studies have tested the sheathing-to-framing connections to determine their response characteristics, determine their resistance, and provide data for analytical modeling; since they have been shown to be a critical element in the wall performance.

A relatively small number of full-scale houses have been tested. Tests have been performed on single- and two-story houses under field and laboratory conditions. In addition, very few experimental studies have been conducted on inter-component connections. Testing of those connections is important, since they are key elements for the wood-frame building to act in an integrated fashion and to provide data for computer modeling.

3.2 Analytical Studies

Analyzing the structural components of a wood-frame building subjected to lateral loads is essential to understand their performance during natural disasters. Since shear walls are the most important elements in resisting lateral loads, they have been extensively studied by several investigators since the early 1970s. Simplified analysis methods and finite element models were developed to predict the nonlinear behavior of the walls under static lateral loading. A few researchers also attempted to predict the dynamic behavior of the walls subjected to earthquake ground motion. Analytical models have also been developed for floors and roofs under uniform pressure.

The development of analytical tools for analyzing complete wood-frame houses started in the mid 1980s. This work included analyzing the different structural components, as well as the inter-component connections in an assembled model. Comparisons with experimental studies were performed to assess the validity of the proposed models and analyses. To date, only limited research has been directed toward the analysis of a complete building or the inter-component connections subjected to different loading combinations.

4 OVERVIEW OF NIST RESEARCH

NIST has developed a research plan to improve the state-of-the-art of wood-frame building analysis tools, based on the current state of research and knowledge presented in the previous two sections. Figure 1 shows a block diagram of the technical approach of the research.

The objective of the NIST project is to develop the metrics and predictive tools necessary for evaluating the structural performance of housing systems during natural disasters, including earthquakes and strong winds. Expected outcomes of this program include enhanced disaster resistance and construction cost reduction by the housing industry.

Using validated three-dimensional finite element models of typical systems, structural performance criteria for complete houses will be developed. The analytical model will include the interaction of the various diaphragms such as shear walls, floors, and roof, as well as inter-component connections. A library of the models for the different diaphragms and connections will be built. Data from prior testing conducted

on wood diaphragms will be used in the model. As mentioned in the previous section, there is minimal data on the performance of inter-component connections, such as those between wall and roof, wall and foundations, and intersecting walls, therefore, this program will test the various connections under monotonic and cyclic loads to characterize their performance and provide the necessary data for modeling.

The developed models will be used not only for conventional wood-frame houses, but also for innovative materials and systems such as structural insulated panels (SIPs), insulated concrete forms (ICFs), and other systems that may be suggested in the future. Testing will be conducted on new systems when modeling data are missing, and the models of their components and connections will be added to the element library.

Once the three-dimensional model is assembled, sensitivity studies will be conducted to establish the baseline performance of conventional houses and the performance of innovative systems. The studies will use deterministic and stochastic procedures to investigate the influence of various parameters on the building performance. Those parameters include building configuration, connection type, loading type, uncertainties in loading, and variations in material and connection properties. The sensitivity studies should help establish performance criteria, determine failure mechanisms, determine probability of failure under a given loading, and identify weak links and over-designed structural components. Comparisons between the performance of conventional and innovative systems will be conducted to assess the merits of each system.

5 CURRENT EXPERIMENTS ON FULL-SCALE WOOD-FRAMES

NIST is conducting experiments to obtain missing data on the performance of inter-component connections. The first phase of experiments will test wall-to-roof component connections similar to those shown in Figure 2. The objectives of this testing are to: 1) provide data for computer modeling, 2) determine the level of uncertainty in their characteristics, and 3) understand their performance, since they have been identified as a weak link in many structural failures. This phase will include various types of wall-to-roof connections such as toe-nailed; and hurricane and seismic, ties and clips.

Prior to the component connection tests, eight full-scale specimens similar to those in Figure 3 are currently being tested. The objectives of this testing are to:

1) understand the in-situ behavior of the wall-to-roof connections in the structure,
2) determine the displacements and forces that will be applied to component connection tests,
3) validate the three-dimensional models of houses, and
4) explore possible failure mechanisms.

The specimens (see Figure 3) represent a center cut through a simple wood-frame house. Each specimen consists of two shear walls of 1.22 m (4 ft) length and 2.44 m (8 ft) height, supporting four roof trusses spanning 4.88 m (16 ft). The shear walls and roof trusses were purchased prefabricated from a local supplier. The shear walls are supported on steel beams rigidly attached to the strong floor. The framing for each shear wall consists of double top plates, single bottom plate, and vertical studs spaced 0.40 m (16 in) on center. All framing members are constructed from 38 x 89 mm (2x4 nominal) spruce-pine-fir, grade No. 2 lumber. 11 mm (7/16 in) thick oriented strand board (OSB) panels are used as outer wall sheathing and are connected to the framing using 38 mm (1.5 in) cement coated staples spaced 76 mm (3 in) on perimeter and 152 mm (6 in) on intermediate studs.

Roof trusses, with a top chord slope of 4:12, are placed 0.40 m (16 in) apart. All truss elements are 38 x 89 mm (2x4 nominal) members. 11 mm (7/16 in) thick OSB sheathing is attached to the trusses using 8d-common nails spaced 0.1 m (4 in). Only toe nailed connections and hurricane clips are being used in these tests to tie the roof trusses to the shear walls.

The specimens will be subjected to monotonic uplift, monotonic lateral, and cyclic lateral loads. Uplift loads are applied using a vertical actuator with a steel loading tree that distributes the load

to ten points on the roof sheathing. Uplift point loads on the roof sheathing are further distributed using 2 x 8 lumber members. Lateral loads will be applied using a horizontal actuator through steel pipes that are connected to the roof trusses at their center of mass. Both the vertical and horizontal actuators push against a steel reaction frame. The specimens are highly instrumented with displacement transducers and load cells to gain maximum information on the response characteristics of the specimens.

At the time of this writing, only two specimens have been tested under uplift load simulating wind effects on structures. The first specimen used a toe-nailed connection (two 16d-common nails) to tie the bottom chord of the roof trusses to the walls, while the second used a stronger hurricane clip to connect the bottom chord of the trusses to the upper plate of the walls' top plate.

For the toe-nailed connection, the specimen failed at one side (south end) on the connection between the trusses and the top plate of the south wall. The failure mode is characterized as nail withdrawal from the top plate which resulted in separation in the bottom wood fibers of the bottom chord as can be seen in Figure 4. Figure 5 presents the uplift load-deformation curve for two of the failed connections.

For the specimen with the stronger hurricane clip connection, failure was observed on one side (north end) between the lower plate of the walls' top plate and the wall studs (see Figure 6) and also in the staples connecting the wall sheathing to the same plate. This is due to the high resistance of the hurricane clip between the truss and the upper plate of the walls' top plate. Figure 7 presents the uplift load-deformation curve for one of the failed connections.

Figures 5 and 7 indicate that the behavior of both connections is highly nonlinear and that once the connections reach their ultimate load they lose a significant portion of their resistance. Comparing Figures 5 and 7, it can be observed that the hurricane clip connection has a higher uplift capacity and a larger failure deformation than the toe-nailed connection. It can also be seen that the residual strength of the hurricane clip connection is equivalent to the capacity of the toe-nailed connection.

6 CONCLUSIONS

NIST researchers are investigating the structural performance of housing systems. The performance of wood-frame houses in past earthquakes and hurricanes indicate that while recent disasters in the United States have resulted in few casualties, they have caused substantial damage and significant economic loss to residential housing. An investigation of the state-of-the-art in experimental and analytical research on wood-frame found that while significant progress has been made in analytical modeling and testing of shear walls and diaphragms, only limited progress has been made on the testing and modeling of complete houses and inter-component connections.

To help improve the performance of wood-frame housing, NIST has started a research program to fill some of the gaps in understanding their structural behavior during natural disasters. The NIST research will include developing experimentally validated, three-dimensional, analytical models to predict the performance of housing units during natural disasters. This model will be used to establish performance characteristics of conventional and innovative housing systems. Testing is being conducted on components for which modeling and performance data are lacking, such as inter-component connections. The current experimental work on full-scale wood-frames has shown that the behavior of wall-to-roof connections is highly nonlinear and that the strength of hurricane clips is much higher than that of toe-nailed connections.

7 REFERENCES

Yancey, C. W., Cheok, G. S., Sadek, F., and Mohraz, B. (1998), "A Summary of the Structural Performance of Single-Family, Wood-Frame Housing," *Technical Report NISTIR 6224,* National Institute of Standards and Technology, Gaithersburg, MD.

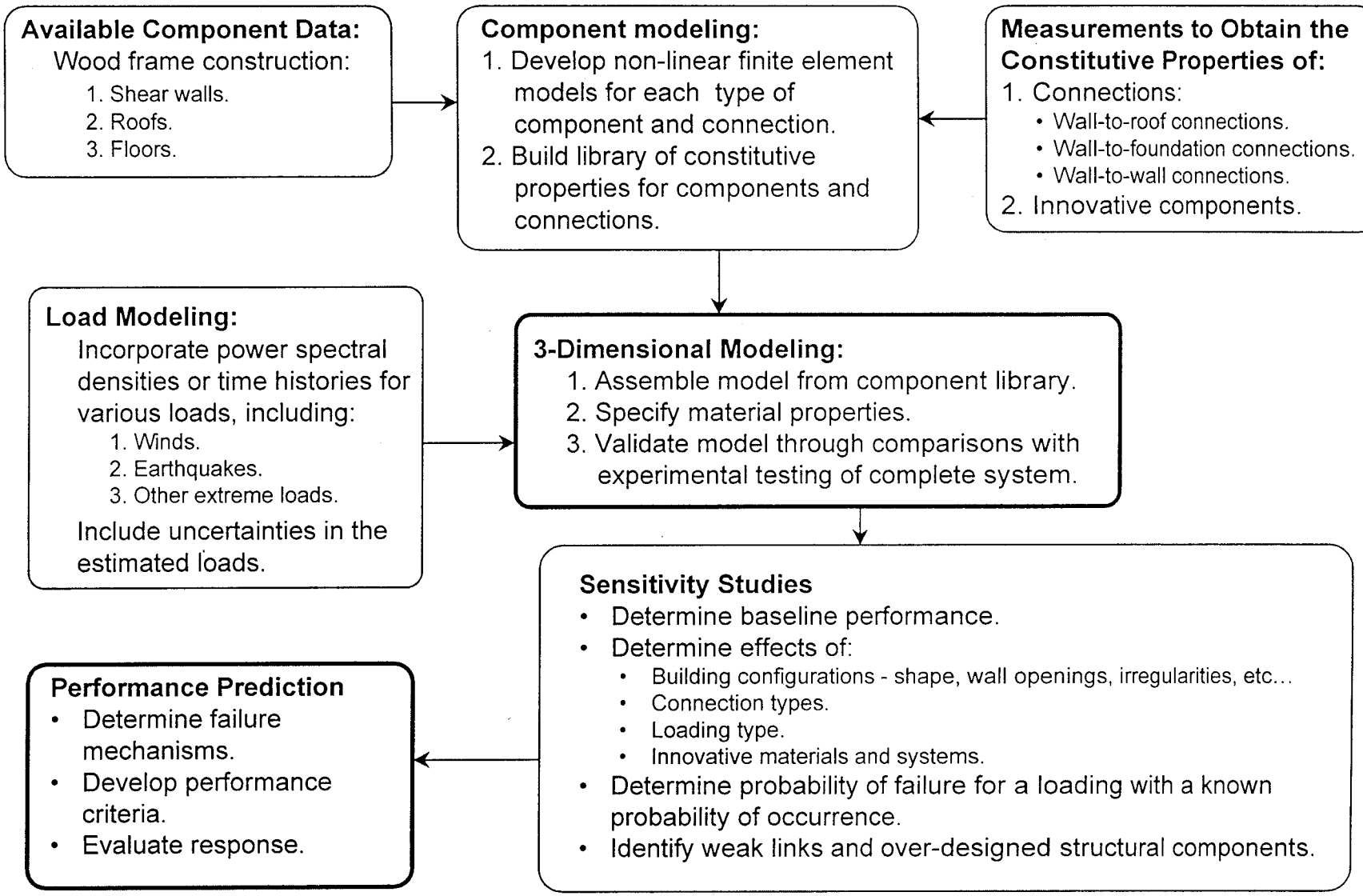

Figure 1. NIST's Research Plan

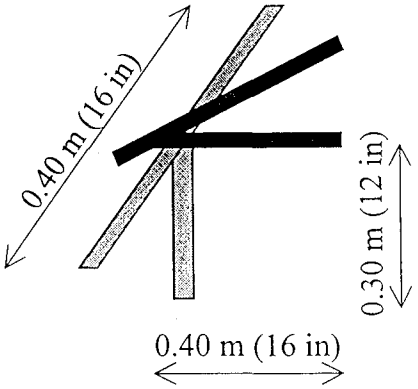

Figure 2. Component Test Specimens for Wall-to-Roof Connections

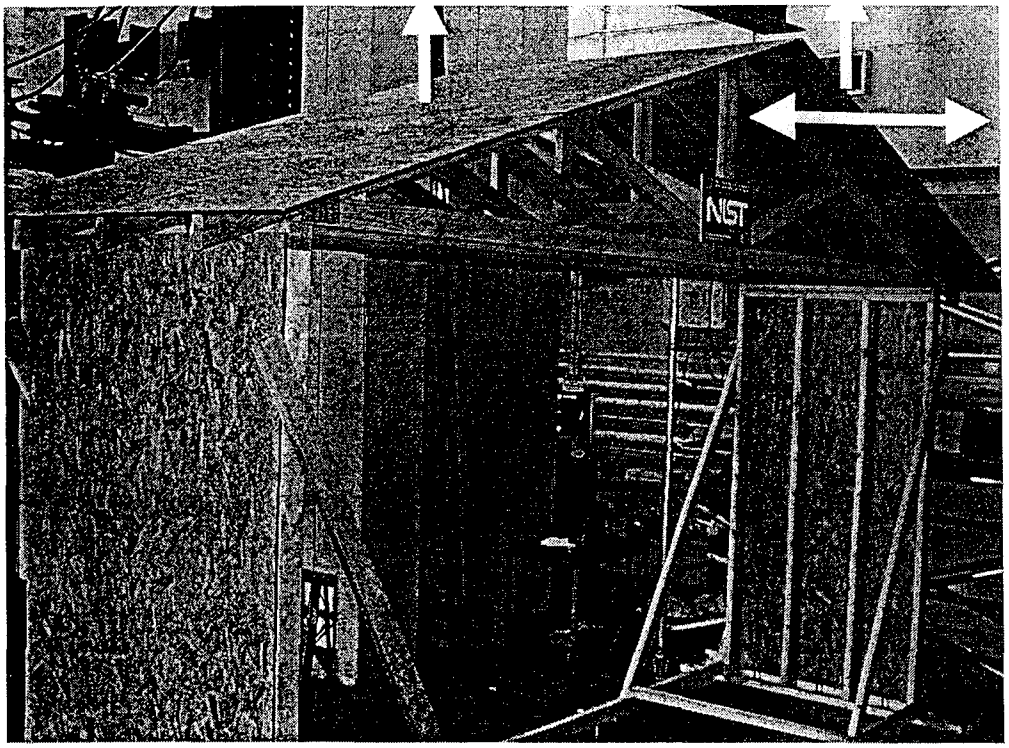

Figure 3. Full-Scale Wood-Frame Specimens

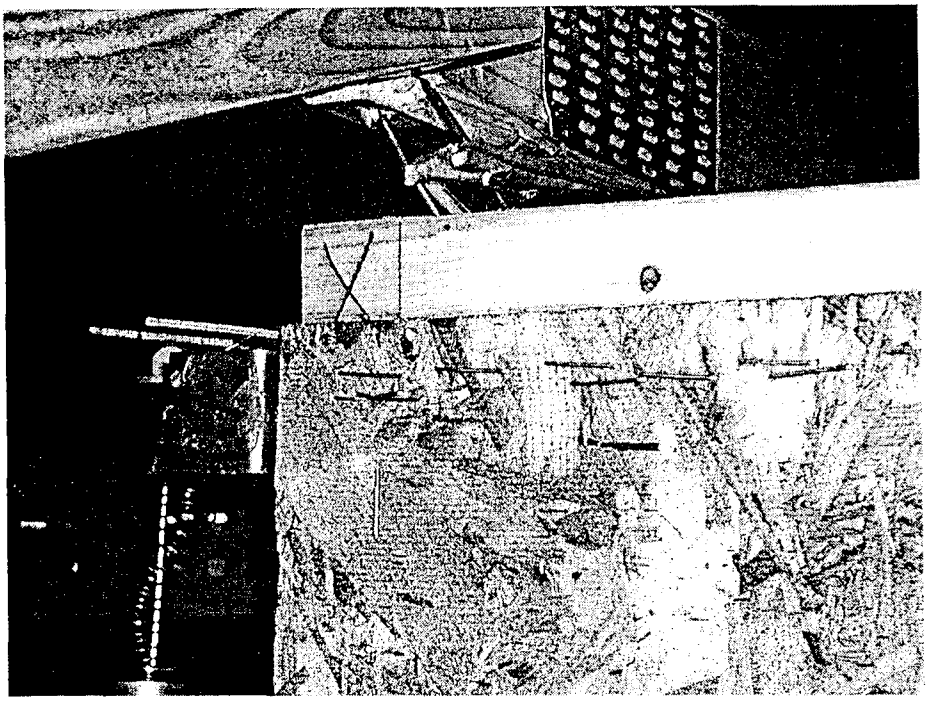

Figure 4. Failure of Toe-nailed Wall-to-Roof Connection

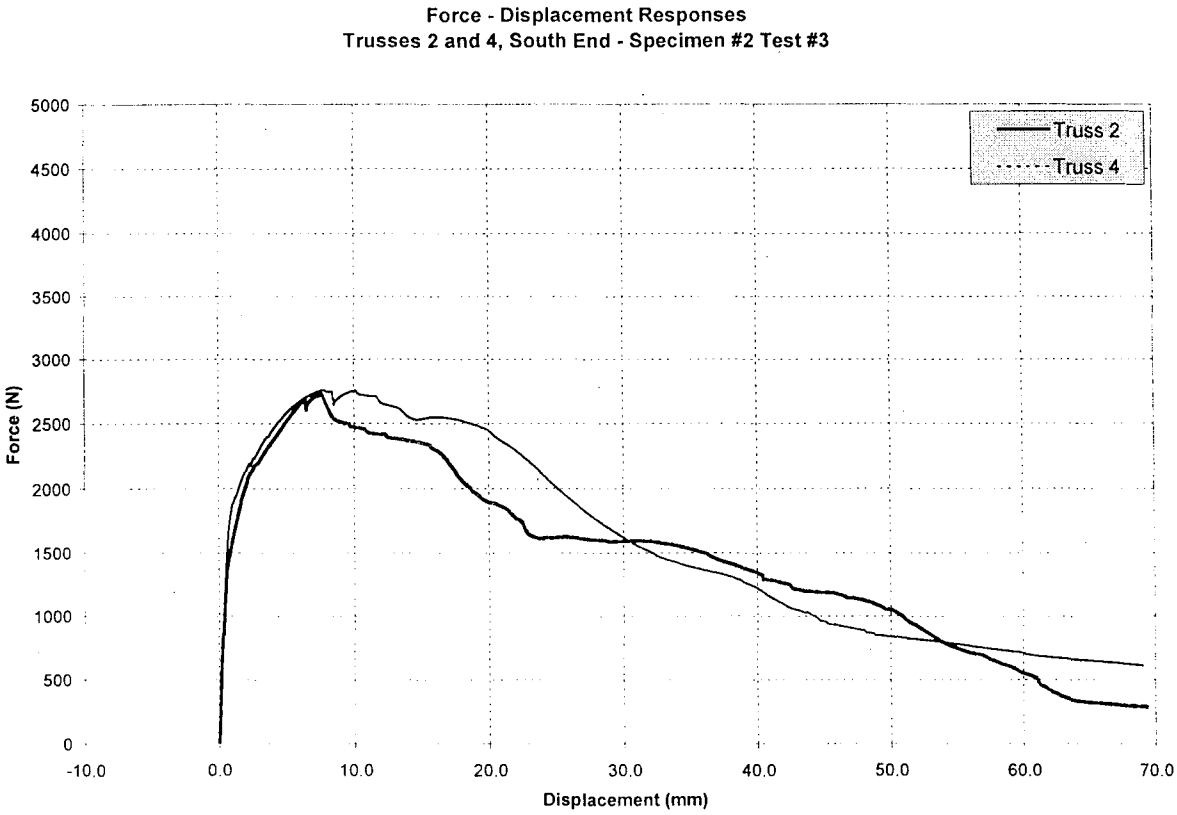

Figure 5. Load Deformation Curve of Toe-nailed Wall-to-Roof Connections

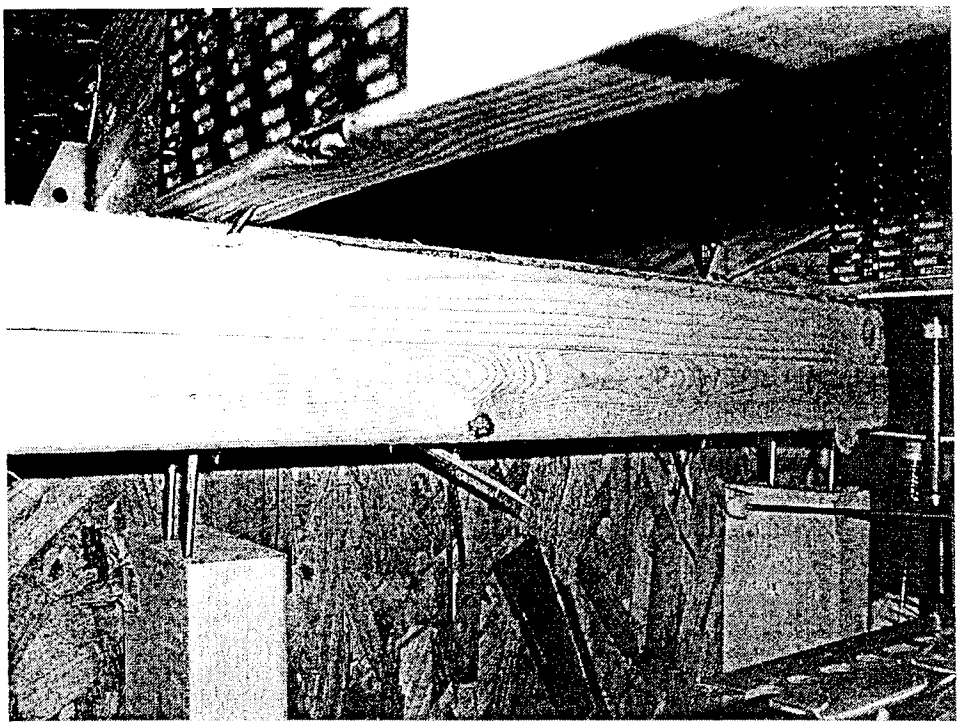

Figure 6. Failure of Wall-to-Roof Connection with a hurricane clip

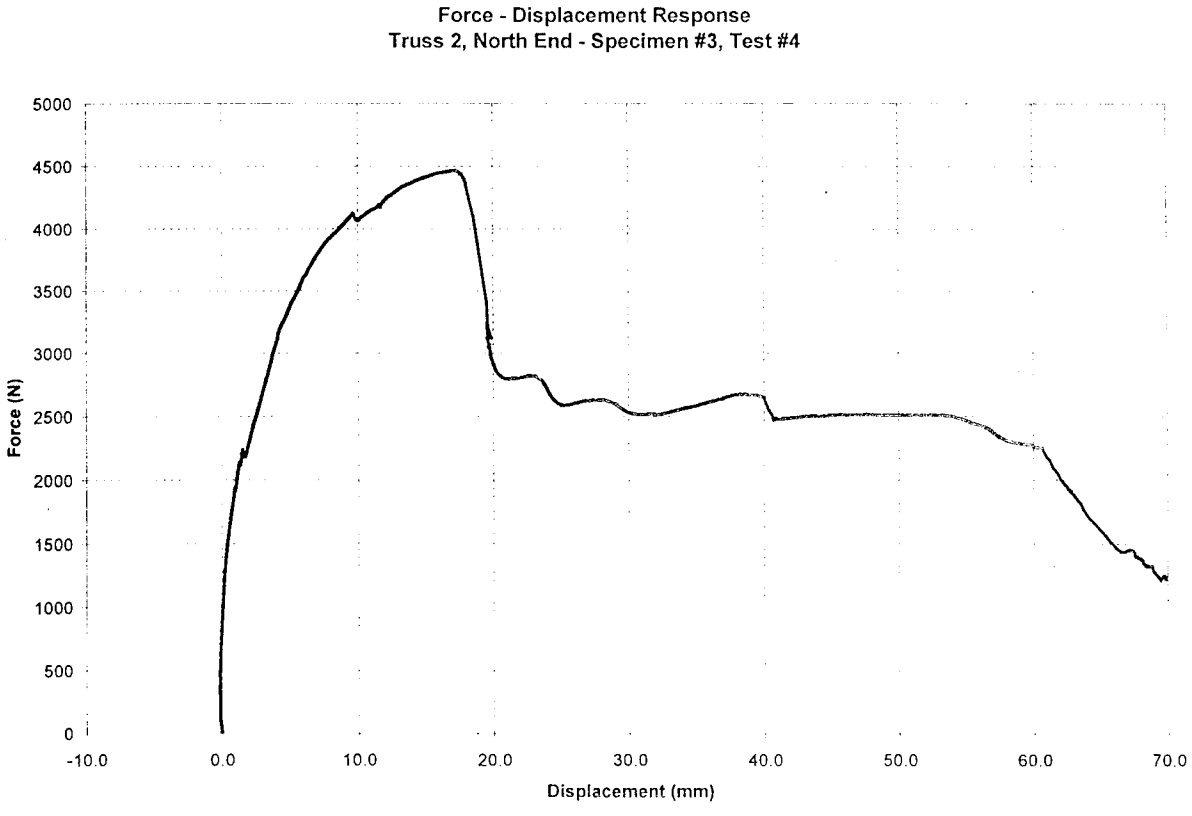

Figure 7. Load Deformation Curve of Wall-to-Roof Connection with hurricane clips

Performance-Based Damage Assessment and Design Verification of U.S. Housing in Extreme Earthquake and Hurricane Events

by

Jay H. Crandell[1] and William Freeborne[2]

ABSTRACT

This paper presents an evaluation of U.S. residential construction with respect to the actual performance of single-family detached dwellings subjected to extreme earthquakes and hurricanes. Design and construction implications are also addressed in a scientifically rigorous approach based on statistical sampling of the affected housing populations, engineering analysis, and fragility modeling. Such an approach is believed to be an effective means to identify performance issues, evaluate the strength of cause-and-effect relationships, and properly focus attention on cost-effective solutions to performance problems that will improve future design methods and construction practices.

KEYWORDS: Houses; hurricanes; earthquake; performance; design; assessment; damage; statistics; fragility.

1.0 INTRODUCTION

In this study, the "experience" of conventional residential construction (light-frame wood) is evaluated with respect to single-family detached (SFD) housing performance in the Northridge Earthquake and Hurricane Andrew using a scientifically sound experimental approach. Major seismic events cause damage to lateral resisting wall systems in conventional wood-frame construction and major wind events often cause damage to roof systems. Since these systems tend to predominate the structural risk to homes in earthquakes and hurricanes, understanding their actual performance is essential to understanding the overall performance of residential construction.

The objective of this paper is to evaluate the actual performance of homes during the Northridge Earthquake and Hurricane Andrew using statistical data on key factors such as construction characteristics, damage frequency, ground motions, wind speed, and system strength estimation. The current approaches to seismic design and wind design are also evaluated by investigating the ability to predict the actual damage and explain certain fundamental cause-and-effect relationships.

2.0 EVENT CHARACTERIZATIONS

2.1 Northridge Earthquake

The Northridge Earthquake occurred at 4:30 a.m. on January 17, 1994. Its epicenter was located in a densely populated area of Los Angeles County near the community of Northridge. Over 30 deaths were reported as a direct result of the tremor, and a total death toll of 58 was attributed to both direct and indirect causes [1]. Fortunately, relatively few deaths were associated with single family dwelling construction even though most people were in their homes at the time of the tremor. Overall property loss estimates range from $20 to $30 billion. While this earthquake was the most costly natural disaster experienced in the United States, its magnitude (Richter Scale M_L = 6.4, Surface Wave Magnitude M_S = 6.8, Moment Magnitude M_W = 6.7) was modest in terms of other more severe earthquakes. The Northridge Earthquake produced an unprecedented set of

[1]Director, Structures and Materials Division, NAHB Research Center, Inc., 400 Prince George's Blvd, Upper Marlboro, MD 20774-8731 (www.nahbrc.org)
[1]Mechanical Engineer, Office of Policy Development and Research, U.S. Department of Housing and Urban Development, 451 Seventh Street, S.W. – Room 8132, Washington, DC 20410 (www.hud.gov)

strong motion records, including more than 250 records considered representative of free field ground motion [2]. The recorded strong ground motions were characterized by a large degree of variation between sites at comparable distances from the source. Several different causes of spatial variation in ground motions have been recognized which are systematic and predictable to some extent. Strong ground motions are influenced by the characteristics of the seismic radiation from the source, by the process of wave propagation between the earthquake source and the recording site, and by local site effects [3].

2.2 Hurricane Andrew

Hurricane Andrew struck a densely populated area of southern Florida on August 24, 1992, with peak winds in excess of 78.2 m/s (175 mph) recorded at one location [4]. Using advanced hurricane modeling techniques and available wind speed data, the estimated over-land wind field of Hurricane Andrew was modeled as shown in Figure 1 [5]. The winds produced by Hurricane Andrew were estimated to have mean recurrence interval of about 300 years [6]. Because of the distance of the housing stock from the shoreline, most of the damage was related to wind, rain, and wind-borne debris — not storm surge.

3.0 DAMAGE ASSESSMENT METHODOLOGY

The objectivity of the damage assessment method hinges on the use of sampling procedures to gain a valid representation of the performance of the population of affected homes and to avoid bias toward less severe or more severe occurrences of damage. This report focuses on the study of single-family detached (SFD) housing. The sampling method and damage rating approach are briefly described below. For a more detailed treatment, the reader is referred to the original studies [7][8].

For the Northridge Earthquake, a 16.1 km (10 mi) radius around the epicenter was selected as a damage zone for study. Postal regions—as defined by five-digit zip codes that fell within the damage zone or intersected its border—were used as the basis for a random selection of homes from property tax records. There were 183,514 SFD home entries in the property tax database for the designated zip codes. Seventy-five sites were randomly selected by street address from the tax record database. The home at the selected address was surveyed along with two homes on either side—a total of five homes per site. The survey teams visited 75 sites resulting in 341 usable survey forms.

For Hurricane Andrew, over 600 randomly sampled homes experiencing the highest winds were assessed using detailed field survey forms. The randomly determined damage study locations are shown in Figure 1. The sample was drawn from a street map. In the first stage, a random sample of map grid areas was made. Within the sampled grids, a random sample of streets was drawn. All homes on the sampled streets were surveyed, with exception of those homes on a street that were not surveyed at the end of a day. A total of 466 survey forms were deemed suitable for analysis.

In each survey, all of the sample homes were visited by one of several assessment teams to document the housing characteristics and the level of performance. Survey forms were used to document about 60 construction characteristics and 30 damage characteristics for each home. Photographs were taken of each assessed property. For each category listed on the survey form, earthquake or wind damage was graded according to four levels of severity:

- NONE: no visible damage;
- LOW: components are stressed, but in functional condition (i.e., minor cracking of stucco or minor loss of roof sheathing);
- MODERATE: evidence of severe stress, permanent deflection, or near failure in any structural system (i.e., severe cracking of stucco or loss of many roof sheathing panels without collapse of the structure or roof system); and,
- HIGH: partial or complete failure (i.e., collapse) of any structural system.

Case studies of rare instances of extreme damage were also conducted for each event, but they are beyond the scope of this paper. Similarly, statistical surveys and case studies were also performed for multi-family low-rise and single-family attached forms of residential construction.

4.0 CONSTRUCTION CHARACTERISTICS AND DAMAGE STATISTICS

4.1 Northridge Earthquake Survey

The SFD housing characteristics are briefly summarized in Table 1. Using information provided by the property tax record database and inspectors with the Department of Building and Safety, it was determined that about 90 percent of the homes in the sample were built prior to the 1971 San Fernando Valley Earthquake when simple prescriptive requirements were normal to SFD home construction. About 60 percent of the surveyed homes were built during the 1950s and 1960s. House age ranged from the 1920s to the early 1990s. SFD homes were typically one-story and nearly two-thirds had an attached garage. Styles of SFD homes ranged from expensive custom homes to affordable, older homes. As expected, all homes surveyed had wood exterior wall framing and most did not use structural sheathing for wall bracing. Instead, wood let-in braces, Portland cement stucco, and interior wall finishes provided lateral resistance. Homes on crawlspace foundations outnumbered those on concrete slabs by almost two-to-one, despite a notable increase in the use of slab-on-grade foundations since the 1960s. Most of the crawlspace foundations used full-height concrete or masonry stem walls, not cripple walls.

The performance of SFD homes is shown in Table 2. The table is broken into observed damage of the homes sampled and estimates of damage for the entire population of homes within the survey area. Confidence intervals at the 95 percent level are shown for each estimate.

Damage to structural elements—foundation, wall framing, and roof framing—was limited to a small proportion of surveyed homes. In general, SFD homes suffered minimal damage to elements that are critical to the safety of occupants. Of the structural elements, damage was most common in the foundation system. The small percentage of surveyed homes that experienced moderate to high foundation damage were located in areas that endured localized ground effects or problems associated with hillside sites. The localized ground effects included fissures or ground settlement that cracked foundations. For hillside sites, partial slope failures contributed to the foundation damage.

Interior and exterior finishes suffered more widespread damage than foundation and framing, with only about half the buildings escaping unscathed. However, the great majority of damage was limited to the lowest rating categories. Stucco was observed on nearly all home exteriors. Damage to stucco usually appeared as hairline cracks radiating from the corners of openings—particularly larger openings such as garage doors—or along the top of the foundation. Interior finish damage paralleled the occurrence of exterior finish (stucco) damage. Resilient finishes—such as wood panel or lap board siding—fared well and often showed no evidence of damage even when stucco on other areas of the same building was moderately damaged.

The Chi-square test was used—at a 95 percent level of confidence—to judge statistical significance of various conditions on the outcome of a home's performance. The inferences initially designated for study by the Chi-square test included observed performance versus:

- peak ground acceleration estimates,
- age of the home,
- roof type
- number of stories, and
- foundation type.

Chi-square analyses requires a large number of observations in each category to produce valid results. Thus, the analysis was limited to the exterior damage rating as the performance indicator since it represented the greatest extent of damage. Also, the low, moderate, and high damage ratings were grouped such that a

damage/no-damage test was applied. Except for foundation type, all inferences were inconclusive.

Using only data from one-story homes, comparison of crawlspace versus slab-on-grade foundation construction shows a significant difference in the level of damage to the stucco used on one-story homes. Single-story homes with slab foundations exhibited damage to exterior finishes in about 30 percent of the cases, while homes on crawlspace foundations with masonry or concrete stem walls approached a 60 percent rate of occurrence. Since the majority of crawlspace homes in the survey area were built before 1960 while nearly three-quarters of slab homes were built after 1960, stucco performance alone may not be sufficient to conclude that one foundation type is necessarily better than another. There may be factors influencing stucco performance other than merely foundation type, such as house age.

Case studies of damage were conducted on 54 SFD homes that experienced rare, severe damage. The most notable sources of structural damage to these case study homes were related to ground conditions (e.g., fissures and settlement) and hillside construction conditions (e.g., weak foundation connections or partial slope failures). Damage to wall finishes, contents, mechanical equipment, masonry chimneys, and masonry privacy fences was much more common.

4.2 Hurricane Andrew Survey

Table 3 summarizes the key construction characteristics of the sampled homes in the Hurricane Andrew study. Most of the homes were one story in height with nominally reinforced masonry walls, wood-framed gable roofs, and composition shingle roofing.

Table 4 summarizes the key damage statistics determined for the sampled homes in Hurricane Andrew. As expected, the most frequent form of damage was related to windows and roofing with 77 percent of the sampled homes suffering significant damage to roof covering materials. Window damage resulting in at least one broken window was realized in 91 percent of the sampled homes. Blown-off roof sheathing was the most significant aspect of the structural damage with 64 percent of the homes losing one or more roof sheathing panels. Loss of windows and roofing in Hurricane Andrew led to widespread and costly water damage to interiors.

In a similar study of Hurricane Opal, wind speeds ranged from about 44.7 m/s to 51.4 m/s (100 to 115 mph) based on peak gusts at a 10m (33 ft.) height and normalized to open terrain over the sample region. Again, roofing damage was the most common form of wind damage, but at a frequency of only 4 percent of the housing stock [9]. Roof sheathing damage was realized in less than 2 percent of the affected housing stock. This data provides a good contrast to that obtained from the Hurricane Andrew study. Aside from the much lower wind speeds in Hurricane Opal, most of the homes were shielded by trees whereas those in South Florida were in typical suburban residential exposure (wind exposure B) and trees, when present, were denuded in the extreme winds of Andrew. The more extensive damage in Hurricane Opal was caused by storm surge to homes and other buildings on the barrier islands.

Some inferences on the Hurricane Andrew data were found to be statistically significant at a 95 percent confidence level. For example, gable roofed homes suffered significantly higher damage on average than their hip-roofed counterparts with respect to the amount of roof damage realized. It should be noted that this difference in vulnerability is not reflected by commensurate differences in wind loads calculated for roof components in ASCE 7 [10]. Also, two-story homes experienced significantly higher average damage than one-story homes with respect to window and water damage, but not roof damage.

The level of damage to walls was very low with about 2 percent of the homes experiencing some significant form of wall structural damage. About 96 percent of the homes were constructed of nominally reinforced masonry walls (i.e. #4 vertical rebar at 2.4 m (8 feet) on center). Interestingly, this amount of reinforcement falls below the minimum reinforcement ratios that are required in current reinforced masonry or

concrete design specifications in the United States. Similarly, roof tie-down failures were reasonably low with 84 percent of the sampled homes experiencing no form of failure to these important elements in high wind regions. About 8 percent of the homes experienced a partial or full roof blow-off failure while most homes had breached envelopes (i.e., broken window glazing and/or a failed garage door) resulting in a higher internal pressure condition according to current design practice represented in ASCE 7.

5.0 STRUCTURAL PERFORMANCE EVALUATION

5.1 Northridge Earthquake

The findings reported herein are summarized from a more thorough evaluation and report on the Northridge Earthquake damage statistics [11]. A total of 49 homes were extracted from the Northridge Earthquake survey discussed previously which met the following criteria:

- one-story, single-family homes;
- stucco exterior wall finish (without structural panel sheathing);
- asphalt composition roof shingles; and
- adequate photographic documentation to characterize the street facing wall configuration.

These criteria resulted in a fairly homogenous, random sample for the purpose of evaluating fundamental relationships between damage and various seismic design factors. The application of findings from this study is limited to the types of homes that meet the above criteria. These homes were of typical construction in the San Fernando Valley with stucco and wood let-in wall bracing. Roughly 80 percent of these homes had crawlspace foundations and 20 percent had slab-on-grade foundations.

Table 5 summarizes the damage to the exterior wall finish of the 49 homes extracted from the survey. The percentages in Table 5 closely coincide to the damage statistics for the complete survey sample of the 341 homes as shown in Table 2.

5.1.1 Solid Wall Ratio (β) vs. Stucco Damage Rating

The value of the solid wall ratio, β, was determined from the photographic documentation of the street-facing side of the sampled houses. It is a simple ratio of the length of solid wall segments (i.e., without openings for windows and doors) to that of the entire wall line. Figure 2 indicates that there is no obvious correlation between the amount of solid stucco wall and the damage rating for the homes in this study. This finding was unexpected. However, there is a possible slight trend when looking at the average β for the NONE and LOW groupings which are 52 percent and 49 percent, respectively. Unfortunately, the variability (scatter) of the data obscures any statistically conclusive finding.

5.1.2 Wall Discontinuities vs. Stucco Damage Rating

Both NEHRP – 97 and UBC – 97 include design provisions for homes constructed with plan irregularities [12][13]. Many of the homes in this study had an *Out-of-Plane Offset* plan structural irregularity. By definition, an out-of-plane offset is a discontinuity in a lateral force resistance path, such as out-of-plane offsets of the vertical elements. This type of irregularity is believed to be associated with substandard performance and current residential construction codes limit a braced wall line offset to 1.2 m (4 ft) for this reason. However, Figure 3 shows no apparent correlation between the number of wall discontinuities on the street facing wall and damage rating for the homes in this study. Figure 4 considers only offsets equal to or greater than 1.2 m (4 ft) as a wall discontinuity. Again, there seems to be no apparent correlation between the stucco damage rating and the number of offsets greater than or equal to 1.2 m (4 ft).

5.1.3 Spectral Response Acceleration vs. Stucco Damage Rating

Data from 9 strong motion stations that recorded ground motions during the Northridge

Earthquake were examined in this study. These 9 stations were in close proximity to the 49 homes investigated in this study. The peak horizontal component for the 0.2 second acceleration response spectra and the 1.0 second acceleration response spectra for 5 percent critical damping were extracted from the data sets for the 9 strong motion ground stations. This data is summarized in Table 6 along with the corresponding return period estimate. The return periods were determined using the U.S. Geological Survey (USGS) hazard curves for each site. The methodology used to create seismic maps and hazard curves is discussed in other reports [14][15].

Ground motion amplification has been observed at the Tarzana – Cedar Hill station in many earthquakes for both strong and weak ground motions. The Tarzana station is located near the crest of a low (20 m) natural hill on the south side of the San Fernando Valley. Topographic effects can explain many features of the observed amplification patterns, but the three dimensional geological structure beneath the hill may also be responsible in part for the very large observed amplification at the top of the hill [16]. For this reason the ground motions at Tarzana were considered anomalous and not used in this study.

The latitude and longitude for each of the 49 houses extracted from the survey were determined. The distance of the homes to the nearest strong motion stations was determined from the latitude and longitude coordinates. The corresponding acceleration response spectra was determined by interpolating between the ground motion stations closest to the house of interest. Figure 5 graphically indicates that there was no apparent correlation between the 0.2 second spectral response acceleration and the stucco damage rating for the sampled homes. Figure 6 suggests that there may be a slight trend between the 1.0 second spectral response acceleration and damage rating on average. The average 1.0 second spectral response acceleration for the NONE and LOW groupings are 40 percent and 46 percent, respectively. It is impractical to consider if the trend is statistically significant since the sample is relatively small and the scatter is relatively large. Although a weakly supported observation, Figure 6 provides an indication that the longer period spectral response acceleration may be the better seismic design parameter for small conventionally built wood-framed buildings such as homes since it appears to better explain the damage.

5.1.4 Case Study – Mecca Avenue

Table 7 summarizes three homes surveyed on Mecca Avenue that were part of the random sample of homes. They were of very similar construction (style) and oriented identically to the ground motion. The three homes summarized in this case study reinforce some of the findings discussed earlier in this paper. The surveyed homes were on the same street and of close proximity to the Tarzana strong motion station. The Tarzana station realized some of the largest ground motion readings during the Northridge Earthquake. In this anecdotal comparison, the damage rating improved with increasing wall discontinuity and decreasing solid wall amount. This finding, though not statistically conclusive, is exactly opposite of conventional engineering theory.

5.2 Hurricane Andrew

The performance of roof sheathing components in Hurricane Andrew was evaluated using principles of engineering and risk modeling and this report summarizes the major findings from the original study [17]. To facilitate the performance evaluation, a Monte Carlo simulation model was developed to predict the frequency of roof sheathing damage (i.e., estimate the percentage of homes experiencing the loss of at least one panel of roof sheathing). The model accounted for variation in sheathing fasteners, construction materials (i.e., framing lumber species and density), South Florida housing characteristics, workmanship effects, and other important parameters affecting the actual sheathing resistance values and wind loads (i.e., surface pressures) experienced. The sheathing pull-off resistance values and variation used in the model were based on tested data with adjustments to account for roof framing lumber used in South Florida [18]. The wind speed over

the sample region (Figure 1) was essentially treated as a deterministic parameter and was based on the modeled range of wind speeds experienced over the sample region (i.e., mean = 72.6 m/s (162.5 mph), COV = 0.01). The wind load provisions of ASCE 7 were used to determine wind pressures on the roof sheathing using a suburban exposure, enclosed building internal pressure condition (i.e., applicable to the attic space prior to sheathing loss), and a wind directionality factor of 0.85.

From the statistical damage survey data discussed previously [8], a sub-set of single-story homes with gable roofs and composition shingle roofing was selected as a homogenous sample for the performance evaluation and model calibration. Of these randomly sampled homes, 69 percent±6 percent (95 percent confidence limits) experienced the loss of at least one panel of roof sheathing, and all were in the 71.5-73.8 m/s (160-165 mph)(peak gust) region of Hurricane Andrew as shown in Figure 1.

The key results of the study are the fragility curves shown in Figure 7 which give predictions of the percentage of homes expected to experience the loss of one or more panels of roof sheathing based on the hurricane magnitude (wind speed). Figure 7 contains four different fragility curves representing different levels of roof sheathing attachment. The curve representing the actual housing population (second from the top) is calibrated to the actual observed roof sheathing damage frequency of 69 percent±6 percent (95 percent confidence limits) at a wind speed of 72.4 m/s (162 mph) (peak gust) with a mix of 6d and 8d sheathing nails representing roof sheathing attachments in the modeled housing population. The model prediction is 71 percent -- tending toward a slight over-estimation of the actual damage frequency.

Some very interesting findings are drawn from the analysis:

- Actual Performance Better Than Minimum Code

The minimum requirement for roof sheathing attachment in the 1991 South Florida Building Code was 6d common nails spaced at 30 cm (12 in) on center in the field of the roof sheathing panels (see top curve in Figure 7) [19]. If this minimum requirement was representative of the entire housing population, the predicted frequency of roof sheathing loss would have been about 92 percent instead of 69 percent of the homes. One may conclude that this minimum code requirement was very insufficient for the South Florida wind climate and that the housing performance was actually better than that implied by the code minimum. However, neither the code-implied performance nor the actual performance is considered acceptable.

- Revised Code Minimum Will Significantly Improve Performance

The next most important observation is that the level of performance expected for new homes constructed under the 1994 South Florida Building Code will be significantly improved (bottom curve in Figure 7) [20]. This improvement is primarily attributed to increasing the roof sheathing attachment requirement to 8d common nails from 6d common nails without any change in workmanship or inspection that may result in improved installation quality. Decreasing the spacing to 15 cm (6 in) on center and requiring sheathing attached to the gable end framing to be nailed at 10 cm (4 in) on center are also important features in the new code. New homes constructed under this revised code provision are predicted to perform with a roof sheathing loss frequency of about 1 percent in the next event equivalent to Hurricane Andrew.

- Benchmark for Acceptable Performance

An acceptable roof sheathing damage frequency may be targeted at about 10 percent of the homes for an event the magnitude of Hurricane Andrew in the South Florida wind climate (see lower box in Figure 7 at 72.4 m/s (162 mph) wind speed). This target is risk-consistent with the generally acceptable performance of standard roof sheathing attachments in typical

extra-tropical wind climates covering most of the non-coastal United States. Thus, a damage frequency of about 10 percent of the homes losing one or more panels of roof sheathing in an event similar to Hurricane Andrew constitutes a respectable goal or target performance for the South Florida housing population. Obviously, the actual frequency of roof sheathing damage (i.e., 64 percent of the all SFD homes) does not meet the proposed benchmark for acceptable performance.

Though not similarly evaluated, the incidence of building collapse (wall racking) or roof blow-off should have a lower target damage frequency because of the more severe consequences. Indeed, the occurrence of this type of damage was documented at a reasonably low level in Hurricane Andrew – 2 percent for wall damage and 8 percent for roof-wall connection damage [8]. (The 2 percent wall damage statistic is primarily associated with wood frame wall construction which comprised about 4 percent of the sampled homes). Of the nominally reinforced masonry homes sampled, no wall failures were documented; extremely rare incidences of severe masonry wall damage, however, were found in the housing population [8].

- Possible Wind Directionality and Shielding Effects

One point of concern following the generation of the fragility curves was related to the level of damage at lower wind conditions. According to the wind map in Figure 1, the maximum wind speeds for Hurricane Andrew were less than about 62.6 m/s (140 mph) for areas north of 88th Street (Kendall Ave.). Kendall Avenue was the northern boundary for the statistical sampling region in the HUD damage survey [8]. This northern boundary of the 'damage zone' was selected because of the lack of any significant damage, particularly roof sheathing loss, proceeding further northward.

As shown in Figure 7, the calibrated MCS model predicts damage frequencies of more than 50 percent at the 62.6 m/s (140 mph) wind speed. One possible reason is that the rate of wind speed decrease in Figure 1 is too low north of the eyewall of Hurricane Andrew (i.e., an error in the hurricane wind field model). This would require that the wind speeds drop from 71.5 m/s (160 mph) to less than about 44.7 m/s (100 mph) at the crossing of Kendall Avenue to agree with a damage level well below 10 percent based on observation in this region (see Figure 7). This wind-speed drop-off may be physically unreasonable, though not implausible. Therefore, it is believed that this drop-off in actual damage relative to the modeled damage is at least in part due to a change in the wind exposure condition (exposure B was used in the model). This change in wind exposure is attributable to two characteristics. First, the areas north of Kendall Avenue were generally older developments with more mature trees which could have shielded the lower buildings (i.e., one-story homes). Second, the wind speeds in this region were low enough that the trees were able to maintain some level of protection during the hurricane without being completely destroyed or denuded. It is also possible that the generally older homes in this region were built using materials and methods that were somewhat more wind resistant.

To test this hypothesis, the MCS model was re-run at the 62.6 m/s (140 mph) wind speed with an additional adjustment to account for possible shielding effects due to the survival of the trees. The calculated wind loads were reduced by 25 percent for shielding which corresponds with the results of a recent wind tunnel study of low-rise structures in a densely built-up (i.e., shielded), exposure B environment [21]. With this adjustment, the MCS model predicted a roof sheathing damage frequency of about 1 percent which agrees reasonably well with the anecdotal observation of very little structural damage north of Kendall Avenue. Thus, the existence of mature trees in a relatively dense mix with development may reduce wind damage significantly, provided the wind speeds do not exceed the ability of the trees to act as barriers.

Some of this disparity may be attributed to an unaccounted increase in wind directionality effect not considered in the model. Proceeding north of the hurricane eyewall, the wind speed

magnitude and range of wind directions experienced are both diminished. Thus, a wind directionality factor of 0.75 (as applicable to extra-tropical wind conditions) may be appropriate as concluded in an extensive analytical wind tunnel study [21].

It is probable that the following factors all contributed to an apparent over-prediction of damage north of the eyewall (outside of the statistical damage study region):

- wind field modeling errors,
- increased reductions in wind load associated with wind directionality,
- increased shielding associated with the survival of trees; and,
- differences in the construction materials and methods used in the generally older homes located north of the eyewall and the sample study region.

6.0 CONCLUSIONS

6.1 General

1. It is feasible and economical to obtain reliable and representative data on housing construction and damage frequencies (i.e., performance) following extreme natural events such as earthquakes and hurricanes.

2. Construction and performance data collected and evaluated as described in this paper may be used to rationally assess performance, identify need for improvement, evaluate the adequacy of engineering methods relative to actual performance, and develop cost-effective solutions related to the real problems associated with natural hazards.

6.2 Northridge Earthquake

1. The single-family housing population performed reasonably well in the Northridge Earthquake with 95.9 percent of the sampled homes receiving a stucco damage rating of NONE or LOW; very few homes exhibited significant structural damage related to life-safety concerns.

2. Despite fundamental structural performance relationships assumed in conventional seismic design practices and theory, there was no obvious or significant correlation between solid wall ratio or spectral response acceleration and the damage rating for the statistically representative sample of homes examined in this study.
3. The findings provide some indication that the long period (1 second) spectral response acceleration is the preferable ground motion parameter for design of small, light-frame structures.
4. This study also confirms that certain irregularities, such as wall out-of-plane offsets, do not have the affect on performance implied by current design and construction provisions.

6.3 Hurricane Andrew

1. Given the magnitude of Hurricane Andrew, the structural (life-safety) performance of the typical South Florida housing stock (i.e., masonry walls with wood frame roofs) was found to be very reasonable with the prominent exception of roof sheathing attachment.

2. Wind loads determined in accordance with ASCE 7 provide a reasonable basis to assess the actual performance of residential roof components given the use of an "enclosed building" internal pressure condition for the determination of roof sheathing loads, the use of a 0.85 wind directionality factor, and appropriate consideration of wind shielding effects.

3. The actual performance of the housing stock was, on average, better than that implied by the governing building code provisions preceding Hurricane Andrew's devastation – though both are considered unacceptable.

4. Revisions to the South Florida Building Code (SFBC) following Hurricane Andrew resulted in roof sheathing attachment provisions that are slightly conservative, but practical and effective.

5. The statistical data on roof-to-wall connection performance in Hurricane Andrew gives ample evidence that the roof tie-down connection (as required by SFBC and executed in practice) was reasonably reliable.

7.0 REFERENCES

[1] National Institute of Standards and Technology, *1994 Northridge Earthquake – Performance of Structures, Lifelines, and Fire Protection Systems*, Gaithersburg, MD, 1994

[2] Grazier, V.M., *Strong Motion Data from Ground-Response Sites and Structures Recorded During the 1994 Northridge Earthquake*, Proceedings Northridge Earthquake Research Conference, Los Angeles, California, 1997.

[3] Somerville, P., *Research Overview on Strong Ground Motion: The 1994 Northridge Earthquake*, Proceedings of the NEHRP Conference and Workshop on Research on the Northridge, California Earthquake of January 17, 1994, Richmond, CA, 1998.

[4] Reinhold, T. A., Vickery, P. J., and Powell, M. D. (1993). "Windspeeds in Hurricane Andrew: myths and reality." *7th U.S. Nat. Conf. on Wind Engrg.*, Univ. of California, Los Angeles, Calif., 553-562.

[5] Vickery, P.J., P.F. Skerlj, A.C. Steckley, and L.A. Twisdale, *Hurricane Wind Field and Gust Factor Models for Use in Hurricane Wind Speed Simulations*, Applied Research Associates, Raleigh, NC, 1997.

[6] Vickery, P.J., P.F. Skerlj, A.C. Steckley, and L.A. Twisdale. *Simulation of Hurricane Risk in the United States Using an Empirical Storm Track Modeling Technique*, Applied Research Associates, Raleigh, NC, 1998. (pending journal publication).

[7] *Assessment of Damage to Residential Buildings Caused by the Northridge Earthquake*, Prepared for the U.S. Department of Housing and Urban Development by the NAHB Research Center, Inc., Upper Marlboro, MD, 1994.

[8] *Assessment of Damage to Single-Family Homes Caused by Hurricanes Andrew and Iniki*, Prepared for the U.S. Department of Housing and Urban Development by the NAHB Research Center, Inc., Upper Marlboro, MD, 1993.

[9] *Assessment of Damage to Homes Caused by Hurricane Opal*, Prepared for the Florida State Home Builder's Association by the NAHB Research Center, Inc., Upper Marlboro, MD, 1996.

[10] *Minimum Design Loads for Building and Other Structures* (ASCE 7-95), American Society of Civil Engineers, New York, NY, 1995.

[11] *Evaluation of Housing Performance and Seismic Design Implications in the Northridge Earthquake*, Prepared for the U.S. Department of Housing and Urban Development by the NAHB Research Center, Inc., Upper Marlboro, MD, June 1999.

[12] *NEHRP Recommended Provisions for Seismic Regulations for New Buildings and Other Structures*, Building Seismic Safety Council, Washington, D.C., 1997.

[13] *Uniform Building Code: Volume 2*, International Conference of Building Officials, Whittier, CA, 1997.

[14] Frankel, A., *Mapping Seismic Hazard in the Central and Eastern United States*,

Seismological Research Letters, Vol. 66, No. 4, pp. 8-21, 1995.

[15] Frankel, A., Mueller, C., Barnhard, T., Perkins, E., Leyendecker, E., Dickman, N., Hanson, S., Hopper, M., *National Seismic Hazard Maps, June 1996: Documentation*, U.S. Geological Survey, Open File Report 96-532, 1997.

[16] Darragh, R.B., Graizer, V.M., Shakal, A.F., *Tarzana, California: Site Response and Characterization*, Proceedings of the NEHRP Conference and Workshop on Research on the Northridge, California Earthquake of January 17, 1994, Richmond, CA, 1998.

[17] *Reliability of Conventional Residential Construction: An Assessment of Roof Component Performance in Hurricane Andrew and Typical Wind Regions of the United States*, Prepared for the U.S. Department of Housing and Urban Development by the NAHB Research Center, Inc., Upper Marlboro, MD, 1999.

[18] Mizzell, D.P. and Schiff, S.D., *Wind Resistance of Sheathing for Residential Roofs*, Clemson University, Clemson, SC, 1994.

[19] *South Florida Building Code*, Dade County, FL, 1991.

[20] *South Florida Building Code*, Dade County, FL, 1994.

[21] Ho, Tat Chiu Eric, *Variability of Low Building Wind Loads*, Ph.D. Thesis, Department of Civil Engineering, The University of Western Ontario, July 1992.

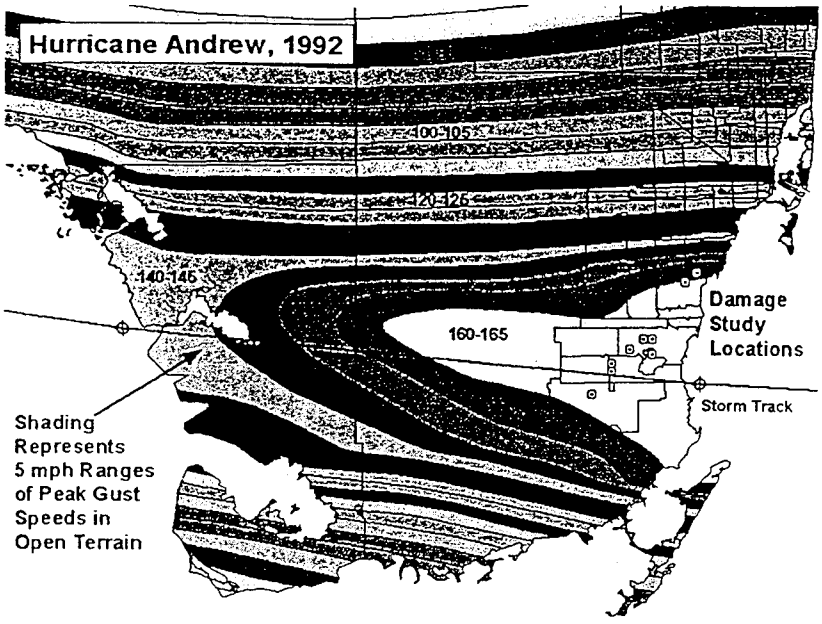

Figure 1
Maximum 3-Second Gust Wind Speeds (mph)
Experienced in Hurricane Andrew at 10 m (33 ft) Elevation over Open Terrain
(Courtesy Applied Research Associates, Raleigh, NC)
1 mph = 0.447 m/s

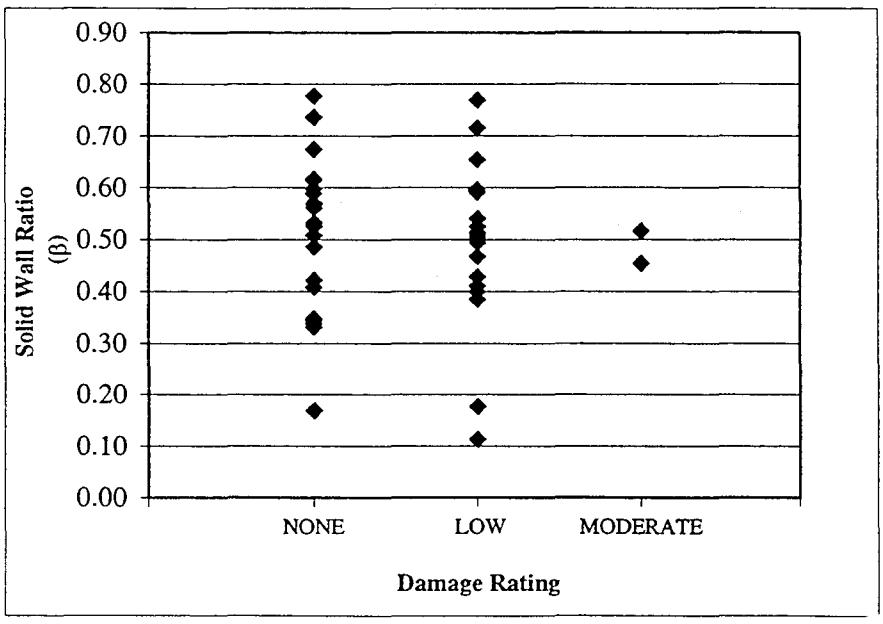

Figure 2
Solid Wall Ratio (β) vs. Damage Rating
(Data Points Represent Individual House Samples)

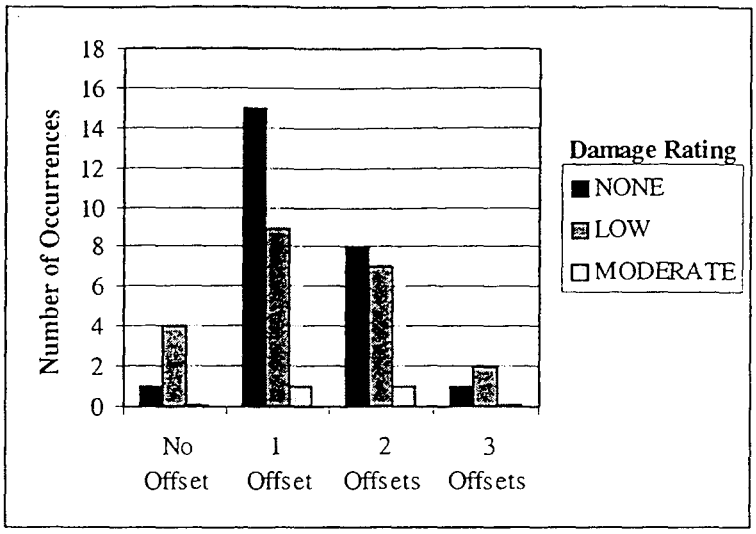

Figure 3
Non-Correlation of Wall Offsets and Damage Rating

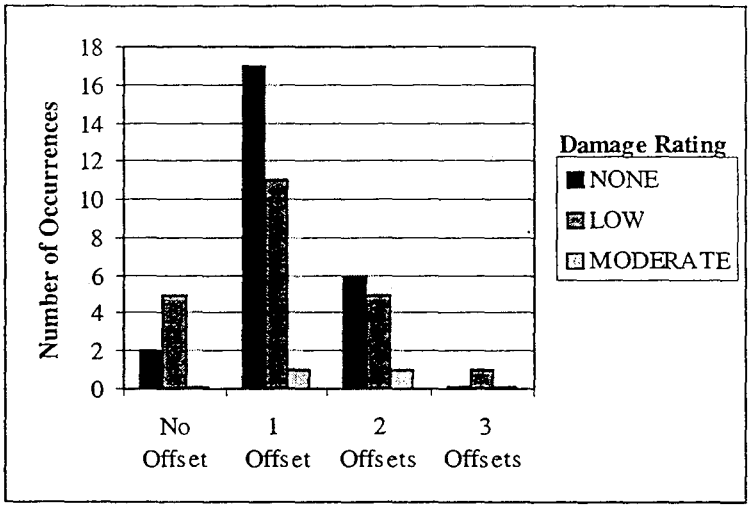

Figure 4
Non-Correlation of Wall Offsets Greater than 1.2 m (4 ft) and Damage Rating

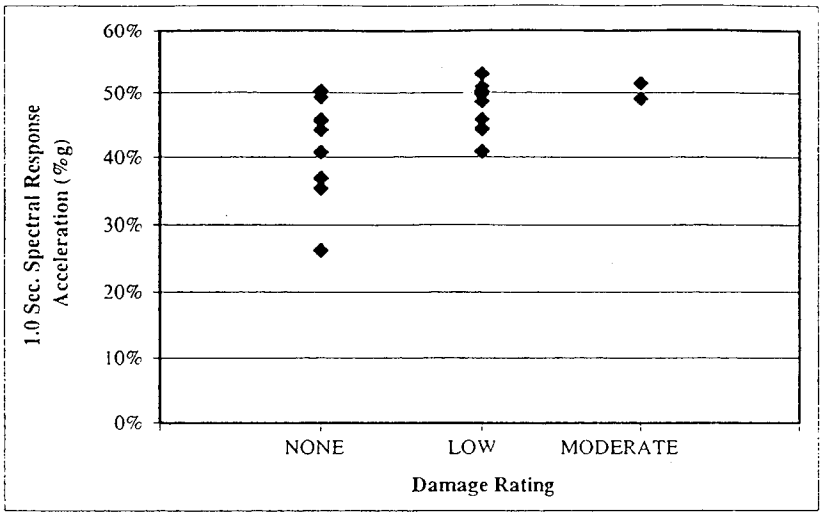

Figure 5
0.2 Sec Acceleration Response Spectra vs. Damage Rating
(Data Points Represent Individual House Samples)

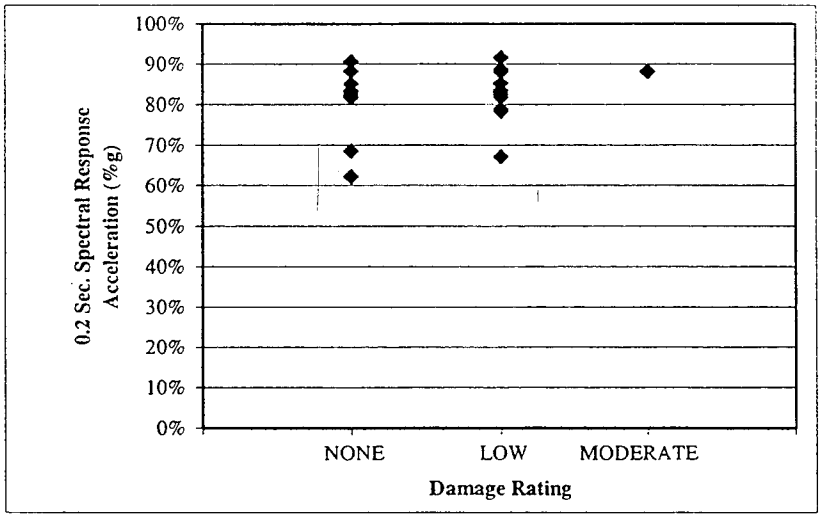

Figure 6
1.0 Sec Acceleration Response Spectra vs. Damage Rating
(Data Points Represent Individual House Samples)

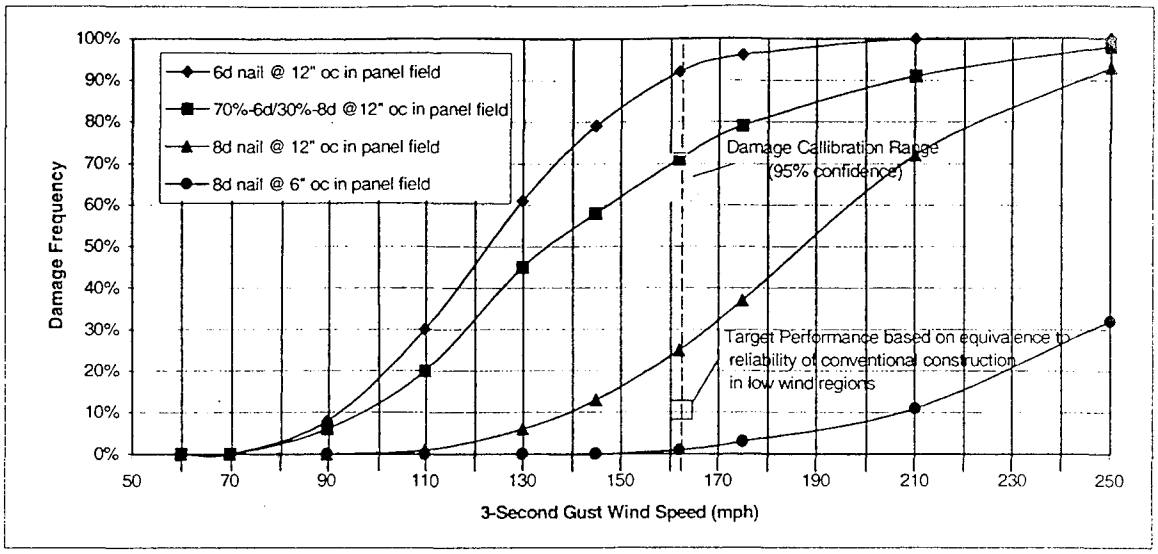

Figure 7
Roof Sheathing Fragility Curves
for One-Story Homes in a Suburban Exposure
(1 mph = 0.447 m/s).

Table 1
Construction Characteristics of SFD Dwellings

COMPONENT	NORTHRIDGE HOMES, 1994
Number of Stories	79% One 18% Two 3% Other
Wall Sheathing	80% None 7% Plywood 13% Unknown
Foundation Type	68% Crawlspace 34% Slab 8% Other
Exterior Finish	50% Stucco/Mix 45% Stucco Only 6% Other
Interior Finish	60% Plaster 26% Gypsum Board 14% Other/Unknown

Table 2
Description of Damage to Single-Family Detached Homes
(Northridge Earthquake)

Observed Damage	Sample Size	No Damage	Low Damage	Moderate Damage	High Damage
Foundation	327	295	26	3	3
Foundation-to-Walls	324	293	24	5	2
Walls	317	311	6	0	0
Roof	328	326	2	0	0
Exterior Finish	306	155	141	9	1
Interior Finish	265	132	122	11	0

Estimated Damage within Survey Area	No Damage	Low Damage	Moderate Damage	High Damage
Foundation	87.9% < **90.2%** < 92.5%	5.9% < **8.0%** < 10.0%	0.3% < **0.9%** < 2.7%	0.3% < **0.9%** < 2.7%
Foundation-to-Walls	88.1% < **90.4%** < 92.7%	5.4% < **7.4%** < 9.4%	0.5% < **1.5%** < 3.6%	0.2% < **0.6%** < 2.2%
Walls	94.0% < **98.1%** < 99.0%	0.9% < **1.9%** < 4.1%	0.0% < **0.0%** < 0.9%	0.0% < **0.0%** < 0.9%
Roof	97.2% < **99.4%** < 99.6%	0.2% < **0.6%** < 2.2%	0.0% < **0.0%** < 0.9%	0.0% < **0.0%** < 0.9%
Exterior Finish	46.7% < **50.7%** < 54.7%	42.1% < **46.1%** < 50.1%	1.6% < **2.9%** < 5.5%	0.1% < **0.3%** < 1.8%
Interior Finish	45.5% < **49.8%** < 54.1%	41.8% < **46.0%** < 50.3%	2.4% < **4.2%** < 7.3%	0.0% < **0.0%** < 1.1%
Foundation	161,300 < **165,600** < 169,800	10,700 < **14,600** < 18,400	600 < **1,700** < 4,900	600 < **1,700** < 4,900
Foundation-to-Walls	161,800 < **166,000** < 170,200	9,900 < **13,600** < 17,300	900 < **2,800** < 6,500	400 < **1,100** < 4,100
Walls	172,600 < **180,000** < 181,700	1,600 < **3,500** < 7,500	0 < **0** < 1,700	0 < **0** < 1,700
Roof	178,400 < **182,400** < 182,700	300 < **1,100** < 4,000	0 < **0** < 1,700	0 < **0** < 1,700
Exterior Finish	85,600 < **93,000** < 100,300	77,200 < **84,600** < 91,900	2,900 < **5,400** < 10,100	100 < **600** < 3,300
Interior Finish	83,500 < **91,400** < 99,300	76,600 < **84,500** < 92,400	4,300 < **7,600** < 13,400	0 < **0** < 2,100

Table 3
Construction Characteristics
of Sampled Single-Family Detached Homes

Component	Hurricane Andrew 1992
No. of Stories	80% One 2% Other 18% Two
Roof Construction	81% Gable 6% Other 13% Hip
Wall Construction	96% Masonry 4% Wood Frame
Foundation Type	100% Slab
Siding Material	94% Stucco 6% Other
Roofing Material	73% Comp. Shingle 18% Tile 9% Other
Interior Finish	Primarily Gypsum Board

Table 4
Percentage of Sampled Single-Family Detached Homes
With 'Moderate' or 'High' Damage Ratings

Component	Hurricane Andrew 1992
Roof Sheathing	24% (64%)*
Walls	2%
Foundation	0%
Roof Covering	77% (99%)[1]
Interior Finish (water damage)	85%

[1]Percentage in parenthesis includes "low" damage rating and, therefore, corresponds to homes with one or more sheathing panels lost or any form of roof covering damage. Other values indicate moderate or high damage ratings, including roof blow-off or similar serious failures (i.e., collapse).

Table 5
Summary of Exterior Finish Wall Damage
to the Sub-Sample of 49 Homes

Damage Rating	Percent of Survey
NONE	55.1
LOW	40.8
MODERATE	4.1
HIGH	0.0

Table 6
Summary of Strong Ground Motion Stations
in Close Proximity to the Sampled Homes

Station Name	Latitude	Longitude	0.2 sec Spectral Response Acceleration (%g)	0.2 sec Return Period (yrs)	1.0 sec Spectral Response Acceleration (%g)	1.0 sec Return Period (yrs)
Century City - LACC Nth	34.064	118.417	88%	292	43%	432
LA - UCLA Grounds	34.068	118.439	90%	301	24%	196
LA - Hollywood Storage Lot	34.090	118.339	100%	281	46%	514
Tarzana - Cedar Hill	34.160	118.534	270%	13,619	79%	1,813
Arleta - Nordhoff Station	34.236	118.439	81%	169	53%	502
Pacoima - Kagel & Canyon	34.288	118.375	76%	116	53%	326
Malibu - Point Dume	34.013	118.800	26%	139	10%	209
Moorrpark - Fire Station	34.288	118.881	63%	108	23%	99
Newhall - Fire Station	34.387	118.530	140%	268	117%	3,021

Table 7
Summary of Homes Surveyed on Mecca Avenue

Address	Solid Wall Ratio, β	No. of Wall Offsets	Closest Station	Damage Rating
#1 Mecca Ave	0.349	2	Tarzana[1]	None
#2 Mecca Ave	0.389	0	Tarzana[1]	Low
#3 Mecca Ave	0.455	0	Tarzana[1]	Moderate

[1]The strong motion readings at the Tarzana ground station were among the largest recorded during the Northridge Earthquake.

American Lifelines Alliance— Reducing Risks to Utility and Transportation Systems from Natural Hazards

by

Stuart Nishenko[1], Tim Sheckler[1], William U. Savage[2], and Douglas Honegger[3]

ABSTRACT

The Federal Emergency Management Agency (FEMA) and the American Society of Civil Engineers (ASCE) have entered into a cooperative agreement to establish the American Lifelines Alliance (ALA) public-private partnership project, with the goal of reducing risks to lifelines (utility and transportation systems) from natural hazards. ALA's objective is to facilitate the development and adoption of national consensus design and retrofit guidelines and standards that, when implemented by lifeline owners and operators, will systematically improve the performance of lifelines to acceptable levels in natural hazard events.

ALA is working with partners on existing non-consensus guidelines, standards, and industry practices, synthesizing and improving them, as appropriate, and shepherding the resulting documents through a formal consensus process. Each project involves (1) a Standards Developing Organization (SDO) for consensus development; (2) representatives from the appropriate sector of the utility or transportation community; and (3) representatives from the relevant manufacturing and technical communities.

ALA is using a general, well-established procedure for assessing the performance of utility and transportation systems subjected to natural hazards, and identifying actions to reduce their risk. When ALA-sponsored consensus guidelines and standards are available to implement this procedure and are applied to a specific utility or transportation system, the likely performance of the system in a natural hazard occurrence is quantified, and guidance for possible mitigation actions is provided.

ALA's initial activities are focused on converting well-established practices within the utility and transportation industries into nationally applicable consensus guidelines and standards. ALA is seeking sponsoring organizations and stakeholders to co-fund and provide in-kind support to mutually beneficial efforts. In some cases, existing practices are not sufficient to be put through a formal consensus process. In these situations, the role of ALA may include funding studies in order to improve or extend practices to the point where national consensus is achievable. ALA is also establishing extensive outreach and implementation activities.

KEYWORDS: American Lifelines Alliance, lifelines, utilities, transportation systems,

[1] Federal Emergency Management Agency, 500 C Street SW, Washington DC 20472
[2] PI/ALA Fellow, Federal Emergency Management Agency, Washington D. C., 20472 and Pacific Gas and Electric Company, San Francisco, CA 94105
[3] 2690 Shetland Place, Arroyo Grande, CA 93420

natural hazards, risk assessment, performance guidelines

1.0 INTRODUCTION

The Federal Emergency Management Agency (FEMA) and the American Society of Civil Engineers (ASCE) have entered into a cooperative agreement to establish the American Lifelines Alliance (ALA) public-private partnership project. The vision of the project is to reduce risks to lifelines (utility and transportation systems) from natural hazards. ALA's objective is to facilitate the creation, adoption, and implementation of American National Standards Institute (ANSI)-approved national consensus design and retrofit guidelines and standards. These documents, when implemented by lifeline owners and operators, will systematically improve the performance of utility and transportation systems to acceptable levels in natural hazard events. Formation of the ALA is in direct response to needs identified over 10 years ago, and is an outgrowth of a request by Congress in the 1990 Reauthorization of the National Earthquake Hazards Reduction Program (NEHRP).

The process that is being developed and implemented by ALA addresses considerations that are unique to or particularly important to transportation and utility systems.

- Each lifeline system is unique in its development history, and each system typically occupies a region that has geographically varying exposure to natural hazards. The evaluation of performance of the system must be able to accommodate the specific components of the system, which may have been designed according to different criteria at different times, and are exposed to site-specific natural hazards.
- Most lifeline systems include networks or multiple components that provide redundancy and resilience when subjected to damage or disruption. As a consequence of this inherent functionality, a given lifeline can tolerate some level of damage while providing adequate performance as far as the users of the lifeline are concerned. The analysis of risk due to natural hazards must incorporate consideration of functionality as experienced by the user of the lifeline system.
- The consensus guidance products that result from ALA activities are being prepared to be used on a voluntary basis by owners and operators of lifelines; but they could also be adopted by lifeline regulators to provide suggested or required guidance for achieving acceptable performance in response to natural hazards. Acceptable performance criteria must be explicitly established by the appropriate stakeholders, including the lifeline agency, its customers or users, and cognizant regulators. Acceptable performance criteria must include considerations of redundancy, and should preferably be characterized in probabilistic terms.

This paper describes the approach to the development of lifeline guidelines and standards being used in ALA. A general procedure commonly being used for natural-hazards risk management serves as a template for ALA product development for all lifelines. At the present time, guideline elements are being developed in several lifeline areas.

Systems suitable for the ALA process include:

Electric power transmission and distribution
Natural gas transmission and distribution
Potable water conveyance and distribution
Wastewater transportation and processing
Oil and liquid fuel handling, transport, and storage
Highways
Railroads
Telecommunications

2.0 ROLE AND SCOPE OF ALA

Under the guidance of a working group, ALA has identified lifeline systems for which non-consensus guidelines, standards, and industry practices exist. ALA is taking these existing documents, synthesizing and improving them,

as appropriate, and shepherding the resulting documents through a formal consensus process to develop nationally applicable guidelines. Each project involves a Standards Developing Organization (SDO) for consensus development, representatives from the appropriate sector of the utility or transportation community, and representatives from the relevant manufacturing and technical communities. Placing each consensus document in an SDO will ensure that the document will be reviewed and updated on a regular basis, so that it remains current with respect to new hazards data, updated system performance evaluation procedures, and changes in society's acceptable levels of risk. ALA is working with a wide range of sponsoring organizations and stakeholders to co-fund and provide in-kind support for specific activities. ALA project working group members and FEMA personnel provide coordination and oversight of these activities.

In some cases, existing practices for natural hazards risk management are not developed enough to be put through a formal consensus process. For example, databases for ice loading hazards have been developed for only the eastern half of the U. S., and procedures for evaluating the performance of water conveyance pipelines have not been comprehensively assembled for the national range of pipe types, soil conditions, levels of ground shaking, and levels of permanent ground deformation. In these and similar situations, the role of ALA includes funding or otherwise encouraging studies and projects that will improve or extend practices to the point where national consensus is achievable.

2.1 General Risk Analysis Procedure

ALA is using a general procedure for assessing the performance of utility and transportation systems subjected to natural hazards, and identifying actions to reduce their risk. The following six steps describe the procedure.

- Identify and quantify the natural hazard
- Identify and quantify the expected damage states of components within the system
- Assess the damage states and functionality of the system components when affected by a natural hazard
- Evaluate system functionality
- Identify and evaluate impacts of reductions of lifeline system functionality and financial or other losses
- Provide guidance to the system owner and others

When ALA-sponsored national consensus standards and guidelines are applied to a specific utility or transportation system, the likely performance of the system in a natural hazard occurrence is quantified, and guidance for possible mitigation actions is provided.

2.2 Implementation of ALA Guidance

ALA is also undertaking programs to encourage the implementation of natural hazards risk reduction measures by system owners and others. These programs consider the many means by which natural hazard risks can be reduced within the diverse types and sizes of lifeline systems, and address owner concerns over budgeting, coordination with other internal programs, management support for risk reduction, and regulatory issues. Also, those who are currently implementing natural hazards risk-reduction programs are being asked to identify particularly useful existing guidelines and standards, as well as barriers to their implementation. ALA is coordinating these efforts with other public/private partnerships such as FEMA's Project Impact.

2.3 Status of ALA Activities

Since its inception in 1998, ALA has developed and begun to carry out the program described above. FEMA funding has been critical in supporting these initial ALA activities:

- An increasingly broad community—from lifeline engineers to regulators to lifeline owners and operators—is being informed of ALA plans and activities. A group of more than 200 Corresponding Advisors has been established to provide input and feedback

on ALA plans.

- Several efforts have been or are being funded by the ALA project to take advantage of well-established industry practices.
  1. An engineering firm is preparing a comprehensive procedure for establishing earthquake vulnerability relationships for potable water conveyance pipelines and related facilities such canals, tunnels, storage tanks, valves, and control instrumentation. The vulnerability relationships determine the probability of specified damage states as a function of pipe or facility characteristics, and earthquake hazard characteristics including soil conditions, peak ground motions, permanent ground deformation, and other relevant parameters. This procedure will be incorporated in a subsequent development of earthquake performance-based design guidance.
  2. An existing standards committee task group is being provided with logistical support to complete development of earthquake performance criteria for gas and liquid fuels transmission pipelines.
  3. An existing ice-loading hazard map that was developed for several regions in the United States is being extended to cover the entire U. S. east of the Rocky Mountains. This map will be available to be incorporated as an appendix of the ASCE 7 Standard, *Minimum Design Loads for Buildings and Other Structures*.
- FEMA, ASCE, and Pacific Gas and Electric Company (PG&E) have established and co-fund a fellowship position at FEMA. The fellowship recipient (One of the authors of this paper) is spending one-quarter time for a year working at FEMA to bring utility expertise into FEMA's Mitigation Directorate in particular support of ALA-related activities.
- Electric power earthquake risk is one topic of the multi-participant, applied earthquake research program established in 1996 by PG&E and the Pacific Earthquake Engineering Research Center (PEER) at the University of California at Berkeley. The California Energy Commission, the California Department of Transportation, and other utilities are also providing research support. Utility-directed studies of the seismic vulnerability of high-voltage substation equipment, seismic interactions that potentially damage interconnected substation equipment, and predictive functionality models for electric power system performance in earthquake scenarios are being conducted, with the goal of incorporating the results into an ALA-developed earthquake design guideline.

4.0 CONCLUSIONS

The American Lifeline Alliance has been established as a major initiative supported by FEMA with the goal of establishing a national consensus process to reduce risks to lifelines (utility and transportation systems) from natural hazards. The ALA effort draws on the experience and expertise of lifelines personnel, consultants, academic researchers, and others to build consensus agreements on practical and effective means to accomplish this goal. With the involvement of many organizations, agencies, and individuals over the next several years, ALA is expected to oversee the development and implementation of consensus guidelines and standards that, over time, will achieve a significant improvement in the performance of lifelines affected by natural hazards.

ACKNOWLEDGEMENTS

The authors acknowledge the input to this paper derived from documents prepared by the ALA Working Group. Thomas McLane provided additional ideas and reviews. The support of FEMA, ASCE, and PG&E is gratefully acknowledged.

Theme 5

Public Health

Public Health Assessments in Post-disaster Settings: Recommendations for a Multidisciplinary Approach

by

Josephine Malilay[1]

ABSTRACT

Rapid assessments of needs and health status have been conducted by the U.S. Centers for Disease Control and Prevention (CDC) in natural disaster settings for gathering information about the status of affected populations during emergencies. A review of 8 such assessments (6 from hurricanes, 1 from an ice storm, and 1 from an earthquake) examines current methods and applications, and describes the use of results by policy makers so assessments in post-disaster settings can be improved.

Seven of the 8 (88%) were performed during or after the third day post-impact (range: 1-70 days, median: 7 days). All addressed demographics, morbidity, and water; 7 concerned food, sanitation, and transportation; and 6 queried access to medical care and electricity. All 8 provided estimates of the proportions of needs; none, however, estimated the extent of needs for the affected population. Of the 8, 5 confirmed a policy decision, such as rescheduling food delivery to an earlier date.

Increasing application of health assessments provides impetus for improving current methodologies; standardizing collection instruments; involving other sectors in emergency relief; and ensuring useful information for decision makers.

KEYWORDS: needs assessments, natural disasters, multidisciplinary assessments

1.0 INTRODUCTION

Obtaining timely, accurate, and reliable information about the needs and health status of affected populations presents a challenge to health workers who must respond appropriately and effectively to catastrophic emergencies and disaster situations. In acute settings such as post-natural disasters--defined as ecologic disruptions exceeding the local capacity to respond and calling for outside assistance--information about changing events and needs becomes critical as large numbers of people may become injured or ill or are killed, populations displaced, living conditions overcrowded, usual sanitation and hygiene compromised, and normal public health programs interrupted or ceased. Such information becomes requisite for emergency officials to make appropriate requests for urgent medical care or relief assistance.

In recent years, rapid health assessments--conducted by program managers to monitor and improve the performance of health-care systems--have become the modi operandi for gathering information about the status of an affected population, particularly during emergency response. Known also as rapid needs assessments or rapid epidemiologic assessments, these assessments represent the first line of epidemiologic response activities in the aftermath of disasters, with results providing the basis for directing relief efforts. Although earlier methods have been largely *ad hoc* and fragmentary, subsequent procedures use epidemiologic study designs and sampling approaches.

[1] Centers for Disease Control and Prevention, National Center for Environmental Health, 1600 Clifton Road, NE (Mailstop E-23), Atlanta, Georgia 30333 USA

The cluster sampling approach for assessing post-disaster needs has gained increasing attention by health subsectors providing initial response activities, such as search and rescue, disaster medicine, and emergency relief. After repeated applications in actual field settings, the design has been modified to yield reasonably accurate results that may be extrapolated to estimate the needs and the magnitude of those needs in an affected community.

Assessments of health needs have been conducted systematically in post-natural disaster settings by the U.S. Centers for Disease Control and Prevention (CDC), a public health agency tasked to address the health consequences of disasters. The specific contents of these assessments are usually at the discretion of the investigators and the local health agency who conduct the actual assessments in the field setting. Usually, with the advice and collaboration of local officials or sponsoring organizations, rapid needs assessments have addressed 1) general needs that may be common among affected populations (e.g., access to transportation and prescription medications), and 2) specific needs that may be germane to local conditions (e.g., access to particular communications media such as a radio station), or to the nature of a particular disaster event (e.g., use of gasoline-powered generators in an ice storm.)

Because the results of rapid health assessments greatly influence the nature of relief activities, a review of past applications allows us to: 1) ascertain strengths and limitations of the assessments; 2) examine the methods employed; and 3) review the usefulness of information generated and the subsequent use of this information by policy makers, so that lessons may be learned to improve health needs assessments in post-disaster settings. This review compares assessments for similarities and differences: 1) across disaster types; 2) within similar disasters; 3) by timing when the assessments are conducted; and 4) in U.S.-based versus international settings. It further identifies decision making actions that have resulted from information gathered, and finally, suggests direction for future assessments of the needs and health status of affected communities.

2.0 METHODS

Post-disaster assessments that were reported in CDC's *Morbidity and Mortality Weekly Report*, a weekly publication of current publication of current domestic and international public health issues, from 1980 through 1999 were reviewed because they applied a systematic methodology in data collection. Selected assessments were compared descriptively for the timing in which they were conducted, their content areas, sampling methodology, and results.

3.0 RESULTS

Thirteen needs assessments from 6 published reports were identified for review. Of the 13, 3 were from Hurricane Andrew in Florida and 2 were from Hurricane Andrew's subsequent strike on Louisiana, USA; 4 were from Hurricane Marilyn in the U.S. Virgin Islands, and 1 was from Hurricane Opal in the Florida panhandle; 1 was from Hurricane Georges in the Dominican Republic; 1 was from a severe ice storm in Maine; and 1 was from a major earthquake in Turkey. Five assessments from 2 separate hurricane events--Marilyn (4 assessments) and Opal (1 assessment)--were described in 1 report. Four assessments from Hurricane Andrew and its effects in 2 states, where assessments were repeated within 7 days of each other, were described in 1 report; a third assessment in one of those states was performed 2 months later and reported separately. The remaining 3 assessments--from an ice storm, Hurricane Georges, and an earthquake--were reported individually. The earliest assessment was published in 1992, the latest in 1999.

Because repeated assessments conducted within days of each other addressed the same basic items for detecting changes in needs, this analysis focuses on information from the first assessment, with the exception of the third and independent assessment related to Hurricane Andrew conducted

in Florida 2 months after the event. Therefore, 8 assessments are represented in this analysis. The Seven (88%) of the 8 assessments concerned climatic disasters, which were concentrated in U.S. states bordering the Gulf of Mexico and a U.S. territory and an island nation in the Caribbean Sea. Only 1 assessment addressed a geologic disaster, a major earthquake in Turkey. Seven of the 8 assessments were performed during or after the third day post-impact (range: 1 day to 70 days, median: 7 days). Assessments in the 2 foreign countries were performed at least 60 days after the disaster event.

3.1 Demographics, Food, Health Care, and Lifeline Systems

All 8 assessments addressed demographics (number and ages of household occupants), morbidity (types and number of sick or injured), and water supply. Seven queried residents about sanitation, food supply, and transportation; 6 inquired about access to medical care and electricity. The contents of the assessments are presented in Table 2.

For climatic disasters, the most frequent issues concerned demographics, morbidity, medical care, food, water, and sanitation. For the survey conducted 2 months after Hurricane Andrew, additional in-depth questions were raised about barriers to adequate care, health insurance, unemployment compensation, public health programs, primary health care including preventive services, nonspecific environmental problems, mental health status, and evacuation behavior. Vulnerable subgroups in the population such as young children, the elderly, pregnant and lactating women, and migrant workers who may have marginal access to relief services were identified in the assessment after Hurricane Georges in the Dominican Republic. Similar to the 2-month survey conducted after Hurricane Andrew, questions after the ice storm were specific for homes without restored electrical power, including sources for generating alternate power and the presence of working carbon Finally, we determined whether findings resulted in actions taken by decision makers such as health characteristics of the study assessments are presented in Table 1.
monoxide detectors.

Although topics for the single geologic event, an earthquake, were similar to those for hurricanes, the striking difference was the question related to disaster-related deaths in the household. No other disaster event presented a question about mortality.

Assessments conducted domestically and abroad were similar in content.

3.2 Populations at Risk

Because the primary intention of a needs assessment is to describe the scope of the needs of affected populations and ideally, the magnitude of those needs, the reports were examined for references to populations at risk. Five of the 8 assessments provided estimates of the pre-event population, usually from the census; 3, assessments from Hurricane Andrew in Florida and Louisiana and Hurricane Opal in the Florida panhandle, did not. All 8 assessments estimated needs based on proportions of needs, using population estimates derived from the demographics portion of the survey. None, however, extrapolated the magnitude of needs to estimate the extent of needs for populations at risk. For example, 52% of respondents from the example of Hurricane Marilyn had access to electrical power, indicating that 48% were without electricity at the time of the assessment. The proportion may represent 480 of 1,000 people, 4,800 of 10,000, or 48,000 of 100,000. Without knowing the population at risk and given that census estimates and electrical power records were unavailable for immediate decision-making, it is difficult to determine the magnitude of the need for electricity at the time of the survey, e.g., whether the utility needed to be restored for the households of 480 or 48,000 persons.

3.3 Actions Taken By Decision Makers

authorities and emergency management officials, and whether such actions were documented in the

report. Five of the 8 assessments confirmed actions in response to the results, such as rescheduling food delivery earlier than planned and discontinuing plans for house to house outreach when most residents had access to a particular radio station. One assessment, from the ice storm, demonstrated that although the lack of electricity was extensive and continued into a second week, most residents were able to meet their needs for food, water, warmth, and sanitation. Two assessments, from Hurricane Opal in Florida and the earthquake in Turkey, did not document any actions taken by decision makers, although results were conveyed to local health authorities.

4.0 DISCUSSION

The primary intention of needs assessment is to provide reasonably accurate and reliable estimates of needs with relatively quick turnaround so that appropriate actions for relief can be taken. However, all but 1 of the assessments actually were conducted ≥ 3 days following the event. Because these data suggest that logistical constraints may delay the arrival of an assessment team in less than 3 days, perhaps local authorities or neighboring institutions or persons should be designated by local authorities to perform assessments in the event of a major disaster. The relative simplicity of the survey instrument and an orientation to survey techniques, including the modified cluster sampling method, could be facilitated in train-the-trainer programs for emergency management, particularly for the health sector. By the same token, a needs assessment may not be realistic or practical to be conducted locally in the first 72 hours post-disaster as people are engaged in search and rescue activities, first aid, and burial of the dead.

Interestingly, all assessments used proportions based on a denominator composed of the sample population to measure the scope, or range, of needs in the surveyed community. Although this Assessments of needs and health status raise other post-disaster interests that may transcend the public health response community, particularly among professions related to prehospital emergency and disaster medicine and engineering for lifeline systems. Among responders from emergency and disaster medicine, information is needed as to what may be considered useful in

is a reasonable first step, the magnitude, or size or extent of those needs should also be estimated to reflect the needs of the entire affected community. This may be accomplished by obtaining estimates of the number of people affected by the disaster from sources such as the census or local authorities. By determining the magnitude of needs of the affected population, estimates can then be derived for response actions, such as the quantity of resources to restore electricity to a certain number of households.

Basic categories of needs and health status were uniform for the most part, particularly with regard to demographic composition of households; health status; medical care; food; water and sanitation; access to lifeline systems; housing damage; and shelter requirements. After 8 applications of the assessments, standardizing the collection, analysis, and interpretation of these elements may be a next step. A recent worldwide attempt, using the experience of nongovernmental organizations (NGOs) in humanitarian assistance, is the Sphere Project, This conglomeration of NGOs produced a charter promulgated by more than 228 organizations from more than 60 countries and identified minimum standards for disaster assistance in water supply and sanitation, nutrition, food aid, shelter and site planning, and health services. Perhaps a similar effort should be spearheaded for performing needs assessments in disaster settings, as has been recommended for situations of complex emergencies. Assessments are performed by many groups that inundate a stricken area to provide aid. The methods for the assessments are frequently undocumented, may not be systematic, and often present difficulty in interpretation and generalization to the entire disaster-affected area. Standardization of the content of needs assessments would facilitate identification of needs and delivery of appropriate services and resources in the aftermath of a disaster.

assessments conducted within 3 days, 3 to 10 days, and more than 10 days after a major disaster. For example, within 3 days of arrival, appropriate activities that may be incorporated in a needs assessment include evaluating patient volumes at emergency medical-care facilities; assessing pharmaceutical stockpiles during the emergency period; and projecting the use of stockpiles so that additional supplies may be requested in anticipation of the volume for future demand and use. Medical outreach teams have been proposed, but the reality of their arrival immediately after a disaster event raises questions about their usefulness during the emergency period. One solution may be to train local personnel to perform such assessments.

Lifeline systems, damage to pre-disaster housing, and types of shelter were addressed in most of the assessments. Usually not directly linked to public health, these topics are nonetheless associated with human health and well-being after a disaster event. For example, a continual supply of electrical power is needed for persons on home health care, storage of medicines requiring refrigeration, and heat and warmth for safe shelter. Almost immediately after a disaster, the integrity of lifeline systems is examined in field assessments, similar to those performed for public health. Including the disciplines that perform these activities in needs assessments for public health may facilitate efficiency, promote the sharing of mutually beneficial information, and consolidate appropriate resources for response.

This review included only assessments performed by CDC and reported in the *Morbidity and Mortality Weekly Report.* Many other assessments are performed in post-disaster settings by local governments, NGOs, international organizations, and military sectors from donor countries. Nevertheless, this review suggests one trend in the increasing frequency of applying post-disaster needs assessments, consistent use of specific issues, and ways in which the methods and the performance of such assessments can be modified to improve overall delivery of assessments in disaster field settings.

5.0 CONCLUSIONS

Although an element of urgency was associated with them, needs assessments in this review were typically conducted within 1 week after disasters occurred. However, this delay did not obviate their utility in the field setting depending on the objectives of the assessments and changes in needs with time. For assessments that may be performed within 72 hours of a disaster, acute needs may be related to immediate response, such as emergency needs, use of emergency services, and identification of appropriate emergency medical personnel. Additional assessments from this time have yet to be conducted for full evaluation. For assessments performed 3-10 days post-disaster, issues focused on demographics, health status, food and water supply, and restoration of utilities and services. Most of the assessments in this review were conducted during this time frame, and may be indicative of the reality of time and logistical constraints when responding to disaster events. Finally, 3 assessments also were conducted more than 1 month after the event. Categories of interest expanded to include others such as barriers to adequate care, mental health status, evacuation and storm preparation behaviors, continuing food, water, and sanitation needs, warmth, and shelter types.

Since 1992, needs assessments are increasingly being applied in the field setting. The widespread use of these techniques for disaster response provides an impetus to improve current methodologies; standardize collection, analysis, and presentation techniques; involve other disciplines who are also working to achieve the same objectives; communicate results clearly to decision makers; ensure that information is useful; and finally, document actions taken by decision makers in response to the results.

6.0 REFERENCES

Anker M. Epidemiological and statistical methods for rapid health assessment: introduction. World health statistics quarterly 1991;44:94-97.

Balthazar JC. The potential of the case-control

method for rapid epidemiological assessment. World health statistics quarterly 1991;44(3):140-144.

Boss LP, Toole MJ, Yip R. Assessments of Centers for Disease Control and Prevention. Rapid health needs assessment following Hurricane Andrew -- Florida and Louisiana, 1992. Morbidity and Mortality Weekly Report 1992;41(37):685-688.

Centers for Disease Control and Prevention. Comprehensive assessment of health needs 2 months after Hurricane Andrew -- Dade County, Florida, 1992. Morbidity and Mortality Weekly Report 1993;42(22):434-437.

Centers for Disease Control and Prevention. Surveillance for injuries and illnesses and rapid health-needs assessment following Hurricanes Marilyn and Opal, September-October 1995. Morbidity and Mortality Weekly Report 1996;45(04):81-85.

Centers for Disease Control and Prevention. Community needs assessment and morbidity surveillance following an ice storm -- Maine, 1998. Morbidity and Mortality Weekly Report 1998;47(17):351-354.

Centers for Disease Control and Prevention. Needs assessment following Hurricane Georges -- Dominican Republic, 1998. Morbidity and Mortality Weekly Report 1999;48(05):93-95.

Centers for Disease Control and Prevention. Community needs assessment and morbidity surveillance following an earthquake -- Turkey, August 1999. Morbidity and Mortality Weekly Report 1999;48(50):1147-1150.

Guha-Sapir D. Rapid assessment of health needs in mass emergencies: review of current concepts and methods. World health statistics quarterly 1991;44(3):171-181.

Gunn SWA. Multilingual dictionary of disaster medicine and international relief. Dordrecht, the Netherlands: Kluwer Academic Publishers, 1990.

mortality, morbidity, and nutritional status in Somalia during the 1991-1992 Famine. Journal of the American Medical Association 1994;272:371-376.

Hlady G, Quenemoen LE, Armenia-Cope RR, et al. Use of a modified cluster sampling methods to perform rapid needs assessment after Hurricane Andrew. Annals of Emergency Medicine 1994;23:719-725.

Leonard RB, Spangler HM, Stringer LW. Medical outreach after Hurricane Marilyn. Prehospital and Disaster Medicine 1997;12(3):189-194.

Lillibridge SR, Noji EK, Burkle FM. Disaster assessment: the emergency health evaluation of a population affected by a disaster. Annals of Emergency Medicine 1993;22:1715-1720.

Malilay J, Flanders WD, Brogan D. A modified cluster-sampling method for post-disaster rapid assessment of needs. Bulletin of the World Health Organization 1996;74:399-405.

Pan American Health Organization. Epidemiologic surveillance after natural disaster. Scientific Publication No. 420. Washington, D.C.: PAHO, 1982.

Smith GS. Development of rapid epidemiological assessments methods to evaluate health status and delivery of health services. International Journal of Epidemiology 1989;18:S2-S15.

The Sphere Project. Humanitarian charter and minimum standards in disaster response. Oxford, United Kingdom: Oxford Publishing, 2000.

Table 1. Characteristics of 8 needs assessments from the Centers for Disease Control and Prevention, *Morbidity and Mortality Weekly Report*, 1980-2000

Characteristic	No. of assessments
Disaster type	
Climatic (hurricane, ice storm)	7
Geologic (earthquake)	1
Timing of assessment	
< 3 days post-event	1
3-10 days	4
> 10 days	3
Number of assessments of same event	
Hurricane Marilyn, U.S. Virgin Islands	4
Hurricane Andrew, Florida	3
Hurricane Andrew, Louisiana	2
Sampling method	
Systematic	1
Cluster	
Modified 1-stage	6
2-stage	1
Estimate of population at risk in disaster zone addressed	
Yes	7
No	1
Type of information provided	
Proportion of needs (%)	8
Extent of needs extrapolated for population at risk	0
Actions taken by decision makers	
Yes, documented	5
No, unneeded	1
Unknown	2

Table 2. Contents of assessments and time frame in which assessments were conducted

Topic	No. of assessments performed within days of event			
	< 3 days n=1	3-10 days n=4	> 10 days n=3	Total
Demographics				
No. and ages of household occupants	1	4	3	8
Vulnerable subgroups				
< 2 years, > 65 years,	1	—	2	3
pregnant female	—	—	2	2
Health status				
Morbidity				
types	1	4	3	8
no. of sick/injured	1	4	3	8
Mortality (no. of deaths)	—	—	1	1
Medical care (Needs and access to prescription medicine)	—	4	2	6
Food supply (Availability)	—	4	3	7
Water supply (Availability, source, and treatment)	1	4	3	8
Sanitation (Access to working toilet)	1	4	2	7
Housing damage	—	2	2	4
Shelter type	—	2	2	4
Access to lifeline systems				
Electricity (Status and sources)	1	4	1	6
Communications	1	4	—	5
Transportation	1	4	2	7

ASSESSMENT MODELS FOR EARTHQUAKE FATALITIES AND AN INTERPRETATION OF THE DEATHS IN THE 1999 KOCAELI, TURKEY, EARTHQUAKE[1]

by

Keishi SHIONO[2]

ABSTRACT

Two models for estimating earthquake fatalities were developed on the basis of existing knowledge in seismology, earthquake engineering, and natural disaster sciences. Those were designed so that disasters in the wide range of built environment are coherently examined with a limited range of input information. The performance accuracy of the models was examined and confirmed acceptable. One of the two models was applied to the discussion on the nature of the fatalities in the Kocaeli earthquake. It was pointed out that the enhancement of structural quality of multi-story apartment buildings is crucial toward the reduction of human losses in future earthquakes.

KEY WORDS: Earthquake Disaster
Damage Estimation
Mortality
Kocaeli Earthquake

1. INTRODUCTION

It is easy to understand that earthquake casualties depend on: 1) earthquake, 2) building collapse, and 3) affected population. Even non-professional people can tell that more victims are killed if an earthquake is more violent; if more buildings collapse; and if more people stay in a building.

Quantitative evaluation of earthquake fatalities, however, has seldom been attempted despite its significance in discussion toward the reduction of human casualties. Though not a few methods for correlating building damage to human losses were developed, those applicability was rather limited. Those were useful only in areas having the same built environment, which is characterized mainly by the construction type of local buildings.

Mass casualty in earthquakes is a serious issue from the viewpoint of global disaster management. With relation to the issue, it is crucial to have an estimation model that can coherently handle disasters in areas with different built environment.

In the first half of this paper, two models for estimating earthquake fatalities, which require only a limited range of input information, but applicable to disasters in the wide range of built environment were developed. In the last half, one of the two models was applied to the discussion on the nature of the fatality in the M7.4 Kocaeli, Turkey, earthquake of August 17, 1999.

2. TWO MODELS

Two models as follows were developed in this study:

1) Distribution model
2) Point model.

---

1) This is a revision of a paper presented in Third Japan-Turkey Workshop on Earthquake Engineering, February 21-25, 2000, Istanbul, Turkey.

2) Department of Civil Engineering, Nagaoka College of Technology, Nagaoka, Niigata 940-8532 Japan

The most significant difference between the two models is found in the method for giving seismic information. It was given by the spatial distribution of seismic intensity in the distribution model, while it was given by a single parameter of the earthquake magnitude in the point model. The point model did not include the spatial variation of seismic intensity in an explicit manner, but one of the relationships used in the model included the attenuation of seismic intensity.

In the point model, population density was given as that for the entire affected area. Building information was given as dominant construction types chosen from a nine-category classification. The classification was done based on the type of principal load-bearing elements and wall material. Detailed explanation is seen in the following section.

The point model is simple, because it was given as a single formula. Only substitution of three independent variables into the formula is required for deriving an estimate. A flaw in the point model lies in the exclusion of spatial relationship, or distance, between an epicenter and affected areas. However, this does not reduce the model's applicability, because most earthquake disasters are attributed to earthquake faults located near affected areas.

In the distribution model, earthquake information was given by the spatial distribution of seismic intensity. The spatial distribution of population density can be included if necessary. Building types were assigned from the nine-category classification, as was done in the point model, and their spatial distribution can be included if necessary. Numerical procedure in the distribution model is more precise in comparison with that in the point model. The numerical procedure in the distribution model, which requires a small computer program, is a little more complicated than that in the point model.

Characteristics of the two estimation models are compared in Table 1.

Only the general ideas for constructing the models and the performance accuracy of the models are described in this paper. Results of case studies for verifying the models are seen in Shiono et al. (1991).

3. DISTRIBUTION MODEL

(1) Structure

Figure 1 shows the flow of calculation in the distribution model. Figure 2 is schematic presentation of the numerical procedure in the distribution model.

Input information was composed of two parts:

1) Earthquake information
2) Regional information.

Earthquake information includes:

1) Surface wave magnitude
2) Epicentral location.

Regional information consists of:

1) Population density
2) Building type (s)
3) Site condition in terms of increment in seismic intensity.

Geographical area in which the three regional data assigned must be coincide with an affected area. Spatial distribution of regional data and a combination of dominant construction types can be included if necessary.

A nine-category classification representing worldwide construction types consists of:

1) Field stone
2) Adobe
3) Cut stone
4) Brick
5) Wood frame with thin infill walls
) Wood frame with thick infill walls
7) Wood
8) Poor-quality reinforced concrete
9) Good-quality reinforced concrete.

Buildings of field stone and adobe correspond to structures classified in Category A of the MSK seismic intensity scale. Buildings of cut stone, brick, and wood frame with infill walls, or half timbered structures, are in Category B. Buildings of wood and good-quality reinforced concrete are in Category C. Buildings of poor-quality reinforced concrete need further discussion to be classified in an appropriate category.

Relationships, or knowledge, used in the distribution model were as follows:

1) Epicentral seismic intensity versus magnitude
2) Attenuation of seismic intensity with distance (Attenuation function)
3) Structural vulnerability of each construction type versus seismic intensity
4) Fatality rate (deaths/population) in each construction type versus collapse rate.

Distribution of seismic intensity was determined from: 1) magnitude versus epicentral intensity relationship, such as Karnik (1965), and 2) an attenuation function, such as Chandra (1979). A simplified approximation of the circular distribution of seismic intensity was employed in this study.

A vulnerability function, which is given as a relationship between seismic intensity and damage extent sustained by a single building, was defined for each construction type, and a set of nine collapse rate functions was generated to represent the total of construction types (Figure 3). Detailed explanation of the procedure for deriving collapse rate functions from vulnerability functions is found in Shiono et al. (1991).

Fatality rare functions were determined based on published survey results, such as Coburn et al. (1989). A set of three functions shown in Figure 4 was used in this study.

(2) Performance

Data from numerous past earthquakes exist to examine performance accuracy of the estimation model. Data were collected from 16 earthquakes (1962-1986) listed in Table 3. In collecting data, any criteria for selecting events was used, so that a performance test can be done with as many data as possible. However, several earthquakes in which damage was limited to sites distant from the epicentral regions, such as the Rumanian earthquake of 1977 and the Mexican earthquake of 1985 were excluded. For these disasters, a simplified approximation of the circular distribution of seismic intensity, which was used in this development, is no longer appropriate.

Death tolls calculated in the distributed model were plotted in Figure 5 in comparison with reported fatalities. A correlation coefficient of 0.84 was obtained between the estimated and reported death tolls for the entire (16) events, and that of 0.90 was obtained for the 13 events in which more than 1,000 lives were lost.

4. POINT MODEL

A simplified method, where spatial variation of seismic intensity was not explicitly included, was constructed and named the point model. A relationship derived from the distribution model, which implicitly includes the attenuation of seismic intensity, was used in the point model. In handling of the point model, programming in computers was not required. Only substitution of three variables, which respectively represent earthquake, building, and demographic characteristics of a disaster, into a single formula was necessary.

Input data to the point model were:

1) Surface wave magnitude
2) Dominant construction type (s) of local buildings
3) Population density (whole disaster area).

Among the three variables, magnitude was chosen as the principal variable, and the relationships between magnitude and fatalities was analyzed. Other two variables representing

buildings and population were used as correction factors.

Figure 6 shows the relationship between magnitude and crude death tolls for the earthquake disasters listed in Table 3. Positive correlation between the two variables are seen, but the plots considerably scattered with a correlation coefficient of 0.46. Logarithms of death toll were used in the calculation of correlation coefficients.

Figure 7 illustrates how magnitude correlates with death tolls when death tolls were adjusted on an assumption that population densities of disaster areas are identical at 38 persons per sq-km. A population density of 38 persons per sq-km was given as the global average of population density. Scattering of the plots reduced, and the correlation coefficient increased up to 0.68.

The relationship between magnitude and deaths calculated in the distribution model is shown in Figure 8. In the calculation for deriving this chart, population density was given at 100 persons per sq-km. Relationships were essentially straight lines, and the lines were nearly parallel to each other. In view of these characteristics, ratios among the fatality rates in various construction types can be admitted constant irrespective of earthquake magnitude. The ratios were determined in Figure 8, and the results are shown in Table 3.

Figure 9 shows how magnitude correlates with fatalities when those were normalized by population density and corrected by construction type. The ratios shown in Table 3 were used for including the difference in vulnerability and lethality among the construction types. Scattering of the plots further reduced, and a correlation coefficient as high as 0.79 was obtained. A correlation coefficient of 0.48 was obtained when only correction by construction type took place, suggesting the significance of simultaneous inclusion of population and building characteristics.

From the regression line derived in Figure 9 with the ratios shown Table 3, the following formula was obtained:

$$D=(2.57 \times 10^{-6}) \times \exp(2.93M) \times (p/38)$$

$$X \begin{cases} 2.2 & \text{(Field stone, Adobe)} \\ 1.0 & \text{(Brick, Cut stone)} \\ 0.33 & \text{(Low-quality reinforced concrete)} \\ 0.12 & \text{(Wood frame with thick infill masonry walls)} \\ 0.026 & \text{(Wood frame with thin infill masonry walls)} \\ 0.0017 & \text{(Wood)} \end{cases} \quad \cdots (1)$$

where,

D: deaths
M: magnitude (Ms)
p: population density of an affected area.

This equation can be applied to disaster areas having two or more dominant construction types. In that case, population density is given for each construction type, as total occupancies in residential buildings of each construction type.

Death tolls calculated in the two models were plotted in Figure 10 in comparison with reported tolls. Relative accuracy of the estimates obtained in the two models can be compared. Correlation coefficients between reported and estimated death tolls were obtained at 0.73 in the point model and at 0.84 in the distribution model, respectively. In the regard of performance accuracy, the point model is almost equal to the distribution model.

5. DEATHS IN THE KOCAELI EARTHQUAKE

The Kocaeli earthquake (M7.4) occurred on August 17, 1999 in the northwestern part of Turkey, and the death toll announced on September 13 was 15,480.

Post-event fatality estimation was done with the point model (Eq. (1)).

Following assumptions were made in the estimation:

1) Brick, half-timber (wood frame with thick infill walls), and poor-quality reinforced concrete were the dominant construction types in the affected area.
2) Brick and half-timber were structural types for single-family houses, while reinforced concrete was that for multi-story apartment buildings.
3) Ten families reside in an apartment building.

With assumed regional data shown in Figure 11 and Table 4, Equation (1) gave an estimated death toll of 15,380. The estimate was acceptable, though further investigation on the regional characteristics is indispensable.

A few additional cases were examined with equation (1), and the result is shown in Figure 12.

The cases represent a probable scenario of future transition in building type accompanying with regional development. The scenario includes, first, the rapid influx of population into industrializing areas, among which is the Kocaeli area severely damaged in the 1999 earthquake, and, second, increased demand for high-occupancy residential buildings, which are supplied as multi-story apartment buildings of reinforced concrete.

In comparison with a population density of 227 persons per sq-km on Stage 0, which represents the 1999 situation, that on Stage 3 is as high as 454 persons per sq-km. The increase in population results in that in the number of multi-story apartment buildings from 30% on Stage 0 to 60% on Stage 3. Increased death tolls on the later stages are attributed to the structural vulnerability in high-occupancy residential buildings of reinforced concrete.

6. CONCLUSIONS

Two models for estimating deaths in the wide range of built environment affected by any given earthquake were constructed. Those are simple and useful requiring a limited range of input information consisting of earthquake, building, and demographic data. Among the two models, one was named the distribution model, and the other the point model. The distribution model includes the spatial variation of input data, while the point model does not. Their performance accuracy was examined and proved acceptable, though the point model was sightly less accurate than the distribution model.

The point model was employed in the post-event estimation of the deaths in the 1999 Kocaeli earthquake. Remarkable agreement between the estimate and the official announcement was obtained, though the building information, or predominant construction types, was rather intuitive.

Death tolls in probable future circumstances of the Kocaeli area due to hypothetical recurrences of the 1999 earthquake were estimated in the point model. Estimated death tolls increase with the progress of regional development accompanied by population influx and increased demand for high-occupancy residential buildings. Structural quality management of high-occupancy residential buildings, or multi-story apartment buildings of reinforced concrete, is crucial toward life safety in future earthquakes.

The author thanks Professor Y. Ohta of Aichi-Shukutoku University and Professor H. Murakami of Yamaguchi University for their valuable contribution to this paper.

REFERENCES

Chandra, U. (1979): Attenuation of intensities in the United States, Bulletin of the Seismological Society of America, Vol. 69, No. 69, pp. 2003-2024

Coburn, A. W., A. Pomonis, and S. Sakai (1989): Assessing strategies to reduce fatalities in earthquakes, Proceedings of International Workshop on Earthquake Injury Epidemiology for Mitigation and Response, July 10-12, 1989, Baltimore, Maryland, pp. P107-P132

Karnik, V. (1965): Magnitude-intensity relationship for European and Mediterranean seismic regions, Stadia Geoph. et Geod., Vol. 9, pp. 236-249

Shiono, K., F. Krimgold, and Y. Ohta (1991): Post-event rapid estimation of earthquake fatalities for the management of rescue activity, Comprehensive Urban Studies, Center for Urban Studies, Tokyo Metropolitan University, No. 44, pp. 61-106

Table 1: Comparison of input data between fatality estimation models

Model	Category of Data			Procedure
	Earthquake	Building Type	Population Density	
Point Model	Magnitude	Predominant Types*	Average for the Whole Disaster Area	Formula
Distribution Model	Seismic Intensity Distribution**	Predominant Types*	Spatial Distribution	Small Program for Personal Computers

* Assigned from a nine-category classification (see the following section).

** Intensity distribution is given based on earthquake magnitude, epicentral distance, and site amplification.

Table 2: Earthquake disasters of which data were used in the verification of the model

	Affected Country	Year	M	Fatalities
1	Iran	1962	7+1/4	12,000 - 15,000
2	Turkey	1966	6.5	2,394
3	Turkey	1967	7.5	89
4	Iran	1968	7.3	7,000 - 10,000
5	Turkey	1970	7.1	1,086
6	Turkey	1971	6.0	57
7	Turkey	1971	6.7	878
8	Iran	1972	7.1	5,000
9	Nicaragua	1972	6.6	5,000 - 11,000+
10	Turkey	1975	6.7	2,385
11	Guatemala	1976	7.5	22,778
12	China	1976	7.8	242,419
13	Turkey	1976	7.4	3,840
14	Algeria	1980	7.3	2,263
15	Italy	1980	6.8	2,735 - 4,689
16	El Salvador	1986	5.4	1,500

Table 3: Ratio of fatality rate in various construction types to that in brick buildings

Building Type	Ratio of Fatality Rate*
Field stone, Adobe	2.2
Brick, Cut stone	1.0
Poor-quality reinforced concrete	0.33
Wood frame with thick infill walls	0.12
Wood frame with thin infill walls	0.026
Wood	0.0017

* Fatality rate in brick building is used as the standard.

Table 4: Assumed built and demographic environment of the Kocaeli area

Construction Type	Relative Number of Buildings	Relative Number of Occupants*	Population Density
Brick	40%	10.1%	24.5
Half-Timber	30%	8.1%	18.4
Poor-Quality RC	30%	81.8%	184.1
Total	100%	100%	227**

* Ten (10) was assumed as the number of families residing in a reinforced concrete apartment building.

** The population density of the affected area was given at 227 persons per sq-km, which is the population density of Kocaeli Province.

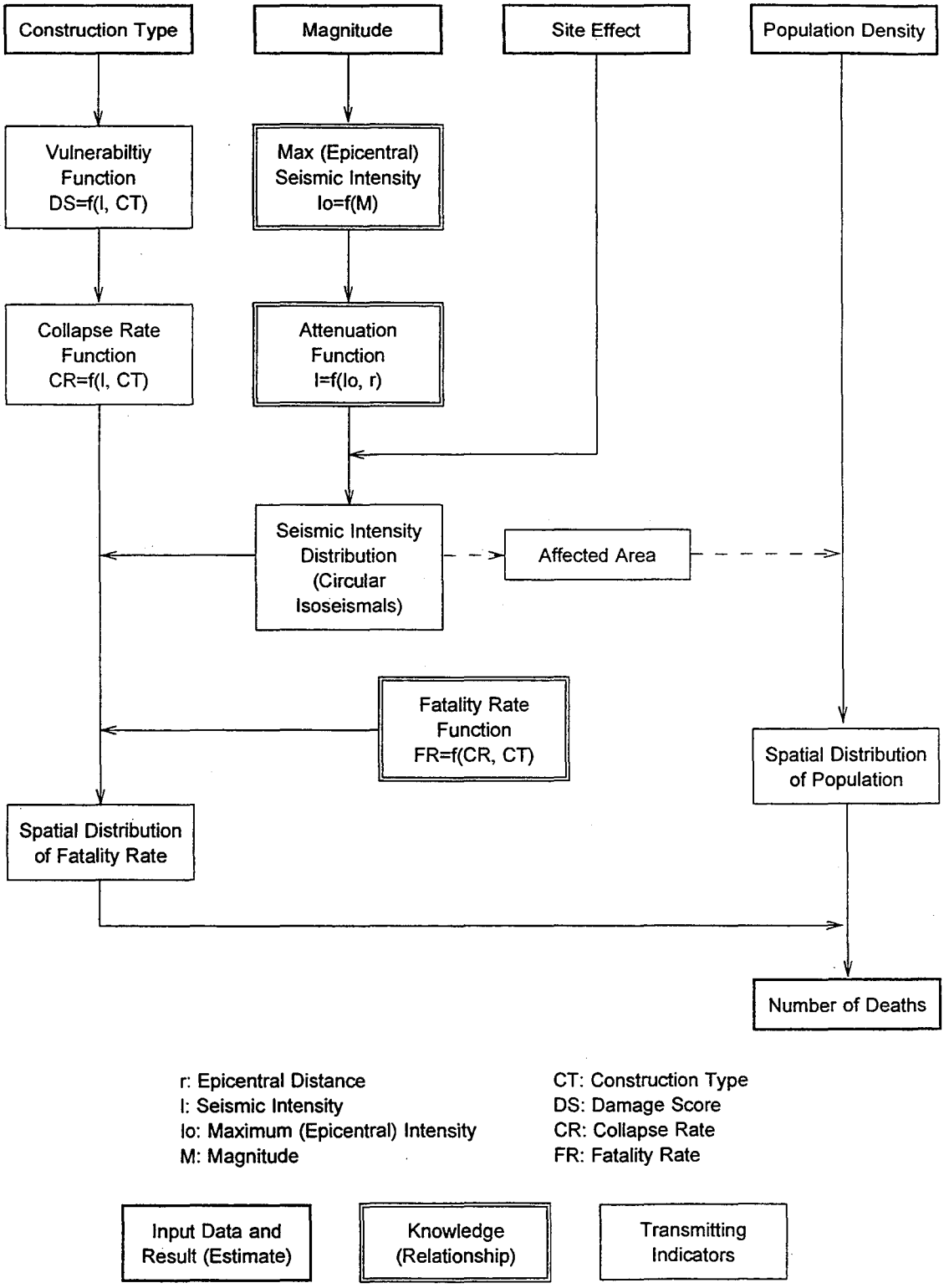

Figure 1: Flow of fatality estimation in the distribution model.

$$D = \int_\theta \int_r f(\rho \cdot V(I))\, d\, r\, d\, \theta$$

D : Total deaths
f : Deaths / sq-km
I : Seismic intensity
V : Collapse rate of buildings
ρ : Population density

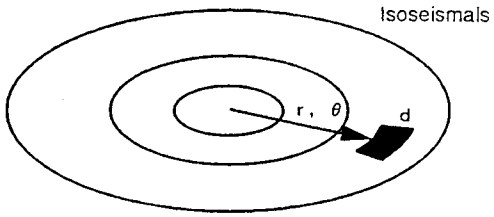

Figure 2: Schematic presentation of fatality estimation in the distribution model.

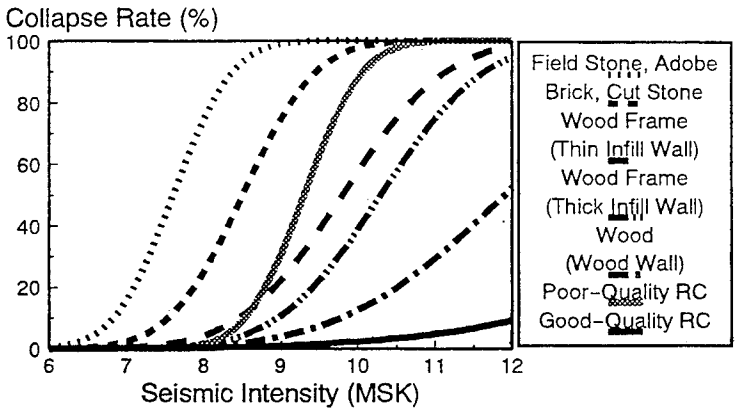

Figure 3: Collapse rate functions.

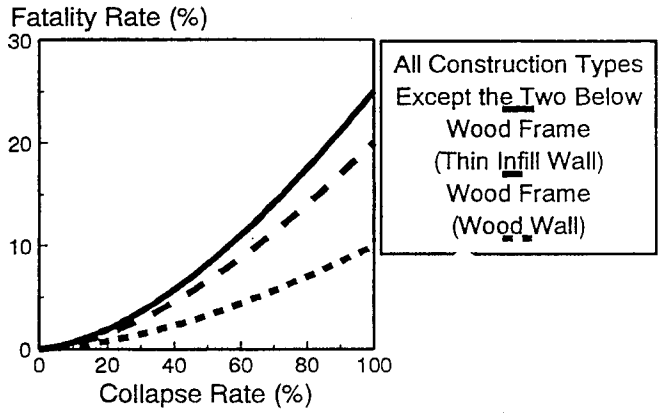

Figure 4: Fatality rate functions.

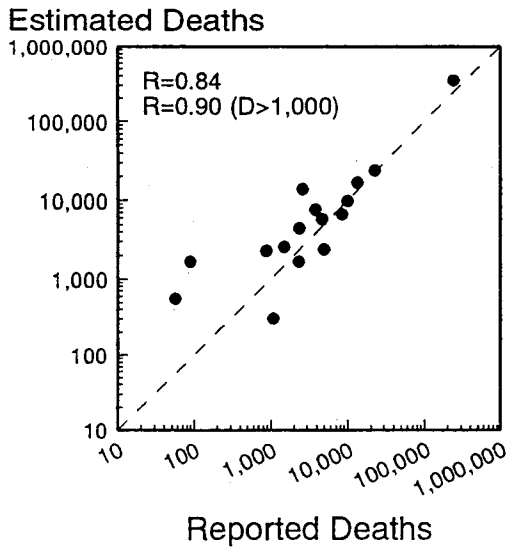

Figure 5: Comparison between reported and estimated death tolls.

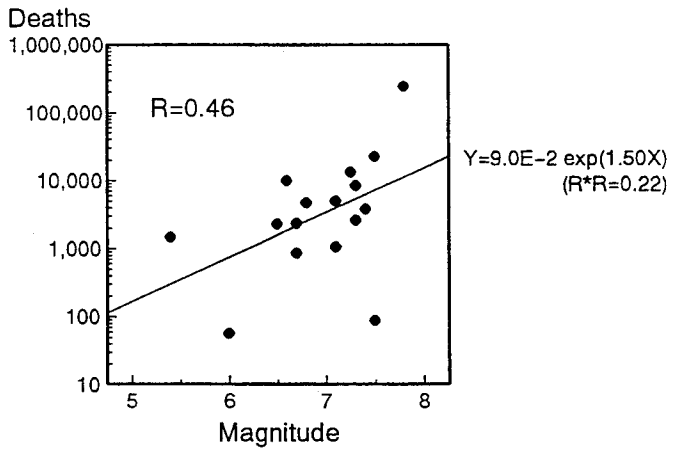

Figure 6: Relationship between earthquake magnitude and fatalities; Crude death tolls are plotted.

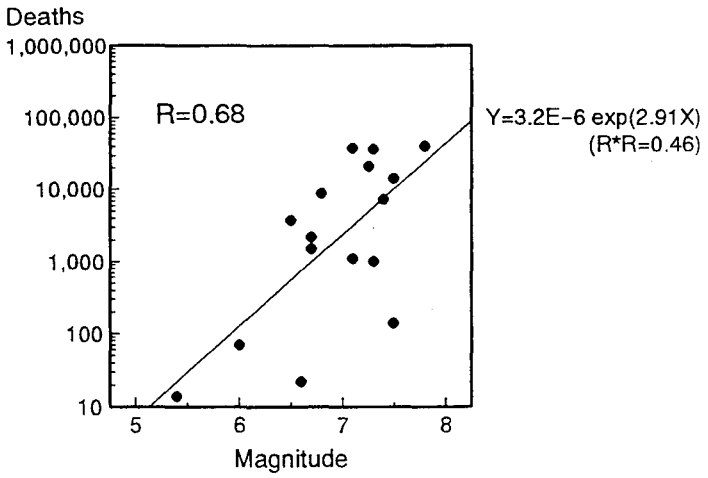

Figure 7: Relationship between earthquake magnitude and fatalities; Death tolls are normalized by the global population density.

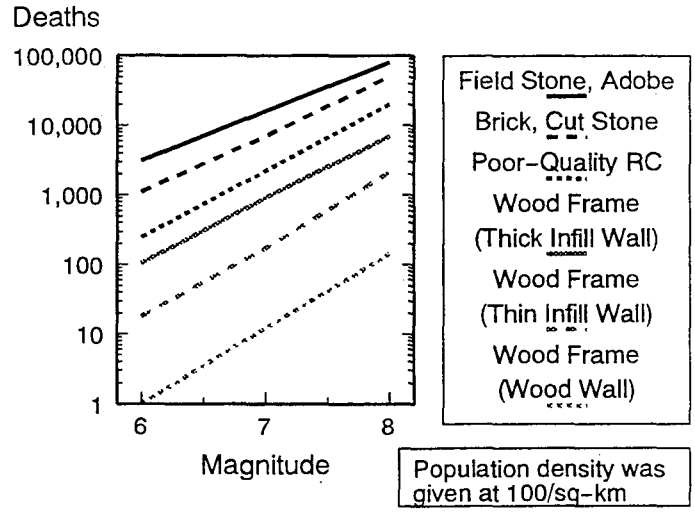

Figure 8: Relationship between earthquake magnitude and fatalities; Population density is normalized at 100 persons per sq-km.

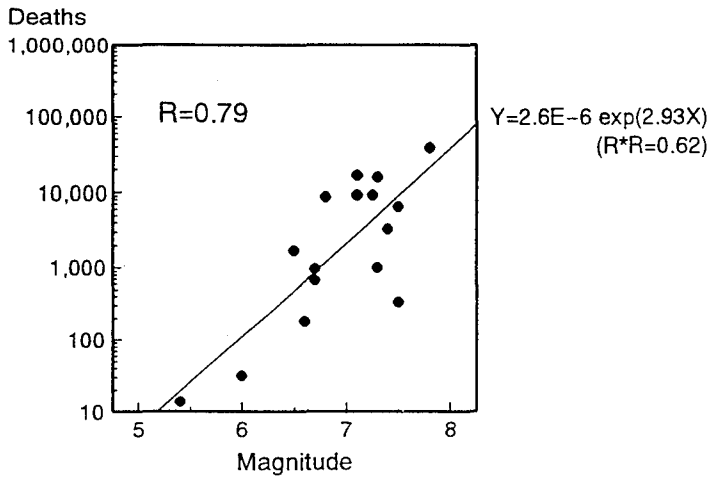

Figure 9: Relationship between earthquake magnitude and fatalities;
Death tolls were normalized by population density and corrected by building type.

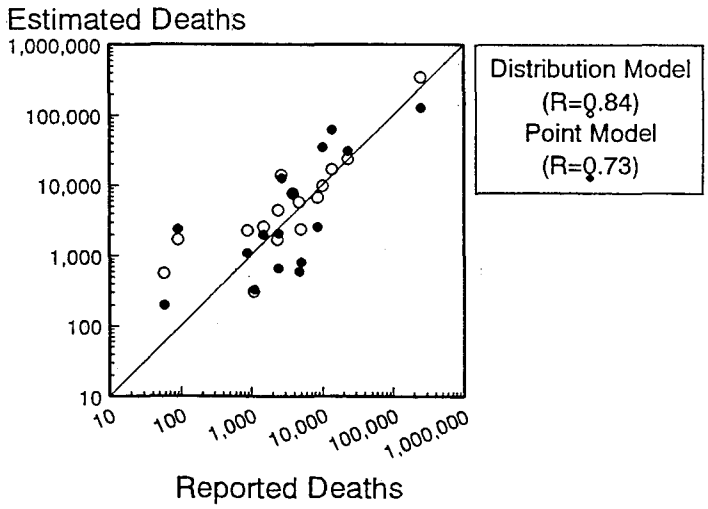

Figure 10: Comparison between recorded and estimated death tolls;
Death tolls estimated in the two models can be compared.

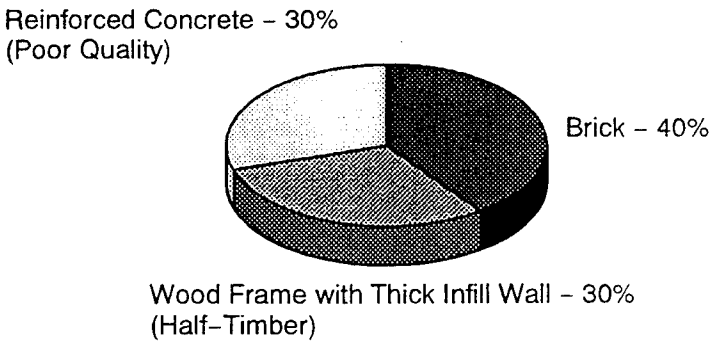

Figure 11: Relative number of buildings by construction type in the affected area of the Kocaeli earthquake.

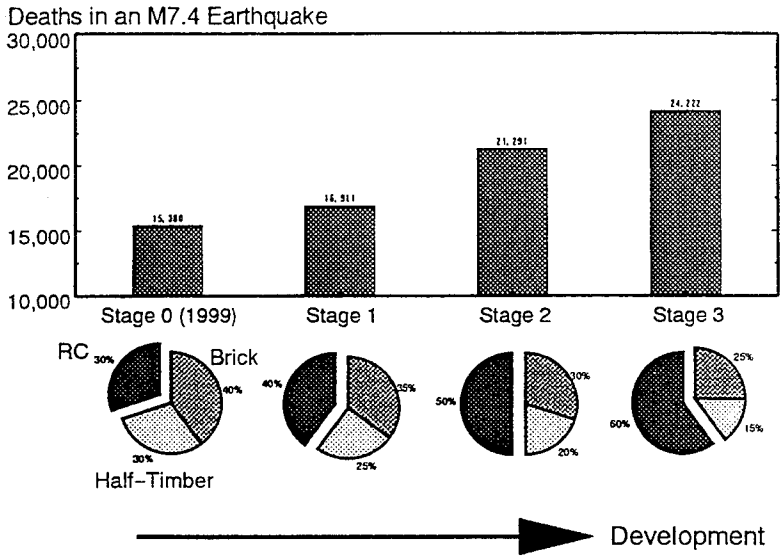

Figure 12: Increase in expected deaths with the progress of regional development.

Predictors For People's Response to a Tornado Warning, Arkansas, March 1, 1997

By

Lina Balluz, MPH, Sc.D.[1], Laura Schieve, MPH, Ph.D.[2], Talmage Holmes, Ph.D.[3], Stephanie Kiezak, MS[1], Josephine Malilay, Ph.D.[1]

ABSTRACT

Nine powerful (F3-F4) tornadoes hit Arkansas from the southeastern to the northeastern part of the state during the afternoon of March 1,1997. The strongest of the tornadoes touched down in Saline and Clark Counties. We assessed factors associated with people's response to the tornado warning issued in Clark and Saline Counties, Arkansas. We conducted a population-based cross-sectional study in Clark and Saline Counties. We administered a comprehensive questionnaire by telephone to all selected individuals who stated they were at home prior to tornado touch down. Factors associated with response to the warning were educational level equivalent to or greater than high school , presence of a basement in the house , hearing a siren , and having prepared a plan to respond when tornadoes occur. A summary of the results and recommendations are presented.

KEYWORDS: Cross-sectional study, Disaster response, Emergency management, Tornado,

INTRODUCTION

Approximately nine powerful tornadoes hit Arkansas from the southwest to the northeast part of the state during the afternoon of March 1, 1997 (National Weather Service, 1997). Damage indicated that two counties (Saline and Clark) had been hit by tornadoes of F4 intensity on the Fujita-Pearson tornado scale (National Weather Service, 1997). These tornadoes were estimated to be one half to one mile wide, with wind speeds in excess of 200 miles per hour (National Weather Service, 1997). Twenty-six The most common sources from which participants learned about tornadic activity are listed in Table 1. People with at least a high school education were more likely to respond to

fatalities and 400 nonfatal injuries were reported (CDC, 1997). Tornadoes are the most frequent adverse weather event likely to result in a disaster in the United States (Noji, 1997). These storms can result in mass-casualty situations for emergency and local medical facilities (Harris, 1992; Glass, 1980; CDC, 1985). Inadequate warning for the population at risk is one of the main contributing factors to tornado-related deaths and injuries. However, little information is available about the public's response to these warnings, such as the percentage of people seeking appropriate shelters after hearing a tornado warnings.

In this study, we present the results of a post-tornado survey of community residents in Arkansas to determine factors associated with appropriate responses to tornado warnings.

METHOD AND RESULTS

We conducted a population-based cross-sectional study of residents of Clark and Saline Counties. These counties were chosen because they sustained the most severe property damage, and experienced the most fatalities and injuries as a result of the tornadoes. We used random-digit dialing to select a sample of residents from these counties. We administered a comprehensive questionnaire to the 146 participants. Of the 146 participants, none were injured during the tornado, and 5 (3.4%) reported damages to their homes. In addition, 140 (95.9%) understood the terms "tornado watch" and "tornado warning". Of those 140 participants, 64 (45.7%) responded to the warning by seeking shelter.

warning (OR=4.2, 95% CI= 1.1-15.5). People living in a house with a basement were more likely to respond than those without a basement (OR=3.8, exact 95% CI=1.1-17.1). In addition, people who responded were more likely to live in an area actually hit by a tornado (OR= 7.2, 95% CI=1.9-40.6), to have heard sirens (OR=4.4, CI=1.3-18.9) and to have prepared a plan of action (OR=2.6, 95% CI=1.1-6.3) than were those who did not respond to the warning. We also looked at when participants first learned of tornado activity and the amount of time they had to respond. Of the 146 participants, 82 (56%) reported first being aware of a tornado threat at least 10 minutes before it passed through the area, and of the 64 who responded to the warnings, 58 (90.6%) reported a response time (time between hearing a warning and seeking shelter) of 5 minutes.

CONCLUSIONS:

Our findings are consistent with other post-disaster investigations that identified factors specifically associated with reducing mortality and injury. We showed that those factors were also associated with seeking appropriate shelters after hearing tornado warnings. We recommend that people who live in tornado-prone areas without underground shelters, should prepare a plan of action to help them respond immediately to tornado warnings in an effective manner. Elements of this plan may include engaging in tornado drills to familiarize members of the household with safety procedures, sources of shelters in the home or outdoors, and keeping specialized weather radios such as those from the National Oceanic and Atmospheric Administration (NOAA) available in the home. Because the frequency of tornado watches may desensitize people to the dangers of tornadoes, we also recommend increased public health education about how to respond to tornado watches and warnings in areas with high tornadic activity. When planning protective actions such as constructing accessible tornado-resistant shelters, and developing tornado-preparedness programs for at-risk populations, emergency management officials should keep in mind that people have limited time to find shelters.

References

1. Centers for Disease Control and Prevention (1997) Tornado-associated fatalities-Arkansas, 1997. MMWR 46(no.19).

2. Centers for Disease Control and Prevention. (1985) Tornado disaster, North Carolina, South Carolina. MMWR 34:205-212.

3. Glass RI, Carven RB, Bergman DJ, et al. (1980) Injuries from the Wichita Falls tornado: implications for prevention. Science 207:734-738.

4. Harris LF. (1992) Hospitalized tornado victims. Ala Med 61:12-16.

5. Noji EK. (1997) The public health consequences of disaster. Oxford University Press.

1

[1]Centers for Disease Control and Prevention, National Center for Environmental health, 1600 Clifton Road, NE, MS E-23, Atlanta, GA, 30333

Table 1. Sources of tornado warnings heard by survey participants who did and did not seek shelter Arkansas, 1997

Sources	Sought shelter		Did not seek shelter	
	Number	Percent	Number	Percent
Television	52	81.2	59	78.6
Siren	46	71.8	42	56.0
Weather changes	32	50.0	30	40.0
Commercial radio	16	25.0	8	10.6

POST-DISASTER CARBON MONOXIDE POISONING: AN EMERGING HEALTH PROBLEM

by

W. Randolph Daley, DVM, MPH[1]

ABSTRACT

Carbon monoxide (CO) is an odorless, colorless gas capable of causing acute injury and death. Following meteorological disasters over the past decade, CO poisoning has become an increasingly recognized problem. Through case descriptions and studies of post-disaster CO poisoning, important risk factors can be recognized and controlled.

Major sources of CO poisoning vary greatly, largely dependent on the type of the disaster. A number of CO sources were important in poisoning cases following recent winter storms in Washington, Tennessee, New York, and Maine. These included gasoline-powered electric generators, charcoal grills, portable gas stoves, and portable space heaters. Following snow storms in Massachusetts, New York, and Pennsylvania, cases of CO poisoning resulted from exposures in idling motor vehicles. Several severe poisoning cases in North Carolina after Hurricane Fran and the first two deaths related to Hurricane Georges in Puerto Rico were due to CO poisoning from generators.

Investigations of these outbreaks of CO poisoning have greatly increased our understanding of the important factors involved. By properly applying this knowledge, future morbidity and mortality from post-disaster CO poisoning can be prevented.

KEYWORDS: carbon monoxide, poisoning, disaster, winter storm, hurricane, epidemiology, environmental exposure.

[1]U.S. Centers for Disease Control and Prevention, National Center for Environmental Health; Mailstop E-23, 1600 Clifton Road, Atlanta, GA 30333

1.0 INTRODUCTION

CO is a byproduct of the incomplete combustion of carbon-based fuels. On inhalation, it causes poisoning through a number of mechanisms, but chiefly by interfering with the oxygen-carrying capacity of hemoglobin in the blood. Treatment consists of providing supplemental oxygen. In severe cases this oxygen should by supplied under hyperbaric conditions.

CO is responsible for more fatalities in the United States each year than any other toxicant. During 1979-1988, from 878 to 1513 deaths per year were attributed to unintentional CO poisoning. Additionally, from 1992 through 1996, an estimated 9,800 cases of CO poisoning One of the first mentions of a CO poisoning outbreak following a weather-related disaster occurred after the great blizzard of February 1978 in eastern Massachusetts. Of 27 storm-related deaths identified by mortality surveillance, 5 were due to CO poisoning in stranded motorists. These individuals presumably continued to run their automobile engines to keep warm.

Nine years later, in October 1987, an outbreak of CO poisoning was again documented following a severe snow storm striking upstate New York. In fact, CO poisoning was the most common storm-related illness diagnosed from the five emergency departments participating in this investigation. It accounted for 22 of 59 non-traumatic storm-related cases seen during the storm and the five following days. The identified CO sources included electric generators, kerosene heaters, and charcoal briquettes used indoors to provide power or heat. It is of note that in this outbreak the occurrence of a cluster of CO poisoning cases was unexpected by the investigators and considered an unusual finding.

Idling motor vehicles again caused CO poisoning after a blizzard in the northeastern United States in January 1996. From January 8 to 9, in Philadelphia, Pennsylvania, CO exposure caused two severe poisoning cases and one fatality. Over the same time period in New York City, 21 severe CO poisoning cases and 1 CO death occurred. In every case the victim became exposed while inside an idling motor vehicle which had an exhaust pipe blocked by snow. The victims were not reported to be stranded but had started their cars before clearing the snow from around them.

involving consumer products were treated annually in hospital emergency rooms. However, the true number of cases seen by emergency physicians is probably far higher.

Though CO exposure is a year-round problem, incidence of poisoning death increases during the winter months. Most unintentional CO poisoning occurs sporadically as a result of motor vehicle exhaust or improperly functioning home heating units. However, outbreaks have occurred increasingly over the last decade following winter storms and other disasters.

2.0 SNOW STORMS

3.0 WINTER WIND AND ICE STORMS

During an ice storm in March 1991, 55 cases of CO poisoning were diagnosed in an emergency department in Rochester, New York. Of these, 16 patients became unconscious. All but one of the patients were treated and released from the emergency department; the other patient was transferred for hyperbaric oxygen therapy. In 67% of cases generators were the source of the CO and in another 17% the CO source was a fuel-powered heater or stove. Other sources included charcoal grills, fire places, and house fires.

A major outbreak of CO poisoning in western Washington State occurred after a severe winter wind storm disrupted electric power service to over 700,000 residents in January 1993. Wind

gusts from this storm reached 88 miles per hour and near freezing temperatures followed. Investigators reviewed records from 53 hospital emergency departments in western Washington. During the day of the storm and the three subsequent days, 81 laboratory-confirmed cases of CO poisoning were identified. These cases represented 30 exposure incidents with a range of one to nine patients per incident. In 15 of these incidents charcoal was the sole or contributing source of CO. Another 12 incidents involved a generator. All patients poisoned by generators were non-Hispanic Caucasians. Almost all patients poisoned by charcoal were Asian or Hispanic, and most did not speak English. No fatal cases were reported The largest documented post-storm outbreak of CO poisoning occurred in Maine after the severe ice storm of January 1998. This storm disrupted electric power service to over 600,000 residents, some for over two weeks. There were 100 laboratory-confirmed cases identified from four emergency departments in the central region of the state. Cases were documented for two weeks following the storm's onset but most occurred during the initial week of the disaster. One patient died and five received hyperbaric oxygen. The cases represented 42 separate exposure incidents with a range of one to eight cases per incident. A generator was the sole or contributing CO source in 30 incidents involving 85 poisoning cases. Eight incidents involved kerosene space heaters, four involved propane space heaters, and two involved portable gas stoves. Charcoal grills were the sole source of CO in two incidents. Six incidents involved two CO sources.

In this outbreak, it was noted that around a third of the population in this region of Maine used a generator during the disaster. Many of these operated the generator inside a garage. Most people who operated generators during this disaster obtained it after the ice storm and had no previous operating experience. Among families using generators, generator location was the strongest risk factor for poisoning. and 43% of cases were treated with hyperbaric oxygen. Warnings issued in the broadcast and print media may have limited the severity of this epidemic.

In Nashville, Tennessee, 13 cases of CO poisoning were identified from an emergency department following an ice storm in February 1994. None of these patients died and five received hyperbaric therapy. Six patients were poisoned by charcoal grills, four by generators, and three by a fuel powered heater or stove. Over half of patients were Asian in a city with a very small Asian community. Most patients were not fluent in English.

Households operating a generator inside a garage or other structure attached to the home were at 19 times greater risk of becoming poisoned by CO. Households operating a generator inside a basement were at 300 times greater risk.

4.0 HURRICANES

CO poisoning has also been noted as an adverse health effect of tropical storms. During the four days immediately after Hurricane Fran in September 1996, 13 cases of CO poisoning were seen in a hyperbaric treatment center in North Carolina. The storm caused loss of electric power to large areas of the state. These cases represented five exposure incidents. All incidents involved use of a generator operated indoors or outdoors near a ventilation source for a home.

In September 1998, Hurricane Georges disrupted electric power service to most of the island of Puerto Rico. Two days following the hurricane a fatal case of CO poisoning occurred due to a generator operated inside a home. The next day another CO fatality resulted from a generator operated outside but near an opening to a store. CO poisoning was not considered a major risk in Puerto Rico at that time. These deaths represented the first two cases of

hurricane-associated mortality following Georges in Puerto Rico.

5.0 CONCLUSION

In the United States, CO poisoning has emerged as a major adverse health effect following disasters. Though especially common after winter storms, it is also becoming a post-hurricane problem. The potential for outbreaks of CO poisoning exists in any disaster resulting in widespread loss of electric power.

Gasoline-powered electric generators have been the CO source in many post-disaster poisoning incidents. Operation of generators inside a home or attached structure is especially risky, but cases also occur from generators operated outside. Increasing availability of generators to the general population in the United States may play a major role in the emergence of post-disaster CO poisoning.

Other CO sources have been important following winter storms. Indoor use of portable fuel-powered heaters and stoves has caused CO poisoning after numerous winter disasters. Charcoal is a potent producer of CO and is very dangerous if used inside. Charcoal grills have frequently caused CO poisoning following winter disasters, especially among Asian and Hispanic Americans. Exhaust from snow-obstructed automobiles has been a particular danger after snow storms.

Cases of post-disaster CO poisoning are almost always preventable. In the aftermath of severe winter storms or any disaster resulting in widespread loss of electric power, public service announcements should be issued concerning the dangers of CO poisoning. These should cover the symptoms of CO poisonings and ways to prevent exposure. Any message should be issued in language appropriate to local communities. Because CO poisoning is easily misdiagnosed, alerts should be sent to medical providers and emergency response personnel detailing diagnostic and therapeutic measures. Interventions connected with CO sources such as warnings, training, and CO detector promotion should also be valuable. Unless preventive measures are taken, outbreaks of post-disaster CO poisoning may become increasingly more common.

6.0 REFERENCES

Ault K. Estimates oi non-fire carbon monoxide poisonings and injuries. Washington, D.C.: U.S. Consumer Product Safety Commission 1997.

Centers for Disease Control and Prevention. Carbon monoxide poisonings associated with snow-obstructed vehicle exhaust systems - Philadelphia and New York City, January 1996. MMWR 1996;45:1-3.

Centers for Disease Control and Prevention. Deaths associated with Hurricane Georges - Puerto Rico, September 1998. MMWR 1998;47:897-8.

Cobb N, Etzel R. Unintentional carbon monoxide-related deaths in the United States, 1979 through 1988. JAMA 1991;266:659-63.

Cohen BA, Stolp BW, Dear BD, Moon RE, Frazier LM. Carbon monoxide poisoning in the aftermath of Hurricane Fran [letter]. Am J Public Health 1999;89:112.

Daley WR, Smith A, Paz-Argandona E, Malilay J, McGeehin M. An outbreak of carbon monoxide poisoning after a major ice storm in Maine. J Emerg Med 2000;18:87-93.

Geehr EC, Salluzzo R, Bosco S, Braaten J, Wahl T, Wallenkampf V. Emergency health impact of a severe storm. Am J Emerg Med 1989;7:598-604.

Glass RI, O'Hare P, Conrad JL. Health consequences of a snow disaster in

Massachusetts, February 6, 1978. Am J Public Health 1979;69:1047-9.

Houck PM, Hampson NB. Epidemic carbon monoxide poisoning following a winter storm. J Emerg Med 1997;15:469-73.

Wrenn K, Connors GP. Carbon monoxide poisoning during ice storms: a tale of two cities. J Emerg Med 1997;15:465-7.

Assessment of Public Health Needs Among Displaced Persons Residing in a Temporary Camp Following the August 1999 Earthquakes in Turkey

by

Dahna Batts-Osborne, MD, FACEP[1]
Lina Balluz, ScD, MPH
Mary Naughton, MD, MPH

ABSTRACT

The Centers for Disease Control and Prevention (CDC) conducted a rapid epidemiologic assessment of the needs of displaced persons affected by the earthquake that struck western Turkey on August 17, 1999, and to evaluate the morbidity that resulted from the disaster. The results of two activities conducted in one severely affected area to assess the public health implications of the disaster for displaced persons in two camps are presented.

KEYWORDS: Turkey earthquake, needs assessment, public health, surveillance

1.0 INTRODUCTION

At approximately 3:02 a.m. on August 17, 1999, an earthquake measuring 7.4 on the Richter Scale struck western Turkey and resulted in official estimates of 17,000 deaths and 10,000 people reported missing. Approximately 24,000 people were injured, and an estimated 600,000 people were left homeless. Numerous aftershocks occurred during the following month, causing further damage and loss. The epicenter was approximately 7 miles southeast of the city of Izmit, near the town of Gölcük. This location indicates that the earthquake occurred on the northernmost strand of the North Anatolian fault system. The earthquake originated at a depth of 10.5 miles and produced at least 37 miles of surface rupture. A community needs assessment was conducted in one camp in addition to a study of clinic visits in two camps, 2 and 6 weeks after the earthquake. The purpose of the assessment was to provide an objective postdisaster measure of needs to decision makers in the affected area.

2.0 METHODS

2.1 Community Needs Assessment

A needs assessment was conducted in Bahececik camp, which had been established by local authorities 1 week after the earthquake in the Gölcük region. Gölcük was thought to be the area most affected by the disaster. This camp had 248 tents. On October 1-2, a household survey using a systematic random sample was conducted, targeting a total of 155 households. A household was defined as a unit of people residing in one tent. One adult from each selected household was interviewed using a standardized questionnaire that focused on demographics, illnesses, injuries, sanitation, shelter, and medical needs.

2.2 Morbidity Review

Morbidity data during the postdisaster phase at Bahcecik camp clinic and Izmir camp clinic in the Gölcük area was characterized. Logbooks were reviewed for two 8-day periods: from August 30 (the first day for which clinic records were available at both sites) through September

[1]Medical Epidemiologist, Centers for Disease Control and Prevention, Atlanta, Georgia 30333, dtb7@cdc.gov

6, 1999, and from September 25 through October 2, 1999.

3.0 RESULTS

3.1 Results of Community Needs Assessment

In Bahcecik camp, 154 households were visited, and interviews were completed for 86 (56%). The survey represented 339 persons with a median household size of four people. Of the 86 households, seven (8%) had a child aged 2 years or younger; nine (10%) reported a household member aged 65 years or older; and three households (4%) reported a pregnant female. Fifty-four (63%) reported damaged and uninhabitable structures, and 22 (26%) reported homes that were completely destroyed.

Of the 86 households, 20 (23%) had a household member who had sustained an injury, and 90% of the injuries were lacerations. Sixty-nine households (80%) reported having at least one ill household member since the earthquake; these 69 households reported a total of 128 ill people. Approximately 32 people (25%) reported depression, but only 14 (44%) sought treatment; 24 (19%) reported respiratory illness, and 23 (96%) requested medical treatment. Twenty (17%) noted chronic diseases, specifically kidney problems, hypertension, and heart disease, and 16 (80%) sought treatment. Thirteen (10%) noted gastrointestinal illness, and 11 (86%) sought treatment. The Bahcecik camp clinic provided medical care for people in 85 (99%) of the surveyed households. Of the 86 households, one (1%) reported an earthquake-related death. This low percentage most likely reflects the fact that Turkish families generally live together in one household and that whole The impact of a disaster on a population varies with the type of disaster. An earthquake of great magnitude is one of the most devastating events in nature. The earthquakes in Turkey caused extensive infrastructure damage and losses worth approximately $6.5 billion. Rapid needs assessment of the affected population is an important initial step of response (1). Results of such an assessment can minimize inappropriate

families either died or survived. It does not reflect the numerous friends, co-workers, and extended family members who were killed.

Piped water was the major source of drinking water, as reported by 81 (94%) households. Seventy-five (87%) of the 86 Bahcecik camp households reported that food was available and was mainly provided by the relief workers in the camp. In 77 (90%) households, people had access to transportation; 83 (97%) households had garbage disposal by municipal collection; and 83 (97%) households had access to showers. Field latrines connected to septic tanks were most commonly used for human waste disposal by households (83 [97%]) and were reported as "clean" or "somewhat clean" in 45 (52%) households. Electricity was not available for 79 (92%) households.

3.2 Results of Morbidity Data

There were 468 logbook entries at Bahcecik camp clinic and 534 entries at Izmir camp clinic for the 8-day period from August 30 through September 6, 1999. During the second 8-day period, September 25 through October 2, 1999, 411 and 669 entries, respectively, were reviewed (Table 1). The overwhelming number of visits were for illnesses, rather than injuries.

The primary illness for both time periods in both tent cities was upper respiratory tract illness, followed by musculoskeletal pain. All other causes, including diarrhea, represented no more than 10% of the total clinic visits (Tables 2 and 3).

4.0 CONCLUSIONS

relief in terms of delays and content. In Bahcecik camp, where 88% of the population was homeless, the primary need was housing. Most inhabitants planned to remain in their tents until they received houses. In addition, the low frequency of gastrointestinal diseases implies that sanitary conditions at the camp were well maintained. This information may control the rumors of epidemics and help local health

authorities focus on allocating resources to reduce crowding, to provide counseling, and to supply appropriate medications, which were public health needs as reflected by the predominance of respiratory diseases and reports of depression. Although 73 (85%) households indicated access to a source of medication, and direct observation showed a well-stocked medication supply area, the most common medications that were needed for diabetes, hypertension, and depression, as well as analgesics and vitamins, were not available, according to persons interviewed.

Other recommendations to the local health authorities based on these activities included providing shelter, heat, and clothing suitable for winter conditions; providing mental health services, social activities, and community jobs to address the increased level of stress in the communities; continuing the current level of medical care; and encouraging reporting of morbidity data from local camp clinics to regional health offices.

5.0 REFERENCES

Guha-Sapir D. Rapid assessment of health needs in mass emergencies: review of current concepts and method. World Health Stat Q 1991;44:171-81

TABLE 1

MORBIDITY BREAKDOWN AT BAHCECIK AND IZMIR CAMPS, TURKEY, 1999

Tent City	Illnesses	(%)	Injuries	(%)	Total
Bahcecik					
Aug.30-Sept. 6, 1999	434	92.7%	34	7.3%	468
Sept. 25-Oct. 2, 1999	382	92.9%	29	7.1%	411
Izmir					
Aug.30-Sept. 6, 1999	492	92.1%	42	7.9%	534
Sept. 25-Oct .2, 1999	628	93.9%	41	6.1%	669

TABLE 2

MORBIDITY AT BAHCECIK CLINIC 2 AND 6 WEEKS AFTER EARTHQUAKE, TURKEY 1999

DIAGNOSIS	BAHCECIK WEEK 2	DIAGNOSIS	BAHCECIK WEEK 6
Upper respiratory tract infection	116 (24.8%)	Upper respiratory tract infection	125 (24.8%)
Musculoskeletal pain	32 (6.8%)	Musculoskeletal pain	25 (6.0%)
Watery diarrhea	28 (6.0%)	Skin Infection	17 (4.1%)
Psychiatric Illness	27 (5.8%)	Dental/oral disease	16 (3.9%)
Hypertension	21 (4.5%)	Hypertension	14 (3.3%)

TABLE 3

MORBIDITY AT IZMIR CLINIC 2 AND 6 WEEKS AFTER EARTHQUAKE, TURKEY 1999

DIAGNOSIS	IZMIR WEEK 2	DIAGNOSIS	IZMIR WEEK 6
Upper respiratory tract infection	126 (20.0%)	Upper respiratory tract infection	168 (21.8%)
Musculoskeletal	61 (9.6%)	Musculoskeletal	52 (6.8%)
Skin rash	41 (6.5%)	Skin infection	24 (3.1%)
Hypertension	40 (6.3%)	Dyspepsia	21 (2.7%)
Lower respiratory tract infection	35 (5.5%)	Lower respiratory tract infection	21 (2.7%)

Wind Storm-related Disaster Deaths in the United States, 1994-8

by

Julie Jacobson. MD

ABSTRACT

Disasters are responsible for deaths every year in the United States. The Center for Disease Control and Prevention (CDC) has partnered with the American Red Cross (ARC) to systematically collect comprehensive information on disaster-related deaths to determine who is at risk in disasters. From January 1, 1994 through December 31, 1998, wind storms were responsible for a majority of these deaths. We found that decedents from wind storm disasters were more likely to be males or the elderly; women and children were not at increased risk. People occupying mobile homes were at a higher risk than individuals occupying single family homes, especially in tornadoes. Decedents in hurricanes were more likely to die from drowning than individuals killed in other wind storm events. By characterizing decedents in wind storm disasters we can work to prevent the unnecessary loss of life from these disasters and focus prevention and mitigation efforts at those at risk.

KEYWORDS: DISASTERS; MORTALITY; HURRICANE; TORNADO

1.0 INTRODUCTION

Since 1986, the American Red Cross (ARC) and the Center for Disease Control and Prevention (CDC) have partnered to provide timely and comprehensive information on disaster-related deaths for public health use. As part of the Federal Response Plan, the ARC is mandated by Congress to provide mass care to all

Disasters cause thousands of deaths each year around the world. The worldwide population at risk from disasters is increasing with more people living in areas vulnerable to disaster events. (World Disaster Report, 1999) This phenomenon is also observed in the United States. By 2010, the number of people will double living in hurricane-prone and seismically active areas. (National Mitigation Strategy, 1995) As advances in technology increase the accuracy of weather prediction, predictions need to be communicated to those at risk to decrease morbidity and mortality. (Noji, 1997) By looking at deaths that result from wind storms we can learn who is at risk of death from these events and improve our ability to prevent adverse health outcomes.

Between 1994-98 in the United States, a total of 861 disaster-related deaths occurred. Of these deaths 92% (791/860) were related to a climatic event; the largest number of deaths, 62% (490/791), were caused by wind storm events. (Jacobson) This report provides a descriptive summary and associated risk factors for death in wind storm disasters from January 1, 1994 through December 31, 1998.

2.0 METHODS

Presidentially-declared natural disasters. Through an agreement with CDC, the ARC response contains a surveillance component, *The American Red Cross- Centers for Disease Control and Prevention Health Impact Surveillance System for Disasters*, which collects information on morbidity and mortality resulting

from these disaster events. (Patrick, 1992). ARC staff actively and passively collect data through medical examiner and coroner's offices, hospital surveillance, home visits, funeral home information, news papers and word of mouth. They then confirm the death through the medical examiner, coroner, or funeral home and fill out a standard surveillance form that records demographic information, the location and cause of death, how the death was related to the disaster, and the death circumstances. As ARC contacts the families of decedents to provide services, additional information may be obtained about the death from surviving family members. Completed forms are forwarded to CDC, where data are cleaned and entered into Epi Info 6.1 and Microsoft Excel for analysis. We described deaths by gender, age, cause of death, and disaster type. Data were compared to US 1996 (median year) census data to calculate risk.

3.0 RESULTS

3.1 TYPE OF DISASTER

From January 1, 1994 to December 31, 1998, 65 wind storm-related deaths occurred in 4 categories; 23 involving tornadoes, 26 hurricanes (involving 7 tropical storms and 10 hurricanes), 12 flood/tornado mixed events, and 4 other storms. The largest number of deaths were attributed to tornadoes with 208 deaths, followed by hurricanes with 194 deaths, flood/tornado mixed events with 79 deaths, and other storms with 9 deaths. Hurricanes had the largest number of deaths per disaster with 14 deaths/disaster (tropical storms 8 deaths/disaster). Tornadoes had the second most deaths with 9 deaths/disaster. The deadliest disaster type however was tornado, with a death rate of 7 per thousand people affected, followed by other storms (2/1000 affected), flood/tornados (1/1000 affected), and finally hurricanes (0.6/1000 affected).

We then compared the demographics and location of death of decedents in the two most severe wind disaster types, tornadoes and hurricanes. (Table 2) Males had a higher risk of death in hurricanes (RR 2.47, 95% CI 1.81- 3.37) and a marginal increase in risk from tornadoes (RR 1.32, 95% CI 1.00-1.74). Elderly (≥65 years)in tornadoes, were the only age group with

3.2 DEMOGRAPHIC INFORMATION

During this 5-year period, 490 people died in wind storm disasters. Decedents had a median age of 41 years (range <1 to 107 years) and were 62% male (299/486). Males had a relative risk of death of 1.73 (95% CI 1.44- 2.08) compared to females. Six percent (30/483) of decedents were <5 years of age, 19% (92/483) were <18 years of age, and 20% (96/483) were ≥65 years of age. Individuals aged ≥65 years had a relative risk of death from disasters of 1.55 (95% CI 1.25- 1.93) when compared to all disaster-related deaths. No other age group showed a statistically significant difference in death rate.

3.3 LOCATION OF DEATH OR FATAL INJURY (TABLE 1)

Deaths from wind storms occurred primarily in single family homes (25%) and outdoors (24%). The remaining deaths occurred in mobile homes (19%), motor vehicles (19%), multi-family dwellings (<1%), and other (including public buildings, boats, etc). To calculate the relative risk of location of death we compared mobile homes and multi-family dwellings to single family homes. The risk of death in a mobile home was 7.89 times (95% CI 5.79- 10.76) that of being in a single family home. Occupying multi-family homes actually had a reduced risk of death 0.03 (95% CI 0.00- 0.18).

3.4 TORNADOES VS. HURRICANES

an elevated risk of death (RR 1.59 95% CI 1.13-2.24). The risk of death in a tornado when in a mobile home was 11.61 times (95% CI 7.82-17.23) that of being in a single family home. This was not the case for hurricanes; no statistical difference was observed between occupying mobile homes and single family homes. Compared to all wind storm-related deaths, tornadoes had a higher risk of a death from trauma (RR 1.28, 95% CI 1.11-2.15) and hurricanes had a higher risk of drowning (RR 1.34, 95% CI 1.06-1.70).

4.0 DISCUSSION/CONCLUSIONS

Most disaster-related deaths in the United States are related to climatic events. Improvements in detection and warning systems over the past 4 decades have been credited with a steady decrease in disaster-related deaths (National Research Council 1994). The effects of these warning systems may be reflected in the differential in death rates by disaster type. Disasters with the least amount of warning time, tornadoes, have the highest death rate (7.2 deaths/1000 affected) and disasters with more warning time, hurricanes, have a lower death rate (0.6 deaths/1000 affected) (Figure 2).

Tornadoes are the most lethal disaster type in the United States with 7.2 deaths per 1000 people affected. In 1952, the National Weather service began broadcasting tornado warnings and since that time the number of deaths from tornadoes has been decreasing (Noji 1997). However, over this 5 year period, the number of deaths from tornadoes and flood/tornado events has risen upward (Figure 1). Historically, North America has the most severe tornado disasters on the earth. (Bohonos 1999) Studies have shown that warning time and access to proper sheltering have the greatest impact on morbidity and mortality (Bohonos 1999, Belville 1987, Carter 1989, Eidson 1990). Occupying mobile homes have repeatedly been shown to be a risk for death. Our data support this with an increased risk of death of 11.61 times when compared to other residences. Therefore, prevention strategies should be directed to 1) occupants of mobile homes and 2) use of timely effective warnings. Mobile homes in tornado prone areas should have safety shelters or safe rooms. All households residing in tornado prone areas should have a National Oceanic and Atmospheric Association (NOAA) Weather Radio to warn them of storm warnings. NOAA radios will turn themselves on when a warning is issued, so even at night or when families are asleep they will be alerted of the risk of oncoming severe weather and be able to take the proper precautions (NOAA 1999). NOAA radios should be as common as smoke detectors.

Hurricanes affected the largest number of people (310,969) and had the third largest number of deaths by disaster type (194) yet were the least deadly (0.6/1000 affected). However, advanced warning systems should allow us to decrease this rate further. One of the most interesting findings with hurricanes was the increased risk of drowning when compared to other wind storm disasters. Hurricanes are mixed events by their very nature involving not only wind, but storm surge and potentially heavy rains. The Saffir/Simpson hurricane scale that is used to determine what areas are evacuated, is based primarily on wind speed and storm surge. Given the increased risk of drowning, some of these deaths could potentially be avoided if rainfall and flooding risk were incorporated into the rating scale.

Males and the elderly are at higher risk of death from wind storm disasters (RR 1.73) than females and all age groups, respectively. This refutes previous findings that women and children are at the greatest risk of death from disasters (Noji 1997). As in previous studies, our findings confirm the increased risk of death for the elderly in wind storm disasters as a whole (RR 1.55) and

in tornadoes specifically (RR 1.59). However, we did not find an increased risk for women and children. Males were at an increased risk in all The ARC CDC Health Impact Surveillance System for Disasters provides us with the first surveillance system for disaster-related deaths that systematically collects data on all disasters with detailed information on the decedent, the cause and circumstances of death in a single data base (Patrick 1992, Storm Prediction Center (SPC) 2000). Although this data may not represent all disaster-related deaths, it is one of the most comprehensive disaster data collection systems. Although it may under-represent the total number of deaths from small disasters and localized events, this system it provides much information on deaths resulting from large scale disasters represented by all Presidentially declared disasters and disasters with a national ARC response.

By looking at deaths that result from disasters, we can learn who is at risk of death from these events and improve our ability to prevent adverse health outcomes (Binder 1987). As the population at risk of injury and death from disasters increases, we need to work to mitigate and prevent these risks. By providing communities at risk with the tools to protect themselves including: 1) NOAA radios for warnings of severe weather and alerts 24 hours a day; 2) knowledge of flood risk areas and safe evacuation routes prior to and during flood events; and 3) safe rooms for people residing in mobile homes, we can decrease the unnecessary loss of life in disasters.

6.0 REFERENCES

Binder S, Sanderson LM. The roll of the epidemiologist in natural disasters. *Ann Emerg Med.* 1987 Sep;16(9):1081-4.

Carter AO, Millson ME, Allen DE. wind storm disaster types.

Epidemiologic study of deaths and injuries due to tornadoes. *Am J Epidemiol.* 1989 Dec; 130(6):1209-18.

CDC. Tornado-Associated Fatalities – Arkansas, 1997. MMWR 1997; 46(19):412-416.

CDC. Risk factors for death in the 27 March 1994 Georgia and Alabama tornadoes. MMWR. 1995;19(2):170-7.

Federal Emergency Management Agency (FEMA). National Mitigation Strategy Partnership for Building Safer Communities. FEMA. December 6, 1995

International Federation of Red Cross and Red Crescent Societies (IFRC). World Disasters Report. IFRC. 1999.

Morrow BH. Women and families in disaster: Emergency management issues and recommendations, Proceedings of the Annual International Conference of the Business Administration, London. 1995 June.

Mulilis JP. Gender and earthquake preparedness A research study of gender issues in disaster management: differences in earthquake preparedness due to traditional stereotyping or cognitive appraisal of threat?. *Austr J of Emerg Managment. 1999 Autumn; 14(1): 41-50.*

NOAA. NOAA Weather Radio the voice of the National Weather Service. Http://www.noaa.gov/nwr/nwr.pdf.

Noji EK. The Public Health Consequences of Disasters. Oxford University Press. 1997.
Belville JD. The National Weather Service warning system. *Ann Emerg Med.* 1987 Sep;16(9):1078-80.

Patrick P. The Red Cross and CDC's Natural-Disaster Surveillance System. *American Journal of Public Health.* December 1992, Vol 82, No. 12.

Pielke RA Jr, Pielke RA Sr. Hurricanes their Nature and Impacts on Society. John Wiley & Sons. 1997.

Sapir DG. Natural and man-made disasters: the vulnerability of women-headed households and children without families. *World Health Stat Q.* 1993;46(4):227-33.

Storm Prediction Center (SPC). Tornadoes and Deaths by Year and Month 1950-1997. http://www.spc.noaa.gov/archive/tornadoes/ustdbmy.html.

Table 1. Location of death or fatal injury in wind-storm fatalities in the United States, 1994-98

Location of death*	Weather-related deaths
Outdoors	24%
Single-family home	25%
Multi-family home	<1%
Mobile home	19%
Motor Vehicle	19%

* remaining deaths occurred in the 'other' category

Table 2. Characteristics of decedents and location of death in tornadoes and hurricanes in the United States, 1994-98

Demographic data	**Tornado**	**Hurricane**
Gender- male	56%	62%
Mean age	40 years	42 years
Location of death* n=396		
Outdoors	18%	29%
Single-family home	29%	27%
Multi-family home	0%	0.1%
Mobile home	32%	5%
Motor Vehicle	7%	23%
Primary causes of death n=488		
Trauma	85%	30%
-head trauma	17%	7%
Drowning	5%	42%

* remaining deaths occurred in the 'other' category

Theme 6

Natural Disasters in the World and the

URBANIZATION AND URBAN DISASTER PREVENTION

by
Tomomitsu FUJII[1)]

ABSTRACT

In Japan, urbanization has been accompanied by the appearance of increasingly advanced and complex social systems. And disasters caused by earthquakes, intensive rainfall and other natural forces that caused property damage and human casualties have evolved into quite complex urban disasters that bring secondary disasters in addition to the primary damage.

This report reexamines past urban earthquake and flood disasters to study changes and features in urban disasters accompanied by urbanization. The report also presents an outline of urban disaster prevention measures that must be promoted to prevent urban disasters and minimize their effects to increase the safety of urban areas.

KEY WORDS: Urbanization
Urban Disaster
Earthquake, Flood
Disaster Prevention Measure

1. INTRODUCTION

The rapid industrialization and urbanization since the beginning of high-speed economic growth in 1955 has concentrated the population in the three huge metropolitan regions around Tokyo, Nagoya, and Osaka. Urbanization has been accompanied by the appearance of advanced social systems and facilities, and by their increasing close interrelationships.

Once social systems and facilities are destroyed or disrupted by natural disasters, not only does the system itself fail, ripple effects cause chain reactions triggering new forms of disasters that did not seen in the past. In this way, disasters that occur in urban area have been transformed and evolved as a by-product of urbanization.

Focusing on natural disasters accompanied by urbanization, this report reexamines past earthquake and flood disasters to study the changes, features and lessons of urban disasters. The report also includes an outline of urban disaster prevention measures against earthquakes and intense rainfalls that must be promoted to prevent urban disasters and minimize their effects considering recent social trends including internationalization, information technology revolution, and aging of society.

2. URBAN DISASTER

2.1 Urbanization

Figure 1 shows changing numbers of human casualties due to past natural disasters. Although continuous implementations of disaster prevention

1) Director-general, Public Works Research Institute, Ministry of Construction
1 Asahi, Tsukuba, Ibaraki 3050804 Japan

measures has been rewarded with a steady fall in the number of casualties, continued concentration of properties and population in urban regions increased their susceptibility against natural disasters. And the 1995 Hyogo-ken Nanbu Earthquake caused the most serious disaster in the recent history of Japan.

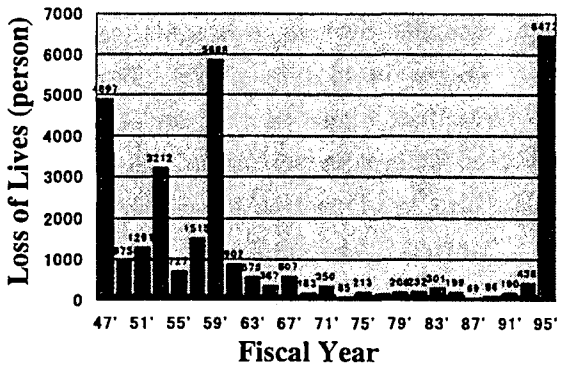

Fig. 1 Human Casualties due to Natural Disasters

In urban regions, new social systems and facilities have appeared and spread to support the socio-economic activities (**Figure 2**). Many of these social systems and facilities have never been exposed to a large-scale disaster and have the potential to cause unpredictable forms of damage and complex chain-reactions of secondary disasters.

Background	Facilities and Functions	Years 30' 50' 70' 90'
Rising Price of Land, Concentration of Population/ Functions	Multistory Buildings	
	Underground Arcade	
	Reclaimed Land	
	Chemical Plant	
Rapid/ Mass Transportation System	Highway System	
	Subway System	
Information Oriented	Online Computer System	
Improvement of Living Condition	Water Supply/ Sewage	
	Convenience Store	
Major Earthquakes		Kanto EQ, Niigata EQ, Hyogo-ken Nanbu EQ

Fig. 2 Appearance of New Social Systems and Facilities

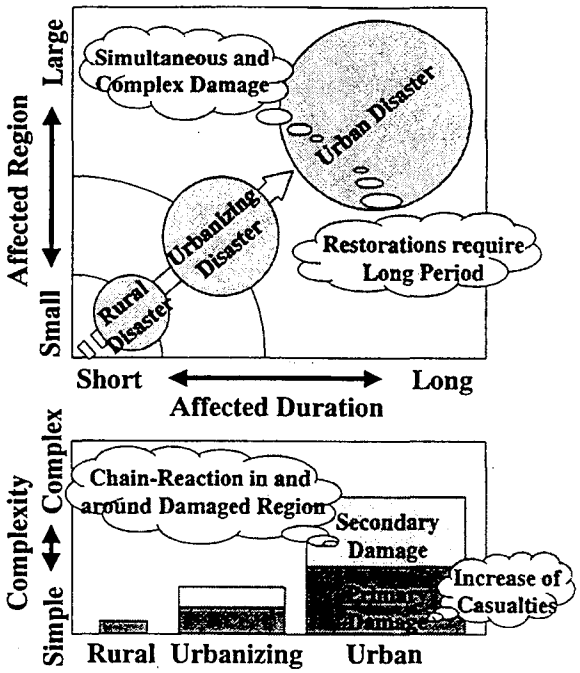

Fig. 3 Evolution and Classification of Natural Disasters (schematic)

2.2 Recent urban disasters

(1) Classification of natural disasters

Figure 3 schematically presents that natural disasters have evolved by focussing on their "effected duration", "effected region" and "complexity of influence". This report categorizes natural disasters as a "rural disaster", an "urbanizing disaster" and an "urban disaster".

1) Rural disaster:

This type means a classical disaster developed in a region where urbanization has not initiated and neither infrastructures nor disaster prevention facilities have been provided. Most of the effects caused are primary damage such as property damages and human casualties. Effected duration and region are limited.

2) Urbanizing disaster:

This type of disaster occurs in rapidly urbanizing

regions where population has been increasing but infrastructures and disaster prevention facilities have not been sufficiently provided. Rapid urbanization in developing countries has increased the frequency of this type of disasters around the world. Although effects caused by the disaster are mainly primary damages, effected duration and region are larger than rural disasters.

3) Urban disaster:

This type of disaster occurs in highly urbanized metropolises and regional core cities. Where the infrastructures are not sufficiently safe, extremely severe primary damage occur, and cause disruption of urban functions as the secondary damage. Because urban functions are highly interdependent and complexes, it is difficult to predict the relationship between the external natural force and the form of damages. Influence of the disaster spread over wide area, and disaster restoration requires long period comparing with previous types of disasters.

(2) Recent urban disasters in Japan

1) Niigata Earthquake (1964/6/16, M 7.5)

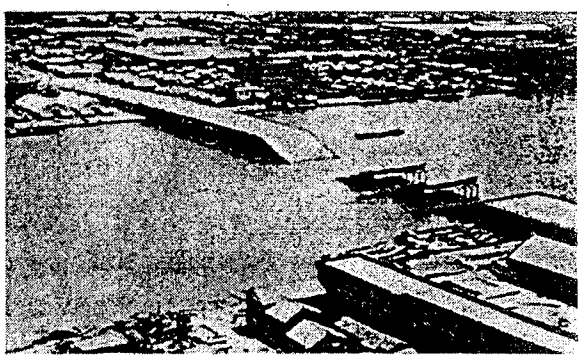

Photo. 1 Failure of Highway Bridge due to Ground Liquefaction

Earthquake disaster developed in the urbanizing Niigata Prefecture caused approximately 470 of casualties, 1,960 of totally destroyed buildings, and failures of highway bridges. Ground liquefaction that occurred over wide areas of soft soil deposit was an unpredictable phenomenon that have never experienced before. And it was pointed out that a ground cave-in and a lateral ground flow induced by the ground liquefaction are likely to enlarge human and property damages. Because most of core cities are placed on soft ground soil deposit in Japan, this disaster experience enforced countermeasures to prevent the ground liquefaction.

2) Miyagi-ken-oki Earthquake (1978/6/12, M 7.4)

Earthquake disaster developed in an urbanized regional core city of Sendai in Miyagi Prefecture caused appropriately 1,350 casualties and severe damages on lifeline facilities for electric power/ gas/ water supply and sewerage. Damage of buildings in newly prepared residential districts and human casualties due to the collapse of block walls were never experienced in previous disasters. Because damages of lifelines influenced daily lives and socio-economic activities for several weeks after the earthquake, upgrading the seismic safety of lifelines was pointed out to be important.

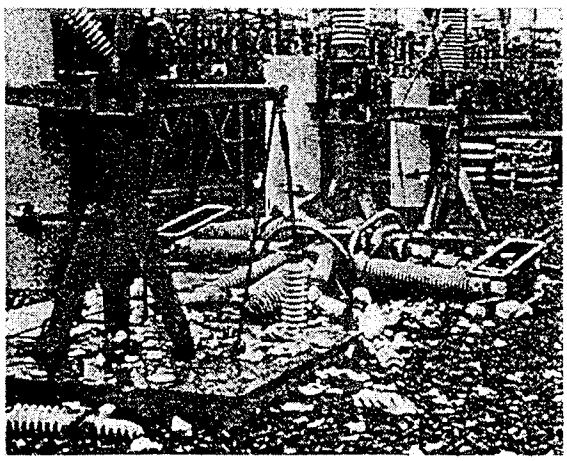

Photo. 2 Damage of Power Plant

3) Nihonkai-Chubu Earthquake (1983/5/26, M 7.7)

Earthquake disaster developed in the urbanized regional core city of Noshiro in Akita Prefecture caused approximately 270 casualties, severe damage on transportation systems including highways and railroads, and lifeline facilities. The fact that about 75% of the casualties were the direct result of Tsunami triggered by the earthquake served as a sharp reminder of the importance of prompt evacuation activities and provision of information to residents following an earthquake. Transportation systems and lifelines were seriously disrupted by damages to embankments and buried pipelines. Because it takes a long time to find out and repair damage of underground facilities, it was pointed out that seismic strengthening of underground facilities is important.

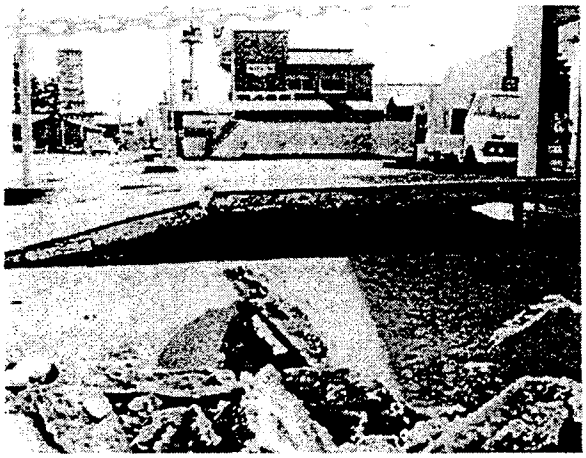

Photo. 3 Up-lift of Underground Gas Storage Tank

4) Intensive Rainfall in Nagasaki Pref. (1982/7/23, 187 mm/ hour)

Flood disaster developed in the urbanized regional core city of Nagasaki caused slope failures and sediment flows around residential districts, and disruptions of highway network. Approximately 1,100 casualties and 600 totally collapsed buildings were developed. Because the City of Nagasaki is located in a peninsula surrounded by the sea, disruptions of highway network temporarily isolated the city and obstructed rescue activities. Even after the flood waters had receded, mountains of debris and abandoned automobiles blocked the streets so that it took a week just to re-open the trunk roads. The disaster was a sharp reminder of the importance to secure the highway network redundancy, and to re-open trunk road promptly after flood disasters.

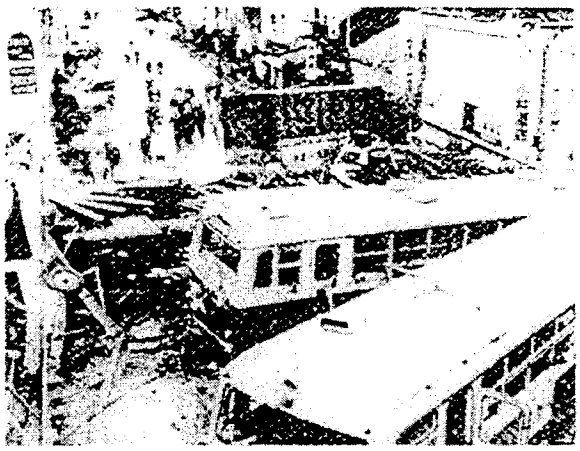

Photo. 4 Closure of Trunk Road due to Flood Debris

5) Hyogo-ken Nanbu Earthquake (1995/1/17, M 7.2)

Hyogo-ken Nanbu Earthquake was one of the largest earthquake disaster developed in highly urbanized region in Japan. Extensive ground motion that was not formerly anticipated caused approximately 5,500 fatalities, 93,000 totally collapsed buildings, catastrophic damage of transportation systems and lifelines, and damage of other industrial facilities. Because disruptions

of arterial highways caused serious and long lasting influence on nationwide transportation activities, importance to provide alternate arterial transportation routes was pointed out. The importance of wide-area improvements to urban districts was also illustrated by the spread of uncontrollable fires that swept through districts with high concentrations of wooden dwellings. Damage to disaster prevention bases and information systems that seriously hampered the urgent response after the earthquake also reminded the importance to prepare appropriate crisis management programs in addition to disaster prevention programs.

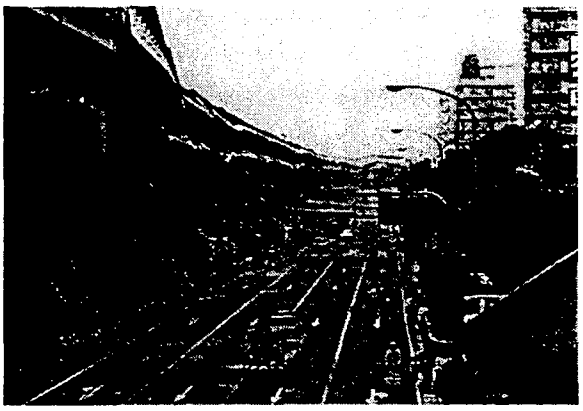

Photo. 5 Disruption of Arterial Viaduct

6) Intensive Rainfall in Fukuoka Pref. (1999/1/29, 122 mm/ hour)

Flood developed in Fukuoka city caused 2 fatalities, and slope failure developed in Hiroshima Pref. caused 31 fatalities and 153 collapsed buildings. Around the Hakata Station where the use of underground space was advanced, an underground arcade and underground station were flooded. In the basement of a nearby office building, people who failed to evacuate promptly were drowned. The flooding cut off transportation routes and caused the failure of power system equipment blacking out the Hakata Station area. This flood clearly indicated that the city was susceptible to the influence of intensive rainfall that exceeded the anticipated amount of rainfall. The flooding of underground space was never experienced before, and reminds the need of flood disaster prevention measures for underground space.

Photo. 6 Flooding of Underground Station

2.3 Features and lessons learned

(1) Features of urban disaster

1) Simultaneity and complexity

In addition to the damage of human lives and properties, complex disasters including city fire, slope failure, tsunami, flooding, lifeline damage, transportation damage, rumors, deteriorate of environment, and other disasters are developed simultaneously. And the form of disasters varies according to topographical conditions, ground conditions, and other unique features of regions.

2) Increase of human casualties

Highly concentrated populations tend to cause an extremely increase of human casualties. Extensive rescue and medical treatment activities are required. Also numbers of emergency facilities for medical treatment and evacuation are needed.

3) Influence to socio-economic activities

Socio-economic activities in urban regions are highly dependent on infrastructures including lifeline facilities, transportation facilities, information related facilities, etc. Once infrastructures lost their functions, serious repercussion may be induced. In the 1995 Hyogo-ken Nanbu Earthquake, for example, disruption of expressway not only cause delayed evacuations, delayed restorations works and traffic congestions in the damaged region but indirectly affected nationwide socio-economic activities. And the damage of port facilities at Kobe not only cause loss of functions but also affected socio-economic status in neighbor countries through import/ export activities.

4) Chain-reaction and expansion of disaster

As a consequence of the highly interdependence of urban functions, primary damage may induce chain-reaction and cause the expansion of secondary damage. For example, urban functions are extremely dependent on electricity, failure of power station affects almost all the urban functions and socio-economic activities as the secondary damage.

5) Difficulty of disaster prediction

Due to the complex relationships between urban functions, damage that does not seem to be related with external natural force may be developed. And due to recently appeared new facilities and functions, unexpected new forms of damage may be developed. In the 1971 San Fernando Earthquake, for example, explosion of gas pipeline and falling-off of curtain walls in high-rise buildings were developed. In the 1978 Miyagi-ken-oki Earthquake, more than half of the fatalities were induced by the collapse of block walls. In the 1995 Hyogo-ken Nanbu Earthquake, malfunctions of fire hydrants prevented firefighters from halting the spread of city fires, and the damage of gas stations help leaving many vehicles abandoned on city streets.

(2) Lessons learned from urban disasters

1) Importance of disaster mitigation planning

Although frequency of large-scale urban disasters is quite low, disaster potentials is extremely high. For promoting countermeasures and securing safety of urban regions against such kind of "low frequency and high influence" disasters, it is quite important to develop appropriate disaster mitigation plans that include risk management measures for damage prevention and crisis management measures for minimizing disaster influences by urgent response works. Also construction of infrastructures must balance the pursuit of advanced functions with consideration of their safety and roles during disasters.

2) Assessment of growing susceptibility

It is essential to carefully study the credible external natural force, and evaluate susceptibility of urban regions. Susceptibility must be appropriately evaluated from the following viewpoints;

a) Distribution and attribute of population:

As the population concentrate to the urban regions, disaster potential increases. As the population increases, residents with various attributes also increase, i.e. elderly, handicapped, foreigners, and infants. As the population increases, relationship in community is likely decline and residents with little experience of disasters are increase. Housing problem enforce long distance commute, and induce huge population gap between daytime and nighttime. Depending on the time disaster occurs, human casualties due to panic and traffic accidents may extensively increase.

b) New facilities/ functions and chain-reactions:
As new facilities/ functions increase, new form of damage and propagation of disaster due to chain-reaction are likely developed. It is therefore essential to evaluate disaster susceptibilities by understanding vulnerability of facilities/ functions and their relationships.

c) Spread of residential districts:
Accompanied with the spread of residential districts, residents living in risky districts from disasters are increasing. Districts with extremely high concentration of wooden dwellings have risk from city fire. Districts along steep slopes have risk from slope failure. Districts with low elevation have risk from flooding and tsunami. And districts formed in reclaimed land have risk from ground liquefaction.

d) Advanced use of urban space:
Accompanied with the lack of land, elevated structures have been constructed for utilizing urban space. Although these structures are necessary in urban regions, vulnerability and risk from disasters must be carefully studied. For example, High-rise buildings have risk from fire, underground facilities including arcade and stations have difficulty in emergency evacuation, and elevated railways and viaducts have risk from earthquakes.

e) Hazardous plants and materials:
As the urban functions concentrated, hazardous plants and materials to sustain urban activities are required. These plants and materials include energy production plants, pharmaceutical and chemical plants, gas storage tanks, petroleum supply bases, gas stations, etc. These plants and materials have risk from explosions and serious environmental problems.

3. DISASTER PREVENTION MEASURES

3.1 Basic concept

The "Disaster Countermeasures Basic Act" was enacted in Nov. 1961 in response to a large-scale disaster caused by the 1959 Ise-wan Typhoon. The Act established the framework for disaster prevention measures in order to protect human lives and properties from external natural forces including earthquakes, tsunamis, windstorms, intensive rainfalls, landslides, floods, high tides, volcanic eruptions, heavy snows, etc. **Figure 4** shows the relationship between disaster prevention plans prepared for national level, Prefectural level, municipal level and citizens' level.

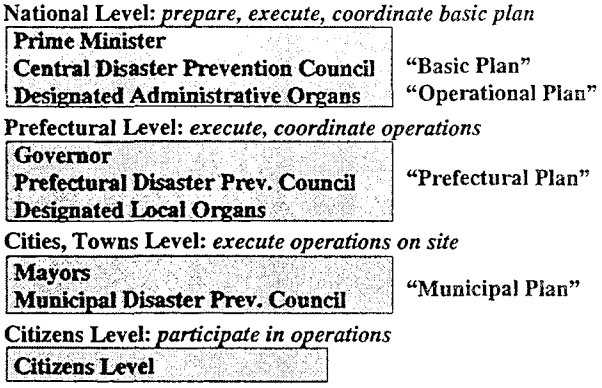

Fig. 4 "Basic Plans for Disaster Prevention" in Japan

Here, the disaster prevention plan was revised following the 1995 Hyogo-ken Nanbu Earthquake. Although disaster countermeasures have been implemented to protect human lives and properties from anticipated natural external forces, the concept of crisis management to minimize the disaster influence was additionally introduced. This is because we must recognize technical difficulties to predict a maximum limit of external

natural forces, and technical/ financial difficulties to completely protect facilities/ functions from damages against catastrophic levels of external natural forces.

3.2 Earthquake disasters

(1) Basic concept for disaster prevention

Although a mechanism of earthquake occurrence have been investigated, it is technically difficult to predict the maximum scale, accurate location and time of earthquakes. And it is financially/ technically unrealistic to attempt protecting facilities/ functions from damage considering catastrophic levels of external earthquake force. In the "Basic Plan for Disaster Prevention" described above, basic concept for preventing damage of structures/ facilities is described as follows (**Table 1**):

Table 1 Basic Concept for Preventing Damage

		Earthquake Motions	
		Ordinary Motion once or twice during lifecycle	Extremely Strong Motion very low probability during lifecycle
Importance	Ordinary Structures	Significant Loss of Functions must be Prevented	Threat to Human Lives Must be Prevented
	Important Structures		Significant Influence To Urgent Activities and Social Activities Must be Prevented

1) External earthquake forces

Two levels of earthquake motions must be considered in the seismic design of structure/ facility. The first level is ordinary motion that has certain probability to strike structure/ facility once or twice during its lifecycle. The second level is extremely strong motion that has very low probability to strike structure/ facility during its lifecycle. The second level of motion includes that generated by interplate earthquakes in the ocean, and that generated by earthquakes due to inland faults.

2) Requirement of safety

Significant loss of functions must be prevented against the first level of ordinary earthquake motion. And serious threat to human lives must be prevented against the second level of extremely strong earthquake motion. In addition, sufficient seismic safety must be provided to structure/ facility that failure of function affect significant influence to urgent response activities and socio-economic activities. The amount of safety must be determined by considering importance of each structure/ facility.

For securing safety of structure/ facility, other than the individual seismic design, it is also important to secure function of systems by increasing system redundancy and providing alternatives.

(2) Disaster mitigation measures

After the 1995 Hyogo-ken Nanbu Earthquake, the Ministry of Construction compiled the "Concept of Urban Planning emphasizing on Seismic Safety". Based on the concept, disaster mitigation measures have been promoted. In addition to the seismic design/ retrofitting of infrastructures/ buildings, following principal policies have been strongly focused.

1) Reduction of vulnerability

The policy includes the reconstruction of vulnerable districts with high concentration of wooden dwellings, establishment of disaster proofing zones, and distribution of open spaces to prevent the spread of city fire.

2) Improvement of core public facilities

For securing urban functions for evacuation, fire fighting and emergency transportations, the policy enforcing implementations of the evacuation route network, emergency transportation route network,

3) Upgrading safety of lifeline facilities

The policy includes construction of common utility ducts accommodating water, gas, electricity, telephone and other pipelines, providing backup water sources needed for fire fighting and daily lives, and improving information systems to collect, analyze, disseminate disaster information.

(3) Technological development

The Public Works Research Institute has been promoting R&Ds for the urban earthquake disaster mitigation. Followings are the principal research themes.

1) Technologies for disaster prevention

- Preparation of seismic hazard map taking effects of inland faults into account
- Evaluation of emergency transportation route seismic performance

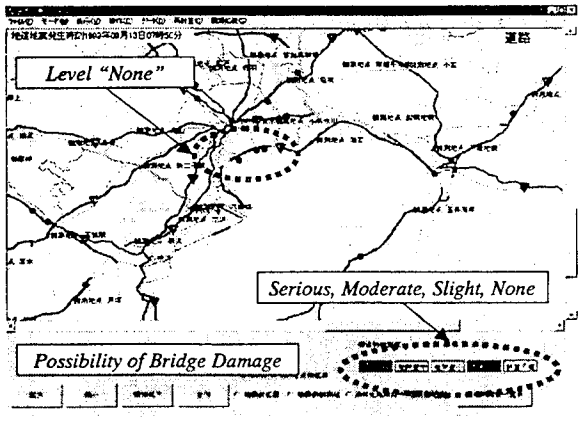

Fig.5 Urgent Damage Estimation Technology (Highway Bridge Damage)

2) Technologies for crisis management

- Urgent damage estimation using ground motion observation network (**Figure 5**)
- Urgent damage detection using advanced information technologies including satellite image and sensors

3.3 Flood disasters

(1) Basic concept for disaster prevention

Conventional measures have been promoted in order to prevent flood-induced damage against anticipated level of rainfalls. Although the frequency of flood disasters has been reduced, the scale of disasters has tented to increase due to the urbanization. The basic concept of flood disaster prevention becomes, therefore, an appropriate control of the relationship between intensive rainfall and induced damage. Based on this basic concept, comprehensive flood disaster mitigation measures are needed in order to create watershed systems where intensive rainfall does not significantly affect the socio-economic activities.

1) External natural force

Relationship between anticipated intensive rainfalls and induced damage in the existing watershed must be carefully studied. Anticipated form, scale and influence of flood disaster must be studied considering past disaster experiences, changes of watershed and safety of related facilities.

2) Requirement of safety

Requirement of the flood frequency reduction and flood-induced damage reduction must be studied considering above described relationships in each watershed. Combination of disaster mitigation facilities must be carefully selected considering the reliability/ deterioration and cost/ effect/ limitation of facilities.

(2) Disaster mitigation measures

Followings are basic approaches for flood disaster mitigation implemented by the Ministry of Construction.

1) Facilities to deal with anticipated floodwater

These include river course improvement, levees, diversion channels, dams, retarding basins, drainage pumping stations, high tide levees, etc.

2) Facilities to reduce damage due to extreme floodwater

These include super levees, forest zones, double levees, emergency drainage gates, and land side channel networks.

3) Measures to reduce floodwater

These include the conservation of water retention/ retarding functions by constructing storage/ infiltration facilities in the watershed, and the control of woody debris and harmful sediment by constructing sediment dams.

4) Reduction of disaster potential in watershed

This approach includes the management of land use, and the promoting of flood-proofing city planning.

5) Improvement of urgent response

This approach includes improvement of urgent warning, dissemination of hazard map, improvement of evacuation by education/ drills.

(3) Technological development

Followings are principal research themes conducted by the Public Works Research Institute for flood disaster mitigation.

1) Technologies for disaster prevention

- Preparation of flood hazard map for displaying distribution of risks in each watershed (**Figure 6**)

2) Technologies for crisis management

- Pre-disaster dissemination of flood information for the awareness/ education of residents
- Post-disaster dissemination of flood information for the effective evacuation activity

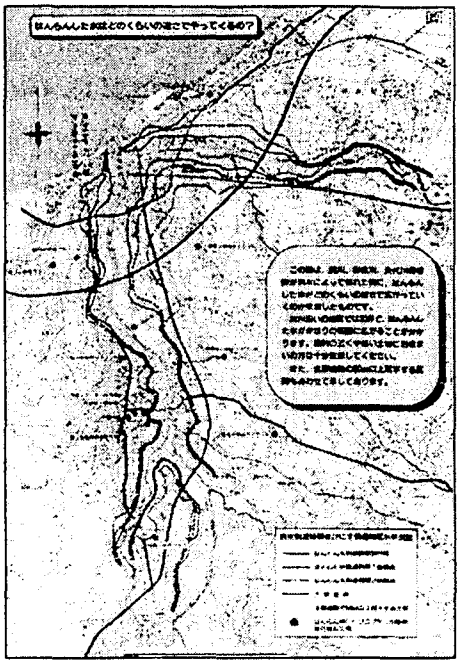

Fig. 6 Flood Hazard Map

4. CONCLUDING REMARKS

This report reexamines past earthquake and flood disasters to study the changes, features and lessons of urban disasters. This report also introduced the basic concept, policy measures and technological development for the urban disaster mitigation in Japan.

Features of urban disaster can be summarized as follows;

1) Highly concentrated population and properties tend to cause an extremely increase of human casualties and structural damages.
2) Once urban infrastructures lost their functions, serious repercussions to socio-economic activities are developed. As the consequence of highly interdependence of urban functions, primary damage induces chain-reaction and

causes the expansion of secondary damage in and around the damaged region.

3) Accompanied with newly appeared urban facilities/ functions and the chain-reaction effects, unexpected forms of damage tend to be developed.

Lessons learned from past urban disasters can be summarized as follows;

1) For securing safety against "low frequency and high influence" urban disasters, it is essential to develop appropriate disaster mitigation plans that include risk management measures for damage prevention and crisis management measures for minimizing damage influence. It is also essential to disseminate appropriate disaster information to public for the better awareness and education.
2) It is essential to assess the susceptibility of existing urban regions. Viewpoints include distribution and attribute of population, newly appeared facilities/ functions, chain-reactions, spread of residential districts, advanced use of urban space, and distribution of hazardous plants and materials.

REFERENCES

1) PWRI: Report on disaster caused by the 1964 Niigata Earthquake, report of PWRI, vol. 125, 1965.6
2) PWRI: Report on disaster caused by the 1978 Miyagi-ken-oki Earthquake, report of PWRI, vol. 159, 1983.3
3) PWRI: Report on disaster caused by the 1983 Nihonkai-chubu Earthquake, report of PWRI, vol. 165, 1985.3
4) Earthquake Engineering Division of PWRI: Report on disaster caused by 1982 Intensive Rainfall in Nagasaki Pref,, technical memorandum of PWRI, vol. 2417, 1986.11
5) PWRI: Report on disaster caused by 1995 Hyogo-ken Nanbu Earthquake, report of PWRI, vol. 196, 1996.3
6) Central Disaster Prevention Council: Basic Plans for Disaster Prevention, 1997.6
7) Ministry of Construction: Concept of Urban Planning emphasizing on Seismic Safety, 1995.4

Effects of the August 17, 1999 Kocaeli (Izmit) Earthquake and the November 12, 1999 Duzce Earthquake, Turkey, on Dams

by

Ellis L. Krinitzsky[1], Mostafiz R. Chowdhury[2], and Ghassan Al-Chaar[3]

ABSTRACT

Three major dams were situated in areas of serious ground shaking, ≥0.2 g, caused by the 1999 Kocaeli and Izmit earthquakes along the North Anatolian Fault in Turkey. The Kirazdere Dam was 1 to 2 km from the fault rupture, and the dam sustained shaking of up to 0.4 g, yet had no damage. The other dams also were not damaged.

KEYWORDS: Turkey, Kocaeli earthquake, Izmit earthquake, dams, earthquake damage

1.0 INTRODUCTION

On August 17, 1999, a powerful earthquake struck Turkey. The shock occurred at 01:39:80 Greenwich Time, 03:01 AM local time. The magnitude was interpreted at the Kandilli Observatory and Earthquake Research Institute of Bogazici University in Istanbul to be M_s:7.8. Additional values were assigned as follows:

m_b	: 6.3 (USGS)
Duration magnitude	: 6.7 (Kandilli)
M_w	: 7.4 (USGS, Kandilli)
Epicenter	: 40.70N, 29.99E (USGS)
Focal Depth	: 11 km

The epicenter occurred about 11 km SE of Kocaeli (Izmit) as shown in Figure 1.

Another strong earthquake occurred at Duzce (Figure 1) three months later, on November 12. This earthquake occurred with 30 km of surface rupture on the North Anatolian fault. It was the same fault that ruptured in the Kocaeli earthquake but its epicenter was about 120 km east of Kocaeli (see Figure 1). Values for the Duzce earthquake are:

M_w	: 7.2 (Kandilli)
M_b	: 6.3 (USGS)
M_s	: 7.5 (USGS)
Epicenter	: 40.76N, 31.16E
Focal Depth	: 10 km

Based on the peak recorded motions, the distribution of aftershocks, and the extent of strong damage, isoseismals were interpreted for the Kocaeli earthquake as shown in Figure 1. The shaking was experienced as a narrow band parallel to the North Anatolian fault. Maximum damage occurred in the central area at Kocaeli (Izmit) but also in pockets along the north and south shores of the Gulf of Izmit, particularly at Karamursel and Golcuk. Shoreline property settled, parts slid into the Gulf, and water encroached onto the land. To the east, notable damage from soil liquefaction was experienced at Sakarya (Adapazari). And damage occurred in the west near Yalova.

2.0 BEHAVIOR OF DAMS

Only two major dams were in the zone in which the isoseismals for the Kocaeli earthquake were equal to or greater than 0.2 g. The locations of these dams are shown in Figure 1. They are Kirazdere (Yuvacik) Dam and Gokce Dam. Kirazdere Dam is within 2 or 3 km of the epicenter and in close proximity to the causative fault. The dam would have experienced peak horizontal motions of 0.3 to 0.4 g. Gokce Dam is in the area

[1] Senior Research Scientist, Geotechnical Laboratory, Engineering Research and Development Center, U.S. Army Corps of Engineers, 3909 Halls Ferry Road, Vicksburg, MS 39180-6199, krinite@mail.wes.army.mil.

[2] Research Civil Engineer, Structures Laboratory, Engineering Research and Development Center, U.S. Army Corps of Engineers, 3909 Halls Ferry Road, Vicksburg, MS 39180-6199, chowdm@mail.wes.army.mil.

[3] Research Civil Engineer, Construction Engineering Research Laboratory, Champaign, IL, g-al-chaar@cecer.army.mil.

of considerable damage and numerous aftershocks in the area of Yalova. Gokce Dam would have experienced motions of at least 0.2 g or greater. This is a reasonable inference though there were no strong motion records in the Yalova area.

2.1 Gokce Dam

Statistics on Gokce Dam are:

Year completed	1988
Height (from foundation)	61.0 m
Height (from river bed)	50.0 m
Crest length	747 m
Reservoir area	1.28 km^2
Reservoir volume	13,250,000 m^3

The dam (Figure 2) is composed of a rock-filled shell having a clay core with upstream and downstream sand filters. The reservoir level during the earthquake appears to have been at about 70 percent. The dam is founded on bedrock.

As noted, the dam is interpreted to have experienced 0.2 g or greater of peak horizontal acceleration. There were no strong motion records in the region. The only observed effect of the earthquake on the dam was a longitudinal crack which developed on the crest. The crack is shown in Figure 3. It was about 7 mm wide at the middle of the dam and was located along the upstream side of the gravel road which runs along most of the crest of the dam. The work was judged by the authors to have been only cosmetic in its effects. Fine cracks, not affecting the structure, were observed in a concrete building at the dam.

The downstream face of the dam was observed to be somewhat irregular as seen in Figure 2. The irregularity is on the order of 1 to 2 m. There was no evidence that this was the result of slumping or other movement. The exposed upstream face appears to have a more uniform appearance. There was also no observed evidence of increased water seepage downstream from the dam. Except for the minor crack along the crest, the dam showed no effects of the earthquake shaking.

2.2 Kirazdere (Yuvacik) Dam

Kirazdere Dam is also known as Yuvacik Dam. Its statistics are:

Year completed	1992
Height (from foundation)	108.5 m
Height (from river bed)	102.5 m
Crest length	390 m
Reservoir area	1.74 km^2
Reservoir volume	5,200,000 m^3

Kirazdere Dam (Figure 4) is of particular interest as the epicenter of the Kocaeli earthquake is within a few kilometers of the site. Figure 5 shows two meters of right lateral strike slip fault movement that was observed within one to two kilometers of Kirazdere Dam. From the isoseismals in Figure 1, the dam is inferred to have experienced 0.3 to 0.4 g of peak horizontal acceleration.

The maximum accelerations recorded from the Izmit station about 10 to 12 km distant were 0.145 g, 0.167 g, and 0.230 in the vertical, north-south and east-west directions, respectively. To utilize these data for the Kirazdere Dam, the acceleration records were scaled to 0.4 g. The acceleration data points were scaled by factor 1.74 (0.4 g/0.230 g), where 0.4 g is the desired scale and 0.23 g is maximum horizontal acceleration measured. Spectral acceleration curves for the scaled acceleration records are shown in Figure 6. From this figure, the predominant frequencies are about 0.35, 0.57, and 0.35 Hz in the vertical, north-south and east-west directions, respectively.

The Kirazdere Dam is earth fill with a clay core, sand and gravel filters, and a rock shell. A road passes along its crest. The dam manager stated that a few cracks resulted from the earthquake. These had the width of about 2 mm and occurred on the gravel road on the crest near the left abutment looking upstream, and were parallel to the axis of the dam. The lengths of these cracks were not observed. The road on the crest is heavily used and the cracks quickly disappeared.

A few hairline cracks were seen in a one-story concrete structure at the dam. No cracking was seen in the concrete of the spillway.

Benches excavated into the left abutment, looking upstream, showed some falling away of material from the stepped benches and small talus accumulations of rockfall debris (see Figure 7). The dam manager explained that some of this material in the talus fell during the earthquake but some of it was there before the earthquake.

The upstream and downstream faces of the dam were straight and uniform. A tunnel which carried a water pipeline from under the dam had experienced a small leak.

The dam appears to have suffered no significant damage from the earthquake. The cracks, and talus on the abutment, were extremely minor.

2.3 Hasanlar Dam

Hasanlar Dam, located about 30 km northeast of Duzce and 15 to 20 km from the fault rupture in the November 12, 1999 earthquake, is included here because of similarities to the Kocaeli event. Statistics for Hasanlar Dam are:

Year completed	1972
Height (from foundation)	72.8 m
Height (from river bed)	70.8 m
Crest length	67 m
Reservoir area	2.85 km^2
Reservoir volume	1,651,000 m^3

Hasanlar Dam (Figure 8) was, like Gokce and Kirazdere Dams, built on bedrock with a clay core, sand and gravel filters, and a rock shell.

The maximum accelerations recorded from the Duzce station were 0.481 g, 0.312 g, and 0.364 g in the vertical, north-south and east-west directions, respectively. To utilize these data on the Hasanlar Dam, the acceleration records were scaled to 0.2 g. The acceleration data points were scaled by factor 0.55 (0.2 g/0.364 g), where 0.2 g is the desired scale and 0.364 g is maximum horizontal acceleration measured. Spectral acceleration curves for the scaled acceleration records are shown in Figure 9. The predominant frequencies are about 0.6, 0.35, and 0.65 Hz in the vertical, north-south and east-west directions, respectively.

Inspection of the dam showed no effects from earthquake shaking.

3.0 CONCLUSIONS

Only two dams experienced earthquake shaking with a PHA≥0.2 g. These were Gokce Dam near Yalova, where the PHA was around 0.2 g, and Kirazdere Dam, southeast of Izmit where the PHA was as much as 0.4 g. An additional dam, Hasanlar, experienced about 0.2 g from the Duzce earthquake. All of the dams are earth embankments on bedrock. None of the dams had any significant damage.

The behavior of Kirazdere Dam, which is located practically at the epicenter of the 1999 Kocaeli earthquake, is of particular interest. The dam experienced a world class earthquake of $M_s = 7.8$. The dam had no damage.

4.0 ACKNOWLEDGMENTS

The authors were greatly helped by Dr. Mustafa Erdik, chairman of the Department of Earthquake Engineering and Director of the Kandilli Observatory and Earthquake Research Institute at Bogazici University, who furnished strong motion instrumental data and background for understanding the earthquake processes in the region. He also provided contacts with Turkish officials for permissions to visit dams.

The resulting data from this research effort, unless otherwise noted, were obtained from research conducted under the Earthquake Engineering Research Program of the U.S. Army Corps of Engineers by the U.S. Army Engineer Research and Development Center. Permission was granted by the Chief of Engineers to publish this information. Opinions expressed in this paper may or may not represent those of the Corps of Engineers.

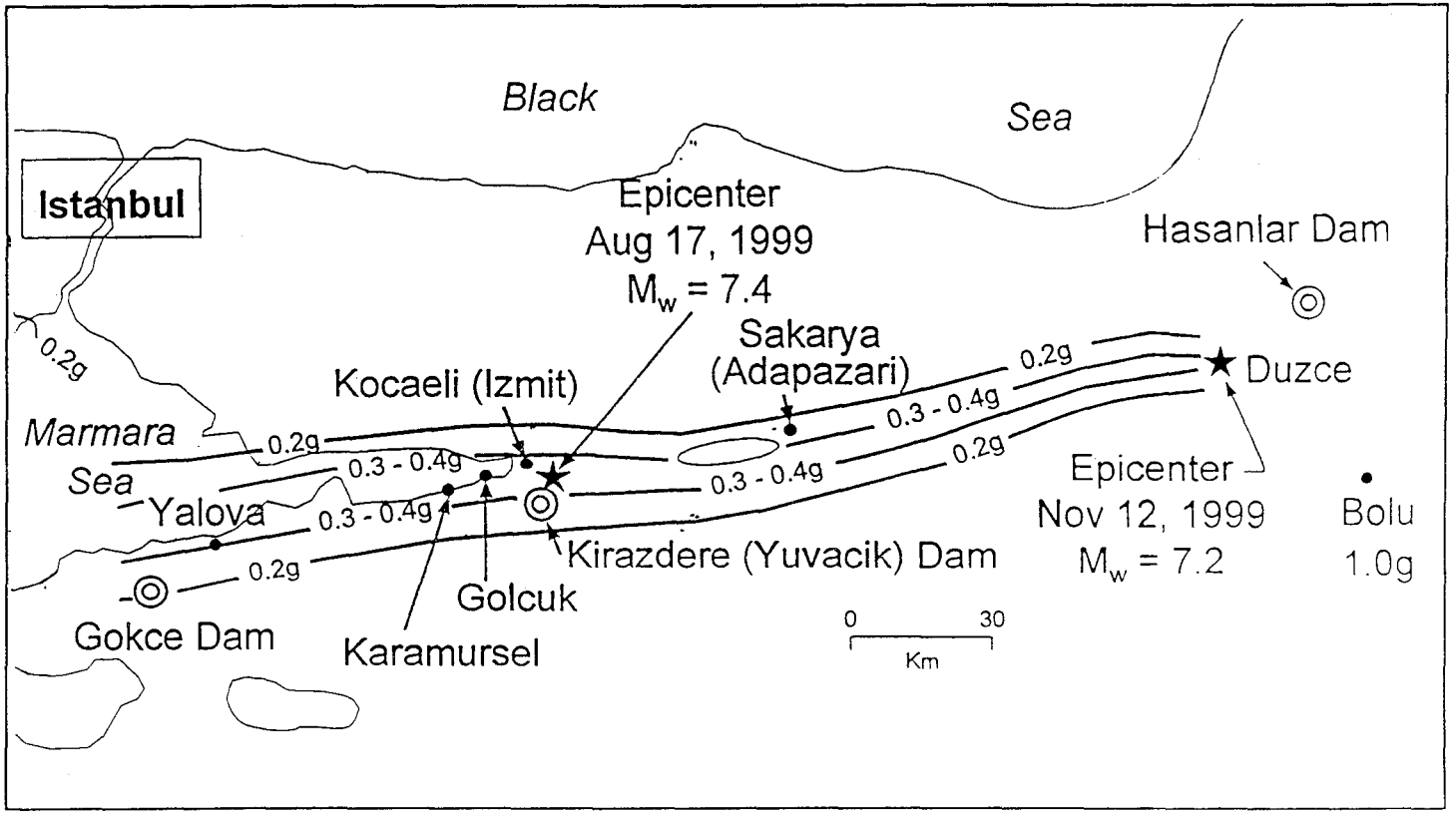

Figure 1. Interpreted isoseismals for the August 17, 1999 Turkey earthquake. Epicenters are shown for both the August 17 and November 12 earthquakes. Dams located in the area of significant shaking from these two earthquakes are Gokce, Kirazdere, and Hasanlar

Figure 2. Downstream view of Gokce Dam near Yalova

Figure 3. Longitudinal crack near the edge of the crest of Gokce Dam on the upstream side. The location is about at the middle of the dam. The width of the crack was about 7 mm at its greatest

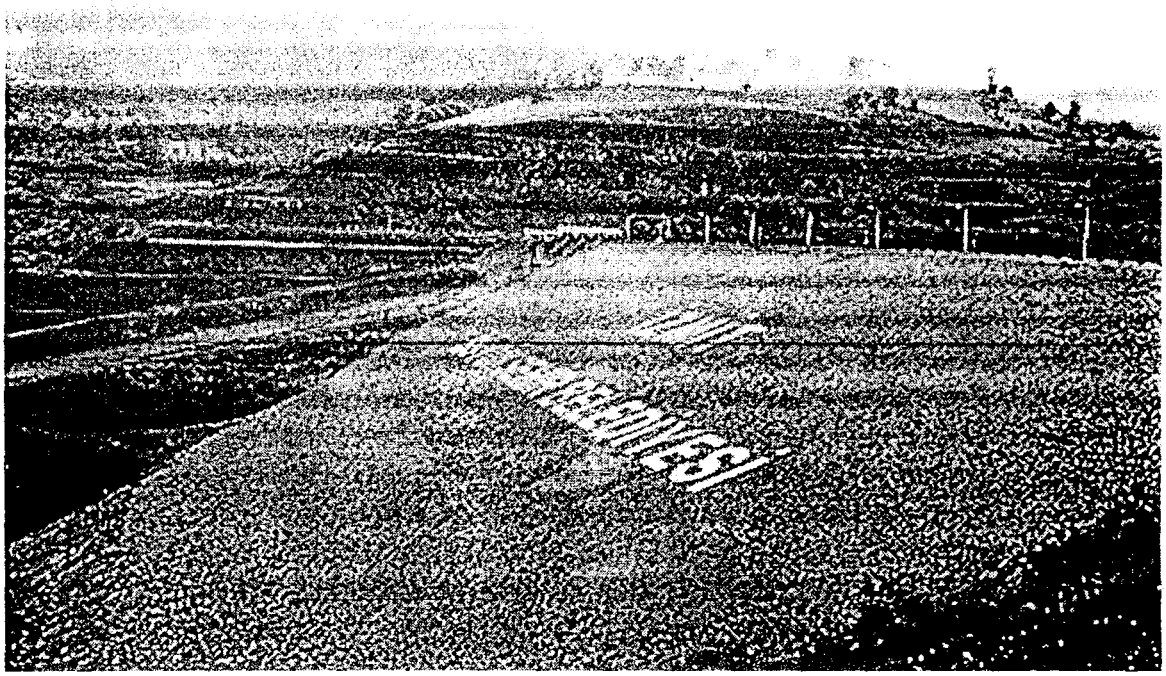

Figure 4. Downstream face of Kirazdere (Yuvacik) Dam

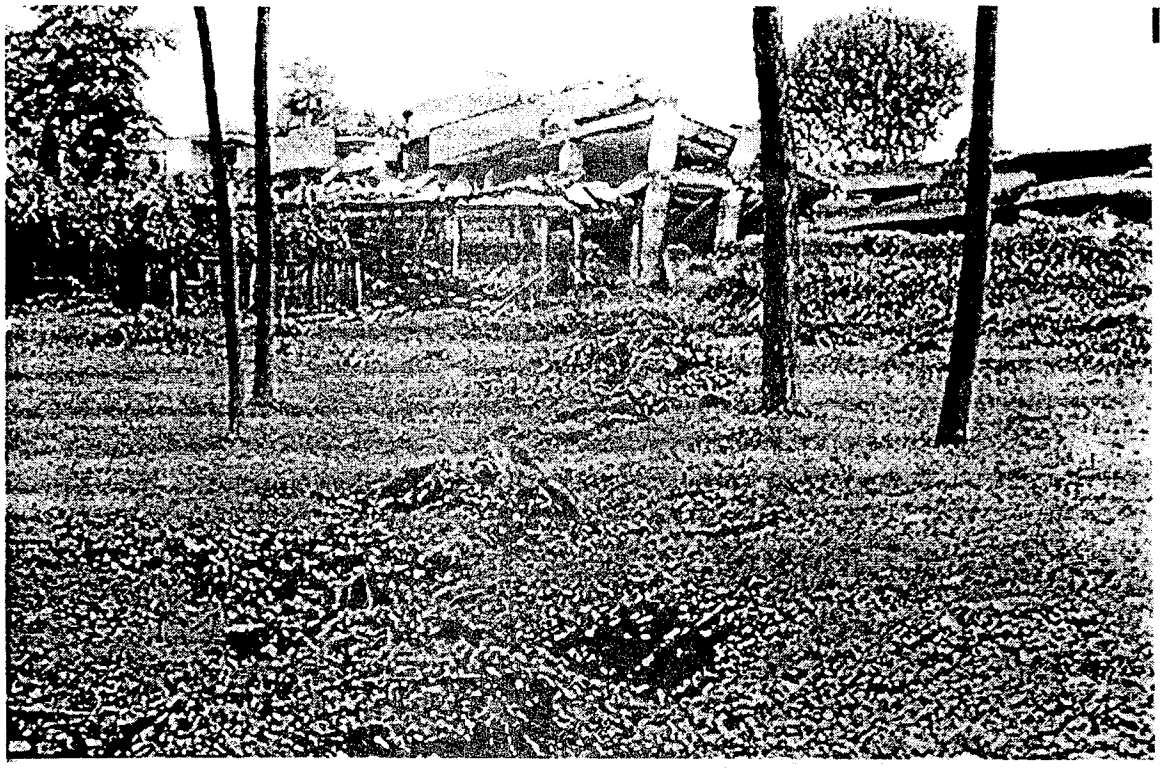

Figure 5. Right lateral strike-slip fault movement of about two meters which occurred within one to two kilometers from Kirazdere Dam

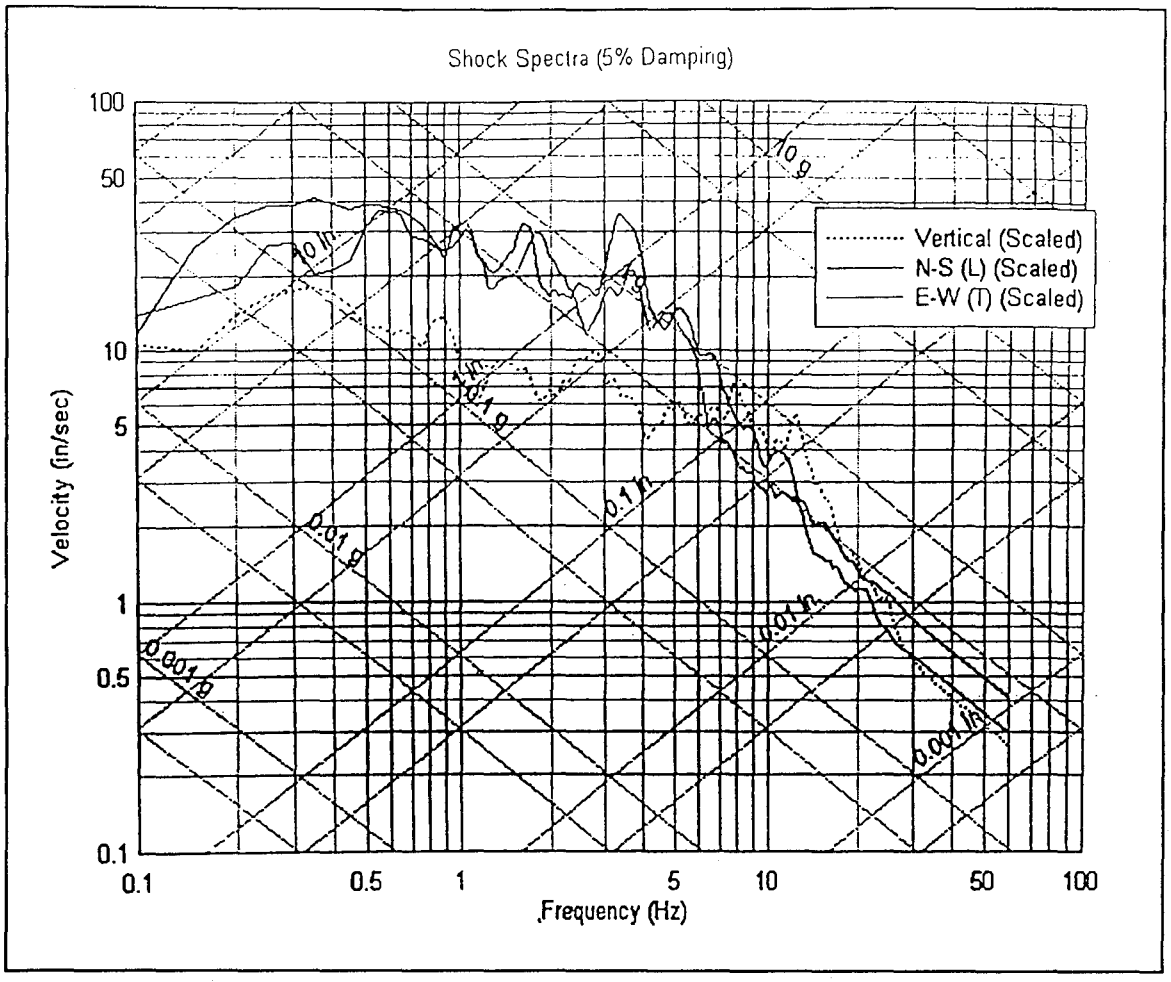

Figure 6. Spectral acceleration for the scaled acceleration time history at the Izmit station developed for Kirazdere Dam

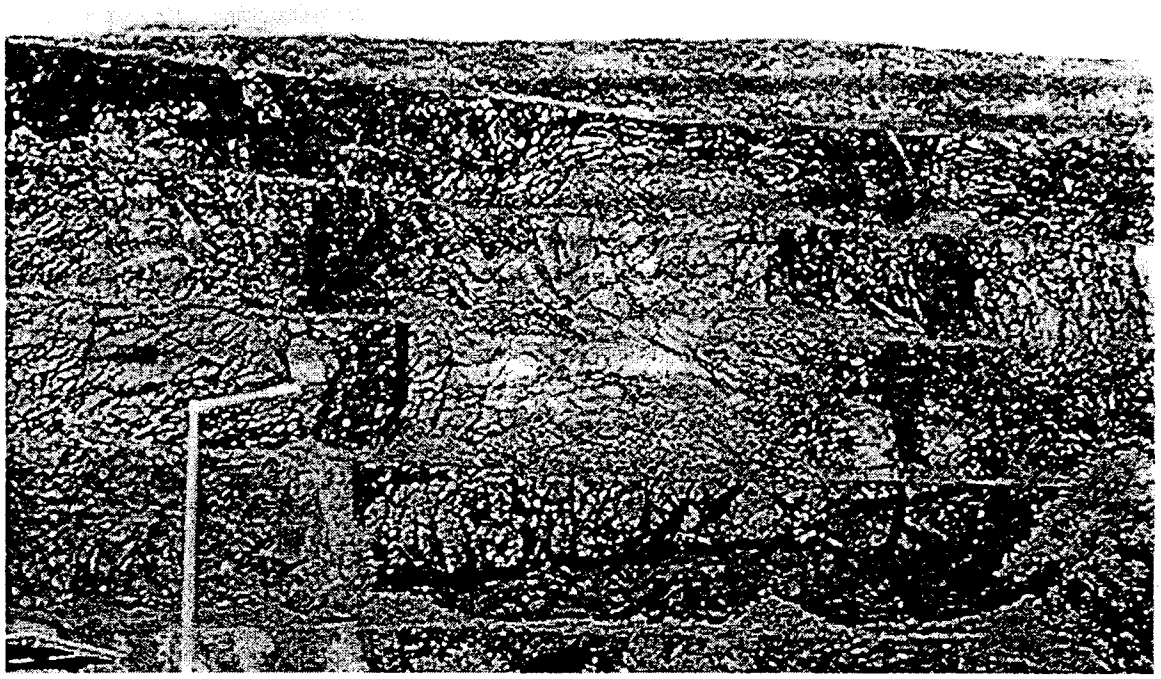

Figure 7. Rockfall debris in the left abutment of Kirazdere Dam

Figure 8. Downstream face of Hasanlar Dam

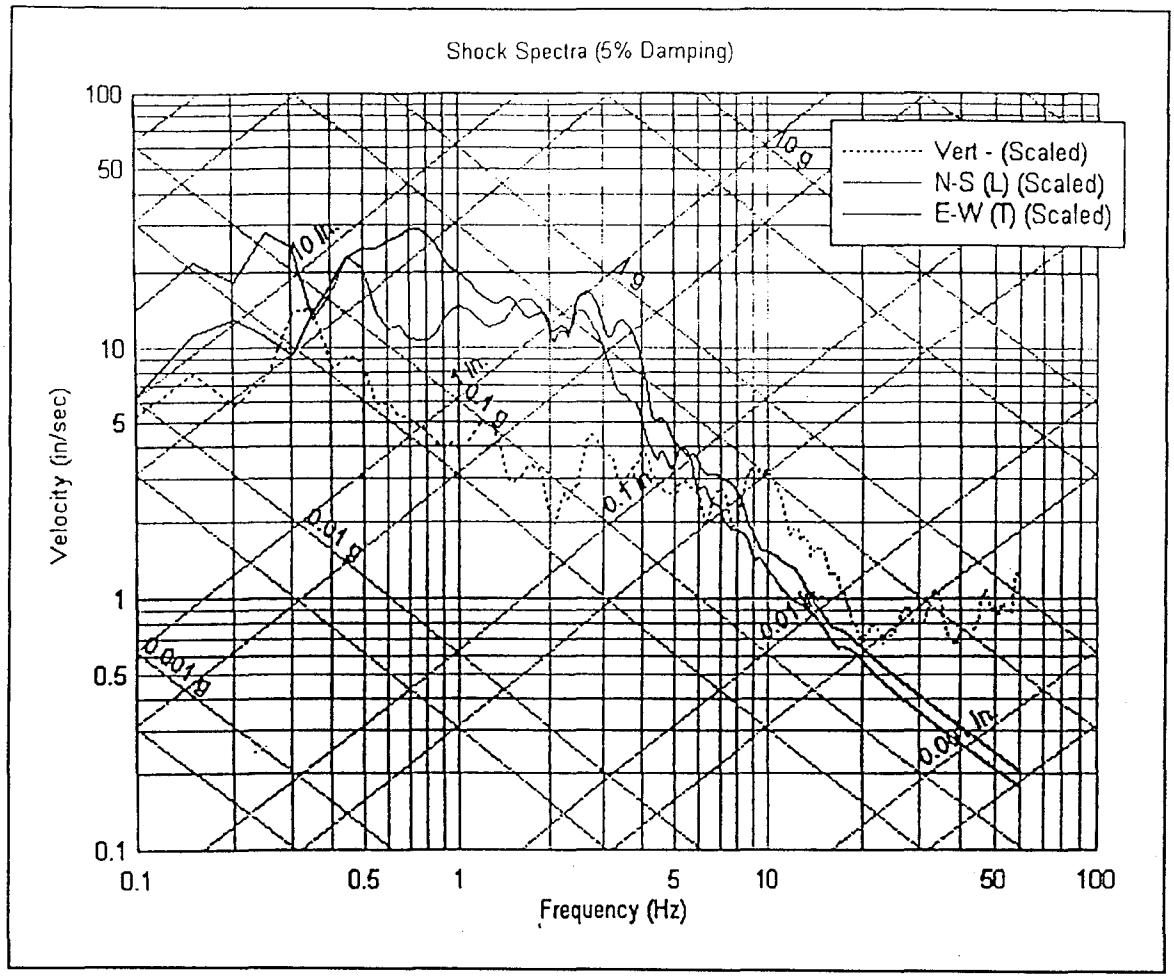

Figure 9. Spectral acceleration for the scaled acceleration time history at the Duzce Station developed for Hasanlar Dam

DAMAGE OF TRANSPORTATION FACILITY IN THE 1999 KOCAELI AND DUZCE, TURKEY EARTHQUAKES AND THE 1999 CHI-CHI, TAIWAN EARTHQUAKE

by

Kazuhiko KAWASHIMA[1] and Gaku SHOJI[2]

ABSTRACT

This paper describes the damage of bridges in the 1999 Kocaeli and Duzce, Turkey, earthquakes and the 1999 Chi-Chi, Taiwan, earthquake. Effect of tectonic ground movement is presented.

Keywords: Seismic Damage, Bridge, Turkey, Kocaeli Earthquake, Duzce Earthquake, Chi-Chi Earthquake

1. INTRODUCTION

Extensive structural damage occurred in the Kocaeli, Turkey, Earthquake (moment magnitude M_w=7.4), August 19, 1999, and the Chi-Chi, Taiwan Earthquake (M_w=7.6), September 21, 1999. About 17,000 and 2,400 victims were induced in the Kocaeli and Chi-Chi earthquakes, respectively. In the Turkey, an earthquake with M_w=7.1 (Bogazici University1999) occurred on 12, November, 1999 in Duzce, about 100km east of the Kocaeli (Duzce earthquake), and about 900 peoples were killed.

In the three earthquakes, the tectonic ground movements as well as strong ground shaking induced significant structural damage in the transportation facility. A damage survey was conducted in Kocaeli earthquake by the first author on September 8 and 9, 1999, and in the Chi-Chi earthquake by the authors on October 9-14, 1999. This paper describes the damage of transportation facility in the Kocaeli and Duzce earthquakes, Turkey, and the Chi-Chi, Taiwan, earthquakes.

2. KOCAELI, TURKEY EARTHQUAKE

(1) Tectonic Ground Movement and Ground Motion in the Damaged Area

In the Kocaeli earthquake, extensive damage of transportation facilities occurred in the Kocaeli and Sakarya region. A part of the right-lateral strike slip Anatolian fault ruptured in east-west direction for about 100km from Golcuk to Duzce. As shown in Fig. 1, since the Trans-European Motorway was almost parallel to the fault, the fault rupture crossed the Motorway at several locations. Damage of road facilities was extensive around the city of Arifiye as shown in Figs. 2 and 3. Arifiye Overpass (No. 3, refer to Fig. 3) and Sakarya Center Bridge (No. 5, refer to Fig. 3) collapsed. Overpasses near Ariyiye Overpass (No. 2, 4 and 5, refer to Fig. 3) suffered minor damage.

Various evidence of right-lateral strike slip rupture was observed in the area (refer to Fig. 3). For example, a 4.3m offset of a concrete fence of an automobile factory (Arbas Arac Kadlama Fabzikasi) was developed at northeast corner (Point D) as shown in Photo 1. In a poplar grove at Point G, the largest fault offset measured from displaced poplar trees that were originally planted in lines was 4.3m, as shown in Photo 2. The fault developed an offset of an about 1m-diameter sewer pipe embedded at Point H, as shown in Photo 3. The offset appeared to be on the order of at least 3m and probably 4m. The fault rupture continued further west parallel to the Motorway and resulted in a 3.6m offset of a 1.4m-diameter drainage pipe at Point I, as shown in Photo 4. The Points G, H and I were close to Arifiye Bridge that collapsed in the earthquake.

1) Professor, Graduate School of Science and Engineering, Tokyo Institute of Technology
2) Research Associate, Graduate School of Science and Engineering, Tokyo Institute of Technology

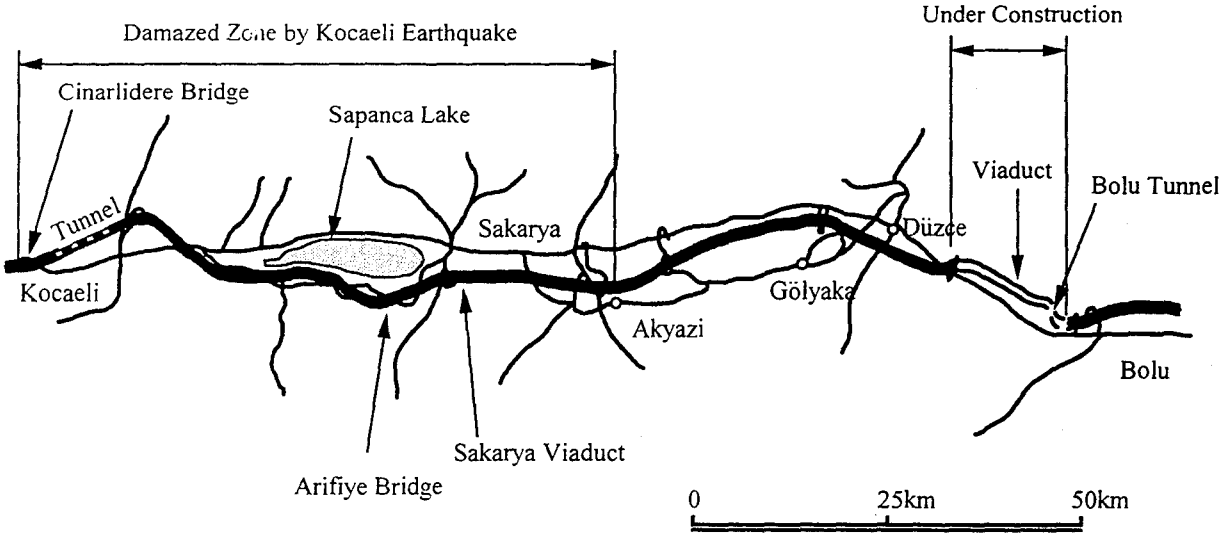

Fig. 1 Damaged Region in the Kocaeli and Duzce Earthquakes, Turkey

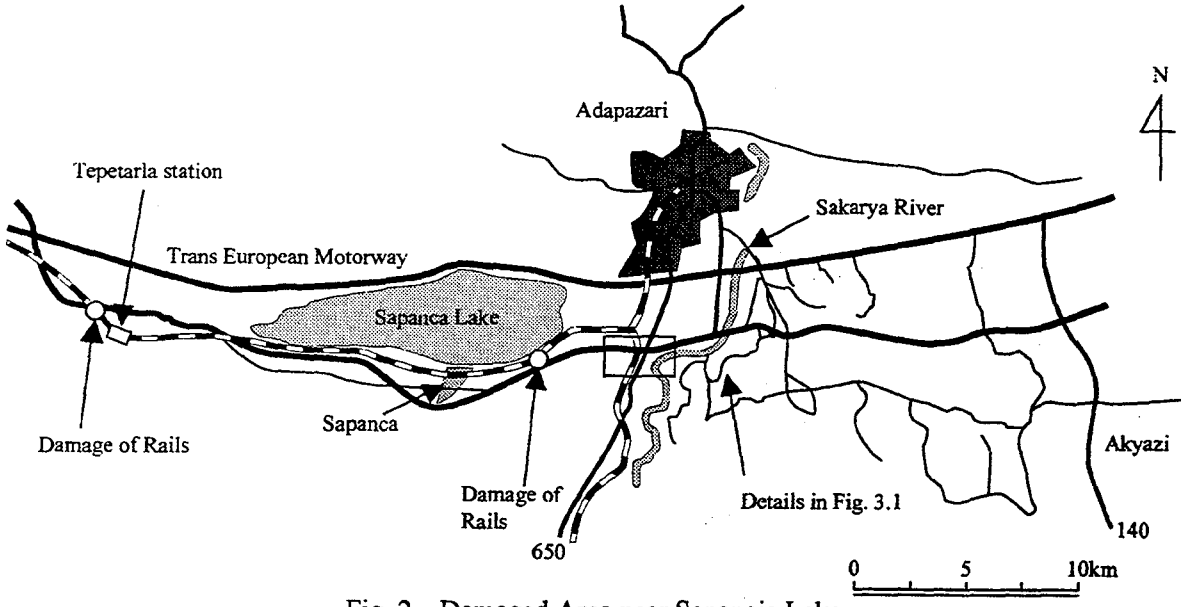

Fig. 2 Damaged Area near Sapancia Lake

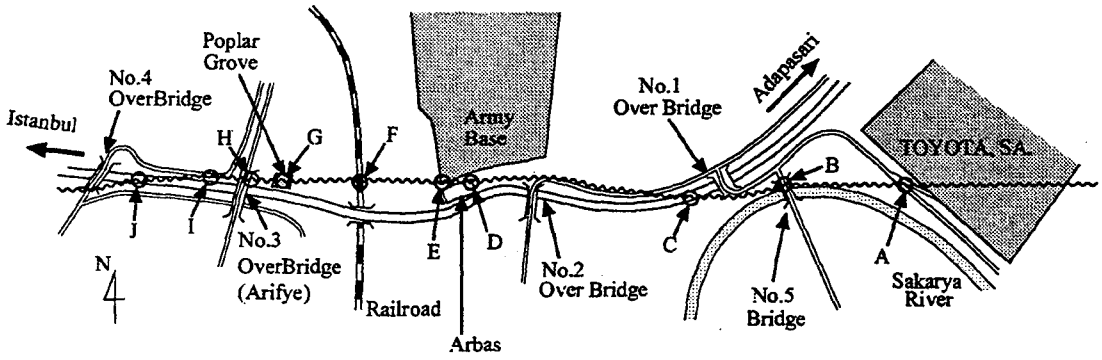

Fig. 3 Damaged Transportation Facilities and Fault-Induced Ground Movement, Kocaeli Earthquake

Photo 1 Offset of a Concrete Fence of 4.3 m at Automobile Factory (Point D, refer to Fig. 3)

Photo 2 Offset of Poplar Grove of 4.3 m (Point G, refer to Fig. 3)

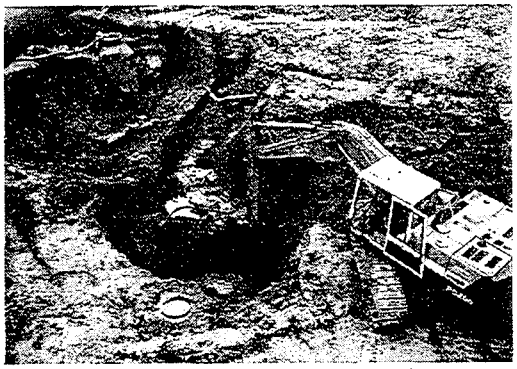

Photo 3 Offset of a Sewage Pipe (Point H, refer to Fig. 3)

Photo 4 Offset of a Drainage Pipe of 3.6 m (Point I, refer to Fig. 3)

Photo 5 Offset of Poplar Trees of 2.5 m near Tepetarla Station (South side (bottom in Photo) was about 1 m lower than the north side (top))

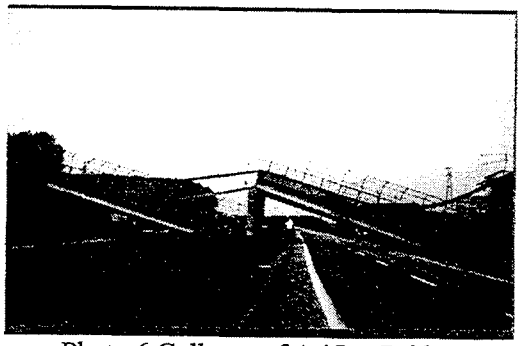

Photo 6 Collapse of Arifiye Bridge (Courtesy of H. Hoashi)

Near Tepetarla Station (refer to Fig. 2) where a large offset of railways occurred, the largest offset measured from offset of poplar trees was 2.5m, as shown in Photo 5. As well as the right lateral slip, an offset of ground surface level of about 1m (south side was lower than the north side) was observed.

Strong motion accelerations were recorded at various locations by Ministry of Public Works and Settlement, Bogazici University and Istanbul Technical University. Fig. 4 shows the ground accelerations recorded at Sakarya, Adapazeri. The fault normal acceleration was not recorded at this site. The peak acceleration of fault parallel component was 4.07m/s^2, and this was the largest

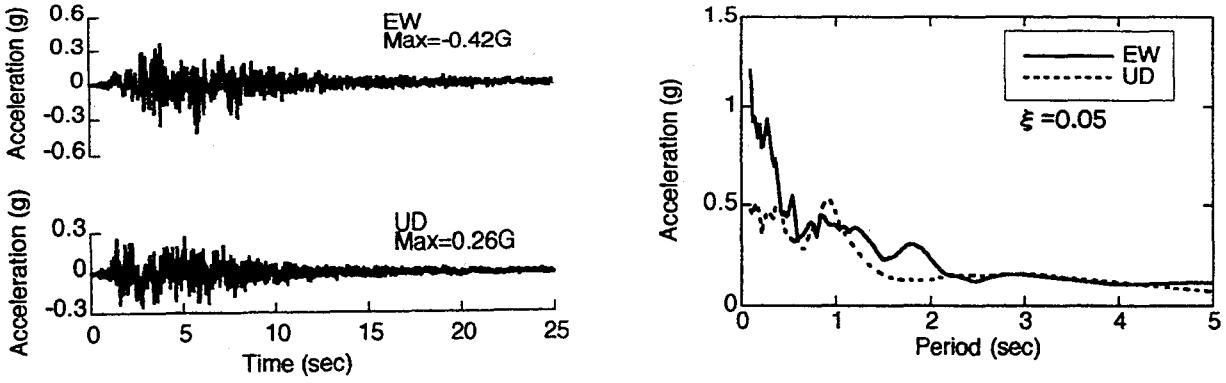

Fig. 4 Ground Motions Recorded at Sakarya, Adapazeri

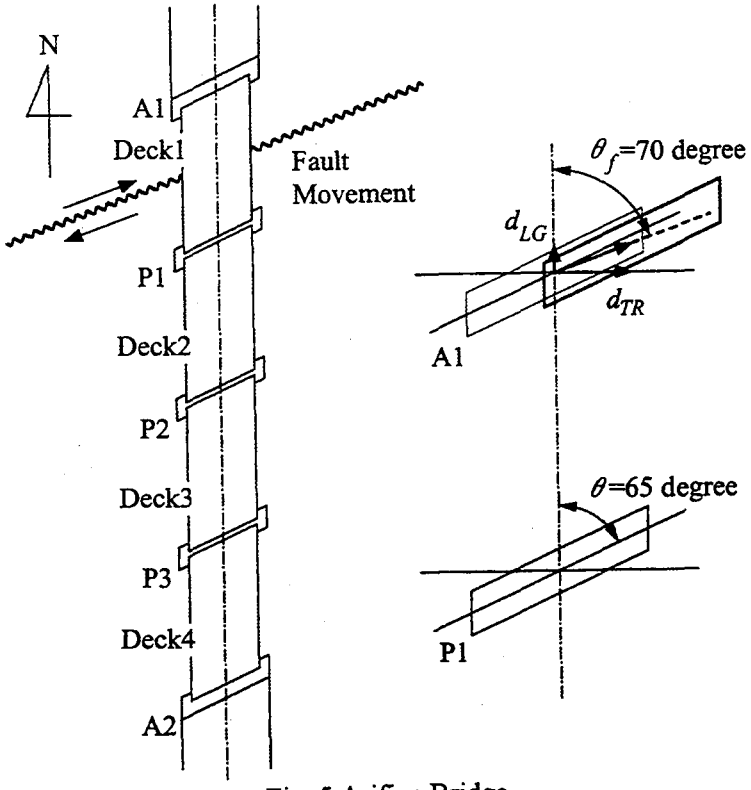

Fig. 5 Arifiye Bridge

acceleration measured in the Kocaeli earthquake. It was rather smaller than the amplitude that is generally generated by a M_w 7.4 earthquake. The response acceleration is over 1g at short natural period, but it decreases sharply as the period increases.

(2) Collapse of Arifiye Overpass

The Arifiye Overpass was of 4 span simply supported prestressed concrete bridge (No. 3, refert to Fig. 3). It was supported by two abutments and 3 wall-type reinforced concrete piers. It was a skewed bridge with a skew angle of 65-degree. The substructures and the decks are denoted herein as A1, P1, P2, P3 and A2, and D1, D2, D3 and D4, respectively, from north to south (refer to Fig. 5). As shown in Photo 6, the D2, D3 and D4 dislodged from their supports at south ends and fell down with the north side still being

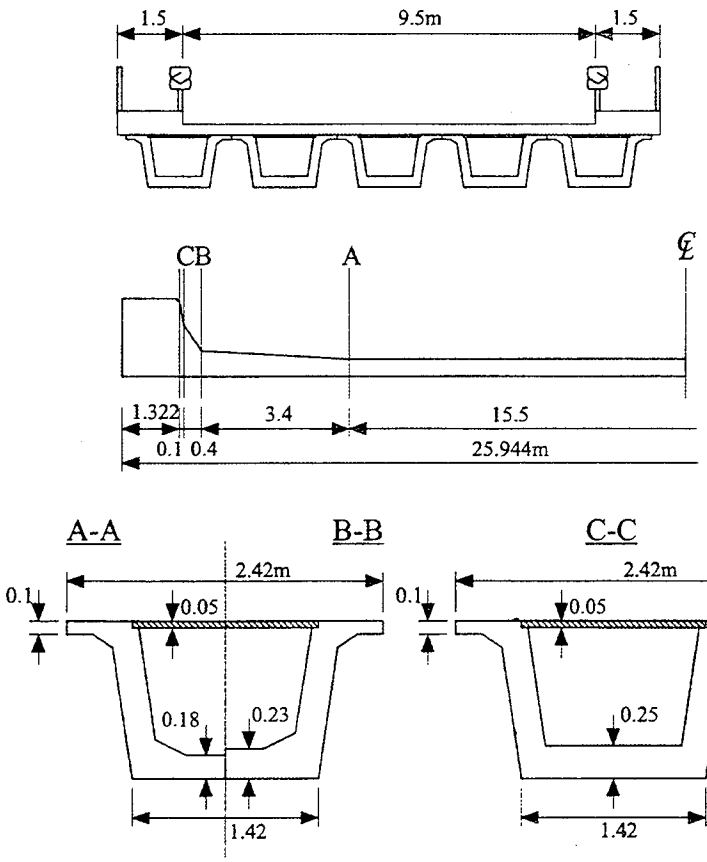

Fig. 6 Cross Section of Arifiye Bridge (Courtesy of F. Inal and H. Hoashi)

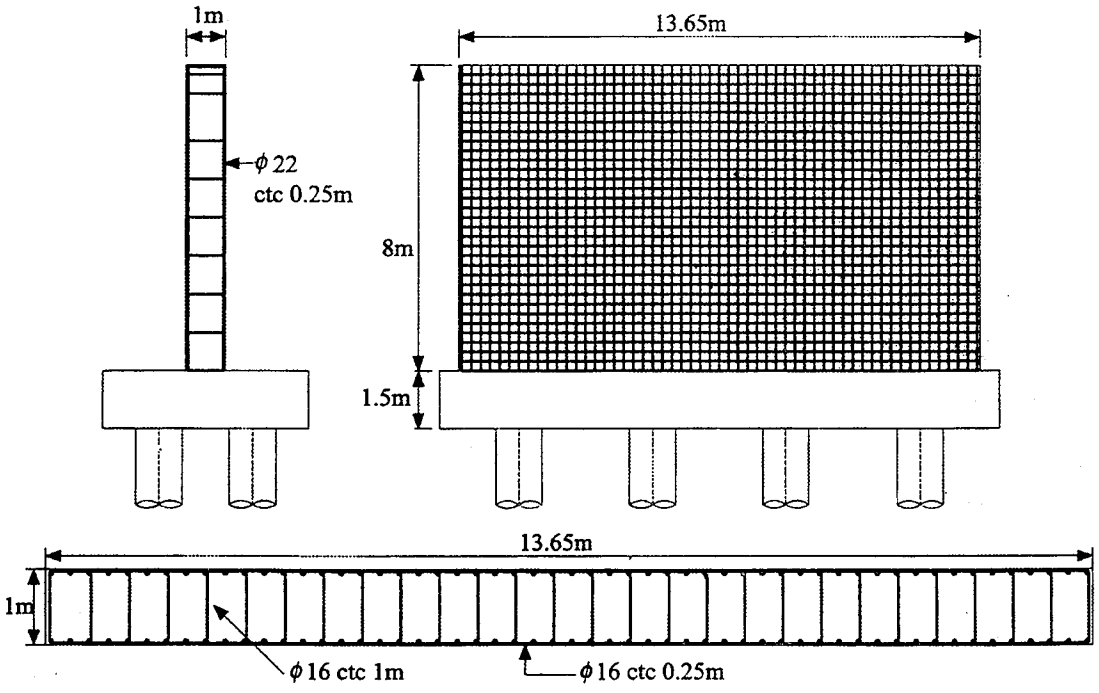

Fig. 7 Section of Piers, Arifiye Overpass (Courtesy of F. Inal and H. Hoashi)

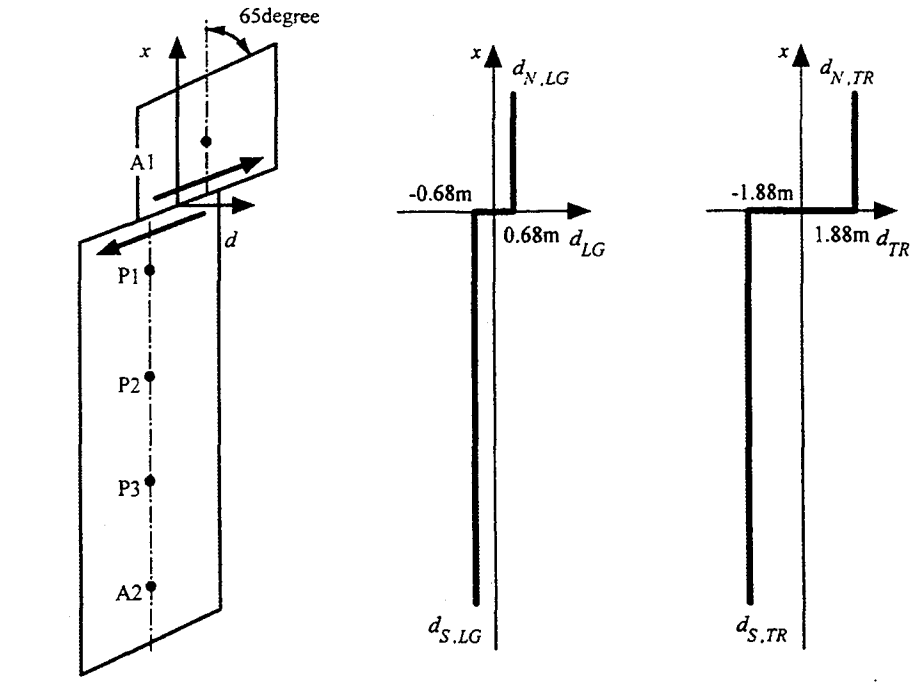

(a) Deformation of Ground (b) Displacement d_{LG} (c) Displacement d_{TR}

Fig. 8 Effect of Fault Movement

supported by the piers. D 1 rested on ground almost horizontally.

The decks were of 5 precast concrete U-beams as shown in Fig. 6. They were supported by 5 elastomeric bearings with 300mm x 300mm and 100mm high per substructure. As shown in Fig. 7, the piers were 1m thick and 14m wide in longitudinal and transverse directions, respectively. The design strength of concrete was 30 MPa. This was a standard overpass in the area. The reinforced concrete footing that supported P1 was 5.3m long and 14m wide in longitudinal and transverse directions, respectively. The footing of P3 was supported by 8 1m-diameter cast-in-place reinforced concrete piles. The piles were reinforced by 12 20mm plain bars. The averaged concrete strength investigated with the Shumit hammer was 56 MPa and 47 MPa at the front wall of A2 and the upper surface of P1 footing, respectively.

As shown in Fig. 5, the fault rupture crossed the bridge between A1 and P1 with an angle θ of about 70-degree. The right-lateral strike-slip fault forced A1 to move in northeast direction with respect to P1-P3 and A2. If one idealizes a ground rupture as shown in Fig. 8 (a), the ground displacement at north and south of the fault rupture, d_N and d_S, may be obtained as $d_N = d_S = D_0/2$, in which D_0 is a relative displacement of ground at the fault rupture. Thus, the ground movement in transverse and longitudinal directions of bridge axis may be written

$$d_{N,TR} = D_0/2 \cdot \sin\theta$$
$$d_{N,LG} = D_0/2 \cdot \cos\theta \quad (1)$$

at the north of fault, and

$$d_{S,TR} = -D_0/2 \cdot \sin\theta$$
$$d_{S,LG} = -D_0/2 \cdot \cos\theta \quad (2)$$

at the south of fault.

Assuming $D_0 \approx 4$m and $\theta \approx 70$-degree, the ground displacements may be obtained from Eqs. (1) and (2) as shown in Fig. 8 (b) and (c). The relative displacement between A1 and P1 in longitudinal direction, d_{LG}, is 1.37m, which is much larger than the seat length of about 0.6 m at A1 and 0.45 m at P1. It seems that D1

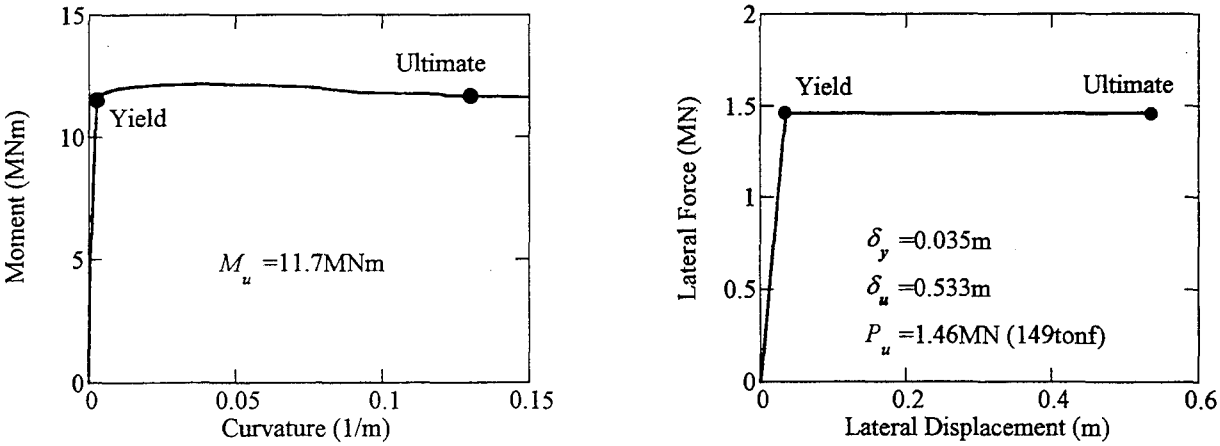

(a) Moment-Curvature Relation

(b) Lateral Force-Lateral Displacement Relation

Fig. 9 Lateral Force vs. Lateral Displacement of Piers, Arifiye Overpass

dislodged from its supports due to such a large relative displacement induced by the fault rupture between A1 and P1. On the other hand, the foundations of P2, P3 and A2 were forced to move in south direction. It appears that such a southward movement of foundations resulted in dislodging D2, D3 and D4 from their support at the north ends.

From the reinforcement presented in Fig. 7 and concrete strength of 30 MPa, the lateral force vs. lateral displacement relation was evaluated based on the standard moment-curvature analysis (Japan Road Association 1996) as shown in Fig. 9. The stress-strain relation of concrete developed by Hoshikuma et al (Hoshikuma et al. 1997) was used to represent the confinement effect. Assuming that the tributary mass of a pier is 5800 kN, the response acceleration that resulted in yielding of piers becomes approximately 0.2 g.

(3) Overpasses around Arifiye Overpass

Near the Arifiye Overpass, there were several overpasses that had the same deck and substructure type to the Arifiye Overpass. In general, their seismic performance was good. For example, the fault crossed a two span simply supported prestressed concrete overpass (No. 1 Overpass, refer to Fig. 3) at its south abutment, after crossing the Motorway at about 50 m west

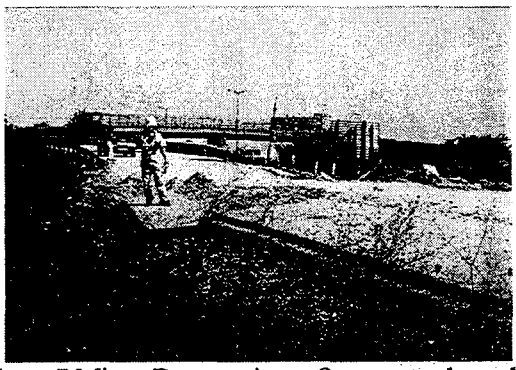

Photo 7 Minor Damage in an Overpass where the Fault Crossed the Overpass at Its Abutment

of the overpass as shown in Photo 7. However, the damage was minor, i.e., only about 50mm-shear deformation of elastomeric bearings occurred associated with the tectonic ground movement.

At a 3 span simply supported overpass (No. 2 Overpass, refer to Fig. 3), located about 400m east of No. 1 Overpass, the deck collided with the north abutment, resulting in crush of a part of concrete parapet wall. About 20-30mm-shear deformation of elastomeric bearings occurred due to the fault movement. A 3 span simply supported overpass located about 400m west of the Arifiye Overpass (No. 4 Overpass, refer to Fig. 3) suffered only minor damage at the parapet wall of the north abutment, although the fault crossed nearby at the south abutment.

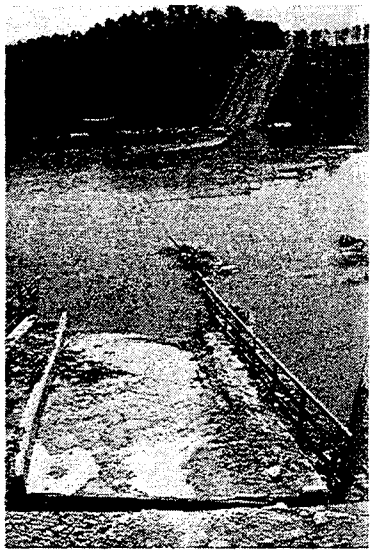

Photo 8 Collapse of Sakarya Central Bridge

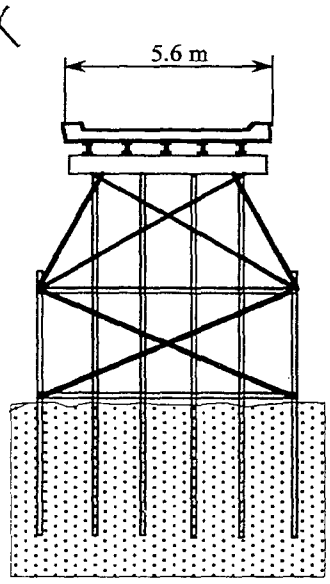

Fig. 10 Sakarya Central Bridge (Courtesy of F. Inal, H. Hoashi and K. Kosa)

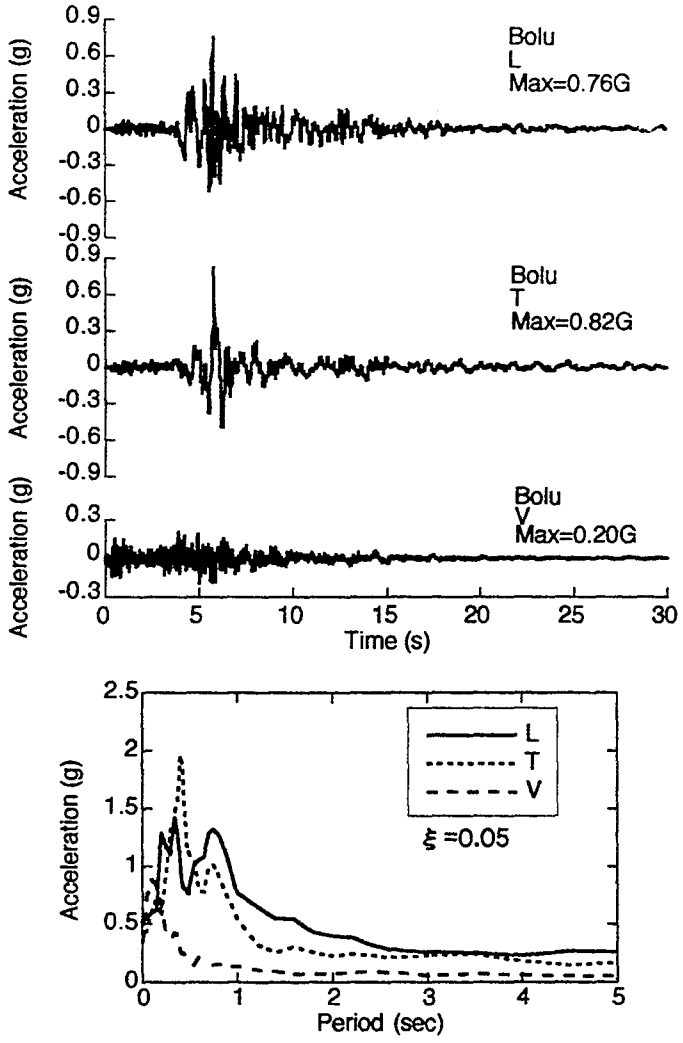

Fig. 11(a) Ground Accelerations Recorded in the Duzce Earthquake

Photo 8 Collapse of Sakarya Central Bridge

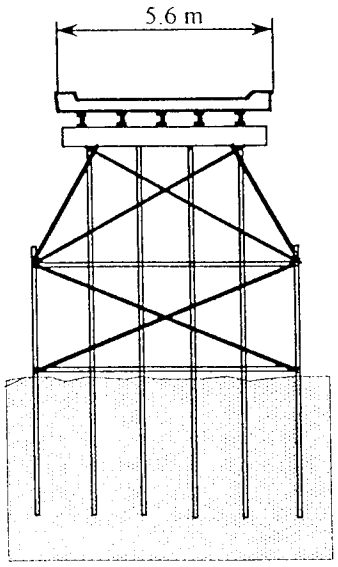

Fig. 10 Sakarya Central Bridge (Courtesy of F. Inal, H. Hoashi and K. Kosa)

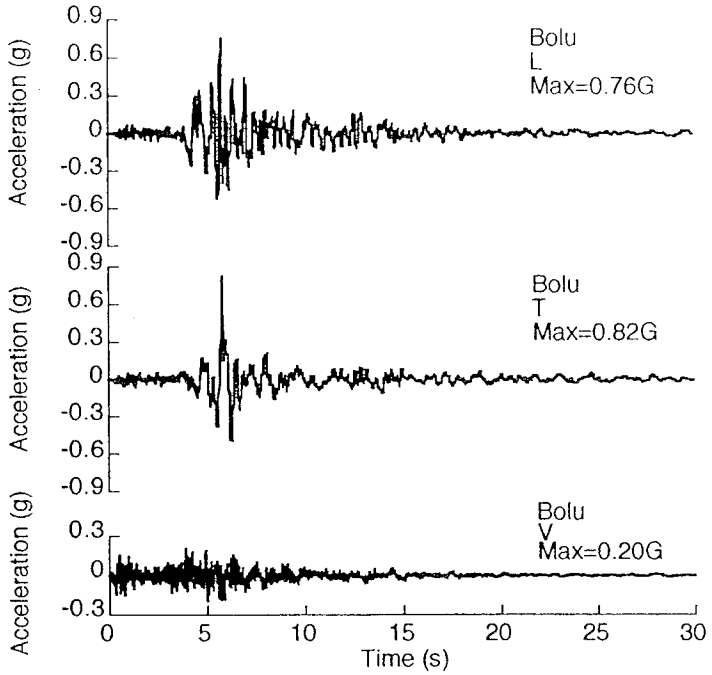

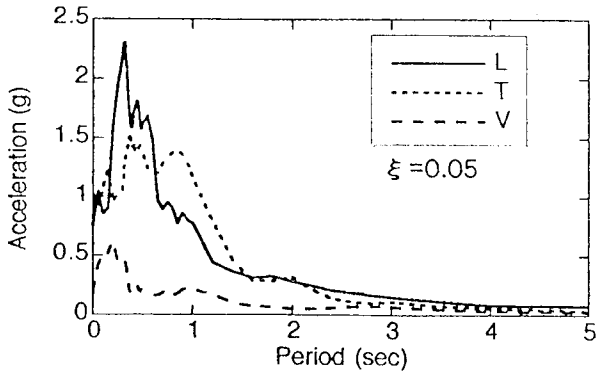

Fig. 11(a) Ground Accelerations Recorded in the Duzce Earthquake

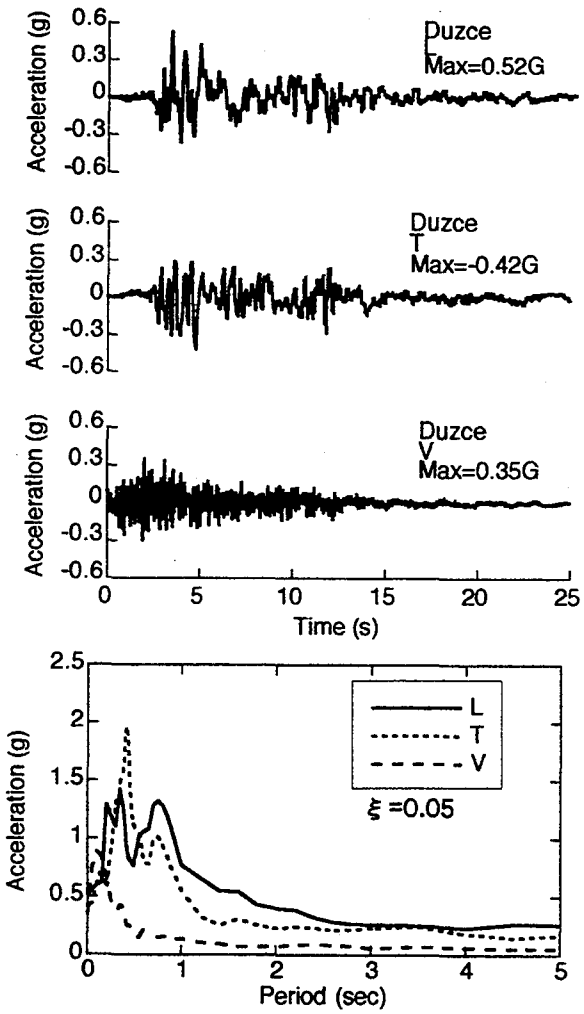

Fig. 11(b) Ground Accelerations Recorded in the Duzce Earthquake

The short wall-type piers, the short bridge span and the large constrain of the rigid abutments to the decks contributed to prevent build-up of the bridge response in the earthquake.

(4) Sakarya Center Bridge

Sakarya Center Bridge, crossing Sakarya river, on a regional road (No. 5 bridge, refer to Fig. 3) collapse as shown in Photo 8. The bridge was 8 span simply supported girders with two Gerber hinges at center. The length was 10m+6@12m+10m=92m. They were supported by steel piles as shown in Fig. 10. It was built 30-35 years ago. The decks collapsed with a span each on both ends tilted on the embankments. The fault crossed the north abutment.

3. DUZCE, TURKEY EARTHQUAKE

Fig. 11 shows ground acceleration recorded at Bolu and Duzce in the Duzce earthquake (Bogazici University 1999). The peal acceleration of lateral components was 0.76 g and 0.82 g at Bolu. Pulses with long durations are included in the record. Response acceleration of 0.05 damping ratio was 2.3 g in the L-component. Fig. 12 shows the ground accelerations recorded at the JMA observatory in the 1995 Hyogo-ken nanbu earthquake.

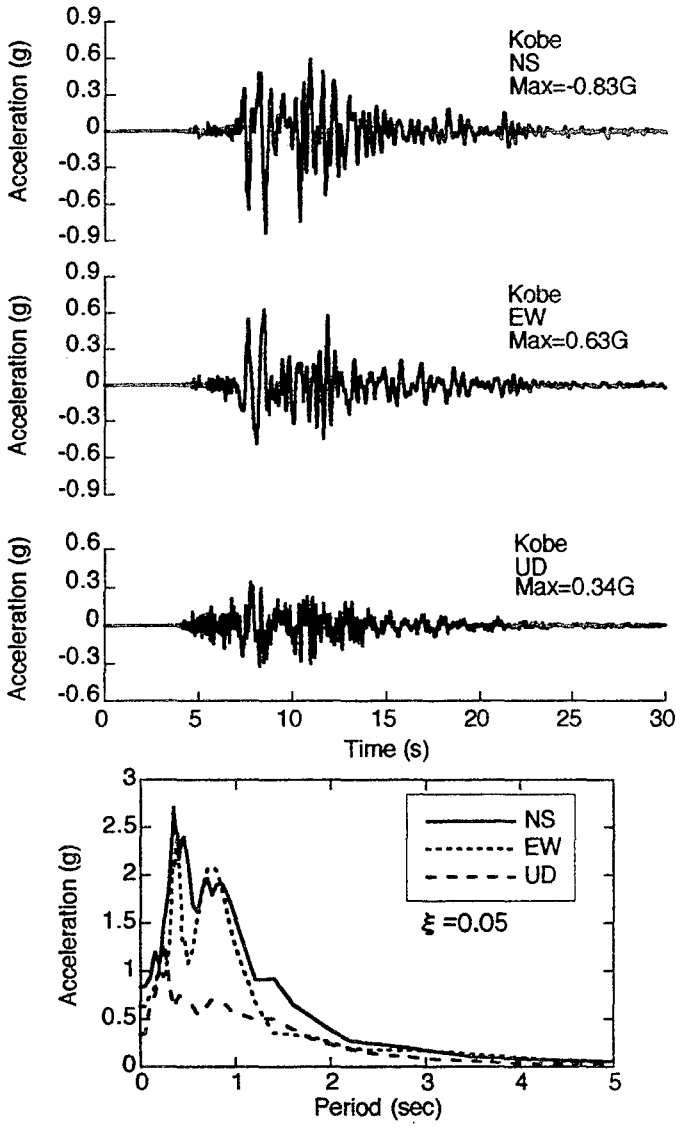

Fig. 12 Ground Accelerations Recorded at JMA Observatory in the 1995 Hyogo-ken Nanbu Earthquake

Photo 9 Damage of 10-Span Bridge, Duzce (Courtesy of H.Hoashi)

Photo 10 Fault that Crossed 10-Span Bridge (Courtesy of H.Hoashi)

Photo 11 Damage at Expansion Joint and Bearings
(Courtesy of H. Hoashi)

Acceleration and time are scaled in the same with Fig. 11. The Kobe observatory record also had several long-period pulses. The response acceleration was over 2.5 g at 0.4 second in the NS (fault normal) component.

A part of the Istanbul-Ankara Motorway that was under construction suffered damage (refer to Fig. 1). A 10-span simply supported prestressed concrete bridge with a total deck length of about 2.1 km suffered damage as shown in Photos 9, 10 and 11. The decks were continuous, which resulted in the continuous behavior of the bridge in an earthquake. The bridge was nearly completion when the earthquake occurred. A fault crossed between two columns resulting in some rotation of the columns. At least two decks were heavily displaced from their original seat.

4. CHI-CHI, TAIWAN EARTHQUAKE

(1) Tectonic Ground Movement and Ground Motion

The earthquake was induced by the Che-Long-Pu Fault. It was a thrust fault, and surface rupture was observed for over 70km between Min-Ju and Tungshih. Eastern Taiwan is a tongue of the Philippine Sea tectonic plate that is over-thrusting the Eurasia plate.

As shown in Fig. 13, damage occurred in Shihkang region, Tungshih region, Taiping, Wufeng and Tsaotun region, Nantou region, Chi Chi region, and Mingchien and Chushan region.

Figs. 14 and 15 show ground accelerations recorded at Shikhkang (TCU068), Taichung (TCU082) and Nantou (TCU076) and their response acceleration of 0.05 damping ratio, respectively. It is seen that several pulsses with longer period are included in the ground accelerations recorded at north. Almost single pulse with the peak acceleration of 4.9 m/s^2 was included in the EW component at Shikhkang. Response acceleration of 0.05 damping ratio is about 1.5g at 0.5 second in this record.

Fig. 16 compares the record at Shikhkang (TCU068) with the ground accelerations recorded at Bolu (L-component) and Duzce (L-component) in the Duzce earthquake (refer to Fig. 11), Sylmar parking lot (NS-component) in the 1994 Northridge earthquake and JMA Kobe observatory in the 1995 Hyogo-ken nanbu earthquake (refer to Fig. 12). It is noteworthy that Shikhkang record had larger response acceleration that the JMA Kobe record at the period over 2 second. The record at Bolu has over 2 g response acceleration at 0.3 second.

In the earthquake, at least eight bridges (Bei-Fong Bridge, Chang-Geng Great Bridge, Shc-Wci Bridge, Yi-Jian Bridge, Wu-Shi Bridge, Pin-Ling Bridge, Mou-Loh-Shi Bridge, Min-Ju Great Bridge, and Tong-Tou Bridge) collapsed, and a number of bridges suffered extensive damage. The tectonic movement along the fault developed most extensive damage. Two bridges significantly damaged by the fault movement and a modern cable-stayed bridge damaged by ground motion effect are described below.

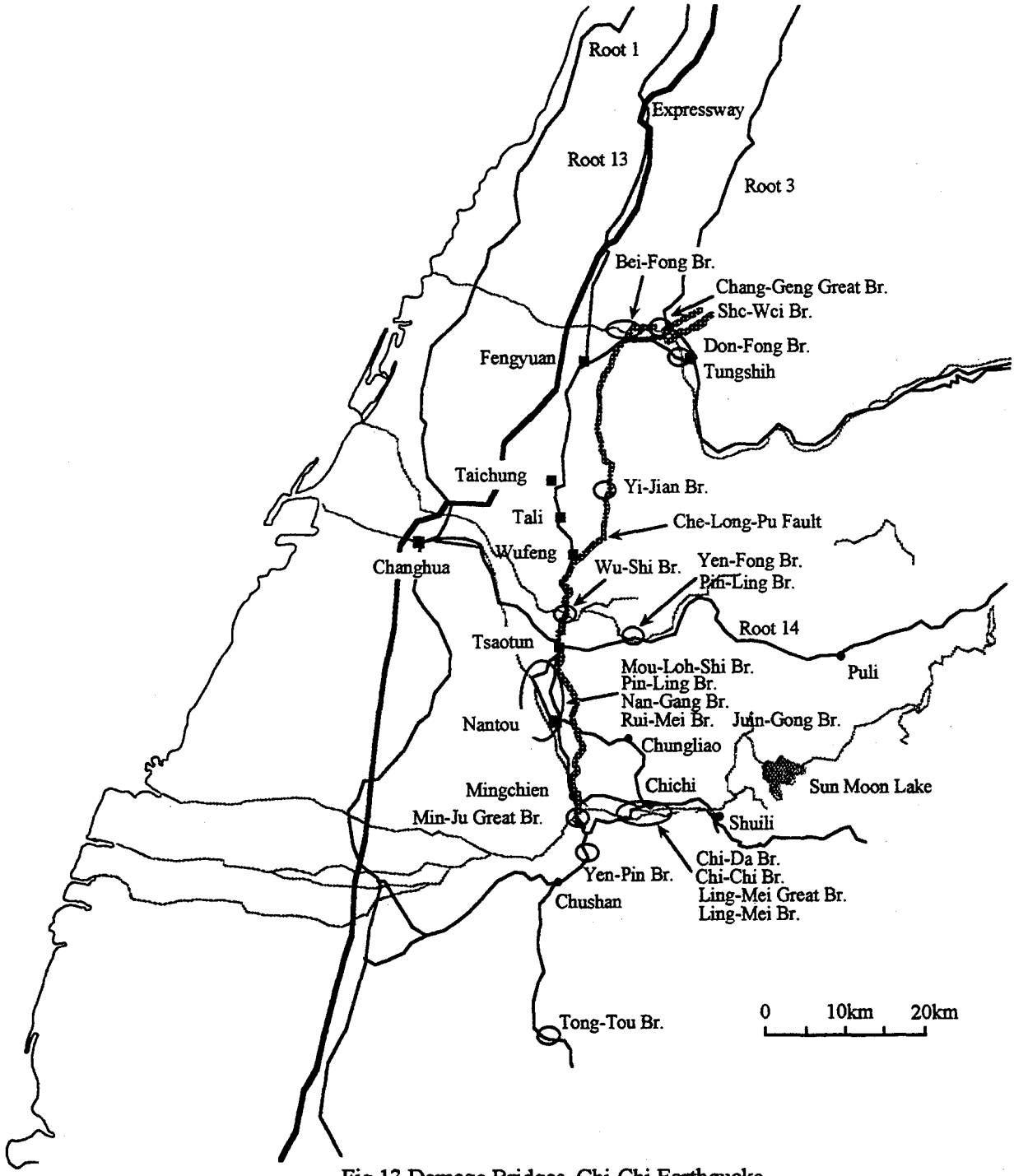

Fig.13 Damage Bridges, Chi-Chi Earthquake

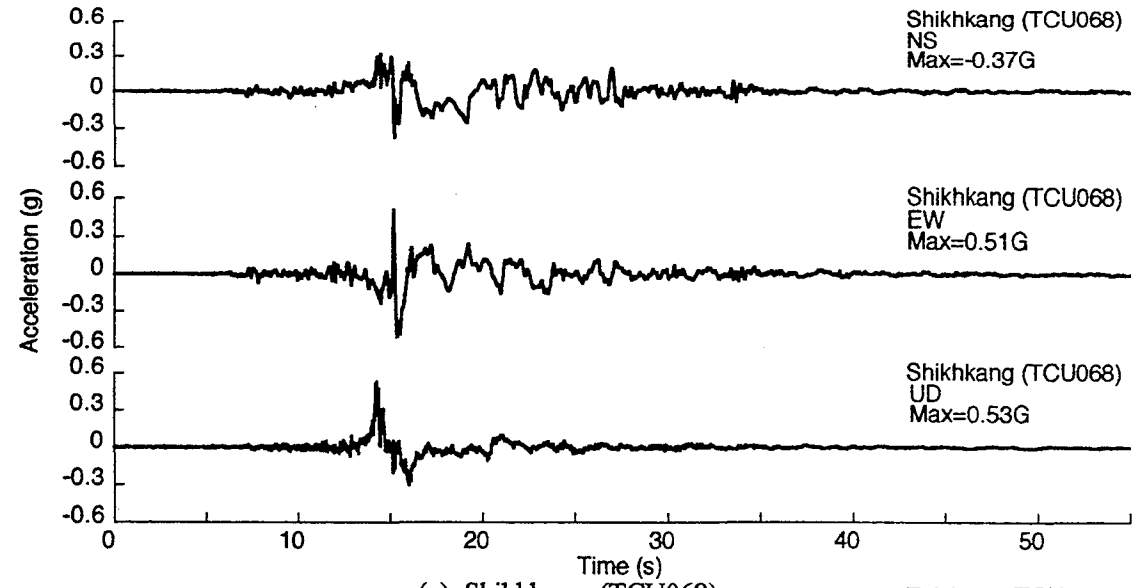

(a) Shikhkang (TCU068)

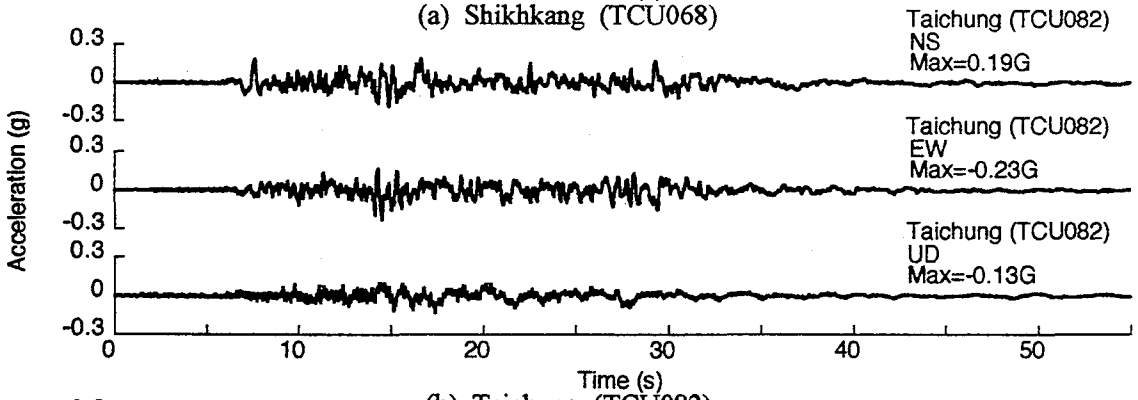

(b) Taichung (TCU082)

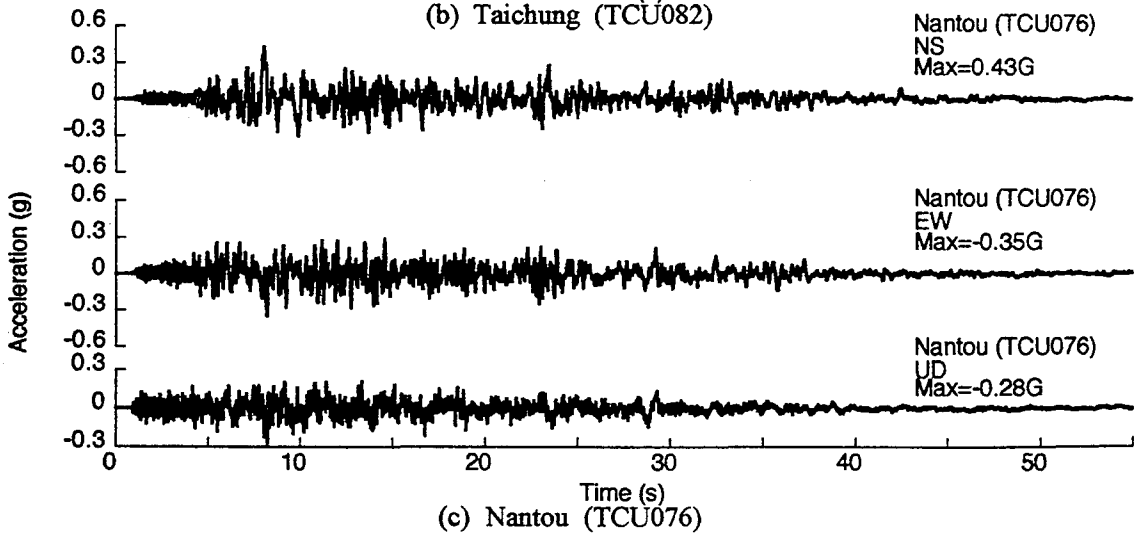

(c) Nantou (TCU076)

Fig.14 Ground Accelerations, Chi-Chi Earthquake

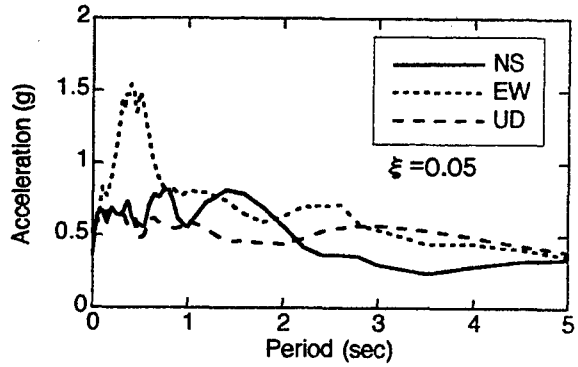

(a) Shikhkang (TCU068)

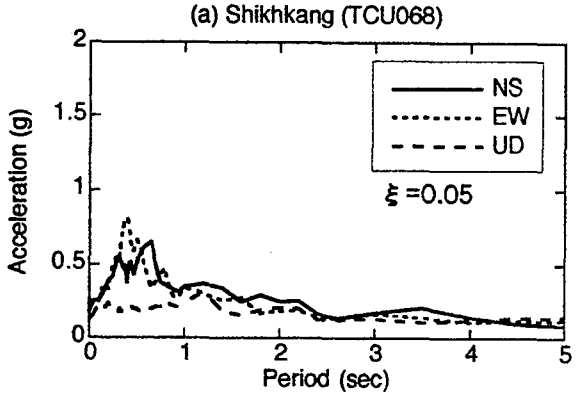

(b) Taichung (TCU082)

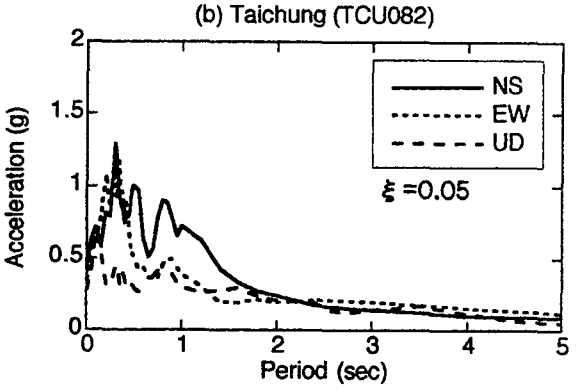

(c) Nantou (TCU076)

Fig.15 Response Accelerations of 0.05 Damping Ratio, Chi-Chi Earthquake

(2) Collapse of Bei-Fong Bridge

Bei-Fong Bridge was located downstream of the Shikhkang Dam, which suffered extensive damage by the fault movement. Due to the fault movement, a waterfall was created about 100m upstream of the bridge. It was of 13-span simply supported I-beam girder, constructed in 1991. The south most three spans collapsed as shown in Fig. 17 with other spans being free from damage. The abutments, piers and decks are numbered herein from north to south. A2, P12 and P11 were upheaved about 3-4m, and P12 and A2 were laterally displaced about 3.5m and 4m, respectively, in downstream direction (west) as shown in Photo 12. It is known that the reversed fault accompanied lateral displacement at many locations. D13 was resting on the slope of river embankment with the north end being dislodged 6.6m south from the original position.

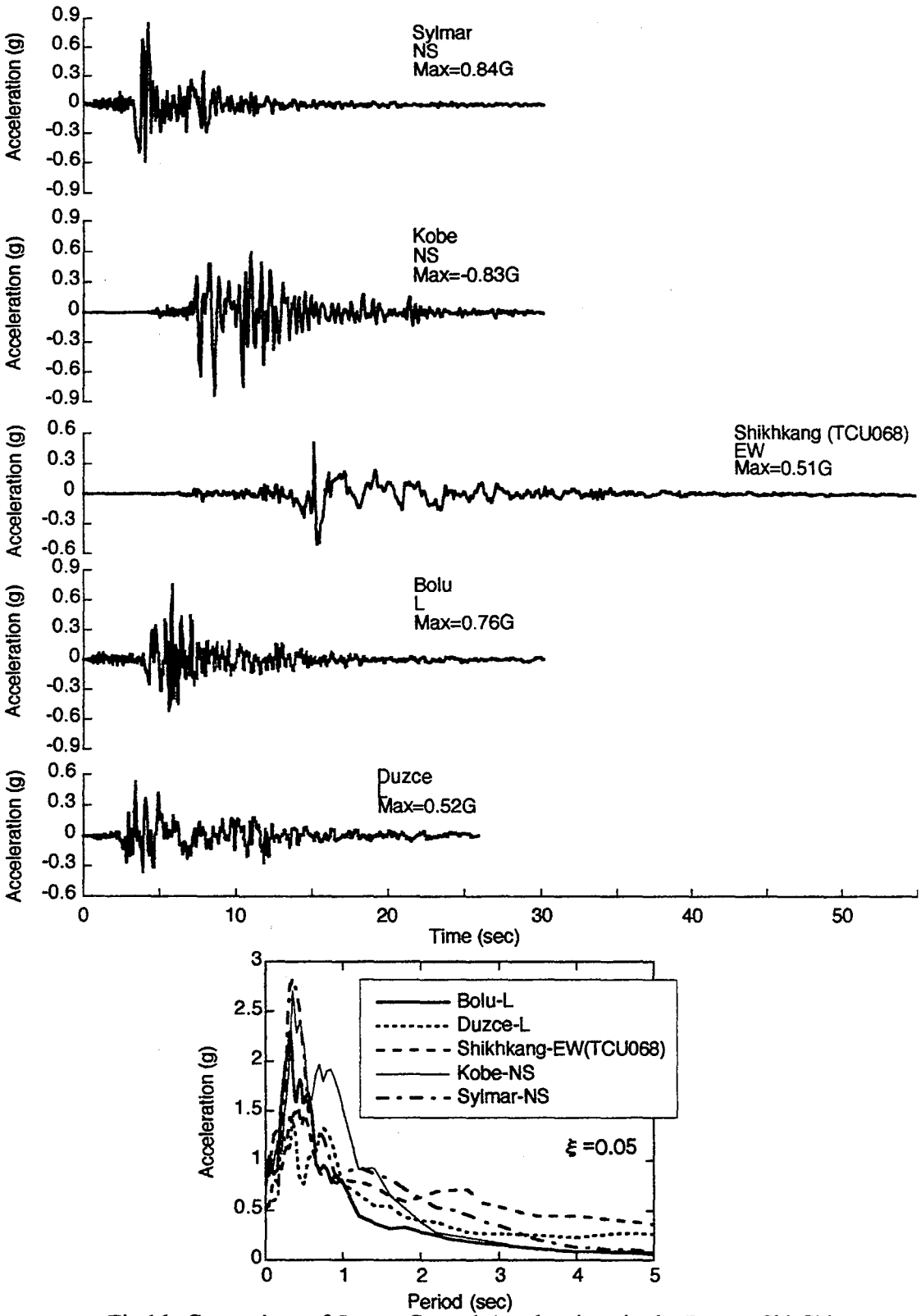

Fig.16 Comparison of Strong Ground Accelerations in the Duzce, Chi-Chi, Hyogo-ken Nanbu and Northridge Earthquakes

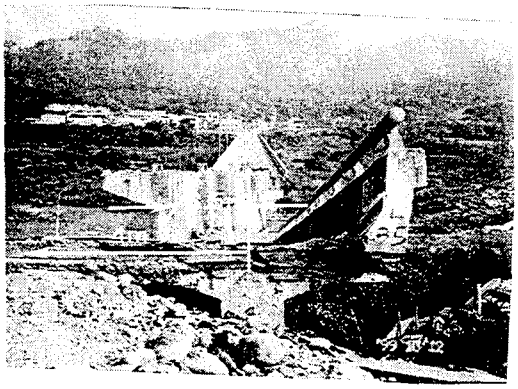

Photo 12 Lateral Movement of A2 and P12, Bei-Fong Bridge

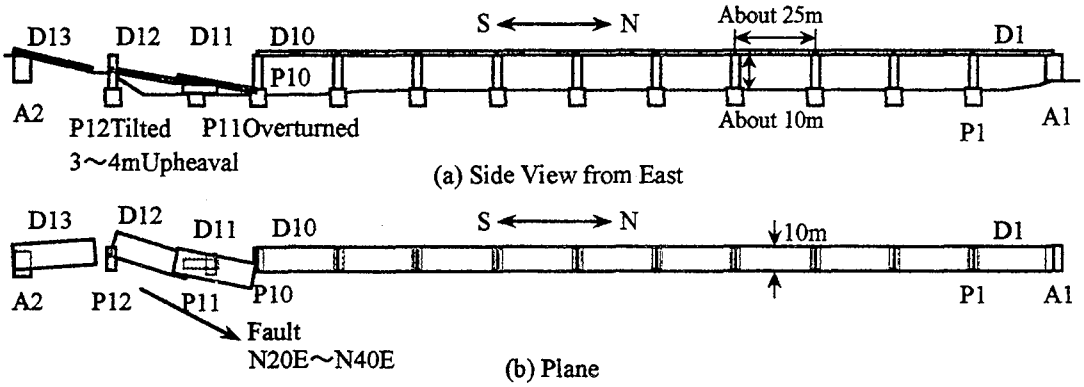

Fig. 17 Damage of Bei-Fong Bridge

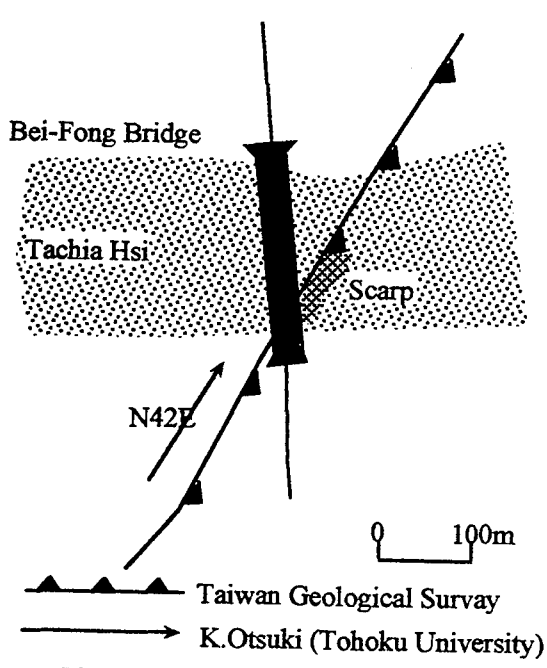

Fig.18 Fault around Bei-Fong Bridge

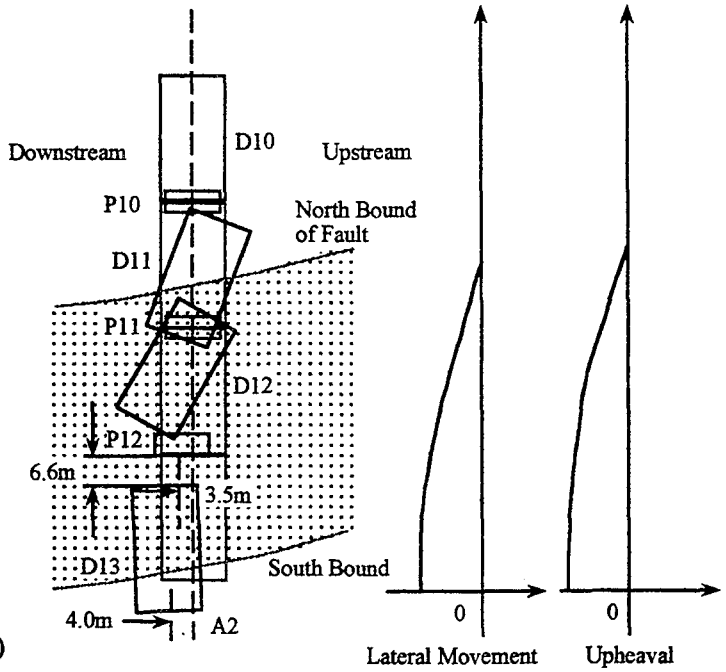

Fig. 19 Fault Movement and Ground Movement, Bei-Fong Bridge

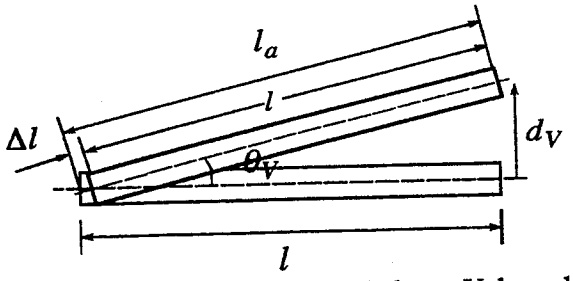

Fig.20 Shortening of Span Length due to Upheaval

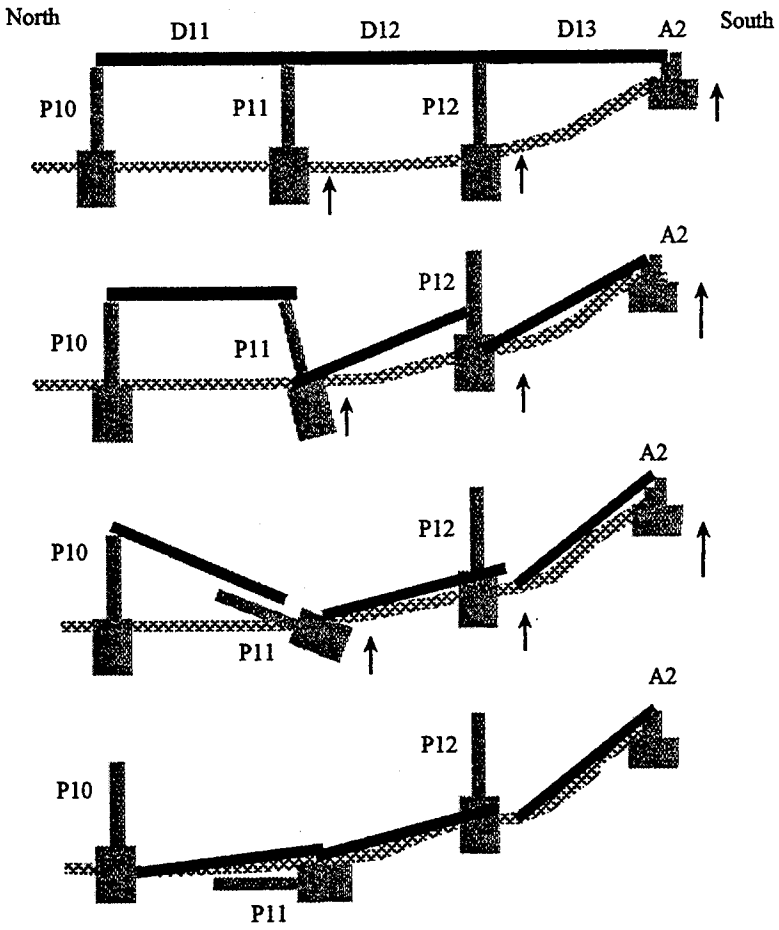

Fig. 21 Collapse Mechanism, Bei-Fong Bridge

Fig. 18 shows the location of fault investigated by the Taiwan Geological Survey and Otsuki, K., Tohoku University. Probably the fault crossed the bridge between A2 and P12 with an angle of about 42-degree. From the fact that P12 was laterally displaced in west, and that D11 and D12 were clockwise rotated (20-40-degree), it appears that the fault movement crossed the bridge in wider zone; perhaps between A2 and P11 as shown in Fig. 19.

If one idealizes the fault movement at south of the fault relative to the north, the transverse and longitudinal displacements of ground may be represented as (refer to Fig. 19)

$$d_{TR} = -D_0 \sin\theta$$
$$d_{LG} = -D_0 \cos\theta \quad (3)$$

in which D_0 is a fault displacement. Substituting $d_{TR} \approx$-4m and $\theta \approx$42-degree into Eq. (3), one obtains $D_0 \approx$-6m and $d_{LG} \approx$-4.5m. The longitudinal displacement $d_{LG} \approx$-4.5m is shorter than the amount of above-mentioned southward dislodgment of D13 at the north end (6.6m), however they are not too much different.

It is interesting to note that the vertical upheaval might not be a serious cause of the dislodgment of decks from their supports. If one idealizes the upheaval at right substructure relative to the left as shown in Fig. 20, the shortening of span length due to the upheaval, Δl, may be written as

$$\Delta l = \frac{1}{\cos\theta_V}(1 - \cos\theta_V) \quad (4)$$

in which θ_V is angle of tilting, and is given as

$$\theta_V = \tan^{-1}(\frac{d_V}{l}) \quad (5)$$

in which l is span length and d_V is amplitude of relative upheaval between two substructures. Assuming $\Delta l \approx$25m and $d_V \approx$3m, one obtains θ_V=6.8 degree and Δl=0.18m. Consequently, shortening of the span length due to upheaval is shorter than the seat length.

Based on the above facts, it appears that the failure of the bridge was triggered by a large tilting of P11 in north direction, caused by fault movement as shown in Fig. 21. D12 dislodged first from P11 at its north end, followed by the dislodgment at south end. This resulted in the complete collapse of D12. D12 finally felt down on the sidewall of P11 at north end with the clockwise rotation associated with right-lateral fault movement. The collapse of P11 resulted in the dislodgment of D11 at its south end. The south end of D11 thus finally felt down on the north end of D12. Increased distance between P12 and A2 resulted in the collapse of D13.

(3) Collapse of Wu-Shi Bridge

Wu-Shi Bridge was of a separated northbound bridge (upstream, east) and a southbound bridge (downstream, west) as shown in Fig. 22. They were of 17-span simply supported PC beam girders. Bridge axis was N20E. The abutments, piers and decks are numbered herein from north to south, and the northbound and southbound bridges are designated by putting E and W, respectively.

The northbound bridge was constructed in 1983, while the southbound bridge was newer than the northbound bridge. As shown in Photo 13, the northbound bridge was supported by wall-type piers with a section of 8.5m x 3m, while the southbound bridge was supported by reinforced concrete piers with a rectangular section of 5m x 2m. For example, in P1W (P1 at the southbound bridge), 32 deformed bars with a diameter of 22mm were placed around the pier, and deformed tie bars with a diameter of 12mm were placed 200mm interval. They were supported by caisson foundations with a diameter of 6m. Deformed 22mm bars from the caissons were spliced with the bars in the piers within 1m from the bottom of piers. Concrete strength measured by the Shumit hammer was about 24MPa.

D1E and D2E collapsed (refer to Fig. 22), and D1W and D2W tilted and settled extensively. Fig. 23 shows damage of piers in the southbound bridge. P1W and P2W failed in shear, as a result of a shear force from east to west. The caisson foundation at P3W suffered shear failure due to a shear from east to west as shown in Photo 14. Damage was significant at P1W and P2W, however other piers also (P3W-P8W, P13W) suffered damage.

On the other hand, damage of P2E and P3E was limited; P2E suffered several shear cracks at midheight as a result of lateral force from north to south. P3E suffered a 100-150mm opening of concrete at 1.5m high from the foundation. P2E and P3E looked as if they settled about 2m relative to the piers in the south beyond P4E. It seems that this was induced by the upheaval in the south of the fault.

A 2m high scarp was observed at about 100m east (upstream) of the bridge. The fault crossed the bridge between P2 (P2E & P2W) and P3 (P3E & P3W) with an angle of about 40-degree

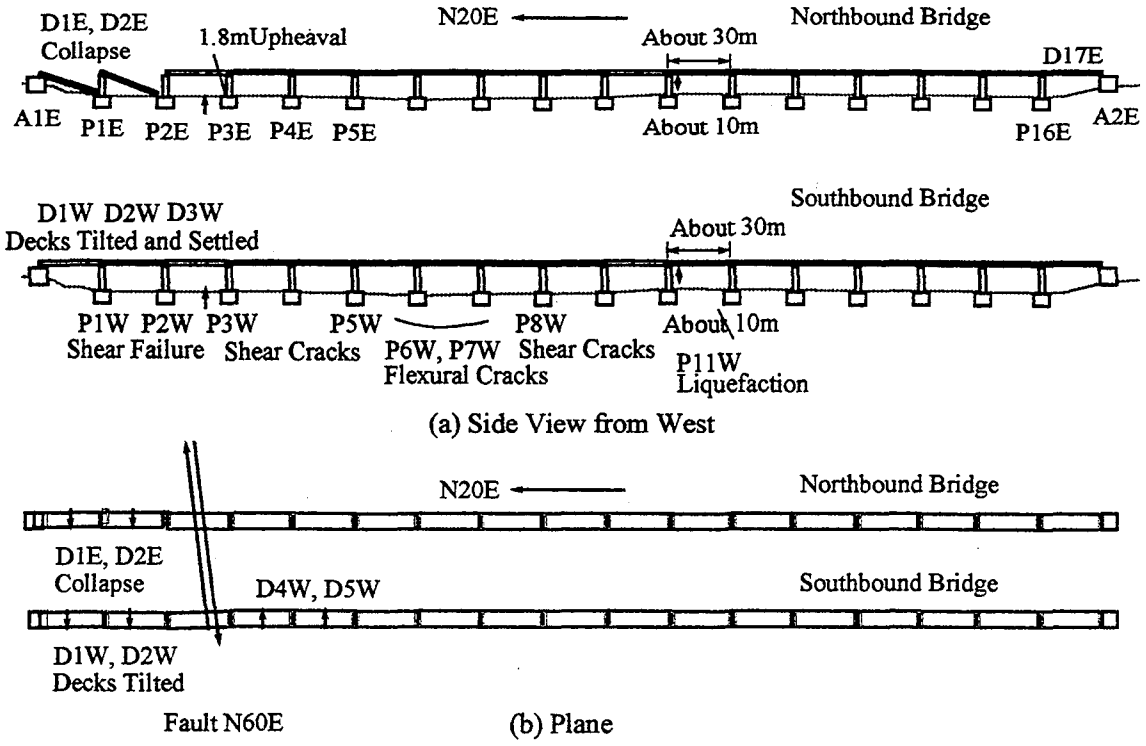

Fig.22 Damage of Wu-Shi Bridge

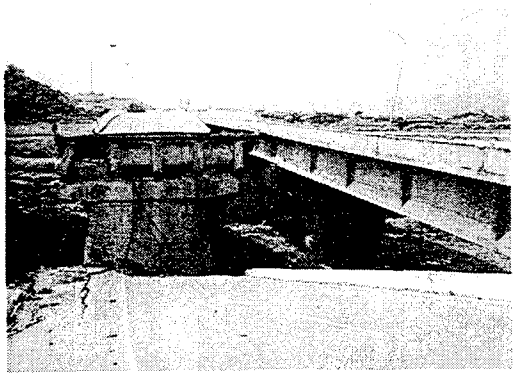

Photo 13 Collapse of Wu-Shi Bridge

(N60E) as shown in Fig. 24. Between P2 and P3, a vertical rupture of about 1m high (piers in south beyond P3 were upheaved) was observed. Photo 15 shows a displacement of P1W and P2W in east direction (transverse direction), relative to other piers in south beyond P3. The displacement was as large as 2m. However it was the ground at south of the fault (between P2 and P3) that moved in the earthquake. Photo 15 should be consequently interpreted that piers at south beyond P3W were forced to be upheaved resulting in the lateral displacement in west direction. It appears that this attributed to the fact that not only P1 and P2, but also most piers from P3 to P16 suffered damage.

Substituting the relative displacement in transverse direction of $d_{TR} \approx 2$m and $\theta \approx 40$-degree into Eq. (3), the fault dislocation may be $D_0 \approx 3.1$m, and relative displacement in longitudinal direction d_{LG} is about 2.4m. It appears that the westward fault movement at south beyond P3W resulted in a lateral force to occur in D1W and D2W in west direction, which, in turn, caused the shear failure in P1W and P2W. It is interesting to note that since the failure of P1W and P2W contributed to absorb the large fault displacement, the decks (D1W and D2W) did not collapse.

In a similar way, a large lateral force applied to D1E and D2E in the northbound bridge, which resulted in some damage at P1E and P2E. Since strength of wall-type piers (P1E and P2E) was large enough, they did not collapse. However,

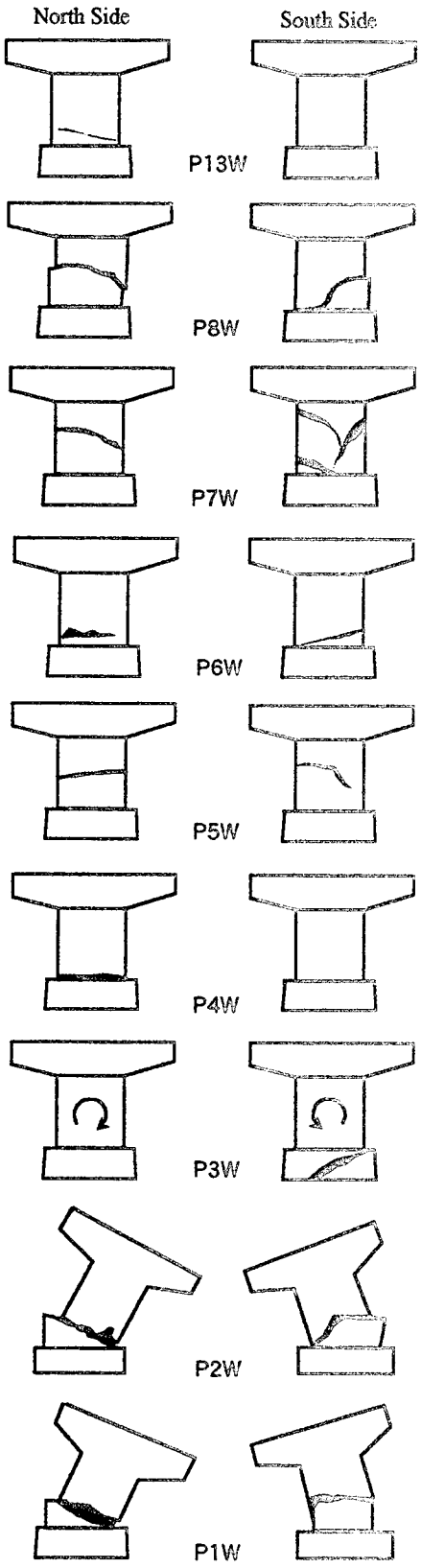

Fig. 23 Failure of Piers, Wu-Shi Bridge

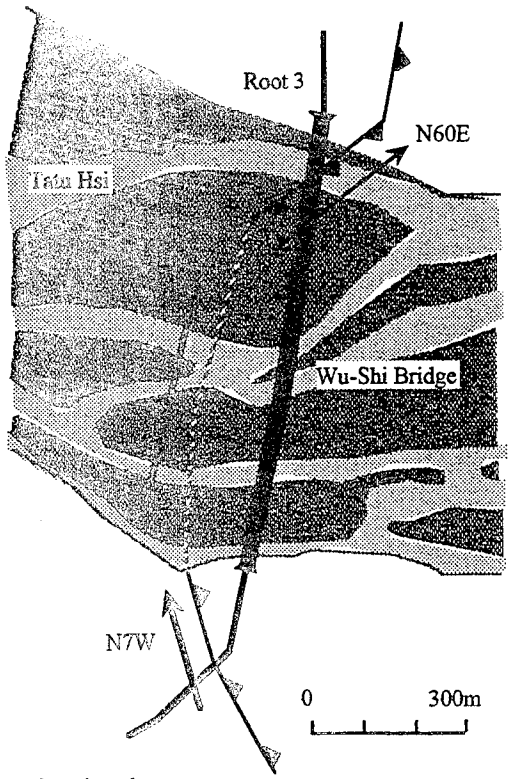

Fig.24 Fault around Wu-Shi Bridge

Photo 14 Failure of Caisson Foundation as a Direct Fault Movement, Wu-Shi Bridge (Courtesy of S. Iwata)

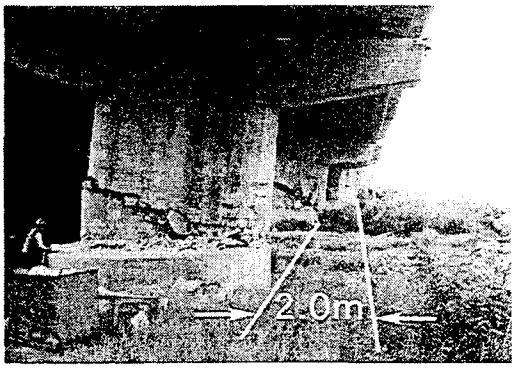

Photo 15 Lateral Movement of P1 and P2, Wu-Shi Bridge

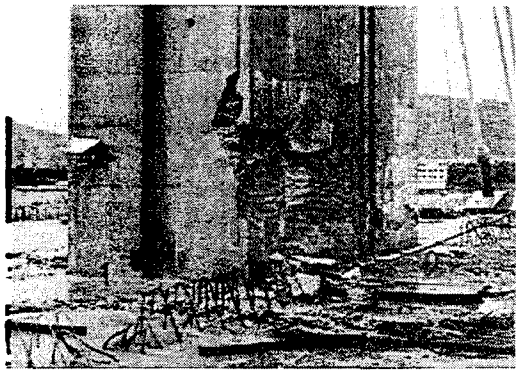

Photo 16 Damage of Tower

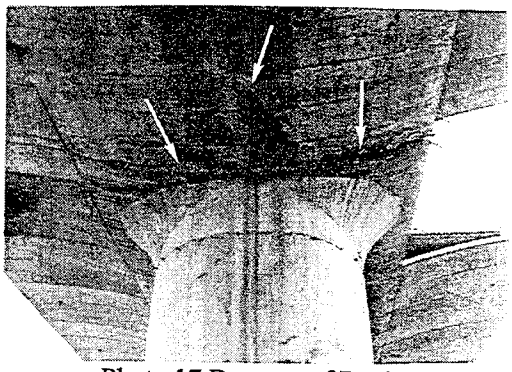

Photo 17 Damage of Deck

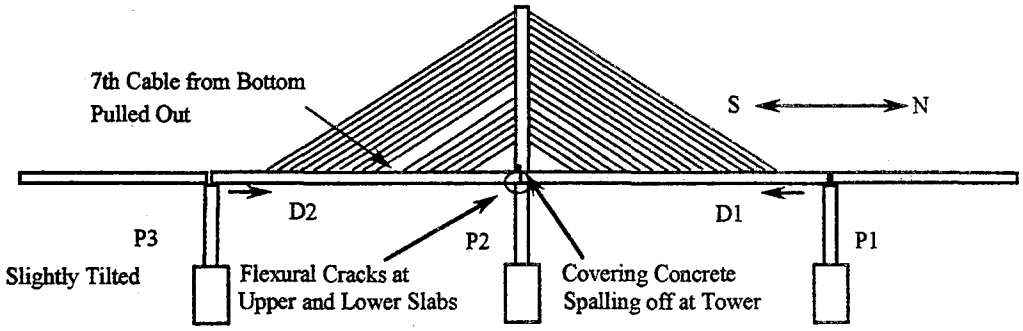

Fig.25 Damage of Chi-Da Bridge

this developed large relative displacements between the piers and the decks, and this resulted in the collapse of D1E and D2E.

It appears that the failure of the caisson foundation at P3W (refer to Photo 14) was developed by a direct fault movement.

(4) Damage of Chi-Da Bridge

A cable-stayed bridge as shown in Fig. 25 suffered damage at the tower, deck and cables. It was a single towered two-span continuous prestressed concrete cable-stayed bridge, and it was under construction. The tower and the decks

were rigidly connected. Multi-cable (17 cables) in double planes was used.

The tower suffered spalling off of covering concrete as shown in Photo 16. Since the damage was more extensive on the surface in transverse direction, it appeared that the damage was developed associated with the tower response in transverse direction. A 100-300mm wide flexural cracks penetrated the upper and lower slabs of the deck at close to the tower as shown in Photo 17. It seemed that the flexural crack occurred due to longitudinal response of the bridge. The 7th cable from bottom suffered damage at its cast-iron coupler, and was pulled out. It appeared that several other cables suffered damage to some extent at the connections. No evidence of a fault movement was observed around the bridge.

5. CONCLUSIONS

Seismic damage of bridges in the 1999 Kocaeli and Duzce, Turkey, earthquakes, and the 1999 Chi-Chi, Taiwan, earthquake was presented. Features of the damage may be summarized as follows:

(1) The tectonic ground movement that crossed bridges resulted in the extensive damage in Kocaeli, Duzce and Chi-Chi earthquakes.
(2) In Kocaeli Earthquake, Arifiye Overpass collapsed due to a fault movement that crossed the bridge with an angle of 65-degree. An increased distance between A1 and P1 resulted in the collapse of D1, and the lateral displacement of foundations forced to move by the fault contributed to the damage of D2, D3 and D4. Because other overpasses on the Trans-Europe Motorway were rested on short and wall-type piers and abutments with large cross sections, damage due to the ground motion was less significant.
(3) In Duzce earthquake, a new and long prestressed concrete bridge supported by high piers suffered damage at their supports. A fault movement that crossed the bridge was observed, and this may be the main reason for damage.
(4) In Chi-Chi Earthquake, at least eight bridges collapsed. Bei-Fong Bridge and Wu-Shi Bridge suffered damage associated with the fault movement. The fault crossed the bridges that resulted in a large lateral force in the piers. Overturning and failure of the piers triggered the collapse of the bridges.
(5) It is interesting in Wu-Shi Bridge to note that the decks supported by stiff wall-type reinforced concrete piers collapsed in the northbound bridge while the decks supported by reinforced concrete piers with smaller rectangular sections did not fall down (although they suffered major damage) in the southbound bridge. Failure of the piers in the southbound bridge contributed to absorb a large relative displacement induced by the fault movement, and as a result, it prevented to have a critical failure. It shows that a certain type of devices or mechanisms that absorb the fault displacement are effective to prevent failure in a bridge subjected to a large fault movement.
(6) A modern cable-stayed bridge suffered extensive damage at the tower and the deck. Since the tower and the decks were simply fixed, this may be a major contribution to the damage

ACKNOWLEDGEMENT

The authors express their sincere appreciation to Fulya Inal and Hiroaki Hoashi, Division of Motorway Bridges, General Directorate of Highways, Ministry of Public Works and Settlements, Turkey for their kind cooperation for providing valuable information. The authors also sincerely appreciate Professor C. H. Loh and K. C. Chang, Center for Earthquake Engineering Research, National Taiwan University, Taiwan for their kind support for the site damage investigation. Kind cooperation of Takao Hashimoto, Chiyoda Consultants, and Takeo Suzuki, Okumura Construction, for the site investigation in Kocaeli Earthquake, and Professor Kazuhiro Iemura, Kyoto University and Shuji Iwata, JR Tokai, for the site investigation in Chi-Chi Earthquake are greatly appreciated. Valuable information for Kocaeli and Chi-Chi earthquakes was provided by Professor Kenji Kosa, Kyushu Technical University.

REFERENCES

Bogazici University Kandilli Observatory and Earthquake Engineering, Home Page, 1999

Hoshikuma, J., Kawashima, K., Nagaya, K. and Taylor, A., Stress-Strain Model for Confined Reinforced Concrete in Bridge Piers. *Journal of Structural Engineering*, 123(5), 624-633.New York: ASCE, 1994.

Japan Road Association, Part V Seismic Design, Design Specifications of Highway Bridges. Tokyo:Maruzen, 1996.

Kawashima, K., Hashimoto, T. and Suzuki, T., *Damage of Transportation Facilities in the Kocaeli, Turkey, Earthquake*. Report No. TIT/EERG 99-7, Tokyo Institute of Technology, Tokyo, 1999.

Kawashima, K., Iemura, H., Shoji, G. and Iwata, S., *Damage of Transportation Facilities in the Chi-Chi, Taiwan Earthquake*. Report No. TIT/EERG 99-8, Tokyo Institute of Technology, Tokyo, 1999.

Lee, W. et al, CWB Free-field Strong Motion Data from the 921 Chi-Chi Earthquake, Vol. 1, Digital Acceleration Files on CD-ROM, 1999

USGS, Implications for Earthquake Risk Reduction in the United States from the Kocaeli, Turkey, Earthquake of August 17, 1999, Geological Survey Circular, 1999

The Performance of theTrans European Motorway Structures During the Nov. 12, 1999 Düzce Earthquake

By

Hamid Ghasemi[1], James D. Cooper[2], Roy Imbsen[3]

ABSTRACT

Almost 3 months after the devastating August 17, 1999 Kocaeli earthquake, another earthquake with a moment magnitude of 7.2 hit Turkey on November 12, 1999. Called the Düzce earthquake, it resulted from a right lateral strike-slip rupture along the secondary Düzce fault. Its epicenter was centered near the town of Düzce, in the province of Bolu. This earthquake caused close to 1000 fatalities and 5000 injuries. The damage to buildings was similar to that sustained during the Kocaeli earthquake. Two viaducts and one tunnel under construction exhibited extensive damage.

The content of this paper is based on a reconnaissance survey, of bridge and tunnel sites along the Trans European Motorway (TEM) segment under construction near Bolu, conducted by the FHWA team dispatched to Turkey on November 28, 1999. During this survey, the roadway alignment and the physical condition of the Bolu Viaducts #1 and #2, and Bolu Bridge #2 were observed; superstructure damage to Viaduct #1 was viewed from the east and west abutments and from atop Piers #4, #5, and #10 (the first expansion joint from the western abutment of the westbound span); Bolu Bridge #2 damage was viewed at the west abutment seat and from atop the first pier east of the western abutment of the eastbound span. Bolu Tunnel damage was viewed from the Elmalik entrance westward to the collapse in both tunnels.

KEYWORDS: Düzce EQ, Kocaeli EQ, fault rupture, near fault effect, energy dissipating units, bearing failure, tunnel collapse

1.0 INTRODUCTION

The November 12, 1999 Düzce earthquake with a moment magnitude of 7.2 was caused by a right lateral strike-slip rupture along the secondary Düzce fault near the town of Düzce *(figure 1)*. This fault is connected to the main segment of the North Anatolian Fault (NAF) by the Elmalik and Asagi Bakacak faults. The length of the surface fault rupture is estimated to be 40 km with an average lateral offset of 4 m along most of its length.

The NAF has been studied as a collaborative effort by both Turkish and U.S. scientists for many years. In particular, U.S scientists have been interested in the NAF because there is a strong similarity between the creep rate and energy release of both the North Anatolian and the San Andreas fault in California *(figure 2)*. Both faults have generated large magnitude earthquakes in the last 100 years.

Figure 3 shows the close proximity of the TEM to the NAFZ which is of outmost importance and depicts the epicenter of the August 17, 1999 Kocaeli Earthquake, located in the town of Golcuk, about 140 km east of Düzce.

[1]Ph.D., Research Structural Engineer, FHWA, Turner-Fairbank Highway Research Center, McLean, VA
[2]P.E., Technical Director, Bridge R&D, FHWA, Turner-Fairbank Highway Research Center, McLean, VA
[3]Ph.D., P.E., D. Engr., President, IMBSEN & ASSOCIATES, INC., Sacramento, CA

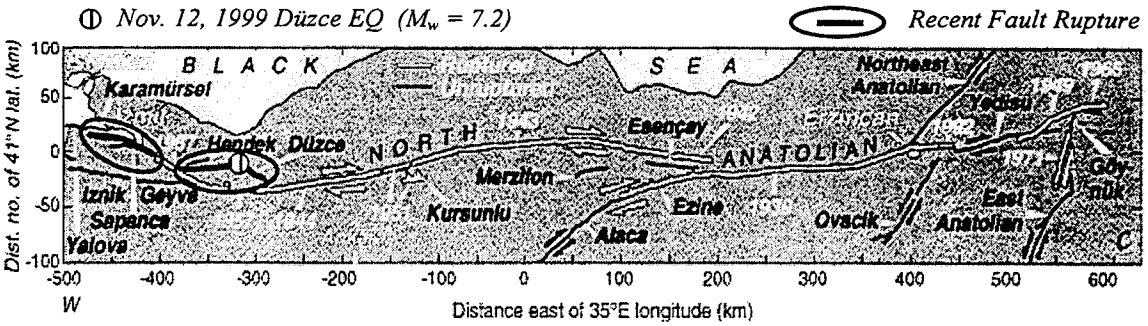

Figure 1: The North Anatolian Fault Zone

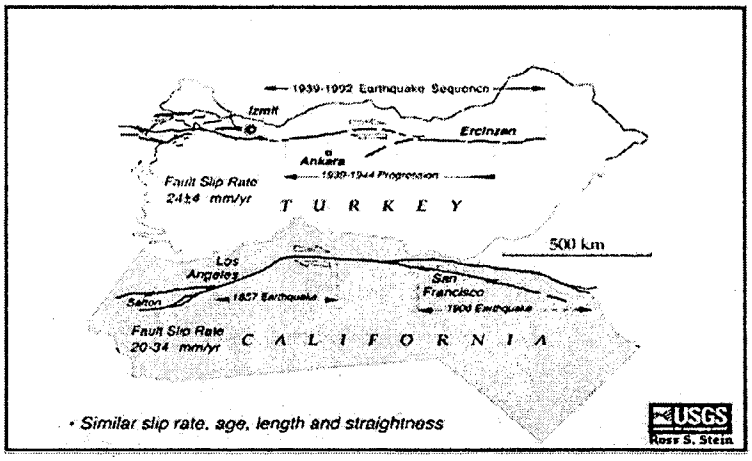

Figure 2: The Comparison of the North Anatolian and San Andreas Faults

At the Düzce station near the epicenter of the Nov. 12 earthquake, Peak Ground Acceleration (PGA) of 1.0g was recorded before the ground motion instrumentation was clipped due to its limitation on recording acceleration above 1.0g. Between these two stations, in the towns of Kaynasli and Bolu, there were two viaducts and one tunnel under construction. It is therefore reasonable to assume that these structures, that were not instrumented, experienced a PGA of at least 0.8g. These structures are part of the last 24 km segment of the Trans European Motorway (TEM) that is scheduled to be completed.

The Düzce earthquake caused considerable damage to the superstructure of Viaduct #1 and to the Bolu tunnel due to the close proximity of fault rupture (near fault effect). A surface fault trace was visible between a segment of Viaduct #1 piers and evidence of high velocity impulses was observed from the earthquake records and at the sites.

There are indications that high velocity impulses or "Fling" effects normal to the direction of rupture of strike-slip faults are produced by near field effects of earthquakes which present special problems for highway structures and tall buildings. These problems are manifested by very large displacements, overturning moments, the occurrence of liquefaction, and other energy sensitive structural responses.

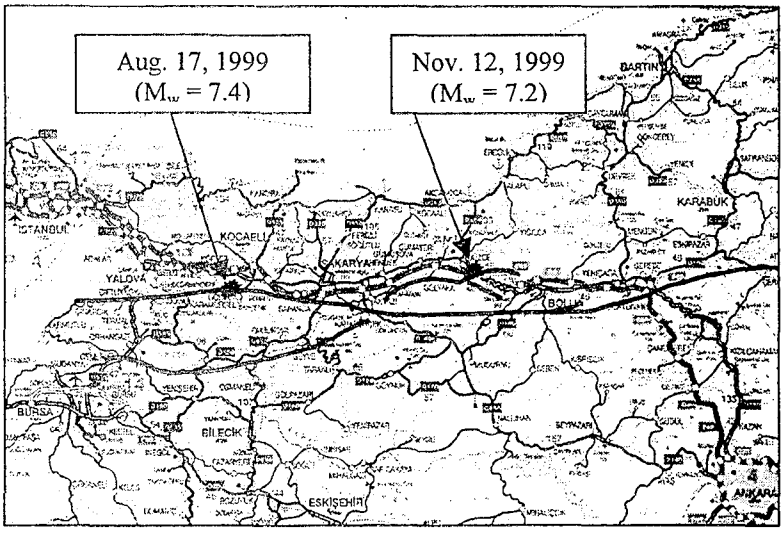

Figure 3: Map showing approximate proximity of the NAFZ to the TEM

2.0 SITES VISITED

2.1 Bolu Viaduct #1

Viaduct #1 with its 59 dual spans and 2.3 km structure length was approximately 95% complete and awaiting installation of expansion joints for completion of the project at the time of the Düzce earthquake (*figure 4*). Its span are 40 m long and consist of 7 lines of simply-supported, prestressed concrete box girders seated on pot bearings with a stainless steel PTFE-slider interface. The deck slab is continuous over 10 spans.

The viaduct's piers are single, octagonal cast-in-place, hollow-core reinforced concrete columns, 4.5x8.0 meters in plan dimension with heights varying from 10 m to about 49 m. They were designed and detailed to provide ductile behavior during earthquakes.

The viaduct had also incorporated an Energy Dissipation Unit (EDU) system, which is installed on each pier cap to accommodate longitudinal thermal movements and to reduce any seismic forces through energy dissipation during a major event.

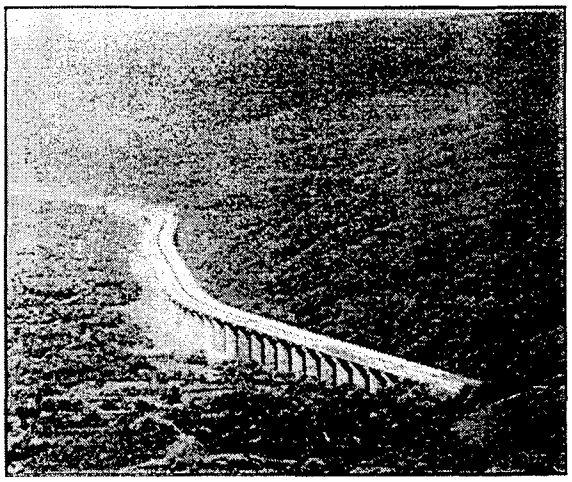

Figure 4: General View of Bolu Viaduct #1

2.1.1 Design Strategy

The design concept for Viaduct #1 involved the application of mixed criteria, using the 1990 AASHTO seismic design guidelines coupled with the design of a hybrid isolation system based on Italian guidelines. The system is comprised of pot bearings with a Teflon-stainless steel sliding interface under each box-girder and an EDU located at the center of each pier-cap which was bolted to a high reinforced concrete pedestal on top of the pier cap and to

the underside of the deck (*figure 5*). The arrangement of EDU's for a 10-span simply supported segment of the viaduct is shown in the Figure 6. Also as shown in Figure 6, the deck slab is continuous over the intermediate supports.

The EDU's consist of C-shaped energy dissipating steel elements which are referred to as crescent moons (*figure 5*). These elements provide hysteretic behavior through yielding of the steel elements. In addition to the crescent moons, a piston and a sliding unit are incorporated into the EDU's at the expansion joints and at the center pier of each 10-span continuous segment.

Cable restrainers were utilized at the expansion joints, (*figure 7*), as a secondary line of defense to prevent the end girders from falling off their supports due to displacements beyond those assumed.

In summary, during normal environmental conditions (i.e., thermal expansion) the viaduct movement is provided for by the PTFE-slider interface of the bearing in conjunction with the sliding unit of the EDU's which is controlled by the piston and is incorporated into the units. However, during the design level earthquake (acceleration of 0.4g), the piston would lock up similarly to a shock absorber and engage all of the EDU's on each 10-span continuous deck segment. This would dissipate the energy induced by the ground motion and also reduce the displacement response and the total force exerted on each pier.

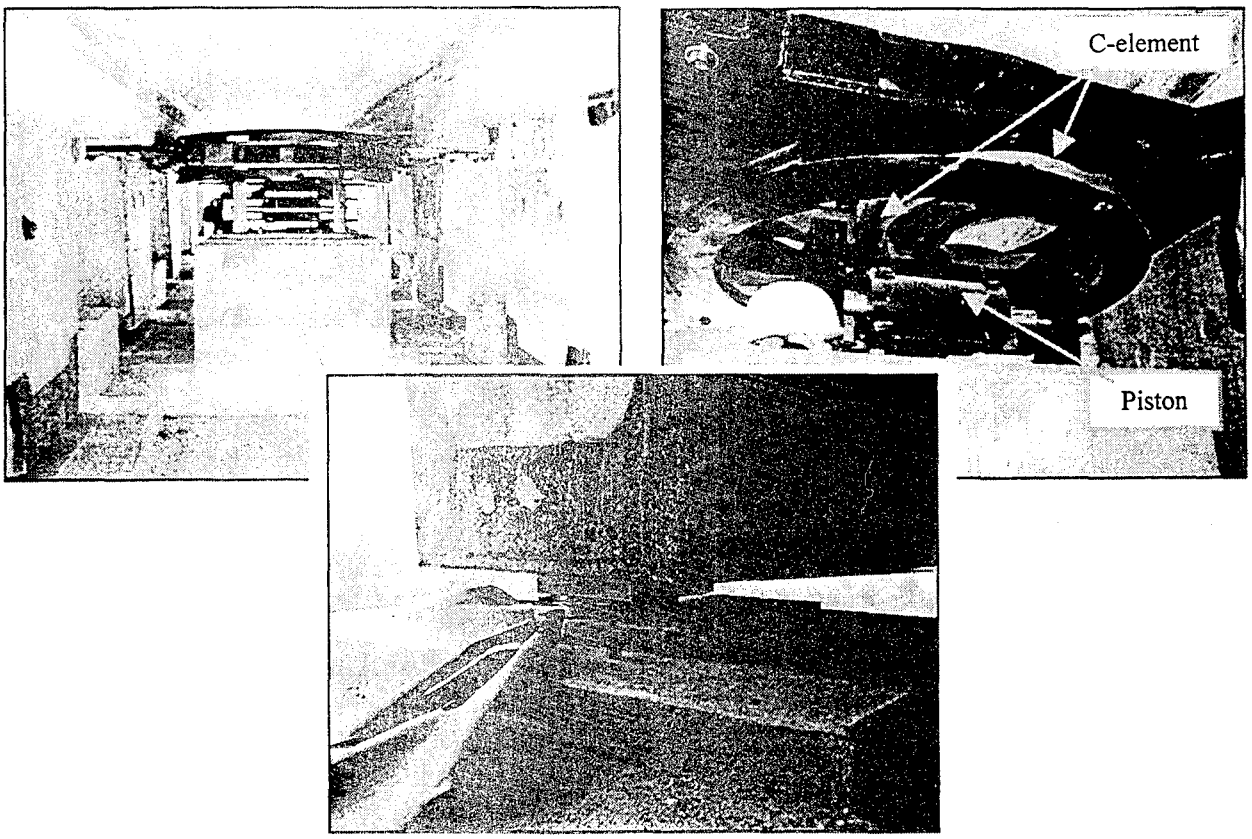

Figure 5: A Pot bearing and an EDU unit

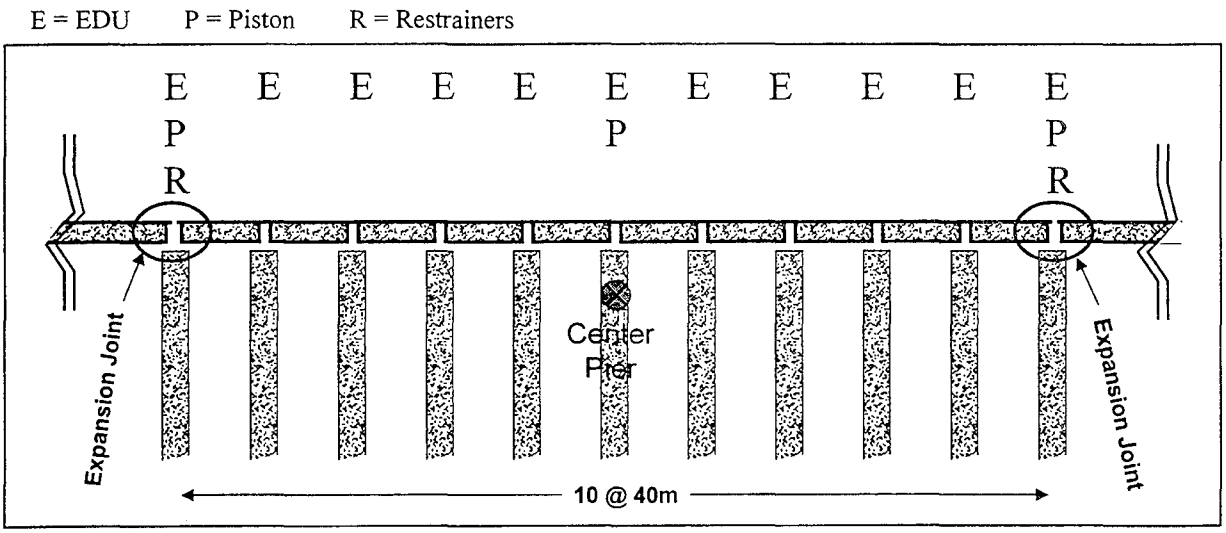

Figure 6: The arrangement of EDU's with and without pistons and cable restrainers

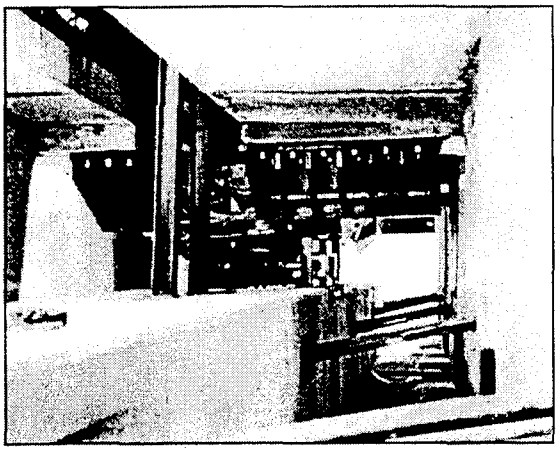

Figure 7: Cable restrainers at the expansion joint

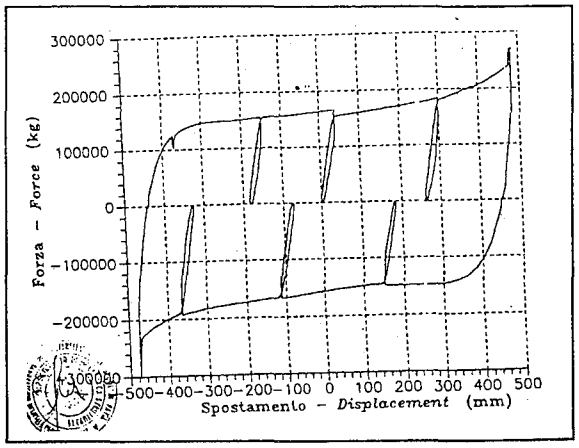

Figure 8- Actual testing result of an EDU at ultimate displacement (±480 mm)

Figure 8 shows a typical force-displacement characteristic of an EDU at the ultimate displacement (±480 mm). The enclosed area is the energy dissipation capability of the unit which was designed for 40% of critical damping.

The team believed that a good seismic design philosophy had been selected with an apparent ductile reserve capacity of the concrete piers for resisting earthquakes beyond the design level earthquake.

2.1.2 Field Observations

1) The surface fault trace was visible sporadically in the valley town of Kaynasli, where Viaduct #1 is located. Faulting caused major destruction to buildings, residential housing and other facilities. The fault trace was also observed at Viaduct #1, where it intersected Pier #45(eastbound), then continued between the two Piers #46 before intersecting Pier #47 (westbound) as shown in Figure 9. Fault rupture movement, estimated to be about 2.5 to 3 m at this location resulted in a rotation of nearly

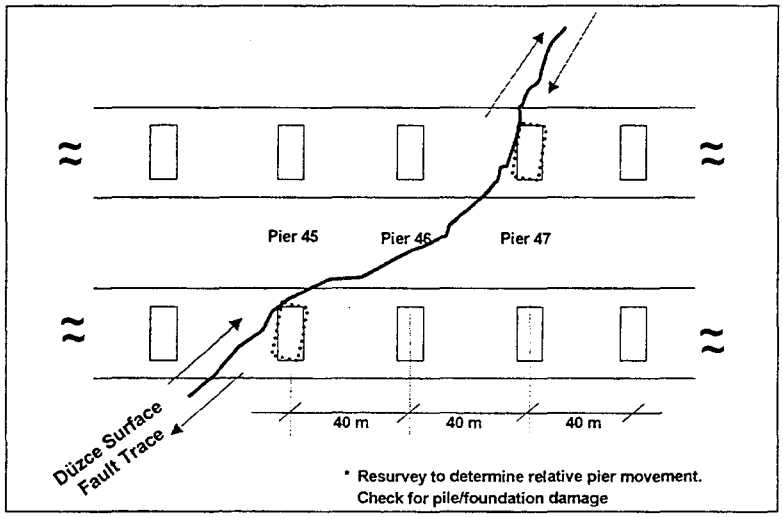

Figure 9: Fault trace between piers 45 and 47

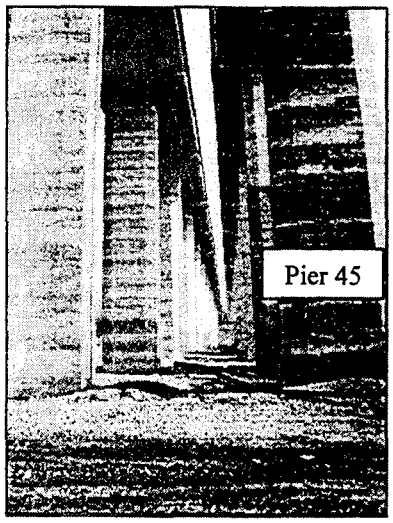

Figure 10: Fault trace

12 degrees at the pile caps of piers #45 (eastbound) and #47 (westbound) about their vertical axes *(figures 9 and 10)*.

2) Significant damage did occur to the EDU's and bearings from surface rupture displacements and ground shaking which caused the superstructure girders to translate on their pier tables, narrowly avoiding total collapse, *(figures 11 through 13)*.

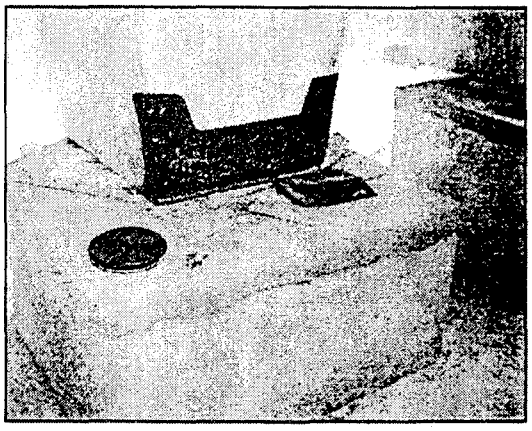

Figure 12: Typical dislodgment of bearing systems

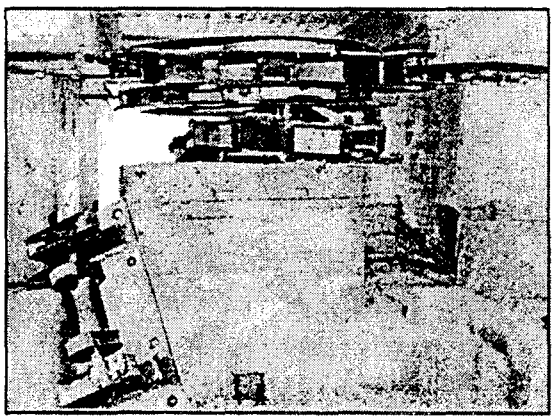

Figure 11: Dislodged EDU, Pier 5

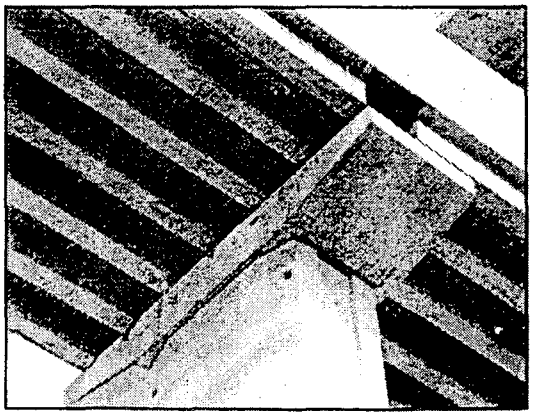

Figure 13: End of facia girder extending beyond pier table

3) Shear keys or blocks used to control transverse girder movement, although severely damaged, appear to have functioned as intended *(figures 14 and 15)*.

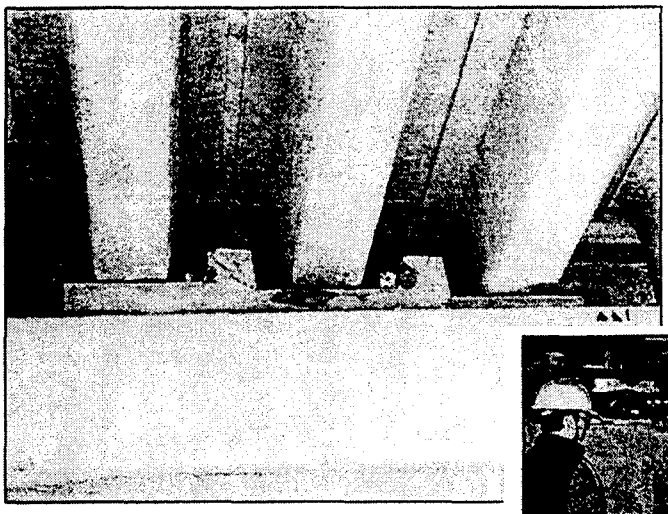

Figure 14- Shear block damage (translational restraint)

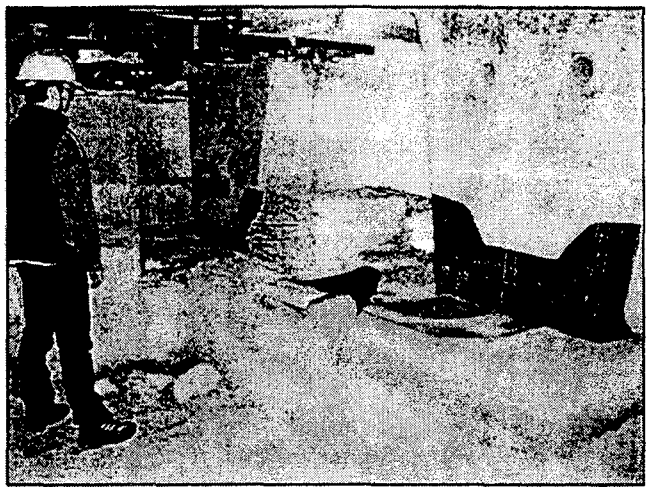

Figure 15: Shear block damage

2.1.3 Damage Scenario

The following outline presents a damage scenario for Viaduct #1. It is based on the field observations made on November 30, 1999 and December 2, 1999.

1) The viaduct was first subjected to a low frequency vibratory motion, which was then followed by a high velocity impulse or "fling" resulting from the near field effect. The surface fault trace was visible at Piers 45, 46 and 47 *(figure 10)*.

2) The fling caused the bearings to be ejected from underneath the box girders after the bearing sliding plate interface area was exceeded *(figure 12)*.

3) On some piers, especially those closer to the fault trace, the fling broke the epoxy bond of the bearing plates to both pier caps and the bottom flange of the box girders. Many of the bearing plates were found on the ground below.

4) On other piers, the stainless steel interface plates, which were epoxied to the bottom bearing plates, were protruding from the edge of the pier cap or were found on the ground below.

5) Almost all of the stainless steel interface plates had a distinct scoring which resembled the number "9". The "9" trace may validate a scenario of a large cyclic motion resulting from the fling effect *(figure 16)*. Also included in Figure 16 are the authors suggestions for

remediation which was made at the time of the site investigation.

6) Upon the loss of the bearings from underneath the girders (and in some instances the steel bearing plates too), the superstructure then dropped approximately 5 cm to rest on the pier caps. That caused an excessive bending moment at the EDU connection to the deck, which resulted in the partial to total binding of the C-elements ring plates (*figures 17 through 19*). The binding action prevented the EDU's from functioning properly.

7) The fling effect possibly sheared off the connection between the EDU and its pier cap as well as the connection to the deck. It is believed that the design of the EDU connections to the Super- and sub-structure was based on the elastic limits of the C-element. The connections for the bearings plates were designed for a force level equal to the dynamic coefficient of friction of the PTFE-sliding bearing (4%).

8) It was also noted that the displacement capacity of the bearings ($\pm$210 mm) was less than those of the EDU units ($\pm$320 mm). Therefore, the EDU's would have never reached their optimum performance.

9) Most of the 10-span superstructure segments moved toward the west abutment. At the 10-span unit which included piers 45, 46, and 47 where the fault trace was visible, three of the girders slid off the cap of Pier # 46 (*figure 13*). This was possibly the result of rigid-body substructure motion to the east. The superstructure rested on PTFE-sliders, had a greater inertial mass relative to the substructure, and therefore was unable to follow the pier's movement. At the same time, the EDU's were probably not functional after the initial velocity impulse, and were unable to control the excess superstructure displacement. Whether the piers, the deck, or both moved can be better determined after a final and precise survey of the bridge is made.

10) It appeared that the piers were not subjected to many flexural cycles of motion as indicated by the lack of flexural cracking in the pier. The only hairlines flexural cracking noted were at Piers #35 and #36. The sudden failure of the bearings and EDU's apparently uncoupled the substructure from the deck's inertial force. This fuse type behavior points out the effectiveness of an isolation approach in protecting substructure elements.

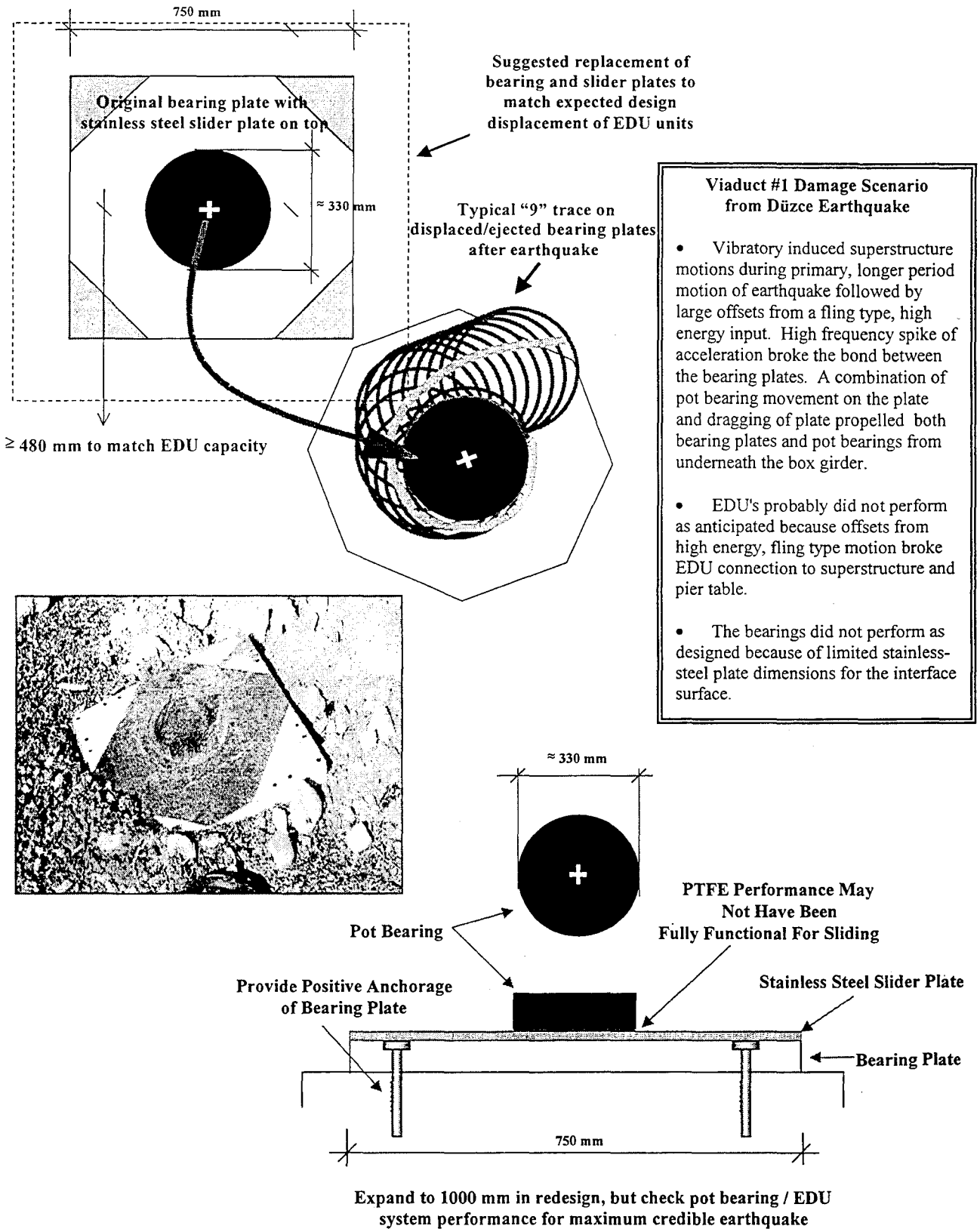

Figure 16: Viaduct #1 Bearing Damage Scenario (based on the site review on 11/30/99)

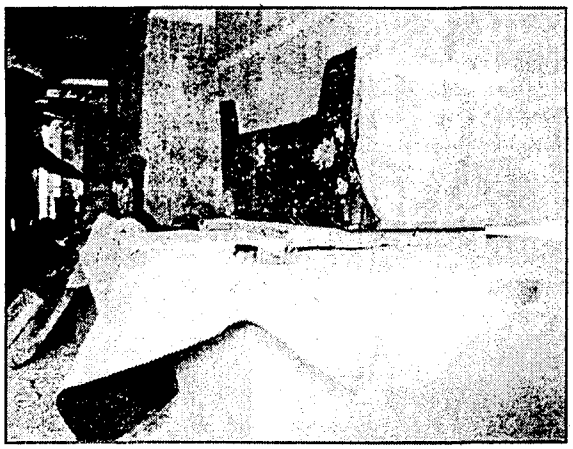

Figure 17: Bearing failure

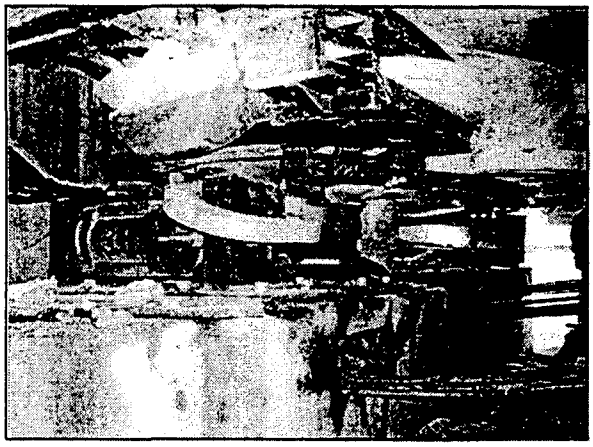

Figure 18: EDU failure

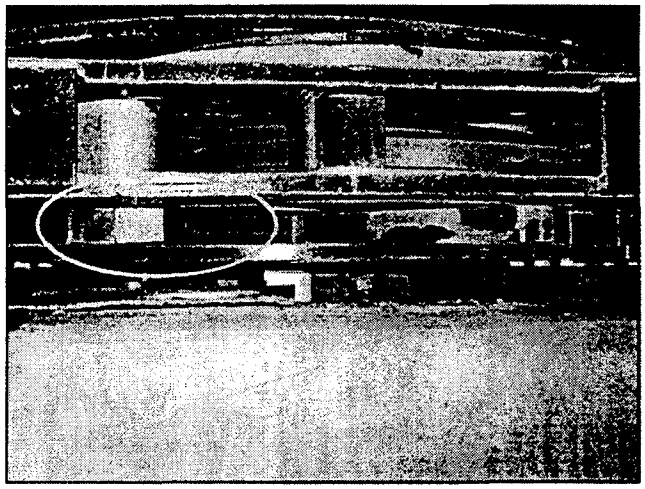

Figure 19: ___ Fractured EDU "C" element

2.2 BOLU BRIDGE #2

Bridge #2 is an in-service, dual 5-span simply-supported prestressed concrete box girder structure having a circular pier column and a very large horizontal radius of curvature *(figure 20)*. The spans sit on rectangular reinforced elastomeric bearing pads and EDU's similar to those used in Viaduct #1 to limit seismic response. The deck slab is continuous over 5 spans.

2.2.1 Field Observations

1) Moderate structural damage occurred to the concrete box girders of Bridge 2. The west end of the eastbound span translated approximately 3-1/2 inches to the north relative to the west abutment, as evidenced by the misalignment of lane striping at the west abutment, *(figure 21)*.

2) Examination at the abutment seat revealed a set of well proportioned steel reinforced rectangular elastomeric bearing pads, *(figure 22)*, and an EDU device that had "worked" during the Düzce Earthquake,(*figure 23)*. One "C" element had compressed to a 23-1/2 inch opening from center of pin to center of pin while the other "C" element extended to an opening of 31 inches. Markings on a bearing plate

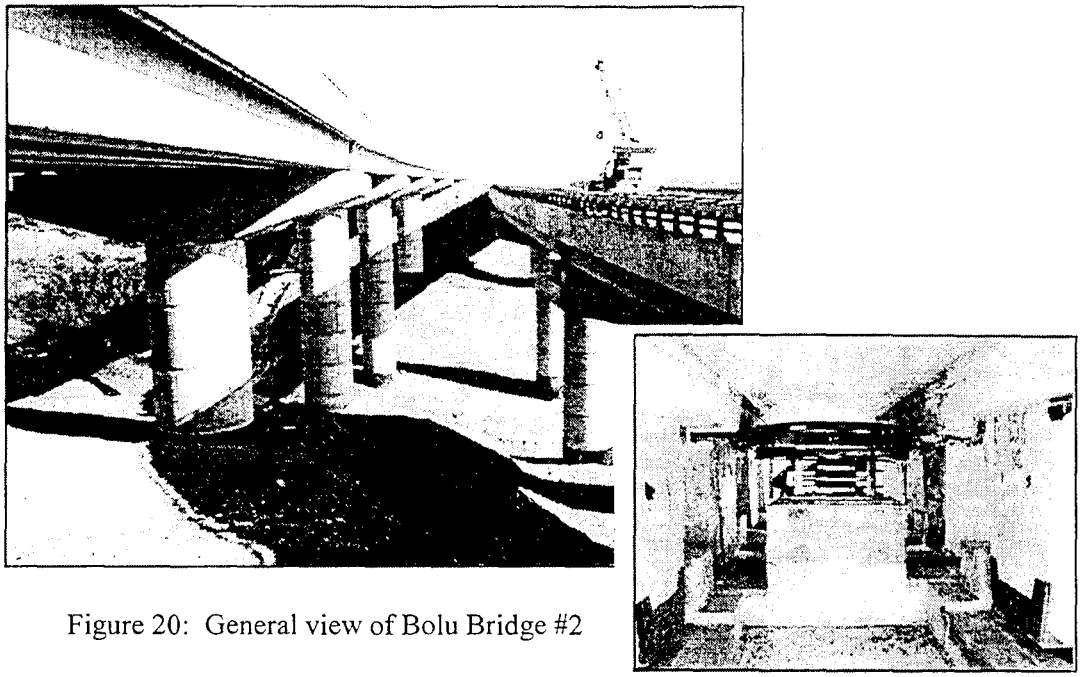

Figure 20: General view of Bolu Bridge #2

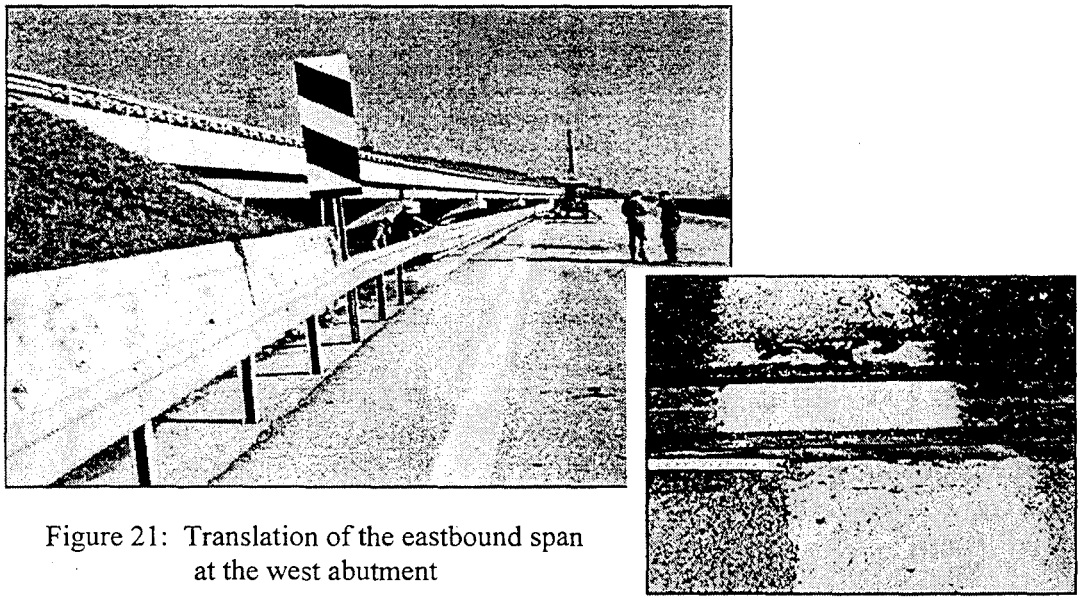

Figure 21: Translation of the eastbound span at the west abutment

indicated that the 12 inch by 27-1/2 inch by 4-1/2 inch thick bearing pad had translated about 6-1/2 inches to the north and about 3-3/4 inches to the west. Movements of the elastomeric bearings allowed the EDU to function and dissipate energy as conceptually designed.

3) Inspection of the eastbound span at the first pier table to the east of the western abutment indicated that the bearings allowed the EDU to "work". It was noted that one of the anchorages of the EDU brackets that was attached to the superstructure appeared to be at incipient failure, that is cracking of the concrete at the EDU anchorage point was noted, (*figure 24*).

Additionally, the grade of the superstructure resulted in a natural 2 inch differential offset between the bracket attachment between spans. This differential distance provides a naturally occurring, biased moment or twisting to occur across the EDU which could bind the top and bottom rings, thus locking the "C" elements and rendering the EDU inoperative.

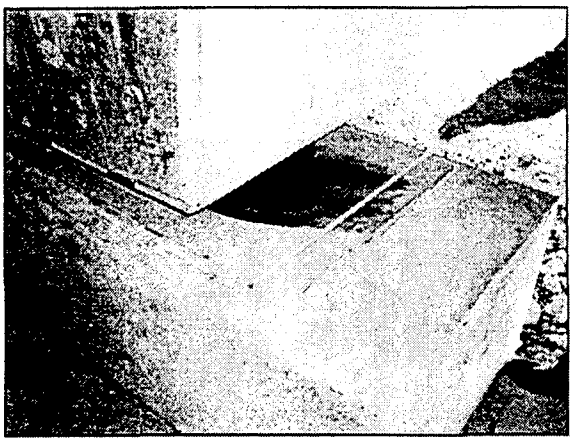

Figure 22: Well proportioned steel-reinforced elastomeric bearing pad showing evidence to translation

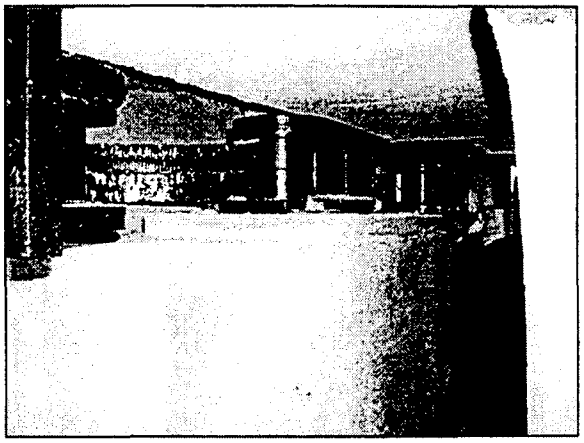

Figure 23: Flaked-off paint of an EDU "C" element that had "worked"

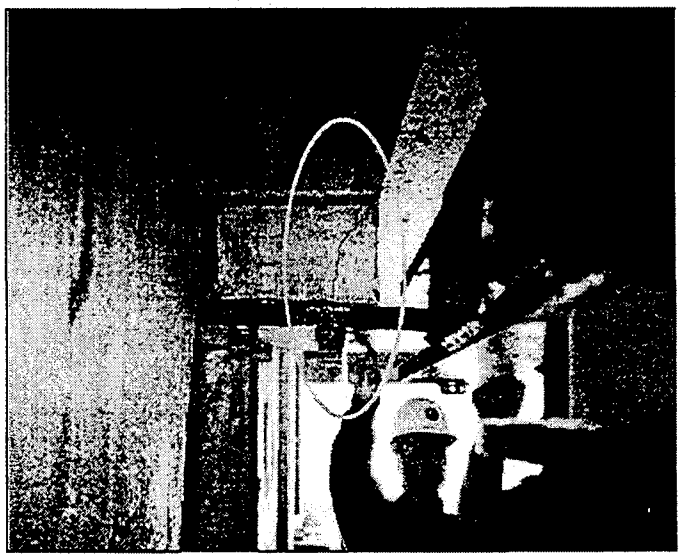

Figure 24: Incipient failure of EDU anchorage point

4) The stable performance of the well proportioned steel reinforced elastomeric bearing pads and bearing plates having sufficient sliding capacity in, all likelihood, allowed the EDU to function, although any additional shaking could have failed the positive attachment of the EDU top brackets to the superstructure. When using isolation/EDU systems, it is imperative to design the independent units (bearings, plates and EDU) to act as a SYSTEM.

2.3 BOLU TUNNELS

At the time of the Düzce earthquake, excavation for 3.3 km twin Bolu Tunnels was about 70% complete with about 30% of the final liner system in place. The Tunnels are located about 35 km east of the epicenter. They both have a width of 12 m, outer and inner heights of 15.3 m and 8.6 m respectively, and outside diameter of 17 m. The bore hole information, field observations and the study of regional geology, reveals that for approximately the first 1.5 km from the Elmalik portal a very soft compressible, clayey type of material exists. The remaining 1.7 km is located in weak to moderately competent rocks. It is also noted that the rock portion of the tunnels is heavily deformed by vertical faults suggesting an existence of a wide brittle shear zone. Figures 25 and 26 show the tunnel portals at Elmalik (east-bound) and at Asarsuyu (west-bound).

2.3.1 Design Approach

The Bolu Tunnels design methodology is based on the New Austrian Tunneling Method (NATM). Each tunnel consists of three layers (from outside inwards) of shotcrete, reinforced concrete and finally an unreinforced concrete layer. The complexity of the site forced the designers to consider 4 options for construction.

Option 1 was to advance by blasting followed by shotcreting over rock. Option 2 was similar to option 1; however, a thicker shotcrete section was required. Due to the continuous deformation of the clay deposit at sections of the tunnels, a third option was considered. This option required 45 cm shotcrete, 60 cm intermediate reinforced concrete and finally a 60 cm of unreinforced concrete lining.

Option 4, as shown in Figure 27, was planned for the worst condition since there was evidence of soil squeezing and also settling of the tunnels due to extremely soft soil. In this option, two pilot bench tunnels with a radius of 2.5 m were excavated along the sides of each tunnel for rigidity and to stabilize the tunnel movement. The pilot bench tunnels were later filled with concrete. In bridge terms, these tunnels act similar to bridge abutments.

The seismic design for the tunnels was based on experience and judgement. The EPA of 0.4g was used in design, which corresponds to a return period of about 500 years.

2.3.2 Field Observation

A very brief visual inspection of the Bolu tunnels was made on December 2, 1999. The inspection consisted of a drive through of both bores from the Elmalik portal to the collapsed sections, approximately 300 meters from the portal entrance, with limited time spent at the face of the collapse and in the structurally incomplete segment leading to the collapse. The collapsed locations are shown in Figure 28. They occurred in a section of tunnel passing through a clay/weak rock zone where a temporary shotcrete lining system was in place.

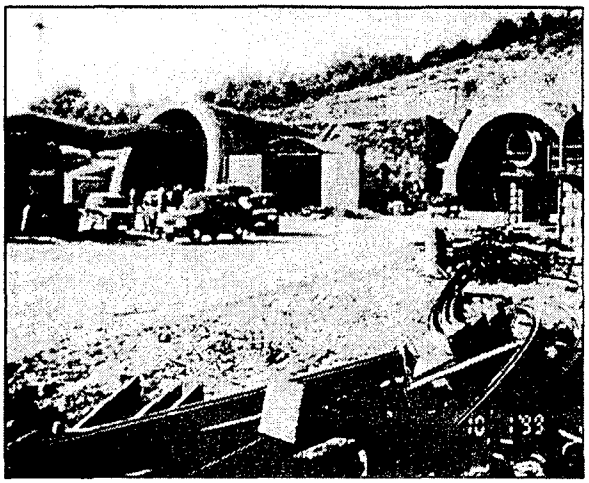

Figure 25: Bolu Tunnel at Elmalik Portal

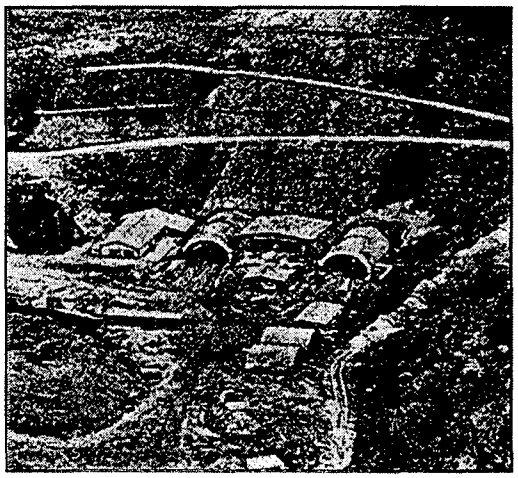

Figure 26: Bolu Tunnel at Asarsuyu Portal

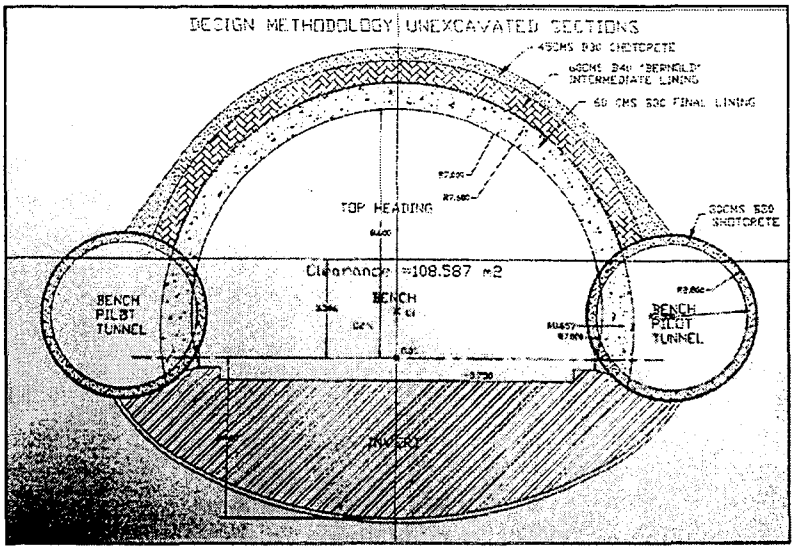

Figure 27: Option 4 tunneling technique

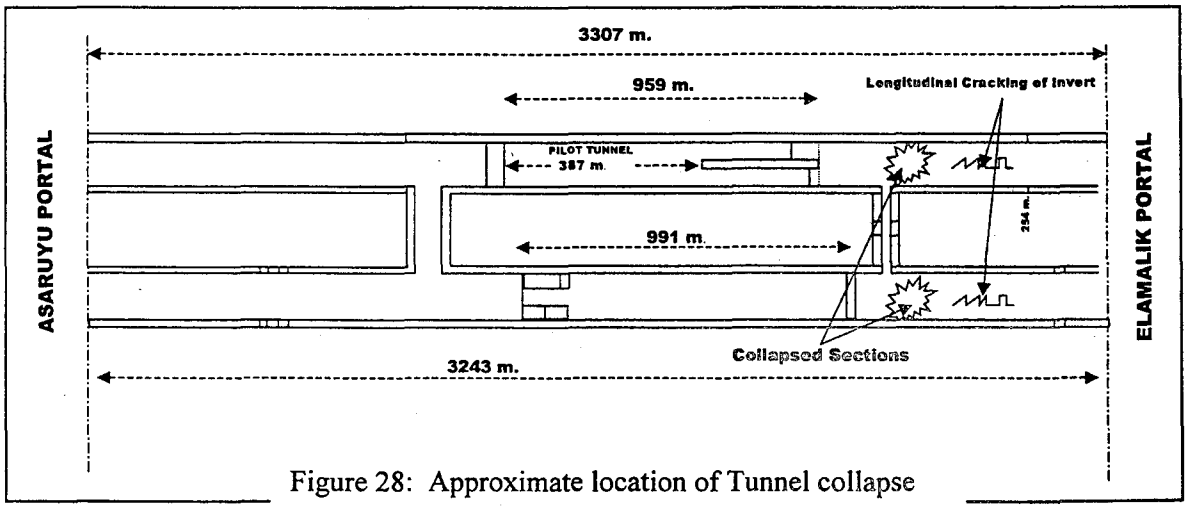

Figure 28: Approximate location of Tunnel collapse

3.0 SUMMARY/CONCLUSIONS

1) The FHWA team inspected the roadway alignment and the physical condition of the Bolu Viaducts #1 and #2, and Bolu Bridge #2. Also, the twin Bolu Tunnels damage was viewed from the Elmalik entrance westward to the collapse.

2) The Düzce earthquake caused considerable damage to the superstructure of Viaduct #1 and to the Bolu Tunnels due to the close proximity of fault rupture (near fault effect). A surface fault trace was visible between a segment of Viaduct #1 piers and evidence of high velocity impulses was observed from the earthquake records and at the sites.

3) The stations at Düzce and Bolu, 30 km apart, recorded PGA of 1.0g and 0.8g respectively. It is therefore reasonable to assume that Bolu Viaduct #1, which was not instrumented, located between these two stations experienced a PGA of at least 0.8g.

4) Significant damage did occur to the EDU's and bearings of Bolu Viaduct #1 from surface rupture displacements and ground shaking which then caused the superstructure girders to translate on their pier tables, narrowly avoiding total collapse.

5) The positive connections of many EDU's to the superstructure and pier cap of Bolu Viaduct #1 were sheared off.

6) Shear keys or blocks used to control transverse girder movement of Bolu Viaduct #1, although severely damaged, appear to have functioned as intended.

7) Moderate structural damage occurred to the concrete box girders of Bridge #2. The west-end of the eastbound span translated approximately 3-1/2 inches to the north relative to the west abutment.

8) Although the bearing pads on Bridge #2 had translated about 6-1/2 inches to the north and about 3-3/4 inches to the west, there was no significant damage to the EDU's and bearings. However, cracking of the concrete was noted at one of the anchorages of the EDU brackets that was attached to the superstructure.

9) Complete closure of both Bolu Tunnel bores was noted about 200 to 300 meters from the Elmalik portal entrances. The collapses occurred in a section of tunnel passing through a clay/weak rock zone where a temporary shotcrete lining system was in place. Severe shotcrete spalling was noted between sets and at the sets along the tunnel wall.

In summary, the close proximity of the fault rupture to the Bolu structures caused significant superstructure movements relative to the substructure which resulted in severe damage to bearings and EDU's, in particular, on Bolu Viaduct #1. However, despite an earthquake larger than design for, and a fault surface rupture under the viaduct, collapse did not occur and the viaduct performed satisfactorily.

Also due to types of damage inflicted on the bridges by the Düzce earthquake, much can be learned by the earthquake engineering and seismological communities. The near fault effect, the behavior of the EDU's and their positive connection to super-and sub-structure are just a few of the factors that can help engineers in designing and retrofitting bridges to resist future NAFZ type seismic activity.

Building Damages in Taiwan Chi-Chi earthquake

by

Masaomi TESHIGAWARA[1], Hiroshi FUKUYAMA[2], Hiroto KATO[3], Mizuo INUKAI[4]

ABSTRACT

This paper describes Building Damages in Taiwan Chi-Chi earthquake. Two Specialist Team of Japan went to Taiwan in order to execute of the emergency risk inspection, etc.

Here, the following are introduced : Disaster situation by both teams and content of the technical assistance cooperation and transition of the earthquake resistant design code of Taiwan. Still, disaster situations, etc. described in this paper are not always an outline of the whole damage, since it is based on limited investigation.

Key Words: Taiwan Chi-chi earthquake
Hyogo-ken Nanbu Earthquake
Building damage
Building Risk Inspection
Building Seismic Code

1. Introduction

Taiwan Chi-Chi earthquake took place in early morning, on September 21st, 1999, with the magnitude 7.7 (U.S. geological survey institute) and with the magnitude 7.3 (Taiwan Central Weather Bureau). This epicenter was near Chichi town, Nantou county in Taiwan. It became a catastrophe of 2,333 deaths, 10,002 injuries and 39 missing persons, and 9,909 complete collapse buildings, 7,575 middle damage buildings (Ministry of the Interior, National Fire Administration, Oct. 13. 2000).

Authors went to Taiwan for 5 days on first of October from 27th of Septembers, which related to execute of the emergency risk inspection, etc. while the disaster situation of the building is investigated in this place, as a Japan Disaster Relief Team specialist team (Team leader : Kazuo Okayama, chief of disaster prevention section, National Land Agency earthquake) for the purpose of investigation on the cooperation needs and recommendation in technical aspect and administration side. And, another team entered into Taiwan for 5 days in the 10 days from sixth of Octobers as Taiwan building risk inspection specialist team (Team leader : Masaomi Teshigawara) formed for the purpose of the guidance recommendation based on experience in Japan in the second risk evaluation of the building which the Taiwan authorities executed in the damaged area. Here, the following are introduced : Disaster situation by both teams and content of the technical assistance cooperation and transition of the earthquake resistant design code of Taiwan. Still, disaster situations, etc. described in this paper are not always an outline of the whole damage, since it is based on limited investigation.

2. Earthquake

(1) Epicenter and scale

Generation : At 1:47 a.m. September 21st, 1999.

The scale : Taiwan Central Weather Bureau announcement: magnitude 7.3

U.S. Geological Survey announcement: magnitude 7.7

1) Head, Structural Division, Department of Structural Engineering, Building Research Institute, Ministry of Construction, Tsukuba-shi, Ibaraki-ken, 305-0802, Japan)
2) Head, Large Scale Structure Testing Division, Department of Production Engineering, ditto.
3) Chief Researcher, Large Scale Structure Testing Division, Department of Production Engineering, ditto.
4) Chief Researcher, Building Engineering Division, International Institute of Seismology and Earthquake Engineering, ditto.

(the moment magnitude are about 10 times more than Hyogo-ken Nanbu Earthquake's)

Epicenter : Near Chi-Chi town, Nantou County, 23.85 N latitude and 120.78 East longitude degrees, 1.1 Km depth (by the Taiwan Central Weather Bureau).

It is said that the Tamoupu-Hsuangtung fault and the Chelungpu fault which pass through the epicenter moved. Anyway they are almost the east rised fault of the north-south direction.

Duration time : About 40 seconds

Maximum acceleration : 984gal (observation point of 10.2 kilometer from the epicenter)

Fault fracture surface : 80 kilo × 40 kilometer.

(2) Seismic intensity distribution

Main shock:

Seismic intensity 6(>250gal):

Nantou county Mingchian Village, Taichung city

Seismic intensity 5(> 80gal):

Hsinchu county Chupei, Tainan county Yungkang, Chiayi city, Ilan city

Seismic intensity 4(> 25gal):

Pingtung county Chiuju, Taitung county Chengkung, Penghu county Makung, Taipei city, Kaohsiung city, Taitung city

Seismic intensity 3(>2.5gal):

Miaoli county Sani, Hualian city

(using 7 class seismic intensity scale in Taiwan which removed seismic intensity of the 7th class from the old 8 class seismic intensity scale of Japan).

The largest aftershock: 7:52 a.m. September 26th, 1999 generation, magnitudes of 6.8.

Seismic intensity of 6:

Nantou county Jihyuetan

Seismic intensity of 5:

Chiayi county Alishan, Tainan county Chiali, Chiayi city

(the seismic intensity of 2 in Taipei City).

The large earthquake in a past :

Miaoli earthquake (in Hsinchu, Taichung) on April 21st, 1935. M 7.1. 3,276 deaths.

(3) Earthquake strong-motion record

In Taiwan, there are some earthquake strong-motion record networks which are Central Weather Bureau Strong-motion Network (CWBSN) with 75 observation points, Institute of Earth Sciences, Academia Sinica (IESAS) with 109 observation points, Central Weather Bureau Earthquake Center (TSMIP) with 600 observation points, etc., and many strong-motion earthquake records have been obtained. Main maximum accelerations of the earthquake annoncement system by the Central Weather Bureau are as follows. With the observation, the maximum acceleration rapidly lowers, as it separates from the epicenter.

Nantou (10.2 km from epicenter)	973gal
Kukeng(28.7 〃)	394 〃
Alishan(27.7 〃)	231 〃
Taichung(34.6 〃)	222 〃
Chiayi(53.3 〃)	166 〃
Jihyuetan(12.7 〃)	165 〃
Hsinchu(107 〃)	94 〃
Kaohsiung(150 〃)	16 〃

The distribution of strong-motion earthquake record and damaged area is shown in Fig. 1.

According to the spectrum of the acceleration and the pseudo velocity by the strong-motion records, a bigger acceleration than Kobe is observed in the short period. And, in another record point, a big velocity is observed in the long period.

3. Damage of buildings

3.1 Outline of damage

Reinforced concrete structures and framed masonry structures are typical type of the buildings in Taiwan. At others are steel structure, steel and reinforced concrete structure, brick structure, wooden structure, soil brick (the dried brick) structure, etc.. It seems that recently reinforced concrete building are almost used.

The damaged building in this earthquake spreads over 200 km. The features does not seem that the building is suffering from heavy damage but the buildings of heavy damage or

collapse are scattered in the buildings of the light damage (Photo 1, 2). However, all buildings on the large fault (photo 3) which exposes from Fengyuan City to Shihkang Village in Taichung County, at Takeng district in the north-east of Taichung City, from Wufeng Village, Taichung County to Tsaotun Town, Nantou County, etc are getting collapsed or inclined damage (photo 4~6). And, we can say that it is also a feature that collapse of high-rise residential building (photo 1, 14) which exceeds 30m high are seen not a few.

In Taichug City which population is about 1,000,000, the exposed fault is 10 km from the center in the city(photo 3). In spite of it, the damage is considerably less than Hyogo-ken Nanbu Earthquake, and infrastructures, etc. almost normally work. The number of the heavy and middle damaged buildings in Taichung City are 496 and 516 buildings, respectively (at present October 13th).

The damage in Taichung City, Taichung County and Nantou County are as follows.

(1) Taichung City

In south of the city, the damage has been limited to the houses in which reclaimed land (photo 14, 15), which has some structural disadvantage at the cross of roads, and the houses in the north near which stands on the fault (photo 3).

(2) Taichung County

In Fengyuan City, Taichung County which was located in north about 30km from Taichung City, Taichung County, there were the fault which reaches less than 5m heigh observed. And, in Tungshih Town (photo 26), a collapse of small-scale houses such as the one-story house was mainly observed, removal works of the collapsed houses were advanced including the most intense district of the damage, and the approach by automobiles was not possible.

(3) Nantou County

We inspected in Mingchian Village (photo 27), Chichi Town (photo 28 and photo 29) and Chungliao Village (photo 30) of west in Nantou County and Nantou City (photo 31). Especially, the failure situation of Chungliao Village is serious. There is some zones surrounded by roads in which almost buildings are collpased which means the extent of the damage. There was the long space between the reinforcement bars from the situation of the failure structure. And the buckling of columns and integration of the oil tin to the under side of beams, etc. were observed as well as in Taichung City.

3.2 Damage outline of the RC building

(1) Damage of the low-rise RC building

There are many cases which the first floor are used for stores, and over the second floor for houses on low-rise building about 2~5 floor (photo 7). Though generally they are the frame structures, the walls are often established in 3 planes except for the part which faced the road. It is the structure with many quantities of the wall which can effectively resist for the earthquake. On the side which faces the road, there are one thing of the 1 span and other thing of the row house type of the multiple-span. It seems to often establish the boundary walls over all layers in the multiple-span houses. Generally the damage of the buildings of this type is comparatively light in photo 8,9. Especially, though the building in photo 9 was under construction near the fault, it was non-damaged. However, large damage such as a collapse was also observed in the buildings without the wall at the corner of the road and the buildings without 2 planes or 3 planes on the first floor. Still, large damage seems to have been generated in the building of framed masonry structure (the structure which established the wall of the brick in the RC frame) which appears the apparently similar structure for the mortar finishing.

In the building in Taiwan, the 1 span is often spent as a public sidewalk, and in this case, over the second floor, it is supported by cantilever beams and columns on the first floor. Therefore, it becomes the depth direction of 1 span of first floor with (over the second floor some) the type

that the wall is not established. In the building with small spans of the depth direction in this investigation, the damage (photo 11) in which this seemed to be a cause was not many, and it seemed to be also observed damage such as a collapse, since it becomes a structural type equal to *pilotis*.

(2) Damage of the middle-rise RC building

Middle-rise building with about 7,8 floor is mainly seen in the city area. In the building (photo 12) in which the wall of first floor becomes little the *pilotis* type for houses, in addition to this, for the over second floor in the building in which the wall is in the corner of road and store, on the first floor there was the damage in which the first floor collapses, and the many buildings of non-damage also exists.

(3) Damage of the high-rise RC building

The high-rise buildings which exceeds the 10th floor is mainly seen in multiple dwelling house in urban area. It is also said that the lower layer floor is used as a commercial building. Some structures are the frame structure which consists of columns and beams, and others are the frame with structural walls which consists of bricks in all frame (photo 13). Damage mainly observed in these buildings is collapse and heavy damage of most lower layer which originates from the destruction of the column of most lower layer which becomes the *pilotis* type (photo 14～16) and collapse and inclination damage of the building which originates for it. And, the shear failure and the buckling failure of columns at the large setback in the middle floor (photo 17), the heavy damage of non-structural members by the excessive deformation, etc. are also observed. There is not always and greatly the damage of low-rise buildings around these high-rise buildings. Still, the high-rise buildings without structural damage also reaches in great numbers.

(4) Comparison of RC building damages between this earthquake and Hyogo-ken Nanbu earthquake

According to the Table 1, the damage of the RC building observed in Hyogo-ken Nanbu Earthquake[1] are also observed in this Chi-chi Earthquake. For example, photo 18 shows a collapse of the soft storey (*pilotis* type) of a elementary school, simultaneously, the shear failure of short columns. Except of these damage features in present earthquake, the following damages are mentioned : Collapse and inclination of the high-rise residential buildings and other buildings right on the fault.

Table 1 Comparison of damage features of RC buildings between Hyogo-ken Nanbu Earthquake and Taiwan Chi-chi Earthquake

Damage features of RC buildings in Hyogo-ken Nanbu Earthquake[1]	Taiwan Chi-chi Earthquake
1) Failure of *pilotis* (storey collapse or heavy damage)	many cases
2) Collapse or heavy damage of first floor, not *pilotis* (the torsional destroy by the irregular arrangement of walls and the shortage of shear capacity, etc.)	many cases
3) Damage of middle storey according to the vertical direction discontinuity of each storey's strength or rigidity	confirmed
4) Shear failure of short columns attached handrail walls and hanging walls	confirmed
5) Severe damage of columns by shortage of hoops and anchoring shortage of hoop end.	confirmed
6) Destroy of connections between main bars	confirmed
7) Collision between buildings	confirmed
8) Destroy of beam-column joints	not confirmed
9) Destroy at the column sections of main bar arrangement discontinuity	not confirmed
10) Fall down of precast concrete roofs	not confirmed
11) Column yield of frames designed for beam yield	many cases

(5) Damages of other building structures

As for frame structure with infilled masonry walls, brick structure (Photo 19), wooden structure (Photo 20), sundried brick structure (Photo 21), the ratio of damage buildings to non-damage buildings were more than the RC building, and these complete collapse buildings were not a few found. And the collapse of the light steel building was also observed.

Still, the damage of the steel reinforced concrete structure building has not been confirmed in this investigation.

(6) Damage of civil engineering structures

The severe damage is also observed in civil engineering structure. Destroy of a dam (Photo 22), collapse of bridge (Photo 23) and destroy of roads by landslides (photo 24), etc. took place. However, important facilities such as the expressway seem to be designed much strong which prepared for the emergency, and heavy damage in this earthquake is not reported.

4. Building seismic design code of Taiwan

Before 1973, the seismic design code of Taiwan, which referred to seismic intensity method of Japan was adopted, and it was allowable stress design for 0.1 design seismic coefficient. After the war, since the values of allowable stress became twice, without the design seismic intensity changing, the base shear coefficient in that time for the ultimate strength of the building is about 0.15. This means that the base shear coefficient is about 1/2 of RC building frame structure of the current standard in Japan.

In 1997, referring to the U.S.A. UBC in 1974, the base shear coefficient method was adopted. It is the allowable stress design method until the revision 1997 in the strength side. By this revision, the base shear coefficient for the design of usual RC building frame structure in the largest zone factor, was 0.084, the ultimate strength coefficient became about 0.13, and it became about 83% of its previous standard.

The base shear coefficient for the design of usual RC building frame structure was revised in 1982. And this coefficient became 0.10 in the largest zone factor including Taichung County, and the ultimate strength was about 0.15. These coefficients were equivalent to ones of the code before 1973. (However, they are this 0.8 times in Nantou County.)

In 1997, the evaluation of the deformation of the building was revised, considering the ground property. The standard base shear coefficient is 0.157, while the ultimate strength design method is adopted to the RC buildings, and load factor for it is 1.403. That is to say, standard base shear coefficient of the ultimate strength became $0.157 \times 1.403=0.22$. Still, as for the steel structure, the allowable unit stress design is adopted, and the design base shear coefficient for this design is 0.196. After this revision, in the region of highest seismicity, the ultimate strength base shear of usual RC building frame structure became about 73% of the base shear in the region where the zone factor is 1 at the current standard of Japan. In Nantou County and Taichung County which are close to this epicenter, since the region horizontal acceleration coefficient is 70% of the maximum value, the required strength is about 50% of Japan. In this revision 1997, the horizontal force in highest seismicity became 1.5 times of the previous one, while the period of the building was less than 0.3 seconds as mentioned above. And the horizontal force became equivalent while the period was more than 1 second, or it was smaller than the previous value depending on the ground classification. In comparison with the standard of Japan, the 70% strength is required in the short period region. And the required strength is about half in the period from 1 second to 2 seconds, in comparison with the type II ground of Japan. Fig. 2 show the relationship between the base shear coefficient and period of the RC building with the biggest capacity by the seismic code after 1982 (Ds=0.3) of Japan and Taiwan.

5. Technical assistance and cooperation

(1) Building emergency risk inspection of Taiwan

The emergency risk inspection shall be carried out by the two phases.

At the 1st phase, in seven field (collapse, inclination, members such as columns and beams, something falling down, effect to the adjacency building, foundation, others (situation of the infrastructure)), each damage is inspected in three ranks (light, middle and heavy). If there is one field of "heavy" or "middle" rank, the mentioned building is inspected as the rank "no entry" or "limited entry" respectively, and the red paper or yellow paper are set respectively. In other case, the green paper is set on it as the rank "safety".

At the 2nd phase, according to the structural method (reinforced concrete, steel, brick, wood), each evaluation items are established, and each items are inspected into three ranks (light, middle and heavy). This inspection method is similar to the emergency damage inspection in Japan.

In Taichung County and Taichung City, the first phase of emergency risk inspection was already done or finishing another several days in 29th of September.

(2) 2nd phase of building emergency risk inspection

After the 1st phase of building emergency risk inspection, there are some problems which are the clarifications of the inspection technique and the enough guidance about for the criterion to the inspectors, etc. in order to promote the second phase. There was a request from the Taiwan authorities about the inspection guidance for 3 days by seminar type which is concerned with the second phase for registered architects who carries out the emergency risk inspection, etc. in Taichung County and Nantou County. The second phase is correspondent to the emergency damage inspection in Japan. The specialist team of Japan was operated for the respond to this request.

By the decision of the high level in the Taiwan authorities on fourth of October, the priority was given to "investigation for the financial support", not the second phase. So, the second phase was not yet prepared, but the specialist team was operating for the initial purpose of guidance and recommendation from the lessons of Japan about the implementation method of the second phase in damaged area for Taiwan authorities.

Problems, guidance and recommendations on the second phase are as follows.

1) Link with financial support

Taiwan authorities had a problem that in a certain local government, the result of the emergency risk inspection was linked with financial support for damage or apartment house payment by Taiwan government. Therefore, some people requested the inspection result "no entry" to inspectors.

The specialist team explained that in Japan, the main purpose of the inspection was the prevention of the secondary disaster by aftershocks, and was not linked with the support to the cost for the reconstruction of housing or, priority occupancy measures to temporary dwellings, etc.

2) Responsibility of structural engineers

The complaints to the responsibility of the structural engineers of the buildings inspected "no entry" was strong.

Explanation about this problem is that the reason of damage should be discussed. For example, the building code should be revised when the higher external force than expected was happened, or some damage should depend on the bad construction works. These means that it is not reasonable that structural engineers should be responsible with the damage. The correct reason of damage should be resolved.

3) Removal of buildings inspected "no entry"

What is the dealing with the case when the owner of the building inspected as "no entry" does not cooperate in its removal ?

The explanation to it is that though there are

no obligation such as the removal even in Japan on the result of the emergency damage inspection, referring to the Building Standards Law, the order of the removal is possible, when this building is considered to be dangerous.

(3) Outline of questions in discussion in Taipei City and seminars

1) Validity of the level of seismicity evaluation index Iso. Seismicity input, region coefficients, etc.
2) Dealing with the building suffered from the damage in the earthquake.
3) Dealing with the building which is not satisfied with the standard.
4) Role of structural engineers or government for retrofitting
5) Relation between minimum strength regulations of the standard and observed ground acceleration, and relation of the collapse buildings,. Possibility of the authorization of the disaster area, etc.
6) Regulation to decide the removal, repairing or retrofitting about inclined buildings.

(4) Suggestions from the Japan side.

1) The clarification of the meaning of the inspection system.
   *The distinction of emergency risk inspection and financial problems such as the support.
2) The improvement in accuracy and reliability of inspection.
   *Training for inspection.
   *Utilization of the lessons from Hyogo-ken Nanbu Earthquake disaster.
3) The utilization of the lessons from damaged area.
   *Respcts of quality control and construction rule.
   *Promotion of structural design and construction quality control by structure engineers and structural designers.
4) Accurate retrofit and repair
   *Enough explanation aobut the distinction of dangerous building and removal building.
   *Utilization of epair and of the retrofit manual of Japan.
   *Utilization of evaluation of seismic capacity for effect of retrofitting.

6. Conclusion

Taiwan side concretely resolve the problems which are notification of the meaning of the inspection system, improvement of accuracy and reliability of the risk inspection, and utilization of the lessons from the damaged area and accurate retrofitting. These activities needs the knowledge and experience of Japan.

So it is desired that the cooperation of science and research collaboration and local government or private cooperation be closely promoted between Japan and Taiwan.

Acknowledgment

The effort of Hideaki YOKOI, Head, Applied Seismology Division, International Institute of Seismology and Earthquake Engineering, Building Research Institute, Ministry of Construction、Japan is greatly appreciated, as for the earthquake dimension of this paper,

[Reference]

(1) "1995 Hyogo-ken Nanbu Earthquake damage investigation report (outline edition)", Building Research Institute, Ministry of Construction, March 1996.

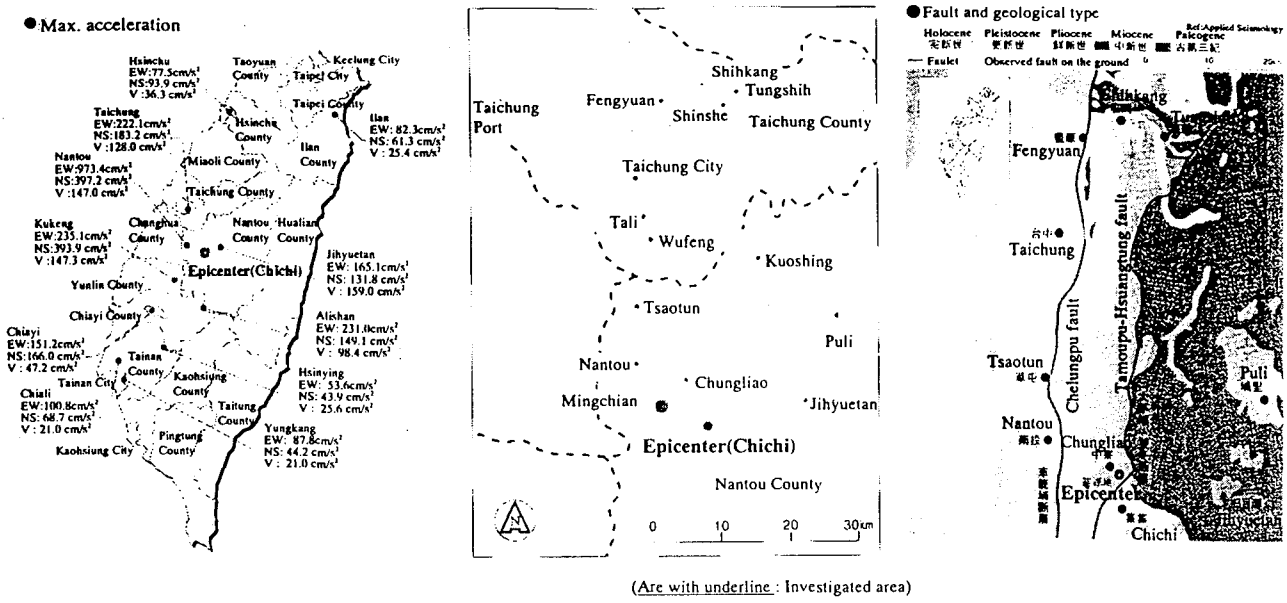

(Are with underline : Investigated area)

Fig.1 Damaged are and maximum accelerations observed
(Ref. 'NIKKEI Architecture', 18 Oct 1999, pp.107-122 in Japanese)

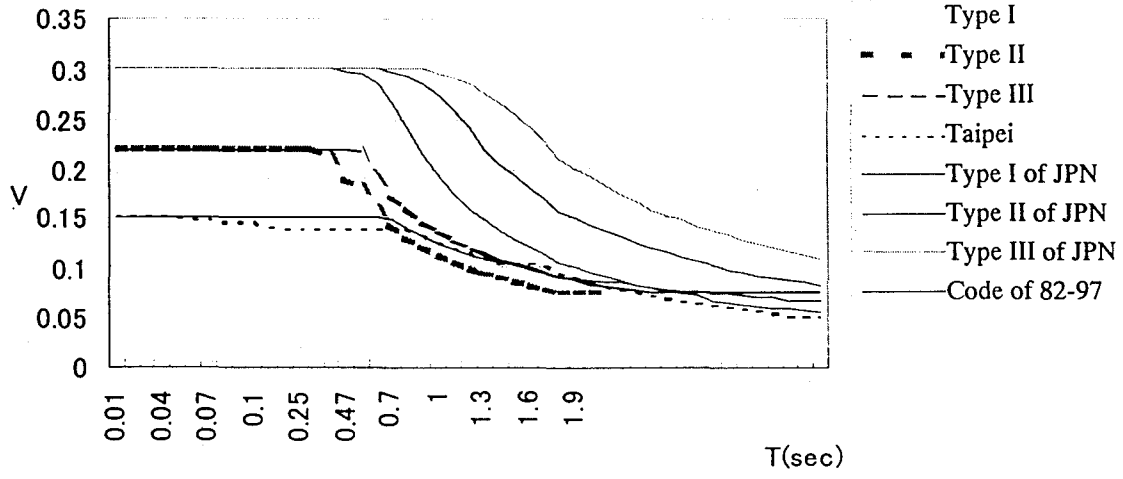

Relationship between minimum design horizontal force V and fundamental period T

Fig.2 Comparison of the design base shear coefficient after 1982 in Taiwan with the vibration coefficient (at Ds=0.3) in Japan.

Photo 1Collapsed high-rise multiple dwelling house (Tungshih, Taichung County).
The 12-floor RC building collapsed by the destruction of the *pilotis* column. The damage of the low-rise building of the vicinity is very greatly nonexistent.

Photo 2 Situation of damage from the sky (Puli, Nantou County)
Though it is comparatively a region of heavy damage, it is the situation that the building that almost buildings are light damage and collapsed is scattered .

Photo 3 Fault (Takeng, Taichung City)
The displacement of 3～5m vertically and about 4～8m horizontally has been generated

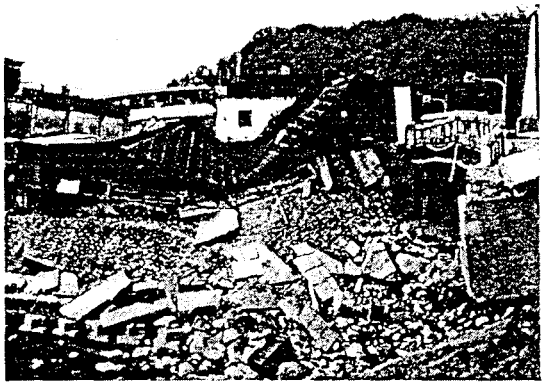

Photo 4 Building collapsed just above fault (Fengyuan City, Taichung County)
Building of brick is perfectly destroyed

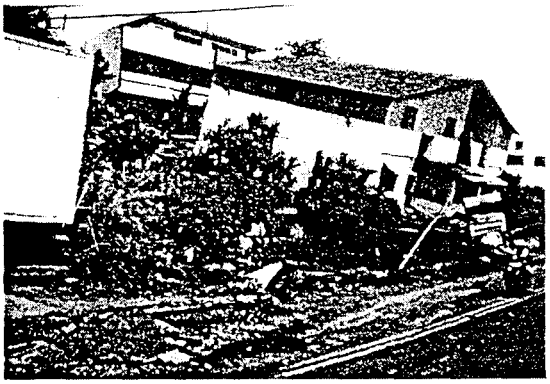

Photo 5 Building just above fault (Fengyuan City, Taichung County)
The ground behind building is rised. The building in this vicinity got same damage

Photo 6 Building just above fault (Shihkang, Taichung County)
RC multiple dwelling house of the new construction inclined by the fault. The pile is not used. The damage of the superstructure is very greatly nonexistent

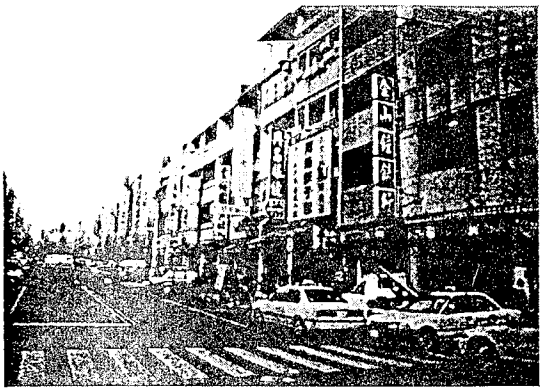

Photo 7 Typical street in Taiwan (Tungshih, Taichung County)
Store on first floor and houses over second floor are used. The 1 span in the roadside of first floor is used as a public road.

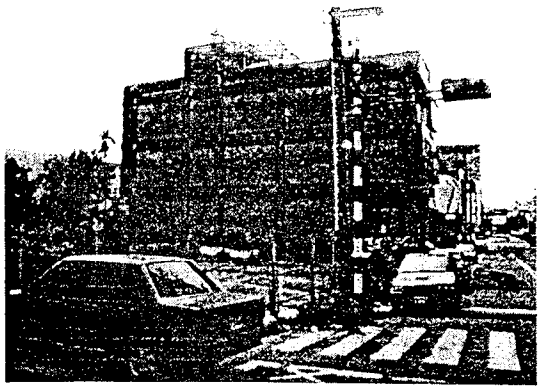

Photo 8 Typical low-rise building (Fengyuan City, Taichun County)
In one direction of the building, RC wall except for the 1 span in the roadside of first floor without the window has been established. Non-damage.

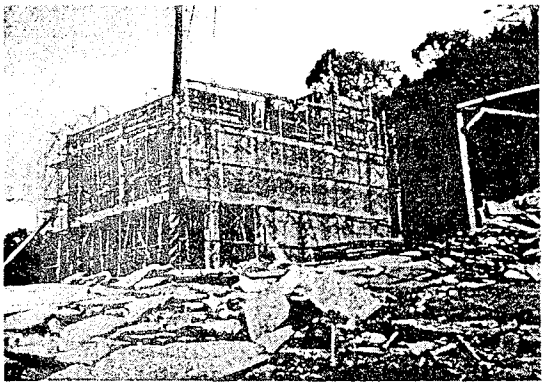

Photo 9 The low-rise building (Fengyuan City, Taichung County)
It is under construction near the fault of photo 4,5. The structure is almost non-damage

Photo 10 The low-rise building (Fengyuan City, Taichung County)
The wall was distributed irregularly even in the low rise, and there was heavy damage in the building with small walls on first floor.

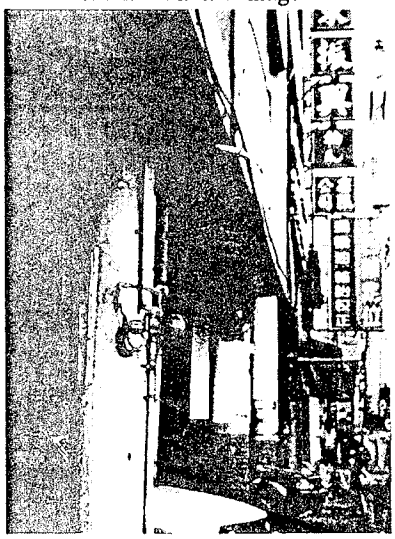

Photo 11 Damage of the column in the first floor setback division (Tungshih, Taichung County)

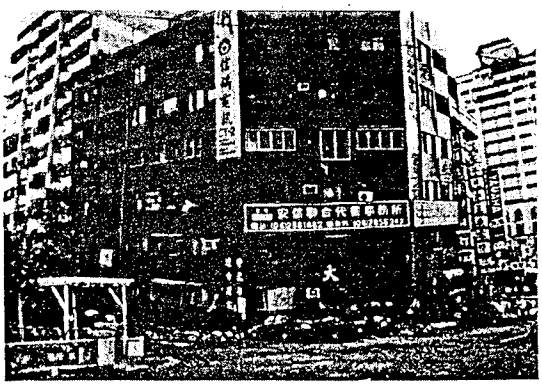

Photo 12 Middle-rise building which is built in the corner lot where first floor collapsed (Taichung City)
By there being small twists by the localization of the wall and wall quantities of first floor, it is supposed destroying the column of first floor. Large damage is not observed in the building in the vicinity.

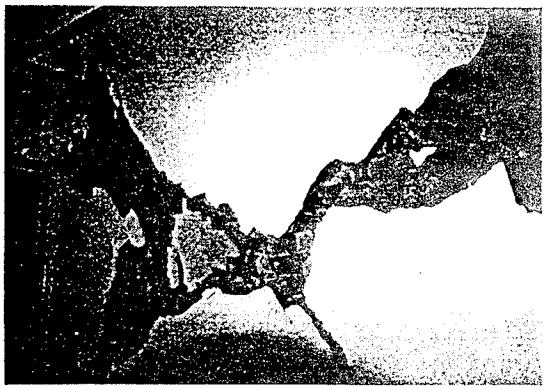

Photo 13 Damage of brick wall of the high-rise residential building (Fengyuan City, Taichung County)
Large response displacement occurs, since there is no RC structural wall, and it is supposed the heavy damage of the brick wall.

Photo 14 High-rise multiple dwelling house in which first floor collapsed (Taichun City)

Photo 15 High-rise multiple dwelling house in which first floor collapsed (Taichung City)
Destruction situation of the first floor column in photo 14. The damage of the lower part is being concentrated at first floor.

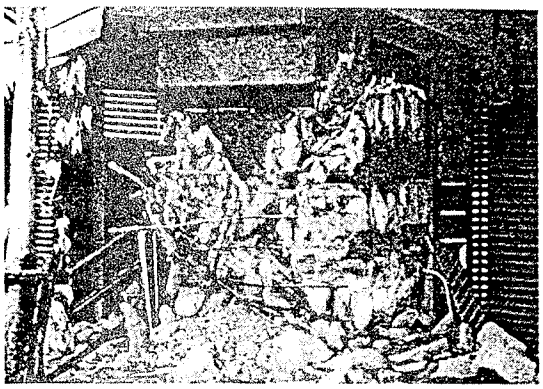

Photo 16 Damage of the first floor column of the high-rise multiple dwelling house (Tunshih, Taichung County)
15-floor building of design and construction equal to photo 1. A collapse was avoided, and the column of first floor has damaged.

Photo 17 Damage of the middle floor of the high-rise multiple dwelling house (Fengyuan City, Taichung County)
The damage is concentrated in the column of the middle floor of the setback largely.

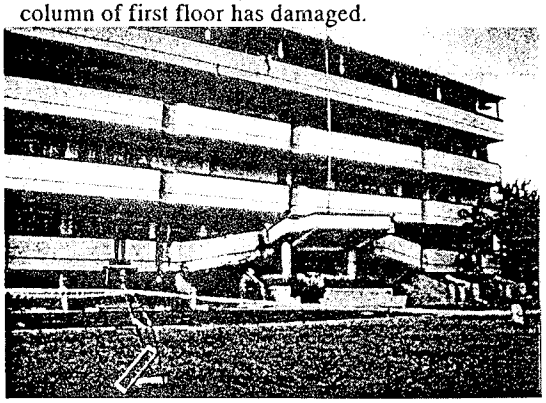

Photo 18 Elementary school in which first floor collapsed (Tunshih, Taichung County)
The wall of first floor was *pilotis* type, and the nonstructural wall was also attached to the column, and it became short column.

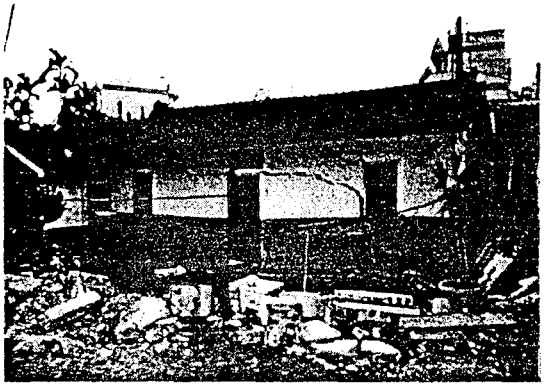

Photo 19 Damage of brick structure (Shihkang, Taichung County)
A collapse was avoided, and large crack was generated in the brick wall. The brick fence of the front has collapsed.

Photo 20 Damage of the wooden building (Tungshih City, Taichung County)
The wooden building of tiled roof is observed. Though the building of the photo remained for an inclination, it was also seen the result to collapse in the vicinity.

Photo 21 Damage of sundried brick structure (Tungshih, Taichung County)
It is completely destroyed. It is near the building of photo 7.

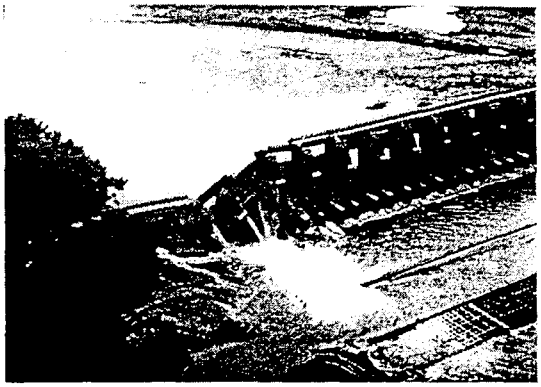

Photo 22 Destruction of a dam (Shihkang, Taichung County)
The fault crossed the dam.

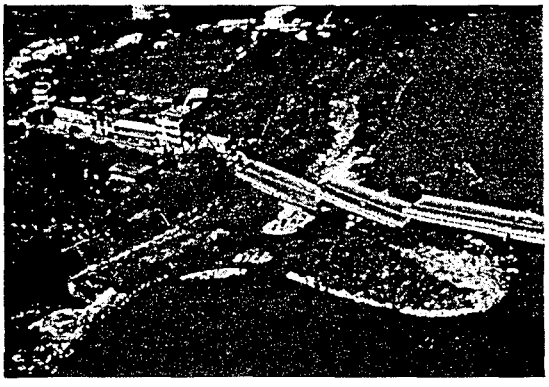

Photo 23 Collapse of bridge (Shihkang, Taichung County)
It is an upstream of photo 22, and collapse is considered to be the effect of the fault. The damage of the bridge was observed not a few.

Photo 24 Landslide in the mountain (near Shuili, Nantou County)
Landslides are being generated in everywhere, and the road has been blocked.

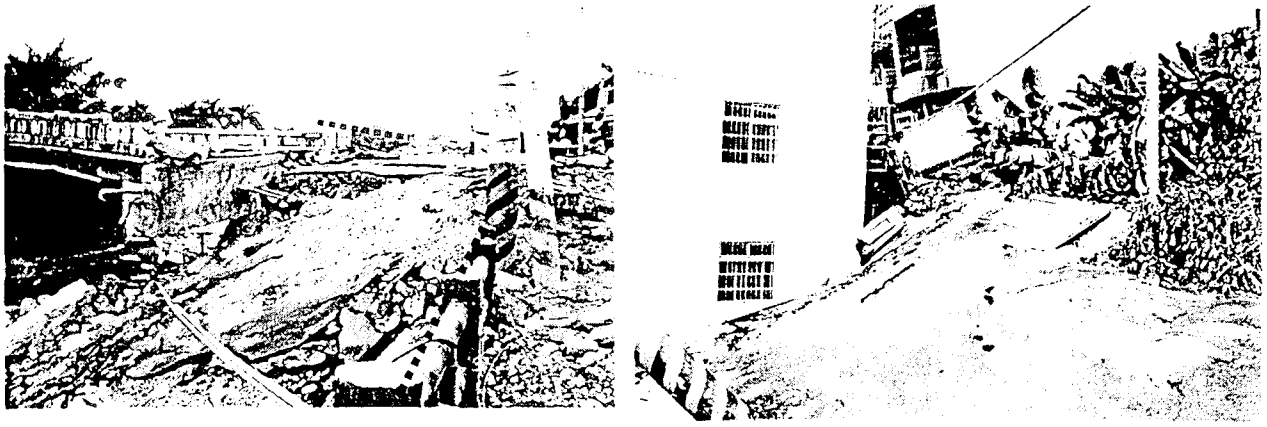

Photo 25 Fault (suburb of Fengyuan City, Taichung county)

The part of the bridge rises and moves to the horizontal direction, too. (The overpass rail which is shown by the red broken line was straight originally.)

The right side at the building which was built across the 9 m road rises and moves to the side of the building on the left side.
The road between buildings disappear and the car in parking is put in.

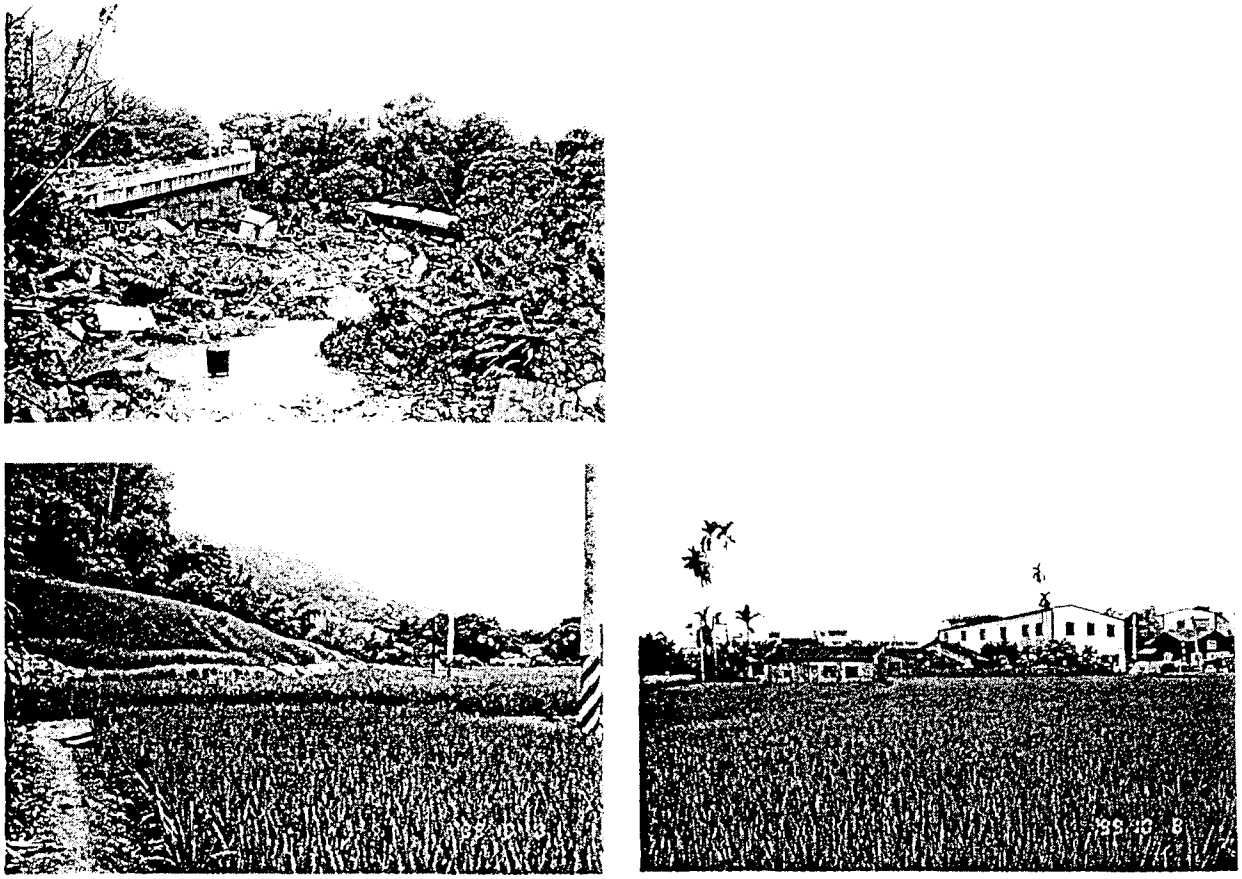

Photo 26 Fault (suburb of Fengyuan City, Taichung county)
The side of the left back at the farm field which was to be plain rises.
The dug rice dies and being discoloring to the brown of it.
The damage on the side (the east side) where the fault rose is big whereas it doesn't seem to suffer heavy damage on the west side.

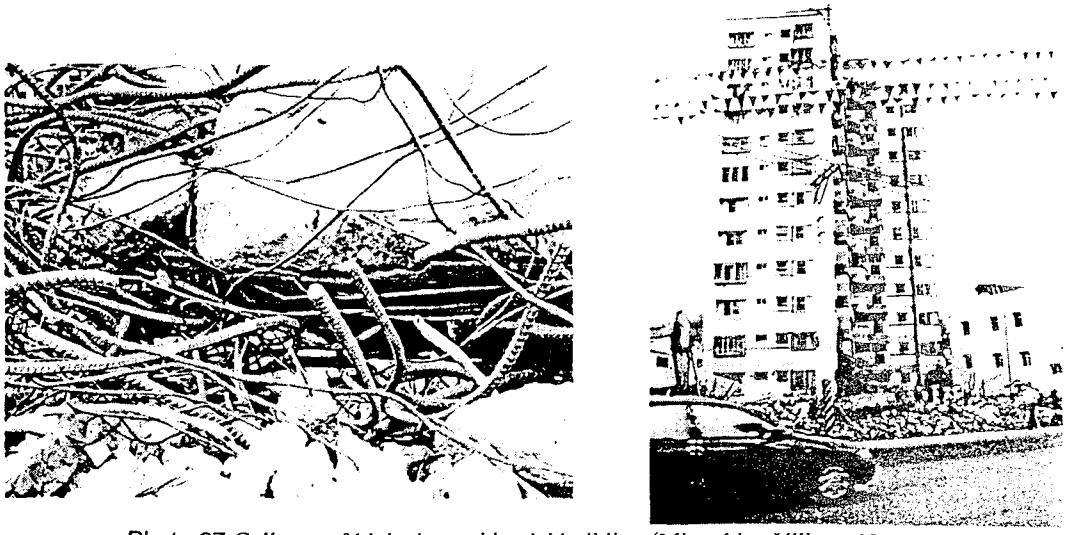

Photo 27 Collapse of high-rise residential building (Mingchian Village, Nantou County)

One of the 12nd floor building RC building falls down while another which is the same as the building in the back is damaged lightly.
During removal work

Photo 28 Collapse of high-rise residential building (Chichi Town, Nantou County)
The top and bottom of plain columns on the 1st floor of the 3rd floor RC residential building floor destroys in bending failure, and it is swaying to the right.

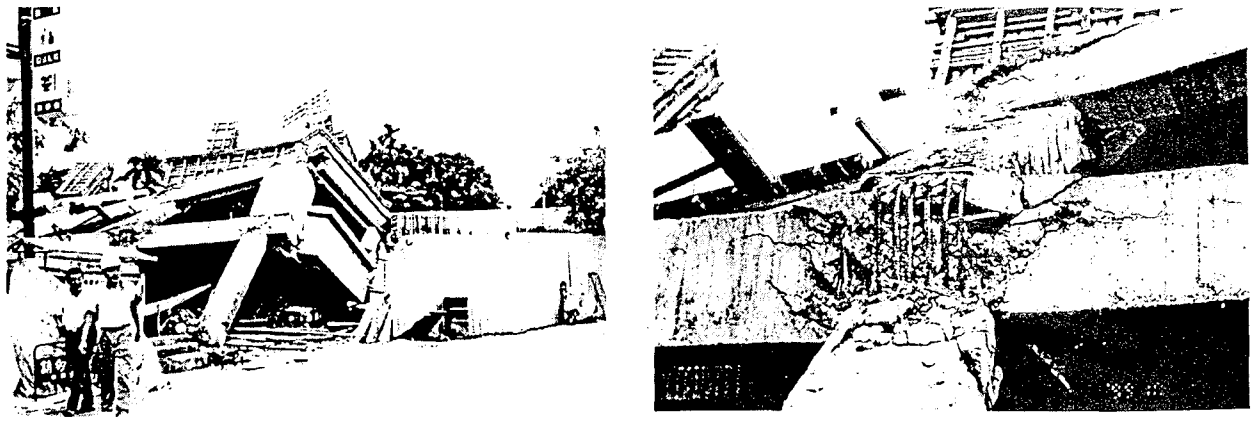

Photo 29 Building damage under construction (Chich Twon, Nantou County)
RC building under construction is finishing the 1st, and 2nd floor of casting concrete and the 3rd floor is casting.

Photo 30 Area where a lot of buildings suffered damage above the heavy (Chungliao Village, Nantou County)
The building which faced a street suffers completely heavy damage.
The oil can in the concrete which was made a topic by the newspaper.
It is explained by the related engineers when the oil can is the one to be using for non-structural parts such as the beam, in order to make wipe and isn't using for the main structure body.

Photo 31 Damage of high-rise multiple building (Nantou City, Nantou County)
About 50 % of the columns which faced a road in the side at the 12nd floor RC buildings which are built in the corner place is being heavy damaged.

Photo 32 Damage of high-rise multiple building (Fengyuan City, Taichung County)

Damage of the three 22nd floor RC residential buildings (the lower floors are commercial facilities) which are built as the surrounding of a court.
Damage of the non- structural walls on the middle floors and damage of the column tops on the 1st floor.

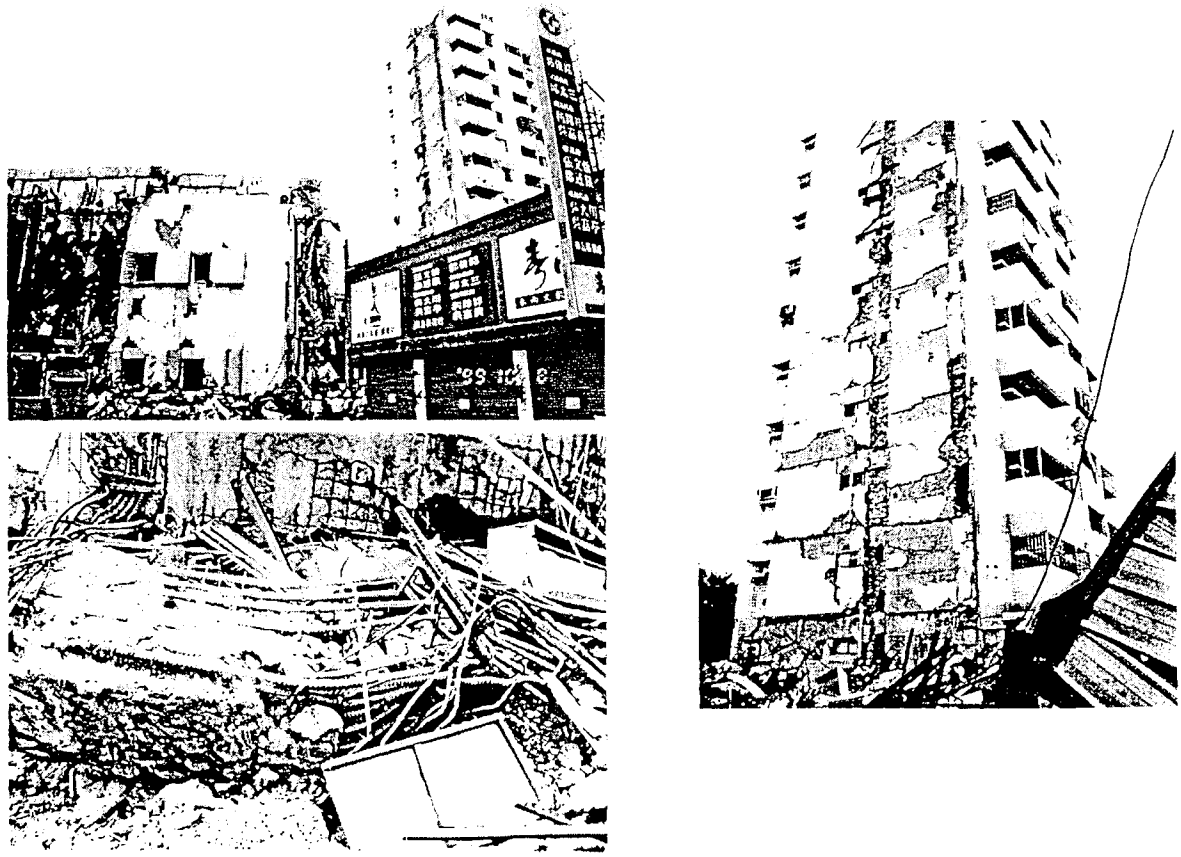

Photo 33 Damage of high-rise residential building (Fengyuan City, Taichung County)

One of the 12nd floor RC residential building which are the same as the right one in this photo falls down in the 1st floor.
Removal work and column.

DAMAGE OF EARTH RETAINING STRUCTURES IN THE 1999 CHICHI, TAIWAN EARTHQUAKE

Ken-ichi TOKIDA[1], Osamu MATSUO[2], Shinya NAKAMURA[3]

ABSTRACT

This paper reports damage to earth retaining structures due to the 1999 Chichi Taiwan earthquake, based on the post-earthquake field survey. Types of retaining structures include conventional concrete retaining walls, geosynthetics-reinforced soil retaining walls and segmental retaining walls. Details of the damage are described and their failure mechanism and implications are discussed.

KEY WORDS: earthquake,
retaining wall,
damage

1. INTRODUCTION

At 1:47 a.m. on September 21st, 1999, a strong earthquake occurred with its epicenter in the Nan-Tou prefecture in central Taiwan. Magnitude of the earthquake is Ml=7.3 (Taiwan central meteorological office) or Ms=7.7 (U.S.G.S.). The earthquake caused fault with a total length of 80 kilometers. It also caused loss of more than 2,400 people's lives and damage to more than 20,000 houses, extensive geo-hazards and damage to various engineered structures. The authors conducted a field survey after the earthquake focusing on damage to soil structures.[1] The survey was conducted as a part of the cooperative research project, "Development of Earthquake and Tsunami Disaster Mitigation Technologies and Their Integration for the Asia-Pacific Region", budgeted by Science and Technology Agency of Japan. This paper briefly describe the damage to several types of retaining walls constructed along roads and their failure mechanisms are discussed. The location of the three sites surveyed in this paper is shown in Figure 1.

2. CONVENTIONAL CONCRETE RETAINING WALLS

Among the types of conventional concrete retaining walls, the leaning- and gravity-type retaining walls seem to be most popularly constructed in Taiwan. A small number of cantilever-type concrete retaining walls and geosynthetics-reinforced soil retaining walls were found within the authors' field survey. The cantilever-type concrete retaining walls were observed in flat areas, not in mountainous/hilly area. This might be due to the fact that this type of retaining walls requires a considerable width of base plate and when constructed in steep slope side the need for setting-back slope cutting would increase the construction cost. For the same reason, the leaning- and gravity-type retaining walls are generally preferred in mountainous/hilly area. Within the survey, no damage to the cantilever-type retaining walls was found. According to Dr. Chou, a local consultant engineer, this type of walls has been usually designed seismically in Taiwan.

In contrast, serious damage to a number of leaning- and gravity-type retaining walls was found in hilly areas. Most of the damaged walls were located on steep slopes and their typical failure modes were sliding and tilting, occasionally associated with collapse at

1) Director, Earthquake Disaster Prevention Research Center, Public Works Research Institute, Ministry of Construction, Tsukuba, Ibaraki-ken, Japan
2) Head, Soil Dynamics Division, ditto
3) Senior Research Engineer, ditto.

construction joint.

Photograph 1 shows the typical damage of the gravity-type retaining wall. The site is located midway of a mountain road connecting Tsaulin and Chushan (Site① shown in Fig.1). As shown in Figure 2, the road is a cut-and-fill constructed on a steep slope with a slope angle of 50 degrees to the horizontal. The retaining wall with a height of about 7 meters was standing almost vertically, thus may be categorized as gravity-type retaining wall. However, they seemed too slender. The base of the walls were insufficiently embedded into the foundation soil and no special treatment to strengthen the bearing capacity was made. It is therefore presumed that the walls had only very small safety margin against external disturbances. Two longitudinal segments of the retaining wall completely tilted down the steep slope and the neighboring segments were distorted as shown in Figure 2. These remaining walls appeared to have tilted back, implying that the base slide movement surpassed the tilt-forward movement.

The downslope foundation soil was loose and trunk of a tree located about 5 meters down from the retaining wall was bent at a height of 1 meter from the ground surface, while the upper part of the trunk standing vertically. In addition, asphalt pavement was overlaid in several layers with a total thickness of 50 cm. These evidences convince us that there had been landslides associated with limited amount of movement during the past heavy rainfalls, which was confirmed by local people as well.

The observations suggest us that the factors leading to collapse of this gravity-type retaining wall would have been:

(a) Foundation soil was potentially unstable to have exhibited landslides during past rainfalls.

(b) No special treatment had been made to strengthen the foundation against bearing failure.

3. GEOSYNTHETICS-REINFORCED SOIL RETAINING WALLS

Photograph 2 shows the cut slope covered by geosynthetics- reinforced soil retaining wall collapsed during the earthquake. The site is located near the front gate of Chi-Nan International University in Pu-Li (Site② shown in Fig.1). As illustrated in Figure 3, the slope with a total height of 80 meters had been cut in a 60-degree slope and was refilled with the geosynthetics-reinforced soil retaining wall to cover the cut slope.

In the damaged zone, the surface was retained with the geosynthetics-reinforced soil retaining walls. The reinforcement, geogrid, was placed in every 80 to 120 centimeters layer, while wrapping around the stack of soil bags at the slope face. The retaining wall was composed of six or seven sub slopes with a height of 10 meters each and horizontal steps of two to three meters wide. The reinforcement length ranged from 4 to 13m as in Fig.3, while the wrap-around length was 1.5 to 1.8 meters, according to the authors' survey. It should be noted that according to local people the upper portion of the original slope failed along an inclined weak layer due to a rainfall during the cut and fill works.

The failure mode looked like the following: the upper five sub-slopes slid down the slope with their configuration maintained, while the bottom one or two sub slopes were hidden behind the overlying sub slopes. At lower portion, wrap-around reinforcements were pulled out and soil bags and interlayer backfill soil spilled out.

Although no detailed information is available at this moment on the failed slope, the authors assume a possible failure mechanism as follows (see Figure 4):

Figures 4(a) and (b) show the forces and stresses acting on the soil retaining wall before and during the earthquake. The resultant force acting on the bottom plane of the wall before the earthquake (denoted as Qs in Figure 4(a)) is given as a sum of the self-weight and

the earth pressure at the interface with the cut slope. During the earthquake, horizontal inertial force acted on the soil retaining wall, thereby the normal stress and shear stress at the interface reduced. These changes would have caused an increase in the vertical component of the resultant force acting on the bottom plane (denoted as Qe in Figure 4(b)), an increase in the horizontal component of Qe, an increase in the inclination of load Qe, and shifting-forward of the load eccentricity. This load, Qe, would have caused bearing capacity failure or excessive deformation of the bottom part of the soil retaining wall rather than the foundation soil (the foundation at this site seemed very stiff). Once the bottom part collapsed or deformed, the downslope deformation would have progressed to the overlying part.

The observations suggest us that bearing capacity at the base of the reinforced soil retaining wall is very important, and sufficient length of reinforcement embedment and wrapping-around are necessary. This type of seismic instability is likely to occur in geosynthetics-reinforced soil retaining walls with short bottom length relative to the height.

4. SEGMENTAL RETAINING WALL

In the middle of the prefectural road No.129 connecting Taichung and Dungshr, there was another type of the reinforced soil retaining wall, i.e., segmental retaining wall which were damaged as shown in Photograph 4 (Site③ shown in Fig.1).

This is a type of retaining wall in which blocks are piled up in the wall surface, FRP (fiber reinforced plastic) connecting rods are inserted between each block to constrain the horizontal movement and geogrids are fixed by the rods. In recent years, it is widely used in North America and Europe, while rarely used in Japan.

Figure 5 shows the cross section of the distorted wall. In this site, the reinforcements (geotextile) were placed with a vertical interval of 80 cm, and four pieces of concrete block with dimensions of 20 cm high, 50 cm wide and 30 cm deep (see Photograph 5) were stacked at the surface. The figure also shows that the stack of concrete blocks buckled out at a mid-height. Disconnection of the reinforcement from the connecting pins and subsequent extrusion of backfill soil were also observed (see Photograph 6). Crushed stone was used behind the facing, presumably for drainage consideration.

Attention should be paid that bulging of the concrete block facing are located at the mid-height of the reinforcement interval. The buckling should have been induced by the earth pressure during the earthquake. If we assume that the facing behaved like a rigid wall, the bending moment due to earth pressure takes maximum at the mid-height. As the reinforcement interval becomes large, the resistance of the block facing against buckling becomes less. Although the design procedure for the facing has not yet been developed, it is conventionally recommended in North America to place reinforcements in every three blocks (Leschchinski, 1999 [2]).

This damaged case suggests us that the interval of 80 cm corresponding to the height of four pieces of block was too large to resist against the earthquake. The authors do not know the reason why an interval of 80 cm was adopted. If an engineer considers that the use of reinforcement with lower strength associated with smaller spacing can be replaced by use of reinforcement with larger strength associated with larger spacing, he would prefer the latter for the reason of cost and workability.

Therefore the observations suggest us that some restrictions seem to be necessary on the interval of the reinforcement. Also sufficient connection strength between each blocks or block and geotextile are crucial.

5. SUMMARY AND CONCLUSIONS

Post-earthquake field survey was conducted for various types of soil retaining structures that were damaged by the 1999 Chichi earthquake. The results of the survey may be summarized as follows:

1) Among the conventional types of concrete retaining walls, damage to gravity-type retaining walls were

frequently found in mountainous areas. Most of the damaged walls were located at potentially unstable steep slopes and they looked slender in proportion to the height. Foundations were not treated properly to strengthen the bearing capacity.

2) Damage to wrap-around type geosynthetics-reinforced soil retaining wall was also observed. Possible reasons for the failure would be sliding failure of the original slope, bearing failure at the base of the reinforced soil retaining wall, and insufficient length of reinforcement embedment and wrapping-around.

3) In the case of damaged segmental retaining walls, large interval of the reinforcements and insufficient connection strength between the segmental wall and the reinforcements seemed to have caused failure.

Furthermore, the results of the field survey suggest us the importance of the following considerations in design and construction of retaining walls.

1) When leaning- or gravity-type retaining walls are constructed in mountainous region, proper evaluation of bearing capacity in the foundation slope and necessary treatment are crucial to secure stability not only during heavy rainfalls but also during earthquakes.

2) Earthquake-resistant design procedure for the wall surface portion should be developed further in the case of segmental retaining wall and geosynthetics-reinforced walls. And appropriate construction work is crucial to the security of these walls.

The case records will be studied further in the form of back-analysis to verify and improve the existing seismic design procedures for the types of soil retaining structures.

The construction works of the reinforced soil wall have been increased in Japan as Fig.6. Therefore, a manual titled as "Design and Construction Manual of Reinforced Soil Using the Geotextile" was issued in February 1993, as a result of cooperative research project between Public Works Res. Inst. and private firms.

Since then, the reinforced retaining walls have been experienced several earthquakes such as Kushiro-oki earthquake in January 1993 and Han-Shin Awaji Earthquake in January 1995 in Japan and demonstrated high performance[3].

The manual was revised in February 2000 based on recent experiences as shown in Appendix 2[4]. The manual will be used effectively for future construction of reinforced soil structures.

REFERENCES

1) O. Matsuo, S. Nakamura: Report of the field survey on the 1999 Chichi Taiwan earthquake, Technical memorandum of PWRI, No.3707, March 2000 (in Japanese)

2) Leschchinski, D. (1999): Private communication to Tatsuoka.

3) F.Tatsuoka, M.Tateyama, and J. Koseki: Performance of soil retaining walls for railway embankments, A Special Issue of Soils and Foundation on Geotechnical Aspects of the January 17, 1995 Hyogoken-Nambu Earthquake, pp.311 – 324, 1996.

4) Public Works Research Center: Design and Construction Manual of Reinforced Soil Using the Geotextile, February 2000 (in Japanese)

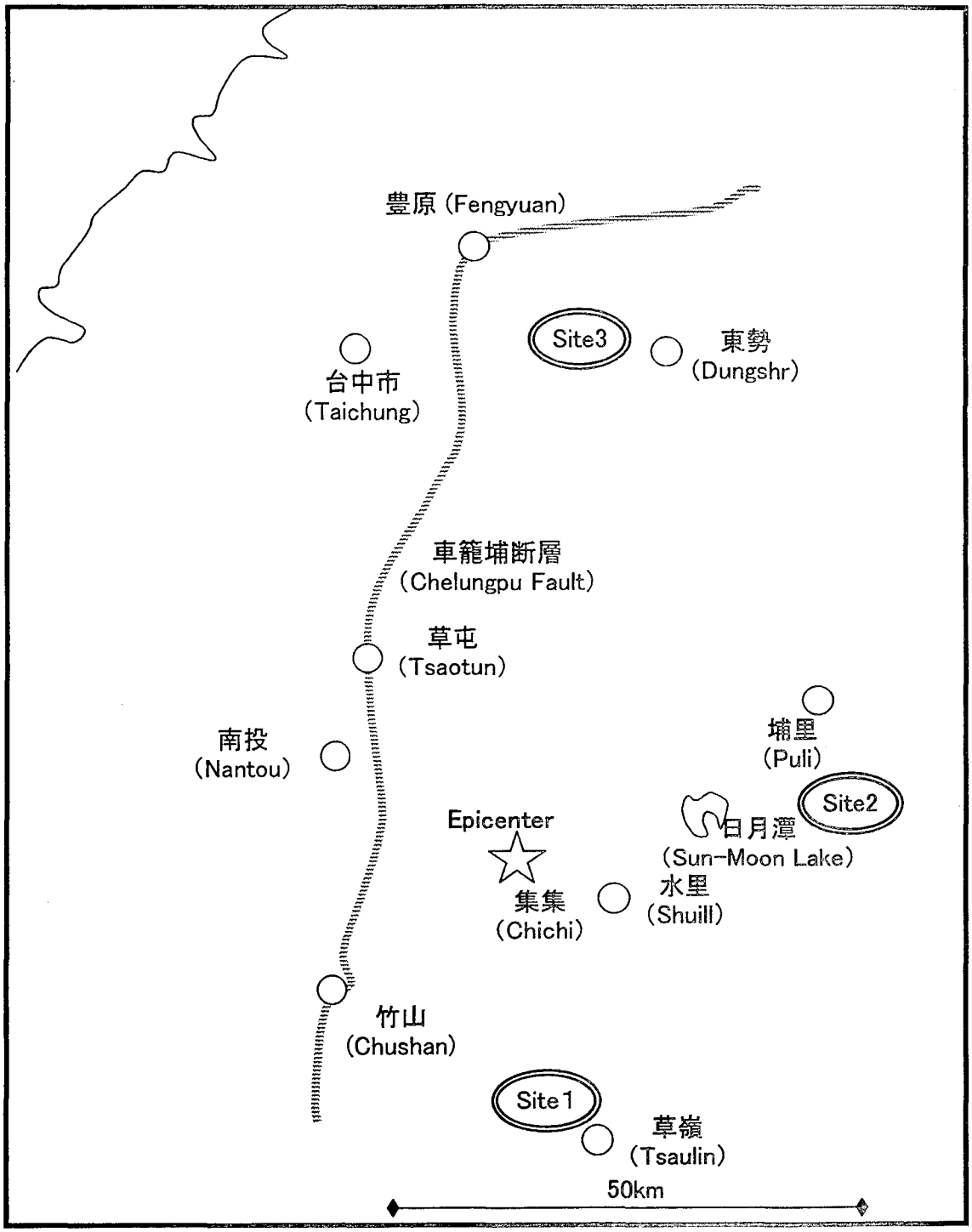

Fig.1 Central part of Taiwan

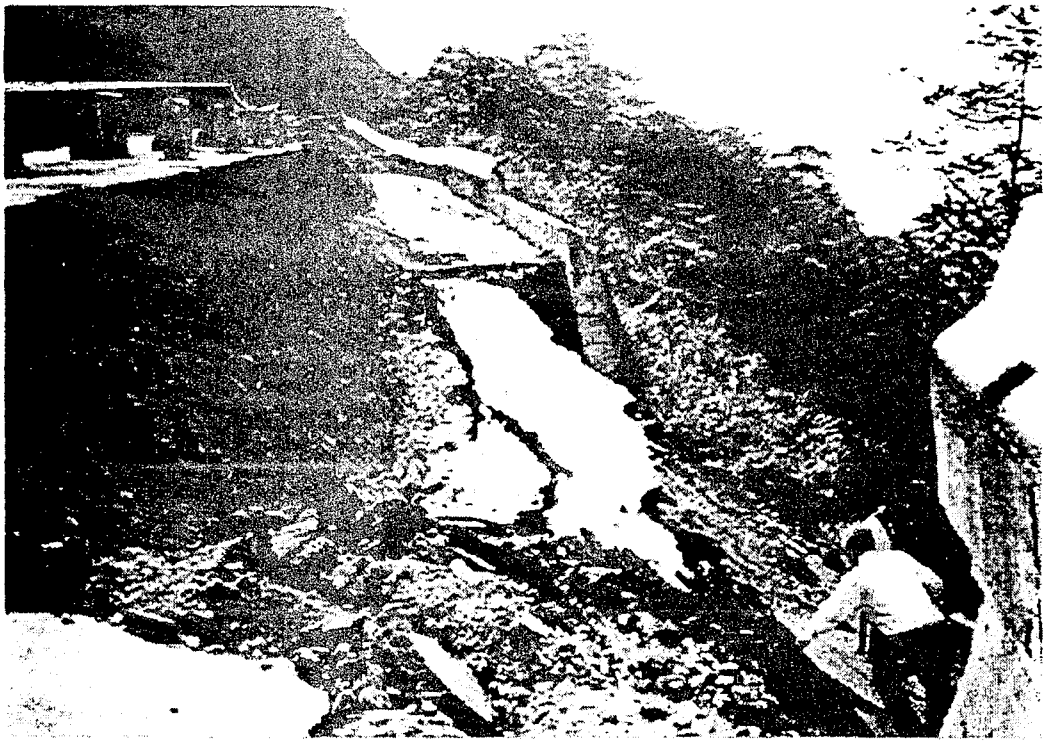

Photo.1 Collapsed gravity-type concrete retaining wall
(Site1 in Fig.1)

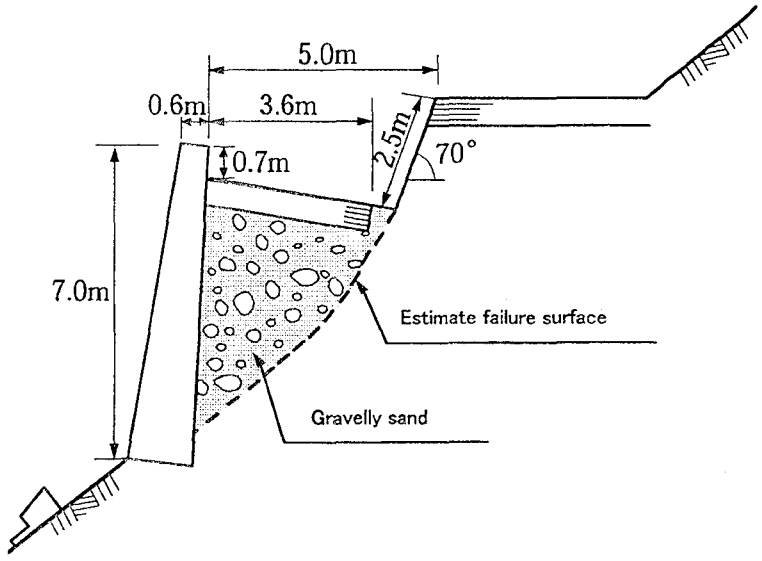

Fig.2 Cross section of collapsed gravity-type concrete retaining wall

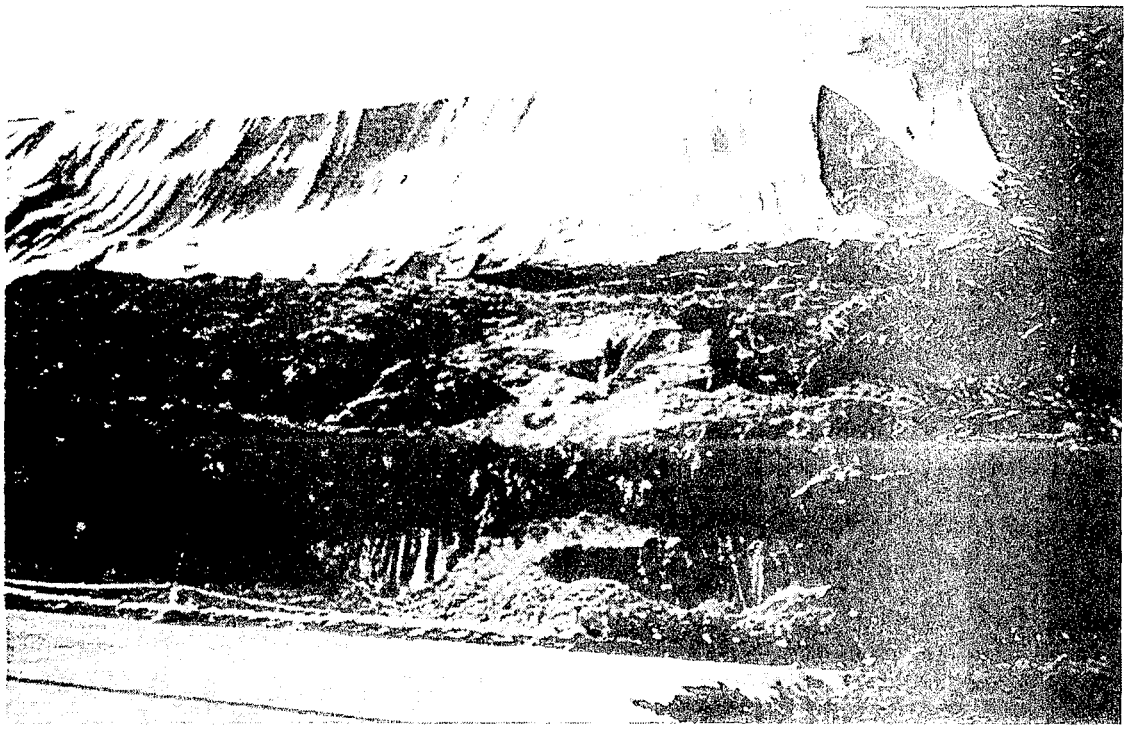

Photo.2 Front view of the collapsed geosynthetics-reinforced soil retaining wall(Site2 in fig.1)

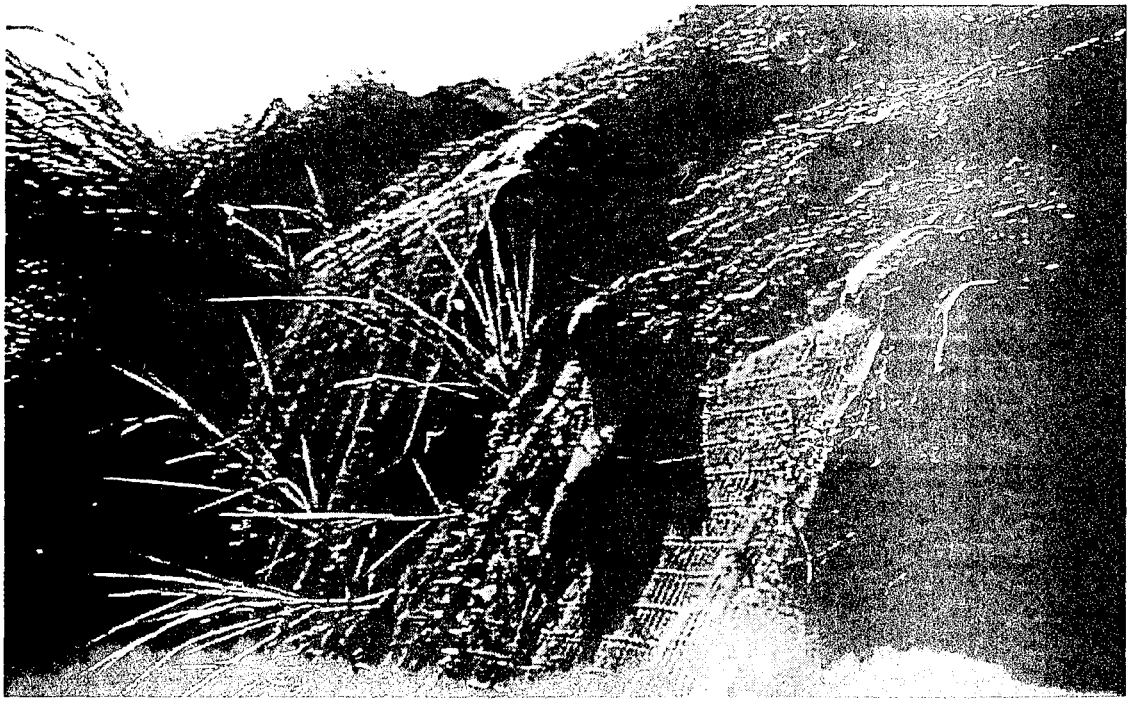

Photo.3 Failure of the reinforcement

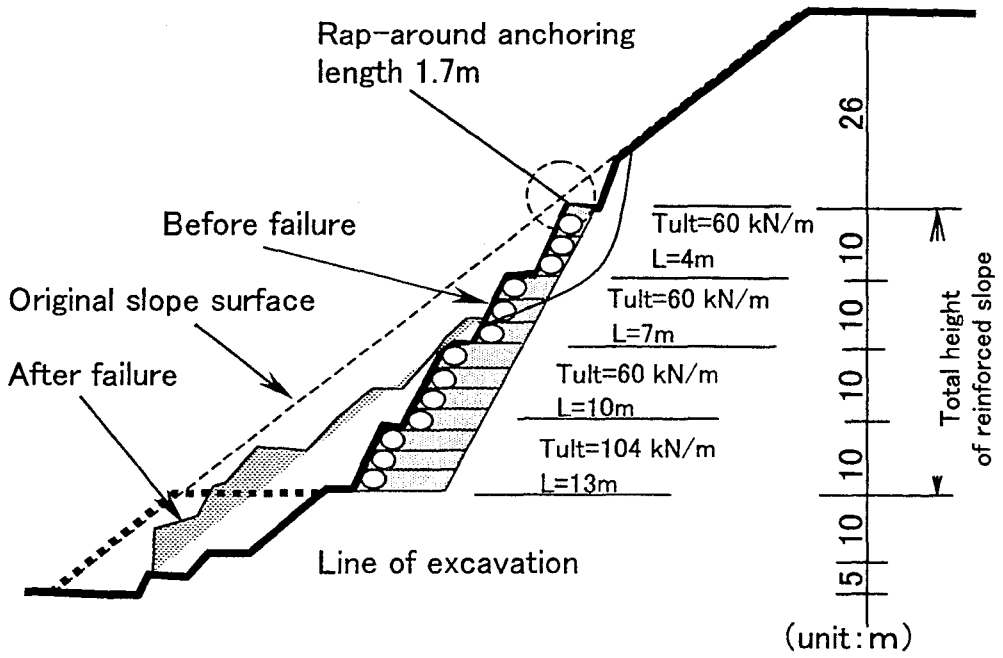

Fig.3 Cross section of the failed geosynthetics-reinforced soil retaining wall

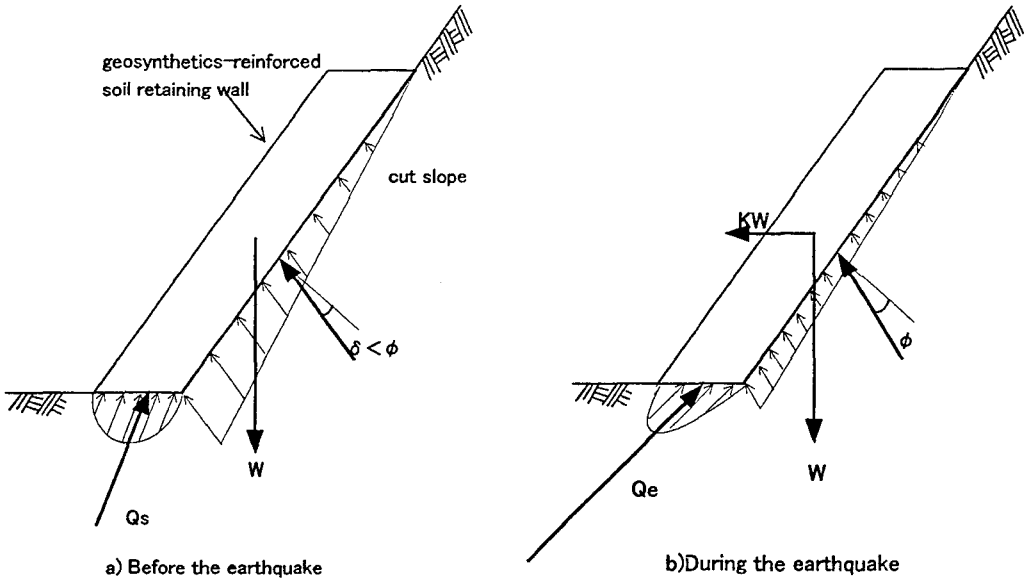

Fig.4 Schematics of forces acting soil retaining wall on the soil retaining wall

Photo.4 Collapsed segmental wall(Site3 in fig.1)

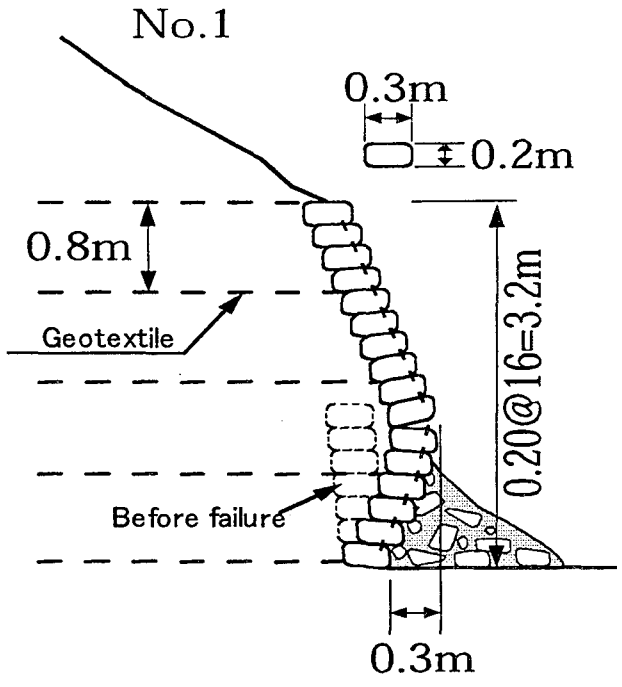

Fig.5 Collapsed segmental retaining wall

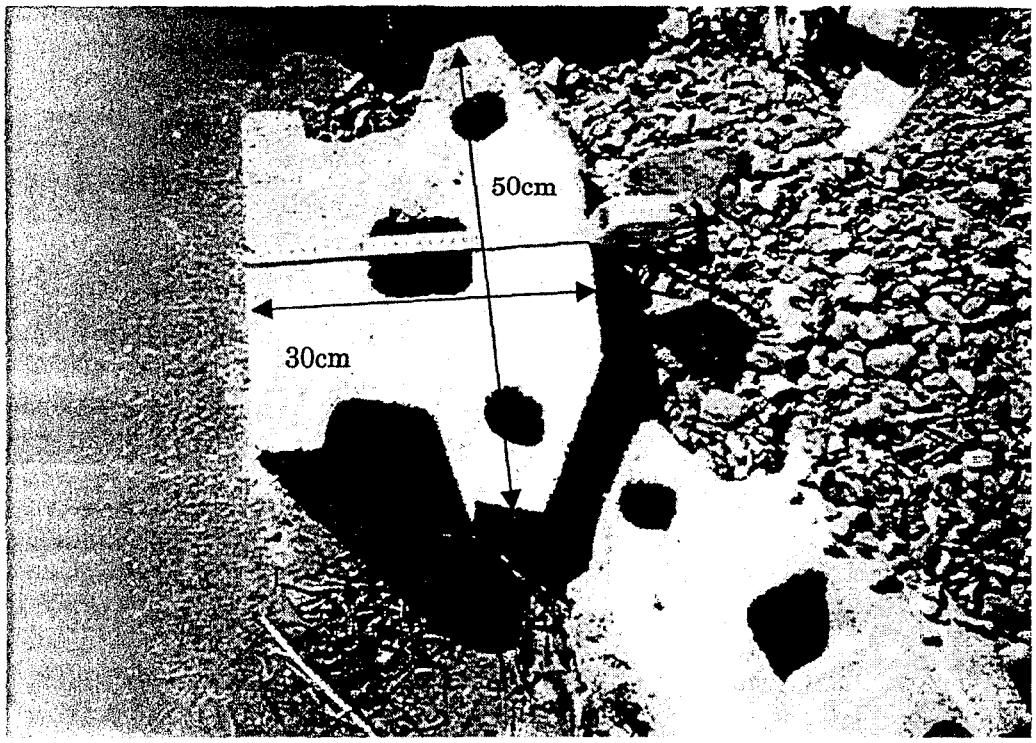

Photo.5 Shape of the block

Photo.6 Close view of the collapsed segmental wall

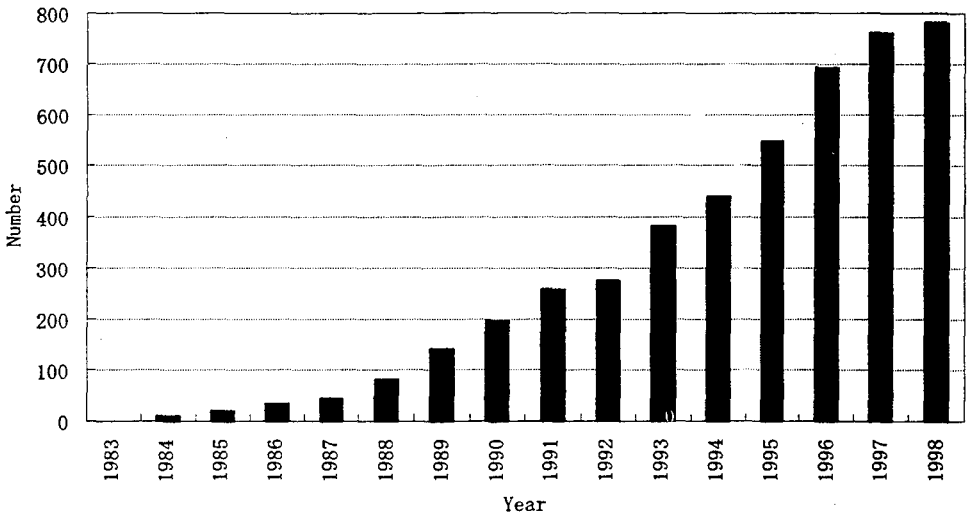

Fig. 6 A trend of construction works of reinforced soil wall in Japan

Appendix1 List of participants of the field survey

Osamu MATSUO: Head, Soil Dynamics Division, Earthquake Disaster Prevention Research Center, Public Works Research Institute, Ministry of Construction, Tsukuba, Ibaraki-ken, Japan
Shinya NAKAMURA: Senior Research Engineer, ditto.
Fumio TATSUOKA: Professor, Department of Civil Engineering, University of Tokyo, Hongo, Tokyo, Japan
Masaru TATEYAMA: Senior Research Engineer, Railway Technical Research Institute, Kokubunji-shi, Tokyo, Japan
Chin-Chuan HUANG: Associate Professor, National Cheng-Kung University, Tainan, Republic of China
Ichiro FURUTA: OYO Corporation, Nagoya-shi, Aichi-pref., Japan

Appendix2 Abstract of the Design and Construction Manual 2000 for Reinforced Soil Using the Geotextile, Japan

The abstract of the revised manual especially on the earthquake design procedure is shown as follows.

Classification of Reinforced Soil Structure

In this manual, the geotextile reinforced retaining soil is divided into two types; reinforced embankment and reinforced soil wall, depending on the slope gradient.

The definitions are given as follows.

(1) A Reinforced Embankment

This applies to the fill with a slope gradient milder than 1: 0.6. In the design, the stability of reinforcing area against earth load is not necessary to be considered. Stability check modes are in Fig.1.

(2) A Reinforced Soil Wall

This applies to the fill with a slope gradient steeper than 1: 0.6. In the design, the stability of reinforced area is examined on sliding, pull-out and rupture modes, induced by earth load. When the height of the reinforced soil is less than 8.0m, the seismic stability examination can be omitted, because it can be functionally safe for the earthquake of the usual scale, conditioned that design and construction are properly made. When the reinforced soil wall is located on crucial link of highway network and is considered, if once damaged, to take long time to restore, the seismic stability check should be carried out. Stability check modes are in Fig.2.

Types of the Reinforced Soil Wall

Typical types of the reinforced soil wall are shown in the manual as wrapping-around type (Fig.3), steel frame type (Fig.4), concrete panel type (Fig.5), concrete block type (Fig.6) and other types (Fig.7).

Earthquake Resistant Design of the Reinforced Soil Wall

Fundamentally, by replacing the seismic load with inertial force, the approach of the usual design is applied. The seismic stability check is based on the pseudo-static seismic force method.

Basic seismic design procedure is in Fig.8. And concrete content is as follows.

1) Design seismic intensity

$k_h = c_z k_{h0}$

k_h: Seismic intensity

k_{h0}: Standard seismic intensity (in Table 1)

c_z: Regional correction coefficient (1.0, 0.85, 0.7)

Table1 Standard horizontal seismic intensity

Type of Ground	I	II	III
Middle scale earthquake	0.12	0.15	0.18
Large scale earthquake	0.16	0.20	0.24

2) Seismic design safety factor.

Table2 Seismic design safety factor for reinforced soil wall

Types of safety factor		Design safety factor	
		Always	Earthquake
Internal stability	Sliding circle	≧1.2	≧1.0
	Tensile force of geotextile	≧1.0	≧1.0
	Pull out of geotextile	≧2.0	≧1.2
External stability	Sliding	≧1.5	≧1.2
	Tilting	e≦L/6	e≦L/3
	Bearing capacity	≧2.0	≧1.5
Wholly stability	Sliding include ground	≧1.2	≧1.0

Notes) e: eccentric distance from the center of the bottom of reinforced soil wall

L: bottom width of reinforced soil wall.

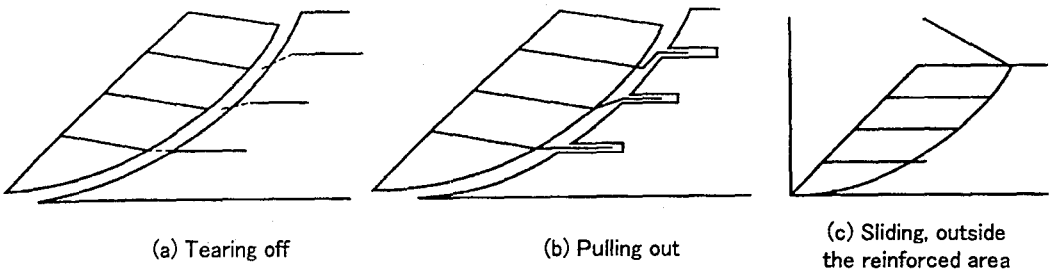

Fig.1 Stability check modes of reinforced embankment

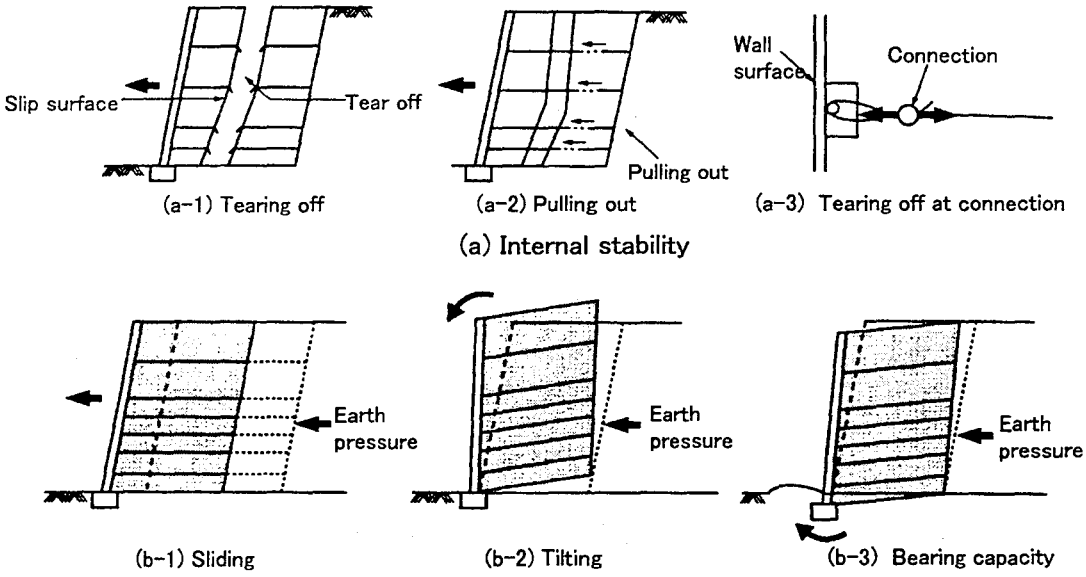

Fig.2 Stability check modes of reinforced soil wall

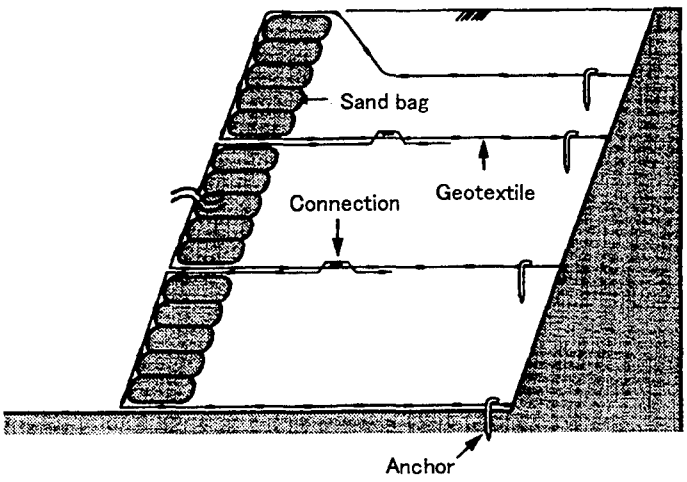

Fig.3 Wrapping-around type

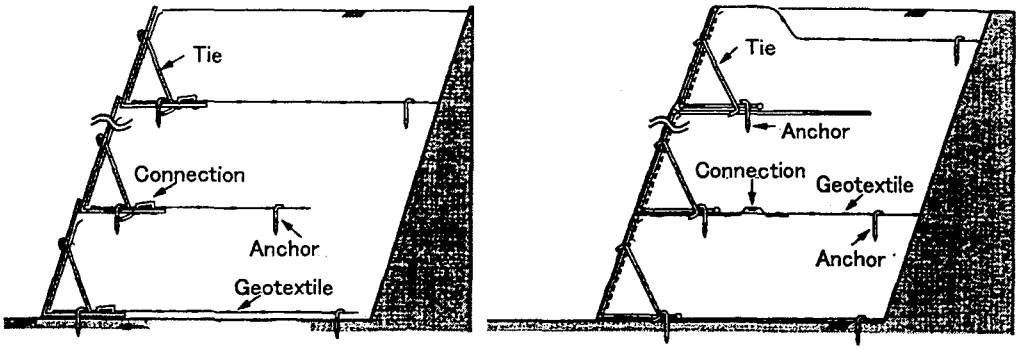

Fig.4 Steel frame type

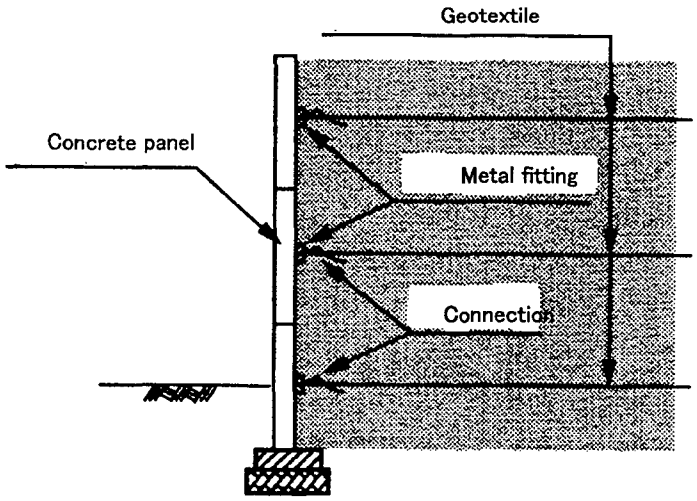

Fig.5 Concrete panel type

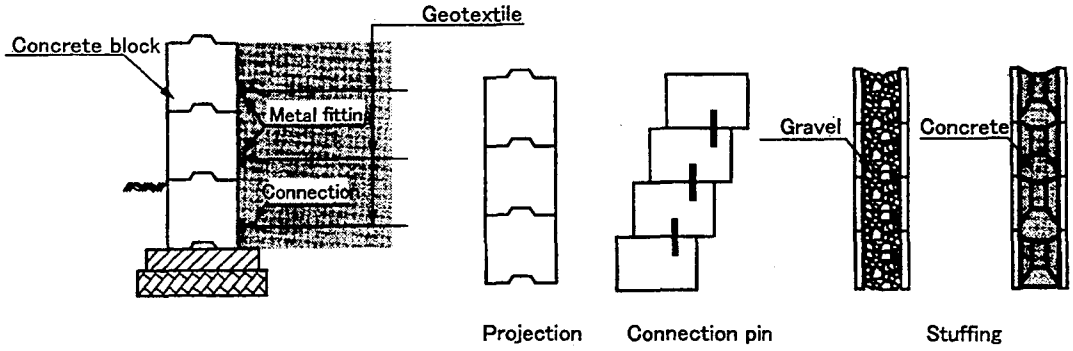

Fig.6 Concrete block type

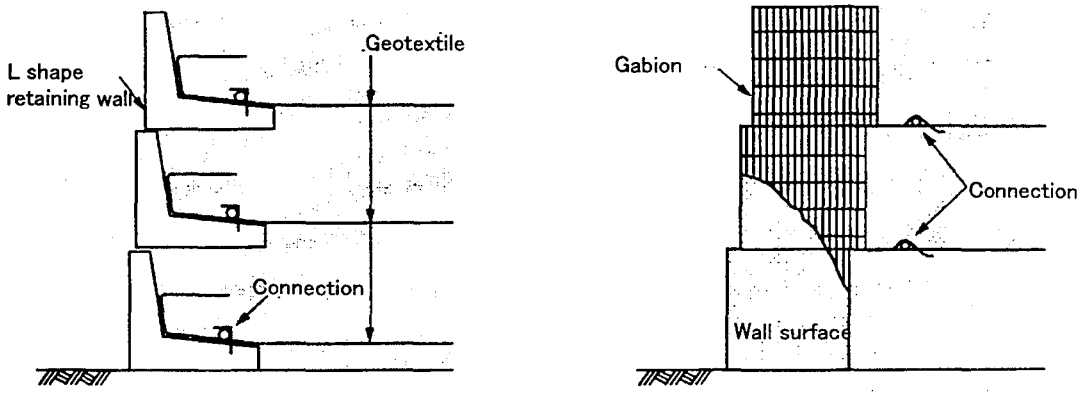

(a) L shape retaining wall type

(b) Gabion type

Fig.7 Other types

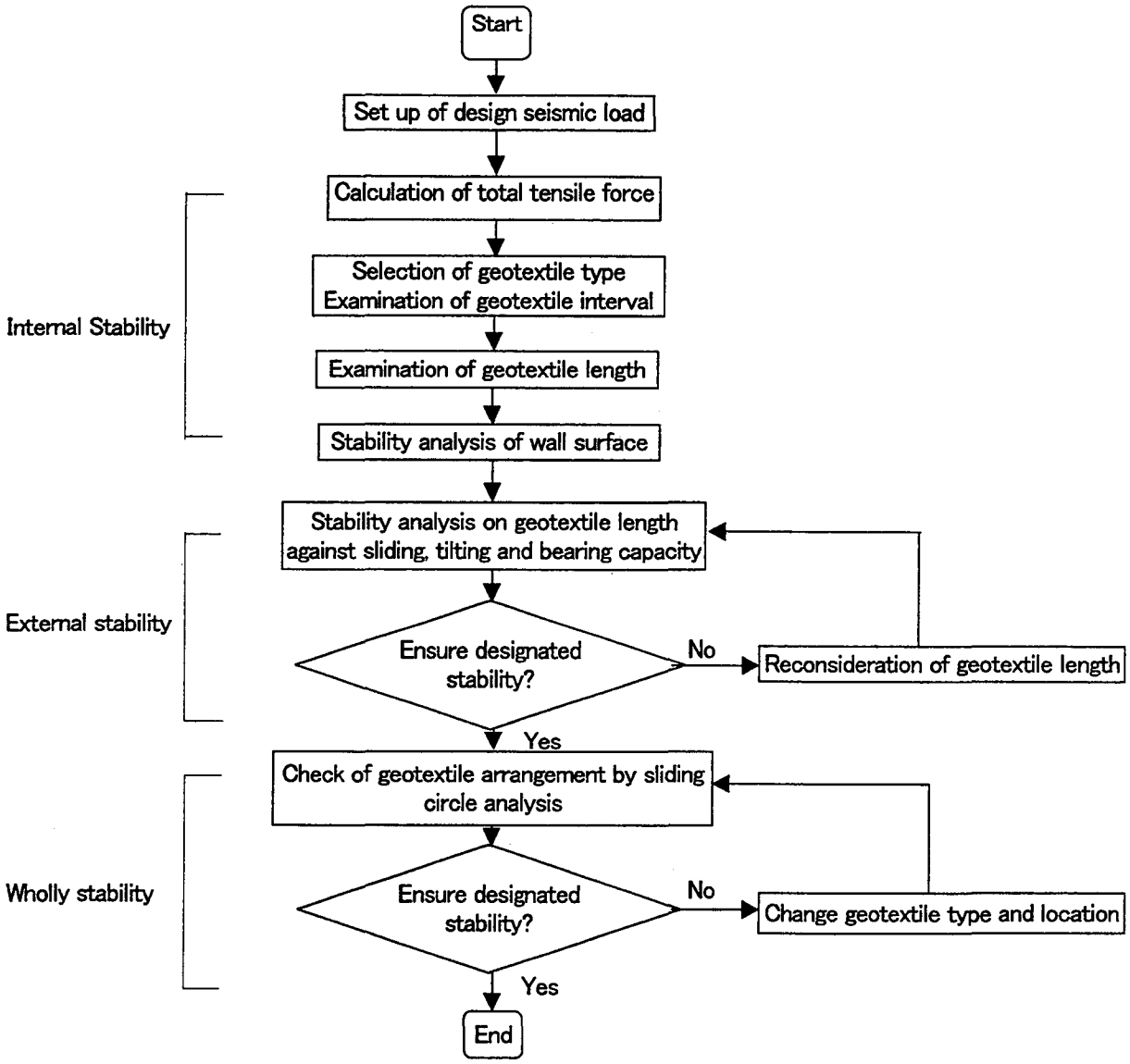

Fig.8 Procedure of seismic design of reinforced soil wall

HURRICANE MITCH RECONSTRUCTION PARTNERSHIPS AND PROGRESS

William E. Roper[1]

[1]Science Advisor for Sensing, Imagery, and Knowledge Systems
National Institute of Standards and Technology

ABSTRACT

A review of reconstruction efforts since Hurricane Mitch occurred and the application of information collected during the response stage are presented. A sample of geospatial technologies applicable to disaster management is presented. The application of Geo-spatial technologies following Hurricane Mitch in Central America is presented. Natural disasters have a major impact, globally and within the United States (U.S.) causing injury and loss of life, as well as economic losses. To better address disaster response needs, new approaches to leverage technological capabilities are described to improve disaster management. Geospatial analysis is one of these important capabilities.

KEY WORDS: Hurricane Mitch; Disaster management; Central America; Information Infrastructure; Disaster recovery; mapping; Geo-spatial library; LIDAR; Geographic Information Systems; Global Positioning System; satellite sensors; 3-D fly through.

1. INTRODUCTION

This paper will focus on an update of the reconstruction efforts that have occurred since the devastation of Hurricane Mitch in the fall of 1998. Particularly, the application of geospatial technology and methods to assist or support recovery and reconstruction activities will be reviewed and assessed. There has been significant capability growth in the geospatial areas of remote sensing, spectral analysis, global positioning systems (GPS), geographic information systems (GIS), and modeling and simulation techniques (Roper, 1998). Each adds important value in characterizing infrastructure, risk areas, disaster zones, and control points that are essential to rapid deployment of scarce resources in the most effective manner.

Natural disasters are a constant threat to mankind on a global scale. Global disaster costs are continuing to rise. Annual global economic costs related to disaster events average $440 billion per year (World Disaster Report, 1996) with floods being the major cause. In the U.S., the number of lives lost due to natural disasters has been decreasing over the last several deceased, largely because of advances in disaster indication and warning capabilities. In terms of damage to property, however, the trend is reversed. For the period 1992-1996, the average cost of natural disasters in the U.S. has been $54.3 billion, with hurricanes and earthquakes tied as the leading cause. These rising costs are the combined result of increased urbanization, particularly in high-risk coastal areas, and the increased complexity and size of our infrastructure.

The loss of life and property continues to rise in many regions of the world because of these events. One example is the Bangladesh weather event of 1970, when a tropical cyclone slammed into its delta region killing 300,000 people (Tobin and Montz, 1997). The crop losses were estimated at $63 million, and more than 280,000 cattle were drown (Burton, Kates, and White, 1993). The rich delta soil is an agricultural

resource that still draws people to settle there; therefore a recurrence of this type of weather event could likely pose a similar disaster.

2. GEOSPATIAL RESEARCH COMMUNITY INVOLVEMENT

The flow of disaster related information could be conceptually shown as a seven-step process as shown in Figure 1. The geospatial research community may have a role in each of these steps, depending on the particular disaster situation.

This could include assistance in defining the problem through current image analysis. Assistance in determining collection and analysis methodologies assists in defining the requirement. A key area of support is providing supporting data in the form of maps, imagery, and spectral information. An even more important support area is data exploitation. This includes the processing of digital data, image integration, feature classification and attribution, classification output, accuracy assessments, and post-processing operations. It is most technically challenging step in process. The decision support phase includes geospatial visualization, merged data analysis, and specialized decision support products. This involves the synthesis of data types in order is generate data layers (such as, soils, vegetation, terrain) along with models and simulation techniques that use the various data layers.

It is during this phase that the concept of virtual forums could take place. These forums would allow expert input from multiple locations to be jointly focused on problem solving for the disaster situation. Within the geospatial community this could include virtual fly-through support showing the impacts of possible decisions on the natural environment, and on the population, including those with special needs. It also could include analysis of changing situational information, and image-based change detection and analysis. In the final two phases, tailored map products and GIS overlay information can be used as integral parts of directives and guidance to disaster managers in the field. These specific products could be maps delineating evacuation routes, area identification for damage assessments, or point locations for water distribution.

The geospatial research community has typically been interdisciplinary, including the natural sciences, engineering, architecture, land use planning, photogrametry, etc. However, in the disaster management arena, broader interdisciplinary teaming will be required. This could include public policy and health specialists at the Federal, state, and local level. It may include other medical specialists, police, National Guard, and communications experts.

The greatest potential for loss reduction is during the mitigation phase (Disaster Information Task Force Report, 1997), when communities can be made more disaster resistant. The largest share of costs, however, are directed toward the recovery phase, where good mitigation principles also need to be put into practice rather than just rebuilding to be impacted by a similar disaster in the future. Geospatial products and location specific tools developed during the response phase of the disaster may be excellent vehicles for planning and implementing effective mitigation.

3. HURRICANE MITCH STORM TRACK AND CHARACTERISTICS

Hurricane Mitch, the strongest October hurricane ever recorded, formed in the southwest Caribbean sea from a tropical wave about 360 miles south of Kingston, Jamica, late on October 21. The system initially moved slowly westward and intensified to a tropical storm (Atlantic Hurricane Summaries, 1999). Mitch

then moved slowly northward. Its course changed to north northwestward on the 23rd and 24th while gradually gaining strength. Early October 24, Mitch became a hurricane. Later that day, as it turned towards the west, Mitch began to intensify rapidly. In about 24 hours, its central pressure dropped 52 MB to 924 MB by the afternoon of October 25. Further strengthening took place and the central pressure reached a minimum of 905 MB about 40 miles southeast of Swan Island on the afternoon of October 26. This pressure is the fourth lowest ever recorded in an Atlantic hurricane this century. It is tied with Hurricane Camille in 1969. This is also the lowest pressure ever observed in an October hurricane in the Atlantic Basin.

At its peak, the maximum winds were estimated to be 180 mph, a strong Category 5 hurricane. After passing over Swan Island, Mitch began to gradually weaken on October 27 while moving slowly west, then southwest toward the Bay Islands off the coast of Honduras. The center passed very near the Island of Guanaja wreaking havoc there. From mid-day on the 27th to early on the 29th, the minimum central pressure rose 59 MB. The center of the hurricane meandered near the north coast of Honduras from late on the 27th through the 28th before making landfall during the morning of the 29th about 70 miles east of LaCeiba with 100 mph winds. Mitch moved southward over Honduras, weakening to a tropical storm early on the 30th. Mitch moved slowly over Honduras and Guatemala on September 30-31, gradually weakening to a depression. The storm generated torrential rains over portions of Honduras and Nicaragua where the associated floods were devastating. Some heavy rains also occurred in neighboring countries.

Although Mitch originally dissipated near the Guatemala/Southeast Mexico border Sunday afternoon, November 1, the remnants continued to produce locally heavy rainfall over portions of Central America and eastern Mexico for the next couple of days. On November 3, a low-level circulation became evident in the eastern Bay of Campeche and an Air Force Reserve reconnaissance aircraft investigating the system reported tropical storm-force winds and a 99-MB central pressure. Mitch had regenerated into a tropical storm on the afternoon of the 3rd while located about 55 miles west-southwest of Campeche, Mexico. Mitch weakened to a depression early on the 4th as it moved inland over the northwest Yucatan Peninsula. The center re-emerged over the south central Gulf of Mexico by mid-morning on the 4th regaining tropical storm strength. Mitch began to accelerate to the northeast as it became involved with frontal zone moving through the aster Gulf of Mexico. Mitch made landfall on the morning of the 5th in southwest Florida near Naples with maximum sustained winds near 60 mph. By mid-afternoon of the 5th, Mitch moved offshore of south Florida and became extra tropical. Figure 2 shows the storm track of Hurricane Mitch.

4. INITIAL GEOSPATIAL SUPPORT OF MITCH RECOVERY ACTIVITIES

4.1 Initial Response Efforts

U.S. military forces were some of the first international support units on the ground conducting recovery operations. As a result, a number of requirements for geospatial products were identified early in the operations (Operations Summary, January 1999). In support of these requests, maps, country studies, water aerial appraisals and other available materials were collected and provided to the U.S. Army Corps of Engineers (USACE) Operations Center for use in immediate recovery operations, planning any additional deployments and future reconstruction efforts. Separate requests for ground water resource data were received from

support elements of the Second Mare Expeditionary Force and two Air Force Red Horse Squadrons (well drilling units) in Honduras. Maps and water area appraisals were provided to two Marine Expeditionary Forces. Water detection data was also provided to the Air Force Unit.

Initial analytical activities focused on assessing road and bridge damage in Honduras. Satellite imagery was reviewed and road and bridge assessment data were tabulated and served over the communication links. These data were keyed to a regional map, provided by the National Imagery and Mapping Agency (NIMA), to which a grid was added as an orientation aid for the user. Photomaps of the Soto Cano Air Base and a slide area along the Chaluteca River in Tegucigalpa were also prepared and provided to the Army Corps of Engineering Operations Center. The 30th Engineer Battalion, also in Honduras, requested specific Digital Topographic Data, and loan of high capacity hard drives to process data. The Topographic Engineering Center imbedded current imagery data on the affected areas onto 14 CDs and provided them to the 30th Engineers. These CDs contained Landsat and Spot imagery (Collier, 1999).

4.2 Joint Government and Private Sector Support

A cooperative effort of U.S. Government agencies and the private sector developed a Digital Atlas of Central America to assist in recovery efforts and planning for reconstruction. The geographic information system (GIS) based product provided a framework for displaying and organizing information in multiple layers useful to those responding to the disaster. Products were produced showing, for example, the path of Hurricane Mitch over a map with country boundaries and color-coding to illustrate terrain elevation (Digital Atlas, January 1999).

4.3 Geospatial Technology Applications

For the initial reconstruction phase, a number of geospatial products are needed to enhance planning and project executio. Virtually all activities associated with the reconstruction effort required large-scale (high resolution) base maps showing topography, drainage, and the location of roads, bridges, and massive sediment deposits from the flooded Rio Choluteca River within the city limits is of particular concern with the fast approaching rainy season. Also a major landslide during Mitch has left a large area of unstable ground immediately above the city. Figure 3 is an airborne image of a major sediment deposit area on the Rio Choluteca River where a major bridge was destroyed and many homes were washed away. Figure 4 shows the integration of the image information into a GIS database for use in planning reconstruction and also to potentially form a future framework for the information infrastructure in this geographic area.

Because of the vulnerability of the city of Tegucigalpa to additional flooding and landslides during the rainy season and the limited time available to put protection measures in place; the majority of the initial effort in developing action plans was placed on short-term solutions to the flooding and landslides. The effort to develop more long-term solutions required substantial additional data gathering and engineering analysis to determine the most cost effective solutions. These studies and data collection efforts have been underway and a series of proposed approaches have been developed. One of the focus areas is the reconstruction sewage treatment system. The report on this project should provide a plan showing the preliminary layout of the sewage collection system, pumping station locations, and location/alternate locations for the treatment plant. This effort would address alternate

treatment plant processes and the reason for selecting a particular process. The report would be coordinated with the city officials and three design review meetings would be held at Tegucigalpa. It was estimated that the report would take 12 months to prepare. For this project topographic maps and existing sewer system plans have been be reviewed and used extensively in developing the alternative treatment plant and system options. The service area and potential locations of the treatment plants have been developed and some construction has been initiated, but the progress over the last year has been slow and is well behind the original plan for reconstruction.

4.4 Summary of Initial Response Lessons From Hurricane Mitch

Hurricane Mitch was a natural disaster of epic proportion to Central America. The recovery and reconstruction efforts have also been of a magnitude not encountered before in that region. For the first time in a major disaster, extensive application of geospatial technology was used to assist in all phases of the recovery. A digital atlas and Geographic Information System was created for the impacted area to form a framework to integrate new data information over time in a systematic manner. Satellite, aircraft, and ground information sources were used to collect data and information to support the recovery activities. A variety of products were successfully generated tailored to user needs in the field and higher-level decision-makers in the recovery effort.

5. INTER AMERICAN DEVELOPMENT BANK RECONSTRUCTION SUPPORT

The Inter-American Development Bank (IDB) approved $597 million in financing for the countries of Central America that suffered severe damage from Hurricane Mitch during the one-year period immediately following one of the worst natural disasters ever suffered by the region. Simultaneously, at the request of Central American governments, the Bank identified more than $280 million in resources for projects that had been approved prior to the impact of storm that could be converted into financing for new programs for disaster recovery. Disbursements to the region reached $540 million in support of reconstruction in Honduras, Nicaragua, Guatemala and El Salvador. A major portion of Bank reconstruction financing was focused on social sector investments.

The IDB resources are part of a commitment by the international community to provide more than $9 billion in humanitarian assistance, long-term financing, and debt relief to countries stricken by Mitch. IDB President Enrique V. Iglesias reiterated that the institution expects to contribute about $3.4 billion over five years to the task of recovery and transformation of Central America, a region with deep and persistent social problems and a high level of vulnerability to natural disasters. "A year ago Central America's peoples suffered a catastrophe of biblical proportions," Iglesias said. "Now they are making progress on the monumental task of rekindling development. Although the challenge ahead is not something that can be resolved quickly and easily, progress is being achieved in the context of democracy and macroeconomic stability with the support of the international community" (Inter American Development Bank Web Page, 2000).

Hurricane Mitch unleashed over Central America in less than a week the equivalent of one year of rainfall on a region parched by eight months of drought. Its destructive force, made worse by diverse environmental problems, triggered massive flooding and landslides. Nearly 10,000 persons died because of the disaster and thousands more disappeared. Millions of Central Americans lost their homes,

their land, and their crops. Infrastructure that had represented decades of investment was swept away. Economic losses rose to more than $5 billion, the equivalent of 17 percent of the region's gross domestic product. The IDB responded immediately to the Central American crisis. The Bank sent technical missions to the four countries most affected by the disaster in order to assist IDB country offices in evaluating the damage, identifying available resources, and preparing the most urgent counter-measures. President Iglesias personally visited the region to learn the priorities of the Central American countries.

In the first few months following the destruction of Mitch, the Bank concentrated its assistance on emergency programs covering a wide program of activities, ranging from help in the preparation of national plans for reconstruction and transformation to support for social programs. Among other projects, the Bank supported rehabilitation of water and sanitation systems, rural roads, bridges, schools, rural health clinics, and other high-priority social services.

At the request of governments of the isthmus, the IDB organized a meeting of donor countries and multilateral organizations to form the Consultative Group for the Reconstruction and Transformation of Central America, an initiative to coordinate international cooperation. The group met at the headquarters of the Bank in Washington, D.C. in early December 1998 to analyze the response to the emergency and the preliminary studies, prepared by the United Nations, on the damage caused by the hurricane. The Consultative Group, chaired by the IDB, met again at the end of May in Stockholm, with support from the Swedish government. There the Central American countries presented their national plans for reconstruction and transformation. During that meeting the donor community also had an opportunity hear the opinions of representatives of diverse civil society organizations from Central America on the impact of Mitch. At the end of the conference, donors pledged more than $9 billion in assistance, an unprecedented amount for this kind of aid effort.

The Central American recovery plans, whose main documents can be accessed on the IDB's website (www.iadb.org), are designed to reactivate the economies, generate productive employment, reduce poverty, and promote the sustainable use of natural resources. They also seek to strengthen the democratic system of government at all levels, encourage the participation in government by the citizenry, and improve the mechanisms of prevention and mitigation of natural disasters.

In response to Mitch the IDB also organized regional workshops attended by officials from Central America and by experts from donor countries on social and environmental vulnerability, the reduction of the risk of natural disasters, and emergency management measures. The Bank also sent several missions to the region to discuss initiatives with the governments to improve the transparency and efficiency in the use of public funds, one of the major concerns of the donor community.

The IDB put special emphasis on programs to alleviate poverty, rehabilitate basic infrastructure, and protect natural resources. These projects are designed to improve the efficiency of services and increase their coverage to include the most vulnerable social groups as well as to encourage decentralization and the participation by the private sector and civil society organizations. One outcome of the financial assistance effort by the IDB has been a net positive flow of resources to the four countries hardest hit by the hurricane. In keeping with the Stockholm agreements, the Bank is due to hold in February a round of consultations at

the national level with Honduras and Nicaragua to analyze the progress in reconstruction and transformation.

In November of 2000, the regional consultative group will meet in Madrid at the invitation of the Spanish government to discuss Central American proposals. This forum will help highlight the region's strategic advantages in terms of its geographic location, access to major markets, and recent economic reforms designed to stimulate trade and investment. At the same time, a series of workshops will be held on regional development. Among the issues that will be discussed are the benefits of furthering Central American integration through road and electricity projects and initiatives to reduce environmental and social vulnerabilities by means of improved management of shared watersheds and the establishment of early warning systems for natural disasters.

6. PRIVATE SECTOR SUPPORT ACTIVITIES

An important component over the overall reconstruction effort in Central America has been voluntary contributions and support from private, commercial and charitable organizations. Such support is usually coordinated through international organizational structures and the host country receiving the support. Several illustrative examples are provided in this section.

6.1 Catholic Relief Services

On September 18, 1999 a bridge donated by J.F. White Construction in Massachusetts was inaugurated yesterday in Moseli, Nicaragua, a small village 250 kilometers north of Managua (Catholic Relief Services Web Page, 2000). Catholic Relief Services, which has an office in Nicaragua, worked with the construction company to relocate the bridge from Massachusetts to Central America. The bridge replaced one that was destroyed one year ago by Hurricane Mitch. The bridge spans the river between the states of Jalapa and San Fernando (Catholic Relief, 1999.

Following last year's hurricane, the Commonwealth of Massachusetts and local construction companies, working with the Archdiocese of Boston, joined forces and donated 37 Bailey bridges and related equipment to Catholic Relief Services for assembly in Honduras and Nicaragua. "Catholic Relief Services is extremely appreciative of the efforts of the Commonwealth of Massachusetts, the Archdiocese of Boston, and the numerous firms and individuals that have helped to make this assistance happen," said Louise Wilmot, Deputy Executive Director of Catholic Relief Services, who attended the ceremony. "This bridge will not only reconnect the 60,000 people who were left isolated since the hurricane destroyed the bridge, it will also link the people of Massachusetts and Moseli."

People in the rural region primarily support themselves through the production of rice, corn, coffee, lumber, and cattle. Without the bridge, they were unable to deliver their products to the markets, resulting in great losses of income. "This is an example of a public/private partnership responding in an innovative and important manner," commented Mark Snyder, Catholic Relief Services' Country Representative in Nicaragua. In Nicaragua, more than 100 bridges on primary and secondary roads were destroyed by the storm leaving many areas completely isolated. "The technical support and the bridges will make a tangible difference in people's lives here," Snyder said.

Catholic Relief Services is the official overseas relief and development agency of the U.S. Catholic community. Founded in 1943, today

the agency provides assistance to needy people in more than 80 countries.

6.2 Environmental Systems Research Institute (ESRI)

As part of the early support to Hurricane Mitch ESRI provided multi-hazard maps and information to emergency response organizations, military, national and local governments. The data will serve as an educational tool across the Central America by sharing geographic knowledge about local hazards and prompting mitigation of those risks (ESRI Web Site, 2000). These same geospatial based information resources can be used to assist in reconstruction and building Disaster-Resistant Communities. The focus is on promoting local preventive measures that will help reduce the loss of lives and property during disaster events. It is a commonsense approach based on three principles--preventive actions must be decided at the local level, private sector participation is vital, and long-term preventive efforts and investments are essential.

Some of the technology applications and methods provided to Hurricane Mitch recovery and reconstruction parallel current efforts in the United States under Project Impact being lead by the Federal Emergency Management Agency (FEMA). FEMA is taking a proactive approach to change the way the public deals with disasters. Project Impact: Building Disaster-Resistant Communities is a nationwide initiative that FEMA launched in October 1997. It helps communities protect themselves from the devastating effects of natural disasters with preventive actions that dramatically reduce disruption and loss. The initiative focuses on promoting local programs that will prevent extensive loss of lives and property during disaster events. It is a commonsense approach based on three principles—preventive actions must be decided at the local level, private sector participation is vital, and long-term preventive efforts and investments are essential.

Local agencies have detailed, hands-on knowledge of local issues, which makes them ideally suited to facilitate disaster planning, mitigation, and preparedness. And currently 120 communities throughout the United States are participating in Project Impact. FEMA is also recruiting other federal agencies and businesses into the program to help get the latest technology and mitigation practices implemented at the local level. Additionally, Project Impact is serving to empower communities as they pursue smart growth strategies while strengthening the federal government's partnership with local government.

A common thread that weaves its way through every phase of Project Impact is GIS. Most of the data requirements for disaster management are of a spatial or geographic nature, and that makes GIS the logical tool. Identifying potential hazards, planning mitigation programs, and assisting in disaster preparedness activities are some of the critically important roles GIS has taken on for the Project Impact communities. With GIS, local agencies can compare maps of hazards such as earthquake faults, fire risk areas, or flood areas to other map data. Locating streets, pipelines, hospitals, residential areas, power lines, and storage facilities in relation to known hazards on maps makes the process seamless.

7. CENTRAL AMERICA RECONSTRUCTION ACTIVITY SUMMARY

Since Hurricane Mitch struck Central America, project participants and local governments have worked to help people recover from the storm's tremendous damage. The four Central American

countries hardest hit by Hurricane Mitch in 1998 have made immense progress. More than 21million storm victims have been assisted through programs in Nicaragua, Honduras, El Salvador and Guatemala.

The first two phases of post-storm operations in the Central America emergency response and rehabilitation are largely finished. In the next phase, project participants will adapt long-term development work to incorporate ongoing recovery work that has at its core the promotion of community organization, building capacity of local governments, and the formation of a trust-based link between communities and their governments. This critical link is needed to achieve a sustainable recovery. Transportation will be one of the focuse areas. There are many remaining bridges and roads that need repair and replacement throughout Central America (Figure 5). Simultaneously, capitalize will continue on its efforts to strategize regionally across the four Central American countries. From the geophysical to the political, the social to the economic, Honduras, Nicaragua, El Salvador and Guatemala share characteristics that should be addressed across national borders (US AID Web Site, 2000).

There remains a commitment to the transformation of Central America over the long term, and programs will continue to work in collaboration with communities, local governments and local nongovernmental organizations -- as well as to advocate at the national and international levels -- ways to improve the lives and livelihoods of the marginalized people of the region. A summary of activities completed and underway in each of the four countries are described in the following sections.

7.1 Nicaragua

Mitch-related activities are being transformed into larger development programs, mirroring the approach used in neighboring countries. The current work includes, categorized as sustainable agriculture and environmental protection; housing repair and reconstruction; temporary employment; and water and sanitation, are summarized below:

Sustainable Agriculture and Environmental Protection: In Matagalpa Department, Agricultural Rehabilitation Project now largely focuses on development rather than rehabilitation activities, although farmers badly affected by Mitch will continue to receive extra assistance until the end of the year. This project helped over 3,000 households rehabilitate and protect their agricultural and forested lands and reestablish crop production. The Agriculture and Environment Project, operational throughout 1999 in León and Matagalpa Departments, helped 1,785 families diversify their food production and reforest about 250 acres of land. It is intended to extend this project for at least an additional year, and link it to agricultural rehabilitation and improvement in Posoltega. There, work will continue through November 2001 with residents of Finca Santa Maria (see housing repair and reconstruction, below) and 1,150 other families in the area to reestablish crop and small livestock production, identify and test alternative crops, and develop irrigation schemes where feasible. The Seeds and Tools Project (Estelí and Matagalpa) included Erosion Control Project (Matagalpa) and La Esperanza Project (Ciudad Darío).

Housing repair and reconstruction: The Vivienda Estelí Project helped 142 homeless families reconstruct their houses. By October, all 142 houses were completed, each with a water tap and a sanitary latrine. Participants in the Estelí Rural Infrastructure Project will soon finish building a road to the small community, after which residents, and the municipal

government of Estelí, will hold an official opening ceremony.

In October 1999, housing reconstruction projects were launched in La Trinidad and Posoltega. In both places, problems obtaining legal title to suitable land delayed project start-up. In La Trinidad, participants will build 49 houses in a jointly planned community. In Posoltega, 350 families will build homes over the course of the next two years. Figure 6 shows some of the reconstruction activities underway. In most cases reconstruction is being done above historical high water lines. There are still some ateas where expedient reconstruction is accuring in the flood plain. The resulting Finca Santa Maria community will include a school, health facilities, green spaces and a water system. Participants also have been engaged in ongoing agricultural rehabilitation and a good local harvest from the first post-Mitch agricultural season was also very positive. Other organizations will contribute counseling through the agricultural training center and several small economic activities project to the residents of the future Finca Santa Maria.

Temporary employment: In Condega, Pueblo Nuevo and San Juan de Limay municipalities of Estelí Department, the Rural Infrastructure Project created short-term employment opportunities through cash for work projects. In October funding was secured for an additional two years of project activities. During the project's first phase, one or more members of more than 2,100 households in 60 communities rebuilt 101 kilometers of road, cleared riverbeds of flood debris, and built retention walls and sewers.

Water and sanitation: The Water and Sanitation Project in Matagalpa and Jinotega that was recently transformed into a one-year development project rehabilitated 65 water systems and 204 wells serving a total of 35,880 people. In Chinandega, the El Viejo Water Project will continue into 2000, providing participants with new water systems and latrines and the training to maintain and repair them. The Betesda Water Project in Posoltega reestablished clean water for 800 people and built 92 latrines. As mentioned above, a water system forms part of the ongoing work in Finca Santa Mario, and also in the Posoltega area.

7.2 Honduras

There were seven Mitch-related projects in Honduras. Four of the projects are now finalized, and two will conclude within a few months. The seventh has evolved into a three-year development project, in line with a longer-term recovery strategy in the Central America region. Among these projects are river channel clearing and construction and stream bank stabilization to reduce the threat of future flooding. Figures 7 and 8 illustrate some of the ongoing projects in this area.

Food for Work: The food for work program began in December 1998 and ended in October 1999. The project encompassed agricultural recovery, environmental rehabilitation, and infrastructure repair and construction in 51 municipalities in 10 departments. In all, 36,000 families received basic food commodities -- maize and beans -- in exchange for their work. An additional 2,000 pregnant or lactating women and children under 5 received supplemental food in the chronically food-poor departments of Lempira and Intibucá. With tools and other relevant supplies participants rehabilitated farmland, restored water and sanitation systems, rebuilt bridges and retaining structures along riverbanks and repaired houses damaged by the storm. With the addition of seeds and tools from many Food for Work participants were able to again produce food for their families. The objectives were to ensure the short-term survival needs of families while

helping them restore their productive capacity and support their economic revitalization. In all cases, Food for Work projects was three-party agreements between project sponsors, participants and municipal governments. Construction and digging tools, seeds and agricultural tools, and other items required by communities in their rehabilitation and construction work were provided This project component was finalized in September 1999.

Resettlement of the Homeless: In early October, heavy rains caused renewed flooding on the Choluteca River. Families were forced from temporary housing into their newly- or partially-built homes in Renacer Marcovia, a community planned and constructed for approximately 3,000 residents of the original Marcovia village, which was destroyed by floods a year ago. Today, 254 houses are complete and 226 houses are nearing completion. The project had installed temporary latrines and water tanks, which served until January 2000 when permanent sanitation systems were built. Renacer Marcovia's population has played an important role in planning the new village's public and residential areas, and has provided all the labor for the cement-block homes.

Reactivating Household Economies (REMAM): As of late October, 177 community credit committees in 150 communities had disbursed loans averaging $195.60 to nearly 2,300 families. More than 70 percent of borrowers had launched small-scale commercial activities, and the remainder opted to begin production or food processing businesses. The REMAM project, an emergency economic rehabilitation program, will continue through January 2000, disbursing loans to a total of 3,000 families in six departments, including the families participating in the Renacer Marcovia project.

In the first phase of the Choluteca and Valle Water and Sanitation project 18 communities repaired or rebuild storm-damaged water systems in eight municipalities of Choluteca and Valle Departments. By the end of October, eight of the water systems had been designed and three systems were under construction. CARE and municipal authorities surveyed and registered as protected areas the fragile watersheds that feed these systems and that provide water for 500,000 people. Watershed management training was provided for municipal authorities, and a signed a agreement was made with the Honduran National Forestry Authority to provide additional training and support to the project. This water, sanitation and environmental protection project will continue until April 2002.

Debris and Sediment Management: The cleanup, removal and disposal of debris and sediment is still underway in the branches and main stems of the major drainage basins. Much progress has been made, but many areas still need attention in order to reduce the risk of future flooding as shown in figure 9.

Hygiene Education for Urban Populations: This work, finalized in September, complemented the Tegucigalpa Child Survival Project by training 800 community members and health workers to deal with water and sanitation issues in disaster situations, to administer water committees, and to manage post-traumatic shock. Nearly 1,500 primary school students learned about health and hygiene through this project component, and residents of 24 urban slums completed infrastructure projects, repairing or building latrines, drainage canals and retaining walls in their neighborhoods. There remain many health and sanitation issues throughout the country as shown in figure 10. In the case of the Villaneuva Water and Sanitation Education Project it helped 1,275 families in

Villanueva municipality overcome water and sanitation problems resulting from the hurricane. Technical assistance was provided and materials to build a 80,000 gallon water storage system, the municipal government and other sponsors installed the principal branches of the water distribution system; and project participants were responsible for installing connections to bring water to their homes or communal taps. Training representatives of the participating communities in system maintenance was also part of the overall process of community organization and participation. Projects will continue in Honduras to address water and sanitation, environmental protection, sustainable agriculture, education and child health.

7.3 El Salvador

Mitch-related emergency and rehabilitation work in El Salvador has transitioned into two longer-term development programs that will assist people in three Eastern and western regions of the country (360,000 people and 163,000 people, respectively) to manage clean water systems, maintain basic sanitation facilities, protect the environment and rehabilitate agricultural systems over the coming years. A third project in Usulután helped 12 families rebuild houses damaged by floods last year. The development programs in El Salvador will focus heavily on water supply, environmental protection and sustainable agriculture.

7.4 Guatemala

The last of the Mitch rehabilitation activities in Guatemala helped residents rebuild 19 suspension footbridges damaged or destroyed by flooding. In all, these bridges provide access to 93 communities and about 4,000 families. Since the hurricane struck, Mitch-related work in Guatemala has included emergency response, water and sanitation system rehabilitation, agricultural recovery, reforestation and watershed protection in the Polochic river basin, Alta and Baja Verapaz Departments. Ongoing development work in Guatemala includes village banks, health, agriculture and environmental protection and education.

8. CONCLUSION

The opportunity to leverage technology in the geospatial area to assist in disaster management has never been greater. There are many tools and processes currently in use that have not been applied to assist in disaster management. Examples include the application of hyperspectral sensor data, use of digital multispectral video, and geospatial 3-D fly-through analysis. All of these capabilities could support and enhance the information available to the disaster management decision-maker.

There are exciting changes expected to occur during the next few years in the few years in the geospatial community. New aircraft and space-based sensor systems are planned that will revolutionize the spectral and spatial resolution of data available for commercial applications. There will be challenges, particularly in the data processing and management area, because of the extremely large spectral databases these new sensors will generate.

The spectral library project also provides an opportunity to expand cooperatively our global understanding of the vegetative and geologic spectral makeup of the earth. The baseline data from this effort would be invaluable in conducting change analysis assessments following a natural disaster, such as an earthquake or hurricane. Using some of the analysis tools described earlier, the analysts and decision-makers could virtually walk into the disaster situation. Other spectral technologies, such as fluorescence, could be used to precisely

locate very small underground gas and oil leaks remotely. Within the next decade, there may be the ability to better harness geospatial analysis capabilities to help reach the vision for the cooperative exchange of timely, relevant information useful during all phases of disaster management - to save lives and reduce economic loss.

9. REFERENCES

Atlantic Hurricane Summaries for 1998, Accu-Weather Service, April 1999

Burton, Ian, Robert W. Kates, and Gilbert F. White, The Environment as Hazard, 2d Edition, New York, NY: The Guilford Press, 1993

Catholic Relief Program, Web Site, www.crp.org, May, 2000

Collier, Vincent, Hurricane Mitch Summary Report, U.S. Army Topographic Engineering Center, March 1999

Digital Atlas of Central America, Version 1.0, Center for Integration of Natural Disaster information, U.S. Geological Survey, February 10, 1999

Disaster Information Task Force Report, Harnessing Information and Technology for Disaster Management, Global Disaster Information Network, 1997

Environmental Systems Research Institute, Web Site, www.ersi.com, May, 2000

Inter-American Development Bank, Web Site, www.iadb.org, April, 2000

Operations Summary, Interagency Support to Hurricane Mitch Reconstruction, U.S. Army Corps of Engineers, January 25, 1999

Roper, William, Geospatial Analysis Support to National Disasters, U.S.-Japan Wind
And Seismic Panel, International Conference, Washington, DC, May 1998

Tobin, Graham A., and Burrell E. Montz, Natural Hazards: Explanation and Integration, New York, NY: The Guilford Press, 1997

United States Aid for International Development, Central America Support and Development Activities, Hurricane Mitch Recovery, Web Site, http://www.info.usaid.gov, May 2000

World Disaster Report, Disaster Relief Task Force, United Nations, March, 1996

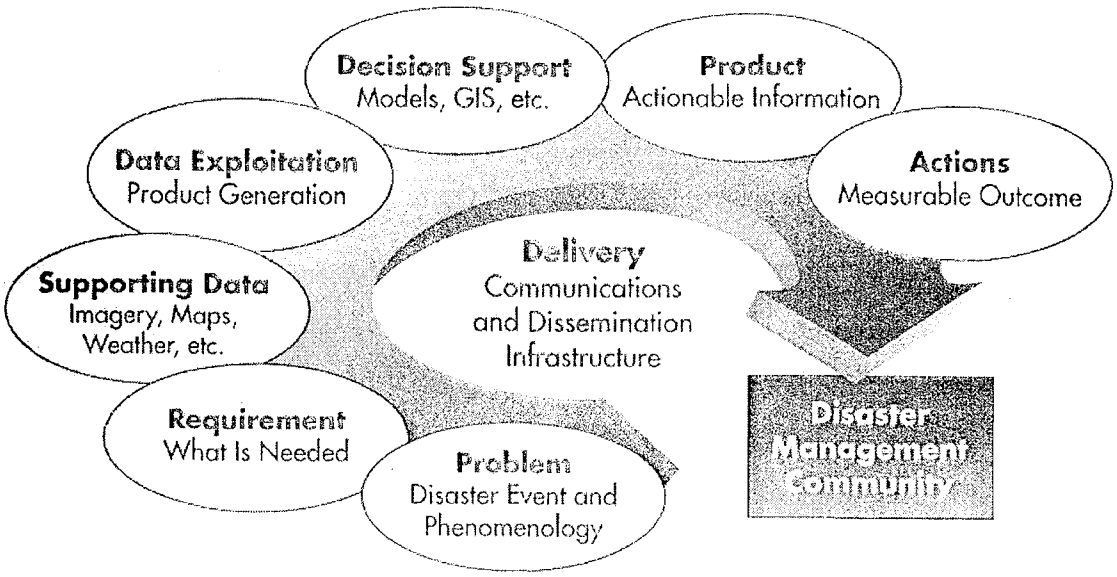

Figure 1: The Primary Elements of Disaster Management

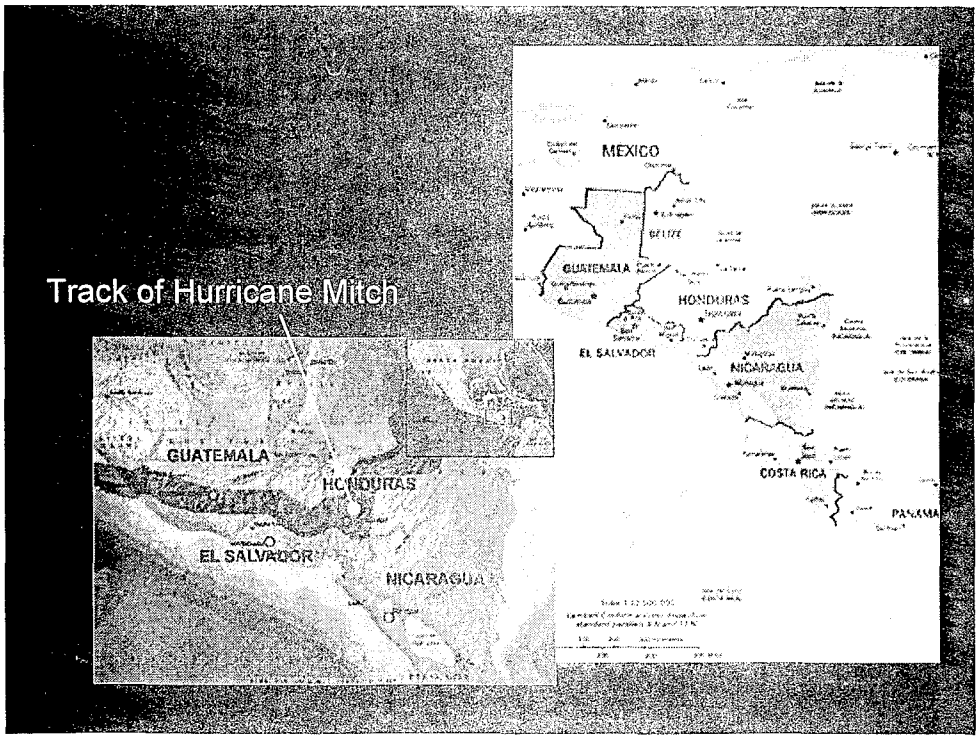

Figure 2: Storm Track of Hurricane Mitch Across Central America

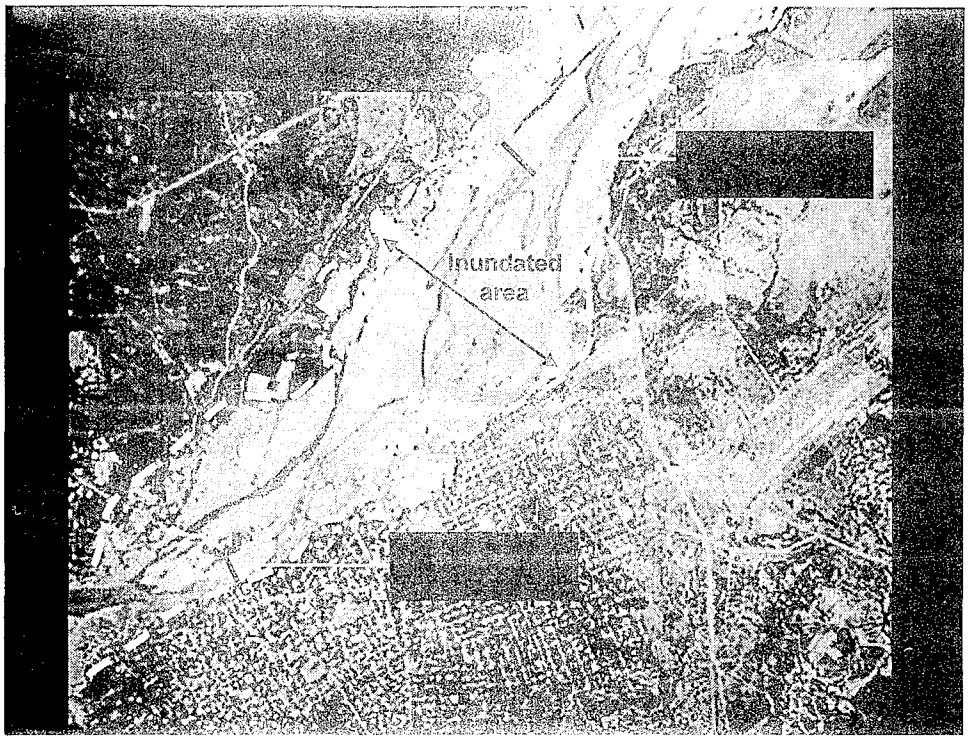

Figure 3: Airborne Sensor Image of Choluteca River Sediment Deposits near Choluteca City

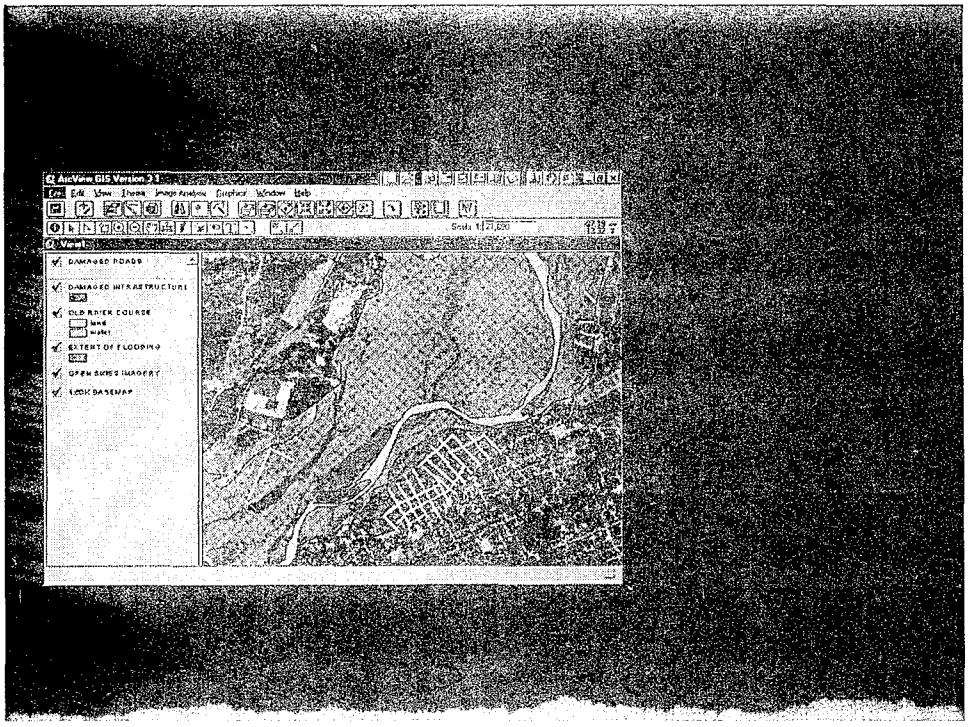

Figure 4: Integration of Imagery into GIS Data Base

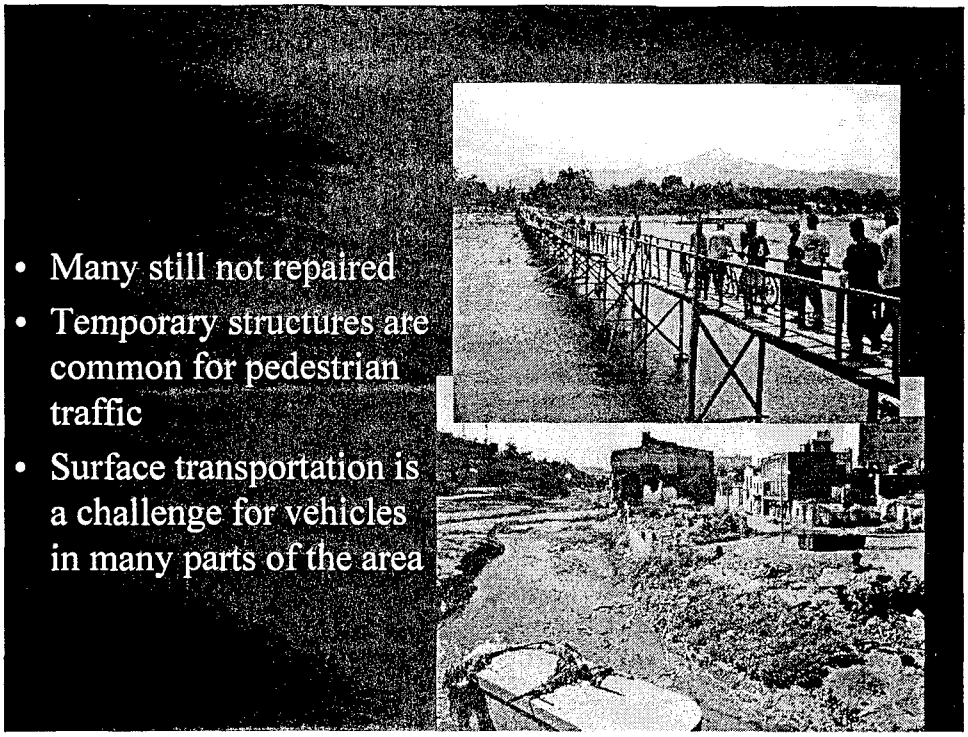

Figure 5: Temporary foot bridges and Damaged Bridge Infrastructure

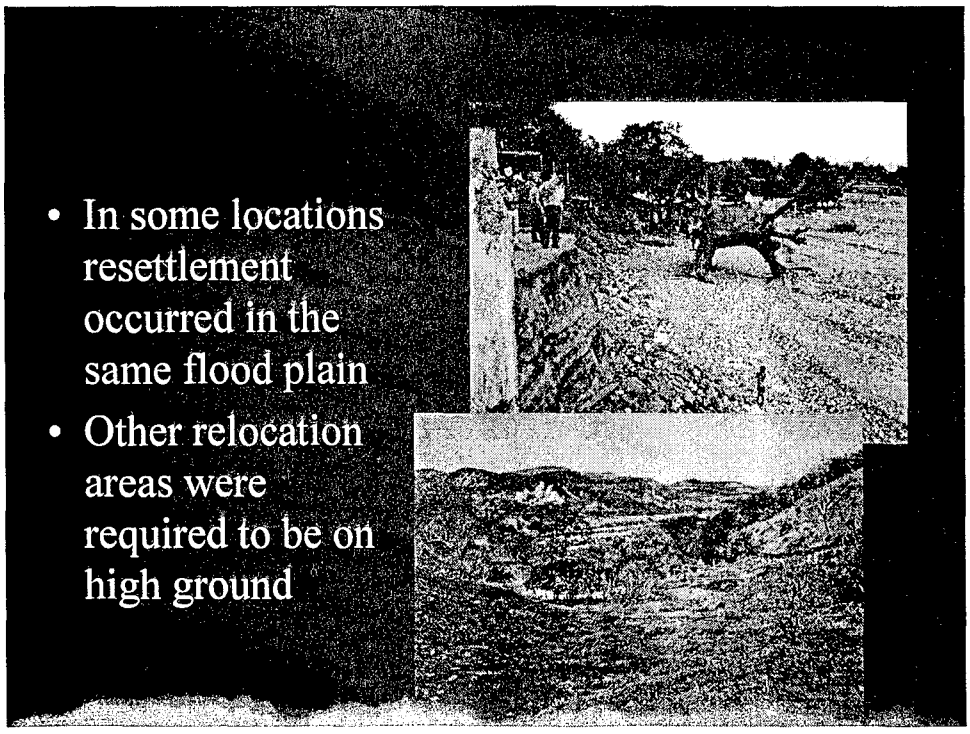

Figure 6: Policy Variations in Resettlement and Relocation Practices

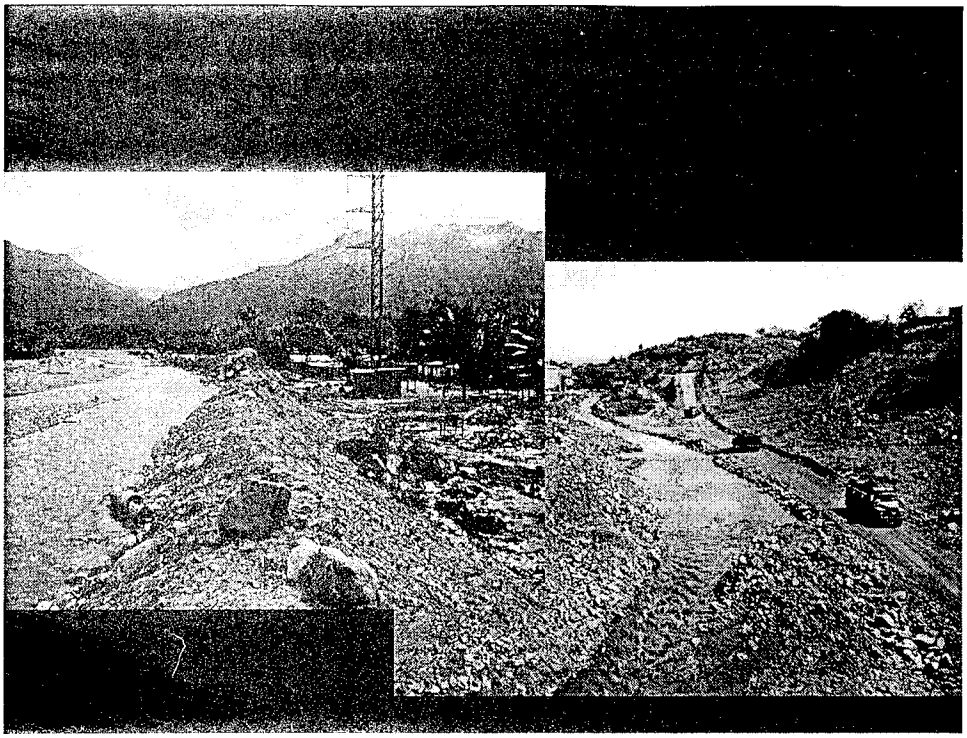

Figure 7: Preparation for Future Flood Protection Through Channel Clearing and Construction

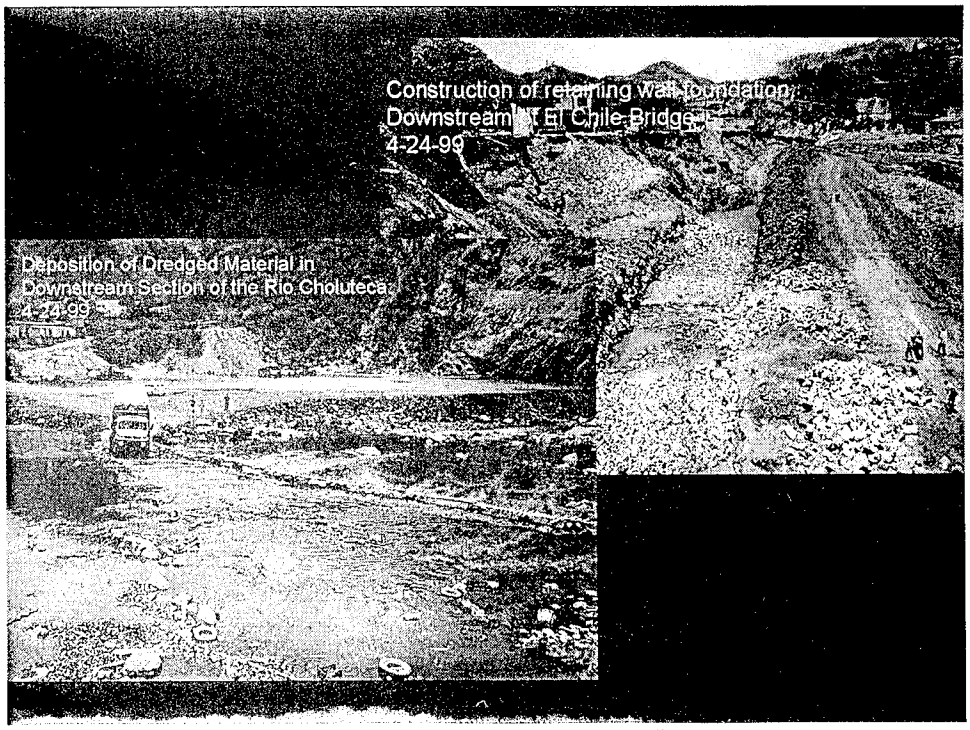

Figure 8: Stream Bank Stabilization Projects

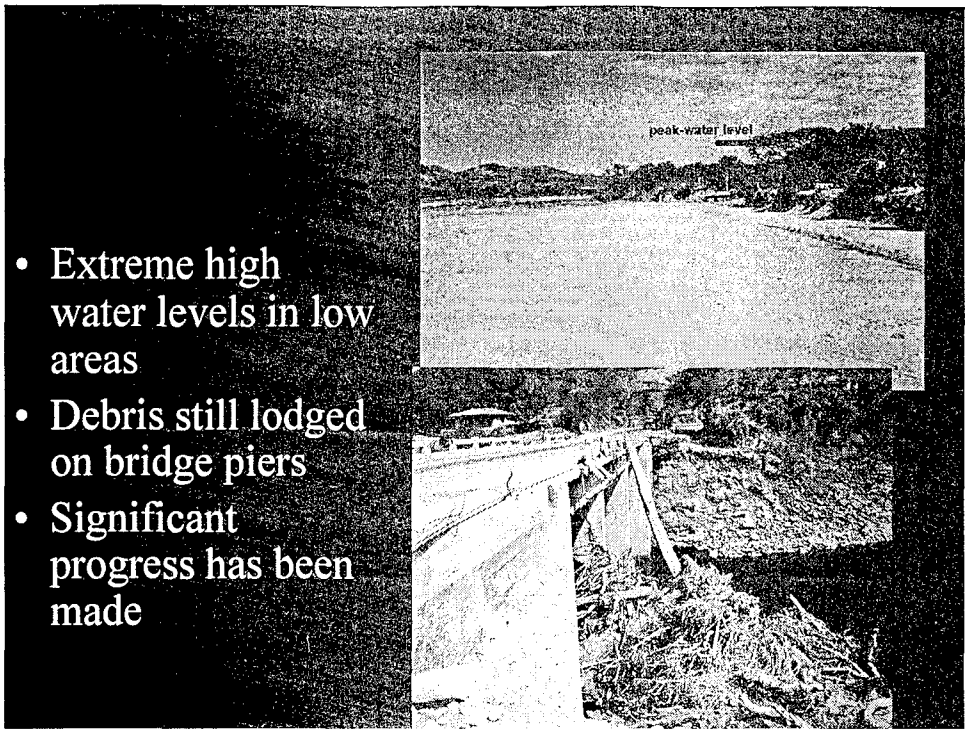

Figure 9: Debris and Sediment Management Challenges Along the Choluteca River

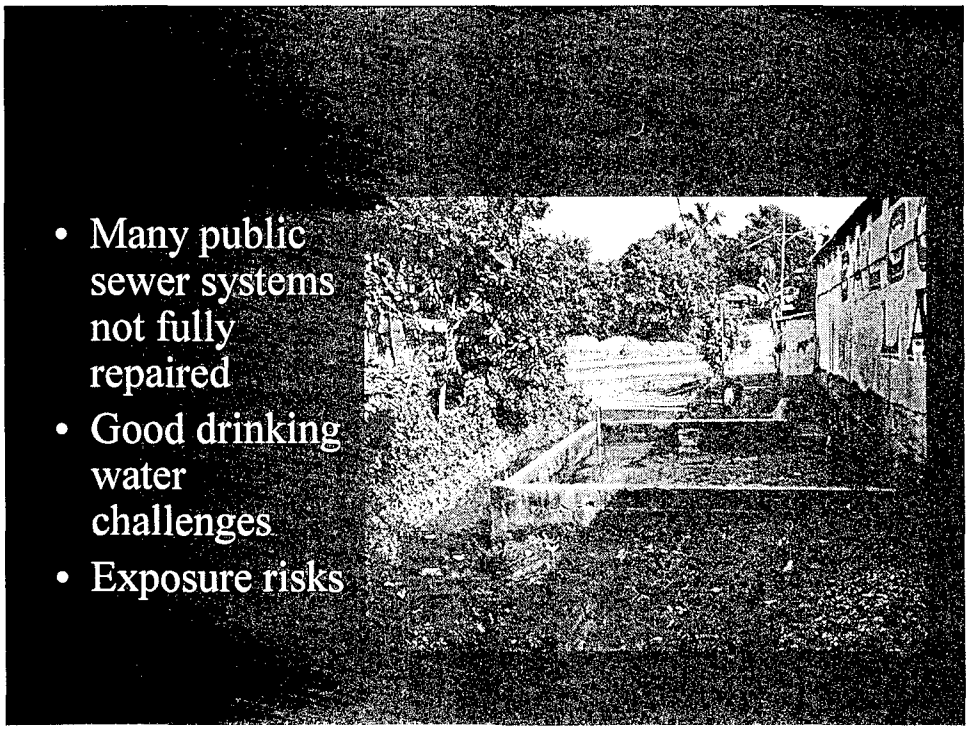

Figure 10: Sanitation and Drinking Water Exposure Risks

Storm Surge Disaster by Typhoon No. 18 in 1999

by

Hiroyasu Kawai [1)]

ABSTRACT

On September 24, 1999, the typhoon No. 18 attacked the west of Japan, and induced storm surge and high waves at the high astronomical tide. According to the tide records, the inundation traces, the witnesses, and the numerical simulation, the meteorological tide anomaly became more than 3 meters in the northern innermost region of Yatsushiro-kai Sea, and became more than 2.5 meters in the western region of Suo-nada Sea. Sea water pushed by the storm surge overflowed and overtopped sea walls, and inundated the houses and the farming lands. Some breakwaters were slided, and parapets were removed from the bases. That was the most enormous storm surge disaster since 1959 in Japan.

KEY WORDS: Astronomical Tide
Inundation
Meteorological Tide Anomaly
Typhoon

1. INTRODUCTION

Japan has several large bays facing the Pacific Ocean, as shown in **Figure. 1**, and some typhoons take routes through the Japan Islands every year. Therefore, the Japanese in the coastal zone have been suffering from storm surge disaster.

After the experience of the tremendous storm surge disaster by the typhoon No. 13 in 1953, the Sea Coast Act of 1956 was issued by the Japanese Government to prevent such disaster. The Committee on Coastal Engineering was also founded in the Japan Society of Civil Engineers. However, unfortunately the typhoon No. 15 in 1959, named *Isewan Typhoon* in Japan, generated large storm surge and high waves in Ise Bay. The coastal dikes were collapsed, and consequently about 5,000 lives were lost.

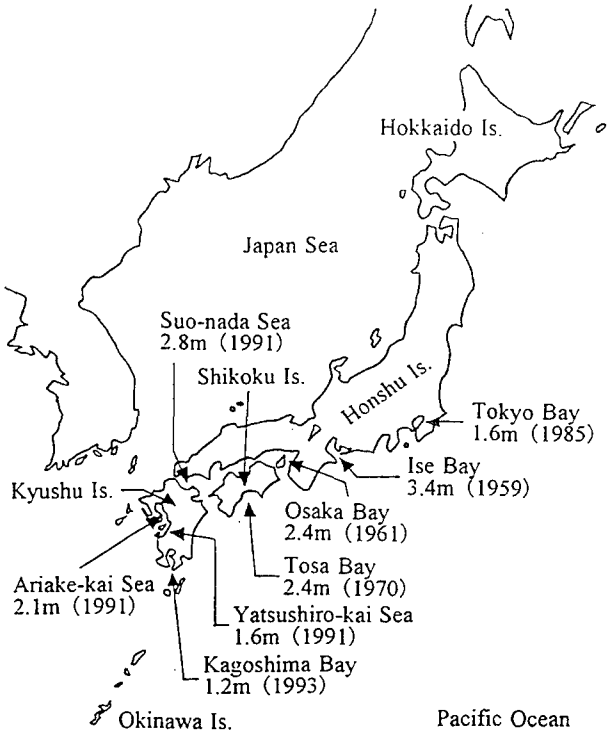

Figure 1 Maximum meteorological tide anomaly in principal bays in Japan between 1945 and 1998

1) Senior Research Engineer, Hydraulic Engineering Division, Port and Harbour Research Institute, Ministry of Transport; 3-1-1, Nagase, Yokosuka, 239-0826, Japan

After these disasters, the countermeasures by structures such as breakwaters, coastal dikes, and tide gates were developed in the principal bays in Japan. As the result, such enormous disasters have not been occurred since 1959 until 1998, although the meteorological tide anomalies shown in **Figure 1** were recorded. However, on September 24 in 1999, many coastal facilities and houses in the western region of Japan were damaged by the typhoon No. 18. That was the most enormous storm surge disaster in Japan since the typhoon No. 15 in 1959.

In this paper, the conditions of the typhoon No. 18 in 1999, and the characteristics of the storm surge in Kagoshima Bay, Yatsushiro-kai Sea, and Suo-nada Sea are reported.

2. TYPHOON NO. 18 IN 1999

Figure 2 shows the route of the typhoon No. 18 in 1999, in comparison with the other principal typhoons affecting the Kyushu region. The typhoon was generated to the south of the Okinawa Island on September 19, and approached the Kyushu Island on September 24. The maximum instantaneous wind velocity of 66.2 m/s was recorded at Ushibuka near the southern entrance of Yatsushiro-kai Sea. The typhoon passed by Yatsushiro-kai Sea, with an atmospheric pressure at the typhoon center of 940 hPa, and at a speed of 40 km/h, in the early morning. The typhoon landed on Omuta in the Kyushu Island, crossed the northern part of the Kyushu Island, went across Suo-nada Sea, and landed again on Ube in the Honshu Island.

The principal typhoons which caused the large meteorological tide anomalies around the Kyushu Island are listed in **Table 1**. The symbol p_c and V represents the atmospheric pressure at the typhoon center and the progression speed, near Yatsushiro-kai Sea, respectively. The typhoon No. 18 in 1999 was one of the strongest typhoons in these several ten years. The progression speed was slightly small.

The astronomical tidal range between the H.W.L. (mean monthly-highest water level) and the L.W.L. (mean monthly-lowest water level) is approximately 4 meters in Yatsushiro-kai Sea. In the case of the typhoon No. 19 in 1991, the meteorological tide anomaly became large at the low astronomical tide. On the other hand, in the case of the typhoon No. 18 in 1999, the meteorological tide anomaly became large at the high astronomical tide, therefore the total tidal level became much higher than the H.W.L.

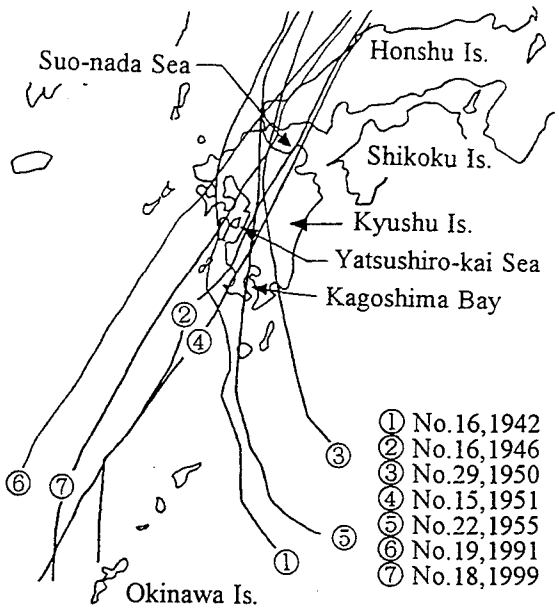

Figure 2 Routes of principal typhoons affecting the Kyushu region

Table 1 Characteristics of principal typhoons

typhoon No.	p_c (hPa)	V (km/h)
① No. 16, 1942	950	45
② No. 16, 1945	930	50
③ No. 29, 1950	965	25
④ No. 15, 1951	945	75
⑤ No. 22, 1955	950	40
⑥ No. 19, 1991	935	50
⑦ No. 18, 1999	940	40

3. NUMERICAL MODEL OF STORM SURGE

(1) Winds Caused by Typhoon

The distribution of the atmospheric pressure in a typhoon is given by the Mayer's formula as follows.

$$p_0 = p_c + \Delta p \exp\left(-\frac{r_0}{r}\right) \tag{1}$$

where, p_c is the atmospheric pressure at the center of a typhoon, Δp is the pressure differential, p_0 is the atmospheric pressure at the point with a radial distance r from the center, and r_0 is the influence radius.

Assuming the above distribution, the gradient wind speed U_{gr} is given by

$$U_{gr} = -\frac{rf}{2} + \sqrt{\left(\frac{rf}{2}\right)^2 + \frac{\Delta p}{\rho_a}\frac{r_0}{r}\exp\left(-\frac{r_0}{r}\right)} \tag{2}$$

where, f is the Coriolis coefficient, ρ_a is the density of atmosphere.

The wind speed is actually reduced by about 30% and the wind direction is changed inward by about 30 degrees, by the friction along sea surface. The actual wind speed, namely marine wind speed, U_1 can be assumed as follows.

$$U_1 = C_1 U_{gr} \tag{3}$$

where, C_1 is the parameter assumed to be 0.70 in this paper.

The movement of a typhoon also generates the winds of which speed U_2 is given by

$$U_2 = \frac{U_1(r)}{U_1(r_0)} V \tag{4}$$

where, V is the progression speed of a typhoon. The directions of the wind component and the typhoon progression are identical.

(2) Propagation of meteorological tidal wave

The propagation of the meteorological tidal wave caused by a typhoon is represented by the non-linear long wave theory. The equation of continuity and the equations of motion can be written by

$$\frac{\partial \eta}{\partial t} + \frac{\partial M}{\partial x} + \frac{\partial N}{\partial y} = 0 \tag{5}$$

$$\frac{\partial M}{\partial t} + \frac{\partial}{\partial x}\left(\frac{M^2}{D}\right) + \frac{\partial}{\partial y}\left(\frac{MN}{D}\right) = +fN - gD\frac{\partial \eta}{\partial x} - \frac{D}{\rho_W}\frac{\partial p_0}{\partial x} + \frac{1}{\rho_W}(\tau_{sx} - \tau_{bx}) + A_h\left(\frac{\partial^2 M}{\partial x^2} + \frac{\partial^2 M}{\partial y^2}\right) \tag{6a}$$

$$\frac{\partial N}{\partial t} + \frac{\partial}{\partial x}\left(\frac{MN}{D}\right) + \frac{\partial}{\partial y}\left(\frac{N^2}{D}\right) = -fM - gD\frac{\partial \eta}{\partial y} - \frac{D}{\rho_W}\frac{\partial p_0}{\partial y} + \frac{1}{\rho_W}(\tau_{sy} - \tau_{by}) + A_h\left(\frac{\partial^2 N}{\partial x^2} + \frac{\partial^2 N}{\partial y^2}\right) \tag{6b}$$

where, t is the time, x and y axes are taken in the horizontal direction, g is the gravity acceleration, ρ_W is the density of sea water, p_0 is the atmospheric pressure on the water surface, A_h is the horizontal eddy viscosity coefficient. D is the water depth, M and N are the flux flows. They are defined by

$$D = h + \eta \tag{7}$$

$$M = \int_{-h}^{\eta} u\,dz \tag{8a}$$

$$N = \int_{-h}^{\eta} v\,dz \tag{8b}$$

where, z axis is taken in the vertical direction, and $z=-h$ at the sea bottom, $z=\eta$ at the water surface. u and v is the component of the velocity in the direction of the x and y axis respectively. Additionally, τ_{sx} and τ_{sy} is the tangential stress along the water surface, and τ_{bx} and τ_{by} is the tangential stress along the sea bottom, in the direction of the x and y axis respectively, defined by

$$\tau_{sx} = \rho_a C_D W_x \sqrt{W_x^2 + W_y^2} \tag{9a}$$

$$\tau_{sy} = \rho_a C_D W_y \sqrt{W_x^2 + W_y^2} \tag{9b}$$

$$\tau_{bx}=\frac{\rho_w g n^2}{D^{7/3}} M\sqrt{M^2+N^2} \qquad (10a)$$

$$\tau_{by}=\frac{\rho_w g n^2}{D^{7/3}} N\sqrt{M^2+N^2} \qquad (10b)$$

where, C_D is the resistance coefficient along the sea surface, W_x and W_y is the wind velocity at 10 meters above the sea surface in the direction of the x and y axis respectively, n is the Manning's roughness parameter.

(3) Finite difference method and grid mesh

In this paper, the governmental equations are solved by a finite difference method with a stacked grid mesh for space successive steps and the leap-frog method for time successive steps.

The regions shown in **Table 2** are combined with each other. The region 1 includes a part of the Pacific Ocean and the East China Sea near the Japan Islands. The storm surge is reproduced during 48 hours, namely from 12:00 on September 22, 1999 to 12:00 on September 24. The time interval between successive steps is 4 seconds.

4. FIELD INVESTIGATION

The tide records are the most reliable data to understand the storm surge. However, only one tide station is available in Kagoshima Bay. A few tide stations are available in Yatsushiro-kai Sea, however there is no in the northern innermost region, in which the large meteorological tide anomaly gave the enormous disaster. Therefore, it is necessary to ask the witnesses in the affected areas the maximum water level and the occurrence time, and to measure the heights of the inundation traces.

In this paper, the field data are classified into four categories shown in **Table 3** by the reliability. The actual tidal level should be near the categories A and B, lower than the category C, and higher than the category D.

Additionally, the damages of the breakwaters, the sea walls, and the coastal dikes were also investigated.

Table 2 Grid Mesh

	region	number of grid points	space interval
Common	1	74 × 75	16.2 km
	2	81 × 87	5.4 km
Kagoshima Bay	3	66 × 57	1.8 km
	4	72 × 96	0.6 km
	5	72 × 126	0.2 km
Yatsushiro-kai Sea	6	57 × 63	1.8 km
	7	132 × 135	0.6 km
	8	96 × 135	0.2 km
	9	150 × 111	0.2 km
	10	81 × 96	0.2 km
Suo-nada Sea	11	114 × 120	1.8 km
	12	186 × 114	0.6 km
	13	120 × 195	0.2 km
	14	213 × 111	0.2 km
	15	102 × 102	0.2 km

Table 3 Classification of field data

category	content
A	- tide record with no error
B	- trace of the maximum water level unaffected by wave runup and wave overtopping
C	- trace of the maximum water level affected by wave runup - trace of the overtopped water
D	- tide record without the peak tidal level - trace of the maximum water level due to tide inside a partially shield building - trace of the maximum water level at the backward of the sea wall or coastal dike

5. STORM SURGE IN KAGOSHIMA BAY

Kagoshima Bay is approximately 70 kilometer long from south to north as shown in **Figure 3**, and is much deeper than the other bays in Japan as shown in **Figure 4**. The majority of the typhoons going through or passing by the Kyushu Island may go up north in almost parallel to the axis of the bay, therefore strong wind blows from the bay entrance to the northern innermost region in the case that a typhoon goes up north at the west side of the bay.

Figure 5 shows the profiles of the meteorological tide anomalies at the principal points. The meteorological tide anomaly became the maximum between 3:00 and 4:00. During the period, the astronomical tidal level was near the M.S.L. (mean sea level), and the total tidal level was near the H.W.L. (mean monthly-highest water level).

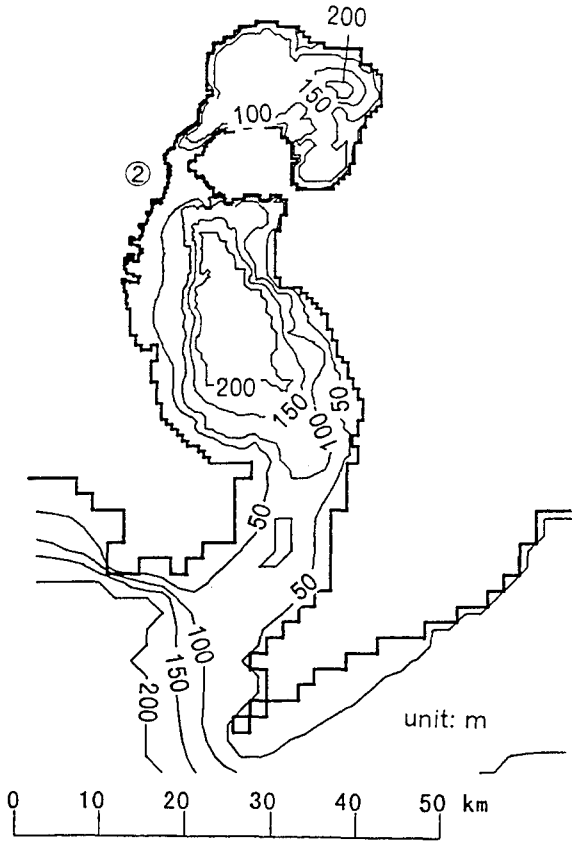

Figure 3 Bathymetry of Kagoshima Bay

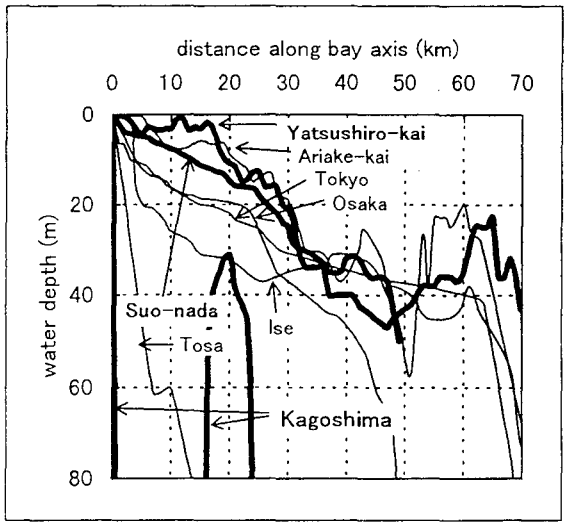

Figure 4 Longitudinal sections of principal bays in Japan

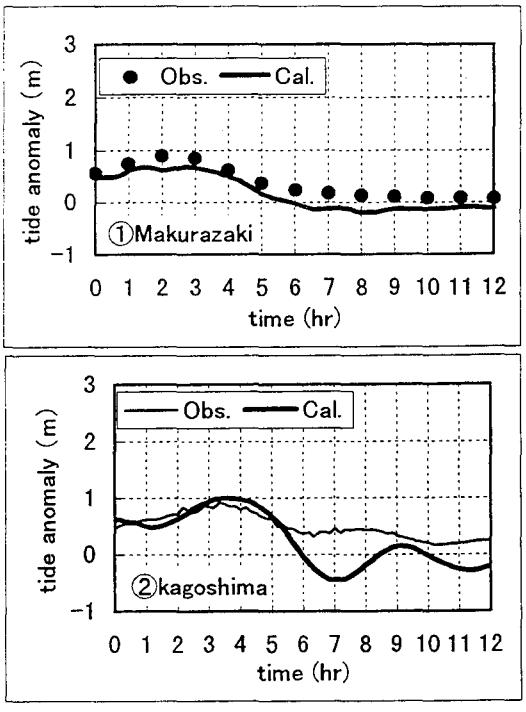

Figure 5 Profile of meteorological tide anomaly in Kagoshima Bay

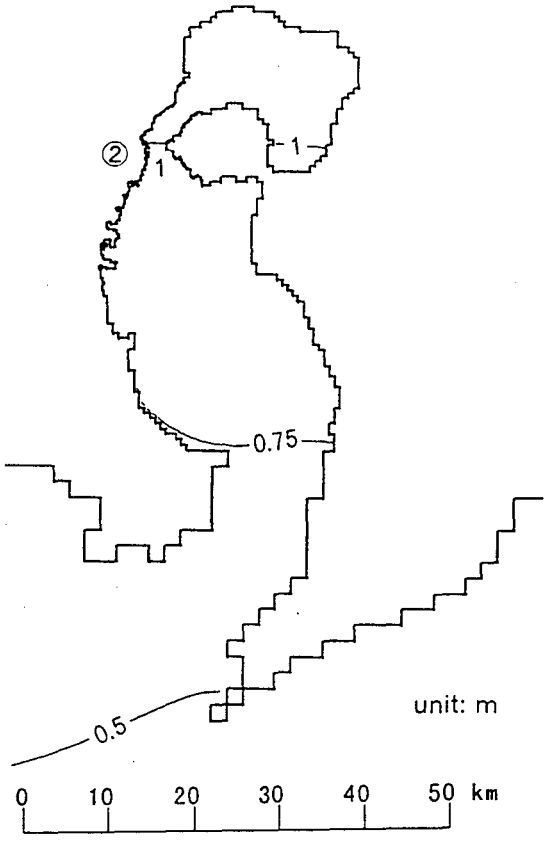

Figure 6 Maximum meteorological tide anomaly in Kagoshima Bay

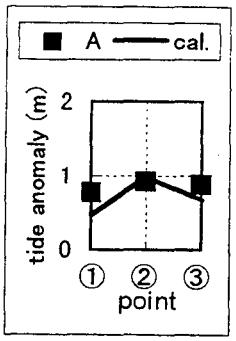

Figure 7 Comparison of meteorological tide anomaly in Kagoshima Bay

Figure 6 shows the distribution of the maximum meteorological tide anomaly in Kagoshima Bay. The maximum meteorological tide anomaly at the bay entrance and in the northern innermost region was around 0.5 meter and 1 meter respectively.

As shown in **Figure 7**, the meteorological tide anomaly reproduced by the numerical model agrees with that observed at the tide stations. In the figure, only the point ② Kagoshima is in Kagoshima Bay. The point ① Makurazaki and ③ Shibushi is in the west side and the east side of the bay respectively.

In the Kagoshima Port, breakwater caissons were slided by high waves.

6. STORM SURGE IN YATSUSHIRO-KAI SEA

Yatsushiro-kai Sea is approximately 60 kilometer long from south to north, as shown in **Figure 8**, that is similar to Kagoshima Bay. However, Yatsushiro-kai Sea is very shallow compared with the other bays in Japan. In the northern innermost region, the water depth is less than 10 meters as shown in **Figure 4**, and the coast line is v-shaped as shown in **Figure 8**.

Figure 9 shows the profiles of the meteorological tide anomalies at the principal points shown in **Figure 8**. There are two tide stations at the point ⑧ Misumi. At the points ⑤ Yatsushiro and ⑧ Misumi in the northern innermost region of Yatsushiro-kai Sea, the first large peak was followed by the smaller second peak. The first peak appeared at around 6:00 near the high astronomical tide. Consequently the total tidal level became much higher than the H.W.L.(mean monthly-highest water level).

Figure 10 shows the distribution of the maximum meteorological tide anomaly reproduced by the numerical model. The maximum mete

orological tide anomaly is about 1 meter at the southern entrance region, 1.6 meters around the point ⑤ Yatsushiro, increases sharply in the northern innermost region. The meteorological tide anomaly is estimated to be at least 3 meters at the point ⑦ Shiranui.

As shown in **Figure 11**, the meteorological tide anomaly reproduced by the numerical model agrees with that observed in the tide stations, and that measured by the field investigation.

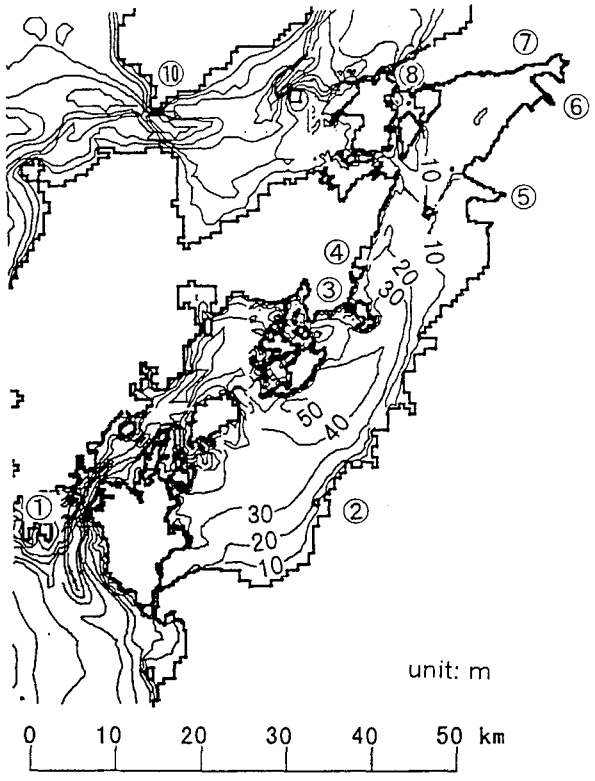

Figure 8 Bathymetry of Yatsushiro-kai Sea

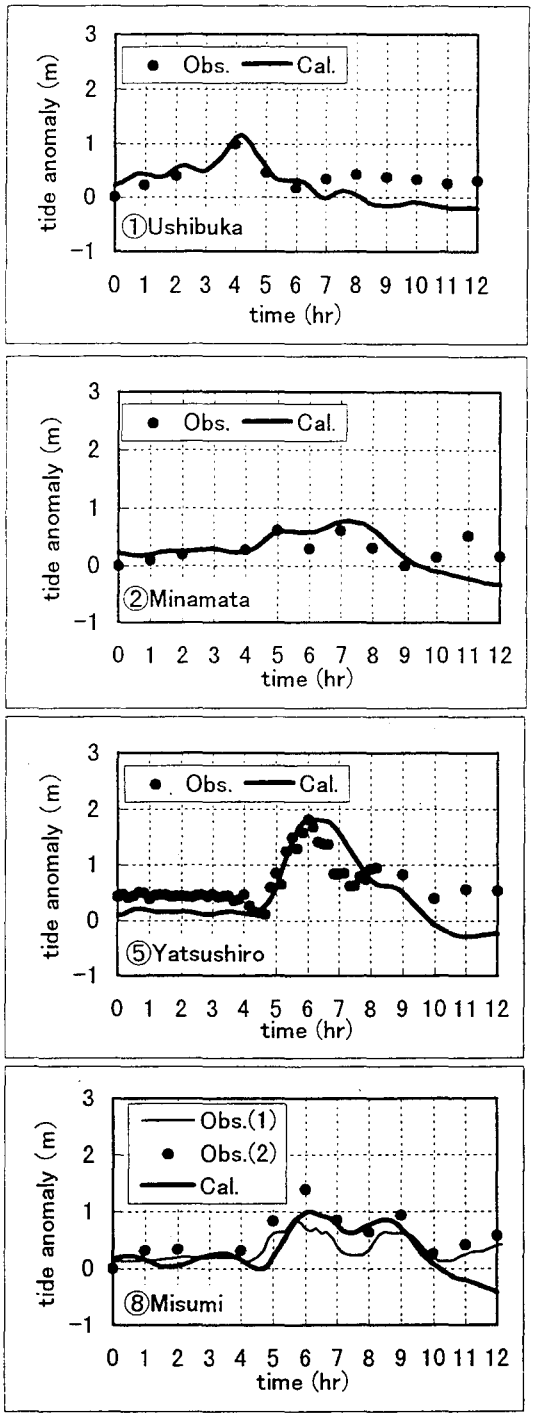

Figure 9 Profile of meteorological tide anomaly in Yatsushiro-kai Sea

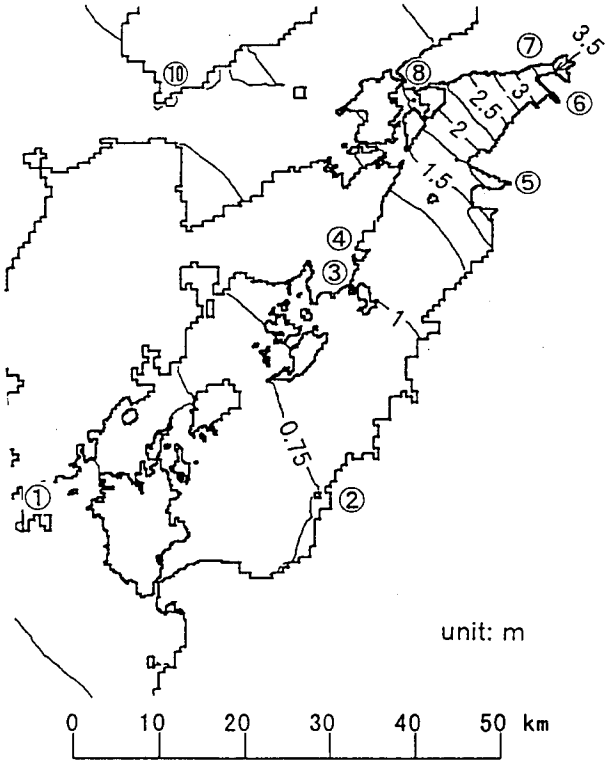

Figure 10 Maximum meteorological tide anomaly in Yatsushiro-kai Sea

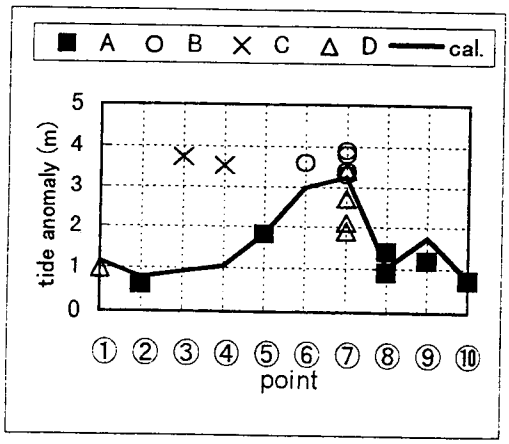

Figure 11 Comparison of meteorological tide anomaly in Yatsushiro-kai Sea
① Ushibuka, ② Minamata, ③ Ryugatake, ④ Himedo, ⑤ Yatsushiro, ⑥ Kagami, ⑦ Shiranui, ⑧ Misumi, ⑨ Kumamoto, ⑩ Kuchinotsu

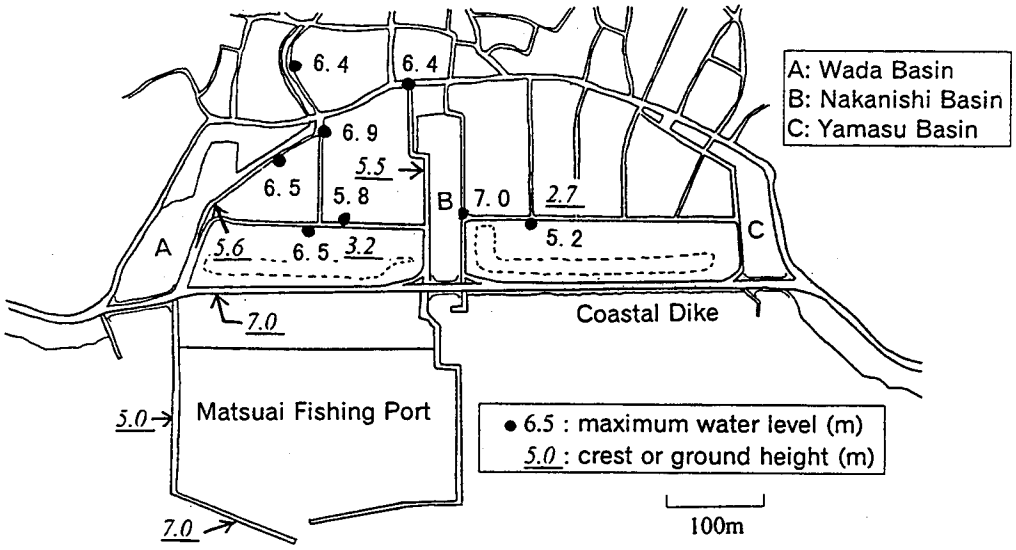

Figure 12 Matsuai Section of Shiranui Town

Figure 12 shows the layout in the Matsuai Section of Shiranui Town, the point ⑦. There is a coastal dike with a height of 7.0 meters above the C.D.L. (chart design level) and three basins for fishing boats are located in the normal direction to the face of the coastal dike. The crests of the seawalls of the basins are 5.5 meters above the C.D.L. Many houses are built around the basins, however the ground levels of some houses are much lower than the crests of the seawalls.

According to the residents, the tidal level might become higher than the crest of the seawalls before 6:00 a.m. Consequently, huge amount of sea water flew over the seawalls, and inundated the houses in ten minutes or so. The area became like a pond. It was difficult for the residents living on the low ground to get aware of the quick rising of the tidal level, because it was dark and the view of the sea was obstructed by the seawalls and the coastal dike.

Photo 1 shows one of the inundated houses. Rice hull on the roof is a trace of the inundation. The inundation height around this house might be 2.6 to 3.3 meters. While most residents living on the first stories of two-storied houses tried to go upstairs, some residents in one-storied house broke the ceiling through and climb on to the roof. Unfortunately 12 people were drowned in the first story.

According to an eyewitness living beside the Nakanishi Basin, the maximum water level might be approximately 7.0 meters above the C.D.L. It means that the meteorological tide anomaly was 3.9 meters. On the other hand, the trace of the overflow could not be found on the coastal dike.

Figure 13 shows the profiles of the astronomical tidal level and the meteorological tide anomaly reproduced by the numerical model. It is reproduced that the total tidal level became higher than the seawalls of the basins before 6:00 and did not exceed the coastal dike.

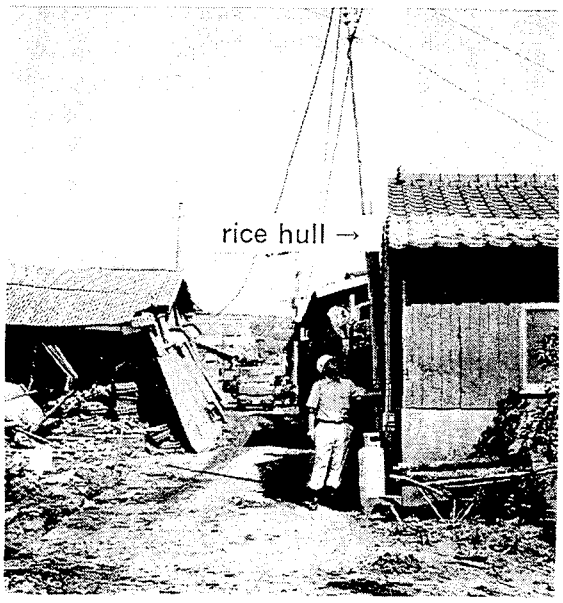

Photo 1 Inundated house

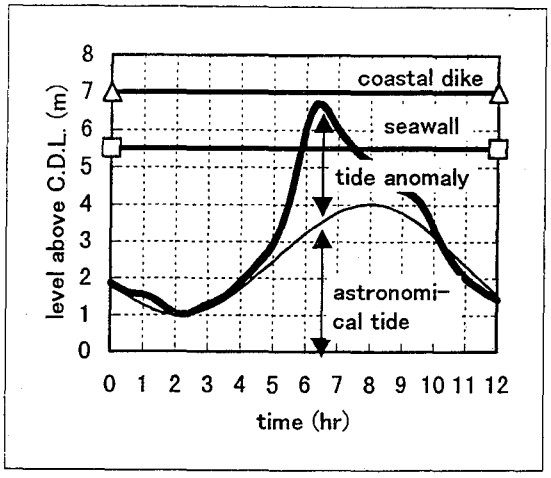

Figure 13 Profile of meteorological tide in Matsuai Section

The houses at the backward of the seawall in the Koyagawachi Section, Ryugatake Town, the point ③ were also inundated by about 1.2 maters. As shown in **Photo 2**, the concrete block wall was collapsed, and the windows on the first stories of the house were completely destroyed. According to the witnesses, the in-

undation began at about 5.00 a.m. and the crest of the seawall at the forward of the houses might be submerged. It was one hour before the inundation in the Matsuai Section.

Figure 14 shows the profiles of the astronomical tide and the meteorological tide anomaly reproduced by the numerical model. The total tidal level might be much lower than the seawall. The incident wave height is estimated by wave hindcasting to be approximately 2 meters. The houses at the first line from the seawall were heavily damaged. Therefore, the area might be inundated mainly by wave overtopping. The witness that the seawall was submerged might mean that waves with long periods overtopped during the storm.

Photo 3 shows the breakwaters in the Odo Port near the inundated houses. The section between A and B was collapsed into sea by the high waves and the high tidal level.

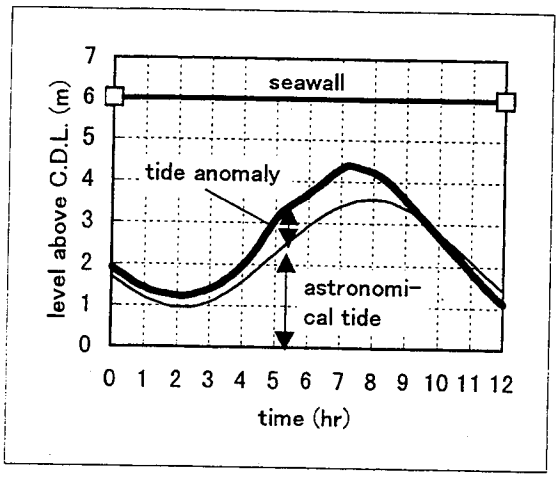

Figure 14 Profile of meteorological tide in Koyagawachi Section

Photo 2 Houses in Koyagawachi Section

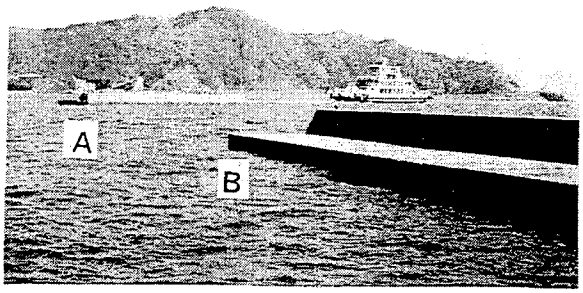

Photo 3 Breakwater in Odo Port

7. STORM SURGE IN SUO-NADA SEA

Suo-nada Sea is approximately 100 kilometer long from east to west, as shown in **Figure 15**. The sea is surrounded by islands, and the axis of the sea is almost normal to the routes of most typhoons approaching the sea. The water depth in the west region is less than 20 meters. Additionally, there are several small v-shaped bays in the northern coast, and the water depth inside the these bays is less than 5 meters.

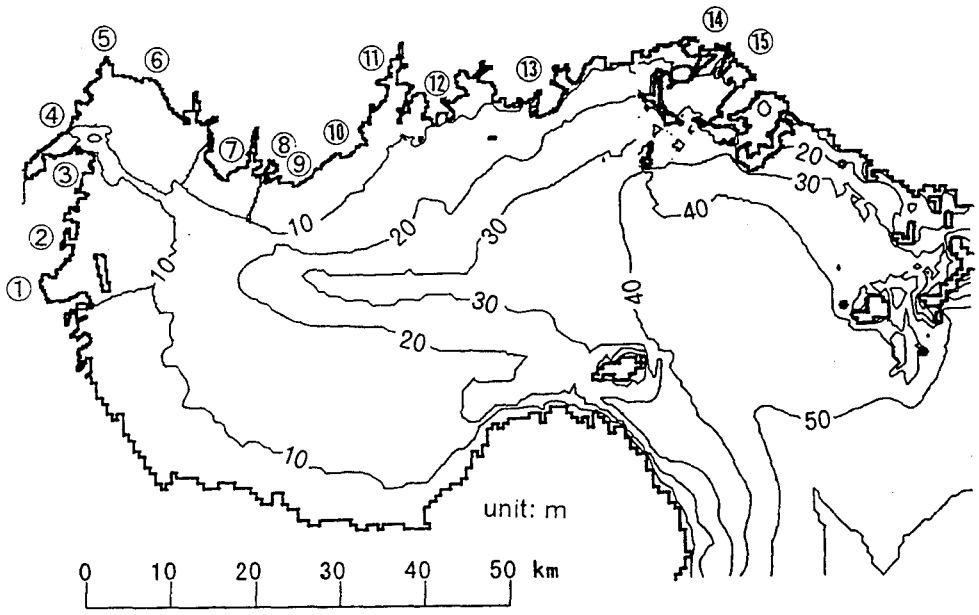

Figure 15 Bathymetry of Suo-nada Sea

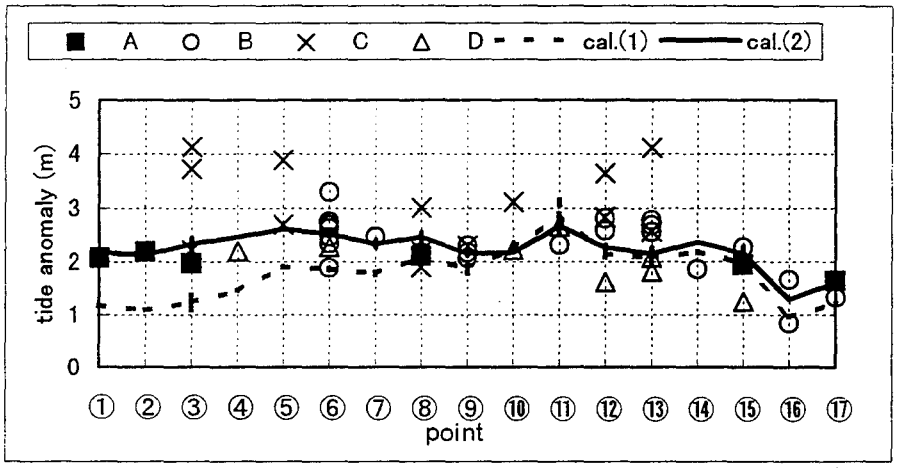

Figure 16 Comparison of meteorological tide anomaly in Suo-nada Sea
① Kanda, ② Shin-Moji, ③ Aohama, ④ Chofu, ⑤ Ozuki, ⑥ Sanyo, ⑦ Onoda, ⑧ West Ube, ⑨ East Ube, ⑩ Ajisu, ⑪ Yamaguchi, ⑫ Aio, ⑬ Hofu, ⑭ Shin-Nanyo, ⑮ Tokuyama, ⑯ Yanai, ⑰ Iwakuni

It is assumed in the numerical model that the wind speed ratios C_1 and C_2 are 0.7 and that sea surface friction changes the marine wind direction by 30 degrees. Such assumptions are adopted in general and are applicable to Kagoshima Bay and Yatsushiro-kai Sea. However, the meteorological tide anomaly computed by the numerical model, described by the dotted line in **Figure 16**, is much smaller than that observed in the tide stations, especially in the western region of Suo-nada Sea.

Suo-nada Sea is long from east to west, and the sea is surrounded by the islands with high

mountains. Therefore, the wind speed and direction estimated with the general assumptions do not necessarily agree with those measured by the wind gauges. By adjusting the wind speed and direction, the meteorological tide anomaly described by solid line in **Figure 16** is obtained.

Figure 17 shows the profiles of the meteorological tide anomalies at the principal points shown in **Figure 15**. There are two tide stations at the point ⑮ Tokuyama. The meteorological tide anomaly became the maximum in the order of the points ① to ⑮, namely from west to east.

Figure 18 shows the distribution of the maximum meteorological tide anomaly reproduced by the numerical model. The maximum meteorological tide anomaly is large in the west region of Suo-nada Sea, especially larger than 2.5 meters around the point ⑥ Sanyo.

In the coast of Suo-nada Sea, many coastal and port facilities were damaged. For example in the artificial island off the Shin-Moji Port, the point ②, the seawalls were leaned and the parapets were put out of joint, by the high waves and the high tidal level, as shown in **Photo 4**. In the Yamaguchi Port, between the points ⑪ and ⑫, the coastal dike was collapsed and consequently the farmland was inundated with sea water.

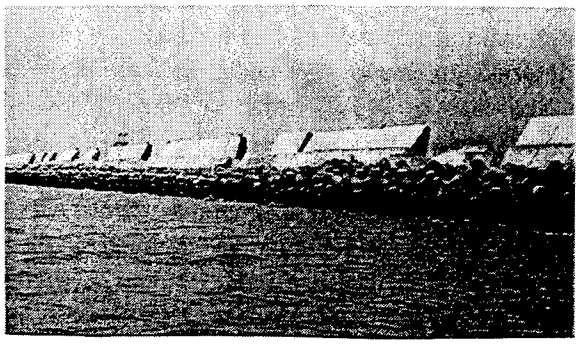

Photo 4 Seawall in the artificial island off the Shin-Moji Port

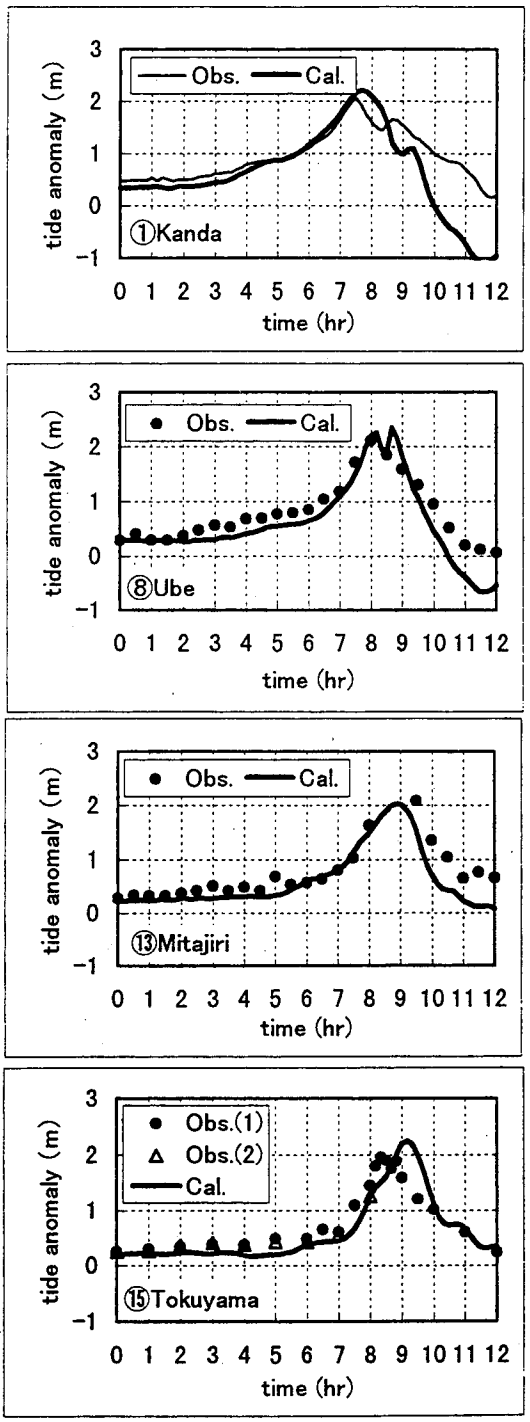

Figure 17 Profile of meteorological tide anomaly in Suo-nada Sea

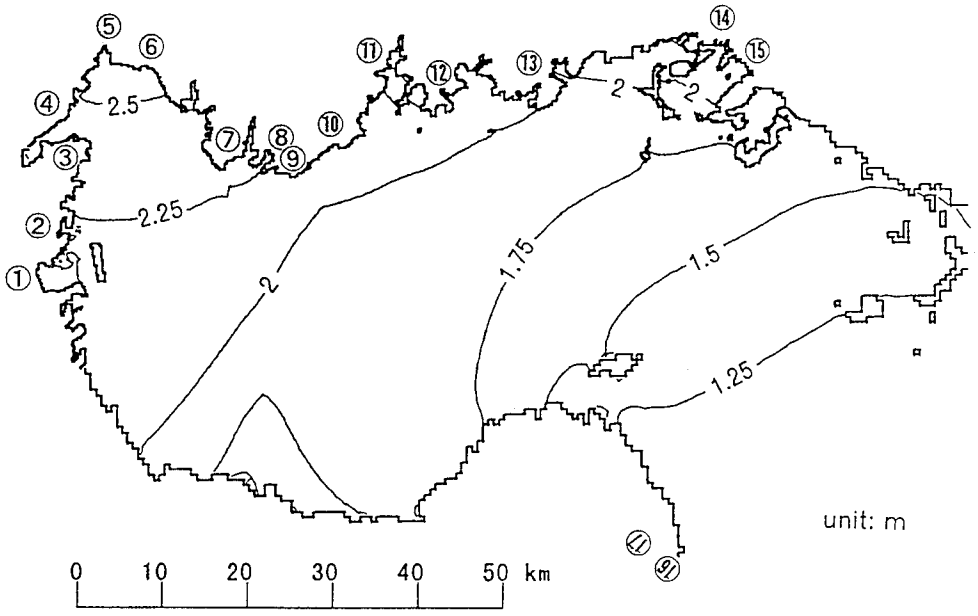

Figure 18 Maximum meteorological tide anomaly in Suo-nada Sea

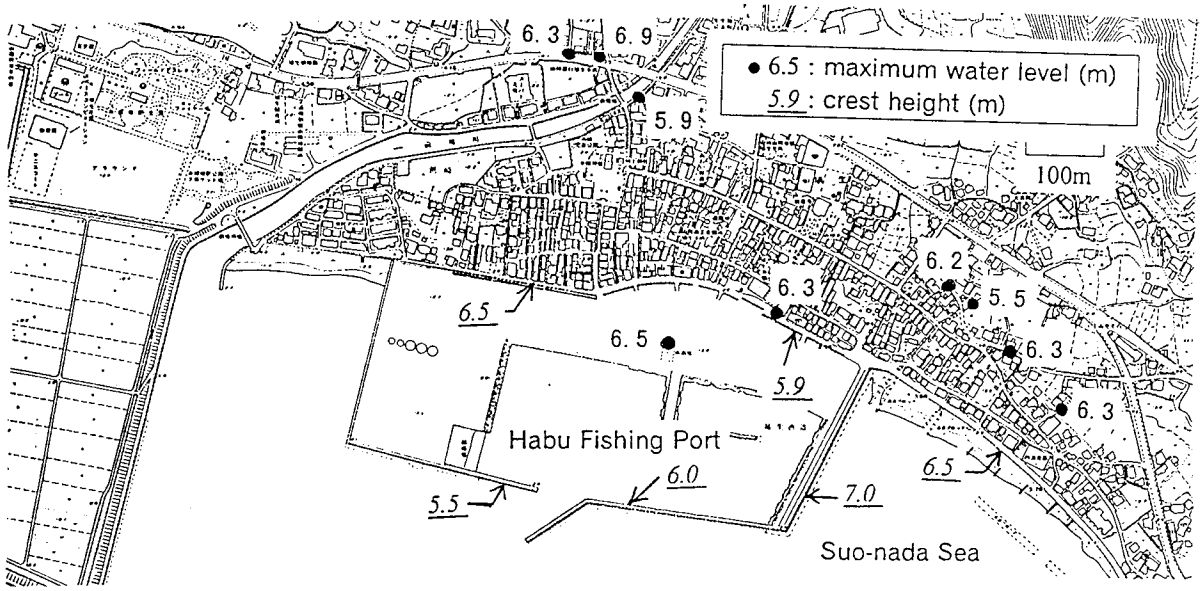

Figure 19 Habu Section of Sanyo Town

Table 4 comparison of conditions in inundated ares

		Yatsushiro-kai Sea		Suo-nada Sea
		Koyagawachi	Matsuai	Habu
Inundation start time		5.00 a.m.	5.50 a.m.	7.30 a.m.
Astronomical tidal level	(C.D.L., m)	+2.2	+3.1	+3.5
Meteorological tide anomaly	(m)	0.9	<3.9	2.5 to 3.0
Total tidal level	(C.D.L., m)	3.1	<7.0	6.0 to 6.5
Crest height of breakwater	(C.D.L., m)	none	5.0 to 7.0	5.5 to 7.0
Crest height of seawall or parapet	(C.D.L., m)	6.0	5.5	5.9 to 6.5
Ground level at the backward	(C.D.L., m)	>5.0	>3.2	>4.8
Maximum inundation height	(m)	1.2	3.3	1.5
Death toll		0	12	0

Figure 19 shows the layout of breakwaters and parapets in the Habu Fishing Port and the residential area at the backward of them. According to the eyewitnesses, the tidal level rose rapidly around 7.30 a.m. The inundation height at the backward of the parapets reached about 1.5 meters. It means that the maximum tidal level was between 6 to 6.5 meters above the C.D.L. (chart design level) and the maximum meteorological tide anomaly was 2.5 to 3 meters. A few fishing boats went over the parapets and attacked the houses. When the tidal level was the maximum, the wind became weak but the wave height was still large.

Table 4 shows the conditions of the inundated areas in Yatsushiro-kai Sea and Suo-nada Sea. In the Habu Section, the inundation began after the sunrise, and the ground level is not so low, therefore no one was drowned there.

8. CONCLUSION

The mail conclusions of this paper are as follows:

(1) By the typhoon No. 18 in 1999 gave enormous storm surge disaster especially in Yatsushiro-kai Sea and Suo-nada Sea.
(2) In Kagoshima Bay, the meteorological tide anomaly became large in the northern innermost region, and the maximum value was about 1 meter.
(3) In Yatsushiro-kai Sea, the meteorological tide anomaly became large in the northern innermost region, and the maximum value was more than 3 meters. The Matsuai Section was inundated by high tidal level due to storm surge.
(4) In Suo-nada Sea, the meteorological tide anomaly became large in the western region, and the maximum value was more than 2.5 meters. Many parapets and coastal dikes were damaged, and the Habu Section was inundated with sea water.

REFERENCES

1. Kawai,H. and T.Hiraishi: Influence of Storm Surge on Failure Probability of Breakwater, Okushiri Tsunami/ UJNR Workshop, Booklet of Abstracts, pp.100-101, 1998.
2. Kawai,H.: Storm Surge in Ise and Mikawa Bay Caused by Typhoon, Proceedings of the 31st Joint Meeting of United States-Japan Panel on Wind and Seismic Effects, 13p., 1999.

APPENDIX

Task Committee Reports

REPORT ON TASK COMMITTEE A
STRONG MOTION DATA AND APPLICATIONS

Date: 19 May 2000

Place: National Institute of Standards and Technology, Gaithersburg, USA

Attendees:	Japan side --	Takashi Nagao (Chairman)	PHRI
		Izuru Okawa	BRI
	U. S. side --	Mehmet K. Çelebi (Acting Chairman)	USGS
		Richard Olsen	ERDC, WES
		Michael Blackford	NOAA/NWS

1. Objective and Scope of Work

To coordinate and promote sharing of strong motion earthquake data among researchers and practicing engineers, and to develop techniques and exchange information for evaluating the destructive effects of earthquake motion.

The scope of work includes:

1. instrumentation,
2. recording, processing, and analyzing strong motion data,
3. engineering characterization of ground motion,
4. design applications, and
5. seismic zonation.

The activities of the Task Committee include:

1. regular exchange of data and publications,
2. creating procedures for disseminating significant strong motion digital data with regard for the rights and expectations of (a) owner, (b) the users of data and (c) the earthquake engineering community,
3. planning and conducting T/C workshops and meetings, and
4. coordinating relevant research activities.

2. Accomplishments

During the 32nd UJNR Panel on Wind and Seismic Effects meeting, presentations made related to the M=7.4 August 17, 1999 Izmit (Turkey) and M=7.2 November 12, 1999 Duzce (Turkey) and M=7.3 September 18, 1999 Chi-Chi (Taiwan) earthquakes revealed the wealth of strong-motion data recorded during these events. The additional data sets will impact earthquake engineering and engineering seismology studies and practices for years to come. These earthquake records enriched the data base for near-fault (<10 km) records by tenfold and they exhibit very large velocities (>300cm/s) and permanent displacements (>8M). These records are in addition to those from the 1994 Northridge and 1995 Great Hanshin earthquakes which had a tremendous impact on various aspects of the strong motion studies, including characterization of near field motion and site response. In addition, activities conducted by Task Committee A members during 1999 and 2000 are:

1. Close monitoring of the on-going changes and new proposals for seismic guidelines and codes, including those of UBC97, NEHRP97 in USA and ISO/WG67 in Japan and the new International Building Code 2000.
2. Contributions of the chairmen and members of Task Committee A to 12th World Conference on Earthquake Engineering (12WCEE; Jan. 2000; Auckland, New Zealand).
3. Official incorporation of COSMOS (Consortium of Organizations for Strong-Motion Observation Systems). This new organization is now planning to work on specific workshops and standardization of strong-motion data bases. Efforts are underway to determine procedures for expanded international participation.
4. Completion of K-net through the efforts of Japan-side Task Committee A members. Its data availability with ease and timely fashion should be a model to both U.S. and Japan strong motion programs for future development. Data is being disseminated with CD_ROMs in both Japanese and English.
5. Beginning of implementation of a new ANSS (Advanced National Seismic Systems) initiative in the United States under the leadership of the USGS. Before end of FY2000 (September 30, 2000), with the funding provided by U.S. Congress, there will be 80 new real-time stations in the United States (40 in Northern California, 20 in Pacific Northwest and 20 in and around Salt Lake City). A brochure describing this initiative was distributed to UJNR members. In future years, this program will deploy additional real-time stations will further help in improving shake maps for use by earthquake response managers.
6. Contributions of the task committee members to the organization of a workshop on "Strong-motion Instrumentation of Civil Engineering Structures" funded by NATO, NSF, USGS, and others (Istanbul, Turkey; June 2 – 5, 1999). Co-director of the workshop, Dr. Çelebi, reported that the proceedings of this workshop is now being finalized.
7. A USGS Report on August 17, 1999 Izmit (Turkey) earthquake [USGS Circular 1193] with contributions from panel members has been distributed to participants of the 32nd Panel Meeting.
8. A USGS Report describing the aims of the ANSS (Advanced National Seismic Systems) has been distributed to the participants of the 32nd Panel Meeting.

3. Future Plans

The future plans include:

(1) Coordination and follow-up, when appropriate, of ongoing US and Japan developments in strong motion recording programs and data dissemination in conjunction with activities of recently established committees and organizations such as COSMOS. Realizing the importance of strong-motion data to earthquake hazard mitigation, T/C A suggests the establishment of links on UJNR Web page to the Web pages of major US and Japan agencies where strong-motion data information are available without restrictions. Coordinate these links also with Cosmos.

(2) Recognizing the increasing emphasis in the engineering and emergency response communities on near-real-time data availability, T/C A will continue to promote the use of, and exchange of information on,new developments in real-time strong motion data acquisition, processing, and notification. This activity will be in conjunction with the proposed TC on Seismic Information Systems. In this context, the task committee will follow with interest the new ANSS (Advanced National Seismic Systems) initiative that is being implemented in the United States.

(3) Drs. Okawa and Çelebi proposed, and the committee accepted, the organization of a 2nd US-Japan Workshop on Soil-Structure Interaction, in Tsukuba, Japan, in March 2001.

(4) Development of recommendations for the Common Agenda, possibly in a workshop regarding US and Japan needs for strong-motion measurements in densely urbanized areas to significantly improve pubic earthquake safety.

(5) Encourage, where and when appropriate, follow-up of ongoing developments in seismic hazard map and seismic guidelines to be generalized for worldwide use.

(6) In coordination with Task Committee G, a joint workshop will be held on Seismic Information Systems and Damage Detection. The time and venue of the workshop will be in coordinated with the Third High Level Forum being planned during Fall 2000.

Report of Task Committee B

TESTING AND EVALUATION PROCEDURES FOR BUILDING SYSTEMS

Date: May 16, 2000

Place: National Institute of Standards and Technology, Gaithersburg, MD

Attendees:	U.S. Side--	H. S. Lew (Chairman)	NIST
	Japan Side--	C. Minowa (Acting Chairman)	NIED
		M. Teshigawara	BRI
		H. Sugita	PWRI

1. Objective and Scope of Work

The objective of the Task Committee is to develop and recommend rational test procedures and to collect performance data of the static and dynamic response of structures through both laboratory testing of prototype structures and filed testing of structures.

The Task Committee:

(1) Plans and conducts workshops and joint meetings to identify research topics and develop joint research programs
(2) Coordinates research projects carried out by various laboratories in the U.S. and Japan. Facilitates publication of research results and implementation of findings in codes and standards.
(3) Facilitates exchange of research personnel, the exchange of technical information and the use of available testing facilities.
(4) Develops uniform testing procedures, including loading history, for comparison of results of tests carried out by various researchers, and for establishment of data base.
(5) Develops guidelines for interpretation of test results to improve the design of structures.
(6) Develops methodology for evaluation and interpretation of test results.

2. Accomplishments

(1) As part of the third phase of the U.S. Precast Seismic Structural Systems Program (PRESS), the testing of the five-story full-scale frame was completed at the University of California at San Diego in August 1999. The results of the testing have been published in the PCI Journal, Nov.-Dec. 1999.

(2) The research program on Composite and Hybrid Structures (CHS) in Japan was completed in early 1998. The Japan Structural Consultant Association has completed applications studies for implementing research results. They are published in the proceedings of the 12 World Conference on Earthquake Engineering in January 2000.

(3) The research program on CHS in the U.S. was initiated in 1995 under the sponsorship of the National Science Foundation. Testing of composite wall systems have been completed.

(4) The sixth and final U.S.-Japan Technical Coordinating Committee meeting on CHS was held in March 2000. The dissemination and archiving of the research results were discussed.

3. Future Plans

(1) Task Committees B and C to hold a joint meeting during the year 2000 to discuss future research plans in the coming decades.

(2) The joint workshop on test procedure, documentation, retrieval of test data, and experimental facilities will be planned in the U.S., in conjunction with the 33rd Joint Panel Meeting.

(3) The Task Committee will consider the future U.S.-Japan Joint Research Program using available testing facilities in both countries including the 3-D Full-Scale Earthquake Testing Facility, which is being constructed at Miki, Japan by the National Research Institute for Earth Science and Disaster Prevention.

(4) The task committee will study the feasibility of establishing a network for live transmittal of experimental testing.

(5) The Task Committee will strongly encourage the CHS program coordinators to prepare reports summarizing the experimental and analytical research activities on CHS in the U.S. and Japan. This report will also recommend the application and implementation of the results in the design and analysis of CHS.

REPORT OF TASK COMMITTEE C

HIGH PERFORMANCE STRUCTURAL SYSTEMS; DESIGN, EVALUATION, RETROFIT AND AUTO ADAPTIVE MEDIA

Date: May 16, 2000

Place: National Institute of Standards and Technology, Gaithersburg, MD, U.S.A.

Attendees:			
	U.S.-side --	H.S. Lew (Acting Chairman)	NIST
	Japan-side --	Masaomi Tesigawara (Acting Chairman)	BRI
		Hideki Sugita	PWRI
		Chikahiro Minowa	NRI

1. Objective and Scope of Work

The objective and scope of work and the future plans of the Task Committee (c) are as follows:

(1) Exchange information and plan, and conduct workshops on new design technologies, evaluation technologies, repair and retrofit techniques.

(2) Study advanced materials and methods for new construction and those for repairing and retrofitting existing structures.

(3) Develop reliable condition assessment systems for new, existing and damaged structures.

(4) Develop and harmonize performance based structural design developed in each country.

(5) Coordinate research projects on design, evaluation and improvement of structures in the U.S. and Japan to minimize duplication and maximize benefits.

2. Accomplishments

(1) The 1st U.S.-Japan Technical Coordinating Committee Meeting on Auto-Adaptive Media (Smart Structural Systems) was held on January 7 – 8, 2000. Research programs of both countries were discussed and planned. Before the meeting, the U.S.-Japan Workshop on Smart Structure Systems was held January 6, 2000.

(2) Conducted the 6th (final) U.S.-Japan Technical Coordinating Committee Meeting on Composite and Hybrid Structural Systems in order to summarize research products and to discuss utilization (Information, dissemination, publication and archiving) of research products, March 2000, USA.

(3) Contributed to the 2nd Grantees Meeting U.S.-Japan coordinating Research in Urban Earthquake Disaster Mitigation on January 22, 2000 at Berkeley, CA to exchange the progress of research.

3. Future Plans
   (1) Develop a reliable methodology for screening and analyzing wind and seismic resistant capacity of existing building including advanced instrumentation technology and expert systems for condition assessment of existing structures.
   (2) Develop a metric system for assessing structural performance and compile a database of advance materials/systems that have potential for improving structural performance of new construction, for use in rehabilitating existing buildings, and for the purpose of quantifying damage.
   (3) Investigate new methods for achieving desired levels of structural performance using advanced materials and systems.
   (4) Continue to encourage participation of consulting engineers, universities, national and local government agencies involved in instrumentation, evaluation, condition assessment, and retrofit and strengthening of existing buildings for seismic and wind resistance.
   (5) Hold the 2nd U.S.-Japan Technical Coordinating Committee Meeting on Auto-Adaptive Media (Smart Structural Systems) before the end of 2000 in U.S.A.

Report of Task Committee D

EARTHQUAKE ENGINEERING FOR DAMS

Date: May 16, 2000

Place:
National Institute of Standards and Technology, Gaithersburg, U.S.A.

Attendees:
U.S. Side-- Robert Hall (Chairman) USAE
Japan Side-- Yoshikazu Yamaguchi (Chairman) PWRI

1. Objective and Scope of Work

To develop technical insights into better understanding of the response of dams to seismic effects, the T/C (D) will plan, promote, and develop research initiatives to assist in assuring seismic safety and economical protective countermeasures against earthquake loading for these structures. The scope of work includes:

(1) Methods of analysis for seismic design of dams including outlet works.
Comparison of design methods and criteria between U.S. and Japan.
Development of "Design Earthquake Ground Motions" for analysis and evaluation of dams.
Assessment of investigation and dynamic analysis methods as tools (modeling, calculation codes).

(2) Dynamic characteristics of dam construction materials and site conditions.
Strength and deformation characteristics during earthquakes (concrete, soil and rock).

(3) For the analysis of observed behavior of dams and outlet works during earthquakes:
- Construct a database that contains measured ground acceleration and dynamic response of dams and outlet works during earthquakes, and other related information which is necessary to evaluate their seismic behavior.
- Investigate the mechanism of damages due to earthquake loading.
- Analytically compare observed behavior during earthquake to the pre-earthquake-resistant design.

2. Accomplishments

(1) In the field of seismic design for embankment dams, Mr. Tomoya Iwashita, PWRI, finished a one-year (August 1998 – August 1999) research at University of California, Berkeley.

(2) T/C (D) conducted the Second U.S.-Japan Workshop on Advanced Research on Earthquake Engineering for Dams in Tokyo, Japan on 7-8 May 1999. The Workshop was attended by 13 U.S. participants and over 100 Japanese participants, and it served as a productive vehicle for technical exchange among scientists, engineers and specialists. The technical sessions focussed on a variety of topics, including dynamic analysis and seismic stability evaluation of concrete and embankment dams, site characterization, vibration testing, and laboratory testing for determination of material properties.

(3) Mr. Tsuneo Uesaka , Mr. Takashi Sasaki and Masahiko Murase, PWRI, visited U.S. Army Engineer Research and Development Center (ERDC) 13-14 March 2000 to discuss the future cooperative research works and to exchange the latest results of research / investigation and technical information about dam earthquake engineering.

3. Future Plans

(1) Exchange of the results of research / investigation and technical information about dam earthquake engineering is encouraged.

(2) Exchange visits to the institutes concerned, of scientists and engineers between U.S. and Japan, is to be extended for the effective communications.

(3) In view of the importance of constructing a database for seismic evaluation of dams and outlet works, cooperative research on the standardization for location and installation of strong motion seismographs, and collection and processing of measured seismic data will be started. Dr. Enrique Matheu (Department of Civil and Environmental Engineering, Louisiana State University) will complete a six-week joint research with PWRI engineers during this year at PWRI. Dr. Matheu will work with PWRI engineers in the initial implementation of the database. This discussion will be useful in developing the proper format of the data, which will be obtained from strong motion instrumentation of dams currently under construction by Ministry of Construction. During the project, he will also work with PWRI engineers in preparing a technical paper on the comparison of U.S. and Japan design standard for concrete dam. A proposal to support this research will be sent by June 2000 to the Japan Science and Technology Agency.

(4) Dr. Michael K. Sharp (U.S. Army Engineer Research and Development Center) will complete a four-week joint research with PWRI during the next year at PWRI to prepare a technical paper on the comparison of U.S. and Japan design standards for embankment dam. The U.S. Army Corps of Engineers through the Earthquake Engineering Program will fund this research effort.

(5) The proceedings of the Second Workshop will be published and distributed to the T/C members and Panel secretariats.

(6) T/C (D) will hold the Third U.S.-Japan Workshop on Advanced Research on Earthquake Engineering for Dams next year in USA. The location and time of the workshop will be determined through correspondence between the chairs of T/C (D). Joint presentations of cooperative research mentioned in (3) will be made at the workshop.

REPORT ON TASK COMMITTEE E

DESIGN FOR WIND AND WIND HAZARD MITIGATION

Date: May 16, 2000

Place: National Institute of Standards and Technology, Gaithersburg, MD, USA

Attendees:	U.S.-side --	Harold R. Bosch (Acting Chairman)	FHWA
		Hiroshi Sato (Co-Chairman)	PWRI
	Japan-side –	Shoichi Saeki	PWRC

1. Objective and Scope of Work

To exchange technical information and to jointly plan, promote and foster research and dissemination, to improve understanding of wind and its effects on structures, establish more rational wind resistant design methods for structures, and to contribute to wind hazard mitigation.

The scope of work includes:

(1) Characterization of strong wind, especially boundary layer extreme winds.

(2) Wind effects (wind loading on and wind-induced response of structures).

(3) Experimental and analytical methods to predict wind and its effects.

(4) Damage and risk assessment.

(5) Wind hazard assessments and wind hazard mitigation.

2. Accomplishments

(1) Held the second Joint Workshop on Design for Wind and Wind Hazard Mitigation at the PWRI on May 24-26, 1999. Twelve US-side Task Committee members and 15 Japan-side members participated in the Workshop. After presenting papers covering wind characteristics; wind flow, pressure and loading; wind-induced response; and wind hazards; the participants separated into three groups: wind characteristics and wind hazards; wind effects on buildings; and wind effects on bridges, and identified research topics of mutual interest. Before and after the Workshop, the participants visited the following technical sites: wind tunnels of Meteorological Research Institute, BRI and PWRI; and the Honshu-Shikoku bridges between Onomichi and Imabari.

(2) The proceedings of the second Workshop were published by PWRI, and distributed to all the Task Committee members.

3. Future Plans

1) Plan the third Workshop in the autumn of 2001, possibly at the University of Washington in the US.

2) Pursue the possibility of collaborative research on the following topics recommended at the second Workshop.

   a) In the field of wind characteristics and wind hazards,
      (1) Wind effects due to complex terrain
      (2) Modeling and validation with full-scale data
      (3) Joint field studies
      (4) Cooperative quick-response post-storm damage assessments
   b) In the field of wind effects on buildings,
      (1) Development of realistic aerodynamic loads for performance-based structural design
   c) In the field of wind effects on bridges,
      (1) Improvement of methods for predicting wind-induced response of cable-suspended bridges with edge girders
      (2) Prediction and mitigation of wind-induced vibration of stay cables

3) Exchange technical information on the following subjects:

   (1) Topographical effects on wind and the use of field measurements, numerical models and geographic information system (GIS) to study these effects.

   (2) Control of wind-induced response of structures.

   (3) Computational fluid dynamics and wind tunnel tests.

   (4) Prediction of wind-induced response of full-scale structures.

   (5) Investigation of wind hazards, including post-storm damage assessment methodologies.

   (6) Wind resistant design codes, standard and recommendations.

REPORT ON TASK COMMITTEE F

DISASTER PREVENTION METHODS FOR LIFELINE SYSTEMS

Date: May 16, 2000

Place: National Institute of Standards and Technology

Attendees:	U.S.-side –	James Cooper (Acting Chairman)	FHWA
		Josephine Malilay	CDC
	Japan-side –	Keiichi Tamura (Acting Chairman)	PWRI

1. Objective and Scope of Work

To improve the performance of lifeline systems during earthquakes and extreme winds, and to promote the development and implementation of technical and non-technical countermeasures, including the capability in damage estimation techniques and inspection procedures, through:

3. Planning and conducting workshops.

4. Facilitating exchange of technical information and personnel.

5. Promoting development of design guidelines and standards.

2. Accomplishments

4) Members of this Task Committee (T/C) participated in the planning and attended the Second High-Level U.S.-Japan Earthquake Policy Cooperation Forum held in Yokohama, Japan in November 1999. The Forum was led by the U.S. Federal Emergency Management Agency and the National Land Agency of Japan, under the U.S.-Japan Natural Disaster Reduction Initiative of the U.S.-Japan Framework for New Economic Partnership (Common Agenda).

3. Future Plans

(1) Encourage collaborative research and development in areas such as: performance prediction and post-earthquake damage assessment of lifeline systems; systems approach to lifeline performance; vulnerability inspection and retrofit techniques; post-earthquake response; and socio-economic impacts of damage to lifeline facilities.

(2) Encourage and strengthen current efforts in both countries for developing seismic design guidelines and standards for lifeline systems. Existing UJNR channels should be fully utilized to facilitate the exchange of relevant information concerning the development of guidelines and standards. Possible collaboration of developing guidelines and standards for

lifeline systems should be pursued.

(3) Continue to explore cooperative opportunities to address post-disaster public health issues as a result of disruption to lifeline systems as a part of the T/C F. T/C F members will make recommendations on the appropriateness of incorporating this topic within the T/C F scope after the appointment of the U.S.-side Chair.

(4) Upon appointment of the U.S.-side Chair, plan and conduct the Eighth Joint Workshop on Disaster Prevention for Lifeline Systems in Japan. Specific location, time, and theme of the workshop will be determined through correspondence between the co-chairs of this task committee.

Report of Task Committee G
SEISMIC INFORMATION SYSTEMS

Date: 17 May 2000

Location: National Institute of Standards and Technology
Gaithersburg, MD U.S.A.

Attendees:	U.S. side	William Roper (co-chairman)	(NIST)
		Stuart Nishenko (co-chairman)	(FEMA)
		Mehmet Celebi	(USGS)
	Japan side	Hideki Sugita (co-chairman)	(PWRI)
		Izuru Okawa	(BRI)
		Akihiro Sanada	(PWRI)
		Masaomi Teshigawara	(BRI)

1. Objective and Scope of Work

The objective of the Task Committee is to plan and coordinate collaborative activities in the following areas:

1. Technically assist the earthquake policy cooperation under the U.S.-Japan Common Agenda for Cooperation in the Global Perspective (Common Agenda).
2. Improve understanding of earthquakes and social impacts through development of seismic information systems.
3. Review the principles, objectives, structures, and methodologies of existing seismic information systems and facilitate practical application in both countries.

These objectives will be achieved through a) planning and conducting workshops, b) planning and conducting cooperative research, c) exchange of information and personnel in administrative and technical fields, and d) introducing research accomplishments to guidelines and standards.

2. Accomplishments

1. The T/C G members participated in the planning and attended the Second High Level U.S.-Japan Earthquake Policy Cooperation Forum (High-Level Forum) that was held under the auspices of the Common Agenda, 10-12 November 1999 in Yokohama, Kanagawa, Japan. The High-Level Forum was led by the NLA and FEMA, and political efforts for the earthquake disaster reduction including the application of seismic information systems were discussed. Recognizing the importance of continuous information exchange, both countries agreed to hold the Third High-Level Forum in 2000.
2. The First U.S.-Japan Workshop on Seismic Information Systems was held at PWRI during 15-16 November 1999. 38 persons including 5 persons from the U.S.-side and 18 persons from the Japan-side participated, and 27 papers were presented during the workshop. Following the workshop, a technical site visit

was conducted at the NLA, the Tokyo Fire Department and the Tokyo Gas Company, Ltd.

3. The Proceedings of the First U.S.-Japan Workshop on Seismic Information Systems are published and will be distributed to the workshop participants and the Secretariat.

3. Future Plans

1. In consideration of the specific topics to be discussed in the Third High-Level Forum, the Task Committee will encourage collaborative activities in the following areas:

- Application of advanced technologies including GIS, GPS, and satellite imaging.
- Strategies to collect, organize, archive, and distribute data from individual information systems.
- Cost-effective technologies for the application of seismic information systems.
- Information systems for tsunami hazard and risk reduction.

2. The Task Committee will pursue the possibility of collaborative research to compare loss estimation methodologies, information system architectures, and risk assessment/crisis management strategies in both countries.
3. The Task Committee will pursue information exchange with other related UJNR T/Cs and Panels on common technologies including earthquake ground motion acquisition, remote sensing of earthquake damage, and tsunami hazard and risk reduction.
4. The Task Committee will conduct the Second U.S.-Japan Workshop on Seismic Information Systems at the USGS facilities in Menlo Park, California in 2000. This workshop will be held in cooperation with Task Committee A and will include damage detection in the agenda. The U.S.-side will propose a date for the workshop that is in coordination with the Third U.S.-Japan High-Level Forum.

Report of Task Committee H
SOIL BEHAVIOR AND STABILITY DURING EARTHQUAKES

Date: May 17, 2000

Place: National Institute of Standards and Technology, Gaithersburg, MD, USA

Attendees:

U.S.-side--	Richard Olsen (Acting Chairman)	WES
Japan-side --	Keiichi TAMURA (Acting Chairman)	PWRI
	Chikahiro MINOWA	NIED

1. Objective and Scope of Work

Government agencies responsible for public works must assure seismic safety and provide economical protection against earthquake hazards.
The objective of the Task Committee (H) is to assist in meeting these needs by enhancing the availability of technology for predicting the dynamic behavior of soils, foundations and earth structures, and analyzing dynamic soil-structure interaction to assure their safe performance during earthquakes.

In accordance with the objective, the scope of work includes:
(1) Exchange information on technological developments, state-of-the-art and practice related to soil behavior and stability during earthquakes,
(2) Exchange information and technical data related to field performance, research, and methods of practice,
(3) Plan and conduct programs of cooperative research and/or workshops in coordination with the proposed or ongoing programs, and
(4) Make other efforts needed including exchange of researchers between U.S. and Japanese research institutes, and publication of research results and recommended practice.

2. Activities

(1) The National Research Institute for Earth Science and Disaster Prevention (NIED), the Building Research Institute (BRI), and Wayne State University (WSU), have continued to work in their cooperative research program "Physical and Numerical Simulation of Structural Damages Due to Liquefaction and Development of Countermeasure Techniques", 1994-2004.

(2) Port and Harbor Research Institute (PHRI), Colorado School of Mines and the New Mexico Resonance Institute (Albquerque, NM) have continued joint

research on application of the Nuclear Magnetic Resonance Imaging (NMRI) method to the study of soil behavior and stability during earthquakes.

(3) Under the auspices of Task Committee "H", Mr. O. Matsuo and Dr. M. Okamura, PWRI researchers in geotechnical earthquake engineering, had a successful visit in August 1999 and December 1999, respectively, to WES and other universities. The purposes of their visit were to collect recent information on evaluating liquefaction potential, experimental techniques of geotechnical centrifuge modeling and related topics, and to discuss possibility of developing cooperative research works.

3. Future Plans

The U.S. and Japan sides will put a focus on exchanging research findings and developing cooperative research works in the following two particular areas in which both Japanese and U.S. researchers are currently conducting the studies.

(1) Seismic stability assessment and design procedures for embankment structures
Japanese researchers are investigating the rationalization of conventional pseudo-static stability analysis procedures and developing predictive procedures of permanent deformation and flow failure.
U.S. researchers are investigating different types of failure mechanisms and the effectiveness of current procedures for liquefaction analysis. Improvement of centrifuge experimentation on embankment structures is a common interest.

(2) Improvement of liquefaction potential assessment procedures
Both the U.S. and Japan currently have procedures for evaluating liquefaction that incorporate many factors. Both sides are currently involved in research to evaluate these factors. In-situ measurement technique by the use of the cone penetrometer is also of common interest for both sides.

The committee also plans an exchange of researchers in the coming year to exchange information and encourage cooperative research activities.

Report of Task Committee I
STORM SURGES AND TSUNAMI

Date: May 17, 2000

Place: National Institutes of Standards and Technology, Gaithersburg, Maryland, U.S.A.

Attendees: U.S.-side --	Michael Blackford, Chairman	NOAA
Japan Side --	Shigeki Unjoh, Acting Chairman	PWRI

Objective and Scope of Work

The objective of this Task Committee is to mitigate damage from storm surge and tsunami through cooperative research and shared technology and information. The primary cause of storm surge is considered to be tropical cyclones (hurricanes, typhoons). The primary cause of tsunami is considered to be sudden sea floor deformation due to earthquakes, landslides, and volcanic activity. Both hazards may cause disasters along coastal regions.

The scope of work of this Task Committee is as follows:

(1) Exchange results of research on storm surge and tsunami occurrence, generation, propagation, and coastal effects. This includes observations on historical, current, and theoretical tsunamis. Of particular interest is the effort by the U.S. and Japan to acquire deep ocean tsunami measurements.

(2) Exchange results and status of storm surge and tsunami activities including analysis of the problem, planning, warning, and engineering approaches.

(3) Exchange information on the development of technologies such as computer programs to predict travel times, landfall locations, wave characteristics, inundation and run-up heights, improved instrumentation, and the use of satellite communication for detection and warning.

(4) Facilitate dissemination through exchanges of literature, technical reports at joint meetings, special workshops, joint projects, and direct interaction among participants. The storm surge research community, which functions through many related societies and international organizations, defines and stimulates work in the field. The Task Committee, through its meetings and workshops, encourages exchanges of ideas and joint study by U.S. and Japanese investigators of tsunami events throughout the world.

Accomplishments

Since the issuance of the last report of this Task Committee U.S. Side members have been active in projects that have resulted in the publication of a number of reports of value to emergency managers and the general public. Two reports of particular interest are, "1997-1999 Activities of the Tsunami Mitigation Subcommittee – A Report to the Steering Committee, National Tsunami Hazard Mitigation Program" and "Surviving a Tsunami – Lessons from Chile, Hawaii, and Japan", U.S. Geological Circular 1187. Through efforts of the Pacific Tsunami Warning Center and the UNESCO/IOC Tsunami Warning System in the Pacific two new water level stations have been installed and placed in operation in Kamchatka and in the northern Kuril Islands.

Data from these stations are relayed through the Japanese GMS satellite to users in Japan, the U.S.A., and Russia. Improved communications methodologies have vastly increased the amount of both seismic and water level real time data available to the Warning Centers. These data help to reduce the time necessary to both issue and cancel tsunami warnings and watches and to reduce the possibility of the issuance of unnecessary warnings.

Future Plans

The Task Committee exchanges information and encourages cooperative research and development on the following subjects:

(1) Cost reduction of deep ocean tsunami detection systems
(2) Accessibility of tsunami detection data in the deep ocean
(3) Investigation of tsunami detection by artificial satellites
(4) Accessibility of gridded bathymetry data in the deep ocean and extension of the database to shallow seas
(5) Development and improvement of numerical models of tsunamis and storm surges
(6) Development of predictive models on scour around structures by tsunamis
(7) Technical support to develop tsunami mitigation programs in Pacific nations
(8) Collecting information (tsunami source, run-up height and damage) for historical and current tsunami in the Pacific

Other

The Task Committee shall hold its Sixth Tsunami Workshop through its joint sponsorship of a tsunami workshop hosted by the NOAA/Pacific Marine Environmental Laboratory to be held in the U.S.A. in 2001.

Report on Task Committee J

WIND AND EARTHQUAKE ENGINEERING FOR TRANSPORTATION SYSTEMS

Date: May 17, 2000

Place: National Institute of Standards and Technology, Gaithersburg, MD, USA

Attendees:	U.S.-side --	Dr. Phillip Yen (Acting Chairman)	FHWA
	Japan-side --	Dr. Hiroshi Sato (Acting Chairman)	PWRI
		Dr. Kazuhiko Kawashima	Tokyo Institute of Technology

1. Objective and Scope of Work

Surface transportation systems play a vital role in the movement of goods and people. Highway bridges are especially influenced by the forces of wind and earthquakes because of their open exposure to those forces.

The objectives of work includes:
(1) To plan, promote and foster research on the behavior of highway bridges when subjected to wind and seismic forces, and
(2) To disseminate research results and provide specifications and guidelines based on the Task Committee's findings.

The scope of work includes:
(1) To focus research on highway bridges without limitation on their size and function, and
(2) To investigate existing and new bridge design, the behavior of whole bridge systems and/or single component of a bridge.

2. Accomplishments

The 15th U.S.-Japan Bridge Engineering Workshop was held during November 9 – 10, 1999, in Tsukuba, Japan. The workshop was attended by 22 U.S. and 65 Japanese participants. The earthquake reports of the Turkey Earthquake and Taiwan Earthquake were held as the special session. The topics of the workshop included: 1) Innovative seismic retrofit technology including the application of new materials and new structural systems, 2) Innovative bridge design concept, e.g., bridges types, materials, life cycle cost analysis. The proceedings of the workshop have been published and will be distributed.

3. Future Plans

(1) The 16th U.S.-Japan Bridge Engineering Workshop will be held in October 2000 at Lake Tahoe, Nevada, U.S.A.

The topics of the workshop will include:

a) Corrosion protection technology of steel and steel materials in concrete.
b) Technology of performance based seismic design and innovative seismic retrofitting for existing bridges.

(2) Encourage coordinated researches on the following topics:

a) Bridge design methodologies which embrace performance based design concepts, limit state design concepts and life cycle costs analyses.
b) Seismic isolation design methodologies considering the dynamic characteristics of isolation devices and their modeling.

(3) Continue to investigate and exchange technical information on the improved seismic retrofitting and strengthening procedures for highway bridges based on experimental, analytical, and field studies, including the development of innovative earthquake protective systems, the evaluation of the seismic performance of total bridge systems, and the development of damage evaluation methods using sensor systems, etc. This exchange should also include information related to the maintenance of existing bridges.

(4) Continue coordinated research project to compare the seismic design criteria and seismic retrofit technologies for bridges in Japan and the U.S.

(5) Encourage research study on seismic and aerodynamic response of long span bridges such as suspension bridges and cable-stayed bridges with emphasis on behavior of composite materials, cable inspection, vibration control, and corrosion protection.

(6) Encourage coordinated research study on system identification techniques, non-destructive evaluation of bridge structures, use and performance materials including new materials, and performance of jointless bridges.

Report on Task Committee K

WIND AND EARTHQUAKE ENGINEERING FOR OFFSHORE AND COASTAL FACILITIES

Date: May 16, 2000

Place: National Institute of Standards and Technology, Gaithersburg, MD, USA

Attendees:

U.S.-side --	Mehmet Çelebi (Acting Chairman)	MMS
Japan-side --	Takashi Nagao (Acting Chairman)	PHRI
	Yoshikazu Yamaguchi	

1. Objective and Scope of Work

To develop technical insights necessary to mitigate damage to offshore and coastal facilities due to extreme wind and seismic effects. The Task Committee will plan, promote and develop research initiatives to meet this objective and will disseminate the results of its research for incorporation into future specifications and design guidelines. Criteria for the design of offshore and coastal facilities differ from their onshore counterparts. These differences arise due to the unique design or mass distribution of the facilities, to the fluid/structure or wind/structure interaction, to the placement of foundation elements in or on soft, fully saturated soils that can be subject to large hydrodynamic pressures, and to the lack of specific environmental data or engineering experience that has been developed for most Onshore Sites.

The scope of work includes:

(1) Sponsoring and conducting workshops and meetings to identify key areas of research opportunities for cooperation and the exchange of knowledge.
(2) Predicting strong motions for offshore and coastal sites including assessing the effects of basin geometry, and linear and nonlinear local geological effects, using actual sea-floor response measurements.
(3) Determining the dynamic response and the interaction of structure/foundation/soil systems to seabed motions and extreme wind forces.
(4) Assessing the dynamic response and behavior of various operational facilities mounted on offshore and coastal structures.
(5) Developing assessment methodologies for earthquakes and other characteristics of potential seismic sources (e.g. faults) for offshore and coastal sites in regards to how these conditions relate to structural design criteria.
(6) Promoting the implementation of new research results into current design and construction processes.
(7) Developing research efforts to include laboratory and field programs to obtain data on the response of offshore and coastal facilities to extreme wind and seismic forces.
(8) Creating performance standards, design specifications, and code recommendations for

(9) applications to new construction as well as remedial action for existing facilities.

2. Accomplishments

(1) Task Committee K held initial planning phase meetings to conduct a third U.S.-Japan workshop. The theme of this workshop will focus on seismic, wind and hazard mitigation techniques for offshore and coastal facilities.

(2) Mr. Nozu, researcher of PHRI, completed research on earthquake resistant technology for offshore and coastal facilities at California Institute of Technology in September 1999.

3. Future Plans

(1) Develop and finalize workshop agenda including invited speakers of the third U.S.-Japan Workshop on Wind and Earthquake Engineering for Offshore and Coastal Facilities.

(2) Coordinate, where possible, on-going research on wind and earthquake engineering for offshore and coastal facilities of interest to the members of the Task Committee K. This includes sharing of research reports and publications, where possible, listed as following.
a) Seismic performance based design concept for onshore and offshore facilities.
b) Rehabilitation/life extension technologies for offshore and port facility.

(3) Task Committee K will work within the framework of the U.S.-Japan Common Agenda Program focusing on the issue of acceptable seismic risk guidelines for ports and harbors.

(4) Task Committee K will coordinate activities with the Pacific Earthquake Engineering Research (PEER) Program on ports and harbors centered at the University of Southern California.

Technical Site Visits

SUMMARY OF THE TECHNICAL SITE VISITS 20-23 MAY 2000

Following the 32nd Joint Meeting of the UJNR Panel on Wind and Seismic Effects, a joint delegation traveled to Puerto Rico to visit four technical sites. Puerto Rico is a self-governing commonwealth of the United States. The delegation visited sites in San Juan and Arecibo in the northern part of the island and traveled to the city of Ponce on the southern coast to visit two sites. The details of these visits are described below.

1. Arecibo Observatory

The delegation visited the Arecibo Observatory on May 21. The Arecibo Observatory is a part of the United States' National Astronomy and Ionospheric Center (NAIC). Cornell University operates the observatory under a cooperative agreement with the National Science Foundation, with additional funding for its operation provided by the National Aeronautics and Space Administration. Mr. José Maldonado hosted the delegation and led the tour of the facility.

The Arecibo radio telescope is the largest single dish radio telescope in the world. The dish measures 305 m in diameter and 51 m deep. The spherical reflecting surface is composed of approximately 40,000 1 m x 2 m panels supported by a network of steel cables. The observatory is located in a large limestone sinkhole in the Karst region near the city of Arecibo. The observatory is used to conduct experiments in the ionosphere, radar studies of nearby planets and asteroids, and to study radio emissions of pulsars and quasars.

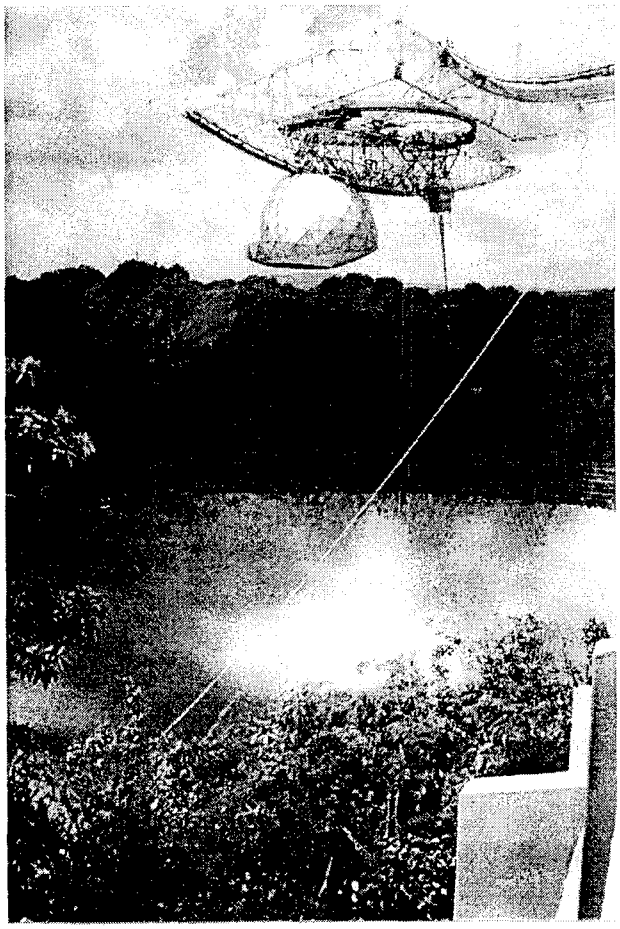

Figure 1: View of Arecibo Observatory showing reflector and antenna platform.

The antenna platform is suspended 137 m above the surface of the dish. The 800,000 kg platform is suspended by cables strung from three reinforced concrete towers. Two of the towers are 80.8 m tall, and the third is 111 m tall. The differing heights were necessary so that the tops of the towers were all at the same elevation. Each tower is back-guyed to ground anchors with a system of seven 8.26 cm steel cables. A separate system of cables connects each corner of the platform to large concrete blocks under the dish. The concrete blocks are attached to jacks, which permit adjustment of the

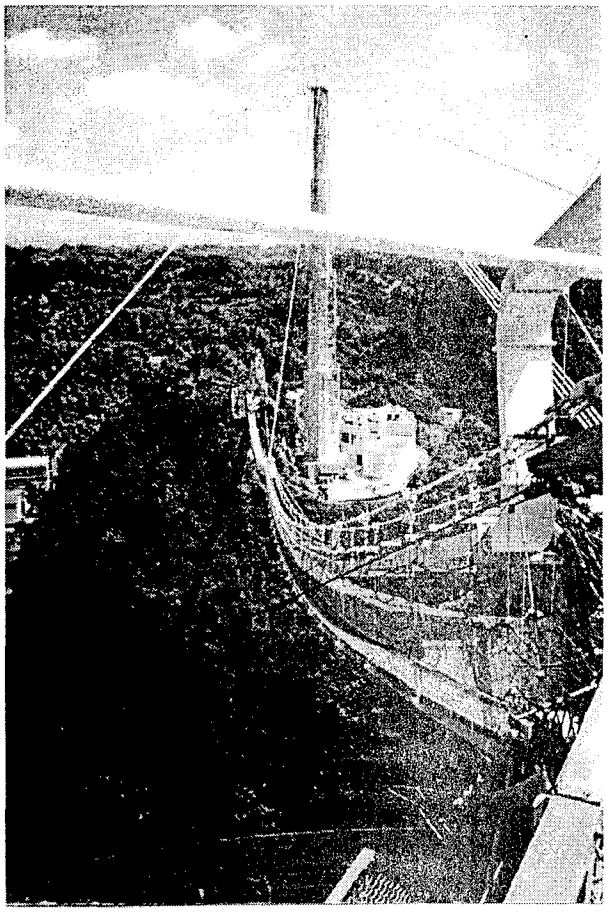

Figure 2: One of three reinforced concrete towers supporting antenna platform. The control building is visible at the lower left and the Visitor Center can be seen at the base of the tower.

height of each corner of the platform with millimeter precision. The triangular frame of the platform supports a circular track from which the azimuth arm is suspended. The circular track allows for the rotation of the azimuth arm in the horizontal plane. The azimuth arm itself is a 100 m long structure that includes a curved track. On one side of the track is mounted the gregorian dome and on the other the carriage house to which a number of linear antennas are mounted. The azimuth arm permits the Gregorian dome or carriage house to be positioned anywhere up to 20° from the vertical. Twenty-six electric motors control the positioning of the azimuth arm, gregorian dome, and carriage house with millimeter precision.

The Arecibo site was selected because of its proximity to the equator, which provided the ability to not only observe the ionosphere but nearby planets as well. The Karst terrain, notable for its large limestone sinkholes provided a natural geometry for the reflector. Construction of the Arecibo observatory was begun in the summer of 1960. The observatory was formally opened three years later in November 1963. The current high precision reflector was installed during an upgrade in 1974 along with a high frequency planetary radar. The gregorian dome was installed as part of major upgrade completed in 1997.

The location of the observatory in Puerto Rico meant that the design and construction had to account for both seismic activity and wind loads due to hurricanes. The antenna platform and tower system is designed to withstand sustained 200 km/h winds. A seismic evaluation of the structure is in progress to verify that the structure is still safe following the addition of the gregorian dome, which added significant mass to the antenna platform. The antenna platform experienced a maximum observed motion of 5 cm during Hurricane Georges in 1998.

The delegation was given a tour of the control room for the observatory and was able to observe an experiment in progress. The delegation was then permitted to walk out to the antenna platform along the personnel access catwalk. The visit to the platform provided

the delegation with a unique perspective of the scale of the structure. The members of delegation had the opportunity to ask specific questions about the design and construction of the observatory and considerations for extreme loads due to wind and seismic events.

Cerrillos and Portugues Dams

The delegation traveled to the city of Ponce on the southern coast of the island to visit two U.S. Army Corps of Engineers dam projects. Ponce, because of its location on the Caribbean coast, and the proximity of the Bucana and Portugues Rivers is subject to flooding during heavy rainfall and has experienced a number of serious floods. The headwaters of both rivers originate in the Central Mountains, and flow southward toward Ponce. The dams and related channel improvements are intended primarily for flood control. Both dams have been designed so that they can be modified to provide water supply to surrounding localities in the future. The reservoirs will also be developed to provide recreation areas for local residents.

The tour began at the field office for the two projects. The delegation was given a presentation on the two dams and related channel improvements by Pablo Vasquez, a civil engineer with the U.S. Army Corps of Engineers site office located near the Cerrillos Dam. The presentation provided an historical context for the two projects including a discussion of the flood events that triggered the projects as well as providing a thorough overview of the projects and some of the key features of the dams, channel improvements and drop structures.

Figure 3: View of Cerrillos Dam embankment.

Following the presentation, Mr. John Conway of the U.S. Army Corps of Engineers took the delegation on a tour of the Cerrillos Dam. The dam consists of a 98.5 m high zoned rockfill embankment with a central clay core flanked by a two-stage filter and supported by zoned rock shells. The axis of the embankment is approximately 474 m long. A 60 m deep, triple line grout curtain was placed beneath the dam along the centerline axis. The crest of the dam is 193.5 m NGVD (National Geodetic Vertical Datun). The minimum flood control pool elevation is 175 m NGVD. An emergency spillway, cut into the right embankment of the dam has a crest of 186.3 m NGVD and is intended to prevent the pool from cresting the main embankment. The outlet works is located in the left abutment of the dam and includes an inclined intake structure, a 5.5 m diameter regulatory outlet tunnel, and a stilling basin. Because the dam is subject to earthquakes, a series of strong motion detectors has been installed at intervals across the dam.

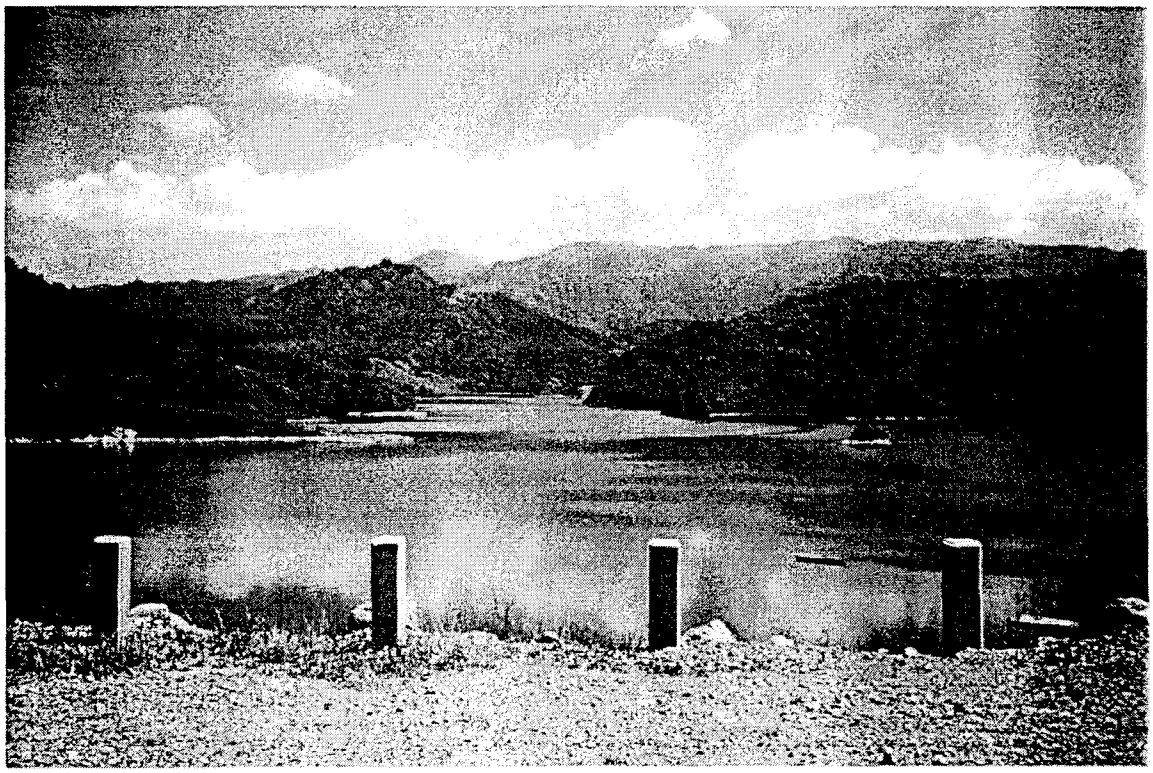

Figure 4: Reservoir created by Cerrillos Dam.

After touring the Cerrillos Dam, the delegation was taken to view the Portugues dam construction site. Construction of the dam itself is scheduled to begin in late 2000. At the site, the rails and moveable platform used to carry equipment for the injection of the grout curtain and the injection pipes were visible. Similar to the Cerrillos dam, a 60 m deep, triple wall grout curtain was also placed for the Portugues Dam.

The Portugues Dam, when complete, will be the first of its kind constructed by the U.S. Army Corps of Engineers. It is a three-centered concrete dam, curved in both the vertical and horizontal directions. The dam will be constructed in two phases, the first to provide

Figure 5: West side of Portugues Dam site. Grout pipes are visible to right of rails.

flood control and recreation and the second to provide water supply. When complete, the dam will have a length of 459 m and a crest height of 82.5 m. The dam will be 13 m wide at the base and 3.7 m wide at its crest.

The delegation was also able to view some of the channel improvements made to both the Bucana and Portugues Rivers. Along the Bucana, it was possible to see sections where rip-rap had been placed to prevent channel erosion during periods of high flow velocities. During the drive to the Portugues Dam, drop structures and concrete channel walls that had been constructed along the Portugues River were visible. From the top of the Cerillos Dam, the realignment of the Portugues River, which changed the location of its confluence with the Bucana River, could be seen.

2. Tren Urbano

On May 23, the delegation toured the alignment of the Tren Urbano urban rail system in the San Juan area. Approximately one-third of Puerto Rico's 3.8 million residents live in the San Juan Metropolitan Area (SJMA), a region of about 1000 km^2. SJMA residents make approximately 3.2 million trips per day, and an estimated 1625 vehicles per square kilometer in the central SJMA combine to produce some of the worst traffic congestion in the world.

The initial phase of the Tren Urbano project will serve the municipalities of San Juan, Bayamón, and Guaynabo. The line will operate 20 hours a day and is expected to serve

115,000 passengers per day. The population density within 0.8 km of the alignment ranges from (4,000 to 8,000)/km^2 and over 30 % of the regional employment will be located within 0.5 km of the train corridor. The Phase I alignment is 17.2 km in length and will have 16 stations. Fifty-two percent of the alignment is elevated, 40 % at grade, and the remaining 8 % underground. The Phase I alignment is scheduled to open in the summer of 2001 at a cost of $1.67 billion.

The delegation began its tour at the Tren Urbano office in Hato Rey. Dr. Dru Desai, of Daniel, Mann, Mendenhall & Johnson, gave an overview presentation of the project, including a discussion of the project requirements, contracting, and construction management. A second presentation oriented the delegation to the alignment and included a videotaped flyover of the Phase 1 alignment.

Following the presentations, the delegation was taken on a tour of the alignment. The tour began at the western terminus of the Phase 1 alignment in Bayamón. The delegation was shown the casting yard where precast concrete segments for the elevated guideway are produced. It was also possible for the delegation to observe the construction of the elevated guideway. The segments are placed using an overhead launching truss and post-tensioned with steel cables. From Bayamón the delegation was taken to Martinéz Nadal to view a station under construction, the maintenance yard, and a section of at-grade rail that will serve as the test track for the system.

Figure 6: Elevated guideways under construction in Bayamón.

From Martinéz Nadal, the delegation was taken to the Tren Urbano office in Río Piedras where it was met by Dr. Rafael Jimenez, Project Director for Tren Urbano. Dr. Jimenez gave a presentation detailing the procurement process and quality assurance/quality control aspects of the project. Following the presentation, the delegation was taken to see the construction of the tunnels and station in Río Piedras. Underground construction was necessary in Rio Piedras due to the presence of a large number of historic buildings and the density of building in the area. Two types of tunnel construction were seen. The Río Piedras station is being constructed using a stacked drift method, where a series of small tunnels are excavated and filled with concrete. Each tunnel is offset slightly from the tunnel immediately below it thus forming an arched vault when complete. The arched

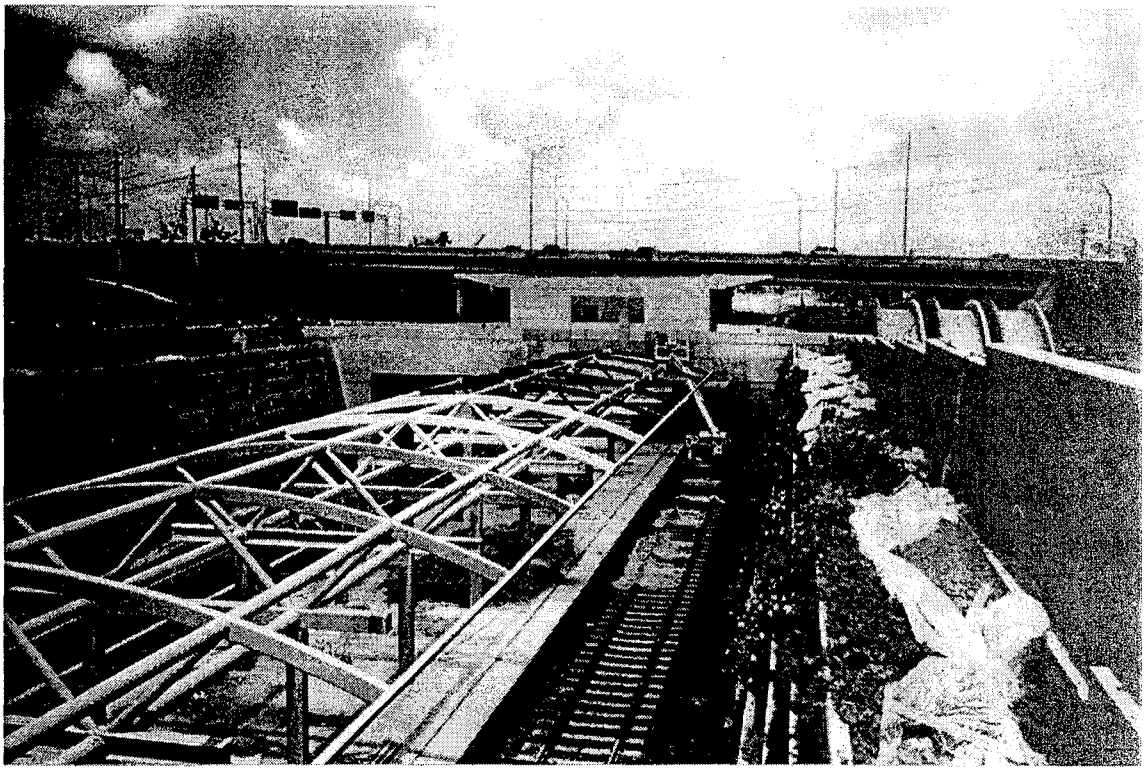

Figure 7: Station under construction in Martinéz Nadal.

vault will house the Río Piedras Station. The delegation was also shown two tunnels formed using the New Austrian Tunneling Method (NATM). These tunnels were bored using a tunneling machine and then lined with precast concrete segments that are gasketed and bolted together and held in place by earth pressure. This construction method provides a level of flexibility to the tunnel enabling it to withstand seismic forces.

Figure 8: Tunnel under construction in Rio Piedras. Precast concrete liner segments are visible.

Each member of the delegation also received information on the design of the structures used on the project, the organization of the Tren Urbano office, the procurement process used, and general information about the Tren Urbano system. This is an impressive project and will be a world-class urban transit system when completed.

NIST Technical Publications

Periodical

Journal of Research of the National Institute of Standards and Technology—Reports NIST research and development in those disciplines of the physical and engineering sciences in which the Institute is active. These include physics, chemistry, engineering, mathematics, and computer sciences. Papers cover a broad range of subjects, with major emphasis on measurement methodology and the basic technology underlying standardization. Also included from time to time are survey articles on topics closely related to the Institute's technical and scientific programs. Issued six times a year.

Nonperiodicals

Monographs—Major contributions to the technical literature on various subjects related to the Institute's scientific and technical activities.

Handbooks—Recommended codes of engineering and industrial practice (including safety codes) developed in cooperation with interested industries, professional organizations, and regulatory bodies.

Special Publications—Include proceedings of conferences sponsored by NIST, NIST annual reports, and other special publications appropriate to this grouping such as wall charts, pocket cards, and bibliographies.

National Standard Reference Data Series—Provides quantitative data on the physical and chemical properties of materials, compiled from the world's literature and critically evaluated. Developed under a worldwide program coordinated by NIST under the authority of the National Standard Data Act (Public Law 90-396). NOTE: The Journal of Physical and Chemical Reference Data (JPCRD) is published bimonthly for NIST by the American Institute of Physics (AIP). Subscription orders and renewals are available from AIP, P.O. Box 503284, St. Louis, MO 63150-3284.

Building Science Series—Disseminates technical information developed at the Institute on building materials, components, systems, and whole structures. The series presents research results, test methods, and performance criteria related to the structural and environmental functions and the durability and safety characteristics of building elements and systems.

Technical Notes—Studies or reports which are complete in themselves but restrictive in their treatment of a subject. Analogous to monographs but not so comprehensive in scope or definitive in treatment of the subject area. Often serve as a vehicle for final reports of work performed at NIST under the sponsorship of other government agencies.

Voluntary Product Standards—Developed under procedures published by the Department of Commerce in Part 10, Title 15, of the Code of Federal Regulations. The standards establish nationally recognized requirements for products, and provide all concerned interests with a basis for common understanding of the characteristics of the products. NIST administers this program in support of the efforts of private-sector standardizing organizations.

Order the **following** *NIST publications—FIPS and NISTIRs—from the National Technical Information Service, Springfield, VA 22161.*

Federal Information Processing Standards Publications (FIPS PUB)—Publications in this series collectively constitute the Federal Information Processing Standards Register. The Register serves as the official source of information in the Federal Government regarding standards issued by NIST pursuant to the Federal Property and Administrative Services Act of 1949 as amended, Public Law 89-306 (79 Stat. 1127), and as implemented by Executive Order 11717 (38 FR 12315, dated May 11, 1973) and Part 6 of Title 15 CFR (Code of Federal Regulations).

NIST Interagency or Internal Reports (NISTIR)—The series includes interim or final reports on work performed by NIST for outside sponsors (both government and nongovernment). In general, initial distribution is handled by the sponsor; public distribution is handled by sales through the National Technical Information Service, Springfield, VA 22161, in hard copy, electronic media, or microfiche form. NISTIR's may also report results of NIST projects of transitory or limited interest, including those that will be published subsequently in more comprehensive form.

U.S. Department of Commerce
National Institute of Standards
and Technology
Gaithersburg, MD 20899–0001